Probing quark mass effects in low-energy hadron physics

Dissertation

zur

Erlangung des Doktorgrades (Dr. rer. nat.)

der

Mathematisch–Naturwissenschaftlichen Fakultät

der

Rheinischen Friedrich–Wilhelms–Universität Bonn

vorgelegt von

Christoph Ditsche

aus

Siegburg

Bonn, Oktober 2012

"The main species of beauty are orderly arrangement, proportion [συμμετρια], and definiteness; and these are especially manifested by the mathematical sciences. And inasmuch as it is evident that these (I mean, e.g., orderly arrangement and definiteness) are causes of many things, obviously they must also to some extent treat of the cause in this sense, i.e. the cause in the sense of the Beautiful."

ARISTOTLE, Metaphysics, 13.1078a–b.*

---

* *Aristotle.* Aristotle's Metaphysics, ed. W. D. Ross. Oxford, Clarendon Press, 1924.
Aristotle. Aristotle in 23 Volumes, Vols. 17 & 18, translated by Hugh Tredennick. Cambridge (MA), Harvard University Press; London, William Heinemann Ltd. 1933, 1989.
`http://perseus.mpiwg-berlin.mpg.de/cgi-bin/ptext?lookup=Aristot.+Met.+13.1078a`

Abstract

Since quarks are confined inside hadrons, their properties as well as their contributions to hadronic observables can be assessed by indirect methods only. As the strength of the strong interaction increases with the spatial distance, the treatment of quantum chromodynamics at low energies in general requires non-perturbative methods like dispersion relations or lattice gauge theory. Based on the fact that the light quark masses are very small with respect to the typical hadronic mass scales for mesons and baryons, furthermore effective field theories can be constructed to describe low-energy properties and dynamics of hadrons perturbatively. The present work is concerned with two particularly interesting hadronic processes that are closely related to the light quark masses. Although distinct theoretical frameworks utilizing different calculational techniques are applied, in both cases the investigations at hand are prerequisites for high-precision analyses of the respective quark-mass effects.

In the first part of this thesis, we investigate higher-order isospin-breaking effects in $\eta \to 3\pi$ decays, namely $\eta \to \pi^0\pi^+\pi^-$ and $\eta \to 3\pi^0$, in chiral perturbation theory. By evaluating the second-order mixed strong and electromagnetic isospin-breaking corrections, we confirm the picture that the electromagnetic contributions are small. Therefore, $\eta \to 3\pi$ is perfectly suited to extract isospin-breaking ratios of light quark masses via comparing theoretical predictions with experimental results. Since for an accurate determination a detailed description of the Dalitz plot distributions is necessary, we study the different effects of higher-order isospin breaking in $\eta \to 3\pi$ on a more general basis. In particular, we investigate corrections to isospin relations between both decay channels at the level of Dalitz plot parameters, showing that the branching ratio of the two partial decay widths entails sizeable uncertainties.

In the second part, we develop a dispersive formalism and a solution strategy for a precision determination of the leading partial waves of the πN scattering amplitude in the low-energy region. They are specifically important to constrain the pion–nucleon σ-term, which measures the light-quark contributions to the nucleon mass and is still a subject of discussion. Starting from hyperbolic dispersion relations, we derive a closed system of Roy–Steiner equations that respects analyticity, unitarity, and especially crossing symmetry. Assuming Mandelstam analyticity, we determine the maximal kinematical ranges of validity of the equations for both the scattering process and the crossed annihilation process $\pi\pi \to \bar{N}N$. To suppress the dependence on the high-energy region, we also introduce subtractions into the Roy–Steiner system, identifying the subtraction constants with πN subthreshold parameters. The S- and P-waves of the crossed process feature prominently in dispersive analyses of the scalar nucleon form factor that is directly linked to the σ-term and the electromagnetic nucleon form factors, respectively. As a first step towards solving the full Roy–Steiner system, we study the solution of these partial waves by using Muskhelishvili–Omnès techniques.

Due to the conceptual and methodological differences, both parts are presented in a self-contained fashion.

Most contents of this thesis have been published under the following references:

- Christoph Ditsche, Bastian Kubis, and Ulf-G. Meißner,
  Electromagnetic corrections in $\eta \to 3\pi$ decays,
  Eur. Phys. J. **C 60** (2009) 83, [arXiv:0812.0344 [hep-ph]].

- Christoph Ditsche, Bastian Kubis, and Ulf-G. Meißner,
  Electromagnetic effects in $\eta \to 3\pi$,
  PoS **CD09** (2009) 043, [arXiv:0910.0210 [hep-ph]].

- Sebastian P. Schneider, Bastian Kubis, and Christoph Ditsche,
  Rescattering effects in $\eta \to 3\pi$ decays,
  JHEP **1102** (2011) 028, [arXiv:1010.3946 [hep-ph]].

- Christoph Ditsche, Martin Hoferichter, Bastian Kubis, and Ulf-G. Meißner,
  Roy–Steiner equations for pion–nucleon scattering,
  JHEP **1206** (2012) 043, [arXiv:1203.4758 [hep-ph]].

Contents

Part I

Isospin-breaking effects in $\eta \to 3\pi$ decays[†]

Chapter 1

Introduction

The decay $\eta \to 3\pi$ is particularly interesting because it is forbidden by isospin symmetry. While the η meson has isospin $I = 0$, according to G-parity three pions (with zero total angular momentum) can only couple to $I = 1$, and thus the decay can only happen via isospin-breaking $\Delta I = 1$ operators. In the Standard Model, there are two such sources of isospin violation: on the one hand strong interactions (with quantum chromodynamics (QCD) as the corresponding locally gauge invariant quantum field theory (QFT)) proportional to the light quark mass difference $\delta = m_d - m_u$ from

$$
\begin{aligned}
\mathcal{H}_{\mathrm{QCD}}(x) &= m_u \bar{u}u(x) + m_d \bar{d}d(x) + m_s \bar{s}s(x) \qquad\qquad \hat{m} = \frac{m_d + m_u}{2} \ , \\
&= \hat{m}\big(\bar{u}u + \bar{d}d\big)(x) - \frac{\delta}{2}\big(\bar{u}u - \bar{d}d\big)(x) + m_s \bar{s}s(x) \ , \qquad \delta = m_d - m_u \ ,
\end{aligned} \tag{1.1}
$$

where for convenience we also define the average light quark mass $\hat{m}$, and on the other hand electromagnetic interactions (as described by quantum electrodynamics (QED)) proportional to the electric charge squared e^2 from

$$
\mathcal{H}_{\mathrm{QED}}(x) = -\frac{e^2}{2} \int \mathrm{d}^4 y \, D^{\mu\nu}(x - y) \, T\big[j_\mu(x) j_\nu(y)\big] \ , \tag{1.2}
$$

where $D^{\mu\nu}(x - y)$ is the photon propagator and $j_\mu(x)$ is the current density containing the charged fields of the theory. A long time ago Sutherland and Bell showed by using soft-pion techniques that the electromagnetic contribution at tree level is much too small to account for the observed $\eta \to 3\pi$ decay rate, which is also known as Sutherland's (soft-pion) theorem [4,5]. Thus, this decay is very sensitive to the non-vanishing light quark mass difference δ and hence potentially yields a particularly clean access to the determination of quark mass ratios. More specifically, neglecting purely electromagnetic contributions, the amplitudes for both the charged ($\eta \to \pi^0 \pi^+ \pi^-$) and the neutral ($\eta \to 3\pi^0$) decay channel are proportional to the inverse of the quark mass double ratio Q^2,

$$
\frac{1}{Q^2} = \frac{m_d^2 - m_u^2}{m_s^2 - \hat{m}^2} = 2\,\frac{\delta}{\hat{m}}\,\frac{\hat{m}^2}{m_s^2 - \hat{m}^2} \ , \tag{1.3}
$$

so that the $\eta \to 3\pi$ decay widths (charged, neutral, and total) are related to Q according to

$$
\Gamma_{\eta \to 3\pi} \propto \frac{1}{Q^4} \ . \tag{1.4}
$$

Moreover, as long as isospin breaking beyond leading order is neglected, both $\eta \to 3\pi$ decay channels can be described by only one amplitude due to the $\Delta I = 1$ selection rule. As a consequence, the ratio of the partial widths for the neutral and the charged decay

$$r = \frac{\Gamma_{\eta \to 3\pi^0}}{\Gamma_{\eta \to \pi^0 \pi^+ \pi^-}} \tag{1.5}$$

must satisfy the inequality $r \leq 3/2$ up to higher-order isospin-breaking corrections. Neglecting furthermore purely electromagnetic corrections again, the (leading) Q-dependence of the amplitude normalizations cancels in the ratio r.

In view of Sutherland's theorem, the strong tree-level amplitude was studied using $(SU(3))$ current algebra and partially conserved axialvector current (PCAC) techniques [6,7], but the (neutral) decay width turned out to be off from the contemporary experimental value by a factor of a few. Already at that time it has been argued that unitarity corrections due to (strong) $\pi\pi$ final-state interaction (FSI) are the driving force behind this blatant discrepancy [8,9]. The PCAC hypothesis and $(SU(3))$ current algebra were later on generalized and cast into a modern form in the framework of $(SU(3))$ chiral perturbation theory (ChPT) [10–12], with the results of current algebra corresponding to the leading-order (LO, $\mathcal{O}(p^2)$, tree-level) ChPT results. As one of the first applications, Gasser and Leutwyler (GL) calculated the strong contribution at next-to-leading order (NLO, $\mathcal{O}(p^4)$, one-loop level) [13]. Although they observed large corrections at NLO (in particular due to $I = 0$ S-wave $\pi\pi$ FSI), their value for the (charged) decay width still differs from experiment by a factor of two.[#1] Using an extension of ChPT including virtual-photon effects [14], Baur, Kambor, and Wyler (BKW) then studied corrections to Sutherland's theorem by evaluating the (purely) electromagnetic contributions in $\eta \to 3\pi$ at one-loop level, i.e. at $\mathcal{O}(e^2 p^2)$, but they found them to be very small [15].[#2] Therefore, strong corrections beyond one loop (see also [16]) were subsequently studied using dispersive methods [17,18], unitarized ChPT [19,20], and eventually with a complete calculation at next-to-next-to-leading order (NNLO, $\mathcal{O}(p^6)$, two-loop level) [21]; all of them finding considerable enhancement compared to the one-loop calculation. Despite these (and others) valiant theoretical efforts and improvements, it still seemed difficult to achieve agreement between the theoretical description of $\eta \to 3\pi$ decays and experimental results for the decay widths and the so-called Dalitz plot parameters of $\eta \to \pi^0 \pi^+ \pi^-$ [22–25] and $\eta \to 3\pi^0$ [26–31].[#3] This is most noticeable for the case of the neutral Dalitz slope α, to which we will refer in the following as the "α-puzzle": ChPT basically fails in accurately reproducing its experimental value $\alpha = -0.0315 \pm 0.0015$ [34], since the theoretical value for α vanishes at leading $\mathcal{O}(p^2)$ and disagrees in sign both at next-to-leading $\mathcal{O}(p^4)$ (irrespective of isospin-breaking corrections, as will be shown in this work) and at two-loop $\mathcal{O}(p^6)$, the result at NNLO (neglecting isospin breaking beyond $\mathcal{O}(\delta)$) at least being compatible with negative values within the given errors.[#4] The branching ratio r, on the contrary, has turned out to

---

[#1]The experimental values for both $\Gamma_{\eta \to \pi^0 \pi^+ \pi^-}$ and $\Gamma_{\eta \to 3\pi^0}$ have changed considerably in time, however, mostly due to the normalization of the total η decay width by the partial width $\Gamma_{\eta \to 2\gamma}$ and therefore not influencing the ratio r much. In fact, the results of [13] were in good agreement with the majority of the then-current experimental results.

[#2]In the framework of $SU(3)$ ChPT including electromagnetism as chosen for this work, the quark masses $m_q \in \{m_u, m_d, m_s\}$ and the electric charge squared e^2 are of the same chiral $\mathcal{O}(p^2)$, whereas $1/Q^2 = \mathcal{O}(p^0)$.

[#3]See in addition [32,33] for the first determination of α and [32] as well as the references given in [23] for former analyses of charged Dalitz plot parameters.

[#4]The rather large errors given in [21], however, are not based on the uncertainties in the bulk of the a

be rather stable with respect to the increasing accuracy in both the experimental determinations [32, 33, 35–38] (see references in [35] for older analyses) and the theoretical predictions; even the LO prediction agrees with the current experimental world average $r = 1.48 \pm 0.05$ [34], which in turn is close to the upper limit of the inequality $r \leq 3/2$ stemming from the $\Delta I = 1$ selection rule.

Based on this situation, the motivation for reconsidering the electromagnetic corrections in $\eta \to 3\pi$ decays at one-loop chiral order as started in [39] and published in [1], hinged on the fact that the authors of [15] neglected terms proportional to $e^2 \delta$, arguing that these are of second order in isospin breaking and therefore expected to be suppressed even further. However, by restricting oneself to terms of the form $e^2 \hat{m}$ and $e^2 m_s$, one excludes some of the most obvious electromagnetic effects, namely real- and virtual-photon contributions as well as effects due to the charged-to-neutral pion mass difference (which is predominantly of electromagnetic origin), both of which scale as $e^2 \delta$. These mechanisms fundamentally affect the analytic structure of the amplitudes in question: in the charged decay channel $\eta \to \pi^0 \pi^+ \pi^-$, there is a Coulomb pole at the boundary of the physical region (i.e. at the $\pi^+ \pi^-$ threshold) corresponding to the exchange of a (soft) virtual photon between the charged pions, while in the neutral decay channel $\eta \to 3\pi^0$, the non-vanishing pion mass difference induces a cusp behavior at the $\pi^+ \pi^-$ threshold due to the opening of an additional physical channel [40] (cf. e.g. [41,42], see also [43,44] for overviews of various examples for threshold cusp phenomena). In contrast, the purely electromagnetic corrections identified in [15] are all polynomials (due to counterterms) or quasi-polynomials (due to kaon loop effects) inside the physical region. Furthermore, Sutherland's soft-pion theorem (assuming $m_u = m_d$, i.e. purely electromagnetic $\eta \to 3\pi$ decays) guarantees that at the so-called soft-pion point these corrections are of $\mathcal{O}(e^2 \hat{m})$ only, and not $\mathcal{O}(e^2 m_s)$; hence at least in this case, in accordance with (1.3), the relative suppression of the hitherto neglected terms at $\mathcal{O}(e^2 \delta)$ (i.e. for $m_u \neq m_d$) is of the order of $\delta/\hat{m} \approx 2/3$ (since $m_d \approx 2m_u$) and therefore these contributions are not a priori negligible. Moreover, the mixed electromagnetic and strong corrections at $\mathcal{O}(e^2 \delta)$ do not spoil the factorization of $1/Q^2$ for both amplitudes and thus enable a consistent application of electromagnetic corrections in the extraction of quark mass ratios from $\eta \to 3\pi$ decays, where for precision studies it is of course important to have *all* electromagnetic corrections under sufficient control. Additional motivation for considering the electromagnetic terms at $\mathcal{O}(e^2 \delta)$ arose from two specific features of the neutral decay channel, namely the cusp phenomenon and the "α-puzzle", as shall also be discussed in the following.

The threshold cusp in $\eta \to 3\pi^0$ encodes information on $\pi\pi$ (re-)scattering in principle in much the same way as the decay $K^+ \to \pi^+ \pi^0 \pi^0$, which at the time of [1] had recently been established as a new means for a precision determination of the $\pi\pi$ S-wave scattering lengths isospin combination $a_0^0 - a_0^2$ multiplying the strength of the cusp in the $\pi^0 \pi^0$ invariant mass distribution at the $\pi^+ \pi^-$ threshold [45–49] (see also the more recent analysis [50]). This difference of scattering lengths, at the same time, is predicted theoretically with tremendous precision [51] by using dispersive methods (namely Roy equations [52,53] in combination with ChPT [54]) and represents a core test of ChPT and our picture of chiral symmetry breaking. However, as in the analogous decay $K_L \to 3\pi^0$ [55], in $\eta \to 3\pi^0$ the cusp is less pronounced than in $K^+ \to \pi^+ \pi^0 \pi^0$ due to the relative strength of the decays into charged and neutral final states. From an experimental point of view, $\eta \to 3\pi^0$ decays had therefore not been

---

priori unknown low-energy constants (LECs) appearing at $\mathcal{O}(p^6)$, which are estimated therein by resonance saturation, but results solely from the chosen fitting procedure.

competitive for a $\pi\pi$ scattering length determination, although from the then-upcoming high-statistics experiments [30,56–58] at least in [58] first (however, not yet statistically significant) indications of the cusp effect have been observed. Since the calculation of [1] is performed at $\mathcal{O}(p^4)$ in chiral perturbation theory, and hence includes the rescattering effect leading to the cusp only at leading order in the quark mass expansion, it is not suited to serve for a precision extraction of $\pi\pi$ scattering lengths, but rather illustrates the phenomenon. In principle, the tailor-made theoretical framework to perform a precision analysis of threshold cusp phenomena is (modified) non-relativistic effective field theory (NREFT), which already then had been worked out up to two loops and including radiative corrections for $\eta \to 3\pi^0$ (along with $K_L \to 3\pi^0$) [59–61] (see also the recent comprehensive analysis [62]). While the NREFT framework is ideally suited to study the FSI dynamics, which are known to be crucial for $\eta \to 3\pi$ decays, it does not allow for a prediction of physical observables without matching to some other source of low-energy information like for instance ChPT. Actually, the ChPT calculation of [1] is in a sense dual to a NREFT calculation, as it predicts electromagnetic effects in those parts of the amplitude that are merely parameterized in the latter.

As far as the neutral Dalitz slope α is concerned, more robust theoretical values had been obtained by using either dispersive techniques [17] (by construction fulfilling unitarity and thus incorporating FSIs to all orders) or unitarization schemes like [20]. Nevertheless, the disagreement between ChPT calculations for α and the experimental value remained an unsolved problem even after the two-loop calculation [21] had been accomplished.[#5] An important shortcoming of both the usual dispersion relations and the existing two-loop calculation, however, is the neglect of higher-order isospin-breaking corrections, especially of electromagnetic contributions entailed in the charged-to-neutral pion mass difference; in particular, it is not yet clear how to consistently incorporate different pion masses in the dispersive machinery. Although presently in fact, there are attempts to deal with this issue either in a new dispersive study [63–65] or using an "analytical" dispersive approach [66,67] (see [65] for a comparison of the different frameworks) these analyses are not yet finished and the final and/or comprehensive results have not been published yet. This situation directly leads to the question of the size of electromagnetic corrections to the ChPT value of α. In fact, also for investigating the "α-puzzle" the combination of NREFT and ChPT together with isospin-breaking considerations turns out to be the ideal tool as will be discussed below.

The evaluation of electromagnetic corrections in $\eta \to 3\pi$ decays including second-order isospin breaking at $\mathcal{O}(e^2\delta)$ as sketched above and published in [1] constitutes the first part of the analysis of higher-order isospin-breaking corrections in $\eta \to 3\pi$ decays presented in this work. For the (chronological) line of argument, here we briefly anticipate the main result of [1]: in general, our investigation confirms the picture, that the $\eta \to 3\pi$ decays are predominantly due to isospin breaking in the strong sector and thus can be used as direct measure for (isospin-breaking) quark mass ratios, in particular Q^2. Although the effects of $\mathcal{O}(e^2\delta)$ are comparable in size to those of $\mathcal{O}(e^2\hat{m})$ analyzed in [15] and, moreover, the most significant change between these electromagnetic corrections occurs particularly in α as a consequence of the cusp effect in $\eta \to 3\pi^0$, the *total* electromagnetic corrections remain at the percent level and thus small throughout for both $\eta \to 3\pi$ decays (as long as "trivial" isospin breaking due to the different pion masses is accounted for in the normalization of the Dalitz

---

[#5]The remarkable agreement of the results of [20] in the framework of unitarized ChPT with experiment (especially for the neutral slope parameter α), however, is not an unbiased prediction, since the input $U(3)$ LECs (differing from the respective perturbative LECs due to the coupled-channel approach) are determined by fitting to several hadronic η and η' decay channels, amongst them $\eta \to 3\pi$ and in particular $\eta \to 3\pi^0$.

plot parameters).[#6] In particular, the corrections at $\mathcal{O}\left(e^2\delta\right)$ that include the cusp effect are by far too small to account for the "α-puzzle".

As the total electromagnetic effects turned out to be small and in view of the progress in exploring and applying the NREFT framework in particular concerning the cusp effect in $\eta \to 3\pi^0$ [71,72] as well as $\eta' \to \eta\pi\pi$ [73], subsequently a dedicated study of the rescattering effects in $\eta \to 3\pi$ decays was conducted [3], wherein by matching the ChPT results at NLO (including higher-order isospin-breaking effects) to a two-loop (modified) NREFT calculation (using the correct empirical $\pi\pi$ scattering parameters for the $\pi\pi$ FSI) a detailed description of the Dalitz plot distributions for both decays is obtained in reasonable agreement with experimental findings. Since NREFT allows for the direct implementation of isospin breaking particularly in all kinematical (i.e. mass) effects — which is much more involved in ChPT, cf. the first part of the present work, and still unexplored in dispersive analyses — it is perfectly suited for investigating the isospin-breaking and FSI-driven $\eta \to 3\pi$ decays. Moreover, compared to potentially very precise but numerically intricate dispersive studies, NREFT calculations yield transparent analytical representations. However, this work is not concerned with the $\eta \to 3\pi$ NREFT calculation presented in [3] itself. Rather, the second part of the analysis of the $\eta \to 3\pi$ higher-order isospin-breaking corrections to be presented in this work deals with the inclusion of "trivial" kinematical isospin-breaking effects, the electromagnetic corrections at $\mathcal{O}\left(e^2\delta\right)$ as derived in [1], and also second-order strong isospin-breaking contributions at $\mathcal{O}\left(\delta^2\right)$ derived in addition to [1] in the combined NREFT+ChPT analysis of [3].

As shown in [3], especially for the "α-puzzle" it is possible to bridge the gap between the ChPT predictions and the dispersive analyses (and moreover, even experimental findings) by a transparent interpretation of the dispersive results of [17], which were obtained in a similar fashion concerning the matching to ChPT at NLO: the discrepancies between ChPT even at higher orders and experiment can be understood as a consequence of the general importance of the $\pi\pi$ FSIs for $\eta \to 3\pi$ decays on the one hand, and the employed value for the $\pi\pi$ scattering lengths parameterizing this rescattering on the other hand. While ChPT calculations at a given chiral order are always restricted to estimates of lower chiral order for these scattering lengths due to the chiral power counting,[#7] the NREFT representation allows to use the phenomenological values, which implicitly include arbitrarily high orders in both the chiral expansion and isospin breaking. In particular, the double rescattering graph with $\pi\pi$ vertices beyond LO is responsible for at least half of the discrepancy between the NNLO ChPT prediction for α and experiment; these effects are of $\mathcal{O}\left(p^8\right)$ at least, but included in the two-loop NREFT framework (as well as in dispersive analyses, however, without higher-order isospin-breaking). Moreover, calculating both decay amplitudes at NLO in ChPT separately

---

[#6]For the neutral decay $\eta \to 3\pi^0$, the contributions to the amplitude at $\mathcal{O}\left(e^2\delta\right)$ have also been derived in [68], which was published, however, after the completion of [39]. Concerning $\eta \to 3\pi^0$, moreover, some *partial* results for electromagnetic corrections at the two-loop level $\mathcal{O}\left(p^6\right)$ have been published: at $\mathcal{O}\left(e^2\delta p^2\right)$, by considering solely the exchange of a virtual photon between intermediate charged pions, it has been "concluded" in [69] that this contribution be sizeable (thus criticizing the NREFT analysis [3] for neglecting it; furthermore ignoring the solution of the "α-puzzle" presented therein), and furthermore at $\mathcal{O}\left(e^2p^4\right)$, by calculating the contributions from the exchange of a virtual photon inside the loop of intermediate charged kaons only, in summary it has been "concluded" in [70] that the decay $\eta \to 3\pi^0$ be mainly driven by electromagnetic isospin breaking and thus could not be used "to determine [quark mass ratios containing] $m_d - m_u$". However, in both cases the "conclusions" are drawn from alarmingly *incomplete* two-loop calculations and are thus invalid; actually, in [69] the authors honestly mention the possibility of cancellations with the remaining contributions at this order, while in [70] it is even explicitly stated that the resulting amplitude is neither finite nor scale-independent.

[#7]For instance, a ChPT amplitude at next-to-leading $\mathcal{O}\left(p^4\right)$ can only include the effect of one $\pi\pi$ rescattering vertex at leading $\mathcal{O}\left(p^2\right)$.

and including second-order isospin-breaking effects at $\mathcal{O}\left(e^2\delta, \delta^2\right)$ consistently, yields access to both strong and electromagnetic isospin-breaking corrections to the $\Delta I = 1$ relation between the amplitudes for the charged and the neutral decay channel. More specifically, in the second part of this work isospin-breaking corrections to the $\Delta I = 1$ relations between leading Dalitz plot parameters of both decay channels are derived and evaluated; in particular for the ratio r, which is reasonably well reproduced even at LO in ChPT, the strong and electromagnetic isospin-breaking effects are expected to be significant in comparison with higher-order chiral corrections. Using these $\Delta I = 1$ relations for Dalitz plot parameters, the numerical results for the Dalitz plot parameters of both decay channels within the NREFT+ChPT framework presented in [3] indicate a tension between the recent KLOE experimental analyses for $\eta \to 3\pi^0$ [30] and $\eta \to \pi^0\pi^+\pi^-$ [25] that, however, cannot be resolved by including isospin-breaking in $\eta \to 3\pi$ beyond leading-order as presented in this work, thus calling for further investigations; besides the aforementioned ongoing theoretical efforts, also new experimental studies have already been announced or are planned in the (near) future for both the neutral [74–78] and the charged [76–81] decay.

This work is organized as follows: in Chap. 2 we briefly review those parts of the formalism of ChPT and $\eta \to 3\pi$ decays that are relevant for both parts of our investigation of isospin-breaking effects in $\eta \to 3\pi$ decays, namely the electromagnetic corrections as discussed in Chap. 3 and the isospin-breaking corrections to the $\Delta I = 1$ amplitude relation as presented in Chap. 4, before we conclude with a summary and a short outlook in Chap. 4. Some technical details are relegated to Apps. A and B.

Chapter 2

Formalism

In this chapter, we collect the formalism and definitions that are needed for the analysis of electromagnetic corrections to the $\eta \to \pi^0 \pi^+ \pi^-$ and $\eta \to 3\pi^0$ decay amplitudes as presented in Chap. 3 as well as for the derivation of isospin-breaking corrections concerning the $\Delta I = 1$ relation between them as discussed in Chap. 4. Note that, unless explicitly stated otherwise, in the following the terms LO, NLO and so forth always denote orders p^2, p^4 etc. of the chiral expansion, and not orders in isospin breaking.

2.1 Chiral perturbation theory preliminaries

A particularly successful approach to describe the interactions of hadrons at low energies is to construct an effective field theory (EFT) which encodes the infrared behavior of QCD. Based upon the approximate chiral symmetry of $\mathcal{L}_{\text{QCD}}$, one can identify the lightest particles in the spectrum with the (pseudo-)Goldstone bosons induced by spontaneous breaking of this symmetry, and their interactions can be written as an simultaneous expansion in small momenta and light quark masses. The corresponding EFT for the strong interactions (of the pseudoscalar mesons) is then chiral perturbation theory [10–12, 82]. Moreover, ChPT can be generalized to include electromagnetic effects systematically [14] (cf. [83], see however [84] concerning the non-uniqueness of the splitting of the Hamiltonian into QCD and QED contributions). Since there are several good introductions to ChPT in the literature, see for instance [85–90], in this section we content ourselves with briefly collecting those definitions and results that are needed in the following.

2.1.1 Chiral perturbation theory with virtual photons

The mesonic Goldstone boson fields are usually collected in the field U according to[#1]

$$U = \exp \frac{i\phi}{F_0} \,, \qquad \phi = \sqrt{2} \begin{pmatrix} \frac{\pi^3}{\sqrt{2}} + \frac{\eta^8}{\sqrt{6}} & \pi^+ & K^+ \\ \pi^- & -\frac{\pi^3}{\sqrt{2}} + \frac{\eta^8}{\sqrt{6}} & K^0 \\ K^- & \bar{K}^0 & -\frac{2\eta^8}{\sqrt{6}} \end{pmatrix} \,. \tag{2.1}$$

[#1]According to the decomposition $\phi = \sum_{a=1}^{8} \lambda^a \phi^a$ in terms of the $SU(3)$ Gell-Mann matrices λ^a and field operators ϕ^a, the ChPT (phase-)convention $\sqrt{2}|\pi^\pm\rangle = |\pi^1\rangle \pm i |\pi^2\rangle$ (corresponding to the adjoint representation of $SU(2)$) for the relation between the pion charge eigenstates and their Cartesian components differs from the usual spherical convention $\sqrt{2}|\pi^\pm\rangle = \mp|\pi^1\rangle - i |\pi^2\rangle$ by an overall sign for $|\pi^+\rangle$. The flavor eigenstate $|\pi^3\rangle$ coincides with the mass eigenstate $|\pi^0\rangle$ only in the limit of $SU(2)$ isospin symmetry (i.e. $\delta = 0$), cf. Sect. 2.1.2.

The (strong) LO effective Lagrangian invariant under chiral symmetry reads

$$\mathcal{L}_{\text{str}}^{\text{LO}} = \frac{F_0^2}{4} \big\langle (D^\mu U)^\dagger D_\mu U + \chi^\dagger U + U^\dagger \chi \big\rangle \,, \tag{2.2}$$

where $\langle ... \rangle$ denotes the trace in flavor space, D_μ is the covariant derivative, and the external scalar and pseudoscalar sources s and p are conventionally combined into[#2]

$$\chi = 2B_0(s + ip) \,, \qquad s = \mathcal{M} + ... \,, \qquad \mathcal{M} = \text{diag}\big(m_u, m_d, m_s\big) \,, \tag{2.3}$$

incorporating the quark mass matrix $\mathcal{M}$ together with the LO low-energy constant B_0, which is related (in combination with F_0) to the chiral quark condensate. The LO LEC F_0, on the other hand, can be identified with the chiral limit of the pion decay constant F_π,

$$F_\pi = F_0\big\{1 + \Delta_{F_\pi}\big\} \,, \qquad \frac{F_K}{F_\pi} = 1 + \Delta_F \,, \tag{2.4}$$

where for later convenience we also define the corrections beyond $\mathcal{O}\big(p^0\big)$ to both the relations between F_0 and F_π as well as between the analogous kaon decay constant F_K and F_π. At NLO, loop diagrams with vertices from the above LO Lagrangian generate infinities that can be absorbed by a renormalization of the (strong) NLO LECs

$$L_i = \Gamma_i \lambda + L_i^r(\mu) \,, \tag{2.5}$$

which are introduced by the NLO effective Lagrangian $\mathcal{L}_{\text{str}}^{\text{NLO}}$ given in [12]. The (scale-dependent) constant λ contains a pole in $d = 4$ space-time dimensions due to dimensional regularization (cf. (A.3)) and the coefficients Γ_i are also given in [12]. Correspondingly, the renormalized LECs depend on the regularization scale μ. All physical observables, however, are finite and scale-independent, which serves as a thorough check in explicit calculations.

Following [14], to include electromagnetism in the framework of mesonic ChPT by adding virtual photons as additional dynamical degrees of freedom, the combined effective Lagrangian up-to-and-including NLO can be written as

$$\mathcal{L}_{\text{eff}} = \mathcal{L}_{\text{str}}^{\text{LO}} + \mathcal{L}_{\text{em}}^{\text{LO}} + \mathcal{L}_{\text{str}}^{\text{NLO}} + \mathcal{L}_{\text{em}}^{\text{NLO}} + \mathcal{O}\big(p^6\big) \,, \tag{2.6}$$

where the local electromagnetic interactions entail the quark charge matrix[#3]

$$\mathcal{Q} = \frac{e}{3} \, \text{diag}\big(2, -1, -1\big) \,, \tag{2.7}$$

and the radiative contributions are described by coupling the photon field A_μ to the meson fields U via minimal substitution of the covariant derivative D_μ. The additional electromagnetic LO effective Lagrangian then takes the form

$$\mathcal{L}_{\text{em}}^{\text{LO}} = -\frac{1}{4} F^{\mu\nu} F_{\mu\nu} + ZF_0^4 \big\langle \mathcal{Q}U\mathcal{Q}U^\dagger \big\rangle \,, \tag{2.8}$$

where $F_{\mu\nu}$ is the electromagnetic field strength tensor and the dimensionless LO LEC Z determines the purely electromagnetic part of the masses of the charged mesons to leading

---

[#2]Supplementing the two diagonal Gell-Mann matrices $\lambda^3 = \text{diag}(1, -1, 0)$ and $\lambda^8 = \frac{1}{\sqrt{3}} \text{diag}(1, 1, -2)$ by $\lambda^0 = \sqrt{2/3}\, \mathbb{1}_3$, $\mathcal{M}$ can be decomposed according to $\mathcal{M} = \frac{m_u + m_d + m_s}{\sqrt{6}} \lambda^0 - \frac{\delta}{2} \lambda^3 - \frac{m_s - \hat{m}}{\sqrt{3}} \lambda^8$, cf. (1.1).

[#3]In analogy to $\mathcal{M}$, also $\mathcal{Q}$ can be decomposed according to $\mathcal{Q} = \frac{e}{2}\big\{\lambda^3 + \frac{\lambda^8}{\sqrt{3}}\big\}$.

chiral order as will be shown in Sect. 2.1.2. Note that we have omitted the gauge-fixing term. The respective NLO Lagrangian is given in [14] and the corresponding electromagnetic LECs are renormalized in analogy to the strong LECs via

$$K_i = \Sigma_i \lambda + K_i^r(\mu) \,, \tag{2.9}$$

with coefficients Σ_i also given in [14]. It shall be stressed here, that throughout this work NLO terms proportional to e^4 (i.e. second-order purely electromagnetic isospin breaking) will be neglected, since they are numerically tiny.

2.1.2 Meson masses and $\pi^0 \eta$ mixing at leading order

In principle, by expanding the LO effective Lagrangian $\mathcal{L}_{\text{eff}}^{\text{LO}} = \mathcal{L}_{\text{str}}^{\text{LO}} + \mathcal{L}_{\text{em}}^{\text{LO}}$ in powers of ϕ one can easily derive the LO meson masses. However, the flavor-neutral states π^3 and η^8 are mixed due to a difference in the light quark masses $m_d - m_u = \delta \neq 0$ according to

$$\frac{B_0}{2} \begin{pmatrix} \pi^3 \\ \eta^8 \end{pmatrix}^T \begin{pmatrix} m_u + m_d & \frac{1}{\sqrt{3}}(m_u - m_d) \\ \frac{1}{\sqrt{3}}(m_u - m_d) & \frac{1}{3}(m_u + m_d + 4m_s) \end{pmatrix} \begin{pmatrix} \pi^3 \\ \eta^8 \end{pmatrix} \,, \tag{2.10}$$

which can be diagonalized by the single rotation angle

$$\epsilon = \frac{1}{2} \arctan\left(\frac{\sqrt{3}}{2} \frac{m_d - m_u}{m_s - \hat{m}} \right) = \frac{\sqrt{3}}{4} \frac{m_d - m_u}{m_s - \hat{m}} + \mathcal{O}(\delta^3) \,, \tag{2.11}$$

leading to the physical meson mass eigenstates[#4]

$$\begin{pmatrix} \pi^0 \\ \eta \end{pmatrix} = \begin{pmatrix} \cos\epsilon & \sin\epsilon \\ -\sin\epsilon & \cos\epsilon \end{pmatrix} \begin{pmatrix} \pi^3 \\ \eta^8 \end{pmatrix} \,. \tag{2.12}$$

To be explicit, the formulae for the LO meson masses and their expansions in the isospin-breaking parameters e^2 and δ up-to-and-including second order read[#5]

$$M_\eta^2 = \frac{B_0}{3}(4m_s + m_d + m_u) + \frac{B_0}{\sqrt{3}}(m_d - m_u)\tan\epsilon + \mathcal{O}(p^4) \tag{2.13}$$

$$= \frac{2B_0}{3}(2m_s + \hat{m}) + \frac{B_0\delta^2}{4(m_s - \hat{m})} + \mathcal{O}(\delta^4, p^4) \,,$$

$$M_{\pi^0}^2 = B_0(m_d + m_u) - \frac{B_0}{\sqrt{3}}(m_d - m_u)\tan\epsilon + \mathcal{O}(p^4) = 2B_0\hat{m} - \frac{B_0\delta^2}{4(m_s - \hat{m})} + \mathcal{O}(\delta^4, p^4) \,,$$

$$M_\pi^2 = B_0(m_d + m_u) + 2F_0^2 Z e^2 + \mathcal{O}(p^4) = 2B_0\hat{m} + 2F_0^2 Z e^2 + \mathcal{O}(p^4) \,,$$

$$M_{K^0}^2 = B_0(m_s + m_d) + \mathcal{O}(p^4) \qquad = B_0(m_s + \hat{m}) + \frac{B_0\delta}{2} + \mathcal{O}(p^4) \,,$$

$$M_K^2 = B_0(m_s + m_u) + 2F_0^2 Z e^2 + \mathcal{O}(p^4) = B_0(m_s + \hat{m}) - \frac{B_0\delta}{2} + 2F_0^2 Z e^2 + \mathcal{O}(p^4) \,,$$

[#4]Note that this description of $\pi^0\eta$ mixing via a single rotation angle is only valid at lowest chiral $\mathcal{O}(p^2)$ [12, 91–93]. The mixing of the octet η^8 and the singlet η^0 to the observed mass eigenstates η and η', on the contrary, is encoded in the strong NLO LEC L_7 [94], i.e. the heavy η' is not a dynamical particle here.

[#5]These equations are of the form of the Gell-Mann–Oakes–Renner relation $M_{GB}^2 \sim B_0 m_q$ [95] stating that the squared Goldstone boson (i.e. meson) masses are given by the product of B_0 (which is a measure for the *spontaneous* breaking of chiral symmetry due to a non-zero chiral quark condensate) and quark masses (breaking chiral symmetry *explicitly* by their non-vanishing values). The linear dependence on the quark masses gives rise to the famous chiral logarithms $\log M_{GB}$.

with M_π and M_K denoting the charged-pion and -kaon masses throughout this work. Thereby, we can read off the charged-to-neutral meson mass differences at LO

$$\Delta M_\pi^2 = M_\pi^2 - M_{\pi^0}^2 = 2F_0^2 Z e^2 + \frac{B_0 \delta^2}{4(m_s - \hat{m})} + \mathcal{O}(\delta^4, p^4) \ ,$$
$$\Delta M_K^2 = M_K^2 - M_{K^0}^2 = 2F_0^2 Z e^2 - B_0 \delta + \mathcal{O}(p^4) \ , \tag{2.14}$$

and it is obvious that the LO electromagnetic contributions to the charged-pion and -kaon masses obey Dashen's theorem [96]

$$\left(\Delta M_\pi^2\right)_{\text{em}} = \left(\Delta M_K^2\right)_{\text{em}} + \mathcal{O}(e^2 m_q) \ . \tag{2.15}$$

Furthermore, we can easily deduce the Gell-Mann–Okubo (GMO) relation [97, 98] including higher-order isospin breaking

$$2M_K^2 + 2M_{K^0}^2 - 2M_\pi^2 + M_{\pi^0}^2 = 3M_\eta^2 - \frac{4B_0 \delta}{\sqrt{3}} \tan\epsilon + \mathcal{O}(p^4) \ , \tag{2.16}$$

which at LO in isospin breaking (i.e. neglecting the term of $\mathcal{O}(\delta^2)$) is fulfilled in nature to a few percent accuracy ($\approx 7\%$ w.r.t. $3M_\eta^2$) and whose dimensionless discrepancy is defined as

$$\Delta_{\text{GMO}} = \frac{2M_K^2 + 2M_{K^0}^2 - 2M_\pi^2 + M_{\pi^0}^2 - 3M_\eta^2}{M_\eta^2 - M_{\pi^0}^2} = -4\sin^2\epsilon + \mathcal{O}(p^2) \ . \tag{2.17}$$

In turn, to replace quark masses and the electromagnetic LEC Z by physical meson masses one may use the relations

$$2B_0 m_s = M_K^2 + M_{K^0}^2 - M_\pi^2 + \mathcal{O}(p^4) = \frac{1}{2}\left(3M_\eta^2 - M_{\pi^0}^2\right) + \mathcal{O}(\delta^2, p^4) \ , \tag{2.18}$$
$$2B_0 \hat{m} = \frac{1}{4}\left[3\left(M_\eta^2 + M_{\pi^0}^2\right) - 2\left(M_K^2 + M_{K^0}^2 - M_\pi^2\right)\right] + \mathcal{O}(p^4) = M_{\pi^0}^2 + \mathcal{O}(\delta^2, p^4) \ ,$$
$$2F_0^2 Z e^2 = -\frac{1}{4}\left[3\left(M_\eta^2 + M_{\pi^0}^2\right) - 2\left(M_K^2 + M_{K^0}^2 + M_\pi^2\right)\right] + \mathcal{O}(p^4) = \Delta M_\pi^2 + \mathcal{O}(\delta^2, p^4) \ .$$

2.1.3 Quark mass ratios

The results of the previous section for the LO meson masses allow to form quark mass ratios determined entirely in terms of observable meson masses,[#6] namely Weinberg's ratios [99]

$$\frac{m_u}{m_d} \approx \frac{2M_{\pi^0}^2 - M_{K^0}^2 + M_K^2 - M_\pi^2}{M_{K^0}^2 - M_K^2 + M_\pi^2} \approx 0.56 \ ,$$
$$\frac{m_s}{m_d} \approx \frac{M_{K^0}^2 + M_K^2 - M_\pi^2}{M_{K^0}^2 - M_K^2 + M_\pi^2} \approx 20.2 \ ,$$
$$\Rightarrow \quad \frac{m_s}{\hat{m}} = 2\frac{m_s}{m_d}\left[1 + \frac{m_u}{m_d}\right]^{-1} \approx \frac{M_{K^0}^2 + M_K^2 - M_\pi^2}{M_{\pi^0}^2} \approx 25.9 \ , \tag{2.19}$$

[#6]In any effective Lagrangian approach as e.g. ChPT, only *ratios* of quark masses can be determined. Using a mass-independent renormalization scheme like $\overline{MS}$, the quark masses are renormalized multiplicatively, so that their dependence on the renormalization scale cancels in quark mass ratios. Moreover, the corresponding (and a priori unknown) LEC, i.e. here B_0, also cancels. Note that by construction the quark masses in ChPT are the same as those in QCD.

which are, however, subject to substantial higher-order corrections.[#7] Other frequently used ratios (see for example [91]) are the single ratio

$$R = \frac{m_s - \hat{m}}{m_d - m_u} \quad \Rightarrow \quad \epsilon = \frac{\sqrt{3}}{4R} + \mathcal{O}(\delta^3) \ , \tag{2.20}$$

that represents the ratio of $SU(3)$ flavor and $SU(2)$ (strong) isospin breaking and naturally appears in the mixing angle ϵ (2.11) and its expansion in $m_d - m_u$, as well as the closely related double ratio (cf. (1.3))

$$Q^2 = \frac{m_s^2 - \hat{m}^2}{m_d^2 - m_u^2} = \frac{m_s - \hat{m}}{m_d - m_u} \frac{m_s + \hat{m}}{m_d + m_u} = \frac{R}{2} \left\{ 1 + \frac{m_s}{\hat{m}} \right\} . \tag{2.21}$$

The latter one is preferable, however, since it is particularly stable with respect to strong higher-order corrections [12],

$$Q^2 = \frac{M_K^2 - M_\pi^2}{\left(M_{K^0}^2 - M_K^2\right)_{\mathrm{str}}} \frac{M_K^2}{M_\pi^2} \left\{ 1 + \mathcal{O}(m_q^2, \delta, e^2) \right\} , \tag{2.22}$$

and furthermore at leading order it is invariant under a shift in the quark masses of the form $m_u \to m_u + \mathrm{const} \times m_d m_s$ and cyclic for m_d and m_s [104].[#8] Moreover, neglecting a tiny term proportional to $(\hat{m}/m_s)^2$, Q represents the major semi-axis of Leutwyler's ellipse [105] relating Weinberg's ratios (2.19),

$$\left(\frac{m_u}{m_d}\right)^2 + \frac{1}{Q^2} \left(\frac{m_s}{m_d}\right)^2 = 1 + \frac{1}{Q^2} \left(\frac{\hat{m}}{m_d}\right)^2 \approx 1 \ , \tag{2.23}$$

since the inverse of the double ratio itself can be written as (cf. (1.3))

$$\frac{1}{Q^2} = 2 \frac{\delta}{\hat{m}} \left(\frac{\hat{m}}{m_s}\right)^2 \left[1 - \left(\frac{\hat{m}}{m_s}\right)^2 \right]^{-1} = 2 \frac{\delta}{\hat{m}} \left(\frac{\hat{m}}{m_s}\right)^2 \left\{ 1 + \mathcal{O}\left(\left(\frac{\hat{m}}{m_s}\right)^2\right) \right\} . \tag{2.24}$$

As the ratio $m_s/\hat{m}$ is accurately known from lattice QCD whereas the ratio m_u/m_d is rather poorly known, cf. [100], a precise determination of Q^2 would also lead to an accurate value of

$$\frac{m_u}{m_d} = \left[4Q^2 - \left(\frac{m_s}{\hat{m}}\right)^2 + 1 \right] \left[4Q^2 + \left(\frac{m_s}{\hat{m}}\right)^2 - 1 \right]^{-1} . \tag{2.25}$$

Using Dashen's theorem (2.15) in order to correct (2.22) for the missing electromagnetic kaon mass contributions, i.e. using $(M_K^2 - M_{K^0}^2)_{\mathrm{em}} = (M_\pi^2 - M_{\pi^0}^2)_{\mathrm{em}}$, the double ratio Q^2 can

---

[#7]While the numerical values in (2.19) correspond to inserting the physical meson masses, averaging three-flavor lattice QCD results (in the $\overline{MS}$ scheme and fixing the running scale at $2\,\mathrm{GeV}$) yields $\frac{m_u}{m_d} = 0.47 \pm 0.04$ and $\frac{m_s}{\hat{m}} = 27.4 \pm 0.4$ [100]; see also [101, 102]. For the single ratio R, the values in (2.19) lead to $R \approx 44.1$ whereas [100] quotes $R = 36.6 \pm 3.8$; from (2.11) thus follows in both cases $\epsilon \approx 1 \times 10^{-2}$, which is in agreement with more sophisticated determinations as e.g. [103] (considering both strong and electromagnetic isospin breaking). In view of $\frac{\delta}{\hat{m}} \approx \frac{2}{3}$ not being small (in contrast to $e^2 \approx \frac{4\pi}{137} \approx \frac{1}{10}$), however, it should be noted that $(SU(2))$ isospin is a good symmetry because the terms proportional to δ are usually *chirally* suppressed.

[#8]These shifts can be compensated by a redefinition of the quark condensate and certain LECs (up to corrections at chiral $\mathcal{O}(p^8)$) and thus lead to the well-known Kaplan–Manohar ambiguity [104]: since these unobservable shifts allow one to move freely on Leutwyler's ellipse (2.23), additional input (e.g. quark mass ratios from baryon mass splittings) is needed in order to extract Weinberg's quark mass ratios (2.19) therefrom (in a given scheme and at a given scale).

be calculated at LO yielding a numerical value of $Q_D \approx 24.2$, which is in accordance with the LO values of the quark mass ratios (2.19). However, Dashen's theorem is subject to potentially large higher-order corrections, see e.g. [106–108], and different models [109–113] yield a range $1 \lesssim \left(M_K^2 - M_{K^0}^2 \right)_{\text{em}} / \left(M_\pi^2 - M_{\pi^0}^2 \right)_{\text{em}} \lesssim 2.5$, which leads to a rather large uncertainty in the numerical value of Q of $Q_D \approx 24.2 \gtrsim Q \gtrsim 20.6$, whereas the recent three-flavor lattice QCD average $Q = 22.8 \pm 1.2$ from [100] (see also references therein) agrees remarkably well with the results $Q = 22.8 \pm 0.4$ [114] and $Q = 23.1 \pm 0.7$ [66] based on KLOE data as well as with the dispersive finding $Q = 22.7 \pm 0.8$ [18].

Due to Sutherland's theorem [4], the dependence of the decay $\eta \to 3\pi$ on the light quark mass difference $m_d - m_u$ is much less prone to be obscured by electromagnetic effects. As will be shown in the next section, the decay amplitudes can be written (at leading chiral order even exactly) in terms of Q^2, and hence an accurate study of this decay can lead to an independent determination of the quark mass ratios. The consideration of higher-order isospin-breaking effects (in particular the re-evaluation of electromagnetic corrections) presented in this work thus allows for an increased precision in this determination.

2.2 $\eta \to 3\pi$ basics

In this section, we discuss some basic properties of $\eta \to 3\pi$ decays, mostly in terms of the decay amplitudes for both the *charged* and the *neutral* channel of $\eta \to 3\pi$,

$$_{\text{out}}\langle \pi^0 \pi^+ \pi^- | \eta \rangle_{\text{in}} = i\,(2\pi)^4 \delta^{(4)}(p_\eta - p_{\text{out}}^c) \mathcal{A}_c(s,t,u) \ ,$$
$$_{\text{out}}\langle 3\pi^0 | \eta \rangle_{\text{in}} = i\,(2\pi)^4 \delta^{(4)}(p_\eta - p_{\text{out}}^n) \mathcal{A}_n(s,t,u) \ . \qquad (2.26)$$

These amplitudes are needed in the following at next-to-leading chiral $\mathcal{O}(p^4)$ and including isospin breaking up to $\mathcal{O}(e^2, e^2\delta, \delta^2)$, which upon neglecting numerically tiny terms at $\mathcal{O}(e^4)$ also corresponds to isospin breaking at next-to-leading order. Since they have been derived in full detail — considering isospin breaking only up to $\mathcal{O}(e^2, e^2\delta, \delta)$, however — already in [39] (and published as part of [1]), neither their derivation nor their explicit forms shall be reproduced here; only the LO amplitudes (which are valid also up-to-and-including $\mathcal{O}(\delta^2)$ without any changes) are stated explicitly, as this will prove valuable for illustrative reasons. The discussion of the *changes* at NLO, however, that are necessary to render the amplitudes given in [1] also valid at $\mathcal{O}(\delta^2)$ is relegated to App. A. For the explicit derivation of the amplitudes we thus refer to [1]; even more details of the calculation are given in [39].

In the following, we first specify our kinematical conventions and then give both LO amplitudes. Subsequently, we discuss the important relation between the charged and the neutral decay amplitude, which is based on the $\Delta I = 1$ selection rule for $\eta \to 3\pi$ decays. Finally, the standard parameterizations for the Dalitz plot distributions of both amplitude squares are discussed with emphasis on "trivial" kinematical isospin breaking.

2.2.1 Kinematics

For the generic $\eta \to 3\pi$ decay

$$\eta(p_\eta) \to \pi_1(p_1) + \pi_2(p_2) + \pi_3(p_3) \ ,$$
$$_{\text{out}}\langle \pi_1 \pi_2 \pi_3 | \eta \rangle_{\text{in}} = i\,(2\pi)^4 \delta^{(4)}(p_\eta - p_{\text{out}}) \mathcal{A}(s_1, s_2, s_3) \ , \qquad (2.27)$$

the on-shell ($p^2 = M^2$) kinematics are given by (with ijk as cyclic permutations of 123)

$$s_i = (p_\eta - p_i)^2 = (p_j + p_k)^2 \,, \qquad p_i^0 = \frac{M_\eta^2 + M_i^2 - s_i}{2M_\eta} \,, \qquad T_i = p_i^0 - M_i \,,$$

$$3s_0 = s_1 + s_2 + s_3 \,, \qquad p_{\text{out}} = p_1 + p_2 + p_3 \,, \qquad \tilde{Q} = T_1 + T_2 + T_3 \,, \qquad (2.28)$$

where T_i denotes the kinetic energy of the respective pion in the η rest frame and $\tilde{Q}$ is the excess energy of the reaction. Taking the first (i.e. always neutral) pion as the odd one, so that the corresponding generic two-by-two scattering amplitude is given by $_{\text{out}}\langle \pi_2 \pi_3 | \eta\, \pi_1 \rangle_{\text{in}} = \,_{\text{out}}\langle \pi_2 \pi_3 | \eta\, \pi^0 \rangle_{\text{in}}$, the kinematical variables s_i can be identified with the usual Mandelstam variables via[#9]

$$s_1 = s \,, \qquad s_2 = t \,, \qquad s_3 = u \,. \qquad (2.29)$$

Since they are related by $3s_0$, only two of them are independent; thus we can choose to work with e.g. s and t or s and $t - u \propto \cos\theta_s$ (as $t + u = 3s_0 - s$ is a function of s again), where $\theta_s = \angle(\mathbf{p_2}, \mathbf{p_3})$ denotes the angle between the 3-momenta of the two non-odd pions. In fact, defining

$$\lambda_{ab}(s) = \lambda\left(s, M_a^2, M_b^2\right) = \left[s - (M_a - M_b)^2\right]\left[s - (M_a + M_b)^2\right] \qquad (2.30)$$

based on the fully symmetric Källén function $\lambda(a, b, c) = a^2 + b^2 + c^2 - 2(ab + bc + ca)$, and

$$\sigma_a(s) = \frac{\lambda_{aa}^{1/2}(s)}{s} = \sqrt{1 - \frac{4M_a^2}{s}} \qquad (2.31)$$

for the case of equal masses, we can write

$$t(s, \theta_s) = \frac{1}{2}\left\{3s_0 - s + \lambda_{\eta\pi^0}^{1/2}(s)\lambda_{23}^{1/2}(s)\frac{\cos\theta_s}{s}\right\} \,, \qquad u(s, \theta_s) = \frac{1}{2}\left\{3s_0 - s - \lambda_{\eta\pi^0}^{1/2}(s)\lambda_{23}^{1/2}(s)\frac{\cos\theta_s}{s}\right\} \,. \qquad (2.32)$$

Specifically, for the charged decay the corresponding Mandelstam variables[#10]

$$s = (p_\eta - p_{\pi^0})^2 \,, \qquad t = (p_\eta - p_{\pi^+})^2 \,, \qquad u = (p_\eta - p_{\pi^-})^2 \,, \qquad (2.33)$$

are related by

$$3s_0^c = s + t + u = M_\eta^2 + M_{\pi^0}^2 + 2M_\pi^2 \,, \qquad (2.34)$$

whereas the Mandelstam variables for the neutral decay read

$$s = (p_\eta - p_{\pi_1^0})^2 \,, \qquad t = (p_\eta - p_{\pi_2^0})^2 \,, \qquad u = (p_\eta - p_{\pi_3^0})^2 \,, \qquad (2.35)$$

and obey the relation

$$3s_0^n = s + t + u = M_\eta^2 + 3M_{\pi^0}^2 = 3s_0^c - 2\Delta M_\pi^2 \,. \qquad (2.36)$$

[#9]Note that these conventions are in line with [1] but differ from [3], where the third pion is the odd one (cf. Fig. 2.1). While this does not affect the amplitudes in terms of s, t, and u, however, there is also a difference concerning the pion charge eigenstates between the usual ChPT convention applied in [1] and the spherical convention (which corresponds to the Condon–Shortley phase convention) used in other theoretical frameworks like e.g. [3,66], see [#1]: the additional sign for the π^+ wave function in the latter convention leads to an overall sign for the charged amplitude, whereas the neutral amplitude remains unchanged.

[#10]In order to ease the notation, we refrain from adding superscript indices c and n to the Mandelstam variables s, t, and u for the charged and neutral decay, respectively, although they differ by definition.
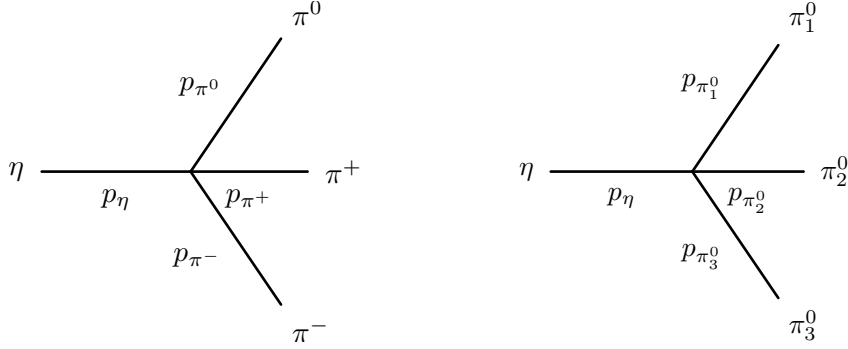
Figure 2.1: Leading-order diagrams for the charged (left) and neutral (right) decay.

For given s, the limits of the corresponding physical region are given by $\cos\theta_s = \pm 1$, so that the charged and neutral $\eta \to 3\pi$ decay widths can be calculated via

$$\Gamma_{c/n} = \frac{S_{c/n}}{256\pi^3 M_\eta^3} \int\limits_{s_-^{c/n}}^{s_+^{c/n}} \mathrm{d}s \int\limits_{t_-^{c/n}(s)}^{t_+^{c/n}(s)} \mathrm{d}t \, \left| \mathcal{A}_{c/n}\big(s, t, u(s,t)\big) \right|^2 , \qquad (2.37)$$

where the s-integration boundaries read

$$s_-^c = 4M_\pi^2 , \qquad s_-^n = 4M_{\pi^0}^2 , \qquad s_+^c = s_+^n = (M_\eta - M_{\pi^0})^2 , \qquad (2.38)$$

and the s-dependent limits for the t-integration are given by

$$t_\pm^c(s) = \frac{1}{2}\left\{ 3s_0^c - s \pm \sigma_\pi(s)\lambda_{\eta\pi^0}^{1/2}(s) \right\} , \qquad t_\pm^n(s) = \frac{1}{2}\left\{ 3s_0^n - s \pm \sigma_{\pi^0}(s)\lambda_{\eta\pi^0}^{1/2}(s) \right\} . \qquad (2.39)$$

The symmetry factor $S_n = 1/3!$ for the neutral decay accounts for the indistinguishable three neutral pions in order to avoid multiple counting of phase space; accordingly $S_c = 1$.

2.2.2 Amplitudes at leading order

At leading chiral $\mathcal{O}(p^2)$ one only has to compute one tree graph each for the charged and the neutral decay, since the fields in the lowest-order Lagrangian are already diagonalized by use of the $\pi^0\eta$ mixing angle ϵ. The corresponding Feynman diagrams are shown in Fig. 2.1.

The charged LO amplitude is then given by

$$\begin{aligned}
\mathcal{A}_c^{\mathrm{LO}}(s) &= -\frac{\sin(2\epsilon)(2s - t - u)}{6F_0^2} - \frac{\cos(2\epsilon)B_0(m_d - m_u)}{3\sqrt{3}F_0^2} - \frac{2\sin(2\epsilon)Ze^2}{3} + \mathcal{O}(p^4) \qquad (2.40)\\
&= -\frac{B_0\delta}{3\sqrt{3}F_\pi^2}\left\{ 2\cos(2\epsilon) - 1 + \frac{3(s - s_0^c) + 2\Delta M_\pi^2}{M_\eta^2 - M_{\pi^0}^2} \right\} + \mathcal{O}(p^4)\\
&= -\frac{B_0\delta}{3\sqrt{3}F_\pi^2}\left\{ 1 + \frac{3(s - s_0^n)}{M_\eta^2 - M_{\pi^0}^2} \right\} + \mathcal{O}(\delta^3, p^4)\\
&= -\frac{B_0\delta}{3\sqrt{3}F_\pi^2}\frac{3s - 4M_{\pi^0}^2}{M_\eta^2 - M_{\pi^0}^2} + \mathcal{O}(\delta^3, p^4) = -\frac{(3M_\eta^2 + M_{\pi^0}^2)(3s - 4M_{\pi^0}^2)}{Q^2 16\sqrt{3}F_\pi^2 M_{\pi^0}^2} + \mathcal{O}(\delta^3, p^4) ,
\end{aligned}$$

where we have first inserted the mixing angle ϵ, then expanded in δ, and finally replaced (at leading chiral order) the quark masses m_s and $\hat{m}$ as well as the LEC Z by physical meson masses via (2.18) and also F_0 by the pion decay constant F_π. Note that the additional electromagnetic term at $\mathcal{O}(e^2\delta)$ cancels the pion mass difference implicitly included in s_0^c. Thus, written in terms of s_0^n, the charged LO amplitude, which depends linearly on s, explicitly displays the Adler zero[#11] at $4M_{\pi^0}^2/3$ (in terms of the neutral pion mass). Moreover, $\mathcal{A}_c^{\mathrm{LO}}$ is completely proportional to $\delta \sim 1/Q^2$ and by using (cf. (2.21) and (2.18))

$$\frac{1}{Q^2} = B_0 \delta \frac{16 M_{\pi^0}^2}{3(3M_\eta^2 + M_{\pi^0}^2)(M_\eta^2 - M_{\pi^0}^2)} + \mathcal{O}(\delta^3, p^4) \tag{2.41}$$

we eventually arrive at the form convenient for the following discussion.

The neutral LO amplitude, on the contrary, contains neither derivatives (i.e. no dependence on Mandelstam variables) nor electromagnetic terms at $\mathcal{O}(e^2\delta)$,

$$\begin{aligned}
\mathcal{A}_n^{\mathrm{LO}} &= -\frac{B_0}{9F_0^2}\left\{ \sqrt{3}(m_d - m_u)\left[2\cos(2\epsilon) + \cos(4\epsilon)\right] - 16(m_s - \hat{m})\cos\epsilon\,\sin^3\epsilon \right\} + \mathcal{O}(p^4) \\
&= -\frac{B_0\delta}{3\sqrt{3}F_\pi^2}\left\{ 1 + 2\cos(4\epsilon) \right\} + \mathcal{O}(p^4) \\
&= -\frac{B_0\delta}{\sqrt{3}F_\pi^2} + \mathcal{O}(\delta^3, p^4) = -\frac{3(3M_\eta^2 + M_{\pi^0}^2)(M_\eta^2 - M_{\pi^0}^2)}{Q^2 16\sqrt{3}F_\pi^2 M_{\pi^0}^2} + \mathcal{O}(\delta^3, p^4) ,
\end{aligned} \tag{2.42}$$

and therefore is a constant proportional to δ, which means in particular that the Dalitz slope α (to be defined in Sect. 2.2.4) vanishes at LO, as already mentioned in Chap. 1.

Note that the LO amplitudes are closely related according to

$$\mathcal{A}_c^{\mathrm{LO}}(s) = \mathcal{A}_n^{\mathrm{LO}}\frac{\hat{a}(s)}{3} + \mathcal{O}(\delta^3, p^4) , \qquad \hat{a}(s) = \frac{3s - 4M_{\pi^0}^2}{M_\eta^2 - M_{\pi^0}^2} = \frac{s - s_A}{s_0^n - s_A} , \qquad s_A = \frac{4M_{\pi^0}^2}{3} . \tag{2.43}$$

2.2.3 Symmetry properties and the $\Delta I = 1$ amplitude relation

Both $\eta \to 3\pi$ decay amplitudes obey general symmetry constraints: while for the charged decay invariance under charge conjugation for both strong and electromagnetic interactions implies that the amplitude $\mathcal{A}_c(s,t,u)$ is symmetric under the exchange of t and u (cf. (2.33)),

$$\mathcal{A}_c(s,t,u) = \mathcal{A}_c(s,u,t) \qquad \Rightarrow \qquad \mathcal{A}_c(s,t-u) = \mathcal{A}_c(s,u-t) , \tag{2.44}$$

the amplitude $\mathcal{A}_n(s,t,u)$ for the neutral decay has to be symmetric under exchange of all pions and thus all Mandelstam variables due to Bose symmetry,

$$\mathcal{A}_n(s,t,u) = S_n\left\{ \mathcal{A}_n(s,t,u) + \text{permutations} \right\} . \tag{2.45}$$

Moreover, the charged and neutral amplitudes can be related at leading order in isospin breaking due to the $\Delta I = 1$ selection rule, as already mentioned in Chap. 1 and as will be shown below. Prior to that, however, it is worthwhile to examine the isospin-violating nature of the $\eta \to 3\pi$ decays carefully.

[#11]Adler zeros are kinematical points, where hadronic amplitudes with a soft pion (i.e. with vanishing 4-momentum) in the final state go to zero due to a chiral $SU(2) \otimes SU(2)$ soft-pion theorem [115, 116], cf. the discussion of Sutherland's soft-pion theorem in Sect. 3.3.

The most concise argumentation considers G-conjugation, which is defined as product of charge conjugation C and a rotation by π around the 2-axis of isospin space, i.e. $G = Ce^{-i\pi I^2}$ with $e^{-i\pi I^2}|I, I^3\rangle = (-1)^{I-I^3}|I, -I^3\rangle$. Thus, the neutral isosinglet η has positive G-parity, $G|\eta\rangle = |\eta\rangle$. Since G-parity is a multiplicative quantum number, from $G|\pi\rangle = -|\pi\rangle$ for the isotriplet π[#12] it follows $G|3\pi\rangle = -|3\pi\rangle$, so that G-parity is not conserved in $\eta \to 3\pi$ decays. In turn, the definition of G-conjugation together with invariance under charge conjugation then yields the selection rule $\Delta I = 1$ for the total isospin.

However, G-parity is a rather subtle combined quantity: in view of the famous Gell-Mann–Nishijima formula $Q = I^3 + Y/2$, which relates the electromagnetic charge to the third component of the isospin and the hypercharge $Y = B + S + \ldots$ containing the baryon number B and all other flavor quantum numbers like for instance the strangeness S, it can be viewed as a generalization of C-parity for neutral particles (or systems) to isomultiplets with zero average electromagnetic charge. The latter constraint is a direct consequence of the fact that G-invariance is strictly valid only for strong interactions in the limit of isospin conservation and thus explicitly broken by electromagnetic interactions. Even though the concept of G-parity can be generalized to some extent (e.g. for neutral antiparticle–particle systems), basically it is designed to explain several phenomenological observations in hadron physics by attributing pertinent G-eigenvalues to the particles (without leading to obvious contradictions, at least) rather than being based on first principles. As a result, it always needs to be supplemented by additional, more fundamental symmetry constraints, since e.g. the (hypothetical) decays of the neutral isosinglet ω with negative G-parity into either $3\pi^+$ or $3\pi^0$ would be perfectly allowed by G-invariance, but are of course forbidden by conservation of charge and total isospin, respectively. Therefore, a reasoning for the isospin breaking in $\eta \to 3\pi$ in terms of the underlying symmetries might be desirable, although (besides being more extensive) this requires some caution, as there are several misconceptions floating around in the literature.

The basic idea is to show that the $\eta \to 3\pi$ decays would be forbidden in the case of isospin conservation: working in the spherical (i.e. charge) basis of the pions where $I^3 = 1, 0, -1$ corresponds to π^+, π^0, π^-, respectively, the (hypothetical) 3π final state with total isospin $I = 0$ (as product of single-particle states $|\pi\rangle$, cf. the multiplicativity of G-parity) is totally antisymmetric with respect to permutations of the three pions, as can be seen either by explicitly constructing the 3π isosinglet or from general group-theoretical considerations (see for instance [117]). Thus, only the combination $\pi^0\pi^+\pi^-$ is allowed (in agreement with charge conservation); moreover, already the Clebsch–Gordan coefficient for the coupling of two pions to the antisymmetric 2π isotriplet (which is the only possibility to subsequently generate the antisymmetric 3π isosinglet) equals zero for $\pi^0\pi^0$,[#13] so that the $\eta \to 3\pi^0$ amplitude vanishes. Due to Bose statistics/symmetry the total (i.e. combined isospin/flavor- and space-) 3π wave

---

[#12]In fact, the negative G-parity of the pion isotriplet (transforming like a vector in isospin space) can be used as the defining property of G-parity, which can therefore be interpreted as parity operation in isospin space. While this naturally agrees with the ChPT convention (i.e. the adjoint representation of $SU(2)$), as in the 3-dimensional Cartesian isospin basis $C = \text{diag}(1, -1, 1)$ and $\exp(-i\pi I^2) = \text{diag}(-1, 1, -1)$ yield $G = -\mathbb{1}_3$, the additional sign for the spherical convention is compensated by adopting $C|\pi^\pm\rangle = -|\pi^\mp\rangle$ in contrast to $C|\pi\rangle = +|\bar{\pi}\rangle$. In both cases, however, the charge eigenstates are just linear combinations of the Cartesian/flavor eigenstates, cf. [#1] and the Gell-Mann–Nishijima relation $Q = I^3 + Y/2$.

[#13]The corresponding Clebsch–Gordan coefficient $\langle 11, 00|11, 10\rangle$ vanishes due to the general symmetry relation $\langle j_1 j_2, m_1 m_2 | j_1 j_2, JM\rangle = (-1)^{J-(j_1+j_2)}\langle j_2 j_1, m_2 m_1 | j_2 j_1, JM\rangle$, cf. e.g. [34]. For the same reason also the decays $\rho^0 \to 2\pi^0$ and $\omega \to 3\pi^0$ are forbidden by isospin symmetry. In fact, these decays (as well as $\omega \to 2\pi^0$ and $\omega \to \eta\pi^0$) are also forbidden by C-invariance, since both ρ^0 and ω are vector particles with negative C-parity ($J^{PC} = 1^{--}$) whereas $C|\pi^0\rangle = +|\pi^0\rangle$.

function (in terms of single-particle states like for the isospin part) must be fully symmetric and thus the spatial part needs to be totally antisymmetric as well.[#14] Choosing the momentum-space representation for the latter, the amplitude for the purely bosonic process $\eta \to \pi^0\pi^+\pi^-$ thus inherits the total spatial antisymmetry under exchange of the momenta of the three pions. Invariance under charge conjugation, however, implies that the amplitude has to be symmetric with respect to interchanging the momenta of the charged pions, cf. (2.44), thereby ruling out a non-vanishing amplitude also for $\eta \to \pi^0\pi^+\pi^-$.

The sources for both strong and electromagnetic isospin breaking were already given in Chap. 1, and in App. B it will be explicitly argued that both (1.1) and (1.2) indeed comprise the $\Delta I = 1$ operators that are necessary due to the $\Delta I = 1$ selection rule for $\eta \to 3\pi$; moreover, it turns out that these operators, like the pions themselves, transform as isovectors. Since the η is an isoscalar, the combination of such $\Delta I = 1$ operators acting on the initial state $|\eta\rangle$ also transforms in analogy to a pion state $|\pi\rangle$. Based on this observation, due to crossing symmetry and neglecting any further isospin breaking, the isospin structure of the generic $\eta \to 3\pi$ amplitude is similar to that of the $\pi\pi$ scattering amplitude, as will also be shown in App. B. Therefore, all results for the latter arising from the isospin structure may easily be transferred to the former. Besides the isospin decomposition of the $\eta \to 3\pi$ amplitude, which is frequently used in the literature but not needed in this work, this entails the well-known $\Delta I = 1$ relation between the charged and the neutral amplitude

$$\mathcal{A}_n(s,t,u) = \mathcal{A}_c(s,t,u) + \mathcal{A}_c(t,u,s) + \mathcal{A}_c(u,s,t) + \mathcal{O}\!\left(e^4, e^2\delta, \delta^2\right) , \qquad (2.46)$$

which we will call $\Delta I = 1$ amplitude relation in the following and which in turn is pivotal for the analysis of (higher-order) isospin-breaking effects in $\eta \to 3\pi$ decays in Chap. 4; its rigorous derivation is also relegated to App. B. Using the spherical convention instead (cf. [#9]) as done in particular in [3], the charged amplitude and thereby the $\Delta I = 1$ amplitude relation pick up a relative sign. In the case of $\pi\pi$ scattering, where the amplitudes do not necessarily carry isospin-breaking prefactors, the corresponding relation is already broken at $\mathcal{O}\!\left(e^2\hat{m}\right)$, see [118].

In all calculations of *both* $\eta \to 3\pi$ decay channels performed in ChPT so far [13, 15, 21] (see also [66, 119]), actually only the amplitude for the charged decay has been calculated explicitly, whereas the neutral one is just deduced by using the relation (2.46), i.e. these calculations are conducted only at leading order in isospin breaking. The fact that (2.46) is not valid in general for isospin breaking beyond leading order, is most easily seen by the fact that e.g. photon loop contributions obviously do not respect this relation. Nevertheless, at leading chiral $\mathcal{O}\!\left(p^2\right)$ (where no such photon loops occur), the relation (2.46) is even fulfilled at $\mathcal{O}\!\left(e^2\delta, \delta^2\right)$ by the LO amplitudes (2.40) and (2.42) if the *neutral* relation (2.36) is used for *all* Mandelstam variables, cf. (2.43):

$$\hat{a}(s) + \hat{a}(t) + \hat{a}(u) = 3\frac{s_0^c - s_A}{s_0^n - s_A} \quad \Rightarrow \quad \mathcal{A}_c^{\mathrm{LO}}(s) + \mathcal{A}_c^{\mathrm{LO}}(t) + \mathcal{A}_c^{\mathrm{LO}}(u) \stackrel{(2.36)}{=} \frac{3\,\mathcal{A}_n^{\mathrm{LO}}}{1 + 2\cos(2\epsilon)} + \mathcal{O}\!\left(p^4\right) .$$
$$(2.47)$$

[#14]Note that, for a three-particle system, this does *not* necessarily imply $(-1)^L = -1$ and thus $L > 0$ for the total angular momentum due to Bose symmetry so that the decay would be forbidden by conservation of angular momentum, since it *is* possible to construct totally antisymmetric 3π spatial wave functions with $L = 0$ but non-zero relative angular momenta between pairs of pions and these 2π states and the respective third pion; the conclusion would be true, however, in the case of a two-particle system. Furthermore, note that in the case of a antiboson–boson state with relative angular momentum L charge conjugation yields $C|\bar{b}b\rangle = (-1)^L|\bar{b}b\rangle$ leading to an additional minus sign for odd values of L. Therefore, the reasoning does not rely on angular momentum considerations at all.

At next-to-leading chiral $\mathcal{O}(p^4)$ and including isospin breaking at $\mathcal{O}(e^2\delta, \delta^2)$, however, the amplitude for the neutral decay channel has to be calculated separately (as is proven by explicitly calculating the non-vanishing corrections to (2.46); cf. (2.49) below and Chap. 4).

From the general symmetry properties (2.44) and (2.45) together with the explicit LO formulae (2.40) and (2.42), one can deduce that the NLO amplitudes may be decomposed as

$$\mathcal{A}_c^{\mathrm{NLO}}(s,t,u) = \mathcal{A}_c^{\mathrm{const}} + \tilde{\mathcal{A}}_c(s) + \bar{\mathcal{A}}_c(s,t) + \bar{\mathcal{A}}_c(s,u) + \mathcal{O}(p^6) \ ,$$
$$\mathcal{A}_n^{\mathrm{NLO}}(s,t,u) = \mathcal{A}_n^{\mathrm{const}} + \tilde{\mathcal{A}}_n(s) + \tilde{\mathcal{A}}_n(t) + \tilde{\mathcal{A}}_n(u) + \mathcal{O}(p^6) \ , \tag{2.48}$$

which is particularly useful for the neutral decay amplitude, where the whole kinematical dependence is contained in the fully crossing symmetric rescattering contributions. These terms (especially the $I = 0$ $\pi\pi$ final-state interactions) are very important and yield about half of the total NLO corrections for $\eta \to 3\pi$ [13]. Furthermore, loops with on-shell intermediate particles (in the s-, t-, or u-channel) give rise to non-vanishing imaginary contributions at $\mathcal{O}(p^4)$. The occurring kaon loops, either in the form of tadpole graphs or as $\bar{K}K$ rescattering diagrams, are important for the expansions in isospin-breaking parameters e^2 (or ΔM_π^2) and δ (cf. the illustrative case of the LO amplitudes in Sect. 2.2.2): the kaon loop contributions entail terms without an isospin-breaking prefactor that, however, can always be collected in the form of implicitly isospin-breaking charged-to-neutral differences of kaon loop functions as will be discussed in App. A.2. By expanding the masses inside the loop functions in terms of the charged-to-neutral kaon mass difference ΔM_K^2 and using (2.14), the isospin-breaking effects of these kaon loop differences can be derived explicitly (cf. (A.11)), although for the discussion of higher-order contributions, namely at $\mathcal{O}(\delta^2)$, it is favorable to avoid these expansions unless it is necessary for the calculation to make the (leading orders in) isospin breaking explicit. In general, we do not expand any loop functions, so that all cuts, even outside the physical region, remain at their exact places; the exceptions to this rule, however, are charged-to-neutral loop differences of pions and kaons at even higher orders in isospin breaking like $\mathcal{O}(e^4, e^2\delta^2, \delta^3)$. Of course, we have checked that our amplitudes $\mathcal{A}_{c/n}^{\mathrm{NLO}}$, which go beyond LO in isospin breaking by considering contributions at $\mathcal{O}(e^2\delta)$ in [1] and additionally at $\mathcal{O}(\delta^2)$ in [3], obey the $\Delta I = 1$ amplitude relation for strong and electromagnetic LO isospin breaking at $\mathcal{O}(\delta)$ and $\mathcal{O}(e^2)$ and also reduce to the (charged) NLO amplitudes given in [13] and [15], respectively; the corresponding neutral amplitudes then agree by construction.

As pointed out above, the NLO amplitudes (2.48) beyond leading order in isospin breaking do not obey the $\Delta I = 1$ selection rule (2.46). However, it is not a priori clear how to consistently write down or to define the terms violating this rule, since the charged-to-neutral pion mass difference $\Delta M_\pi^2 = \mathcal{O}(e^2)$ affects even the relation between the Mandelstam variables in the two channels at $\mathcal{O}(e^2\delta)$ (as $3s_0^c - 3s_0^n = 2\Delta M_\pi^2$; cf. (2.36) and Sect. 2.2.4). Just for the purpose of illustration, we show here the part of the deviation at $\mathcal{O}(e^2\delta)$ proportional to the various low-energy constants, using $s + t + u = 3s_0^n$:

$$\mathcal{A}_n^{\mathrm{NLO}}\Big|^{\mathrm{LEC}} - \Big[\mathcal{A}_c^{\mathrm{NLO}}(s,t,u) + \mathcal{A}_c^{\mathrm{NLO}}(t,u,s) + \mathcal{A}_c^{\mathrm{NLO}}(u,s,t)\Big]^{\mathrm{LEC}}$$
$$= \frac{3M_\eta^2 + M_{\pi^0}^2}{\sqrt{3}Q^2 F_\pi^2 M_{\pi^0}^2}\bigg\{ \Delta M_\pi^2 (M_\eta^2 - 3M_{\pi^0}^2)\frac{L_3}{F_\pi^2}$$
$$+ e^2\bigg[\frac{3}{4}\big(M_\eta^2 + M_{\pi^0}^2\big)(K_3^r - K_4^r/2) - M_\eta^2 K_6^r + \frac{3}{2}\big(3M_\eta^2 - M_{\pi^0}^2\big)\big(K_{10}^r + K_{11}^r\big)\bigg]\bigg\}$$
$$= \mathcal{O}(e^2\delta) \ . \tag{2.49}$$

The higher-order isospin-breaking corrections to the $\Delta I = 1$ amplitude relation will be discussed in detail in Chap. 4.

2.2.4 Dalitz plot distributions and the branching ratio

For comparison with experimental analyses of $\eta \to 3\pi$ decays, the squared absolute value of the pertinent amplitude is conventionally expanded as a polynomial around the center of the so-called Dalitz plot [120, 121] in terms of the corresponding symmetrized (cf. the general symmetry properties (2.44) and (2.45)) and dimensionless coordinates. Based on the generic $\eta \to 3\pi$ kinematics (2.28), we therefore define the convenient abbreviations

$$\tilde{Q}_c = M_\eta - M_{\pi^0} - 2M_\pi \,, \qquad \tilde{Q}_n = M_\eta - 3M_{\pi^0} \,, \qquad \tilde{R}_{c/n} = \frac{2M_\eta}{3}\tilde{Q}_{c/n} \,,$$

$$\tau = \frac{\tilde{R}_n - \tilde{R}_c}{\tilde{R}_c} = \frac{\tilde{Q}_n - \tilde{Q}_c}{\tilde{Q}_c} = \frac{2(M_\pi - M_{\pi^0})}{\tilde{Q}_c} = \frac{2M_\eta}{M_\pi + M_{\pi^0}}\frac{s_0^c - s_0^n}{\tilde{R}_c} = 6.86 \times 10^{-2} \,. \quad (2.50)$$

For the charged decay channel one conventionally uses

$$x = \sqrt{3}\,\frac{T_{\pi^+} - T_{\pi^-}}{\tilde{Q}_c} = \frac{u - t}{\sqrt{3}\tilde{R}_c} \,, \qquad (2.51)$$

$$y = \frac{3T_{\pi^0}}{\tilde{Q}_c} - 1 = \frac{(M_\eta - M_{\pi^0})^2 - s}{\tilde{R}_c} - 1 = \frac{s_0^c - s}{\tilde{R}_c} + \tau\left\{1 - \frac{M_\pi + M_{\pi^0}}{2M_\eta}\right\} = \frac{s_0^n - s}{\tilde{R}_c} + \tau \,,$$

while for the fully symmetric neutral decay channel one introduces polar coordinates at the center of the Dalitz plot via

$$z = \frac{2}{3}\sum_{i=1}^{3}\left[\frac{3T_i}{\tilde{Q}_n} - 1\right]^2 = \frac{2}{3}\sum_{i=1}^{3}\left[\frac{s_i - s_0^n}{\tilde{R}_n}\right]^2 = \frac{2}{3}\sum_{i=1}^{3}\left[\frac{s_i^2 - (s_0^n)^2}{\tilde{R}_n^2}\right] = x_n^2 + y_n^2 \,,$$

$$x_n = \sqrt{z}\,\cos\varphi \,, \qquad y_n = \sqrt{z}\,\sin\varphi \,. \qquad (2.52)$$

It is important to note that the definitions of x_n and y_n agree with those of x and y only for $M_\pi = M_{\pi^0}$, which is, loosely speaking, sometimes referred to as the "isospin limit" for the isospin-breaking $\eta \to 3\pi$ decays (i.e. neglecting isospin-breaking corrections due to the charged-to-neutral pion mass difference $\Delta M_\pi^2 = \mathcal{O}(e^2, \delta^2)$ beyond the leading strong or electromagnetic effects taken into account, cf. e.g. [13,15,21,66]). Experimental data is then fitted to the standard parameterizations of the Dalitz plot distributions for the amplitude squares

$$\left|\mathcal{A}_c(x,y)\right|^2 = \left|\mathcal{N}_c\right|^2\left\{1 + ay + by^2 + dx^2 + fy^3 + gyx^2 + \dots\right\} \,,$$

$$\left|\mathcal{A}_n(z,\varphi)\right|^2 = \left|\mathcal{N}_n\right|^2\left\{1 + 2\alpha z + 2\beta z^{3/2}\sin(3\varphi) + 2\gamma z^2 + \dots\right\} \,, \qquad (2.53)$$

where $\left|\mathcal{N}_c\right|^2$ and $\left|\mathcal{N}_n\right|^2$ are the normalizations and $\{a, b, d, f, g, \dots\}$ and $\{\alpha, \beta, \gamma, \dots\}$ are the Dalitz plot parameters describing the energy dependence of the observable *squares* of the charged and the neutral decay amplitude, respectively. Note that for the charged channel odd terms in x are forbidden by charge conjugation symmetry (2.44), while for the neutral channel according to Bose symmetry (2.45) the linear combination of Mandelstam variables must be fully symmetric and is thus just constant due to $s + t + u = 3s_0^n$, so that any dependence on it can be absorbed in the normalization. For the latter, moreover, the term proportional to $\sin(3\varphi)$
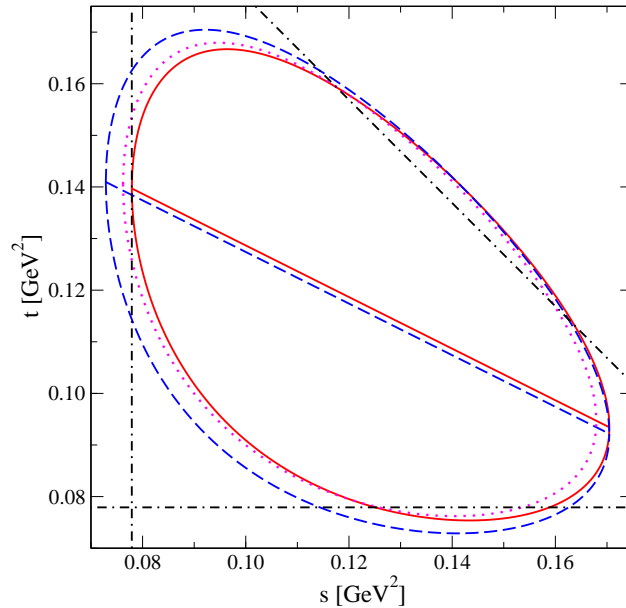
Figure 2.2: Boundaries of the physical regions for the $\eta \to 3\pi$ decays $\eta \to \pi^0\pi^+\pi^-$ (full/red), $\eta \to 3\pi^0$ (dashed/blue), and $\eta \to \pi^0\pi^+\pi^-$ with an average pion mass $\overline{M_\pi^2} = (M_{\pi^0}^2 + 2M_\pi^2)/3$ (dotted/magenta). Also shown are the lines with $t = u$ for both the charged and the neutral decay as well as the thresholds at $4M_\pi^2$ in all three kinematical channels (dashed-dotted/black).

explicitly reflects the threefold angular symmetry, which also follows from $\mathcal{A}_n(s, t, u)$ being fully symmetric in s, t, and u, whereas the accompanying factor $z^{3/2}$ ensures the expected cubic dependence on the Mandelstam variables; the relation $z^{3/2}\sin(3\varphi) = -y_n^3 + 3y_n x_n^2$ then reveals the close analogy to the charged parameterization. Therefore, the neutral parameterization exhibits an "accidental" rotational symmetry only upon neglecting terms of $\mathcal{O}(z^{3/2})$. Of the parameters beyond quadratic order in $(x_{(n)}, y_{(n)})$ for both decays, only the cubic parameters for $\eta \to \pi^0\pi^+\pi^-$ have been measured so far (by the KLOE collaboration [25]) and solely f has been found to differ from zero with statistical significance. Nevertheless, besides the upcoming new analyses of the charged parameters, in view of future very-high-statistics measurements for $\eta \to 3\pi^0$ (cf. Chap. 1 each), also a determination of β and probably even γ might not be beyond the realm of possibility.

By using $M_\pi = M_{\pi^0}$ and thus $\tilde{Q}_n = \tilde{Q}_c$, however, one neglects "trivial" but sizeable isospin breaking in the normalizations of the Dalitz plot variables for the charged and the neutral channel that — depending on the choice of the isospin limit of the pion mass — are at worst due to $(M_\eta - 2M_\pi - M_{\pi^0})/(M_\eta - 3M_{\pi^0}) = 0.94$ and $(M_\eta - 3M_{\pi^0})/(M_\eta - 3M_\pi) = 1.11$, respectively. In particular, a theoretical prediction for the (negative) neutral slope α is lowered in absolute value by about 22% if the charged-pion mass is used. Taking $M_\pi \neq M_{\pi^0}$ into account, in turn, it is important to take care of the precise definition of the center of the Dalitz plot for the charged decay, since the point $s = t = u = s_0^c$ does not completely coincide with the point $x = y = 0$ (where all kinetic energies T_i are equal): $s = t = u = s_0^{c/n}$ corresponds to $x_n = y_n = 0$ for the neutral decay, but $x = 0$ and $y = 5.14 \times 10^{-2}$ for the charged decay [16]. Note that, like for the charged LO amplitude (2.40), the implicit contribution from ΔM_π^2 may be canceled in (2.51) by using s_0^n in lieu of s_0^c (which furthermore turns out to be favorable for analyzing higher isospin-breaking corrections to the $\Delta I = 1$ amplitude

relation in Chap. 4). Moreover, the different pion masses affect the kinematical boundaries of the $\eta \to 3\pi$ Dalitz plots (i.e. of the physical regions) as depicted in Fig. 2.2: in addition to the charged and the neutral decay phase spaces (cf. Sect. 2.2.1) we have also drawn the allowed phase space for the decay $\eta \to \pi^0 \pi^+ \pi^-$ using an average pion mass $\overline{M_\pi^2} = (M_{\pi^0}^2 + 2M_\pi^2)/3$, so that $s + t + u = M_\eta^2 + 3\overline{M_\pi^2} = 3s_0^c$ is exactly reproduced and the corresponding average excess energy $\overline{Q_c} = M_\eta - 3\overline{M_\pi^2}^{1/2}$ is a reasonably good approximation of $\tilde{Q}_c$ as $(\overline{Q_c} - \tilde{Q}_c)/\tilde{Q}_c = -4 \times 10^{-4}$. This approximation is sometimes (e.g. [21, 66]) used in the literature, since at leading order in isospin breaking it is, strictly speaking, not possible to consistently account for the different pion masses in both $\eta \to 3\pi$ decays (featuring at $\mathcal{O}(e^2\delta)$, cf. the discussion preceding (2.49)), although sizeable deviations at the border of the charged Dalitz plot are clearly visible. For later convenience, in Fig. 2.2 we furthermore indicate the threshold for the production of two charged pions in all three kinematical channels s, t, and u as a vertical, horizontal, and diagonal dashed line, respectively, as well as the lines with $t = u$ (separating each the maximal and minimal limits $t_+^{c/n}$ and $t_-^{c/n}$ of (2.39), respectively). Concerning the derivation of the decay amplitudes in ChPT (cf. Sect. 2.2.2 and App. A.2), in order to obtain an unambiguous and explicit ordering of the isospin-breaking parameters δ and e^2 (or, up to higher-order corrections, $1/Q^2$ and ΔM_π^2) together with a minimal set of different meson masses squared (using the GMO relation (2.16)), we choose the neutral pion mass M_{π^0} and the η mass M_η, since at leading chiral order these masses, in contrast to all other pseudoscalar meson masses, comprise neither strong nor electromagnetic corrections at leading order in isospin breaking, cf. (2.13). In addition to this reasoning and besides the previously observed cancellations of isospin-breaking contributions due to ΔM_π^2 in (2.40) and (2.51) by using s_0^n for both decays, this choice is also motivated by the fact the these masses correspond to (most of) the asymptotic states in the processes under investigation; furthermore they feature naturally in the next-to-leading order $\pi^0\eta$ mixing (see [1]) as well as in the soft-pion considerations in Sect. 3.3.[#15] Consequently, for comparison with results for $\eta \to 3\pi$ at leading order in isospin breaking, we define the isospin limit of the pion mass to coincide with the *neutral*-pion mass.

In view of these important "trivial" kinematical isospin breaking effects, especially for the neutral-to-charged ratio r (1.5) of partial decay widths $\Gamma_{n/c}$ (2.37), it is remarkable how well the approximate relation $r \leq 3/2$ — and in particular its limiting case $r = 3/2$ — is actually fulfilled: this approximation arises from the $\Delta I = 1$ amplitude relation (2.46), i.e. at LO in isospin breaking, if one applies the "isospin limit" $M_\pi = M_{\pi^0}$ also to the integrations over the whole phase spaces, which we abbreviate here by $\int \mathrm{d}\Pi_{n/c}$ (excluding symmetry factors $S_{n/c}$)

$$r = \frac{\Gamma_n}{\Gamma_c} = S_n \frac{\int \mathrm{d}\Pi_n |\mathcal{A}_n(s,t,u)|^2}{\int \mathrm{d}\Pi_c |\mathcal{A}_c(s,t,u)|^2} \leq \frac{1}{3!} \frac{\int \mathrm{d}\Pi_n (3|\mathcal{A}_c(s,t,u)|)^2}{\int \mathrm{d}\Pi_c |\mathcal{A}_c(s,t,u)|^2} \approx \frac{3^2}{3!} \frac{\int \mathrm{d}\Pi_c |\mathcal{A}_c(s,t,u)|^2}{\int \mathrm{d}\Pi_c |\mathcal{A}_c(s,t,u)|^2} = \frac{3}{2} \, ,$$
(2.54)

so a sizeable deterioration is to be expected due to neglecting the different phase space boundaries as shown in Fig. 2.2.[#16] For the real case $M_\pi \neq M_{\pi^0}$, in fact, the roughly 12% smaller

---

[#15]For the latter, this choice also represents the best possible separation of (strong) $SU(3)$ isospin breaking due to $1 \gg \hat{m}/m_s \approx 4\%$, cf. (2.19) as well as (2.24) and (2.41).

[#16]First, it is important to note that the 2-dimensional neutral phase space integration is symmetric in s, t, and u. The inequality then follows by using the triangle inequality for the modulus $|\mathcal{A}_n(s,t,u)|$ written in terms of the charged amplitude via (2.46) and subsequently employing Hölder's inequality in order to split the integrals over the six "kinematically mixed" products of amplitude moduli like e.g. $2|\mathcal{A}_c(s,t,u)||\mathcal{A}_c(t,u,s)|$, so that each integral yields the same contribution by virtue of the crossing-invariant phase space. If the charged amplitude is independent of the Mandelstam variables, the inequality turns into an equality, of course.

charged phase space *accidentally* balances to a large extent the overestimation corresponding to the upper limit of the inequality, since the experimental average $r = 1.48 \pm 0.05$ [34] is rather close to $3/2$. Taking into account the correct phase spaces, the LO amplitudes of Sect. 2.2.2 yield a value of $r^{\mathrm{LO}} = 1.509$, which is even above (and *accidentally* very close to) the upper limit of the inequality $r \leq 3/2$,[#17] whereas the NLO amplitudes (which will be discussed in Chap. 3; here, we consider the isospin-symmetric (GL) versions of the NLO amplitudes, cf. Tab. 3.3 in Sect. 3.4.3) yield $r^{\mathrm{NLO}} = 1.442$ in agreement with $r^{\mathrm{NLO}} = 1.43 \pm 0.03$ of [13]. This corresponds to a relative change of more than 4% between LO and NLO and thus illuminates the importance of different (non-linear) functional dependences of the amplitude *squares* on Mandelstam variables that are merely estimated in (2.54). When going from NLO to NNLO, on the contrary, the fact that r increases by less than 1% [21],[#18] indicates that the higher chiral orders affect the normalizations of the $\eta \to 3\pi$ amplitudes (which mostly cancel in the ratio r up to combinatorial factors due to the $\Delta I = 1$ amplitude relation) rather than the shapes of the Dalitz distributions. Besides these purely kinematical effects of isospin breaking, however, there are also higher-order corrections to r stemming from respective corrections to the $\Delta I = 1$ amplitude relation itself that due to the modulus always increase the value of r and thus do not spoil the estimation in (2.54). As the isospin-breaking normalization by the quark mass double ratio Q^2, which mainly drives the $\eta \to 3\pi$ decays, cancels already in the ratio of amplitudes (except for purely electromagnetic contributions, cf. (1.4)), and in view of the rather sizeable changes between $\mathcal{O}(p^2)$ and $\mathcal{O}(p^4)$ on the one hand and the fact that at LO the $\Delta I = 1$ amplitude relation (2.46) is *accidentally* valid even beyond LO in isospin-breaking on the other hand, r is expected to be particularly sensitive on higher-order isospin-breaking effects at NLO (which will be discussed in Chap. 4).

Finally, we wish to comment on the validity of the polynomial expansion (2.53) in particular for the neutral decay channel. The boundary of the Dalitz plot for $\eta \to 3\pi^0$ in terms of the symmetrized coordinates x_n and y_n follows from the maximal and minimal values (cf. (2.39))

$$x_+^n(y_n) = \frac{1}{\sqrt{3}\tilde{R}_n}\sigma_{\pi^0}\big(s_n(y_n)\big)\lambda_{\eta\pi^0}^{1/2}\big(s_n(y_n)\big) = -x_-^n(y_n)\,, \qquad s_n(y_n) = s_0^n - \tilde{R}_n y_n\,, \quad (2.55)$$

within the limits $y_\pm^n = y_n(s_\mp^n)$ and is shown in Fig. 2.3. The dotted lines denote the three symmetry axes at $\varphi \in \{\pi/6, \pi/2, 5\pi/6\}$, which can easily be seen from $y_n \propto s - s_0^n$ defining one of the three symmetry axes and the others being located symmetrically around the $x_n \propto (u - s_0^n) - (t - s_0^n)$ axis; hence, the three kinematical points with $z = 1 = -y_-^n$ correspond to one of the pions being at rest and the other two being emitted back-to-back. The dotted circle depicts the beginning of the rapid decrease of pure phase space for radii $\sqrt{z} > y_+^n =$

[#17]This value agrees with $r^{\mathrm{LO}} = 1.51$ as given in [13]. However, in contrast to a statement made in [21], the LO result for r when neglecting the phase space differences is *not* exactly 1.5, but $1.405 = 0.931\,r^{\mathrm{LO}}$ (using $\int d\Pi_n$). This deviation is smaller than the 12% phase space effect, since the amplitudes are squared inside the integrals. Especially in this context it is interesting to note that $\int d\Pi_n y_n(s) = 0$, which would yield — upon erroneously not squaring the amplitudes — a value of *exactly* 1.5, since the normalized charged LO amplitude $\hat{a}(s) = (s - s_A)/(s_0^n - s_A) = 1 - y_n(s)/y_n(s_A)$ obeys $\hat{a}(s) + \hat{a}(t) + \hat{a}(u) = 3$ for $s + t + u = 3s_0^n$ (cf. (2.47), in concordance with considering the neutral phase space). This property of the neutral Dalitz plot distribution follows from the neutral phase space being totally symmetric in all Mandelstam variables together with the peculiar crossing property of $\hat{a}(s)$ (which in turn derives from its linear dependence on s, t, and u) and reflects its *accidental* rotational symmetry at LO that is not preserved at higher orders in contrast to the generally expected threefold angular symmetry, see (2.53). In analogy, the property $\int d\Pi_{c/n} x_{(n)}(s) = 0$ for both the charged and the neutral distribution corresponds to the $t \leftrightarrow u$ symmetry for both decays.

[#18]Note that [21] uses the average pion mass $\overline{M_\pi^2}$ and a slightly different value of M_η, affecting the numerically value of both $\Gamma_{n/c}$ and in particular r at any chiral order.
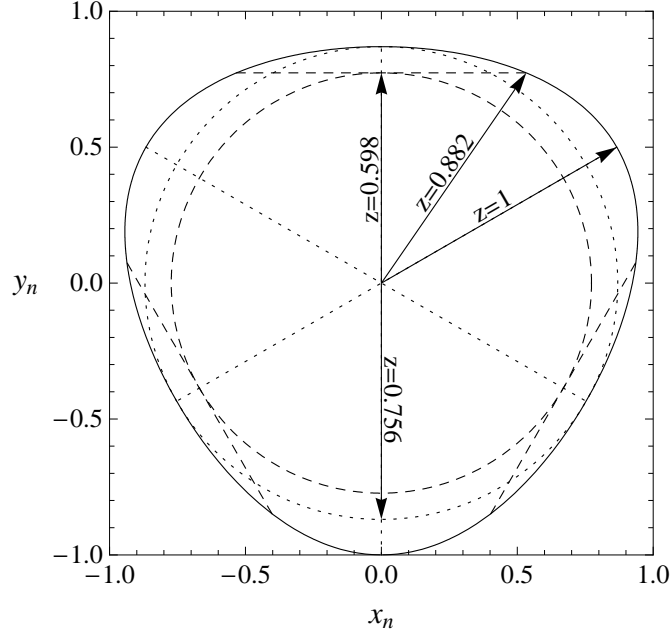
Figure 2.3: Boundary of the $\eta \to 3\pi^0$ Dalitz plot. Dotted: symmetry axes and biggest enclosed circle. Dashed: cusps at $s_i = 4M_\pi^2$ and corresponding circle. Arrows indicate specific z values. See main text for details.

$y_n(4M_{\pi^0}^2) = 0.870 = \sqrt{0.756}$. This deviation from the circular shape due to the relativistic kinematics also affects the angular weighting in the integration over the physically allowed ranges of φ in order to arrive at the radial distribution $\mathrm{d}\Gamma_n/\mathrm{d}z$; since on the one hand $\sin(3\varphi)$ is odd in φ and thus vanishes upon integration over the full range $\varphi \in [0, 2\pi)$, but on the other hand $\varphi = 0$ does not coincide with one of the symmetry axes, the term proportional to β cancels in the radial distribution only inside the dotted circle. Accordingly, in [3] both the (yet unmeasured) higher-order neutral Dalitz plot parameters β and γ are predicted to be very small, but different from zero. It is important to note that the cusps due to $\pi^+\pi^- \to \pi^0\pi^0$ final state rescattering occur at $s_i = 4M_\pi^2$ and not at a single z value (see also Fig. 2.2); the smallest and the largest values of z crossing the cusp lines ($z = 0.598$ and $z = 0.882$, respectively) are indicated at the corresponding arrows (cf. the discussion in [122]).[19] Therefore, the polynomial representation for the neutral Dalitz plot distribution (2.53) is only valid for $\sqrt{z} < y_n(4M_\pi^2) = 0.773 = \sqrt{0.598}$, i.e. inside the dashed circle. The importance of $M_\pi \neq M_{\pi^0}$ especially at the "trivial" kinematical level is also nicely illustrated by the relative size of the annulus between the two circles compared to the total neutral phase space (which is rather small for both $\eta \to 3\pi$ decays, cf. the excess energy $\tilde{Q} = M_\eta - 3M_\pi \approx M_\pi$, compared to e.g. $\eta' \to 3\pi$, where $\tilde{Q} = M_{\eta'} - 3M_\pi \approx M_\eta$; see for instance [123] for a graphical demonstration).

---

[19]Due to the total symmetry of the neutral amplitude under exchanges of pions, it actually suffices to consider a sixth of the neutral Dalitz plot, e.g. the region between the arrows for $z = 1$ and $z = 0.598$ (i.e. $\varphi \in [\pi/6, \pi/2]$) shown in Fig. 2.3, since all events can be mapped into it by a proper choice of the outgoing momenta, cf. the symmetry factor $S_n = 1/6$ in (2.37). Moreover, when considering the differential distribution $\mathrm{d}\Gamma_n/\mathrm{d}s$ (i.e. the neutral decay spectrum w.r.t. to the invariant mass s of the non-odd pair $\pi_2^0\pi_3^0$), this procedure increases the number of neutral pion pairs in the vicinity of the cusp region by a factor of 3, see for instance [61].

Chapter 3

Electromagnetic corrections in $\boldsymbol{\eta \to 3\pi}$ decays[*]

As discussed in Chap. 1, in this chapter we investigate the electromagnetic corrections in both $\eta \to \pi^0 \pi^+ \pi^-$ and $\eta \to 3\pi^0$ decays at next-to-leading chiral $\mathcal{O}(p^4)$ and including second-order isospin breaking at $\mathcal{O}(e^2\delta)$. However, in order to avoid overlap with [39] (wherein the corresponding amplitudes have been derived), here we reproduce neither the derivation of these decay amplitudes nor their explicit forms as both published in [1]. In the following we rather present the further analytical improvements and results beyond [39], namely the rigorous treatment of real-photon radiation (i.e. bremsstrahlung) together with the subtraction of the corresponding universal soft-photon corrections (enabling the matching to experimental analyses) in the soft-photon approximation on the one hand and analyzing the corrections to Sutherland's soft-pion theorem [4, 5] for the electromagnetic corrections on the other hand, as well as the numerical results published in [1]. Nevertheless, the needed loop functions are given explicitly in App. A.1 for convenience. We want to stress here again, that *all* results (analytical and numerical) presented in this chapter are solely based on the decay amplitudes at $\mathcal{O}(e^2, e^2\delta, \delta, p^4)$ — i.e. without terms at $\mathcal{O}(\delta^2)$, cf. Sect. 2.2 — in accordance with [1].

3.1 Real-photon radiation

For the charged decay at next-to-leading chiral $\mathcal{O}(p^4)$ photon loops occur. More specifically, in addition to the self-energy contributions to the NLO propagators of the charged pions, there are vertex corrections due to the coupling of a virtual photon at the meson vertex and one of the charged pions as well as triangle diagram contributions describing the exchange of a virtual photon in the final state between the charged pions. These virtual-photon contributions typically entail infrared (IR) divergences that we keep track of by introducing a finite photon mass m_γ; alternatively one might use dimensional regularization also in the infrared.[#1] The self-energy of the charged pions contributes to both the corresponding IR-finite mass and IR-divergent wave-function renormalization, while the two instantiations of the vertex correction diagram yield the same IR-finite contribution $\mathcal{A}_c^{\pi\gamma}(s)$ to the charged amplitude (cf. [1] for

---

[*]Most contents of this chapter have been published in [1, 2].

[#1]Either way, there are no photon tadpole contributions Δ_γ (cf. e.g. (A.2) for $m_\gamma \to 0$); see also Sect. 4.2.
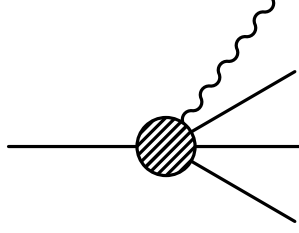
Figure 3.1: Real-photon radiation diagram.

details). The triangle diagram contribution

$$\mathcal{A}_c^{\pi\pi\gamma}(s) = \frac{e^2(3M_\eta^2 + M_{\pi^0}^2)}{Q^2 16\sqrt{3} F_\pi^2 M_{\pi^0}^2} \left\{ (3s - 4M_{\pi^0}^2)\left[2(s - 2M_\pi^2)G(s) + J_{\pi\pi}(s) + 2\frac{\Delta_\pi}{M_\pi^2} - \frac{1}{8\pi^2} \right] \right.$$
$$\left. + (s - 2M_\pi^2)\left[3\frac{\Delta_\pi}{M_\pi^2} - \frac{1}{4\pi^2} \right] \right\} + \mathcal{O}(e^2\delta^2, p^6) \tag{3.1}$$

contains the triangle loop function $G(s)$ (given in (A.9)), which has some interesting features: both the real and the imaginary part are IR-divergent; while the IR divergence in the real part is canceled against bremsstrahlung contributions, the imaginary part can be resummed in the IR-divergent Coulomb phase. Furthermore, $G(s)$ is finite in the ultraviolet, but it contains a kinematical singularity at the threshold $s = s_-^c = 4M_\pi^2$ (i.e. $\sigma_\pi = 0$, cf. (2.31)), the Coulomb pole. From (3.1) one can infer that its contribution to the full NLO amplitude is given by

$$\mathcal{A}_c^{\text{pole}} = \mathcal{A}_c^{\text{LO}} e^2 \frac{1 + \sigma_\pi^2}{16\sigma_\pi} . \tag{3.2}$$

Note that the prefactor of the triangle loop function and hence the Coulomb pole is proportional to the charged LO amplitude (2.40).

In general, infrared divergences due to virtual-photon radiation are canceled by the inclusion of real-photon radiation — so-called bremsstrahlung as depicted in Fig. 3.1 — on the cross-section level. For this purpose, we utilize the soft-photon approximation, which amounts to neglecting the real-photon momentum in the overall energy and momentum conservation. The results for general n-body decays with the radiation of one additional real photon of maximum energy E_{max} can be found e.g. in [124], which also uses a finite photon mass as a regulator; radiative corrections for the largely analogous decay $K_L \to \pi^0\pi^+\pi^-$ in the framework of ChPT are discussed in [125]. Adapting the results of [124] to $\eta \to \pi^0\pi^+\pi^-\gamma$ yields an effective bremsstrahlung contribution to the amplitude squared of the form

$$|\mathcal{A}_c|^2 \frac{e^2}{2\pi^2} \left[\log\frac{m_\gamma}{2E_{\text{max}}} \left\{ 1 - \frac{1 + \sigma_\pi^2}{2\sigma_\pi} \log\frac{1 + \sigma_\pi}{1 - \sigma_\pi} \right\} + F(s, t, u) \right] . \tag{3.3}$$

Here, the maximum photon energy E_{max} (in the η rest frame) is given by

$$E_{\text{max}} = \min\left\{ E_{\text{kin}}, E_{\text{cut}} \right\} , \qquad E_{\text{kin}} = \frac{M_\eta^2 - \left(M_{\pi^0} + \sqrt{s} \right)^2}{2M_\eta} , \tag{3.4}$$

where E_{kin} is the maximal kinematically allowed limit, and the value of the photon cutoff energy E_{cut} is set to a typical detector resolution. This kinematical constraint leads to a

logarithmic divergence at the upper limit $s = s_+^c = (M_\eta - M_{\pi^0})^2$, signaling that very close to the boundary of the phase space the $\mathcal{O}(e^2)$ approximation (i.e. the assumption of only one soft photon being radiated) becomes unreliable. The function $F(s, t, u)$ is given by

$$F(s, t, u) = f(1) + f(-1) - \int_{-1}^{1} \mathrm{d}z\, \frac{1 + \sigma_\pi^2}{1 - z^2 \sigma_\pi^2}\, f(z) \,,$$

$$f(z) = \frac{1 + z\nu}{4\omega(z)} \log \frac{1 + z\nu + \omega(z)}{1 + z\nu - \omega(z)} \,, \qquad \omega(z) = \sqrt{\kappa^2 + 2z\nu + z^2(\varsigma^2 + \nu^2)} \,,$$

$$\nu = \frac{t - u}{s + M_\eta^2 - M_{\pi^0}^2} \,, \qquad \kappa = \frac{\sqrt{\lambda_{\eta\pi^0}}}{s + M_\eta^2 - M_{\pi^0}^2} \,, \qquad \varsigma = \frac{2 M_\eta \sqrt{s}\, \sigma_\pi}{s + M_\eta^2 - M_{\pi^0}^2} \,, \qquad (3.5)$$

and represents contributions that are finite in the limit $m_\gamma \to 0$.

Computing the charged amplitude squared and collecting the IR-divergent parts consistently with respect to both the chiral order and the power counting in e^2 we obtain

$$- |\mathcal{A}_c|^2 \frac{e^2}{2\pi^2} \log \frac{m_\gamma}{M_\pi} \left\{ 1 - \frac{1 + \sigma_\pi^2}{2\sigma_\pi} \log \frac{1 + \sigma_\pi}{1 - \sigma_\pi} \right\} \,, \qquad (3.6)$$

so that by comparing (3.3) and (3.6) it is clear that the inclusion of real-photon radiation indeed cancels the IR divergences.

We have been intentionally vague above about the amplitude $\mathcal{A}_c$ to be inserted in (3.3) and (3.6). As a matter of principle, our calculation is only fully consistent for the lowest-order amplitude $\mathcal{A}_c^{\mathrm{LO}}$ to be multiplied with electromagnetic corrections factors. However, as is conventionally done in ChPT calculations, we only chirally expand the amplitudes to a specific chiral order and we do not re-expand their squares. This way, even when disregarding numerically tiny terms of $\mathcal{O}(e^4)$, we do include interference terms of radiative corrections with strong loop corrections. As a consequence, in order to achieve the cancellation of all IR divergences, the bremsstrahlung terms in (3.3) need to be included with the prefactor

$$|\mathcal{A}_c|^2 \to \mathcal{A}_c^{\mathrm{LO}} \left\{ \mathcal{A}_c^{\mathrm{LO}} + \mathrm{Re}\, \mathcal{A}_c^{\mathrm{NLO}} \big|_{e=0} \right\} \,. \qquad (3.7)$$

3.2   Subtraction of universal soft-photon corrections

The kinematical singularities in the radiative corrections both at $s = 4M_\pi^2$ for (3.2) and at $s = (M_\eta - M_{\pi^0})^2$ for (3.3) are part of the so-called universal (soft-photon) corrections that can even be resummed to all orders in the fine structure constant [124, 126, 127]. In order to perform a meaningful fit of the Dalitz plot distribution (cf. the discussion in Sect. 2.2.4), these universal corrections are usually already applied in the analysis of the experimental data. Thus, in order to enable the matching (or application) of the electromagnetic corrections under consideration to experimental analyses, we also need to account for the universal corrections in the soft-photon approximation by subtracting the corresponding parts of our charged amplitude (square) in the following way before predicting experimental observables:

- The both infrared and kinematically divergent imaginary part of the triangle loop function $G(s)$ can be resummed to the (divergent) Coulomb phase. As an overall phase factor is unobservable, $\mathrm{Im}\, G(s)$ is omitted.

- We subtract the Coulomb pole, whose leading approximation is given in (3.2).

- Furthermore, we subtract the $e^2 \log E_{\text{max}}$ singularity of (3.3) in the form

$$\left|\mathcal{A}_c\right|^2 \frac{e^2}{2\pi^2} \log \frac{M_\eta}{2E_{\text{max}}} \left\{ 1 - \frac{1+\sigma_\pi^2}{2\sigma_\pi} \log \frac{1+\sigma_\pi}{1-\sigma_\pi} \right\} , \tag{3.8}$$

which is the $\mathcal{O}\!\left(e^2\right)$ approximation of the resummed correction factor, see [124, 127].

In this manner, we obtain a charged amplitude *square* free of kinematical singularities. In particular, $\operatorname{Re} G(s)|^{\text{no pole}}$ contains only even powers of σ_π and is hence analytic in s, cf. (A.9).

Nevertheless, in order to illustrate the size of the various corrections, it is useful to plot (real and imaginary parts of) *amplitudes* in Sect. 3.4.1, although, as already discussed in Sect. 3.1, in principle they cannot be made IR-finite in a consistent way. However, we can remedy this problem by hand using the replacement

$$m_\gamma \to M_\eta \tag{3.9}$$

in the charged decay amplitude in order to mimic the net effect of both adding bremsstrahlung and subtracting universal corrections, compare (3.3), (3.6), and (3.8).[#2] Of course, this does not take into account the finite contributions $F(s,t,u)$, which can only be added at the level of squared amplitudes. Furthermore, in Sect. 3.4.1 we retain the threshold divergences (Coulomb pole and phase) for illustrative reasons.

3.3   Corrections to Sutherland's soft-pion theorem

As a final analytic result concerning the electromagnetic corrections at $\mathcal{O}\!\left(e^2\delta\right)$, we want to comment on Sutherland's soft-pion theorem [4, 5]. Explicitly, this theorem (assuming $m_u = m_d$) states that for the limit of one of the three pions to be soft, the (electromagnetic) amplitude for $\eta \to 3\pi$ is expected to vanish, i.e.

$$\lim_{p_i \to 0} \left(\mathcal{A}(s_1, s_2, s_3)\right)_{\text{em}} = \mathcal{O}\!\left(e^2 p_i^2\right) = \mathcal{O}\!\left(e^2 M_i^2\right) , \tag{3.10}$$

where M_i is understood to denote the (off-shell) mass $M_i(p_i) = (p_i^2)^{1/2}$ that for vanishing 4-momentum p_i also goes to zero. Generalizing the on-shell kinematics (2.28) accordingly, from $p_i \to 0$ immediately follows $s_i = M_\eta^2$ and $p_i^0 = |\mathbf{p_i}| = T_i = 0$, which explains the notion of π_i being soft. Conventionally choosing for convenience the odd pion π_1 (corresponding to a π^0 for both decays, cf. [5]) and using the conservation of 4-momentum in the η rest frame, in addition to $s_1 = M_\eta^2$ we can infer $p_2^0 = p_3^0 = M_\eta/2$ and thus $s_2 = s_3 = (M_2^2 + M_3^2)/2$ so that $s_1 + s_2 + s_3 = M_\eta^2 + M_2^2 + M_3^2 \neq 3s_0$ for $p_1 \to 0$ or $M_1 \to 0$ (i.e. $M_{\pi^0} \to 0$ for the charged decay if $M_\pi \neq M_{\pi^0}$ is considered).[#3] In general, soft-pion theorems are solely based on symmetry principles and independent of a specific Lagrangian; e.g. both Sutherland's theorem and Adler's theorem on amplitude zeros [115, 116] have been developed prior to QCD or ChPT. From a modern point of view, however, soft-pion theorems are naturally valid in

---

[#2]Strictly speaking, however, m_γ is supposed to be small in contrast to M_η.

[#3]Hence, also for the definition of these $\eta \to 3\pi$ soft-pion points in the Mandelstam plane at least in principle care needs to be taken as soon as one allows for different pion masses, cf. the discussions in Sects. 2.2.3 and 2.2.4.

the limit of chiral $SU(2) \otimes SU(2)$ symmetry, where *all* pions are massless and soft, and the corrections are then given as higher chiral orders in powers of $p^2 = M^2_{(\pi^0)}$.[#4]

Accordingly, and also in order to compare with the result of [15],[#5] here we simply define the soft-pion points for both $\eta \to 3\pi$ decays via $s = 3s_0^{c/n}$ and $t = u = 0$, respectively (thus preserving $s + t + u = 3s_0^{c/n}$), followed by splitting off ΔM^2_π and then taking the limit $M_{\pi^0} \to 0$. To be more specific, the corrections to the soft-pion theorem (3.10) can therefore be calculated by *simultaneously* performing the following expansions of both amplitudes (which entail in particular expansions of the corresponding loop functions or directly of their charged-to-neutral differences, cf. (A.11), in the pertinent kinematical regime):

- expansion in all Mandelstam variables around the corresponding soft-pion point,[#6]

- expansion in powers of isospin-breaking parameters (rewriting M_π, M_{K^0}, and M_K in terms of M_{π^0} and M_η via the GMO formula (2.16) and consistently neglecting both higher chiral and isospin-breaking orders),

- expansion in M_{π^0} around the soft-pion limit $M_{\pi^0} = 0$ (effectively expanding in $M^2_{\pi^0}/M^2_\eta$).

Alternatively, at a given chiral order, one may work in terms of quark masses and simultaneously expand in isospin-breaking parameters and the average light quark mass $\hat{m}$ (thus effectively expanding in $\hat{m}/m_s$ as well as δ/m_s and e^2/m_s) by using e.g. at leading chiral order

$$\frac{M^2_{\pi^0}}{M^2_\eta} = \frac{3}{2}\frac{\hat{m}}{m_s} + \mathcal{O}\left(\left(\frac{\hat{m}}{m_s}\right)^2, \left(\frac{\delta}{m_s}\right)^2, p^2\right) . \tag{3.11}$$

For illustration purposes, we give the particularly important example (cf. (A.11) and (A.7))

$$\bar{J}_{K^0 K^0}\left(3s_0^c\right) = \frac{1}{8\pi^2}\left\{1 - \sqrt{2}\arctan\frac{1}{\sqrt{2}}\right\} + \frac{1}{24\pi^2}\left\{1 - \frac{3}{\sqrt{2}}\arctan\frac{1}{\sqrt{2}}\right\}\left[\frac{B_0\delta}{M^2_\eta} - 3\frac{\Delta M^2_\pi}{M^2_\eta}\right]$$
$$+ \mathcal{O}\left(\frac{\hat{m}}{m_s}, e^2\delta, \delta^2\right) , \tag{3.12}$$

which furthermore demonstrates the fact that also $3s_0^c = 3s_0^n + 2\Delta M^2_\pi$ generates electromagnetic contributions.

[#4]As an instructive example consider the Adler zeros: in the two-flavor chiral limit, it can be shown (by using PCAC) that the $\eta \to 3\pi$ amplitude goes to zero for vanishing 4-momentum of a charged pion; i.e. for $p_{\pi^+} \to 0$ or $p_{\pi^-} \to 0$ the charged amplitude develops the two Adler zeros at $t = M^2_\eta + \mathcal{O}(M^2_{\pi^0})$ and $u = s = \mathcal{O}(M^2_{\pi^0})$ or $u = M^2_\eta + \mathcal{O}(M^2_{\pi^0})$ and $s = t = \mathcal{O}(M^2_{\pi^0})$, respectively. These zeros are related by crossing and due to the $t \leftrightarrow u$ symmetry of the charged amplitude they can be combined as $s_A = \mathcal{O}(M^2_{\pi^0})$ and $(t - u)^2_A = (M^2_\eta + \mathcal{O}(M^2_{\pi^0}))^2$. By virtue of the $SU(2) \otimes SU(2)$ symmetry, both these positions and the corresponding zeros $\mathcal{A}_c(s_A, (t - u)_A) = \mathcal{O}(M^2_{\pi^0})$ are protected from being of $\mathcal{O}(M^2_\eta)$ and are thus small. At leading chiral order, from (2.40) one can read off $s_A^{(\text{LO})} = 4M^2_{\pi^0}/3$ (and thus $(t - u)^2_A = (M^2_\eta - M^2_{\pi^0})^2$, yielding in fact a line of zeros in the Mandelstam plane), whereas at NLO one usually takes the zero of $\text{Re}\,\mathcal{A}_c$ as approximation for the Adler zero.

[#5]In [15], both $s = M^2_\eta + 3M^2_\pi = 3s_0$ and $t = u = 0$ as well as $s = M^2_\eta$ and $t = u = 0$ are stated for the $\eta \to 3\pi$ soft-pion point, which, however, is (self-)consistent only if *all* pion masses are sent to zero.

[#6]Technically, due to our definition of the soft-pion point, one can first replace both t and u by $(3s_0^{c/n} - s)/2$ (thereby ensuring $t = u$) and then needs to expand in s around $3s_0^{c/n}$ only. Note that for the charged channel one has to be be careful when expanding the "divergent" parts of the amplitude proportional to $1/t$ and $1/u$, which also contain loop functions leading to powers of t and u upon expansion.

As shown in [15] (also assuming $m_u = m_d$), at chiral $\mathcal{O}(p^4)$ the correction of $\mathcal{O}(e^2 m_q)$ at the soft-pion point $s = 3s_0$ and $t = u = 0$ for $\eta \to 3\pi$ indeed scales as $e^2 \hat{m}$, and not as $e^2 m_s$. Explicitly, we find for the purely electromagnetic amplitudes (i.e. neglecting terms of $\mathcal{O}(e^2\delta)$, denoted by BKW) for both decays in this approximation

$$
\mathcal{A}_c^{\mathrm{BKW}} \overset{\mathrm{SP}}{=} \frac{2B_0\hat{m}}{\sqrt{3}F_\pi^2} \left\{ \frac{5\Delta M_\pi^2}{16\pi^2 F_\pi^2} \left(1 - \sqrt{2}\arctan\frac{1}{\sqrt{2}} \right) \right.
$$
$$
\left. + \frac{4e^2}{3} \left[3(K_3^r - K_4^r/2) - (K_5^r + K_6^r) + (K_9^r + K_{10}^r) \right] \right\} + \mathcal{O}\left(e^2\hat{m}\frac{\hat{m}}{m_s} \right) , \quad (3.13)
$$

$$
\mathcal{A}_n^{\mathrm{BKW}} \overset{\mathrm{SP}}{=} \frac{2B_0\hat{m}}{\sqrt{3}F_\pi^2} \left\{ \frac{\Delta M_\pi^2}{16\pi^2 F_\pi^2} \left(1 - \sqrt{2}\arctan\frac{1}{\sqrt{2}} \right) \right.
$$
$$
\left. + \frac{4e^2}{3} \left[3(K_3^r - K_4^r/2) - (K_5^r + K_6^r) + (K_9^r + K_{10}^r) \right] \right\} + \mathcal{O}\left(e^2\hat{m}\frac{\hat{m}}{m_s} \right) , \quad (3.14)
$$

where $\overset{\mathrm{SP}}{=}$ denotes the evaluation at the soft-pion point and the K_i^r are to be evaluated at the scale $\mu = M_{K^0}$, which has been chosen here just for convenience. For comparison, the additional terms at $\mathcal{O}(e^2\delta)$ (denoted by DKM) are found to be (again at $\mu = M_{K^0}$)

$$
\mathcal{A}_c^{\mathrm{DKM}} \overset{\mathrm{SP}}{=} -\frac{2B_0\delta}{\sqrt{3}F_\pi^2} \left\{ \frac{\Delta M_\pi^2}{M_\eta^2} \left[1 + \frac{4}{3}\left(\Delta_{\mathrm{GMO}} + \Delta_F + \frac{M_\eta^2}{F_\pi^2}L_3 \right) \right. \right.
$$
$$
\left. + \frac{M_\eta^2}{16\pi^2 F_\pi^2} \left(\frac{2}{3}\log\frac{M_{\pi^0}}{M_{K^0}} - \frac{9}{2}\log\frac{4}{3} + 5 + \frac{7}{4\sqrt{2}}\arctan\frac{1}{\sqrt{2}} + 2\pi i \right) \right]
$$
$$
- \frac{e^2}{8\pi^2} \left[\left(1 + 2\log\frac{M_{\pi^0}}{M_\eta} + \pi i \right)\log\frac{m_\gamma}{M_\eta} \right.
$$
$$
\left. - \log^2\frac{M_{\pi^0}}{M_\eta} - \frac{\pi^2}{3} + \frac{9}{4} + \frac{\pi}{4}i + \log\frac{M_{\pi^0}}{M_{K^0}} + \frac{1}{4}\log\frac{4}{3} \right]
$$
$$
\left. - \frac{4e^2}{3} \left[(K_1^r + K_2^r) - \frac{7}{2}(K_3^r - K_4^r/2) + (K_5^r + K_6^r) - (K_9^r - 2K_{10}^r - 3K_{11}^r) \right] \right\}
$$
$$
+ \mathcal{O}\left(e^2\delta\frac{\hat{m}}{m_s} \right) , \quad\quad\quad (3.15)
$$

$$
\mathcal{A}_n^{\mathrm{DKM}} \overset{\mathrm{SP}}{=} -\frac{2B_0\delta}{\sqrt{3}F_\pi^2} \left\{ \frac{\Delta M_\pi^2}{M_\eta^2} \left[\frac{8}{3}\Delta_F + \frac{M_\eta^2}{16\pi^2 F_\pi^2} \left(\log\frac{M_{\pi^0}}{M_{K^0}} + 2\log\frac{4}{3} + 3 + \frac{1}{4\sqrt{2}}\arctan\frac{1}{\sqrt{2}} - \pi i \right) \right] \right.
$$
$$
\left. - \frac{4e^2}{3} \left[\frac{3}{16\pi^2} + (K_1^r + K_2^r) - 5(K_3^r - K_4^r/2) + (K_5^r + K_6^r) - (K_9^r - 5K_{10}^r - 6K_{11}^r) \right] \right\}
$$
$$
+ \mathcal{O}\left(e^2\delta\frac{\hat{m}}{m_s} \right) . \quad\quad\quad (3.16)
$$

The comparison of (3.13)–(3.16) demonstrates explicitly that terms of $\mathcal{O}(e^2\delta)$ are relatively suppressed only by $\delta/\hat{m} \approx 2/3$ and not by another small isospin-violating parameter. Furthermore, only the terms in (3.15) and (3.16) entail chiral logarithms; the chiral logarithms squared in (3.15) are due to the expansion of the triangle loop function $G(s)$ of (A.9) around the soft-pion point (note that $G(s)$ only occurs with the prefactor $e^2\delta$ and that the subtraction

of universal corrections would only be meaningful at the level of squared amplitudes):

$$G\left(3s_0^c\right) = -\frac{1}{8\pi^2 M_\eta^2}\left\{\frac{\pi^2}{3} + \log^2\frac{M_{\pi^0}}{M_\eta} - \log\frac{m_\gamma}{M_\eta}\left[2\log\frac{M_{\pi^0}}{M_\eta} + \pi i\right]\right\} + \mathcal{O}\left(\frac{\hat{m}}{m_s}, e^2, \delta\right) \ . \ (3.17)$$

3.4 Numerical results

In this section, we present the numerical results for the charged and the neutral decay as published in [1], based on the corresponding NLO amplitudes at $\mathcal{O}\left(\delta, e^2, e^2\delta\right)$ given therein[#7] and the numerical input collected in App. A.3. Note that for all numerical evaluations, the isospin-breaking kaon loop differences are not expanded (cf. Sect. 2.2.3) and for strong isospin breaking only the parameter Q is employed.

As already mentioned in Chap. 1, throughout this chapter we focus on the electromagnetic contributions to $\eta \to 3\pi$ decays and do not aim at a particularly reliable representation of the purely strong amplitude, since it is well known that one has to go beyond one-loop order to obtain a valid representation of the latter [17–21]. The $\mathcal{O}(\delta)$ part in our calculation corresponds precisely to the one-loop representation of [13], which thus serves as a useful reference point to quantify the different electromagnetic corrections in the following. For this purpose, we only consider uncertainties in these electromagnetic contributions and disregard higher-order strong corrections: since the electromagnetic low-energy constants K_i^r are not very well known, we regard their input (and not unknown corrections of higher order in the chiral expansion) as the dominant source of uncertainty; see App. A.3 for a description of how we vary the K_i^r. However, for some numbers, which marked by an asterisk in the following, we are forced to deviate from our standard procedure to estimate the errors; the respective details are also relegated to App. A.3. All error bands in this section refer to this variation.

3.4.1 Amplitudes

In the following, we compare the results for the one-loop amplitudes of $\mathcal{O}(\delta)$ (henceforth denoted by GL) [13], those with effects of $\mathcal{O}\left(e^2\right)$ added (BKW) [15], and the results of the present investigation up-to-and-including effects of $\mathcal{O}\left(e^2\delta\right)$ (DKM). The GL and BKW amplitudes are also evaluated with our prescription of the isospin limit (i.e. using the neutral pion mass, cf. the discussion in Sect. 2.2.4) as well as with our choice of numerical input (cf. App. A.3) in order to facilitate comparison with the higher-order DKM corrections. For illustration purposes, in this section we plot the amplitudes along the lines $t = u$ (i.e. $x_{(n)} = 0$), which thus have also been drawn in Fig. 2.2.[#8]

In Fig. 3.2 we separately display the real and the imaginary parts of the charged GL, BKW, and DKM decay amplitudes. The infrared divergences in the amplitude are cured by hand according to (3.9), whereas the kinematical singularities at $s = 4M_\pi^2$ are retained here for

---

[#7]We refrain from repeating this numerical analysis with the amplitudes amended by the contributions at $\mathcal{O}\left(\delta^2\right)$ (cf. Sect. 2.2), since these additional terms are never enhanced compared to δ/m_s w.r.t. the leading $\mathcal{O}(\delta)$ terms, as discussed in App. A.2. Therefore, we expect the second-order strong effects for $\eta \to 3\pi$ decays to be numerically negligible (cf. [#7] in Sect. 2.1.3), in particular w.r.t. the uncertainties concerning the electromagnetic corrections. Moreover, in Chap. 4 we will argue that the contributions at $\mathcal{O}\left(\delta^2\right)$ to the higher-order isospin-breaking corrections in $\eta \to 3\pi$ decays — cast into a form that is particularly useful in combination with other theoretical approaches yielding more robust representations of the amplitudes like e.g. (modified) NREFT — drop out entirely.

[#8]Note that for additionally $s = s_0^{c/n}$ (i.e. $t = u = 0$), this corresponds to the respective soft-pion point.

Figure 3.2: Real and imaginary parts of the charged amplitudes GL (dashed/black), BKW (dot-dashed/blue), and DKM (full/red) for $t = u$. The inserts show the region close to the two-pion thresholds. The line widths in the real part indicate the error bands due to a variation of the electromagnetic LECs. The vertical lines show the limits of the physical region.

illustration. By our choice of the isospin limit for the pion mass, the threshold cusp in the GL amplitude is artificially removed from the physical threshold energy to $s = 4M_{\pi^0}^2$. According to (2.40) the leading-order charged decay amplitude is linear in s, which also dominates the energy dependence at NLO. The additional BKW contributions are purely real for both decay channels, as no pion rescattering diagrams contribute at that particular order and thus the imaginary parts of GL and BKW coincide with each other for both decays. Furthermore, all imaginary parts are independent of any low-energy constants and are therefore plotted without an error range. Since it is hard to identify cusps or the Coulomb pole in plots over the full kinematically allowed range, Fig. 3.2 also contains inserts where we show the amplitudes close to the two-pion thresholds. Here, the expected features in the amplitudes are clearly visible: the $\pi^0\pi^0$ cusp at $4M_{\pi^0}^2$ outside the physical region as well as the Coulomb pole and phase divergence at the $\pi^+\pi^-$ threshold.

The numerical results for the neutral GL, BKW, and DKM decay amplitudes are shown in an analogous way in Fig. 3.3. The vertical dotted lines indicate the physical region in s for $t = u$ for the neutral decay, hence the lower bound is now at the $\pi^0\pi^0$ threshold. The leading-order decay amplitude for $\eta \to 3\pi^0$ is constant, see (2.42), and also at NLO the dependence on s is weak. Figure 3.3 shows that the size of the additional contributions in DKM is comparable to or even larger than those in BKW. We find the expected cusp at the energy of the $\pi^+\pi^-$ threshold inside the physical region, although the overall variation is very small. As for the comparable decay $K_L \to 3\pi^0$, the strength of the cusp might be rather small for a very precise determination and an extraction of $\pi\pi$ scattering lengths thereby. However, we wish to point out that the cusp strength, which is proportional to the combination of scattering lengths $a_0^0 - a_0^2$ parameterizing the $\pi\pi$ FSIs as already mentioned in Chap. 1, is underestimated here: while the present one-loop ChPT calculation corresponds to the leading-order value $(a_0^0 - a_0^2)^{\mathrm{LO}} = 9M_\pi^2/(32\pi F_\pi^2) = 0.205$ [128],[#9] the matching of the Roy equations solution to

---

[#9]To be more precise, the cusp strength in our calculation is determined by the leading-order scattering length for $\pi^+\pi^- \to \pi^0\pi^0$ including isospin breaking, which is given by $(s_-^c - M_{\pi^0}^2)/(32\pi F_\pi^2) = (a_0^0 - a_0^2)^{\mathrm{LO}} \times \{1 + \Delta M_\pi^2/(3M_\pi^2)\}$ [118], increasing the isospin-symmetric value by about 2%. Note that for historical reasons
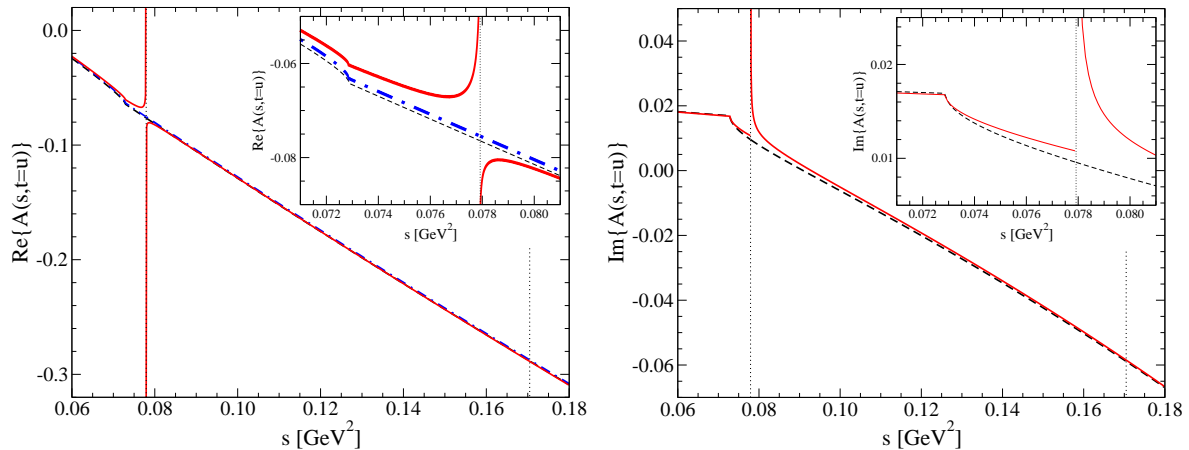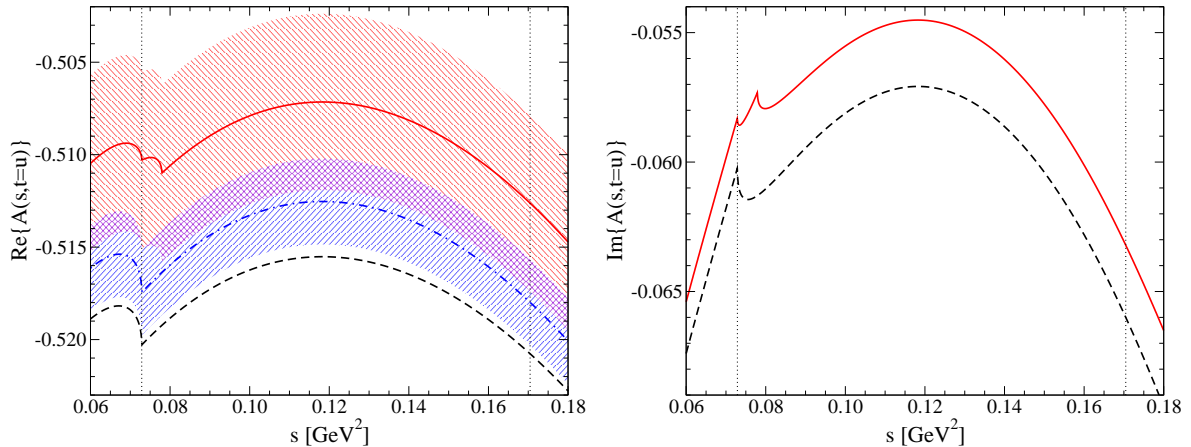
Figure 3.3: Real and imaginary parts of the neutral amplitudes GL (dashed/black), BKW (dot-dashed/blue), and DKM (full/red) for $t = u$. The hatched regions denote the error bands due to a variation of the electromagnetic LECs. The vertical lines show the limits of the physical region.

the next-to-next-to-leading chiral representation yields $(a_0^0 - a_0^2)^{\text{NNLO}} = 0.265 \pm 0.004$ [51,54], thereby increasing the cusp strength considerably. Furthermore, the cusp in $\eta \to 3\pi^0$ is considerably less pronounced than in $K^+ \to \pi^+\pi^0\pi^0$, much as in $K_L \to 3\pi^0$ [60]. For these two reasons, we refrain from displaying the decay spectra $d\Gamma/ds$, which would be the preferred observable for an extraction of $\pi\pi$ scattering lengths.

From Figs. 3.2 and 3.3 we can conclude that the relative sizes of the electromagnetic corrections in the BKW and DKM amplitudes with respect to the strong GL result are of comparable size, and thus the BKW estimate of the electromagnetic effects, neglecting $m_u \neq m_d$, is not a very accurate representation. However, the conclusion that the overall electromagnetic contributions remain rather small is still valid.

3.4.2 Dalitz plot parameters

As discussed in Sect. 2.2.4, in principle the Dalitz plot parameters are defined by expanding the squared absolute values of both decay amplitudes around the "center" of the corresponding Dalitz plot according to the standard parameterizations (2.53). Here, however, we fit these Dalitz plot distributions to discretized grids (of roughly 200×200 points) of squared amplitudes over the whole physical region (by using a uniform weighting of the thereby generated "data" points), since such a fitting procedure is usually employed in experimental analyses. In order to quantify the fit quality for the GL, BKW, and DKM amplitudes, we normalize a fictitious χ^2 to 1 for the GL amplitudes and only regard the relative changes, with the electromagnetic effects switched on successively. The errors on the corrections to the various Dalitz plot parameters are estimated by again varying the electromagnetic low-energy constants K_i^r as described in App. A.3. Since the resulting errors are always larger than the fit errors on the extracted parameters, we can safely neglect the latter.

---

the isospin limit of the scattering lengths is defined in terms of the *charged*-pion mass, however, not affecting this relative increase.

	$|\mathcal{N}_c|^2$	a	b
GL	0.0325	-1.279	0.396
BKW	-0.0004 ± 0.0003	-0.008 ± 0.001	$+0.006 \pm 0.001$
	$= (-1.1 \pm 0.9)\%$	$= (+0.6 \pm 0.1)\%$	$= (+1.4 \pm 0.2)\%$
DKM	$-0.0008 \pm 0.0002^*$	-0.009 ± 0.005	$+0.006 \pm 0.003$
	$= (-2.4 \pm 0.7^*)\%$	$= (+0.7 \pm 0.4)\%$	$= (+1.5 \pm 0.7)\%$

d	f	g	χ^2/ndf
0.0744	0.0126	-0.0586	$\equiv 1$
$+0.0011 \pm 0.0004$	-0.0003 ± 0.0001	-0.0010 ± 0.0003	1.03
$= (+1.5 \pm 0.5)\%$	$= (-2.2 \pm 0.4)\%$	$= (+1.7 \pm 0.6)\%$	
$+0.0033 \pm 0.0003^*$	$+0.0001 \pm 0.0001$	$-0.0038 \pm 0.0009^*$	1.63
$= (+4.4 \pm 0.4^*)\%$	$= (+0.5 \pm 0.6)\%$	$= (+6.4 \pm 1.5^*)\%$	

Table 3.1: Normalization and Dalitz plot parameters for $\eta \to \pi^0 \pi^+ \pi^-$ for the GL [13], BKW [15], and DKM (present work) amplitudes. All electromagnetic corrections are given as shifts (both absolute and relative) with respect to the strong result (GL). The asterisk indicates a non-standard error estimation. See main text for details.

The fit results for the normalization and the Dalitz plot parameters a–g of the charged decay channel are shown in Tab. 3.1 for the GL, BKW, and DKM amplitudes, where we quote the successive electromagnetic corrections corresponding to BKW and DKM both as shifts of absolute size and as relative shifts in percent with respect to the strong one-loop result GL [13]. Note that the universal radiative corrections producing kinematical singularities have been subtracted in the DKM amplitude according to the prescription given in Sect. 3.2. In general, Tab. 3.1 shows that electromagnetic corrections affect the Dalitz plot parameters at the percent level; in most cases, the errors given are of the same order as the central shifts. The normalization tends to get reduced compared to the purely strong amplitude, while the various slope parameters a–g are slightly increased in magnitude. The *relative* shifts in d and g are more sizeable than especially in a and b for the reason that the strong contribution to the x-dependent Dalitz plot parameters is suppressed to next-to-leading order in the chiral expansion (as is obvious from the purely s-dependent tree-level amplitude (2.40)). While the overall effects are still very small, we note that, throughout, the corrections of $\mathcal{O}(e^2)$ do not represent a valid estimate of the dominant electromagnetic corrections, as those of $\mathcal{O}(e^2\delta)$ are of the same order of magnitude — sometimes with the same sign, sometimes both effects tend to cancel. The quality of the polynomial Dalitz plot fit is comparable throughout.

A few comments concerning the cubic Dalitz plot parameters f and g are in order. In general, f is highly correlated with a in the fits. In the electromagnetic corrections, we observe that the influence of the low-energy constants on f and g is rather small, which is obvious from the fact that the counterterms only lead to terms constant and linear in s; we therefore do not consider the electromagnetic shifts thus obtained very reliable. In particular, all errors due to the K_i^r in the parameters d, f, and g are only indirectly induced by the variation in the normalization and by the implicit inclusion of higher-order effects in the squared amplitude.

	$|\mathcal{N}_n|^2$	$10^2 \times \alpha$	χ^2/ndf
GL	0.269	1.27	$\equiv 1$
BKW	-0.003 ± 0.002	$+0.05 \pm 0.01$	0.99
	$= (-1.1 \pm 0.9)\%$	$= (+3.7 \pm 0.5)\%$	
DKM	-0.009 ± 0.005	-0.002 ± 0.01	6.20
	$= (-3.3 \pm 1.8)\%$	$= (-0.2 \pm 1.0)\%$	
DKM(cusp)	-0.009 ± 0.005	$+0.06 \pm 0.01$	0.35
	$= (-3.3 \pm 1.8)\%$	$= (+5.0 \pm 1.1)\%$	

Table 3.2: Normalization and Dalitz plot parameters for $\eta \to 3\pi^0$ for the GL [13], BKW [15], and DKM (present work) amplitudes. The results for the latter are also shown with the fit of the Dalitz plot region restricted as to exclude the cusps at the charged-pion thresholds (DKM(cusp)). All electromagnetic corrections are given as shifts (both absolute and relative) with respect to the strong result (GL). See main text for details.

Note that, without subtracting the kinematical singularities due to universal corrections (cf. Sect. 3.2), in particular the fit results for f become nonsensical.

We now turn to the neutral channel $\eta \to 3\pi^0$. The results for the normalization and the Dalitz plot parameter α are collected in Tab. 3.2. Here, in addition to the results using the GL, BKW, and DKM amplitudes, we also discuss a variant of our result taking into account that the DKM amplitude displays features incompatible with a simple polynomial fit — namely the cusps at the charged-pion thresholds: by DKM(cusp) we denote a fit to the part of the Dalitz plot with $z < 0.598$ chosen such that the border region from the cusp outward is excluded and a polynomial representation of the Dalitz plot distribution is actually valid, cf. Sect. 2.2.4. In general, the corrections of $\mathcal{O}(e^2\delta)$ are even bigger than those of $\mathcal{O}(e^2)$ and the uncertainties due to the K_i^r are on the 1%-level throughout. As for the charged decay channel, the normalization is reduced by electromagnetic corrections by a few percent. Concerning the slope α, the cusp effect leads to the single biggest modification of any Dalitz plot parameter: trying to fit the cusp with the polynomial parameterization reduces α by 4% (compare DKM to BKW in Tab. 3.2), while excluding the cusp region increases it again by more than 5%. The latter shift is in qualitative agreement with the findings in [68], where α is determined from the curvature at the center of the Dalitz plot. The significance of this non-analytic structure is also reflected in the fit quality as quantified by the χ^2/ndf values given in Tab. 3.2: with the cusp included, the fit becomes worse by a factor of 6 (DKM), while excluding it makes it even better than the fit of the GL distribution (DKM(cusp)); of course, this is not surprising, as in fact the parameterizations (2.53) are defined as expansions of the squared amplitudes around the respective "center" of the corresponding Dalitz plot, i.e. around $z = 0$ for the neutral decay. Taking into account that the cusp strength is underestimated by about 30% as discussed in Sect. 3.4.1, these numbers should be scaled accordingly. However, the cusp effect is by far too weak to contribute significantly to an explanation of the long-standing sign discrepancy for α between ChPT calculations and experimental determinations, as we had already anticipated in the discussion of the "α-puzzle" in Chap. 1.
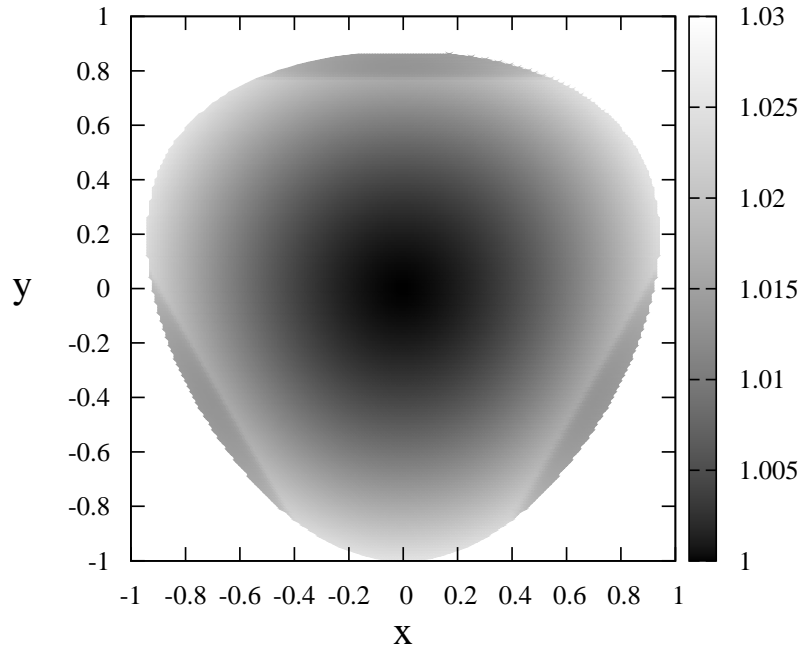
Figure 3.4: $\eta \to 3\pi^0$ Dalitz plot distribution corresponding to the full NLO amplitude (DKM), including the cusp structures at the $\pi^+\pi^-$ thresholds. Here, $x \equiv x_n$ and $y \equiv y_n$.

The $\eta \to 3\pi^0$ Dalitz plot is displayed graphically in Fig. 3.4 for our central result, i.e. the complete one-loop amplitude including electromagnetic corrections up to $\mathcal{O}(e^2\delta)$ (DKM). The cusp structures at the $\pi^+\pi^-$ thresholds are clearly visible, demonstrating that decay spectra with respect to s, t, and u are most sensitive to the cusp effect, not with respect to the radial coordinate z (as discussed in Sect. 2.2.4, see Fig. 2.3).

3.4.3   Decay widths, branching ratio, and quark mass double ratio

The results for the charged and neutral decay widths calculated according to (2.37) are shown in Tab. 3.3. The strong widths calculated at one loop underestimate the experimental values significantly, so again, the electromagnetic corrections are given as relative corrections to the strong result (GL). For the charged decay, the width is reduced moderately by about 2%. In addition, we also show a variant of the DKM amplitude (denoted by DKM(uc)) where the universal corrections are *not* subtracted, i.e. the Coulomb pole at s_-^c and the kinematical bremsstrahlung singularity at s_+^c are included; in this case, the reduction of the width is only about 1%. In the neutral channel, the shifts in the width are completely dominated by the corrections to the normalization of the amplitude, cf. Tab. 3.2. The total corrections up-to-and-including $\mathcal{O}(e^2\delta)$ are about a factor of 3 larger than those estimated by BKW, and the total reduction of the neutral width by electromagnetic effects is in good agreement with the one found in [68].

From these widths one can determine the $\eta \to 3\pi$ branching ratio $r = \Gamma_n/\Gamma_c$ already defined in (1.5) at the different orders in isospin breaking. The resulting electromagnetic corrections are also given in Tab. 3.3. For the BKW corrections, the ratio is nearly constant compared to the strong result (GL), as both widths are shifted by almost the same amount.

	Γ_c	Γ_n		$r = \Gamma_n/\Gamma_c$
Γ^{GL}	$154.5\,\mathrm{eV}$	$222.8\,\mathrm{eV}$	r^{GL}	1.442
$\Delta\Gamma^{\mathrm{BKW}}$	$(-1.5 \pm 1.3)\,\mathrm{eV}$	$(-2.5 \pm 2.0)\,\mathrm{eV}$	Δr^{BKW}	-0.002 ± 0.018
	$= (-1.0 \pm 0.9)\%$	$= (-1.1 \pm 0.9)\%$		$= (-0.1 \pm 1.2)\%$
$\Delta\Gamma^{\mathrm{DKM}}$	$(-2.9 \pm 0.7^*)\,\mathrm{eV}$	$(-7.3 \pm 4.0)\,\mathrm{eV}$	Δr^{DKM}	$-0.020 \pm 0.028^*$
	$= (-1.9 \pm 0.5^*)\%$	$= (-3.3 \pm 1.8)\%$		$= (-1.4 \pm 1.9^*)\%$
$\Delta\Gamma^{\mathrm{DKM(uc)}}$	$(-1.5 \pm 0.7^*)\,\mathrm{eV}$		$\Delta r^{\mathrm{DKM(uc)}}$	$-0.033 \pm 0.028^*$
	$= (-1.0 \pm 0.5^*)\%$			$= (-2.3 \pm 1.9^*)\%$

Table 3.3: Decay widths $\Gamma_{c/n}$ for the charged and neutral decay channel and branching ratio $r = \Gamma_n/\Gamma_c$. The electromagnetic corrections for the BKW and DKM amplitudes are expressed relative to the strong GL result. The asterisk indicates a non-standard error estimation. DKM(uc) denotes the DKM amplitude without subtraction of the universal corrections.

	$\eta \to \pi^0\pi^+\pi^-$	$\eta \to 3\pi^0$
ΔQ^{BKW}	$(+0.24 \pm 0.22)\%$	$(+0.28 \pm 0.22)\%$
ΔQ^{DKM}	$(+0.48 \pm 0.12^*)\%$	$(+0.84 \pm 0.46)\%$
$\Delta Q^{\mathrm{DKM(uc)}}$	$(+0.24 \pm 0.12^*)\%$	

Table 3.4: Electromagnetic corrections to the extraction of the quark mass double ratio Q^2 for both the charged and neutral decay channel. See main text for details.

Including all radiative corrections (DKM), r is reduced by 1.4%, with an uncertainty of about the same size. Without subtraction of the universal corrections, the effect on r is somewhat larger, about 2.3%.

Finally, as anticipated in Chap. 1, we can read off the corrections for the quark mass double ratio Q^2 from the relation (1.4), although, strictly speaking, this relation does not hold for the purely electromagnetic terms of $\mathcal{O}(e^2\hat{m})$, i.e. the BKW contributions and higher-order corrections like those at $\mathcal{O}(e^4)$. Given the smallness of the electromagnetic corrections and the size of the uncertainties, however, the additional error in factorizing Q^{-2} in the complete amplitude can be safely neglected. The resulting shifts in Q as collected in Tab. 3.4 are to be interpreted in the following way: extracted naively according to (1.4), Q would be shifted compared to the purely strong value according to Tab. 3.4, i.e. generally increased. Therefore, the opposite shift has to be applied in order to purify the extraction of Q via (1.4) by comparing a calculated width (e.g. at NLO and assuming Dashen's theorem to be valid) with a real measurement (necessarily including electromagnetic effects) according to

$$\Gamma_{c/n} = \left(\frac{Q_D}{Q}\right)^4 \Gamma_{c/n}^D . \tag{3.18}$$

The electromagnetic corrections in Tab. 3.4 are below half a percent for the charged channel, while in the neutral channel applying the electromagnetic corrections reduces Q by about 1%.

Chapter 4

Isospin-breaking corrections to the $\Delta I = 1$ amplitude relation**

As outlined in Chap. 1, the main motivation for the study to be presented in the following was to recast the results of [1] for the electromagnetic corrections in $\eta \to 3\pi$ decays in ChPT at NLO as presented in Chap. 3 in such a way that they can readily be combined with other theoretical frameworks, which yield a more robust description of the $\eta \to 3\pi$ decays by accounting for the important $\pi\pi$ FSIs more comprehensively than it is feasible in ChPT. In particular, the goal was to make contact with the (modified) NREFT calculation at two-loop-order, which was finally conducted in [3]. However, some of the isospin-breaking effects considered in [1] can be incorporated equally well or even much better in the NREFT framework employed in [3], namely "trivial" kinematical isospin-breaking effects as discussed in Sect. 2.2.4 (i.e. normalization issues and the use of physical meson masses inside the loop functions) on the one hand, and the possibility to use phenomenological values for the $\pi\pi$ scattering lengths parameterizing the $\pi\pi$ rescattering (which is the key to solve the "α-puzzle" as explained in Chap. 1, cf. also the comment on the cusp strength in Sect. 3.4.1) on the other hand. Nevertheless, the *normalization* of the $\eta \to 3\pi$ amplitudes needs to be fixed by other means in order to make predictions for physical observables (which is also true for the ongoing dispersive analyses [63, 67]), since it is proportional (up to small purely electromagnetic contributions) to unobservable quark masses in form of the strong isospin-breaking difference $\delta = m_d - m_u$. The missing information on the quark masses is then usually introduced to the framework by matching to ChPT at some order, and in the case at hand the (modified) NREFT framework is matched to ChPT at NLO. Thus, for combined analyses of both the charged and the neutral decay, it is particularly important to have the isospin-breaking corrections for the normalizations under control — especially when the $\Delta I = 1$ amplitude relation shall be used. We want to stress again that this work is not concerned with the NREFT calculation itself, but rather with the "non-trivial" higher-order isospin-breaking contributions to the ChPT amplitudes as well as with their matching to NREFT in order to achieve the combined NREFT+ChPT framework as presented in [3].

More specifically, this chapter deals with isospin-breaking corrections to the $\Delta I = 1$ relation (2.46) between the amplitudes for $\eta \to \pi^0\pi^+\pi^-$ and $\eta \to 3\pi^0$, which is usually employed in combined analyses of both $\eta \to 3\pi$ decay channels. As this relation is strictly valid at leading order in strong ($\mathcal{O}(\delta)$) or electromagnetic ($\mathcal{O}(e^2)$) isospin breaking, for investigating

---

**Most contents of this chapter have been published in [3].

corrections to it, one needs to calculate both amplitudes independently and including higher-order isospin-breaking effects. According to the discussion in Sect. 2.2.3, at chiral $\mathcal{O}(p^4)$ in addition to the mixed strong and electromagnetic effects at $\mathcal{O}(e^2\delta)$ (as considered Chap. 3) also second-order strong effects at $\mathcal{O}(\delta^2)$ must be taken into account, whereas the numerically tiny second-order electromagnetic terms at $\mathcal{O}(e^4)$ are neglected throughout. Therefore, a re-inspection of the derivation of both $\eta \to 3\pi$ NLO amplitudes (as published in [1]) concerning potential additional contributions at $\mathcal{O}(\delta^2)$ is necessary. While the details of this re-consideration are relegated to App. A, here we briefly summarize the main findings: fortunately, as already indicated in [1], the main sources for such terms are charged-to-neutral differences of kaon loop functions (whose higher-order contributions were not considered therein because they are not predominantly of electromagnetic origin, cf. (A.11)), so that for this purpose only few changes need to be applied to the amplitudes of [1].[#1] However, a thorough derivation of the amplitudes including second-order isospin breaking (except for terms at $\mathcal{O}(e^4)$) raises an additional issue with the meson decay constants that was not foreseen in [1]; for details we refer to App. A.2.

Besides the obvious question how strongly the $\Delta I = 1$ amplitude relation is violated at second order in isospin breaking, the basic idea for the following is to formulate these higher-order isospin corrections in a way they can easily be employed in a framework allowing for a reliable comparison with phenomenology. In general, the ideal level for matching between experimental analyses on the one side and theoretical descriptions on the other side is provided by the Dalitz plot distributions themselves or, to a somewhat lesser extent, by their expansions and parameters as introduced explicitly in Sect. 2.2.4 (cf. (2.53), but see also the discussion on the validity of a polynomial representation for $\eta \to 3\pi^0$ therein). Thus, after first explaining how the $\Delta I = 1$ amplitude relation (2.46) can be understood consistently at second-order in isospin breaking at all, in the following we derive the corresponding $\Delta I = 1$ relations including isospin-breaking corrections between the lowest Dalitz plot parameters of both decays, namely for the normalizations and the leading slopes. Subsequently, these corrections are worked out analytically based on the enhanced one-loop ChPT amplitude as explained above, and finally, they are evaluated numerically with regard to the application within the combined NREFT+ChPT framework as discussed above and in Chap. 1 (i.e. as published in [3]).

We anticipate here that, according to the scheme explained in the following sections, the higher-order isospin-breaking corrections to the $\Delta I = 1$ relation for the Dalitz plot normalizations are going to be of chiral $\mathcal{O}(p^4)$ (i.e. without contributions from the tree-level amplitudes) and therefore small. Accidentally, it turns out that for both the corrections to the $\Delta I = 1$ relations between the normalizations and between the lowest Dalitz plot slopes the contributions stemming from $\mathcal{O}(\delta^2)$ cancel completely; even more, due to the convenient form they are eventually given in, these corrections are of purely electromagnetic origin. This is then (besides the decreasing relative numerical importance of higher-order isospin-breaking effects in general) the reason why also from an analytical point of view we regard a re-evaluation of the numerical analysis of [1] with the enhanced amplitudes to be irrelevant, cf. [#7] in Sect. 3.4.

[#1]By not replacing the kaon masses inside the loop functions (i.e. not expanding the loop functions around the neutral kaon mass) in the derivation of the amplitudes of [1], the corresponding higher-order isospin-breaking effects are implicitly included, which substantially eases the derivation of the $\mathcal{O}(\delta^2)$ contributions (by explicitly expanding the isospin-breaking kaon loop differences as discussed in App. A.2).

4.1 $\Delta I = 1$ relations for Dalitz plot parameters

The goal of this section is to rewrite the second-order isospin-breaking corrections to the $\Delta I = 1$ relation (2.46) between the *amplitudes* for the neutral and the charged decay at chiral $\mathcal{O}(p^4)$ and up-to-and-including $\mathcal{O}(e^2, e^2\delta, \delta^2)$ in isospin breaking in terms of corrections for relations between neutral and charged Dalitz plot parameters, which are defined via expansions of the amplitude *squares* according to (2.53). In particular, we will derive a relation for the normalizations $\mathcal{N}_{c/n}$ as well as a relation concerning the neutral slope α. For this purpose, it is important to recall that the symmetry properties of the Dalitz plot distributions $|\mathcal{A}_{c/n}(x_{(n)}, y_{(n)})|^2$ in terms of Dalitz plot coordinates $x_{(n)}$ and $y_{(n)}$ as discussed in Sect. 2.2.4 are mere consequences of the general symmetries of the corresponding amplitudes $\mathcal{A}_{c/n}(s, t, u)$ in terms of Mandelstam variables as examined in Sect. 2.2.3 and thus must also be valid for the expansions of these amplitudes.

However, as argued at the end of Sect. 2.2.3, beyond first order in isospin breaking it is not a priori clear how to appropriately relate the Mandelstam variables for the two decay channels (due to contributions from $s_0^c - s_0^n \propto \Delta M_\pi^2 = \mathcal{O}(e^2)$, cf. the discussion preceding (2.49)), which in turn is necessary for the expansion around a *common* "center" of the Dalitz plot as a prerequisite for relating the Dalitz plot expansions of both channels: whereas the $\Delta I = 1$ relation (2.46) unambiguously yields the neutral amplitude in terms of the charged one but not the other way round, which suggest using the neutral relation (2.36) for the Mandelstam variables according to the asymptotic particles being η and $3\pi^0$ for the neutral decay, the question of consistency arises, as already in the derivation of the charged amplitude the Mandelstam variables have been replaced via the charged relation (2.34). It was also mentioned already in Sect. 2.2.3 that by using the neutral prescription the LO amplitudes accidentally obey the $\Delta I = 1$ relation even at second-order in isospin breaking, so that all corrections to it are necessarily of chiral $\mathcal{O}(p^4)$ and therefore small — provided this consistency problem can be solved. The crucial point now is the fact that the charged amplitude only depends on s and the difference $t - u$, which together with the following observations motivates an expansion of *both* amplitudes around the kinematical point $s = s_0^n$ and $t = u$ (i.e. preserving $s + t + u = 3s_0^{c/n}$):

- This *common* "center" of the Dalitz plot corresponds to $s = t = u = s_0^n$ or $x_n = y_n = \sqrt{z} = 0$ for the neutral channel, but to $s = s_0^n$ and $t = u = s_0^n + \Delta M_\pi^2$ or $x = 0$ and $y = \tau \neq 0$ in the charged case, cf. (2.51); moreover it corresponds to a physical point for *both* decays in contrast to e.g. $s = t = u = s_0^n$ for the charged decay.

- This expansion scheme respects the general symmetry properties (2.44) and (2.45). In particular for the charged amplitude, expanding in $t - u$ ensures that any shift in the identical expansion point for t and u away from the expansion point for s cancels at the level of Mandelstam variables (in terms of which the $\Delta I = 1$ amplitude relation is actually formulated) irrespective of whether (2.34) or (2.36) is used, thus solving the consistency problem. At the level of Dalitz plot coordinates $x_{(n)}$ and $y_{(n)}$, however, we then have to take care of effects stemming from $y \neq 0$ at the "center".

- Furthermore, this expansion scheme is also in line with our convention for the isospin limit of the pion mass to coincide with M_{π^0} (leading to an unambiguous ordering in isospin-breaking parameters) as motivated in Sect. 2.2.4 and employed in [1]; cf. the partially similar expansion scheme applied in Sect. 3.3.

- Written in terms of $s - s_0^n$, the implicit contributions of ΔM_π^2 cancel completely in the charged LO amplitude (2.40) (so that the corrections to the $\Delta I = 1$ relation between the normalizations $\mathcal{N}_{c/n}$ are of $\mathcal{O}(p^4)$ as anticipated), whereas in the charged Dalitz plot coordinates (2.51) (i.e. the expansion variables of the standard parameterization (2.53)) they cancel up to normalization-related effects due to $\tau \propto \tilde{R}_n - \tilde{R}_c$.

Thereby, the neutral relation (2.36) can be used consistently for *all* Mandelstam variables in the $\Delta I = 1$ amplitude relation (2.46), after the amplitudes have been expanded according to this scheme. However, we also need to expand in τ in order to disentangle the "trivial" kinematical isospin-breaking effects due to the definition of this specific "center" for both Dalitz plots from the "non-trivial" isospin-breaking effects entailed in the amplitudes. For this purpose, we define the abbreviations

$$\tilde{s} = (s - s_0^n), \qquad \tilde{t} = (t - s_0^n), \qquad \tilde{u} = (u - s_0^n), \tag{4.1}$$

so that by additionally expanding in τ the amplitudes thereby take the form

$$
\begin{aligned}
\mathcal{A}_c(s,t,u) &= \tilde{\mathcal{N}}_c\Big\{1 + \tilde{a}\tilde{s} + \tilde{b}\tilde{s}^2 + \tilde{d}(t-u)^2 + \tilde{f}\tilde{s}^3 + \tilde{g}\tilde{s}(t-u)^2 + \dots\Big\} \\
&= \mathcal{N}_c\Big\{1 + \bar{a}y + \bar{b}y^2 + \bar{d}x^2 + \bar{f}y^3 + \bar{g}yx^2 + \dots + \mathcal{O}(\tau^2)\Big\}, \\
\mathcal{A}_n(s,t,u) &= \mathcal{N}_n\Big\{1 + \tilde{\alpha}\big[\tilde{s}^2 + \tilde{t}^2 + \tilde{u}^2\big] + \tilde{\beta}\big[\tilde{s}^3 + \tilde{t}^3 + \tilde{u}^3\big] + \tilde{\gamma}\big[\tilde{s}^4 + \tilde{t}^4 + \tilde{u}^4\big] + \dots\Big\} \\
&= \mathcal{N}_n\Big\{1 + \bar{\alpha}z + \bar{\beta}\underbrace{z^{3/2}\sin(3\varphi)}_{-y_n^3 + 3y_n x_n^2} + \bar{\gamma}z^2 + \dots\Big\},
\end{aligned}
\tag{4.2}
$$

where the relations between the different sets of expansion parameters for both amplitudes up-to-and-including first order in τ are given by (for $M_\pi = M_{\pi^0}$ and thus $\tau = 0$, we reproduce the results derived in [21]; note that we do not need to explicitly expand the overall normalization factors according to $\tilde{R}_c = \tilde{R}_n/(1+\tau)$)

$$
\begin{aligned}
\mathcal{N}_c &= \tilde{\mathcal{N}}_c \times \bar{\mathcal{N}}_c, & \bar{\mathcal{N}}_c &= 1 + \tau\tilde{R}_c\tilde{a}, & \bar{a} &= -\tilde{R}_c\frac{\tilde{a} + 2\tau\tilde{R}_c\tilde{b}}{\bar{\mathcal{N}}_c}, \\
\bar{b} &= \tilde{R}_c^2\frac{\tilde{b} + 3\tau\tilde{R}_c\tilde{f}}{\bar{\mathcal{N}}_c}, & \bar{d} &= 3\tilde{R}_c^2\frac{\tilde{d} + \tau\tilde{R}_c\tilde{g}}{\bar{\mathcal{N}}_c}, & \bar{f} &= -\tilde{R}_c^3\frac{\tilde{f}}{\bar{\mathcal{N}}_c}, & \bar{g} &= -3\tilde{R}_c^3\frac{\tilde{g}}{\bar{\mathcal{N}}_c}, \\
\bar{\alpha} &= \frac{3}{2}\tilde{R}_n^2\tilde{\alpha}, & \bar{\beta} &= \frac{3}{4}\tilde{R}_n^3\tilde{\beta}, & \bar{\gamma} &= \frac{9}{8}\tilde{R}_n^4\tilde{\gamma}.
\end{aligned}
\tag{4.3}
$$

Here, the factor $\bar{\mathcal{N}}_c$ with the leading contribution originating from the linear slope $\tilde{a}$ reflects our definition of a common "center" for both Dalitz plots, and the corrections to $\bar{f}$ and $\bar{g}$ would entail higher-order parameters. The relations between these *amplitude* expansion parameters and the usual Dalitz plot parameters of the amplitude *squares* as defined in (2.53) are then easily shown to be

$$
\begin{aligned}
a &= 2\operatorname{Re}\bar{a}, & b &= |\bar{a}|^2 + 2\operatorname{Re}\bar{b}, & d &= 2\operatorname{Re}\bar{d}, \\
& & f &= 2\operatorname{Re}\big\{\bar{a}\bar{b}^* + \bar{f}\big\}, & g &= 2\operatorname{Re}\big\{\bar{a}\bar{d}^* + \bar{g}\big\}, \\
\alpha &= \operatorname{Re}\bar{\alpha}, & \beta &= \operatorname{Re}\bar{\beta}, & \gamma &= \operatorname{Re}\bar{\gamma}.
\end{aligned}
\tag{4.4}
$$

By virtue of the $\Delta I = 1$ amplitude relation (2.46) we thus can write

$$\mathcal{A}_n(s,t,u) = 3\tilde{\mathcal{N}}_c\left\{1 + \frac{1}{3}\left(\tilde{b} + 3\tilde{d}\right)\left[\tilde{s}^2 + \tilde{t}^2 + \tilde{u}^2\right] + \frac{1}{3}\left(\tilde{f} - 3\tilde{g}\right)\left[\tilde{s}^3 + \tilde{t}^3 + \tilde{u}^3\right] + \ldots\right\}$$
$$+ \mathcal{O}\left(e^4, e^2\delta, \delta^2\right) , \tag{4.5}$$

so that by comparison with (4.2) we can immediately read off the corresponding $\Delta I = 1$ relations at leading-order in isospin-breaking between the normalizations and the leading slope parameters of the *amplitudes*, namely[#2]

$$\mathcal{N}_n = 3\tilde{\mathcal{N}}_c , \qquad \tilde{\alpha} = \frac{1}{3}\left(\tilde{b} + 3\tilde{d}\right) , \qquad \tilde{\beta} = \frac{1}{3}\left(\tilde{f} - 3\tilde{g}\right) . \tag{4.6}$$

The generic (i.e. strong and electromagnetic) higher-order isospin-breaking corrections to these lowest $\Delta I = 1$ amplitude parameter relations, which we will call $\Delta I = 1$ Dalitz relations in the following, can then be written as[#3]

$$\Delta_{\tilde{\mathcal{N}}} = \mathcal{N}_n - 3\tilde{\mathcal{N}}_c \qquad \Rightarrow \qquad \mathcal{N}_n = 3\frac{\mathcal{N}_c}{\tilde{\mathcal{N}}_c}\left\{1 + \frac{\Delta_{\tilde{\mathcal{N}}}}{\mathcal{N}_n} + \mathcal{O}\left(\left(\frac{\Delta_{\tilde{\mathcal{N}}}}{\mathcal{N}_n}\right)^2\right)\right\} ,$$

$$\Delta_{\tilde{\alpha}} = \tilde{\alpha} - \frac{1}{3}\left(\tilde{b} + 3\tilde{d}\right) \quad \Rightarrow \quad \Delta_\alpha = \mathrm{Re}\,\Delta_{\bar{\alpha}} = \frac{3}{2}\tilde{R}_n^2\,\mathrm{Re}\,\Delta_{\tilde{\alpha}} , \tag{4.7}$$

where we refrain from explicitly introducing the analogous corrections $\Delta_{\tilde{\beta}}$ and Δ_β, since β is even not yet measured at all.

Using (4.3) and (4.4), from (4.6) one can also derive relations between the usual (real) Dalitz plot parameters, which in general, however, additionally entail contributions from the imaginary parts of the complex amplitude expansion parameters that are not observable directly. Nevertheless, neglecting all higher-order isospin-breaking corrections except for the normalization, the corresponding relation for the neutral slope α can be written as an inequality containing only the usual Dalitz plot parameters according to (reducing to the result of [21], if moreover $\tilde{Q}_n = \tilde{Q}_c$ is used)

$$\alpha = \frac{\tilde{Q}_n^2}{4\tilde{Q}_c^2}\left\{b - |\bar{a}|^2 + d\right\} = \frac{\tilde{Q}_n^2}{4\tilde{Q}_c^2}\left\{b - \frac{a^2}{4} + d\right\} - \left(\frac{\tilde{Q}_n}{2\tilde{Q}_c}\mathrm{Im}\,\bar{a}\right)^2 \leq \frac{\tilde{Q}_n^2}{4\tilde{Q}_c^2}\left\{b - \frac{a^2}{4} + d\right\} . \tag{4.8}$$

Here, the equality only holds for $\mathrm{Im}\,\bar{a} = 0$, which is the case at leading chiral $\mathcal{O}(p^2)$ (where $\bar{a}$ is the only non-vanishing $\eta \to 3\pi$ amplitude expansion parameter in (4.2), see also [#2]) and thus resembles the current algebra prediction $b = a^2/4$, which also follows directly from (4.4). In order to derive the corrections at $\mathcal{O}(\tau)$, we denote the parameters at $\mathcal{O}(\tau^0)$ (i.e. for instance those in (4.8)) by the subscript "iso" and use the replacements at LO in isospin breaking that

---

[#2]Of course, there is no relation at linear order in Mandelstam variables due to the symmetry (2.45) of the neutral amplitude, cf. the discussion after (2.53). While the relation between the normalizations follows at LO already, the leading slope for the charged channel at LO reads $\tilde{a} = 3/(M_\eta^2 - M_{\pi^0}^2) = 1/(s_0^n - s_A)$, cf. (2.43).

[#3]Using the spherical convention instead leads to an additional sign in the $\Delta I = 1$ amplitude relation (2.46). However, this sign only affects the relation between the normalizations in (4.6), whereas the relations between the higher parameters (in particular the one for the neutral slope) remain unchanged. Furthermore, this change of horses does *not* alter the sign of the correction $\Delta_{\tilde{\mathcal{N}}}$ in (4.7), if the changeover is made by explicitly adapting the sign in front of the *charged* normalization, as done in [3].

result from (4.3) and (4.4) (keeping $|\bar{a}|^2 = a^2/4 + (\operatorname{Im}\bar{a})^2$ just as abbreviation),

$$\bar{a}_{\mathrm{iso}} = \bar{a} + \tau\big(2\bar{b} - \bar{a}^2\big) \quad \Rightarrow \quad a_{\mathrm{iso}} = a + \tau\big(2b - a^2\big) , \quad \operatorname{Im} a_{\mathrm{iso}} = \operatorname{Im} a + \tau\big[2\operatorname{Im}\bar{b} - a\operatorname{Im}\bar{a}\big] ,$$

$$\bar{b}_{\mathrm{iso}} = \bar{b} + \tau\big(3\bar{f} - \bar{a}\bar{b}\big) \quad \Rightarrow \quad b_{\mathrm{iso}} = b + \tau\big(3f - ab\big) ,$$

$$\operatorname{Im} b_{\mathrm{iso}} = \operatorname{Im} b + \frac{\tau}{2}\Big[6\operatorname{Im}\bar{f} - a\operatorname{Im}\bar{b} - \big(b - |\bar{a}|^2\big)\operatorname{Im}\bar{a}\Big] ,$$

$$\bar{d}_{\mathrm{iso}} = \bar{d} + \tau\big(\bar{g} - \bar{a}\bar{d}\big) \quad \Rightarrow \quad d_{\mathrm{iso}} = d + \tau\big(g - ad\big) ,$$

$$\operatorname{Im} d_{\mathrm{iso}} = \operatorname{Im} d + \frac{\tau}{2}\big[2\operatorname{Im}\bar{g} - a\operatorname{Im}\bar{d} - d\operatorname{Im}\bar{a}\big] . \tag{4.9}$$

Thereby, the relation (4.8) — upon neglecting $\mathcal{O}\big(\tau^2\big)$ as well as Δ_α — takes the form

$$
\begin{aligned}
\alpha &= \frac{1}{4}\bigg\{ b - |\bar{a}|^2 + d + \tau\Big[2(1-a)\big(b - |\bar{a}|^2 + d\big) + ad - 4\operatorname{Im}\bar{a}\operatorname{Im}\bar{b} + 3f + g\Big]\bigg\} \\
&= \frac{\tilde{Q}_n^2}{4\tilde{Q}_c^2}\bigg\{ b - |\bar{a}|^2 + d - \tau\Big[2a\Big(b - |\bar{a}|^2 + \frac{d}{2}\Big) + 4\operatorname{Im}\bar{a}\operatorname{Im}\bar{b} - 3f - g\Big]\bigg\} \\
&= \frac{\tilde{Q}_n^2}{4\tilde{Q}_c^2}\bigg\{ b - \frac{a^2}{4} + d - \tau\Big[2a\Big(b - \frac{a^2}{4} + \frac{d}{2}\Big) - 3f - g\Big]\bigg\} - \bigg(\frac{\tilde{Q}_n}{2\tilde{Q}_c}\Big\{\operatorname{Im}\bar{a} + \tau\Big[2\operatorname{Im}\bar{b} - a\operatorname{Im}\bar{a}\Big]\Big\}\bigg)^2 \\
&\le \frac{\tilde{Q}_n^2}{4\tilde{Q}_c^2}\bigg\{ b - \frac{a^2}{4} + d - \tau\Big[2a\Big(b - \frac{a^2}{4} + \frac{d}{2}\Big) - 3f - g\Big]\bigg\} , \tag{4.10}
\end{aligned}
$$

where in the first line we have also expanded the overall normalization $\tilde{Q}_n/\tilde{Q}_c = 1 + \tau$ for illustration. It is important to note that the inequalities (4.8) and (4.10) are strictly valid at the respective orders in isospin breaking. Therefore, Dalitz plot parameter values from theoretical determinations without higher-order isospin-breaking contributions must obey the inequality (4.8), i.e. in particular the results of ChPT at *any* chiral order regardless of the "α-puzzle" already discussed in Chap. 1. Accordingly, one may easily check that in fact *all* sets of NLO parameter values given in Tabs. 3.1 and 3.2 indeed fulfill *both* inequalities — irrespective of the different small electromagnetic corrections, independent of the normalization factor $\tilde{Q}_n^2/\tilde{Q}_c^2$ amplifying the RHS of (4.8) by about 14%, and also even for using the largest value of α in Tab. 3.2 (which better represents the definition via an expansion at the "center" of the Dalitz plot rather than fitting the Dalitz plot parameterization to the whole phase space, cf. Sect. 3.4.3).[#4] Throughout, similar to the normalization prefactor, the additional terms at $\mathcal{O}(\tau)$ in (4.10) turn out to loosen the constraint by increasing the RHS with respect to (4.8). Including second-order isospin-breaking corrections consistently by moreover accounting for Δ_α in (4.10), also experimentally determined Dalitz plot parameter values are expected to (approximately) fulfill the corresponding *equation*. As thoroughly discussed in [3], the imaginary parts of the amplitude expansion parameters (in particular $\operatorname{Im}\bar{a}$), which are generated by $\pi\pi$ FSIs on the one hand but also depend on the usual Dalitz plot parameters on the other hand, can be replaced in (4.10) (and (4.8)) using information on $\pi\pi$ scattering as input for the NREFT framework in order to obtain relations between experimentally observable Dalitz

---

[#4]Note that an unfortunate misprint in the (first) preprint version of the two-loop ChPT analysis [21] (neglecting isospin-breaking corrections beyond $\mathcal{O}(\delta)$ and using the average pion mass $\overline{M_\pi^2}$) has been corrected in the published version: the inequality symbol in the relation corresponding to (4.8) was erroneously twisted. The statement made in [21] that all sets of Dalitz plot parameters given therein be in agreement with the (corrected) relation, however, is *not* true (any more): whereas the LO results are fine, neither the results at NLO nor those at NNLO obey the correct inequality.

plot parameters only. As the numerical investigations of [3] shall not be reproduced here, we only want to mention that the analysis in [3] shows a significant tension between the most recent KLOE neutral [30] and charged [25] Dalitz plot parameters, which has been verified subsequently by [66] and is still unresolved.

Finally, in analogy to (4.8) we give the relation for β at LO in isospin breaking except for the overall normalization (for $\tilde{Q}_n = \tilde{Q}_c$ recovering the result of cf. [66]),

$$
\begin{aligned}
\beta &= \left(\frac{\tilde{Q}_n}{2\tilde{Q}_c}\right)^3 \left\{ g - f + \frac{a}{2}\left(b - |\bar{a}|^2 - d\right) + 2\,\mathrm{Im}\,\bar{a}\left(\mathrm{Im}\,\bar{b} - \mathrm{Im}\,\bar{d}\right) \right\} \\
&= \alpha \frac{\tilde{Q}_n}{2\tilde{Q}_c}\frac{a}{2} + \left(\frac{\tilde{Q}_n}{2\tilde{Q}_c}\right)^3 \left\{ g - f - ad + 2\,\mathrm{Im}\,\bar{a}\left(\mathrm{Im}\,\bar{b} - \mathrm{Im}\,\bar{d}\right) \right\},
\end{aligned}
\tag{4.11}
$$

where the term depending on imaginary parts, however, cannot readily be estimated in order to derive a physically observable inequality in analogy to (4.8), although in principle also $\mathrm{Im}\,\bar{d}$ can be replaced along the lines of [3] as mentioned above. Furthermore, the analog of (4.10) may easily be deduced using the replacements of (4.9).

4.2 Isospin-breaking corrections to the $\Delta I = 1$ Dalitz relations

In this section, we explicitly derive the higher-order isospin-breaking corrections $\Delta_{\tilde{\mathcal{N}}}$ and $\Delta_{\tilde{\alpha}}$ to the lowest $\Delta I = 1$ Dalitz relations defined in (4.7) by expanding both NLO $\eta \to 3\pi$ decay amplitudes of [1] — amended by the second-order strong isospin-breaking effects as explained in App. A.2 — around $s = s_0^n$ and $t = u$ according to (4.2) as motivated and explained in the previous section. As before, numerically tiny terms of $\mathcal{O}(e^4)$ are neglected throughout.

With the application of these results in combination with the NREFT framework in mind, we first briefly comment on the matching procedure between (modified) NREFT and ChPT in [3] (more details can be found e.g. in [62]). The employed NREFT framework is based on expanding in both a formal non-relativistic parameter (in effect expanding in pion 3-momenta and kinetic energies in the η rest frame) and the phenomenologically small effective range parameters for $\pi\pi$ (re-)scattering perturbatively with respect to a consistent power counting scheme, thus yielding a Lagrangian framework. Accordingly, the $\pi\pi$ FSIs, which already in the low-energy region above threshold lead to imaginary contributions to the amplitudes by virtue of unitarity cuts, are explicitly accounted for, while all other (meson) loop effects — namely kaon loops, loops involving η, tadpoles, and self-energy contributions — are parameterized by effective couplings; in fact, the term "non-relativistic" only refers to this subsumption of effects due to inelastic thresholds outside the physical decay region into point-like effective coupling constants, whereas inside the physical region the expressions are fully covariant and exhibit the correct non-analytic low-energy behavior. Comparing the NREFT tree-level amplitudes (i.e. the polynomial parts of the NREFT representations) with the amplitude expansions (4.2), one can derive matching relations for the tree-level couplings in terms of the amplitude expansion parameters. This then allows for matching to ChPT at the "center" of the Dalitz plot via the respective expansions of the ChPT amplitudes at NLO, which in turn contain all the loop effects merely parameterized by the NREFT. For this purpose, however, the following additional steps have to be taken into account on the ChPT side:

- The (non-analytic) imaginary parts due to pion loops in the ChPT and the NREFT amplitudes are identical and by choosing an appropriate matching procedure as explained

in [3] (effectively fixing the NREFT $\pi\pi$ rescattering parameters at their current algebra values) they drop out in the matching relations and can thus be omitted here.

- For the radiative corrections due to real and virtual photons, we have to match the (amended) ChPT result of [1] to the corresponding non-relativistic representation, which is analogous to [61] (for $K \to 3\pi$). As a result, both the Coulomb pole and phase have to be subtracted from the chiral representation at the amplitude level (cf. the subtraction of universal (soft-photon) corrections as discussed in Sect. 3.2) and no bremsstrahlung contributions are to be included at the level of amplitude squares; the finite photon mass m_γ, which was introduced in [1] as regulator for the IR divergences, has to be replaced according to $m_\gamma \to M_\pi/\sqrt{e}$ so that $\log(m_\gamma^2/M_\pi^2) \to -1$.

Here, some remarks concerning the cancellation of IR divergences are in order: as discussed in Sect. 3.1, in ChPT calculations of e.g. cross sections, the IR divergences, which arise at the amplitude level from virtual-photon corrections and can be tamed by using either a finite photon mass as IR regulator or dimensional regularization also in the IR, cancel with corresponding divergences from real-photon radiation (bremsstrahlung) at the level of amplitude squares. Assuming the subtraction of universal corrections (cf. Sect. 3.2) to be applied already on the experimental side as done in [3], however, the explicit inclusion of bremsstrahlung is not necessary when matching ChPT to the (modified) non-relativistic framework, since the virtual-photon diagrams in both theories exhibit the same IR behavior and thus contain the same IR divergences, see [61] (the physical reason for this cancellation being of course the identical IR behavior of both theories). While the present work (as well as the ChPT calculations of virtual-photon contributions in $\pi\pi$ scattering [118, 129] that also go into the analysis of [3]) uses a finite photon mass m_γ, according to [61] NREFT calculations are simplified considerably if the threshold expansion is applied on the basis of dimensional regularization (at the expense, however, of complicating the identification of IR singularities). By comparing the explicit result for the triangle loop function $G(s)$ as given in (A.9) with the one stated in [61] one can infer that the transition between both regularization schemes can be made by replacing[#5]

$$\log \frac{m_\gamma^2}{M_\pi^2} \to -32\pi^2 \lambda_{\mathrm{IR}} - 1 + \log \frac{\mu_{\mathrm{IR}}^2}{M_\pi^2} \; . \tag{4.12}$$

Since both theories are IR-complete, both the infrared divergences λ_{IR} and the dependence on the corresponding scale μ_{IR} must ultimately cancel already at the amplitude level and can hence be omitted in this matching prescription on the ChPT side, rendering the relations we are aiming for (as well as the matching relations to $\pi\pi$ scattering given in [3]) IR-finite and independent of the IR scale. Thus, for the NREFT-related calculation of $\Delta_{\tilde{\mathcal{N}}}$ and $\Delta_{\tilde{\alpha}}$, we can simply apply $\log(m_\gamma^2/M_\pi^2) \to -1$ as already stated above in $G(s)$ of (A.9) as well as in the charged NLO tree-like amplitude (A.17) (which contains the IR-divergent charged-pion wave-function renormalization, cf. App. A.2).

As the following expansion of the amplitudes in particular involves rather lengthy expansions (up to third order) of the various loop functions, it is useful to apply the discussed modifications before expanding: according to the generic formulae for the loop functions given in App. A.1, the respective forms for the case at hand of the two-pion loop function (e.g. for

---

[#5]Note that the definitions of $G(s)$ differ by an overall sign. Furthermore, in [3] the IR scale μ_{IR} was not mentioned explicitly in this matching prescription; however, alike the IR singularity λ_{IR} it cancels anyway.

$\pi^+\pi^-$) and the triangle loop function are given by (with $\sigma_\pi \in (0,1)$ in the physical decay region and Spence's function Li as defined in (A.10))

$$\tilde{J}_{\pi\pi}(s) = \operatorname{Re} \bar{J}_{\pi\pi}(s) = \frac{1}{16\pi^2}\left\{2 - \sigma_\pi \log\frac{1+\sigma_\pi}{1-\sigma_\pi}\right\},$$

$$\tilde{G}(s) = M_\pi^2 \operatorname{Re} G(s)\Big|_{\text{dim. reg.}}^{\text{no pole}} = \frac{1-\sigma_\pi^2}{64\pi^2\,\sigma_\pi}\left\{\operatorname{Li}\frac{1-\sigma_\pi}{1+\sigma_\pi} - \operatorname{Li}\frac{1+\sigma_\pi}{1-\sigma_\pi} + \log\frac{1+\sigma_\pi}{1-\sigma_\pi}\right\}, \quad (4.13)$$

where for later convenience the representation of the triangle loop function is rescaled by a factor of M_π^2 (or, upon neglecting relative corrections of $\mathcal{O}(e^2)$, by $M_{\pi^0}^2$). The other occurring two-meson loop functions just follow from reducing the general forms stated in App. A.1 to the kinematical regime $s \approx s_0^n$ (and thus $t = u = (3s_0^{c/n} - s)/2 \approx s_0^n$) with

$$4M_{\pi^0}^2 < 4M_\pi^2 < s_0^n = \frac{M_\eta^2}{3} + M_{\pi^0}^2 < (M_\eta - M_{\pi^0})^2 < 4M_K^2 < 4M_{K^0}^2, \quad (4.14)$$

which corresponds to the expansion at the common "center" of the Dalitz plot as discussed in the previous section, and are thus all real. Hence, when matching to NREFT, the corrections $\Delta_{\tilde{\mathcal{N}}}$ and $\Delta_{\tilde{\alpha}}$ are going to be real, whereas without this matching prescription they would be complex. More specifically, the calculational scheme consists of two simultaneous expansions up-to-and-including second order for both amplitudes:

- the expansion in Mandelstam variables around the common "center" of the Dalitz plot at $s = s_0^n$ and $t = u$ in order to determine the normalizations and amplitude expansion parameters according to (4.2),[#6]

- and the expansion in isospin-breaking parameters according to the unambiguous ordering scheme discussed in Sect. 2.2.4 (again, neglecting terms of $\mathcal{O}(e^4)$), where in particular the t- and u-channel loop functions in the charged amplitude require an additional expansion in the argument $t = u = s_0^n + \Delta M_\pi^2$.

Together, these expansions then lead to derivatives up to third order of loop functions, which, however, can be rewritten in terms of the original loop functions themselves. Since the calculation of the necessary derivatives is tedious but straightforward, here, we only give one simple example based on (4.13),

$$\frac{\mathrm{d}}{\mathrm{d}s}\tilde{G}(s) = -\frac{1}{M_\pi^2}\left(\frac{1-\sigma_\pi^2}{4\sigma_\pi^2}\right)^2\left\{2\sigma_\pi^2\frac{1+\sigma_\pi^2}{1-\sigma_\pi^2}\tilde{G}(s) + \tilde{J}_{\pi\pi}(s) - \frac{2+\sigma_\pi^2}{16\pi^2}\right\}. \quad (4.15)$$

When taking neutral-to-charged differences in order to derive the corrections $\Delta_{\tilde{\mathcal{N}}}$ and $\Delta_{\tilde{\alpha}}$ via (4.7), corresponding differences of loop functions occur (in addition to the kaon loop

---

[#6]On a rather technical note, we keep $t = u$ (corresponding to the common part of the symmetries of both amplitudes) fixed during the expansions by replacing both t and u in both amplitudes by s, s_0^n, and ΔM_π^2 via (2.34) or (2.36), respectively, so that we are effectively left with one kinematical expansion only (i.e. in $\tilde{s}$ around 0).

function differences (A.11) without isospin-breaking prefactors mentioned before), e.g.[#7]

$$
J_{\eta\pi}(s) - J_{\eta\pi^0}(s) = -\frac{\Delta M_\pi^2}{M_\eta^2}\tilde{\lambda}_{\eta\pi^0}^{-1}\left\{\left(\frac{s}{M_\eta^2} + 1 - \rho\right)\left[\bar{J}_{\eta\pi^0}(s) - \frac{1}{16\pi^2}\right] - \frac{\frac{s}{M_\eta^2} - 1 + \rho}{1 - \rho}\frac{\log\rho}{16\pi^2}\right\}
$$

$$
+ \mathcal{O}\left(\left(\Delta M_\pi^2\right)^2, p^2\right) ,
$$

$$
\bar{J}_{\eta\pi^0}(s) = \frac{1}{32\pi^2}\left\{2 + \left(\frac{1 - \rho}{\frac{s}{M_\eta^2}} - \frac{1 + \rho}{1 - \rho}\right)\log\rho - \frac{\tilde{\lambda}_{\eta\pi^0}^{1/2}}{\frac{s}{M_\eta^2}}\log\frac{\frac{s}{M_\eta^2} - 1 - \rho + \tilde{\lambda}_{\eta\pi^0}^{1/2}}{\frac{s}{M_\eta^2} - 1 - \rho - \tilde{\lambda}_{\eta\pi^0}^{1/2}}\right\}
$$

$$
\tilde{\lambda}_{\eta\pi^0}\left(\frac{s}{M_\eta^2}\right) = \frac{\lambda_{\eta\pi^0}(s)}{M_\eta^4} = \left[\frac{s}{M_\eta^2} - \left(1 - \sqrt{\rho}\right)^2\right]\left[\frac{s}{M_\eta^2} - \left(1 + \sqrt{\rho}\right)^2\right] , \qquad \rho = \frac{M_{\pi^0}^2}{M_\eta^2} ,
$$

$$
\tag{4.16}
$$

where for convenience we have defined the dimensionless and numerically small ratio $\rho \approx 1/16$. Now, we also expand all charged-to-neutral mass differences inside the loop functions and omit any higher-order isospin-breaking corrections,[#8] since besides yielding more compact formulae in general this is particularly useful in the case of $\Delta_{\tilde{\mathcal{N}}}$: once all isospin-breaking effects are unambiguously disentangled and made explicit by these expansions, the corrections to relations stemming from the $\Delta I = 1$ amplitude relation, which is valid at LO in isospin breaking, are necessarily of NLO in isospin breaking, i.e. of $\mathcal{O}\left(e^2\delta, \delta^2\right)$; due to the accidental validity of the $\Delta I = 1$ amplitude relation at leading chiral $\mathcal{O}\left(p^2\right)$ also for these terms, the correction $\Delta_{\tilde{\mathcal{N}}}$ is of $\mathcal{O}\left(p^4\right)$. As by neglecting terms of $\mathcal{O}\left(e^4\right)$ throughout the calculation moreover $\Delta_{\tilde{\mathcal{N}}} \propto \delta$, we can thus conveniently factor out the (real) neutral *leading-order* normalization $\mathcal{N}_n^{\text{LO}} = \mathcal{A}_n^{\text{LO}} \propto \delta$, cf. (2.42), and quote the result as the ratio $\Delta_{\tilde{\mathcal{N}}}/\mathcal{N}_n$ below. In a similar fashion, the neglect of purely electromagnetic second-order terms proportional to e^4 allows for easily dividing by the (real) LO normalizations in the derivation of the amplitude expansion parameters $\tilde{\alpha}$, $\tilde{b}$, and $\tilde{d}$ that are needed for $\Delta_{\tilde{\alpha}}$, which is of $\mathcal{O}\left(p^{-2}\right)$. Explicitly, we thereby find[#9]

$$
\frac{\Delta_{\tilde{\mathcal{N}}}}{\mathcal{N}_n} = e^2\left\{\frac{2(1 - 3\rho)}{3\rho}\tilde{G}(s_0^n) + \tilde{J}_{\pi^0\pi^0}(s_0^n) + \frac{3}{16\pi^2}\left(\log\frac{M_{\pi^0}^2}{\mu^2} - 1\right)\right.
$$

$$
\left. - \frac{4}{3(1 - \rho)}\left[3(1 + \rho)(K_3^r - K_4^r/2) - 4K_6^r + 6(3 - \rho)(K_{10}^r + K_{11}^r)\right]\right\}
$$

$$
+ \frac{\Delta M_\pi^2}{3(1 - \rho)F_\pi^2}\left\{\frac{29 - 111\rho - 9\rho^2 + 27\rho^3}{8(1 + 3\rho)}\bar{J}_{K^0K^0}(s_0^n) + \frac{3\rho(1 + 22\rho + 9\rho^2)}{(1 - 9\rho)(1 + 3\rho)}\bar{J}_{\eta\pi^0}(s_0^n)\right.
$$

$$
- \frac{7 + 21\rho - 495\rho^2 + 243\rho^3}{(1 - 9\rho)(1 + 3\rho)}\tilde{J}_{\pi^0\pi^0}(s_0^n) - 32L_3 + \frac{8(3 - \rho)}{1 - \rho}\frac{F_\pi^2}{M_\eta^2}\Delta_F
$$

$$
+ \frac{1}{16\pi^2}\left[6(3 - 2\rho)\log\frac{M_{\pi^0}^2}{\mu^2} + \frac{2(1 + 2\rho - \rho^2)}{1 - \rho}\log\frac{3 + \rho}{4\rho} - \frac{3(3 - 26\rho - \rho^2)}{(1 - 9\rho)(1 - \rho)}\log\rho\right.
$$

$$
\left.\left.+ \frac{53 - 357\rho + 351\rho^2 + 81\rho^3}{4(1 - 9\rho)}\right]\right\} + \mathcal{O}\left(e^2p^2\right) ,
$$

$$
\tag{4.17}
$$

[#7]Unfortunately, the formula for $\bar{J}_{\eta\pi}(s)$ given in [3] contains a typographical error, cf. $\bar{J}_{\eta\pi^0}(s)$ in (4.16).

[#8]In particular, we do not need to use the unphysical loop function $\Delta_{3\eta\pi^0}$ introduced in App. A.2 any longer.

[#9]In [3], the ratio ρ as well as the results for $\Delta_{\tilde{\mathcal{N}}}/\mathcal{N}_n$ and $\Delta_{\tilde{\alpha}}$ are given in terms of the charged pion mass, the difference being of $\mathcal{O}\left(e^4\right)$ anyway. Furthermore, therein and here we only state the dominant errors, whereas the whole omitted terms are given by $\mathcal{O}\left(e^2\delta, \delta^2, p^4\right)$ and $\mathcal{O}\left(e^2\delta, \delta^2, p^0\right)$, respectively.

which of course comprises the terms proportional to the (finite) strong LEC L_3 or any of the electromagnetic LECs already stated in (2.49), as well as

$$
\begin{aligned}
\Delta_{\tilde{\alpha}} =\; & \frac{e^2}{(1-9\rho)^2(1-\rho)(1+3\rho)^2} \frac{3}{M_\eta^4} \Bigg\{ \frac{7 - 102\rho - 504\rho^2 + 1926\rho^3 - 3375\rho^4}{32\pi^2(1-9\rho)} \\
& + 12\rho(1+63\rho^2)\tilde{G}(s_0^n) - \frac{1 - 14\rho - 138\rho^2 + 234\rho^3 - 1107\rho^4}{1-9\rho} \tilde{\bar{J}}_{\pi^0\pi^0}(s_0^n) \Bigg\} \\
& + \frac{\Delta M_\pi^2}{(1-\rho)(1+3\rho)^2 F_\pi^2} \frac{3}{M_\eta^4} \Bigg\{ \frac{3(3+\rho)(957 - 5240\rho - 1398\rho^2 - 288\rho^3 + 81\rho^4)}{4096(1+3\rho)} \bar{J}_{K^0 K^0}(s_0^n) \\
& + \frac{\rho^2(221 - 3612\rho + 32022\rho^2 - 32076\rho^3 - 2187\rho^4)}{8(1-9\rho)^3(1+3\rho)} \bar{J}_{\eta\pi^0}(s_0^n) \\
& - \frac{3\rho(3 - 124\rho + 1794\rho^2 - 7596\rho^3 + 9315\rho^4)}{(1-9\rho)^3(1+3\rho)} \tilde{\bar{J}}_{\pi^0\pi^0}(s_0^n) \\
& - \frac{1}{128\pi^2(1-9\rho)^3} \Bigg[\frac{\rho^2(37 + 237\rho - 2025\rho^2 + 3159\rho^3)}{1-\rho} \log\rho \\
& - \frac{1}{256}\Big(243 - 39737\rho + 540471\rho^2 - 729333\rho^3 + 3630825\rho^4 - 1810107\rho^5 \\
& + 85293\rho^6 + 59049\rho^7 \Big) \Bigg] \Bigg\} + \mathcal{O}\big(e^2 p^{-2}\big) \,,
\end{aligned}
\tag{4.18}
$$

which in turn is free of LECs at this chiral order, being a pure loop effect and thus a prediction in terms of well-known parameters only. First of all, both results (4.17) and (4.18) are divergence-free and independent of the scale μ. While the scale-independence of $\Delta_{\tilde{\alpha}}$ is explicitly seen, that of $\Delta_{\tilde{\mathcal{N}}}/\mathcal{N}_n$ can be checked by using the scale-dependence of the electromagnetic LECs K_i^r as given in App. A.3. Furthermore, as already anticipated before, these corrections turn out to be completely of electromagnetic origin (up to corrections from $\mathcal{O}(\delta^3)$ at the amplitude level), i.e. they are not affected by taking into account the additional terms of $\mathcal{O}(\delta^2)$ in the amplitudes as explained in App. A.2. Note that in both cases we have made extensive use of the Gell-Mann–Okubo relation (2.16) to simplify the results (4.17) and (4.18), thereby neglecting higher-order terms in the isospin-breaking parameters e^2 and δ.

For the numerical evaluation we employ the same numerical input as in Chap. 3, which is collected in App. A.3. The uncertainties in the electromagnetic LECs completely dominate the error on $\Delta_{\tilde{\mathcal{N}}}/\mathcal{N}_n$, in particular in comparison with the alterations induced by using the charged pion mass instead and/or rewriting the mass of the η in terms of pion and kaon masses via the GMO relation. For $\Delta_{\tilde{\alpha}}$, being independent of any LECs at NLO, we quote an uncertainty solely due to these different schemes for the evaluation of the meson masses; however, we consider the error thus obtained rather underestimated. In total, we find

$$
\frac{\Delta_{\tilde{\mathcal{N}}}}{\mathcal{N}_n} = (-0.7 \pm 1.5)\% \,, \qquad \Delta_{\tilde{\alpha}} = (0.035 \pm 0.003)\,\text{GeV}^{-4} \quad \Rightarrow \quad \Delta_\alpha = (1.4 \pm 0.1) \times 10^{-4} \,.
\tag{4.19}
$$

We want to stress again that these are the numerical results in the form pertinent for (and used in) the NREFT+ChPT analysis [3], i.e. including the modifications described above, which in particular affect the loop functions and their expansions, leading to $\Delta_{\tilde{\alpha}}$ being real so that $\Delta_\alpha = \Delta_{\bar{\alpha}} = (3/2)\tilde{R}_n^2 \Delta_{\tilde{\alpha}}$. Therefore, these numbers cannot easily be compared to the numerical ChPT results presented in Sect. 3.4 (irrespective of the additional analytical

difference of $\mathcal{O}(\delta^2)$ at the amplitude level). In view of the small central values for both corrections, however, we refrain from repeating the calculation without the NREFT-motivated changes, which would in particular involve more cumbersome expansions of the two-pion and the triangle loop functions leading to complex numerical results.

Let us first discuss the correction Δ_α. When matching to ChPT at NLO without taking second-order isospin-breaking fully into account, the result for α in terms of the charged slopes according to (4.10) is too small even if the "trivial" kinematical effects of isospin breaking and all isospin-breaking contributions of higher charged slopes are included (cf. the discussion in the previous section); the amount Δ_α of this discrepancy, however, is numerically tiny in comparison with the differences between the ChPT results up to two-loop order and experiment (i.e. the "α-puzzle"): compared to the experimental world average of $\alpha = -0.0315 \pm 0.0015$ (i.e. $\pm 5\%$) [34], it corresponds to an effect of less than half a percent and thus is very small even for an isospin-breaking correction.[#10] By thoroughly accounting for the $\pi\pi$ FSIs in the two-loop (modified) NREFT formalism, the NREFT+ChPT analysis [3] including this tiny correction yields $\alpha = -0.025 \pm 0.005$ (also corresponding to an relative uncertainty of $\pm 5\%$, whereas the included correction Δ_α amounts to a relative effect of about 0.6%), which is in (marginal) agreement with the experimental value and thus finally solves the "α-puzzle".

The situation is quite different, however, as far as the correction $\Delta_{\tilde{\mathcal{N}}}/\mathcal{N}_n$ between the normalizations is concerned. As already discussed in Chap. 1, in contrast to the individual partial decay widths $\Gamma_{n/c}$, the neutral-to-charged ratio r of these partial widths turns out to be relatively stable with respect to the chiral order, one reason being the fact that the quark-mass-dependent normalization as a major source of uncertainties in the determination of the decay widths drops out up to the correction $\Delta_{\tilde{\mathcal{N}}}/\mathcal{N}_n$ (in the "isospin limit" $M_\pi = M_{\pi^0}$ of $\eta \to 3\pi$ decays). Since the widths are proportional to the squared absolute values of the normalizations, according to (4.7) the normalization correction $\Delta_{\tilde{\mathcal{N}}}/\mathcal{N}_n$ gives rise (in this limit) to a correction factor of approximately $[1 + 2\Delta_{\tilde{\mathcal{N}}}/\mathcal{N}_n]$ for the ratio r so that the central value of $\Delta_{\tilde{\mathcal{N}}}/\mathcal{N}_n$ leads to a decrease of r by about 1.4%. This correction is also included in the final result $r = 1.40 \pm 0.01(\pi\pi) \pm 0.04(\Delta_{\tilde{\mathcal{N}}})$ of [3], which is in agreement with the experimental findings (see below) and moreover shows that for r the total uncertainty in the NREFT+ChPT framework is dominated by the uncertainty in $\Delta_{\tilde{\mathcal{N}}}/\mathcal{N}_n$ as the error induced by the parameterization of $\pi\pi$ rescattering (for the two-loop NREFT representation) is very small. In this context, however, it is remarkable that with $r = 1.432 \pm 0.026$ (fit) and $r = 1.48 \pm 0.05$ (average) two rather different "experimental" values are given by [34]. In fact, the impact of the *uncertainty* in $\Delta_{\tilde{\mathcal{N}}}/\mathcal{N}_n$ on the ratio r is one of the key results here: while e.g. in [66] a value of $r = 1.475 \pm 0.015$ (i.e. $\pm 1\%$, resembling $r^{\mathrm{NNLO}} = 1.47$ of [21] due to matching to two-loop ChPT) is reported and the authors claim that this result be stable against isospin-breaking corrections, the present analysis on the contrary shows that — based on the present knowledge of low-energy strong and electromagnetic interactions — *any* calculation of r *inevitably* entails an uncertainty in r of about 2% to 3%. Admittedly, one might argue that for the numerical evaluation of $\Delta_{\tilde{\mathcal{N}}}/\mathcal{N}_n$ one should divide by the NLO value of the neutral normalization rather than only by the LO one as analytically done here due to the chiral power counting; according to $\Gamma_c^{\mathrm{LO}} \approx 66\,\mathrm{eV}$ and $\Gamma_c^{\mathrm{NLO}} \approx 160\,\mathrm{eV}$ (both evaluated at $Q = Q_D$ as employed in the present work) the numerical result for $\Delta_{\tilde{\mathcal{N}}}/\mathcal{N}_n$ would then be divided by a factor of $\sqrt{160/66} \approx 1.5$ so

---

[#10]It is interesting to note that calculating the parameter $\tilde{\alpha}$ itself with errors in analogy to those of $\Delta_{\tilde{\alpha}}$ yields $\tilde{\alpha} = (4.3 \pm 0.2)\,\mathrm{GeV}^{-4}$ so that numerically the relative correction amounts to $\Delta_{\tilde{\alpha}}/\tilde{\alpha} = (0.8 \pm 0.1)\%$; thus the correction to $\tilde{\alpha}$ induced by $\Delta_{\tilde{\alpha}}$ is largely counterbalanced by the effect of $\Delta_{\tilde{\mathcal{N}}}/\mathcal{N}_n$ in total, cf. (4.5).

that the rescaled relative error of $\Delta_{\tilde{\mathcal{N}}}/\mathcal{N}_n$ is about 1%, leading to an uncertainty in r of 2% at least.[#11] Nevertheless, we prefer the more conservative error estimate, which is consistent with the chiral power counting for the relative correction $\Delta_{\tilde{\mathcal{N}}}/\mathcal{N}_n$. A comparison with the averaged experimental error then shows that presently both experiment and theory can determine r with a precision of about $\pm 3\%$ only. In view of the differences between the "experimental" values as well as between the results of distinct theoretical frameworks like e.g. [3] and [66] on the one hand and the relative changes between predictions of ChPT at different orders (while going from LO to NLO yields a decrease of about 4%, the additional effects at NNLO amount to an increase of less than 1%, as discussed in Sect. 2.2.4) this uncertainty proves to be substantial.

[#11]According to (3.18), using a 5% smaller Q-value leads to about 20% larger results for $\Gamma_{c/n}$ in ChPT calculations, e.g. $\Gamma_c^{\mathrm{NLO}} \approx 197\,\mathrm{eV}$ for $Q = 22.8$ (cf. the discussion in Sect. 2.1.3), being somewhat closer to experimental findings. Of course, such a relative shift does not affect the rescaling of $\Delta_{\tilde{\mathcal{N}}}/\mathcal{N}_n$.

Chapter 5

Conclusion

In the first part of this work, we have re-evaluated the electromagnetic contributions to $\eta \to 3\pi$ decays at next-to-leading $\mathcal{O}(p^4)$ in ChPT, thus calculating the corrections to Sutherland's theorem [4, 5] and extending an earlier analysis [15], which neglected terms of $\mathcal{O}(e^2\delta)$. Terms of this order, however, contain essential non-analytic structures affecting the Dalitz plot distribution, in particular real- and virtual-photon corrections in $\eta \to \pi^0\pi^+\pi^-$ as well as the cusps due to $\pi^+\pi^-$ intermediate states in the $\pi\pi$ FSIs for $\eta \to 3\pi^0$; furthermore, the terms at $\mathcal{O}(e^2\delta)$ are of second order in isospin breaking and hence violate the $\Delta I = 1$ relation between the charged and the neutral decay amplitude that is usually employed in combined analyses of both $\eta \to 3\pi$ decay channels. At the soft-pion point, we have explicitly shown that these additional terms are not suppressed by an additional small isospin-breaking parameter, but only by a factor of $\delta/\hat{m} \approx 2/3$. Numerically, we have calculated the respective corrections to the various Dalitz plot parameters, the partial decay widths $\Gamma_{n/c}$, and thereby the branching ratio r; moreover, we derived the resulting correction for an extraction of the quark mass double ratio Q^2. In order to facilitate comparison with experimental results or application to experimental studies, for the charged decay both bremsstrahlung and the subtraction of universal corrections have explicitly been taken into account (in the soft-photon approximation), since in experimental analyses these effects are inevitable or usually applied, respectively. Although the effects at $\mathcal{O}(e^2\delta)$ are of the same size as those at $\mathcal{O}(e^2\hat{m})$ analyzed in [15], the total electromagnetic corrections remain small (i.e. at the percent level) throughout, provided that "trivial" kinematical isospin breaking due to the charged-to-neutral pion mass difference is accounted for. The most significant changes occur in the $\eta \to 3\pi^0$ Dalitz plot slope α, which is slightly more affected by the presence of the cusps than the other parameters. However, the cusp effect is by far not sufficient to explain the sign discrepancy between chiral predictions and experimental results (i.e. the "α-puzzle"), as especially in this case the purely electromagnetic and the mixed strong and electromagnetic contributions almost cancel. Nevertheless, the results can serve as electromagnetic correction factors in precision studies of $\eta \to 3\pi$ decays and in particular for the determination of the quark mass double ratio Q^2.

In [3], we subsequently bridged the gap between ChPT and phenomenology (as well as dispersive analyses) by using the (modified) NREFT formalism: at two-loop accuracy and with the correct empirical $\pi\pi$ scattering parameters for the FSIs, we obtained a reasonable approximation to the full dispersive resummation of rescattering effects, so that by matching to ChPT at $\mathcal{O}(p^4)$ we found a transparent interpretation of the dispersive results obtained in a similar fashion [17] and thus eventually solved the long-standing "α-puzzle". In the second part of this work, concretely, we have discussed how the electromagnetic corrections derived

in [1] (together with additional second-order strong isospin breaking at $\mathcal{O}(\delta^2)$) can be included in the NREFT calculation of [3]. Although the non-relativistic framework itself provides access to investigating most of the isospin-breaking effects even beyond leading order, due to the necessary matching to ChPT the results of the first part of this work are complementary to the NREFT machinery, as they predict the polynomial terms and their higher-order isospin-breaking corrections in the NREFT amplitudes. After explaining how to amend the ChPT amplitudes at NLO as given in [1] by including also the terms at $\mathcal{O}(\delta^2)$, we have thoroughly investigated the effect of "trivial" kinematical isospin breaking in the expansion of the amplitudes that correspond to the usual parameterizations of the Dalitz plot distributions, where special care needs to be taken of the definition of the "center" of the charged Dalitz plot. Starting from the well-known and usually employed $\Delta I = 1$ amplitude relation between the neutral and the charged amplitude, we have then derived (in a self-consistent fashion) relations between the amplitude expansion parameters and therefrom between the usual Dalitz plot parameters on the one hand as well as the respective isospin-breaking corrections to these relations on the other hand. Based on the (amended) ChPT amplitudes at NLO, we have analytically calculated the corrections to both the relations between the normalizations and between the parameters at quadratic order in Mandelstam variables (i.e. concerning the neutral slope α) in the form needed for the combined NREFT+ChPT framework; remarkably, both corrections turn out to be purely electromagnetic effects. The numerical evaluation of these "non-trivial" isospin-breaking contributions has shown that the relative effect on the normalization and on α is both of the order of 1%. Thereby, in [3] we were able to conclude in summary that, apart from the important "trivial" kinematical effects mentioned before, higher-order isospin-breaking corrections to the $\eta \to 3\pi$ Dalitz plot parameters are very small. However, as far as the ratio r of the partial decay widths is concerned, we have demonstrated that any current theoretical analysis *necessarily* entails an relative error on r of about 3%.

A future improvement on the theoretical side would be to combine the NREFT+ChPT analysis of [3] with dispersive techniques, for instance with the upcoming dispersive analysis [64,65]: as already indicated in Chap. 1, in combined dispersive analyses for both $\eta \to 3\pi$ decay channels, which are in principle well suited for extracting e.g. the Dalitz plot parameters as they entail elastic $\pi\pi$ rescattering to all orders by construction, it is at least very difficult (if possible at all) to accommodate the different pion masses. Therefore, it would be extremely useful to match the dispersive machinery to the non-relativistic representation in order to obtain a reliable description of the whole physical Dalitz plot, since the latter allows to implement higher-order isospin breaking comprising in particular the non-analytic cusp effect near the boundaries of the $\eta \to 3\pi^0$ Dalitz plot. More specifically, the NREFT+ChPT representation can be used in a two-step procedure to first "purify" experimental data from isospin-breaking effects in order to produce isospin-symmetric input for a subsequent dispersive analysis. This combination should then provide the best-possible representation of the $\eta \to 3\pi$ decay amplitude also for a precision extraction of the quark mass double ratio Q^2.

On the experimental side, of course, new high-statistics measurements of both $\eta \to \pi^0\pi^+\pi^-$ and $\eta \to 3\pi^0$ (preferably combined in order to reduce systematic uncertainties) are called for: since for the charged decay channel only one modern determination of Dalitz plot parameters exists up to now [25], new precise experimental information should allow to settle the controversy concerning the internal consistency of the KLOE results on the Dalitz plot parameters, i.e. the tension between the direct experimental determination of α [30] and a determination in terms of the charged parameters based on the $\Delta I = 1$ amplitude relation including second-order isospin-breaking corrections as discussed in the present work. In principle, a

similar analysis is also possible for the higher-order Dalitz plot parameters that have not been measured yet, e.g. in particular the neutral higher slope β (which is not influenced by $\mathcal{O}\big(p^6\big)$ LECs). This together with the cusp effect, which starts to show up in current experimental analyses, justifies also an investigation of the neutral decay channel; the combination of both channels, finally, would then be able to yield a more robust and precise value for the branching ratio r. Fortunately, for both processes new experimental studies are in progress, upcoming, or at least envisaged [74–81].

Due to the fact that the standard polynomial Dalitz plot *parameterizations* are not able to account for non-analytic effects like the cusps in $\eta \to 3\pi^0$, a matching/comparison between experiment and theory on the level of the Dalitz plot *distributions* themselves will be strongly favorable (especially for the future theoretical high-precision program mentioned above), as soon as the respective data are provided by experiments.

Appendix A

$\eta \to 3\pi$ decay amplitudes at next-to-leading order

As already mentioned in Sect. 2.2, in this appendix, we do not explicitly state the complete formulae for the $\eta \to 3\pi$ decay amplitudes at next-to-leading chiral $\mathcal{O}(p^4)$ and considering isospin breaking up-to-and-including $\mathcal{O}(e^2, e^2\delta, \delta^2)$, but rather discuss in detail the *changes* that need to be applied to the amplitudes as given in [1] in order to include also second-order strong isospin breaking at $\mathcal{O}(\delta^2)$. Note that, upon neglecting numerically tiny terms of $\mathcal{O}(e^4)$, the amended amplitudes are thus valid at next-to-leading order *both* in the chiral expansion and in isospin breaking. Prior to that for convenience, we collect the basic loop functions needed in this work, whereas after this investigation of the additional contributions at $\mathcal{O}(\delta^2)$, we specify the numerical input used throughout the numerical evaluations.

A.1 Loop functions

The basic meson loop functions are defined by[#1]

$$\Delta_a = \frac{1}{i} \int \frac{\mathrm{d}^d k}{(2\pi)^d} \frac{1}{M_a^2 - k^2} \ ,$$

$$J_{ab}(s) = J_{ba}(s) = \frac{1}{i} \int \frac{\mathrm{d}^d k}{(2\pi)^d} \frac{1}{\left[M_a^2 - k^2\right]\left[M_b^2 - (k-q)^2\right]} \ , \qquad s = q^2 \ . \tag{A.1}$$

The tadpole "function" Δ_a (in terms of the number of dimensions d and the renormalization scale μ) is given by

$$\Delta_a = 2M_a^2 \left\{ \lambda + \frac{1}{16\pi^2} \log \frac{M_a}{\mu} \right\} \ , \tag{A.2}$$

with the scale-dependent constant λ containing the part that is divergent in $d-4$,

$$\lambda = \frac{\mu^{d-4}}{16\pi^2} \left\{ \frac{1}{d-4} - \frac{1}{2} \Big(\log(4\pi) + \Gamma'(1) + 1 \Big) \right\} \ , \tag{A.3}$$

where $-\Gamma'(1) = \gamma_E \approx 0.5772$ is the Euler–Mascheroni constant. The symmetric two-point loop function $J_{ab}(s)$ can be split up according to

$$J_{ab}(s) = \bar{J}_{ab}(s) + J_{ab}(0) \ , \qquad J_{ab}(0) = -2\lambda - 2k_{ab} \ , \tag{A.4}$$

[#1]All propagators are to be understood in the causal form $-i/(M^2 - k^2 - i\varepsilon)$ with $\varepsilon \to 0$.

with the scale-dependent constant ("function") k_{ab} and the scale-independent function $\bar{J}_{ab}(s)$,

$$k_{ab} = \frac{1}{16\pi^2 \, \Delta_{ab}} \left\{ M_a^2 \log \frac{M_a}{\mu} - M_b^2 \log \frac{M_b}{\mu} \right\} ,$$

$$\bar{J}_{ab}(s) = -\frac{1}{16\pi^2} \left\{ \left(\frac{\Delta_{ab}}{s} - \frac{\Sigma_{ab}}{\Delta_{ab}} \right) \log \frac{M_a}{M_b} - 1 \right.$$
$$+ \frac{\sqrt{\lambda_{ab}}}{s} \left[\frac{1}{2} \log \frac{s - \Sigma_{ab} + \sqrt{\lambda_{ab}}}{s - \Sigma_{ab} - \sqrt{\lambda_{ab}}} - \pi i \, \theta \Big(s - (M_a + M_b)^2 \Big) \right] \theta \big(\lambda_{ab} \big)$$
$$\left. + \frac{\sqrt{-\lambda_{ab}}}{s} \left[\arctan \frac{\Delta_{ab} + s}{\sqrt{-\lambda_{ab}}} - \arctan \frac{\Delta_{ab} - s}{\sqrt{-\lambda_{ab}}} \right] \theta \big(-\lambda_{ab} \big) \right\} , \tag{A.5}$$

where besides $\lambda_{ab}(s)$ of (2.30) and the usual Heaviside function $\theta(x)$ we used the abbreviations

$$\Sigma_{ab} = M_a^2 + M_b^2 , \qquad \Delta_{ab} = M_a^2 - M_b^2 . \tag{A.6}$$

In the case of equal masses $M_a^2 = M_b^2$, the above relations simplify to (cf. (2.31))

$$k_{aa} = \frac{1}{16\pi^2} \left(\log \frac{M_a}{\mu} + \frac{1}{2} \right) ,$$

$$\bar{J}_{aa}(s) = -\frac{1}{16\pi^2} \left\{ -2 + \sigma_a \log \frac{\sigma_a + 1}{\sigma_a - 1} \, \theta(-s) + \sigma_a \left[\log \frac{1 + \sigma_a}{1 - \sigma_a} - \pi i \right] \theta \big(s - 4M_a^2 \big) \right.$$
$$\left. + 2\sqrt{-\sigma_a^2} \, \text{arccot} \sqrt{-\sigma_a^2} \, \theta \big(-\sigma_a^2 \big) \right\} . \tag{A.7}$$

The triangle loop function $G(s)$ corresponding to the loop integral involving two charged-pion propagators and one virtual-photon propagator (introducing a finite photon mass here),

$$\frac{1}{i} \int \frac{\mathrm{d}^d k}{(2\pi)^d} \frac{1}{\big[M_\pi^2 - (k + q_a)^2 \big] \big[M_\pi^2 - (k - q_b)^2 \big] \big[k^2 - m_\gamma^2 \big]} , \tag{A.8}$$

evaluated in the relevant kinematical region $s > 4M_\pi^2$ above the $\pi\pi$ threshold (i.e. $\sigma_\pi \in (0,1)$) and up to corrections at $\mathcal{O}\big(m_\gamma^2 \big)$, can be written as[#2]

$$G(s) = -\frac{1}{8\pi^2 \, s\sigma_\pi} \left\{ \frac{\pi^2}{3} + \text{Li} \frac{2\sigma_\pi}{1 + \sigma_\pi} + \frac{1}{4} \log^2 \frac{1 - \sigma_\pi}{1 + \sigma_\pi} - \frac{1}{2} \log \frac{m_\gamma^2}{s\sigma_\pi^2} \left[\log \frac{1 - \sigma_\pi}{1 + \sigma_\pi} + \pi i \right] \right\} \tag{A.9}$$

$$= -\frac{1}{16\pi^2 \, s\sigma_\pi} \left\{ \pi^2 + \text{Li} \frac{1 + \sigma_\pi}{1 - \sigma_\pi} - \text{Li} \frac{1 - \sigma_\pi}{1 + \sigma_\pi} + \pi i \log \frac{4\sigma_\pi^2}{1 - \sigma_\pi^2} + \log \frac{m_\gamma^2}{M_\pi^2} \left[\log \frac{1 + \sigma_\pi}{1 - \sigma_\pi} - \pi i \right] \right\}$$

using either the usual dilogarithm Li_2 or Spence's function Li (cf. e.g. [130]) according to

$$\text{Li}(z) = -\int_1^z \mathrm{d}t \, \frac{\log t}{t - 1} = \text{Li}_2(1 - z) , \qquad \text{Li}_2(z) = -\int_0^1 \mathrm{d}t \, \frac{\log(1 - zt)}{t} . \tag{A.10}$$

In the second representation of $G(s)$ given in (A.9), the real part of the Coulomb pole, i.e. the kinematical divergence at the $\pi\pi$ threshold (where $\sigma_\pi = 0$), resides solely in the term proportional to π^2; furthermore, it is convenient for the comparison of different IR regularization schemes as discussed in Sects. 3.1 and 4.2.

[#2]Note that the result in [118] contains a typographical error and uses a different sign convention for Li.

A.2 Amplitudes at second order in isospin breaking

In order to derive the additional contributions at $\mathcal{O}(\delta^2)$, in principle one needs to reconsider all contributions to the charged and the neutral NLO amplitudes as given in [1]. However, based on the important observation that the LO amplitudes (2.40) and (2.42) are valid up to corrections of $\mathcal{O}(\delta^3)$, already in [1] it was pointed out that corrections at second-order in strong isospin breaking are to be expected solely from expanding the implicitly isospin-breaking charged-to-neutral kaon loop differences (mentioned already in Sect. 2.2.3) in terms of the isospin-breaking parameters as needed in order to achieve an explicit and unambiguous disentanglement of strong and electromagnetic isospin breaking up to the desired orders (at a given chiral order), cf. Sects. 2.2.2 and 2.2.4. According to the generic meson loop functions given in App. A.1, the expansions of the kaon loop function differences for the tadpole functions $\Delta_K - \Delta_{K^0}$ and the two-point functions $J_{KK} - J_{K^0 K^0}$ read (cf. (A.2) and (A.5))

$$\Delta_K - \Delta_{K^0} = \Delta M_K^2 \left[\frac{\Delta_{K^0}}{M_{K^0}^2} + \frac{1}{16\pi^2} \right] + \frac{\left(\Delta M_K^2\right)^2}{32\pi^2 M_{K^0}^2} + \mathcal{O}\left(e^2 \delta^2, \delta^3, p^4\right) \, ,$$

$$J_{KK}(s) - J_{K^0 K^0}(s) = -2 \frac{\Delta M_K^2}{s - 4M_{K^0}^2} \left[\bar{J}_{K^0 K^0}(s) - \frac{1}{8\pi^2} \right]$$

$$- 2 \left[\frac{\Delta M_K^2}{s - 4M_{K^0}^2} \right]^2 \left[\bar{J}_{K^0 K^0}(s) + \frac{s - 8M_{K^0}^2}{32\pi^2 M_{K^0}^2} \right] + \mathcal{O}\left(e^2 \delta^2, \delta^3, p^2\right) \, , \quad \text{(A.11)}$$

where the charged-to-neutral kaon mass difference ΔM_K^2 is understood to be evaluated at leading chiral order via (2.14). Since the terms of $\mathcal{O}(\delta^2)$ are not of electromagnetic origin, they have been disregarded in the analysis of [1]; nevertheless, it was noted therein that their suppression with respect to the leading isospin-breaking terms is never enhanced compared to $\Delta M_K^2 / M_{K^0}^2$. We want to stress again, however, that in general we do not expand in charged-to-neutral mass differences (or, effectively, replace masses) inside loop functions, unless this is inevitable like in Sect. 4.2. Thereby, using the physical meson masses, all cuts (even outside the physical region) remain at their exact places, which is important for instance for the cusp effect in $\eta \to 3\pi^0$, see Sect. 2.2.4; furthermore, no implicit higher-order isospin-breaking effects are neglected without need in numerical evaluations. Moreover, as already indicated in Sect. 2.2.3, especially for the kaon loop differences it is favorable not to perform these expansions until it is necessary: besides yielding shorter formulae, most of the amplitude contributions given in [1] are therefore also valid at $\mathcal{O}(\delta^2)$. Unfortunately, it turned out that the full amplitudes of [1] are neither finite nor scale-independent at this particular second order in strong isospin breaking. Therefore, a thorough re-analysis of all contributions was necessary, which eventually revealed an inconsistency concerning the definition of the isospin limit for the meson decay constants in ChPT at NLO to be discussed below.

Accordingly, we initially collect all parts of the $\eta \to \pi^0 \pi^+ \pi^-$ and $\eta \to 3\pi^0$ amplitudes that — in the explicit form they are given in [1] — are also valid up-to-and-including $\mathcal{O}(\delta^2)$ in Tab. A.1, where we also indicate the terms containing differences of kaon loop functions without isospin-breaking prefactors.[#3] Here, we merely skip through these contributions very cursorily; for the precise definitions of these quantities as well as their relations to the full

---

[#3]Of course, in analogy also differences of pion loop functions contain both electromagnetic and strong isospin-breaking effects, cf. (2.14), which are, however, beyond the accuracy we are concerned with, since these differences are always accompanied by isospin-breaking prefactors.

quantity	valid up to $+\mathcal{O}(e^4, \dots)$	$\Delta_K - \Delta_{K^0}$	$J_{KK} - J_{K^0 K^0}$
$Z_\eta,\ Z_{\pi^0}$	$+\mathcal{O}(e^2\delta, \delta^2, p^4)$		
Z_π	$+\mathcal{O}(\delta^2, p^4)$		
$\Delta_M,\ \Delta_Z$	$+\mathcal{O}(e^2\delta, \delta^2, p^6)$		
Δ_Q	$+\mathcal{O}(e^2\delta, \delta^2, p^4)$		
$\epsilon_4,\ Z_{\pi^0\eta}$	$+\mathcal{O}(e^2\delta^2, \delta^3, p^4)$	$\times$	
$\mathcal{A}^{\mathrm{LO}}_{\pi^0\eta}$	$+\mathcal{O}(\delta^2, p^4)$		
$\mathcal{A}^{\mathrm{ct}}_{c/n}$	$+\mathcal{O}(e^2\delta^2, \delta^3, p^6)$		
Δ_{GMO}	$+\mathcal{O}(\delta^2, p^4)$		
$\mathcal{A}^{\mathrm{tad}}_{c/n}$	$+\mathcal{O}(e^2\delta^2, \delta^3, p^6)$	$\times$	
$\mathcal{A}^s_c,\ \mathcal{A}^{stu}_n$	$+\mathcal{O}(e^2\delta^2, \delta^3, p^6)$	$\times$	$\times$
$\mathcal{A}^t_{\pi^0\pi},\ \mathcal{A}^t_{K^0 K}$	$+\mathcal{O}(e^2\delta^2, \delta^3, p^6)$		
$\mathcal{A}^t_{\eta\pi}$	$+\mathcal{O}(\delta^3, p^6)$		
$\mathcal{A}^{\pi\gamma}_c,\ \mathcal{A}^{\pi\pi\gamma}_c$	$+\mathcal{O}(e^2\delta^2, p^6)$		

Table A.1: Validity of the NLO contributions to the $\eta \to 3\pi$ decay amplitudes as given in [1]. Marks denote contributions of corresponding kaon loop function differences without isospin-breaking prefactors. See main text for details.

amplitudes we refer to [1]: first of all, there are no $\mathcal{O}(\delta)$ contributions to the NLO wave function renormalization Z-factors (following from the full/dressed NLO propagators, the implicit $\pi^0\eta$ mixing contained in Z_π being of higher order in isospin breaking) that multiply the LO amplitudes (2.40) and (2.42), which in turn are already proportional to δ. Similarly, the NLO renormalization corrections Δ_M, Δ_Z, and Δ_Q to the LO amplitudes (due to the replacement of quarks masses and the LO electromagnetic LEC Z by meson masses), which hence also carry a prefactor of δ, do not entail terms at $\mathcal{O}(\delta)$. The quantities ϵ_4 and $Z_{\pi^0\eta}$ that multiply the isospin-conserving leading-order amplitudes

$$\mathcal{A}^{\mathrm{LO}}_{\pi^0\eta} \in \left\{ \mathcal{A}^{\mathrm{LO}}_{\pi^0 \to \pi^0\pi^+\pi^-}, \mathcal{A}^{\mathrm{LO}}_{\eta \to \eta\pi^+\pi^-}, \mathcal{A}^{\mathrm{LO}}_{\pi^0 \to 3\pi^0}, \mathcal{A}^{\mathrm{LO}}_{\eta \to \eta 2\pi^0} \right\} \tag{A.12}$$

in order to account for $\pi^0\eta$ mixing at next-to-leading chiral order, in contrast, do not contain purely strong $\mathcal{O}(\delta^2)$ terms except those already implicitly included via the kaon tadpole difference. The counter-term contributions $\mathcal{A}^{\mathrm{ct}}_{c/n}$ (corresponding to tree graphs with NLO vertices and thereby introducing NLO strong and electromagnetic LECs) give rise only to higher-order corrections,[#4] and the Gell-Mann–Okubo correction Δ_{GMO} defined in (2.17), which is used to eliminate the dependence on some strong LECs in the previously addressed parts and thus goes always along with some isospin-breaking prefactor, does not yield additional corrections at $\mathcal{O}(\delta)$. The remaining loop contributions can be divided into purely mesonic diagrams and

---

[#4]The counter-term contributions $\mathcal{A}^{\mathrm{ct}}_{c/n}$ are given explicitly only in [39] but not in [1], since they are fully included in the total NLO tree-like amplitudes $\mathcal{A}^{\mathrm{tree}}_{c/n}$ as defined and explained in [1], cf. (A.17) and (A.19).

loops involving virtual photons, which in any case do not lead to effects at $\mathcal{O}(\delta^2)$ beyond those comprised in kaon loop differences: while $\mathcal{A}_c^{\text{tad}}$ corresponds to summing up all pertinent diagrams with a meson tadpole at the (LO) vertex, for the rescattering contributions (denoted by Mandelstam variables as superscripts) we employ the respective symmetry properties of the amplitudes as discussed in Sect. 2.2.3, so that we can identify $\mathcal{A}_n^{stu} = \tilde{\mathcal{A}}_n$ for the fully symmetric neutral amplitude, compare (2.48), whereas for the $t \leftrightarrow u$ symmetric charged decay one needs to consider the s-channel and one of the other two kinematical channels, e.g. the t-channel (again, there is no implicit $\pi^0\eta$ mixing for $\mathcal{A}_{\eta\pi}^t$ at this order in isospin breaking, cf. Z_π), separately.[#5] Finally, the photon loop contributions $\mathcal{A}_c^{\pi\gamma}$ and $\mathcal{A}_c^{\pi\pi\gamma}$, which have already been discussed in Sect. 3.1, are necessarily proportional to e^2 at least.

Now, we are prepared to discuss the necessary changes at $\mathcal{O}(\delta^2)$ that are not simply accounted for by just expanding the kaon loop function differences up to this order as discussed above. Obviously, we still need to consider those contributions to the full amplitudes that are not listed in Tab. A.1, namely the NLO renormalization corrections to the meson decay constants, i.e. Δ_{F_π} and Δ_F as defined in (2.4), which enter the full tree-like amplitudes $\mathcal{A}_{c/n}^{\text{tree}}$. As it turns out, special care needs to be taken of these quantities: while Δ_{F_π} is needed in order to renormalize the replacement of the bare Goldstone boson decay constant F_0 by the pion decay constant F_π in the LO amplitudes, the correction Δ_F to the ratio of the kaon and the pion decay constants is introduced to eliminate further LECs.[#6] Consequently, both quantities always carry a prefactor of δ. As the physical value of F_π ($F_\pi = 92.2\,\text{MeV}$ [131], cf. Sect. A.3) has been extracted from decays of charged pions with electromagnetic corrections already taken into account (and in analogy for F_K, see also [132] and [93]), we use the charged-pion decay constant in the absence of electromagnetism, so that in [1] the relation of F_π to F_0 is as given in Ref. [12] (where electromagnetic corrections are neglected as well) for the isospin limit; accordingly, we also use the correction Δ_F without isospin breaking as given therein. More specifically, in [12] these quantities are defined to be isospin-symmetric at the level of *quark* masses, i.e. using only $\hat{m}$ and m_s, whereas the tadpole loop contributions to them are written therein in terms of *meson* masses for convenience. Neglecting terms proportional to e^2 or δ, according to (2.13) one can easily identify at leading chiral order $M_\pi^2 = 2B_0\hat{m}$ and $M_K^2 = B_0(m_s + \hat{m})$ both for the charged meson masses and the meson masses in the isospin limit, when replacing these quark-mass isospin-symmetric meson masses inside the loop functions by physical meson masses. If one were to neglect only electromagnetic corrections at LO, the charged pion mass is fine, whereas for the kaons only the average mass excludes strong corrections. However, as soon as such corrections to the meson masses are considered as in [1], one is forced to use the neutral masses (cf. the discussion of or conventions for the isospin limit and the ordering scheme in isospin-breaking parameters in Sect.2.2.3), which in turn lead to strong effects at $\mathcal{O}(\delta^2)$ and $\mathcal{O}(\delta)$ for the pions and the kaons, respectively. While these effects, in combination with the prefactor of δ mentioned above, are beyond the scope of [1], this prescription for the kaon tadpoles contained in Δ_{F_π} and Δ_F affects the amplitudes at $\mathcal{O}(\delta^2)$: in fact, without the following amendment, both amplitudes are neither finite nor independent of the renormalization scale at this order.

[#5]When comparing to (2.48), note that in the case of the charged amplitude also the total NLO tree-like amplitude $\mathcal{A}_c^{\text{tree}}$ (A.17) contains kinematical dependences.

[#6]Both L_7 and L_8 can be eliminated simultaneously in terms of Δ_{GMO}, while L_5 can be replaced by Δ_F; the dependences on K_7 and K_8 are already canceled by the NLO renormalization corrections Δ_M and Δ_Z.

According to the relation (cf. (2.18))

$$
\begin{aligned}
B_0(m_s + \hat{m}) &= \frac{1}{8}\Big[3\big(M_\eta^2 + M_{\pi^0}^2\big) + 2\big(M_K^2 + M_{K^0}^2 - M_\pi^2\big)\Big] + \mathcal{O}\big(p^4\big) \\
&= \frac{1}{2}\Big[M_K^2 + M_{K^0}^2 - 2F_0^2 Z e^2\Big] + \mathcal{O}\big(p^4\big) \\
&= \frac{1}{4}\Big[3M_\eta^2 + M_{\pi^0}^2\Big] + \mathcal{O}\big(\delta^2, p^4\big) \ ,
\end{aligned}
\tag{A.13}
$$

these effects at $\mathcal{O}\big(\delta^2\big)$ — spuriously introduced in [1] — can be avoided by using the (however unphysical) tadpole function (cf. (A.2))

$$
\Delta_{K^0} \to \Delta_{3\eta\pi^0} = \Delta_a\Big|_{4M_a^2 = 3M_\eta^2 + M_{\pi^0}^2} \ ,
\tag{A.14}
$$

which is isospin-symmetric and finite at $\mathcal{O}(\delta)$, in the definitions of Δ_{F_π} and Δ_F instead of Δ_{K^0} as used in [1]. Thereby, contrary to [1] we have to use

$$
\begin{aligned}
\Delta_{F_\pi} &= \frac{1}{F_\pi^2}\left\{6(M_\eta^2 + M_{\pi^0}^2)L_4 + 4M_{\pi^0}^2 L_5 - \Delta_{\pi^0} - \frac{\Delta_{3\eta\pi^0}}{2}\right\} + \mathcal{O}\big(e^2, \delta^2, p^4\big) \ , \\
\Delta_F &= \frac{1}{F_\pi^2}\left\{3(M_\eta^2 - M_{\pi^0}^2)L_5 + \frac{1}{8}\Big[5\Delta_{\pi^0} - 3\Delta_\eta - 2\Delta_{3\eta\pi^0}\Big]\right\} + \mathcal{O}\big(e^2, \delta^2, p^4\big) \ ,
\end{aligned}
\tag{A.15}
$$

leading to slightly modified NLO tree-like amplitudes $\mathcal{A}_{c/n}^{\text{tree}}$, which are stated explicitly in the two following sections. Of course, we have explicitly verified that the correspondingly modified full NLO amplitudes $\mathcal{A}_{c/n}^{\text{NLO}}$ (see [1] for the precise definitions) are both finite and scale-independent also at $\mathcal{O}\big(\delta^2\big)$.

A.2.1 $\eta \to \pi^0\pi^+\pi^-$ decay amplitude

In comparison with the formula for the total NLO tree-like amplitude $\mathcal{A}_c^{\text{tree}}$ as given as equation (A.22) in [1], applying the corrections to include all contributions at $\mathcal{O}\big(\delta^2\big)$ as discussed in the previous section amounts to changing the seventh line according to

$$
\begin{aligned}
&(11M_\eta^2 - 3M_{\pi^0}^2)\frac{\Delta_K}{2} + (5M_\eta^2 + 7M_{\pi^0}^2)\frac{\Delta_{K^0}}{2} \\
&= \frac{1}{2}(3M_\eta^2 - 5M_{\pi^0}^2)(\Delta_K - \Delta_{K^0}) + (4M_\eta^2 + M_{\pi^0}^2)(\Delta_K + \Delta_{K^0}) \\
&\to \frac{1}{2}(3M_\eta^2 - 5M_{\pi^0}^2)(\Delta_K + \Delta_{K^0} - 2\Delta_{3\eta\pi^0}) + (4M_\eta^2 + M_{\pi^0}^2)(\Delta_K + \Delta_{K^0}) \\
&= \frac{1}{2}(11M_\eta^2 - 3M_{\pi^0}^2)(\Delta_K + \Delta_{K^0}) - (3M_\eta^2 - 5M_{\pi^0}^2)\Delta_{3\eta\pi^0} \ .
\end{aligned}
\tag{A.16}
$$

Moreover, the tadpole function $\Delta_{3\eta\pi^0}$ enters in lines 10 and 17 both via $\Delta_{K^0} \to \Delta_{3\eta\pi^0}$. Although the latter changes only affect even higher orders in isospin breaking, so that one could also just keep the original Δ_{K^0} up to corrections of $\mathcal{O}\big(e^2\delta^2\big)$, we use $\Delta_{3\eta\pi^0}$ throughout for the sake of clarity.

The full formula for the charged decay then reads

$$
\mathcal{A}_c^{\text{tree}} = \frac{\Delta_K - \Delta_{K^0}}{6\sqrt{3}F_\pi^4}\left[\frac{(3s - 4M_{\pi^0}^2)2M_\eta^2}{M_\eta^2 - M_{\pi^0}^2} - (2M_\eta^2 - M_{\pi^0}^2)\right]
$$

$$
+ \frac{e^2(3s - 4M_{\pi^0}^2)4M_{\pi^0}^2}{9\sqrt{3}F_\pi^2(M_\eta^2 - M_{\pi^0}^2)}\left[3(K_3 - K_4/2) - (K_5 + K_6) + (K_9 + K_{10})\right]
$$

$$
- \frac{1}{Q^2 2\sqrt{3}F_\pi^2 M_{\pi^0}^2}\Bigg\{
$$

$$
\times (3s - 4M_{\pi^0}^2)\Bigg[\frac{3M_\eta^2 + M_{\pi^0}^2}{8} + \frac{M_\eta^2}{2}\Delta_{\text{GMO}} + \frac{(3M_\eta^2 + M_{\pi^0}^2)M_{\pi^0}^2 + \Delta M_\pi^2 6M_\eta^2}{3(M_\eta^2 - M_{\pi^0}^2)}\Delta_F
$$

$$
+ \frac{1}{24F_\pi^2}\Bigg((\Delta_\pi - \Delta_{\pi^0})(21M_\eta^2 + M_{\pi^0}^2) + \frac{3M_\eta^2 + M_{\pi^0}^2}{M_\eta^2 - M_{\pi^0}^2}\Big\{\frac{1}{2}(11M_\eta^2 - 3M_{\pi^0}^2)(\Delta_K + \Delta_{K^0})
$$

$$
- (3M_\eta^2 - 5M_{\pi^0}^2)\Delta_{3\eta\pi^0} - (M_\eta^2 + M_{\pi^0}^2)(\Delta_\pi + \Delta_{\pi^0}) - 3(3M_\eta^2 - M_{\pi^0}^2)\Delta_\eta\Big\}
$$

$$
+ \frac{\Delta M_\pi^2 6M_\eta^2}{M_\eta^2 - M_{\pi^0}^2}\Big\{4(\Delta_K - \Delta_\pi) + 2\Delta_{3\eta\pi^0} - 5\Delta_{\pi^0} + 3\Delta_\eta\Big\}\Bigg)\Bigg]
$$

$$
- (3M_\eta^2 + M_{\pi^0}^2)\Bigg[\frac{M_{\pi^0}^2}{3}\Delta_{\text{GMO}} + \frac{\Delta M_\pi^2(M_\eta^2 + M_{\pi^0}^2)}{M_\eta^2 - M_{\pi^0}^2}\Delta_F
$$

$$
- \frac{L_3}{2F_\pi^2}\Big((s - M_\eta^2)(s - 2\Delta M_\pi^2) + 2tu - (3s + 2\Delta M_\pi^2)M_{\pi^0}^2\Big)
$$

$$
+ \frac{1}{96F_\pi^2(M_\eta^2 - M_{\pi^0}^2)}\Big((\Delta_\pi - \Delta_{\pi^0})(5M_\eta^4 - 40M_\eta^2 M_{\pi^0}^2 - 13M_{\pi^0}^4)
$$

$$
+ 4(M_\eta^4 + 11M_\eta^2 M_{\pi^0}^2 + 4M_{\pi^0}^4)(\Delta_K + \Delta_{K^0}) - 2(M_\eta^4 + 48M_\eta^2 M_{\pi^0}^2 - M_{\pi^0}^4)\Delta_\eta
$$

$$
- (M_\eta^4 + 15M_{\pi^0}^4)(\Delta_\pi + \Delta_{\pi^0}) + \Delta M_\pi^2 4\Big\{3(M_\eta^2 + M_{\pi^0}^2)(2\Delta_{3\eta\pi^0} - 5\Delta_{\pi^0} + 3\Delta_\eta)
$$

$$
- 2(3M_\eta^2 - 11M_{\pi^0}^2)\Delta_K - 4(3M_\eta^2 + M_{\pi^0}^2)\Delta_\pi\Big\}\Big)\Bigg]
$$

$$
- e^2(3s - 4M_{\pi^0}^2)\Bigg[\frac{15M_\eta^2 + M_{\pi^0}^2}{64\pi^2} - 3M_\eta^2\frac{\Delta_K - \Delta_\pi}{M_\eta^2 - M_{\pi^0}^2} + \frac{3M_\eta^2 + M_{\pi^0}^2}{3}\left(\frac{3}{64\pi^2}\log\frac{m_\gamma^2}{M_\pi^2}\right.
$$

$$
+ \frac{3}{4}\frac{\Delta_\pi}{M_\pi^2} + (K_1 + K_2) + K_5 - \frac{M_{\pi^0}^2}{3}\frac{3(K_3 - K_4/2) - (K_5 + K_6) + (K_9 + K_{10})}{M_\eta^2 - M_{\pi^0}^2}\Bigg)
$$

$$
- \left(2M_\eta^2 - \frac{M_{\pi^0}^2}{3}\right)(K_3 - K_4/2) - M_\eta^2(K_9 - 5K_{10} - 6K_{11})\Bigg]
$$

$$
+ e^2(3M_\eta^2 + M_{\pi^0}^2)\Bigg[\frac{M_{\pi^0}^2}{16\pi^2} - 2M_{\pi^0}^2\frac{\Delta_K - \Delta_\pi}{M_\eta^2 - M_{\pi^0}^2} + \frac{3}{4}\Delta_\pi + \frac{3}{2}(M_\eta^2 - M_{\pi^0}^2)(K_3 - K_4/2)
$$

$$
- \frac{M_{\pi^0}^2}{3}K_5 - M_\eta^2 K_6 + 3(M_\eta^2 + M_{\pi^0}^2)(K_{10} + K_{11})\Bigg]\Bigg\} + \mathcal{O}(e^2\delta^2, \delta^3, p^6)\ . \tag{A.17}
$$

A.2.2 $\eta \to 3\pi^0$ decay amplitude

For the neutral decay in analogy, the amplitude $\mathcal{A}_n^{\text{tree}}$ given as equation (A.25) in [1] needs to be modified in the sixth line according to

$$(\Delta_K - \Delta_{K^0}) \to (\Delta_K + \Delta_{K^0} - 2\Delta_{3\eta\pi^0}) \,. \tag{A.18}$$

Together with the related optional (higher-order) change $\Delta_{K^0} \to \Delta_{3\eta\pi^0}$ in line 10, the complete formula takes the form

$$
\begin{aligned}
\mathcal{A}_n^{\text{tree}} = {} & \frac{(\Delta_K - \Delta_{K^0})M_{\pi^0}^2}{2\sqrt{3}F_\pi^4} + \frac{e^2 4M_{\pi^0}^2}{3\sqrt{3}F_\pi^2}\left[3(K_3 - K_4/2) - (K_5 + K_6) + (K_9 + K_{10})\right] \\
& - \frac{1}{Q^2 2\sqrt{3}F_\pi^2 M_{\pi^0}^2}\Bigg\{ \\
& \times (3M_\eta^2 + M_{\pi^0}^2)\Bigg[\frac{3}{8}(M_\eta^2 - M_{\pi^0}^2) + M_{\pi^0}^2\Delta_F \\
& \quad + \frac{1}{32F_\pi^2(M_\eta^2 - M_{\pi^0}^2)}\Bigg((\Delta_\pi - \Delta_{\pi^0})3\frac{27M_\eta^6 - 47M_\eta^4 M_{\pi^0}^2 + 69M_\eta^2 M_{\pi^0}^4 + 15M_{\pi^0}^6}{3M_\eta^2 + M_{\pi^0}^2} \\
& \quad - 2\frac{51M_\eta^6 - 199M_\eta^4 M_{\pi^0}^2 - 51M_\eta^2 M_{\pi^0}^4 + 7M_{\pi^0}^6}{3M_\eta^2 + M_{\pi^0}^2}\Delta_\eta - (3M_\eta^4 - 19M_{\pi^0}^4)(\Delta_\pi + \Delta_{\pi^0}) \\
& \quad - 4(M_\eta^2 - M_{\pi^0}^2)(3M_\eta^2 - 5M_{\pi^0}^2)\Delta_{3\eta\pi^0} + 2(9M_\eta^4 - 36M_\eta^2 M_{\pi^0}^2 - 5M_{\pi^0}^4)(\Delta_K + \Delta_{K^0})\Bigg) \\
& \quad - \frac{e^2}{3}\Bigg(3(M_\eta^2 - M_{\pi^0}^2)(K_1 + K_2) - 6(M_\eta^2 + M_{\pi^0}^2)(K_3 - K_4/2) \\
& \quad + (3M_\eta^2 + M_{\pi^0}^2)(K_5 + K_6) - 7M_{\pi^0}^2(K_9 + K_{10})\Bigg)\Bigg] \\
& + (3M_\eta^4 - 9M_\eta^2 M_{\pi^0}^2 - 2M_{\pi^0}^4)\Bigg[\frac{\Delta_{\text{GMO}}}{2} \\
& \quad + \frac{\Delta M_\pi^2}{M_\eta^2 - M_{\pi^0}^2}\Bigg(2\Delta_F + \frac{1}{4F_\pi^2}\Big\{4(\Delta_K - \Delta_\pi) + 2\Delta_{3\eta\pi^0} - 5\Delta_{\pi^0} + 3\Delta_\eta\Big\}\Bigg) \\
& \quad + e^2\Bigg(3\frac{\Delta_K - \Delta_\pi}{M_\eta^2 - M_{\pi^0}^2} - \frac{3}{16\pi^2} + 3(K_3 - K_4/2) + (K_9 - 5K_{10} - 6K_{11})\Bigg)\Bigg]\Bigg\} \\
& + \mathcal{O}\big(e^2\delta^2, \delta^3, p^6\big) \,.
\end{aligned}
\tag{A.19}
$$

A.3 Numerical input

Here, we give the input data as used for the numerical evaluation of the $\eta \to 3\pi$ decay amplitudes both in Chap. 3 (excluding $\mathcal{O}(\delta^2)$) and Chap. 4 (including $\mathcal{O}(\delta^2)$).

For the meson masses and decay constants we employ the values given in Tab. A.2,[#7] where for the kaon decay constant in fact we use $F_K = 1.193\,F_\pi$ relying on Standard Model

---

[#7]Note the change of M_η in comparison with older values; in particular $M_\eta = 547.3\,\text{MeV}$ is used in [21].

p	π^0	π	K	K^0	η
M_p [MeV]	134.98	139.57	493.68	497.61	547.85
F_p [MeV]		92.2	110.0*		

Table A.2: Meson masses and decay constants according to [131]. See main text for details.

i	1	2	3	4	5	6	9	10	11
$10^3 \times K_i^r$	-2.7	0.7	2.7	1.4	11.6	2.8	0*	4.0	1.3
$4 \times \Sigma_i$	3	$4Z$	-3	$8Z$	-9	$6Z$	-1	$1+6Z$	$1/2$

Table A.3: Electromagnetic LECs at NLO and scaling coefficients. See main text for details.

electroweak couplings [133] (also being in agreement with recent three-flavor lattice QCD averages [100–102]). The electric charge and the quark mass double ratio are evaluated using

$$e^2 = \frac{4\pi}{137.036} \, , \qquad Q = 24.2 \approx Q_D \, , \tag{A.20}$$

and the photon cutoff energy E_{cut} is set to a typical detector resolution of $10\,\text{MeV}$. For the only strong LEC not expressed in terms of physical observables, we use the (finite) value [134][#8]

$$L_3 = -3.5 \times 10^{-3} \, . \tag{A.21}$$

As we concentrate on the electromagnetic corrections in this article, we do not consider uncertainties for L_3. For the remaining next-to-leading order electromagnetic low-energy constants K_i^r, we rely on the estimates in [112, 113, 136] (cf. [137] and see also [110, 138] for further alternatives; for the recent status of lattice QCD(+QED) results on strong and electromagnetic LECs see [100]) using the Feynman gauge and given at the scale $\mu = M_\rho = 0.770\,\text{GeV}$ as collected in Tab. A.3.[#9] Since no number for K_9^r is offered, we use $K_9^r = 0$ according to the earlier evaluation [137].

The uncertainties in the K_i^r are difficult to assess, but they are the dominant sources of uncertainties for the electromagnetic corrections. Hence, we adopt the following procedure: since the values of the renormalized LECs at two different scales are related by

$$K_i^r(\mu_2) = K_i^r(\mu_1) + \frac{\Sigma_i}{16\pi^2} \ln \frac{\mu_1}{\mu_2} \, , \tag{A.22}$$

it appears natural to use correlated errors due to a variation of scale according to

$$K_i^r \to K_i^r \pm \frac{\Sigma_i}{16\pi^2} \, , \tag{A.23}$$

where the respective coefficients according to [14] are also displayed in Tab. A.3. This procedure has the advantage that the resulting error estimate is invariant under a redefinition

---

[#8]Note that a recent global fit of all L_i^r including resonance estimates for the strong LECs at two-loop order yields $10^3 \times L_3 = -3.04 \pm 0.43$ [135], whereas lattice QCD yields results only for those L_i^r (or combinations thereof) that depend on quark masses, i.e. not for L_3.

[#9]Unfortunately, the value for K_5^r was not given in [1].

of the effective electromagnetic NLO Lagrangian, in contrast to a more naive uncorrelated variation of all K_i^r according to $K_i^r \pm 1/16\pi^2$. However, in some cases (most notably for the normalization of the DKM amplitude for $\eta \to \pi^0\pi^+\pi^-$), an accidental cancellation between the various Σ_i when applying (A.23) leads to an unrealistically small error. In those cases, we have replaced the Σ_i by 1 in (A.23) and marked the corresponding errors, thus obtained in a non-standard way, by an asterisk in Tables 3.1, 3.3, and 3.4.

Appendix B

Derivation of the $\Delta I = 1$ amplitude relation

In this appendix, we derive the important $\Delta I = 1$ amplitude relation (2.46) by explicitly proving the corresponding necessary statements made in Sect. 2.2.3 (cf. [13, 139, 140]).

To begin with, we explicitly demonstrate that the sources for both strong and electromagnetic isospin breaking as given in Chap. 1 comprise the necessary $\Delta I = 1$ operators. For this purpose, let us recall the fact that the pions transform like (iso-)vectors under isospin rotations; more specifically, in the Cartesian basis $\pi^k \mapsto R^{ka}\pi^a$ with $R \in O(3)$ (i.e. under the representation $\mathcal{D}^1$ of $SU(2)$).

The strong isospin-breaking operator from $\mathcal{H}_{\text{QCD}} = \bar{q}\mathcal{M}q$ in (1.1) entails the difference $(\bar{u}u - \bar{d}d) = \bar{q}\lambda^3 q$, where $\mathcal{M}$ denotes the quark mass matrix defined in (2.3), $\lambda^3 = \text{diag}(1, -1, 0)$ is the third Gell-Mann matrix, and $q = (u, d, s)^T$ collects the light and strange quark field operators. The latter transform as $q \mapsto Uq$ with $U \in SU(3)$, so that $\bar{q}\lambda^n q \mapsto \bar{q}U^\dagger\lambda^n Uq$. For pure u–d isospin rotations, i.e. $\lambda^n = \text{diag}(\tau^n, 0)$ with Pauli matrices τ^n for $n \in \{1, 2, 3\}$ and $U = \text{diag}(V, 1)$ with $V \in SU(2)$, one has

$$\left(U^\dagger\lambda^n U\right)^\dagger = U^\dagger\lambda^n U = \text{diag}\left(\tilde{V}, 0\right) = \tilde{R}^{nd}\lambda^d \,, \tag{B.1}$$

where $\tilde{V} \in SU(2)$, $\text{tr}\,\tilde{V} = 0$, $d \in \{1, 2, 3\}$, and some real 3×3 coefficient matrix $\tilde{R}$, since the Gell-Mann (Pauli) matrices form a basis of the traceless $SU(3)$ $(SU(2))$ matrices. From

$$\text{tr}\left\{U^\dagger\lambda^k U U^\dagger\lambda^l U\right\} = \text{tr}\left\{\lambda^k\lambda^l\right\} = 2\delta^{kl} \,, \tag{B.2}$$

which is valid for all λ^a with $a \in \{1, 2, \ldots, 8\}$, on the one hand and

$$\text{tr}\left\{U^\dagger\lambda^k U U^\dagger\lambda^l U\right\} = \text{tr}\left\{\tilde{R}^{km}\lambda^m \tilde{R}^{ln}\lambda^n\right\} = \tilde{R}^{km}\tilde{R}^{ln}2\delta^{mn} = 2(\tilde{R}\tilde{R}^T)^{kl} \tag{B.3}$$

on the other hand, one can conclude that $\tilde{R}\tilde{R}^T = \mathbb{1}$ and hence $\tilde{R} \in O(3)$, too. Thus, these pure isospin rotations can be uniformly described by a matrix $R \in O(3)$ *both* for the pions and the light quarks, i.e. the operator $\bar{q}\lambda^n q$ transforms exactly as a pion, $\bar{q}\lambda^n q \mapsto R^{nd}\bar{q}\lambda^d q$, and carries the quantum numbers $I = 1$ and $I^3 = 0$ (the latter following from $\bar{q}q$ being neutral, cf. the Gell-Mann–Nishijima formula $Q = I^3 + Y/2$ discussed in Sect. 2.2.3). Accordingly, it generates transitions between states with $\Delta I = 1$ and $\Delta I^3 = 0$, thus violating the conservation of the total isospin but conserving its third component (i.e. the electromagnetic charge).

The electromagnetic isospin-breaking operator corresponding to $\mathcal{H}_{\text{QED}}$ in (1.2), in turn, comprises a virtual-photon propagator and two electromagnetic currents, which in terms of the quark field operators and the quark charge matrix defined in (2.7) read $j_\mu = \bar{q}\frac{Q}{e}\gamma_\mu q$, thus also containing the difference $\bar{q}\lambda^3 q$. Furthermore, according to the Gell-Mann–Nishijima formula these currents can be decomposed into an isovector component j_μ^3 and an isoscalar component j_μ^Y as $j_\mu = j_\mu^3 + j_\mu^Y/2$. Since the product $j_\mu j_\nu$ is even under charge conjugation, only the interference term $(j_\mu^3 j_\nu^Y + j_\mu^Y j_\nu^3)$ (corresponding to $I = 1$) carries the proper G-parity of -1. Moreover, from charge conservation it is clear that it must have $I^3 = 0$, so that again $\Delta I = 1$ and $\Delta I^3 = 0$.

Therefore, we can conclude that for *both* strong and electromagnetic leading-order isospin breaking the corresponding operator transforms as an isovector like the pions and is neutral, which means that it carries the isospin component index 3 (referring to the Cartesian basis). Since the pion states in the charge basis and the Cartesian basis are simply linear combinations of each other, see [#1] of Chap. 2, we can generically write (cf. (2.27))

$$i\,(2\pi)^4\delta^{(4)}(p_\eta - p_{\text{out}})\mathcal{A}^{klm}(s_1, s_2, s_3) = \langle\pi_1^k\pi_2^l\pi_3^m|\eta\rangle = \langle\pi_1^k\pi_2^l\pi_3^m|\widehat{\mathcal{O}}_{e^2,\delta}^{\,n=3}|\eta\rangle + \mathcal{O}(e^4, e^2\delta, \delta^2) \;, \tag{B.4}$$

where the three outgoing pions have to be in a state with total $I = 1$ and $I^3 = 0$. Neglecting isospin-breaking corrections beyond the leading order already contained in $\widehat{\mathcal{O}}_{e^2,\delta}^{\,n=3}$, we have invariance under isospin rotations,[#1]

$$A^{klm,n} = i\,(2\pi)^4\delta^{(4)}(p_\eta - p_{\text{out}})\mathcal{A}^{klm,n}(s_1, s_2, s_3) = \langle\pi_1^k\pi_2^l\pi_3^m|\widehat{\mathcal{O}}_{e^2,\delta}^{\,n}|\eta\rangle = R^{ka}R^{lb}R^{mc}R^{nd}A^{abc,d} \;. \tag{B.5}$$

Defining row vectors of the rotation matrix R via $w^a = R^{ka}$, $x^b = R^{lb}$, $y^c = R^{mc}$, and $z^d = R^{nd}$ depending on the isospin indices $k, l, m, n \in \{1, 2, 3\}$ (thus at least two of the four vectors $\mathbf{w}, \mathbf{x}, \mathbf{y}, \mathbf{z}$ are identical), the previous equation can be rewritten as

$$f(\mathbf{w}, \mathbf{x}, \mathbf{y}, \mathbf{z}) = w^a x^b y^c z^d A^{abc,d} \;. \tag{B.6}$$

Another rotation by R then amounts to the inverse rotation R^T acting on each of the four argument vectors,

$$f(\mathbf{w}, \mathbf{x}, \mathbf{y}, \mathbf{z}) \mapsto w^a x^b y^c z^d R^{ao}R^{bp}R^{cq}R^{dr}A^{opq,r} = (R^T\mathbf{w})^o(R^T\mathbf{x})^p(R^T\mathbf{y})^q(R^T\mathbf{z})^r A^{opq,r}$$
$$= f(R^T\mathbf{w}, R^T\mathbf{x}, R^T\mathbf{y}, R^T\mathbf{z}) \;, \tag{B.7}$$

and since f is required to be invariant under such rotations, it can only depend on scalar products of these vectors. As f depends linearly on all of its arguments, moreover, we can decompose it according to

$$f(\mathbf{w}, \mathbf{x}, \mathbf{y}, \mathbf{z}) = (\mathbf{z} \cdot \mathbf{w})(\mathbf{x} \cdot \mathbf{y})A_1 + (\mathbf{z} \cdot \mathbf{x})(\mathbf{w} \cdot \mathbf{y})A_2 + (\mathbf{z} \cdot \mathbf{y})(\mathbf{w} \cdot \mathbf{x})A_3 \;, \tag{B.8}$$

where the scalar products reduce to e.g.

$$(\mathbf{z} \cdot \mathbf{w})(\mathbf{x} \cdot \mathbf{y}) = (R^{nd}R^{kd})(R^{lb}R^{mb}) = (RR^T)^{nk}(RR^T)^{lm} = \delta^{nk}\delta^{lm} \tag{B.9}$$

and in analogy for the others, so that

$$A^{klm,n} = \delta^{nk}\delta^{lm}A_1 + \delta^{nl}\delta^{mk}A_2 + \delta^{nm}\delta^{kl}A_3 \;. \tag{B.10}$$

[#1]In principle, the following relations with general n also apply to $\pi\pi$ scattering.

With the definitions $A_i = i\,(2\pi)^4 \delta^{(4)}(p_\eta - p_{\text{out}})\mathcal{A}_i$ (cf. (B.5)) we therefore have

$$\langle \pi_1^k(p_1)\pi_2^l(p_2)\pi_3^m(p_3)|\widehat{\mathcal{O}}_{e^2,\delta}^{\,n}|\eta(p_\eta)\rangle = i\,(2\pi)^4 \delta^{(4)}\big(p_\eta - (p_1 + p_2 + p_3)\big) \tag{B.11}$$

$$\times \Big[\delta^{nk}\delta^{lm}\mathcal{A}_1(s_1, s_2, s_3) + \delta^{nl}\delta^{mk}\mathcal{A}_2(s_1, s_2, s_3) + \delta^{nm}\delta^{kl}\mathcal{A}_3(s_1, s_2, s_3)\Big]\,.$$

From the invariance of the full amplitude $\mathcal{A}^{klm,n}(s_1, s_2, s_3)$ under permutations of the outgoing pions we can conclude for each pion π_i with $i \in \{1, 2, 3\}$ by simultaneously interchanging both the isospin indices and the 4-momenta of the *other* two pions (thus also interchanging the respective Mandelstam variables), that $\mathcal{A}_i$ is invariant under this operation whereas the other two amplitudes are interchanged, e.g. for $i = 1$

$$l \leftrightarrow m \quad \text{and} \quad p_2 \leftrightarrow p_3 \quad (s_2 \leftrightarrow s_3) \quad \Rightarrow \quad \mathcal{A}_1(s_1, s_2, s_3) = \mathcal{A}_1(s_1, s_3, s_2) \quad \text{and}$$
$$\mathcal{A}_2(s_1, s_2, s_3) = \mathcal{A}_3(s_1, s_3, s_2) \tag{B.12}$$

and in analogy for the cyclic permutations of 123. Combining these relations yields

$$\mathcal{A}^{klm,n}(s_1, s_2, s_3) = \delta^{nk}\delta^{lm}\mathcal{A}_1(s_1, s_2, s_3) + \delta^{nl}\delta^{mk}\mathcal{A}_1(s_2, s_3, s_1) + \delta^{nm}\delta^{kl}\mathcal{A}_1(s_3, s_1, s_2)\,, \tag{B.13}$$

resembling the structure of the $\pi\pi$ scattering amplitude for general n, and for the special case $n = 3$ corresponding to $\eta \to 3\pi$ we can read off (cf. (B.4))

$$\mathcal{A}^{311}(s_1, s_2, s_3) = \mathcal{A}^{322}(s_1, s_2, s_3) = A_1(s_1, s_2, s_3) + \mathcal{O}\big(e^4, e^2\delta, \delta^2\big)\,,$$
$$\mathcal{A}^{333}(s_1, s_2, s_3) = A_1(s_1, s_2, s_3) + \mathcal{A}_1(s_2, s_3, s_1) + \mathcal{A}_1(s_3, s_1, s_2) + \mathcal{O}\big(e^4, e^2\delta, \delta^2\big)\,. \tag{B.14}$$

With $|\pi^0\rangle = |\pi^3\rangle$ (up to isospin breaking corrections, cf. Sect. 2.1.2 and [1] of Chap. 2) and

$$|\pi^\pm\rangle = \frac{1}{\sqrt{2}}\Big\{|\pi^1\rangle \pm i|\pi^2\rangle\Big\} \quad \Rightarrow \quad |\pi^0\rangle|\pi^+\rangle|\pi^-\rangle = \frac{1}{2}|\pi^3\rangle\Big\{|\pi^1\rangle|\pi^1\rangle + |\pi^2\rangle|\pi^2\rangle\Big\} \tag{B.15}$$

leading to the identifications[2]

$$\mathcal{A}_n(s_1, s_2, s_3) = \mathcal{A}^{333}(s_1, s_2, s_3)\,, \qquad \mathcal{A}_1(s_1, s_2, s_3) = A_c(s_1, s_2, s_3)\,, \tag{B.16}$$

we thus can eventually infer the $\Delta I = 1$ amplitude relation (2.46).

---

[2] Using the spherical convention (i.e. the Condon–Shortley phase convention), on the contrary, the additional sign for $|\pi^+\rangle$ yields $\mathcal{A}_1(s_1, s_2, s_3) = -A_c(s_1, s_2, s_3)$ and thus an overall sign on the RHS of the $\Delta I = 1$ amplitude relation (2.46).

Part II

Roy–Steiner equations for πN scattering[‡]

Chapter 6

Introduction

Pion–nucleon (πN) scattering is one of the most basic and fundamental processes in hadron physics. On the theoretical side it serves as the prototype reaction of meson–baryon scattering, and on the experimental side its good accessibility has enabled the collection of a large data basis. Consequently, a cornucopia of methods (e.g. dispersion relations, resonance models, quark models, and chiral perturbation theory (ChPT), just to name a few) have been utilized in a multitude of investigations for many decades. Nevertheless, the πN scattering amplitude is still not known to sufficient precision in the low-energy region.[#1] This imbalance is most evident in the scalar-isoscalar sector, which features the so-called pion–nucleon σ-term $\sigma_{\pi N}$, whose value is a measure of the light quark contribution to the nucleon mass (and it can also be related to its strange-quark contribution), see e.g. the classical paper [146]. To be specific, $\sigma_{\pi N}$ is defined as the value of the nucleon form factor $\sigma(t)$ of the scalar quark current $\hat{m}(\bar{u}u + \bar{d}d)$, which is thus also called the scalar form factor of the nucleon, at zero momentum transfer t and hence explicitly reads

$$\sigma_{\pi N} = \sigma(0) \, , \qquad\qquad \hat{m} = \frac{m_u + m_d}{2} \, ,$$

$$\sigma(t) = \frac{1}{2m}\big\langle N(p')\big|\hat{m}(\bar{u}u + \bar{d}d)\big|N(p)\big\rangle \, , \qquad\qquad t = (p' - p)^2 \, , \qquad (6.1)$$

where $\hat{m}$ denotes the average light quark mass and m the nucleon mass. Besides its pivotal role in accounting for quark-mass effects in low-energy hadron physics, the πN σ-term has also gained renewed interest as it parameterizes the spin-independent cross section for possible dark matter candidates scattering off nuclei [147, 148] (for a recent review cf. [149]). In principle, lattice quantum chromodynamics (QCD) would be the method of choice to pin down $\sigma_{\pi N}$ via a precise ab initio calculation — however, a direct computation of the scalar form factor necessarily involves contributions from quark-line disconnected diagrams (that feature importantly in isoscalar quantities in general) which is not yet under sufficient control. Similarly, the indirect extraction of the σ-term from the derivative of the nucleon mass is still hampered with systematic uncertainties related to the chiral extrapolations utilized, see e.g. [150]. Therefore, in this work we follow an alternative approach, namely setting up the powerful, dispersive machinery of Roy–Steiner (RS) equations, that will ultimately allow for a precise determination of the πN scattering amplitude in the low-energy region.

[#1]The exceptions, however, are the S-wave scattering lengths, which can be extracted with high precision from the beautiful data on pionic hydrogen and pionic deuterium, see [142–145].

Roy–Steiner equations, more specifically, are coupled integral equations for partial-wave amplitudes (partial waves) interrelated by crossing symmetry and unitarity relations, that are based on hyperbolic dispersion relations (HDRs), a particular kind of dispersion relations along hyperbolae in the Mandelstam plane. Generally, dispersion relations are a widely used tool that is built upon very general principles, such as Lorentz invariance, unitarity, crossing symmetry, and analyticity (the latter being closely related to causality). There are multiple uses of dispersion relations — they can be used for instance to stabilize extrapolation of experimental data to threshold and allow for a continuation into unphysical regions, as it is e.g. required for the extrapolation of the πN scattering amplitude to the so-called Cheng–Dashen point [151], which in turn is crucial for the extraction of the σ-term. Unitarity constraints, as a matter of principle, can most conveniently be formulated in terms of partial waves. Combining the dispersive concepts with the formalism of partial-wave decomposition leads to the framework of partial-wave dispersion relations (PWDRs), which together with unitarity constraints allows to study processes at low energies with high precision. We just mention a few examples. The most prominent example is of course pion–pion ($\pi\pi$) scattering, which is intimately linked to the spontaneous and explicit chiral symmetry breaking in QCD. Moreover, the pion–pion system, is special as all three channels are identical (i.e. $\pi\pi \to \pi\pi$). Roy equations [52] are the appropriate PWDRs (based on so-called fixed-t dispersion relations), that make explicit use of the full crossing symmetry. They have been extensively studied in the last years [53,152–156], leading to a determination of the fundamental $\pi\pi$ scattering amplitude at low energies with unprecedented precision. The crossing properties are different, however, for the simplest scattering process in QCD involving strange quarks, namely pion–kaon (πK) scattering, where only two channels are identical and one needs to account for both $\pi K \to \pi K$ and $\pi\pi \to \bar{K}K$. Generally, processes involving non-identical particles (so that crossing symmetry intertwines different physical processes) cannot be tackled using conventional Roy equations. For this reason, a combination of fixed-t and hyperbolic dispersion relations was used in [157,158] to construct PWDRs for all channels of πK scattering, which are also referred to as Roy–Steiner equations. As far as crossing symmetry and isospin quantum numbers are concerned, the pion–kaon system is similar to the pion–nucleon case considered here: crossing symmetry relates the s-/u-channel ($\pi N \to \pi N$) and the t-channel ($\pi\pi \to \bar{N}N$) amplitudes, with the s-channel amplitudes being relevant e.g. for σ-term physics, while the t-channel amplitudes feature prominently in the dispersive analysis of the nucleon form factors. In this work, however, we solely consider HDRs, an approach that has already proven useful in the recent construction of RS equations for $\gamma\gamma \to \pi\pi$ [159].

In the low-energy region, the pion–nucleon amplitude is well represented by its projections onto the lowest partial waves, i.e. its S- and P-waves projections, in each channel. Due to the spin of the nucleon, in this approximation one has six partial waves in the s- and u-channel, commonly denoted as $f_{0+}^{\pm}(s)$, $f_{1+}^{\pm}(s)$, and $f_{1-}^{\pm}(s)$, where the superscript $I = \pm$ refers to the isospin, $l \in \{0, 1\}$ in the subscript to the orbital angular momentum, and the $\pm$ to the total angular momentum $j = l \pm 1/2$. Similarly, there are three t-channel S- and P-waves, called $f_+^0(t)$ and $f_\pm^1(t)$, where the superscript refers to total angular momentum J and the subscript $+/-$ to parallel/antiparallel antinucleon–nucleon helicities, such that there is one wave with even and two with odd isospin due to Bose symmetry. It was pointed out in [160] how to generalize the Roy equations for $\pi\pi$ scattering to these nine lowest partial waves of the πN system based on fixed-t dispersion relations. Here, we follow a somewhat different path by utilizing hyperbolic dispersion relations as pioneered by Hite and Steiner a long time ago [161]. The main advantage of HDRs is that they combine the s- and the t-channel (i.e. all three)

physical regions, which is obviously not true for e.g. usual fixed-t dispersion relations. This is most important, since it is known that a reliable continuation to the subthreshold region in dispersion theory can only be made by using input information also from the t-channel, cf. e.g. [162–165]. Furthermore, the knowledge of the absorptive (i.e. imaginary) parts in the hyperbolic dispersion relations is needed only in regions where the corresponding partial-wave expansions converge, and HDRs are considered the best choice fulfilling these requirements that yields still manageable angular kernels without introducing kinematical cuts into the amplitudes [161]. In addition, the underlying hyperbolic relation $(s - a)(u - a) = b$ (with a and b real-valued parameters) also explicitly respects the $s \leftrightarrow u$ crossing symmetry of the πN amplitude. Moreover, examining the domain of validity of the dispersion relations based on the assumption of Mandelstam analyticity, better convergence properties can be achieved with HDRs due to the tunable parameters a and b. Last but not least, HDRs are found to be especially powerful for determining the σ-term [162].

Another important issue is the possibility to subtract dispersion relations. This can be advantageous for various reasons: first, in some cases the asymptotic behavior of the integrand is such that subtractions have to be performed to ensure convergence of the dispersive integral. Similarly, if the high-energy behavior is not known, it can be subsumed in subtraction constants, which are a priori unknown. In some cases, these subtraction constants can be related to phenomenology or the parameters of a low-energy effective field theory like e.g. ChPT. Second, one can even introduce subtractions that are not necessarily required by the asymptotic behavior in order to lessen the dependence on high-energy input, however, at the expense of introducing the corresponding subtraction polynomials. Third, subtracting the dispersion relations is especially useful in the πN case, since subtracting at the so-called subthreshold point allows for a relation to the subthreshold expansion (the subtraction constants can be identified with the subthreshold parameters in this case) and is convenient for the continuation to the Cheng–Dashen point. Additionally, such subtractions are particularly well suited for the t-channel subproblem to be discussed later on. In what follows, we will consider unsubtracted as well as subtracted versions of the RS equations.

The derivation of the (subtracted) RS equations for the πN system is given by a series of steps: first, one expands the s-/t-channel absorptive parts of the (subtracted) HDRs in s-/t-channel partial waves, respectively. Second, one projects the full, partial-wave-expanded HDRs onto both s- and t-channel partial waves, resulting in a closed system of coupled integral equations in the form of partial-wave hyperbolic dispersion relations (PWHDRs) for both channels — the RS equations. The corresponding subset of the RS equations for either the s-channel partial waves $f_{l\pm}^I(s)$ or the t-channel partial waves $f_\pm^J(t)$ together with the according unitarity relation then constitutes what we will refer to as the s- and t-channel part of the RS system in the following, respectively. The closed system of RS equations exhibits the following general structure: it features the nucleon-pole-term (i.e. Born-term) contributions, integrals over the imaginary parts of the s-(and u-)channel as well as integrals over t-channel absorptive parts, both from the corresponding threshold to infinity.[#2] The generic properties of the equations are then determined by the integral kernels, that result from the original HDR kernels via this successive partial-wave expansion and projection scheme. In particular, these kernel functions automatically incorporate the analytic properties expected for general PWDRs: in the equation for each partial wave, the corresponding kernels for the given channel

---

[#2]In fact, the t-channel integrals start at the $\pi\pi$ threshold rather than at the $\bar{N}N$ threshold, i.e. below the physical region of $\pi\pi \to \bar{N}N$, which has important consequences for the t-channel part of the RS system.
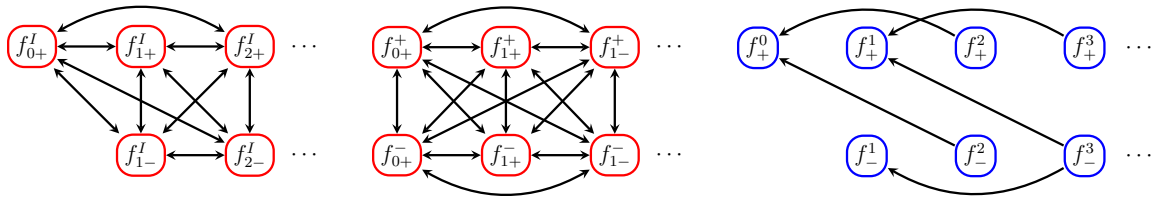
Figure 6.1: Recoupling structure of the s- and t-channel partial waves in the Roy–Steiner system for πN scattering. Left: s-channel, integral kernels only. Center: s-channel, integral kernels and unitarity relations. Right: t-channel, independent of unitarity relations. See main text for details.

consist of the self-coupling, singular Cauchy kernel corresponding to the right-hand cut and an analytic remainder involving in addition the coupling to (at least in principle) all other partial waves of the given channel, while the coupling to the partial waves of the other channel is always analytic. The remainder (together with these crossed-channel terms) contains all left-hand-cut contributions for the channel at hand, especially the contributions from all higher partial waves (i.e. those partial waves not taken into account dynamically) usually called driving terms. The recoupling structure of the partial waves of a particular channel as encoded in the integral kernels turns out to be quite different for s- and t-channel, see Fig. 6.1: while in the s-channel (left) basically all partial waves are coupled with each other (only the even and odd isospin states $I = +$ and $I = -$ are not intertwined by the kernels), for the t-channel (right) the recoupling scheme is much simpler, since Bose symmetry enforces the separation of partial waves with even and odd J (corresponding in our case to t-channel isospin states $I_t = 0$ and $I_t = 1$, respectively, which in turn relate to $I = +$ and $I_t = 1$). Moreover, only higher partial waves contribute to lower ones (thereby qualifying the recoupling scheme also as an ordering scheme), and the $f_+^J(t)$ do not affect the $f_-^J(t)$. However, the interrelation of the partial waves of a given channel is not only determined by the integral kernels but also by the corresponding unitarity relations. In fact, the s-channel unitarity relations are diagonal only in the s-channel isospin basis $I_s \in \{1/2, 3/2\}$ and thus they mix up the $I = \pm$ states yielding the complicated (though symmetric) scheme displayed in Fig. 6.1 (center).[#3] Fortunately, for the t-channel the unitarity relations are diagonal already for the $f_\pm^J(t)$ so that the recoupling structure shown in Fig. 6.1 (right) is also valid for the complete t-channel part of the RS system, which will enable us to recast the t-channel subproblem into the form of a Muskhelishvili–Omnès (MO) problem [166, 167]. Once the t-channel MO problem is solved, the remaining s-channel RS equations take the form of Roy-type equations, so that known results concerning existence and uniqueness of solutions [168, 169] may be transferred as well.

Next, we will outline the strategy to solve the (subtracted) RS system as depicted in Fig. 6.2: generally, in both the s- and t-channel part of the RS system one actually solves the equations in the low-energy region (not necessarily physical) and for the lowest partial waves only, while the amplitudes in the high-energy region as well as higher partial waves are needed as input. The separation between both energy regions occurs at the so-called matching points s_{m} and t_{m} in the s- and t-channel, respectively. Here, we generically introduce l_{d} and J_{d} to specify the partial waves that are taken into account dynamically (i.e. those with $l \leq l_{\mathrm{d}}$

[#3]Working in the I_s isospin basis, conversely, the kernels couple $I_s = 1/2$ and $I_s = 3/2$ states leading to effectively the same recoupling structure.
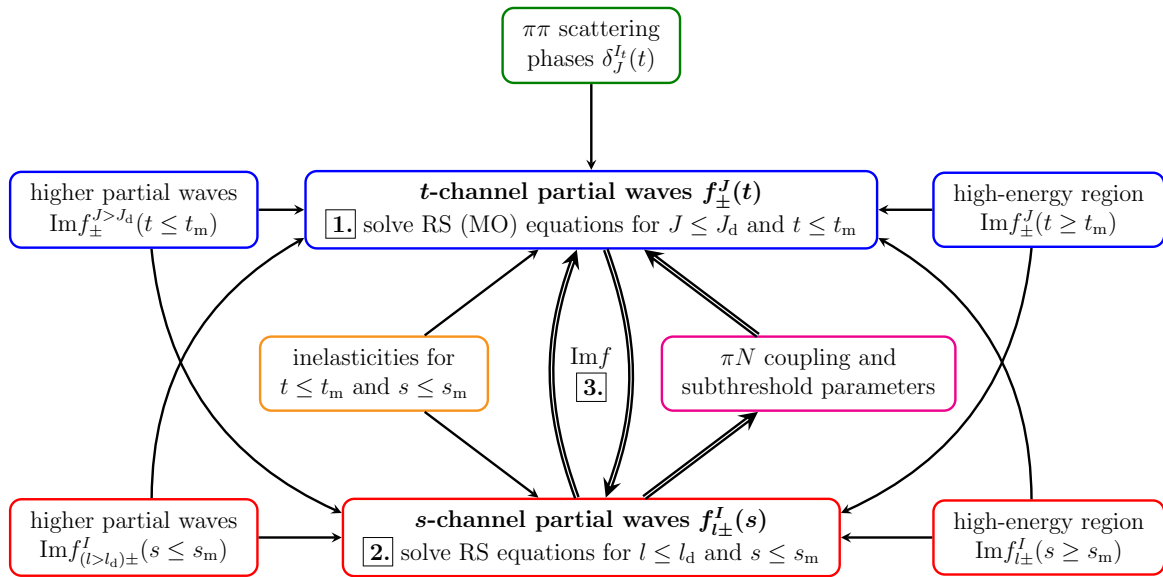
Figure 6.2: Flowchart of the solution strategy for the Roy–Steiner system for πN scattering. Double arrows denote iteration (third step). See main text for details.

and $J \leq J_{\mathrm{d}}$ are solved for). In practice, also the sums over all partial waves in the high-energy regions need to be truncated at some maximal values of l and J. Alternatively, in the asymptotic regions the amplitudes may not be decomposed into partial waves but rather modeled by Regge theory. While the s-channel partial waves are needed as input only in the physical region, where they are well known, the t-channel partial waves are needed already above the $\pi \pi$ threshold and thus far in the unphysical region. Thus, one first solves the t-channel part of the (subtracted) RS system by solving the corresponding MO problem for the lowest, less well determined t-channel partial waves using the better known s-channel partial waves and $\pi \pi$ phase shifts as input (along with starting values for the πN coupling constant as well as the pertinent subtraction constants that enter the subtracted HDRs as parameters) in order to arrive at reasonable solutions for t-channel partial waves as a starting point. Then, one uses these t-channel MO solutions to solve the s-channel part, thereby determining new values for the constants at hand. Subsequently, the preceding steps are iterated until self-consistency of the partial wave solutions and the according parameters is reached and the results have converged. Eventually, the final aim of solving the full (subtracted) RS system for pion–nucleon scattering is a precise determination of the lowest partial waves for both channels in the low-energy region as well as the pertinent low-energy parameters, such as the πN coupling constant and the subthreshold parameters, and to provide reliable theoretical errors for the fundamental πN scattering amplitude for the first time.[#4]

Due to the complexity of the full problem, we will not yet solve the whole set of RS equations in this work, but concentrate on the t-channel part of the RS system as a first step. The solution of this t-channel subproblem is interesting by itself, as it features in the dispersive analysis of the nucleon electromagnetic form factors as well as the scalar form factor, which

---

[#4]Note that in principle the RS framework furthermore allows for systematic improvements, e.g. by solving for higher partial waves, introducing more subtractions, or incorporating more information on inelasticities.

is, in turn, essential for the extraction of the σ-term. At present, in the unphysical region only the KH80 solution [170, 171] (which is by now more than thirty years old) has been used. It is, however, well-known that this solution does not include more recent and precise data and that the πN coupling constant used there differs significantly from more modern determinations. Furthermore, no analysis of the theoretical uncertainties is performed (apart from an iteration uncertainty, cf. Sect. 15.2.2), which is an absolute requirement for any modern theoretical investigation. In fact, it has even been pointed out that the KH80 analysis seems to suffer from internal inconsistencies [162, 165, 172]. Finally, a consistent set of partial-wave amplitudes for all channels is especially important as far as the σ-term determination is concerned.[#5] Therefore, a new t-channel solution is needed as a first step for solving the full, closed system of coupled PWHDRs.

Our solution strategy for the t-channel MO equations follows [158], however, there is a major difference between $\pi\pi \to \bar{K}K$ and $\pi\pi \to \bar{N}N$ as far as inelasticities in the unitarity relation are concerned, since the pseudophysical region in the πN case is much larger due to the large nucleon mass. In both cases, the first non-negligible contribution besides $\pi\pi$ intermediate states originate from $\bar{K}K$, which play an important role for the S-wave in view of the occurrence of the $f_0(980)$ resonance. For $\pi\pi \to \bar{K}K$ the inelasticities can simply be accounted for by using phase-shift solutions for the corresponding partial waves, while physical input for $\pi\pi \to \bar{N}N$ is only available above the two-nucleon threshold. In this work we will content ourselves with the single-channel approximation of the MO problem. Although we derive a generalized (single-channel) MO formalism with a finite matching point to include also inelastic effects, it turns out that for P-, D-, and higher partial waves even the additional approximation of elasticity (beyond $\pi\pi$) yields reasonable results, while the S-wave turns out to require a full solution of the underlying two-channel Omnès problem, which is discussed in [173].

This work is organized as follows: in Chap. 7 we specify our basic conventions and review the specific HDRs for the Lorentz-invariant amplitudes of πN scattering. The explicit derivation of the s- and t-channel RS equations is then described in full detail in Chaps. 8 and 9, respectively. In Chap. 10 we determine the range of convergence of the RS equations, while Chap. 11 contains a discussion of the treatment of the asymptotic regions in the dispersion integrals. In Chap. 12 we derive the partial-wave unitarity relations for both the s- and t-channel and collect the previous results to state the complete RS system of πN scattering. Subsequently, we explain how the t-channel part of the RS system can be cast into the form of a MO problem by virtue of the threshold behavior of the t-channel partial waves. Chap. 13 deals with the issue of introducing pertinent subtractions to the RS system and thereby the t-channel MO problem. Subtracting at and expanding around the subthreshold point leads to sum rules for the corresponding subthreshold parameters as well as once- and twice-subtracted HDRs, based on which the pertinent analytic results of the previous chapters are also extended to the once- and twice-subtracted cases. In Chap. 14 we derive the generalized (single-channel) MO formalism with both non-vanishing inelasticities and a finite matching point. Chap. 15 is dedicated to the explicit solution of the t-channel MO problem: first, we derive the explicit analytical solutions for the lowest t-channel partial waves. Then we collect all necessary input and discuss the numerical results, including their application to nucleon form factors. Finally, we conclude this work by summarizing the results and giving a short outlook in Chap. 16.

[#5] According to [163], the best method for extracting the sigma term from scattering data is to use partial-wave analyses with strong dispersive constraints and subsequently perform an analytic continuation from the s-channel physical region to the Cheng–Dashen point (preferably along different paths), evaluating the important nearby left-hand cut contributions via t-channel partial waves.

Chapter 7

Preliminaries

7.1 Kinematics

In general, we take the s-channel reaction to be $a + b \to c + d$ and the t-channel reaction to be $a + \bar{c} \to \bar{b} + d$ (or equivalently $\bar{b} + d \to a + \bar{c}$ due to time reversal invariance of strong interactions) with the usual Mandelstam variables

$$
\begin{aligned}
s &= (p_a + p_b)^2 = (p_c + p_d)^2 \ , \\
t &= (p_a - p_c)^2 = (p_d - p_b)^2 \ , \\
u &= (p_a - p_d)^2 = (p_c - p_b)^2 \ ,
\end{aligned}
\tag{7.1}
$$

which are interrelated by the sum of all masses according to

$$
s + t + u = m_a^2 + m_b^2 + m_c^2 + m_d^2 = \Sigma \ . \tag{7.2}
$$

Hence, unless stated otherwise, u is always to be understood as a function of s and t via

$$
u(s,t) = \Sigma - s - t \ . \tag{7.3}
$$

The cosines of the center-of-mass-system (CMS) scattering angles for s- and t-channel read

$$
z_s = \cos \theta_s = \frac{1}{\nu_s} \left\{ (t - u) + \frac{(m_a^2 - m_b^2)(m_c^2 - m_d^2)}{s} \right\} \ , \tag{7.4}
$$

$$
z_t = \cos \theta_t = \frac{1}{\nu_t} \left\{ (s - u) + \frac{(m_a^2 - m_c^2)(m_b^2 - m_d^2)}{t} \right\} \ , \tag{7.5}
$$

with the definitions

$$
\nu_s = 4 p_s^f p_s^i \ , \qquad \nu_t = 4 p_t^f p_t^i \ , \tag{7.6}
$$

where $p^i = |\mathbf{p}^i|$ and $p^f = |\mathbf{p}^f|$ are the magnitudes of the corresponding initial and final CMS 3-momenta. Note that for translating $a + b \to c + d$ into a Feynman diagram, we use the non-cyclic convention (pictorially: $\genfrac{}{}{0pt}{}{a}{b} \times \genfrac{}{}{0pt}{}{c}{d}$, with time going rightwards) yielding (7.1) in order to stick to the usual πN conventions of [171] rather than using the cyclic convention (pictorially: $\genfrac{}{}{0pt}{}{a}{b} \times \genfrac{}{}{0pt}{}{d}{c}$) which leads to symmetric kinematical relations for the s-, t-, and u-channel and is therefore sometimes used in the literature. The cyclic convention is especially favorable when all four particles are identical like e.g. in the case of $\pi\pi$ scattering. It leads for example to a minus

sign in front of the mass term for z_s in (7.4) (cf. [174]) but also to different isospin crossing matrices (compare [174] with [52], see also Sect. 7.2). The non-cyclic convention, on the other hand, is well-suited for $s \leftrightarrow u$ crossing symmetric situations like e.g. πN scattering, with $t = 0$ corresponding to an undeflected pion (i.e. forward scattering) in both the s- and u-channel and thus $z_s(t = 0) = 1 = z_u(t = 0)$ rather than $z_s(t = 0) = 1 = -z_u(t = 0)$ for the cyclic convention (cf. [174]). The physical regions for the s-, t-, and u-channel reactions are restricted to kinematical regions yielding a non-negative value of the Kibble function [175]

$$\Phi = stu - \Sigma^2(\phi_s s + \phi_t t + \phi_u u) = \frac{s}{4}\nu_s^2(1 - z_s^2) = \frac{t}{4}\nu_t^2(1 - z_t^2) , \qquad (7.7)$$

where the three coefficients are given by

$$\Sigma^3 \phi_s = (m_a^2 m_b^2 - m_c^2 m_d^2)(m_a^2 + m_b^2 - m_c^2 - m_d^2) ,$$
$$\Sigma^3 \phi_t = (m_a^2 m_c^2 - m_b^2 m_d^2)(m_a^2 + m_c^2 - m_b^2 - m_d^2) ,$$
$$\Sigma^3 \phi_u = (m_a^2 m_d^2 - m_b^2 m_c^2)(m_a^2 + m_d^2 - m_b^2 - m_c^2) . \qquad (7.8)$$

Furthermore, based on the totally symmetric Källén function

$$\lambda(a, b, c) = a^2 + b^2 + c^2 - 2(ab + bc + ca) , \qquad (7.9)$$

we can define the generic kinematical function

$$\lambda_x^{PQ} = \lambda\big(x, M_P^2, M_Q^2\big) = \big[x - (M_P - M_Q)^2\big]\big[x - (M_P + M_Q)^2\big] , \qquad (7.10)$$

and for equal masses

$$\sigma_x^P = \sigma\big(x, M_P^2\big) = \frac{\sqrt{\lambda_x^{PP}}}{x} = \sqrt{1 - \frac{4M_P^2}{x}} . \qquad (7.11)$$

In the case of πN scattering, we have $m_a = m_c = M_\pi$ for the pion and $m_b = m_d = m_N = m$ for the nucleon and introduce the general definitions[#1]

$$\Sigma = 2(m^2 + M_\pi^2) = 2s_0 , \quad \nu(s,t) = \frac{s - u}{4m} = \frac{2s + t - \Sigma}{4m} = \frac{2(s - s_0) + t}{4m} ,$$
$$W^2 = s , \qquad \nu_B(t) = -\frac{s + u - 2m^2}{4m} = \frac{t - 2M_\pi^2}{4m} = \nu(s = m^2, t) , \quad (7.12)$$

with W as the total CMS energy, as well as the abbreviation

$$\lambda_x = \lambda_x^{\pi N} = \lambda\big(x, m^2, M_\pi^2\big) = \big[x - s_-\big]\big[x - s_+\big] , \qquad s_\pm = W_\pm^2 = (m \pm M_\pi)^2 , \qquad (7.13)$$

where W_- and W_+ denote the pseudothreshold and threshold energies, respectively. Note that we will always use the masses of [176], where the isospin limit is defined via the charged particles, i.e. $M_\pi \equiv M_{\pi^\pm}$ for the pion mass and $m \equiv m_{\rm p}$ for the nucleon mass (later also $M_K \equiv M_{K^\pm}$ for the kaon mass). Further related useful definitions and relations read

$$\Sigma_\pm = m^2 \pm M_\pi^2 , \qquad \Sigma_+ = s_0 , \qquad \Sigma_- = W_+ W_- , \qquad \Sigma_-^2 = s_+ s_- , \qquad \Sigma = s_+ + s_- = 2s_0 . \qquad (7.14)$$

[#1]For more on πN kinematics and for πN conventions in general we refer to [171]. Note that the convention for ν therein and which we have adopted here differs from the choice $\nu = s - u$ of e.g. [161].

For the elastic s-channel reaction $\pi N \to \pi N$ with CMS momentum $p_s^f = q = p_s^i$, CMS total energy W, and CMS nucleon energy E the kinematics above threshold (i.e. for $s \geq s_+$) are given by

$$\nu_s(s) = 4q^2 = s - \Sigma + \frac{\Sigma_-^2}{s} \,, \qquad\qquad q(s) = \sqrt{\frac{\lambda_s}{4s}} \,,$$

$$z_s(s,t) = 1 - \frac{s + u - \Sigma}{2q^2} = 1 + \frac{t}{2q^2} \,, \quad E(\pm W) = \pm\sqrt{m^2 + q^2} = \frac{s + \Sigma_-}{2(\pm W)} = \pm E(W) \,. \quad (7.15)$$

For the t-channel reaction $\pi\pi \to \bar{N}N$ (or equivalently $\bar{N}N \to \pi\pi$) with CMS momenta $p_t^i = q_t$ (pions) and $p_t^f = p_t$ (nucleons) the kinematics above threshold (i.e. for $t \geq 4m^2 = t_N$) simplify to

$$\nu_t(t) = 4p_t q_t \,, \qquad\qquad q_t(t) = \sqrt{\frac{t}{4} - M_\pi^2} = \frac{\sqrt{t}}{2}\sigma_t^\pi = +iq_- \,,$$

$$z_t(s,t) = \frac{s-u}{\nu_t} = \frac{2s + t - \Sigma}{4p_t q_t} = \frac{m\nu}{p_t q_t} \,, \qquad p_t(t) = \sqrt{\frac{t}{4} - m^2} = \frac{\sqrt{t}}{2}\sigma_t^N = +ip_- \,, \quad (7.16)$$

where below the corresponding two-particle thresholds t_π and t_N one has to use the quantities

$$q_-(t) = \sqrt{M_\pi^2 - \frac{t}{4}} \geq 0 \quad \forall t \leq t_\pi = 4M_\pi^2 \,, \qquad p_-(t) = \sqrt{m^2 - \frac{t}{4}} \geq 0 \quad \forall t \leq t_N = 4m^2 \,,$$
$$(7.17)$$

whose phases are constrained in general to $p_t q_t = -p_- q_-$ and fixed here by convention. In order to be able to write down relation that are valid in all kinematical ranges we can use the general, always real but potentially negative quantities

$$q_t^2(t) = \frac{t - t_\pi}{4} = -q_-^2(t) \,, \qquad p_t^2(t) = \frac{t - t_N}{4} = -p_-^2(t) \,, \qquad (7.18)$$

from which roots in the corresponding regimes may be taken.

The Kibble function Φ describing the boundaries between physical (real) and unphysical (imaginary) CMS scattering angles simplifies for πN scattering to

$$\frac{\Phi}{t} = su - \Sigma_-^2 = 4sq^2(1 + z_s) = 4p_t^2 q_t^2(1 - z_t^2) \,, \qquad (7.19)$$

such that the boundaries are given by

$$\Phi = -s\Big[u - (\Sigma - s)\Big]\Big[u - \frac{\Sigma_-^2}{s}\Big]$$
$$= \frac{t}{4}\Big[t - \Big(\Sigma - 2\sqrt{(2m\nu)^2 - \Sigma_-^2}\Big)\Big]\Big[t - \Big(\Sigma + 2\sqrt{(2m\nu)^2 - \Sigma_-^2}\Big)\Big] = 0 \,, \qquad (7.20)$$

and the corresponding physical regions are shown in Fig. 7.1, which also clearly shows the $s \leftrightarrow u$ crossing symmetry.

The four Lorentz-invariant amplitudes $A^\pm(s,t)$ and $B^\pm(s,t)$ describing πN scattering in the isospin limit, as well as the related amplitudes $D^\pm(s,t)$ convenient for low-energy theorems are defined in (7.22). These amplitudes are real inside the Mandelstam subthreshold triangle defined by the lines $s = s_+$, $u = s_+$, and $t = t_\pi$, i.e. below the thresholds for the physical s- and u-channel reactions and below the $\pi\pi$ scattering threshold, including in particular the small
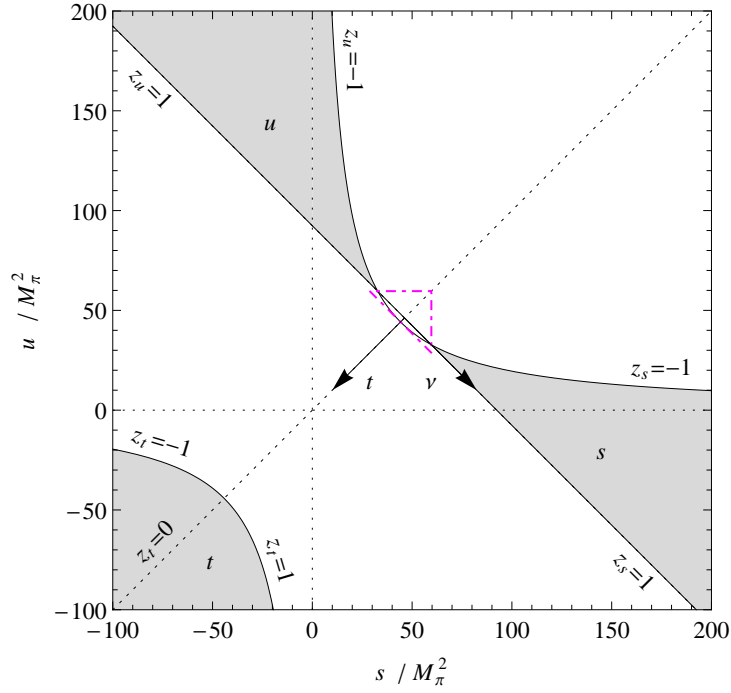
Figure 7.1: Physical regions for s-, t-, and u-channel reactions of πN scattering (shaded) and subthreshold triangle (dot-dashed) enclosing subthreshold lens.

on-mass-shell (on-shell) but unphysical lens-shaped low-energy region close to $(\nu = 0, t = 0)$ (so-called subthreshold lens, cf. Fig. 7.1) especially important for πN scattering low-energy theorems.[#2]

The analytic structure of the invariant amplitudes governs the analytic structure of both the s- and t-channel partial-wave amplitudes, for details we refer to [171] and references therein. Here, we only mention the different analytic structures of the s-channel πN scattering invariant amplitudes (in the complex s-plane)

- right-hand cut (RHC):
  physical s-channel cut along $s \geq s_+$,

- nucleon pole:
  at $s = m^2$ from s-channel nucleon-exchange pole term $1/(s - m^2)$,

- crossed cut:
  along $s \leq s_-$ as combination of u-channel cut $s \leq s_-$ and t-channel cut $s \leq -\Sigma_-$,

- left-hand cut (LHC):
  collective name for all cuts in the unphysical region, i.e. for $\operatorname{Re}\{s\} < s_+$.

[#2]Note that $t \leq 0$ is necessary for both the s- and u-channel reaction to be physical as can be easily seen for the s-channel from $t = -2q^2(1 - z_s)$ with $q \geq 0$ and $|z_s| \leq 1$ (and due to $s \leftrightarrow u$ crossing symmetry in analogy for the u-channel). Thus, for the u-channel reaction from $u \geq s_+$ follows $s \leq s_-$. Demanding both $s \geq s_+$ and $u \geq s_+$ yields $t \leq -4mM_\pi = s_- - s_+$.

In addition, the mapping between the complex s- and q^2-planes involves a circular cut in the complex s-plane at $|s| = \Sigma_- = s_{(+)}s_{(-)}$, where $s_{(+)}(q^2)$ and $s_{(-)}(q^2)$ are the two solutions

$$s_{(\pm)}(q^2) = 2q^2 + \Sigma_+ \pm 2\sqrt{(q^2 + m^2)(q^2 + M_\pi^2)} \tag{7.21}$$

for a given q^2 (note the cut for $-m^2 \le q^2 \le -M_\pi^2$) with $s_{(+)}(0) = s_+$ and $s_{(-)}(0) = s_-$. This circular cut becomes relevant once amplitudes are considered as functions of q^2 rather than s, e.g. for the partial waves. The additional analytic structures of the s-channel partial-wave amplitudes due to the partial-wave projection are[#3]

- kinematical cuts:
  for $s \le 0$ from terms depending on $W = \sqrt{s}$ in the partial-wave projection formula,

- short nucleon cut:[#4]
  along $\Sigma_-^2/m^2 \le s \le m^2 + 2M_\pi^2$ from evaluating the u-channel nucleon-exchange pole term $1/(u(s, z_s) - m^2)$ for $z_s = \pm 1$,

- circular-cut contributions:
  due to t-channel exchange of particles with mass $m_t \ge 2M_\pi$, i.e. from evaluating $1/(t(s, z_s) - m_t^2)$ for $z_s = \pm 1$ and $m_t^2 = t_\pi$,

- crossed-cut contributions for $s \le 0$ and singularities at $s = 0$:
  from the partial-wave projection of the aforementioned u- and t-channel exchanges.

Finally, some kinematical points of specific interest for low-energy πN scattering are (see for instance [171] and [179])

- (s-channel) threshold point at $(s = s_+, t = 0, u = s_-) \equiv (\nu = M_\pi, \nu_B = -M_\pi^2/(2m))$:
  expansion point for the threshold expansion yielding e.g. the scattering lengths,

- Cheng–Dashen point at $(s = u = m^2, t = 2M_\pi^2) \equiv (\nu = 0, \nu_B = 0)$:
  pivotal for pion–nucleon σ-term physics, since the Born-term-subtracted amplitude[#5] $\bar{D}^+(\nu = 0, t = 2M_\pi^2) = A^+(\nu = 0, t = 2M_\pi^2) - g^2/m$ is related to $\sigma_{\pi N}$ by a low-energy theorem [151, 160, 180–182],[#6]

- (s-channel) subthreshold point at $(s = u = s_0, t = 0) \equiv (\nu = 0, \nu_B = -M_\pi^2/(2m))$:
  expansion point for the subthreshold expansion yielding the subthreshold parameters (cf. Sect. 13.1); w.r.t. corresponding soft-pion theorems also called Adler–Weisberger [180, 183, 184] or "anti Cheng–Dashen" [115, 116, 151, 185] point, the latter due to the phenomenological observation $\bar{D}^+(\nu = 0, t = 0) \approx -\bar{D}^+(\nu = 0, t = 2M_\pi^2)$ which is also in line with assuming both pions to be soft.[#7]

[#3]In [177] it was shown how to construct PWDRs solely via the singularity structure in the complex s-plane.

[#4]Actually, there are two short nucleon cuts as discussed in the appendix of [178]. The second one, however, is situated on an unphysical sheet.

[#5]For the invariant amplitudes, a bar usually denotes the subtraction of the corresponding pseudovector Born term, while a tilde denotes the subtraction of the pertinent pseudoscalar Born term.

[#6]Note that since $z_s^{\mathrm{CD}} = z_s(m^2, 2M_\pi^2) = -M_\pi^2/(4m^2 - M_\pi^2) \approx -5.56 \times 10^{-3}$ is close to zero, the amplitudes at the Cheng–Dashen point are dominated by the (s-channel) S-wave.

[#7]The general definition $\nu_B(t, q_i^2, q_f^2) = (t - q_i^2 - q_f^2)/(4m)$ with 4-momenta q_i and q_f for the pion in the initial and final state, respectively, reduces for the on-shell case $\nu_B(t, M_\pi^2, M_\pi^2) = \nu_B(t)$ to (7.12), while e.g. the case of two soft pions (i.e. $q_i \to 0$ and $q_f \to 0$) yields $\nu_B = t/(4m)$. Thus, the preferable choice of variables in the low-energy region, which is independent of soft-pion considerations, is (ν, t), see also [185].

7.2   Isospin structure

The most general Lorentz-invariant and parity-conserving T-matrix element for the process $\pi^a(q) + N(p) \to \pi^b(q') + N(p')$ with isospin indices a and b is given in terms of Lorentz-invariant amplitudes A, B, and D according to (in the conventions of [171])

$$T_{fi}^{ba}(s,t) = \frac{1}{2}\{\tau^b, \tau^a\} T_{fi}^+(s,t) + \frac{1}{2}[\tau^b, \tau^a] T_{fi}^-(s,t) = \delta^{ba} T_{fi}^+(s,t) + i\epsilon_{bac}\tau^c T_{fi}^-(s,t) \ ,$$

$$T_{fi}^I(s,t) = \bar{u}_f(p')\left\{ A^I(s,t) + \frac{\slashed{q}' + \slashed{q}}{2} B^I(s,t) \right\} u_i(p) = \bar{u}_f(p')\left\{ D^I(s,t) - \frac{[\slashed{q}', \slashed{q}]}{4m} B^I(s,t) \right\} u_i(p) \ ,$$

$$D^I(s,t) = A^I(s,t) + \nu(s,t) B^I(s,t) \ , \qquad I \in \{+, -\} \ , \tag{7.22}$$

where we have introduced the isospin index $I = +/-$ for the part that is even/odd under interchange of a and b and the normalization is fixed via the spin-averaged CMS differential cross section (see also the discussion in Sect. 7.3)

$$\frac{\mathrm{d}\bar{\sigma}_{\pi N \to \pi N}^I}{\mathrm{d}\Omega} = \frac{1}{2}\sum_{f,i}\left| \frac{T_{fi}^I}{8\pi W} \right|^2 \ . \tag{7.23}$$

Furthermore, the πN scattering amplitudes $\mathcal{A}$ have definite crossing properties under interchange of s and u for fixed t, i.e. under change of sign of ν, such that one can work with amplitudes according to

$$\tilde{\mathcal{A}} = \begin{cases} \mathcal{A} = \mathcal{A}_{\mathrm{ev}} & \text{if } \mathcal{A}(\nu,t) = +\mathcal{A}(-\nu,t) \ , \\ \frac{\mathcal{A}}{\nu} = \frac{\mathcal{A}_{\mathrm{od}}}{\nu} & \text{if } \mathcal{A}(\nu,t) = -\mathcal{A}(-\nu,t) \ , \end{cases} \tag{7.24}$$

which are even functions of ν and thus free of kinematical square root branch cuts in the complex t-plane originating from ν_t. The invariant amplitudes A and B are then related to $\mathcal{A}_{\mathrm{ev/od}}$ via

$$\mathcal{A}_{\mathrm{ev}}(\nu^2, t) = \begin{cases} A^+(\nu^2, t) \ , \\ B^-(\nu^2, t) \ , \end{cases} \qquad \mathcal{A}_{\mathrm{od}}(\nu, t) = \begin{cases} A^-(\nu, t) \ , \\ B^+(\nu, t) \ , \end{cases} \tag{7.25}$$

where the isospin even and odd parts have definite parity under pion-crossing

$$A^\pm(\nu, t) = \pm A^\pm(-\nu, t) \ , \qquad B^\pm(\nu, t) = \mp B^\pm(-\nu, t) \ , \tag{7.26}$$

which is why the isospin index $I \in \{+, -\}$ will be called crossing index, too. Therefore, the amplitudes A^I and B^I can be written as linear combinations

$$\mathcal{A}^\pm = \frac{1}{2}(\mathcal{A}_- \pm \mathcal{A}_+) \qquad \text{for } \mathcal{A} \in \{A, B\} \tag{7.27}$$

of the amplitudes for the accurately measurable reactions with a proton as target particle

$$\mathcal{A}_\pm = \mathcal{A}(\pi^\pm p \to \pi^\pm p) \ , \qquad \mathcal{A}_0 = \mathcal{A}(\pi^- p \to \pi^0 n) \ . \tag{7.28}$$

Due to isospin invariance and by virtue of the Wigner–Eckart theorem (here the special case for tensors of rank zero)

$$\langle I, I_3 | \mathcal{A} | I', I_3' \rangle = \mathcal{A}^I \delta_{II'} \delta_{I_3 I_3'} \ , \tag{7.29}$$

where $I = \sqrt{\mathbf{I}^2}$ denotes the total isospin and $I_3 = (\mathbf{I})_3$ its third component, the amplitudes of all ten πN scattering reactions can be written in terms of only two independent matrix elements with total s-channel isospin index $I_s \in \{1/2, 3/2\}$. In agreement with [171] (i.e. using the usual Condon–Shortley phase convention for the Clebsch–Gordan coefficients [176], but the non-cyclic kinematical convention according to Sect. 7.1) we assign the isospin-doublets of both the nucleons and antinucleons according to the fundamental (2-dimensional) representation of the Lie-algebra of $SU(2)$

$$|p\rangle = \left|\frac{1}{2}, \frac{1}{2}\right\rangle , \qquad |n\rangle = \left|\frac{1}{2}, -\frac{1}{2}\right\rangle , \qquad |\bar{n}\rangle = \left|\frac{1}{2}, \frac{1}{2}\right\rangle , \qquad |\bar{p}\rangle = \left|\frac{1}{2}, -\frac{1}{2}\right\rangle , \tag{7.30}$$

and the isospin-triplet of the pions (i.e. their charge/spherical[#8] eigenstates) according to

$$|\pi^+\rangle = |1, 1\rangle , \qquad |\pi^0\rangle = |1, 0\rangle , \qquad |\pi^-\rangle = |1, -1\rangle , \tag{7.31}$$

which leads to the following properties under charge conjugation C

$$C|p\rangle = |\bar{p}\rangle , \qquad C|n\rangle = -|\bar{n}\rangle , \qquad C|\pi^\pm\rangle = -|\pi^\mp\rangle , \qquad C|\pi^0\rangle = |\pi^0\rangle . \tag{7.32}$$

Thus, the relations between the spherical and the Cartesian components of the pion-multiplet are given by

$$|\pi^\pm\rangle = \mp\frac{1}{\sqrt{2}}(|\pi_1\rangle \pm i|\pi_2\rangle) , \qquad |\pi^0\rangle = |\pi_3\rangle . \tag{7.33}$$

Note that the standard ChPT conventions for the pions

$$|\pi^\pm\rangle = \frac{1}{\sqrt{2}}(|\pi_1\rangle \pm i|\pi_2\rangle) , \qquad |\pi^0\rangle = |\pi_3\rangle , \tag{7.34}$$

which follow from the alternative assignment

$$|\pi^+\rangle = -|1, 1\rangle , \qquad |\pi^0\rangle = |1, 0\rangle , \qquad |\pi^-\rangle = |1, -1\rangle \qquad \Rightarrow \qquad C|\pi\rangle = |\bar{\pi}\rangle , \tag{7.35}$$

corresponding to the adjoint (3-dimensional) representation of the Lie-algebra of $SU(2)$, differ by an additional sign for the $|\pi^+\rangle$ wave function from the spherical convention which we will adopt in the following. By decomposing the initial and final isospin states of the πN system into linear combinations of eigenstates $|I_s, (\mathbf{I}_s)_3\rangle$ in the spherical convention, e.g.

$$|\pi^+ p\rangle = \left|\frac{3}{2}, \frac{3}{2}\right\rangle , \qquad |\pi^- p\rangle = \sqrt{\frac{1}{3}}\left|\frac{3}{2}, -\frac{1}{2}\right\rangle - \sqrt{\frac{2}{3}}\left|\frac{1}{2}, -\frac{1}{2}\right\rangle ,$$

$$|\pi^0 n\rangle = \sqrt{\frac{2}{3}}\left|\frac{3}{2}, -\frac{1}{2}\right\rangle + \sqrt{\frac{1}{3}}\left|\frac{1}{2}, -\frac{1}{2}\right\rangle , \tag{7.36}$$

we can readily obtain the relations between the πN isospin amplitudes

$$\mathcal{A}_+ = \mathcal{A}(\pi^+ p \to \pi^+ p) = \mathcal{A}(\pi^- n \to \pi^- n) = \mathcal{A}^+ - \mathcal{A}^- = \mathcal{A}^{3/2} ,$$

$$\mathcal{A}_- = \mathcal{A}(\pi^- p \to \pi^- p) = \mathcal{A}(\pi^+ n \to \pi^+ n) = \mathcal{A}^+ + \mathcal{A}^- = \frac{1}{3}(2\mathcal{A}^{1/2} + \mathcal{A}^{3/2}) ,$$

$$\mathcal{A}_0 = \mathcal{A}(\pi^- p \to \pi^0 n) = \mathcal{A}(\pi^+ n \to \pi^0 p) = -\sqrt{2}\mathcal{A}^- = -\frac{\sqrt{2}}{3}(\mathcal{A}^{1/2} - \mathcal{A}^{3/2}) ,$$

$$\mathcal{A}(\pi^0 p \to \pi^0 p) = \mathcal{A}(\pi^0 n \to \pi^0 n) = \mathcal{A}^+ = \frac{1}{3}(\mathcal{A}^{1/2} + 2\mathcal{A}^{3/2}) ,$$

$$\mathcal{A}^+ + 2\mathcal{A}^- = \mathcal{A}^{1/2} . \tag{7.37}$$

[#8]The Lie-algebras of $SU(2)$ and $SO(3)$ are isomorphic.

From these we can infer the so-called isospin triangle relation

$$\mathcal{A}_+ - \mathcal{A}_- = \sqrt{2}\mathcal{A}_0 \, , \tag{7.38}$$

and the relations for the isospin even/odd amplitudes with $I = +/-$ and the amplitudes in the s-channel isospin basis $I_s \in \{1/2, 3/2\}$ can be summarized in matrix notation as

$$\begin{pmatrix} \mathcal{A}^+ \\ \mathcal{A}^- \end{pmatrix} = C_{\nu s} \begin{pmatrix} \mathcal{A}^{1/2} \\ \mathcal{A}^{3/2} \end{pmatrix} \, , \qquad \begin{pmatrix} \mathcal{A}^{1/2} \\ \mathcal{A}^{3/2} \end{pmatrix} = C_{s\nu} \begin{pmatrix} \mathcal{A}^+ \\ \mathcal{A}^- \end{pmatrix} \, , \qquad C_{\nu s} = \frac{1}{3} C_{s\nu} = \frac{1}{3} \begin{pmatrix} 1 & 2 \\ 1 & -1 \end{pmatrix} \, . \tag{7.39}$$

The s-channel isospin amplitudes with $I_s \in \{1/2, 3/2\}$ and the corresponding u-channel isospin amplitudes with $I_u \in \{1/2 = N, 3/2 = \Delta\}$ can be shown to obey the $s \leftrightarrow u$ crossing isospin relations (cf. [174])

$$\begin{pmatrix} \mathcal{A}^{1/2} \\ \mathcal{A}^{3/2} \end{pmatrix} = C_{su} \begin{pmatrix} \mathcal{A}^N \\ \mathcal{A}^\Delta \end{pmatrix} \, , \qquad \begin{pmatrix} \mathcal{A}^N \\ \mathcal{A}^\Delta \end{pmatrix} = C_{us} \begin{pmatrix} \mathcal{A}^{1/2} \\ \mathcal{A}^{3/2} \end{pmatrix} \, , \qquad C_{su} = C_{us} = \frac{1}{3} \begin{pmatrix} -1 & 4 \\ 2 & 1 \end{pmatrix} \, , \tag{7.40}$$

and combining this with (7.39) yields

$$\begin{pmatrix} \mathcal{A}^+ \\ \mathcal{A}^- \end{pmatrix} = C_{\nu u} \begin{pmatrix} \mathcal{A}^N \\ \mathcal{A}^\Delta \end{pmatrix} \, , \qquad C_{\nu u} = C_{\nu s} C_{su} = \frac{1}{3} \begin{pmatrix} 1 & 2 \\ -1 & 1 \end{pmatrix} \, , \qquad C_{u\nu} = C_{\nu u}^{-1} = \begin{pmatrix} 1 & -2 \\ 1 & 1 \end{pmatrix} \, . \tag{7.41}$$

For the t-channel reactions, the $|\bar{N}N\rangle$ isospin states are superpositions of the four states $|I_t = 1, (\mathbf{I}_t)_3\rangle$ and $|I_t = 0, 0\rangle$

$$|\bar{n}p\rangle = |1, 1\rangle \, , \qquad\qquad |\bar{p}p\rangle = \frac{1}{\sqrt{2}}\big(|1, 0\rangle - |0, 0\rangle\big) \, ,$$

$$|\bar{p}n\rangle = |1, -1\rangle \, , \qquad\qquad |\bar{n}n\rangle = \frac{1}{\sqrt{2}}\big(|1, 0\rangle + |0, 0\rangle\big) \, , \tag{7.42}$$

from which follows[#9]

$$|1, 0\rangle = \frac{1}{\sqrt{2}}\big(|\bar{n}n\rangle + |\bar{p}p\rangle\big) \, , \qquad |0, 0\rangle = \frac{1}{\sqrt{2}}\big(|\bar{n}n\rangle - |\bar{p}p\rangle\big) \, , \tag{7.43}$$

whereas the decomposition of the $|\pi\pi\rangle$ isospin states reads

$$|\pi^+\pi^0\rangle = \frac{1}{\sqrt{2}}\big(|2, 1\rangle + |1, 1\rangle\big) \, , \qquad |\pi^+\pi^-\rangle = \frac{1}{\sqrt{6}}|2, 0\rangle + \frac{1}{\sqrt{2}}|1, 0\rangle + \frac{1}{\sqrt{3}}|0, 0\rangle \, ,$$

$$|\pi^-\pi^0\rangle = \frac{1}{\sqrt{2}}\big(|2, -1\rangle - |1, -1\rangle\big) \, , \qquad |\pi^0\pi^0\rangle = \sqrt{\frac{2}{3}}|2, 0\rangle - \frac{1}{\sqrt{3}}|0, 0\rangle \, , \tag{7.44}$$

but since $\bar{N}N$ only couples to $I_t = 0$ and $I_t = 1$, the $I_t = 2$ terms do not contribute here and we are left with a symmetric isosinglet

$$|0, 0\rangle = \frac{1}{\sqrt{3}}\big(|\pi^+\pi^-\rangle + |\pi^-\pi^+\rangle - |\pi^0\pi^0\rangle\big) \, , \tag{7.45}$$

[#9]Note that (7.42) and (7.43) are in perfect agreement with the usual Clebsch–Gordan coefficients [176], but differ from [171] where different conventions are used in these and corresponding equations. In particular, the analog of (7.48) in [171] seems to (exceptionally) follow the cyclic kinematical convention. Nevertheless, all other relations, especially the crossing matrix (7.49) and the important relations (7.50), are identical.

and an antisymmetric isotriplet

$$|1,1\rangle = \frac{1}{\sqrt{2}}\left(|\pi^+\pi^0\rangle - |\pi^0\pi^+\rangle\right), \qquad |1,0\rangle = \frac{1}{\sqrt{2}}\left(|\pi^+\pi^-\rangle - |\pi^-\pi^+\rangle\right),$$

$$|1,-1\rangle = \frac{1}{\sqrt{2}}\left(|\pi^0\pi^-\rangle - |\pi^-\pi^0\rangle\right). \tag{7.46}$$

By strictly using the non-cyclic kinematical convention together with the properties under charge conjugation (7.32) we can get the t-channel amplitudes from the s-channel ones via crossing

$$\mathcal{A}_\pm = -\mathcal{A}(\bar{p}p \to \pi^\pm\pi^\mp), \qquad \mathcal{A}_0 = \mathcal{A}(\pi^+n \to \pi^0 p) = -\mathcal{A}(\bar{n}p \to \pi^+\pi^0) = \mathcal{A}(\bar{n}p \to \pi^0\pi^+), \tag{7.47}$$

which together with the s-channel isospin relations (7.37) on the one hand and the t-channel isospin decompositions above on the other hand yields the following relations for the reactions with a proton as target particle

$$\mathcal{A}(\bar{p}p \to \pi^+\pi^-) = -\mathcal{A}_+ \qquad = -\mathcal{A}^+ + \mathcal{A}^- = -\mathcal{A}^{3/2} \qquad = -\frac{1}{\sqrt{6}}\mathcal{A}^0 + \frac{1}{2}\mathcal{A}^1,$$

$$\mathcal{A}(\bar{p}p \to \pi^-\pi^+) = -\mathcal{A}_- \qquad = -\mathcal{A}^+ - \mathcal{A}^- = -\frac{1}{3}(2\mathcal{A}^{1/2} + \mathcal{A}^{3/2}) = -\frac{1}{\sqrt{6}}\mathcal{A}^0 - \frac{1}{2}\mathcal{A}^1,$$

$$\mathcal{A}(\bar{n}p \to \pi^+\pi^0) = -\mathcal{A}_0 \qquad = \sqrt{2}\mathcal{A}^- \qquad = \frac{\sqrt{2}}{3}(\mathcal{A}^{1/2} - \mathcal{A}^{3/2}) \quad = \frac{1}{\sqrt{2}}\mathcal{A}^1,$$

$$\mathcal{A}(\bar{p}p \to \pi^0\pi^0) = \frac{1}{2}(\mathcal{A}_+ + \mathcal{A}_-) = \mathcal{A}^+ \qquad = \frac{1}{3}(\mathcal{A}^{1/2} + 2\mathcal{A}^{3/2}) \quad = \frac{1}{\sqrt{6}}\mathcal{A}^0. \tag{7.48}$$

Thereby we can easily deduce the $s \leftrightarrow t$ crossing isospin relations (cf. [174])

$$\begin{pmatrix} \mathcal{A}^{1/2} \\ \mathcal{A}^{3/2} \end{pmatrix} = C_{st} \begin{pmatrix} \mathcal{A}^0 \\ \mathcal{A}^1 \end{pmatrix}, \qquad\qquad C_{st} = \begin{pmatrix} \frac{1}{\sqrt{6}} & 1 \\ \frac{1}{\sqrt{6}} & -\frac{1}{2} \end{pmatrix},$$

$$\begin{pmatrix} \mathcal{A}^0 \\ \mathcal{A}^1 \end{pmatrix} = C_{ts} \begin{pmatrix} \mathcal{A}^{1/2} \\ \mathcal{A}^{3/2} \end{pmatrix}, \qquad\qquad C_{ts} = \frac{2}{3}\begin{pmatrix} \frac{\sqrt{6}}{2} & \sqrt{6} \\ 1 & -1 \end{pmatrix}, \tag{7.49}$$

and the fact that $\mathcal{A}^+$ and $\mathcal{A}^-$ have well-defined quantum number $I_t = 0$ and $I_t = 1$, respectively,

$$\begin{pmatrix} \mathcal{A}^+ \\ \mathcal{A}^- \end{pmatrix} = C_{\nu t} \begin{pmatrix} \mathcal{A}^0 \\ \mathcal{A}^1 \end{pmatrix}, \qquad C_{\nu t} = C_{\nu s}C_{st} = \begin{pmatrix} \frac{1}{\sqrt{6}} & 0 \\ 0 & \frac{1}{2} \end{pmatrix}, \qquad C_{t\nu} = C_{\nu t}^{-1} = \begin{pmatrix} \sqrt{6} & 0 \\ 0 & 2 \end{pmatrix}. \tag{7.50}$$

Combining charge conjugation C with a rotation by π around the 2-axis of isospin space

$$e^{\pm i\pi I_2}|I,I_3\rangle = (-1)^{I-I_3}|I,-I_3\rangle, \tag{7.51}$$

one can define G-conjugation as (again in the conventions of [171])

$$G = Ce^{-i\pi I_2}, \tag{7.52}$$

which leads to

$$G|\pi\rangle = -|\pi\rangle \quad \Rightarrow \quad G|\pi\pi\rangle = |\pi\pi\rangle, \tag{7.53}$$

and hence the antinucleon–nucleon initial state in the reaction $\bar{N}N \to \pi\pi$ that we are interested in has to be an eigenstate[#10] of G with eigenvalue (G-parity) $+1$, i.e. it can only couple to states with an even number of pions. The result for charge conjugation of an antifermion–fermion or antiboson–boson pair

$$C|\bar{f}f\rangle = (-1)^{L+S}|\bar{f}f\rangle , \qquad C|\bar{b}b\rangle = (-1)^{L}|\bar{b}b\rangle , \tag{7.54}$$

together with (7.51) yields

$$G|\bar{N}N\rangle = (-1)^{J+I_t}|\bar{N}N\rangle , \tag{7.55}$$

from which we can conclude that for reactions with a two-pion final state (i.e. $G = +1$) only the combinations (J even, $I_t = 0$) and (J odd, $I_t = 1$) are allowed. The same combinations arise from the symmetry properties of the isosinglet (7.45) and the isotriplet (7.46) due to the fact that the exchange of two pions in an orbital state with total angular momentum $J = L$ yields a factor of $(-1)^J$. According to (7.50) this leads to the following selection rules for the partial wave decomposition of the t-channel amplitudes: the partial-wave expansion of the amplitudes $\mathcal{A}^{I=+/-}$ or $\mathcal{A}^{I_t=0/1}$ contains only partial waves with even/odd J, respectively, and the transition between the two sets of amplitudes involves the isospin crossing coefficients $c_J = 1/\sqrt{6}$ and $c_J = 1/2$ with

$$c_J = \begin{cases} \frac{1}{\sqrt{6}} & \text{if } J \text{ is even} , \\ \frac{1}{2} & \text{if } J \text{ is odd} . \end{cases} \tag{7.56}$$

7.3 Unitarity and partial-wave amplitudes

In this section we will combine the principle of unitarity with the general helicity partial-wave formalism in order to consolidate the ground on which the partial-wave unitarity relations for πN scattering will be derived later on (cf. Sect. 12.1).[#11] Especially for the additional inelastic contributions to the so-called extended t-channel unitarity relation it will prove essential to take care of the prefactors due to kinematics and indistinguishability of particles accompanying the partial-wave amplitudes.[#12]

From the unitarity of the S-matrix

$$S^{\dagger}S = \mathbb{1} , \qquad S = \mathbb{1} + iT \quad \Rightarrow \quad T - T^{\dagger} = iT^{\dagger}T , \tag{7.57}$$

by taking matrix elements and inserting a complete set of intermediate states one can easily obtain the general unitarity relation

$$\langle f|T|i\rangle - \langle f|T^{\dagger}|i\rangle = i\sum_{\{j\}} \int d\Pi_{n_j}^{(j)}\langle f|T^{\dagger}|j\rangle\langle j|T|i\rangle , \tag{7.58}$$

where $d\Pi_{n_j}^{(j)}$ denotes the n_j-particle Lorentz-invariant phase space (LIPS) for intermediate state j which in the case of n_j identical intermediate particles implicitly includes an additional

---

[#10] Only isospin multiplets with vanishing mean electromagnetic charge $\bar{Q} = 0$ (i.e. $\bar{I}_3 = 0$) are eigenstates of G-conjugation.

[#11] Besides [171] for πN specifics, a good point of reference for general scattering conventions as well as the partial-wave formalism is [186].

[#12] Potentially along with additional factors as following e.g. from isospin considerations, see for instance (7.56) and Sect. 12.1.

symmetry factor $1/S_{n_j}^{(j)} = 1/n_j!$ in order to avoid multiple counting in the phase space integral. From 4-momentum conservation

$$\langle f|T|i\rangle = (2\pi)^4 \delta^{(4)}(\Sigma p_f - \Sigma p_i) T_{fi} \;, \tag{7.59}$$

one can immediately infer the generalized optical theorem for the invariant amplitudes T_{fi}

$$T_{fi} - T_{if}^* = i \sum_{\{j\}} \int d\Pi_{n_j}^{(j)} (2\pi)^4 \delta^{(4)}(\Sigma p_j - \Sigma p_i) T_{jf}^* T_{ji} \;, \tag{7.60}$$

where overall 4-momentum conservation $\delta^{(4)}(\Sigma p_f - \Sigma p_i)$ is implicitly imposed. If the process is invariant under time reversal, as it is the case for strong interactions, (7.60) takes the form

$$2i \operatorname{Im} T_{fi} = i \sum_{\{j\}} \int d\Pi_{n_j}^{(j)} (2\pi)^4 \delta^{(4)}(\Sigma p_j - \Sigma p_i) T_{fj}^* T_{ji} \;. \tag{7.61}$$

Under the additional assumption of hermitian analyticity of the S-matrix (i.e. that the amplitudes T_{fi} obey the Schwarz reflection principle $T_{fi}^*(s) = T_{fi}(s^*)$ and are real on part of the real axis; this property is therefore also called real analyticity in the literature) it follows

$$\operatorname{Disc} T_{fi}(s) = \lim_{\epsilon \to 0} \left[T_{fi}(s + i\epsilon) - T_{fi}(s - i\epsilon) \right] = i \lim_{\epsilon \to 0} \left[\operatorname{Im} T_{fi}(s + i\epsilon) - \operatorname{Im} T_{fi}(s - i\epsilon) \right]$$
$$= 2i \lim_{\epsilon \to 0} \operatorname{Im} T_{fi}(s + i\epsilon) \;, \tag{7.62}$$

which corresponds to the physical limit for the s-channel process (defined as usual as approaching the physical cut from above in the complex plane; the dependence on t being suppressed here).[#13] Hence, (7.61) can also be proven in the framework of perturbation theory to all orders via the Cutkosky cutting rules [187, 188].

We are interested in two-by-two scattering $a + b \to c + d$ for the case that only two-particle on-shell intermediate states $j_1 + j_2$ contribute to the sum in (7.58). Thus we need the integration over the intermediate two-particle LIPS and the corresponding intermediate 4-momentum conservation.[#14] In the CMS the momenta are given by $|\mathbf{p}_a| = |\mathbf{p}_b| = |\mathbf{p}_i| = p_i$ for the initial and $|\mathbf{p}_1| = |\mathbf{p}_2| = |\mathbf{p}_j| = p_j$ for the intermediate particles and the energies $(p_P)^0 = E_P$ obey $E_a + E_b = \sqrt{s} = E_1 + E_2$. The CMS result of this integration, which is valid for both elastic $p_i = p_j$ and inelastic $p_i \neq p_j$ two-particle intermediate contributions to two-by-two scattering unitarity, then reads

$$\int d\Pi_2^{(j)} (2\pi)^4 \delta^{(4)}(p_1 + p_2 - p_a - p_b)$$
$$= \frac{1}{S_2^{(j)}} \int \frac{d^4 p_1 d^4 p_2}{(2\pi)^4 (2\pi)^4} \delta(p_1^2 - m_1^2) 2\pi \theta(E_1) \delta(p_2^2 - m_2^2) 2\pi \theta(E_2) (2\pi)^4 \delta^{(4)}(p_1 + p_2 - p_a - p_b)$$
$$= \frac{1}{S_2^{(j)}} \int \frac{d^3 p_1 d^3 p_2}{2E_1(2\pi)^3 2E_2(2\pi)^3} (2\pi)^4 \delta^{(4)}(p_1 + p_2 - p_a - p_b) = \frac{1}{S_2^{(j)}} \frac{1}{8\pi} \frac{2p_j}{\sqrt{s}} \int \frac{d\Omega_j}{4\pi} \;, \tag{7.63}$$

[#13]In general, the matrix elements are functions of the components of the external 4-momenta, but due to 4-momentum conservation, Lorentz invariance, and the on-mass-shell condition for the external particles the Lorentz-invariant amplitudes for n external lines depend on $(3n - 10)$ invariant variables only (cf. [174]). For two-by-two scattering with 4 external lines this reduces to e.g. two of the three Mandelstam variables: $T_{fi}(s,t)$.

[#14]The integration runs over physically distinguishable configurations only. Hence, for n_j identical particles, one must either restrict the integration to nonequivalent configurations or divide by the symmetry factor $S_{n_j}^{(j)}$ after integrating over all sets of momenta. We will always use the latter convention as it is favorable for performing the angular integrations.

where the CMS quantities for the on-shell intermediate state are given by

$$p_j = \frac{\lambda^{1/2}(s, m_1^2, m_2^2)}{2\sqrt{s}} > 0 \; , \qquad E_1 = \frac{s + m_1^2 - m_2^2}{2\sqrt{s}} > 0 \; , \qquad E_2 = \frac{s + m_2^2 - m_1^2}{2\sqrt{s}} > 0 \; , \tag{7.64}$$

and the 4-momentum states are normalized according to

$$\langle p' | p \rangle = 2E_{\mathbf{p}}(2\pi)^3 \delta^{(3)}(\mathbf{p}' - \mathbf{p}) \tag{7.65}$$

for both bosons and fermions, which corresponds to the following normalization of spinors

$$\bar{u}^r(p) u^s(p) = 2m\delta^{rs} \; , \qquad \bar{v}^r(p) v^s(p) = -2m\delta^{rs} \; . \tag{7.66}$$

Hence, with one particular intermediate state j the optical theorem (7.61) takes the form

$$\mathrm{Im}\, T_{fi} = \frac{1}{S_2^{(j)}} \frac{1}{16\pi} \frac{2p_j}{\sqrt{s}} \int \frac{\mathrm{d}\Omega_j}{4\pi} T_{fj}^* T_{ji} \; , \tag{7.67}$$

where for equal masses $m_j = m_1 = m_2$ the kinematical phase space factor simplifies to

$$\frac{2p_j}{\sqrt{s}} = \frac{\lambda^{1/2}(s, m_j^2, m_j^2)}{s} = \sqrt{1 - \frac{4m_j^2}{s}} = \sigma(s, m_j^2) = \sigma_s^j \; . \tag{7.68}$$

The differential cross section for two-by-two scattering $a + b \to c + d$ is given by

$$\mathrm{d}\sigma_{fi} = \frac{1}{2E_a 2E_b |\mathbf{v}_a - \mathbf{v}_b|} \mathrm{d}\Pi_2^{(f)} (2\pi)^4 \delta^{(4)}(p_c + p_d - p_a - p_b) \big| T_{fi} \big|^2 \; , \tag{7.69}$$

where the invariant amplitude T_{fi} is dimensionless and the final-state two-particle LIPS $\mathrm{d}\Pi_2^{(f)}$ is completely analogous to (7.63) (with particles $c + d$ instead of $j_1 + j_2$ and thus replacing $\mathbf{p}_j$ by $\mathbf{p}_f$ with $|\mathbf{p}_c| = |\mathbf{p}_d| = |\mathbf{p}_f| = p_f$). The preceding flux factor, that is related to the relative velocity $|\mathbf{v}_a - \mathbf{v}_b|$ and thus frame-dependent, reads in the CMS

$$\frac{1}{2E_a 2E_b |\mathbf{v}_a - \mathbf{v}_b|} = \frac{1}{4\sqrt{(p_a \cdot p_b)^2 - m_a^2 m_b^2}} = \frac{1}{4p_i\sqrt{s}} \; , \qquad p_i = \frac{\lambda^{1/2}(s, m_a^2, m_b^2)}{2\sqrt{s}} \; , \tag{7.70}$$

This leads to the usual CMS-form of the differential cross section (assuming here the particles c and d to be distinguishable; $p_f = p_i$ for elastic scattering)[#15]

$$\frac{\mathrm{d}\sigma_{fi}}{\mathrm{d}\Omega} = \frac{p_f p_i}{\pi} \frac{\mathrm{d}\sigma_{fi}}{\mathrm{d}t} = \frac{p_f}{p_i} \frac{\big|T_{fi}\big|^2}{64\pi^2 s} = \frac{p_f}{p_i} \left| \frac{T_{fi}}{8\pi\sqrt{s}} \right|^2 \; . \tag{7.71}$$

Including the spin s_P for all involved particles, the general spin-averaged differential cross section reads

$$\frac{\mathrm{d}\bar{\sigma}_{fi}}{\mathrm{d}\Omega} = \frac{1}{(2s_a + 1)(2s_b + 1)} \sum_{s_c, s_d; s_a, s_b} \left| \sqrt{\frac{p_f}{p_i}} \frac{T_{fi}^{s_c, s_d; s_a, s_b}}{8\pi\sqrt{s}} \right|^2 \; . \tag{7.72}$$

[#15] From the generalized optical theorem (7.60) for the case $f = i$ one can infer the usual optical theorem relating the imaginary part of the invariant amplitude to the total cross section for the initial state i going to any possible final state, which is the reason for the imaginary part of the invariant amplitude also being called absorptive part. For $a + b \to c + d$ this situation corresponds to forward scattering (i.e. $t = 0$) and from (7.67) and (7.71) one may easily reproduce the usual form $\sigma_i^{\mathrm{tot}}(s) = \lambda^{1/2}(s, m_a^2, m_b^2)\, \mathrm{Im}\, T_{ii}(s, t = 0)$.

Now consider the problem of partial wave decomposition in the presence of spin. The T operator for two-by-two scattering can be diagonalized by using the eigenstates of total angular momentum J as basis, which can be achieved most easily in the CMS via the helicity formalism [189]. With λ_P denoting the helicity of the corresponding particle, one can take the T-matrix elements in the basis of single particle momenta and helicities

$$\langle p_c, p_d; \lambda_c, \lambda_d|T(s)|p_a, p_b; \lambda_a, \lambda_b\rangle = (2\pi)^4\delta^{(4)}(p_c + p_d - p_a - p_b)T_{fi}^{\lambda_c,\lambda_d;\lambda_a,\lambda_b}(s,t) , \qquad (7.73)$$

and with respect to our normalization of 4-momentum states (7.65) and by applying the respective phase space integration (7.63), these matrix elements and thereby the differential cross section for a specific reaction can be written in terms of states of relative motion in the CMS for both incoming and outgoing particle pairs (cf. (7.72) and [189])

$$T_{fi}^{\lambda_c,\lambda_d;\lambda_a,\lambda_b}(s,t) = \frac{(4\pi)^2\sqrt{s}}{\sqrt{p_f p_i}}\langle\theta,\varphi;\lambda_c,\lambda_d|T(s)|\theta_0,\varphi_0;\lambda_a,\lambda_b\rangle ,$$

$$\frac{\mathrm{d}\sigma_{fi}^{\lambda_c,\lambda_d;\lambda_a,\lambda_b}(s)}{\mathrm{d}\Omega} = \left|\frac{2\pi}{p_i}\langle\theta,\varphi;\lambda_c,\lambda_d|T(s)|0,0;\lambda_a,\lambda_b\rangle\right|^2 = \left|\sqrt{\frac{p_f}{p_i}}\frac{T_{fi}^{\lambda_c,\lambda_d;\lambda_a,\lambda_b}(s,t)}{8\pi\sqrt{s}}\right|^2 , \qquad (7.74)$$

where the z-axis is chosen along the incident momentum $\mathbf{p}_a$ (i.e. $\theta_0 = 0$ and w.l.o.g. one can also choose $\varphi_0 = 0$) and θ, φ are the polar angles of $\mathbf{p}_c$ in this frame. These new matrix elements then can be expanded in partial waves of the T-matrix in the helicity basis

$$\langle\theta,\varphi;\lambda_c,\lambda_d|T(s)|0,0;\lambda_a,\lambda_b\rangle = \frac{\sqrt{S_f S_i}}{4\pi}\sum_J(2J+1)\langle\lambda_c,\lambda_d|T^J(s)|\lambda_a,\lambda_b\rangle D^{J\,*}_{\lambda_a-\lambda_b,\lambda_c-\lambda_d}(\varphi,\theta,-\varphi),$$

$$\langle\lambda_c,\lambda_d|T^J(s)|\lambda_a,\lambda_b\rangle = T^J_{\lambda_c,\lambda_d;\lambda_a,\lambda_b}(s) , \qquad (7.75)$$

where $D^{j\,*}_{mm'}(\varphi,\theta,-\varphi) = e^{i(m-m')\varphi}d^j_{mm'}(\theta)$ are the Wigner functions[#16] and we have added explicit symmetry factors S_i and S_f to the partial-wave expansion of [189] in order to take care of identical particles in the initial and final state. The sum runs over integer/half-integer values of J for an even/odd number of half-integer spins present in the initial or final state and the scattering plane is conventionally fixed at $\varphi = 0$ (cf. e.g. [171]). Due to the invariance of strong interactions under time reversal and parity these helicity partial waves obey the symmetry properties

$$T^J_{\lambda_a,\lambda_b;\lambda_c,\lambda_d}(s) = T^J_{\lambda_c,\lambda_d;\lambda_a,\lambda_b}(s) = T^J_{-\lambda_c,-\lambda_d;-\lambda_a,-\lambda_b}(s) . \qquad (7.76)$$

Writing for a generic two-by-two reaction $ab \to cd$

$$\left[S^J_{\{\lambda\}}(s)\right]_{ab\to cd} = S^J_{\lambda_c,\lambda_d;\lambda_a,\lambda_b}(s) = \delta_{\lambda_a,\lambda_c}\delta_{\lambda_b,\lambda_d} + iT^J_{\lambda_c,\lambda_d;\lambda_a,\lambda_b}(s) = \mathbb{1}_{\{\lambda\}} + i\left[T^J_{\{\lambda\}}(s)\right]_{ab\to cd} , \qquad (7.77)$$

where the unity operator has to be removed for inelastic reactions, one obtains for the differential cross section (cf. (7.72), (7.74), and (7.75))

$$\mathcal{M}^{\{\lambda\}}_{ab\to cd} = \frac{\sqrt{S_f S_i}}{2p_i}\sum_J(2J+1)\left[T^J_{\{\lambda\}}(s)\right]_{ab\to cd}d^J_{\{\lambda\}}(\theta) ,$$

$$\frac{\mathrm{d}\sigma^{\{\lambda\}}_{ab\to cd}}{\mathrm{d}\Omega} = \left|\mathcal{M}^{\{\lambda\}}_{ab\to cd}\right|^2 , \qquad \frac{\mathrm{d}\bar{\sigma}_{ab\to cd}}{\mathrm{d}\Omega} = \frac{1}{(2s_a+1)(2s_b+1)}\sum_{\{\lambda\}}\left|\mathcal{M}^{\{\lambda\}}_{ab\to cd}\right|^2 . \qquad (7.78)$$

[#16]A very good reference on Wigner functions and a comparison of the different conventions used in the literature is given in [190].

This normalization ensures that no symmetry factors occur in the elastic unitarity relations for the partial waves (cf. e.g. (7.81)), since they always cancel with the symmetry factor implicitly included in (7.58).[#17] We will consider explicitly the example of $\pi\pi \to \pi\pi$ with $\bar{K}K$ and $\bar{N}N$ intermediate states in Sect. 12.1. Expanding already the single particle momentum matrix elements (7.73), which reproduces the standard normalizations for spinless processes and $\pi N \to \pi N$, the partial-wave expansion reads

$$T_{fi}^{\lambda_c,\lambda_d;\lambda_a,\lambda_b}(s,t) = \sqrt{S_f S_i}16\pi \sum_J (2J+1)\tilde{T}_{\lambda_c,\lambda_d;\lambda_a,\lambda_b}^J(s)d_{\lambda_a-\lambda_b,\lambda_c-\lambda_d}^J(\theta) \ . \tag{7.79}$$

In the case of spinless particles, with $d_{00}^J(\theta) = P_J(\cos\theta)$ and $J = l$ the expansion simplifies to

$$T_{fi}(s,t) = \sqrt{S_f S_i}16\pi \sum_{J=0}^{\infty}(2J+1)\tilde{T}_{fi}^J(s)P_J(\cos\theta) \ . \tag{7.80}$$

For elastic scattering $ab \to ab$ (hence $S_i = S_f$ and $p_i = p_f = p$), below the inelastic threshold only the initial two-body channel contributes to the sum over physical intermediate states in (7.58) and the partial-wave expansion (7.79) together with the angular integration (7.63) and time reversal invariance (7.76) leads to the general elastic unitarity relation for the corresponding partial waves

$$\tilde{T}^J(s) - \tilde{T}^{J\,\dagger}(s) = 2i\,\mathrm{Im}\,\tilde{T}^J(s) = 2i\frac{2p}{\sqrt{s}}\tilde{T}^{J\,\dagger}(s)\tilde{T}^J(s) \ , \tag{7.81}$$

where $\tilde{T}^J(s)$ is a $(2s_a+1)(2s_b+1) \times (2s_a+1)(2s_b+1)$ matrix in helicity space and all potential symmetry factors cancel. If the particles are spinless or if the matrix $\tilde{T}^J(s)$ is diagonal in some appropriate basis (as it is e.g. for $\pi N \to \pi N$ in the isospin basis $I_s \in \{1/2, 3/2\}$), we arrive at

$$\mathrm{Im}\,\tilde{T}_{fi}^J(s) = \frac{2p}{\sqrt{s}}\big|\tilde{T}_{fi}^J(s)\big|^2 \ , \tag{7.82}$$

which is solved by a parameterization of $\tilde{T}_{fi}^J(s)$ via the real phase shift $\delta_{fi}^J(s)$

$$\tilde{T}_{fi}^J(s) = \frac{\sqrt{s}}{2p}\sin\delta_{fi}^J(s)e^{i\delta_{fi}^J(s)} \ , \tag{7.83}$$

where (7.82) and (7.83) are valid for each diagonal element $\tilde{T}_{fi}^J(s)$ of $\tilde{T}^J(s)$. For s above the lowest inelastic threshold s_{inel} these equations have to be modified by introducing real inelasticities $0 \le \eta_{fi}^J(s) \le 1$ via

$$\tilde{T}_{fi}^J(s) = \frac{\sqrt{s}}{2p}\frac{\eta_{fi}^J(s)e^{2i\delta_{fi}^J(s)} - 1}{2i} \ , \qquad \mathrm{Im}\,\tilde{T}_{fi}^J(s) = \frac{2p}{\sqrt{s}}\big|\tilde{T}_{fi}^J(s)\big|^2 + \frac{\sqrt{s}}{8p}\Big[1 - \big(\eta_{fi}^J(s)\big)^2\Big] \ , \quad (7.84)$$

with $\eta_{fi}^J(s) < 1$ for $s > s_{\mathrm{inel}}$ due to additional intermediate states contributing in (7.58). These partial waves are then related to the diagonal elements of the corresponding S-matrix according to

$$S_{fi}^J(s) = \eta_{fi}^J(s)e^{2i\delta_{fi}^J(s)} = 1 + i\frac{4p}{\sqrt{s}}\tilde{T}_{fi}^J(s) \ . \tag{7.85}$$

Note the kinematical factor between the $\tilde{T}_{fi}^J$ and the T-matrix partial waves (7.77).

[#17] Note that in addition no symmetry factors occur in the relation between the differential cross section and the squared matrix element.

7.4 Hyperbolic dispersion relations

There are several excellent general introductions to S-matrix theory and dispersion theory[#18] available in the literature, see for instance [174, 192–197]. Even specific processes are extensively studied in the literature: see e.g. [174, 196, 198] for the simple and thus pedagogical case of $\pi\pi$ scattering, [174, 196, 197] for πN scattering, and [199] particularly for $\pi\pi \to \bar{N}N$. Hence, before reviewing the formalism for the particular case at hand, i.e. hyperbolic dispersion relations for πN scattering, we will content ourselves with a very brief synopsis of the basic underlying ideas in the following (see [191] for the corresponding references)

S-matrix theory started to become popular in the late 1950s[#19] as a program for (dynamically) determining the S-matrix for strong interactions by starting from very general first principles and assumptions, since at that time strong interactions were thought to become uncontrollably strong at short distances in (local) quantum field theory (QFT). For this purpose also observations of (quantum) field theory and perturbation theory were generalized to postulates (e.g. that imaginary parts of scattering amplitudes correspond to the propagation of on-mass-shell intermediate states). With the advent of QCD and especially asymptotic freedom in the early to mid 1970s, however, the interest in the S-matrix program waned rapidly, although it should be stressed that there is no contradiction whatsoever between QFT/QCD and S-matrix theory. In fact, the latter can generally be thought of as an on-mass-shell field theory and many of its concepts and assumptions are frequently used hitherto.[#20] Besides further symmetry principles of the specific scattering process under consideration (e.g. isospin), the foundations of S-matrix theory are given by the postulates of

- Lorentz invariance,

- unitarity,

- crossing symmetry,

- and "maximal" hermitian analyticity

for the S-matrix and thus the Lorentz-invariant scattering amplitudes. While unitarity, which amounts to nothing else but probability conservation, can easily be implemented in the formalism (in particular for partial-wave amplitudes, cf. Sect. 7.3), it is difficult to precisely formulate

---

[#18]Although these two terms are frequently used in a synonymical way in the literature, in fact they comprise a variety of conceptually rather different theories and theoretical programs, which, however, share a good deal of the calculational (i.e. especially dispersive) techniques. An excellent overview on both the differences and overlaps of the miscellaneous specific theoretical approaches during the historical development of the general field is given in [191], which thereby proves valuable as literature survey. For the sake of simplicity, however, we will generically use the term S-matrix theory in the following. Moreover, [191] is concerned with the interrelation and the (at least historical) rivalry between S-matrix theory and (local) quantum field theory as a case study for a philosophical discussion (though being fairly technical at the same time) on the construction and, in particular, the selection of theories in modern physics.

[#19]Its roots can be traced back to Heisenberg in the 1930s, though.

[#20]A very good example for the strong interrelation between these two different theoretical approaches is the Lehmann–Symanzik–Zimmermann (LSZ) formalism of causal asymptotic field theory as a means of implementing the general principles of S-matrix theory. Moreover, together with the more speculative concept of duality (i.e. that any hadronic scattering amplitude may be considered either as the sum of direct-channel resonances or as the sum of crossed-channel Regge exchanges), S-matrix theory lead to the bootstrap model for strong interactions (or even the notion of nuclear democracy), which was the starting point for the development of modern string theory.

the *assumption* of so-called "maximal" hermitian analyticity, which is linked to the physical principle of causality and is crucial for the possibility of analytic continuation and thus for the validity of dispersion relations. More specifically, it is assumed that the S-matrix elements for a given channel of a scattering process are functions that are analytic (actually: hermitian analytic, cf. Sect. 7.3) in the corresponding (squared CMS) energy except for those singularity structures that are enforced by the other principles, namely particle poles (corresponding to the exchange of stable particles, as motivated by leading-order perturbation theory) and unitarity (i.e. physical) cuts as well as crossed-channel cuts (as already mentioned in Sect. 7.1), hence the term "maximal" (hermitian) analyticity. In principle, there are rigorous derivations of analyticity properties of scattering amplitudes based on quantum field theoretical micro-causality, however, such proofs are straightforward only for the forward scattering of massless particles; for e.g. πN elastic scattering analyticity in s is only proven at fixed (physical) momentum transfer t for a limited range of t [200] (see also [201] for a review of rigorous proofs of analyticity properties). In the most optimistic scenario of the S-matrix program, these fundamental principles — together with suitable asymptotic boundary conditions needed for the convergence of the dispersion relations — would be sufficient to (uniquely) specify the scattering amplitudes. After these general remarks, we now will turn to the case at hand.

For invariant amplitudes with definite $s \leftrightarrow u$ crossing properties (for fixed t, i.e. (ν, t) are the "natural" variables) like πN scattering, it was shown in [161] (and references therein) that the requirements that the parameterizations of the integration paths in the dispersive integrals correspond to curves in the Mandelstam plane so that

- the curves pass through both the direct and all crossed channels
  (enabling the lowest partial waves to catch most of the important contributions),

- the curves do not enter the double spectral regions
  (ensuring the convergence of the partial-wave expansions/projections, cf. Chap.10),

- the parameterization does not introduce kinematical cuts into the invariant amplitudes,

- and the resulting integral kernels are reasonably simple

inevitably lead to equilateral hyperbolae in the (s, u) Mandelstam plane with hyperbola parameter b and asymptotes $s = a$ and $u = a$,

$$(s - a)(u - a) = b \, . \tag{7.86}$$

To be specific, considering t as the independent variable and $\nu = (s-u)/(4m)$ to be a function of t and the curve parameters yields the relation (the linearity in b being a consequence of the last of the above requirements)

$$t = g(s; a)b + h(s; a) \, , \qquad g(s; a) = -\frac{1}{s - a} \, , \qquad h(s; a) = \Sigma - s - a \, , \tag{7.87}$$

from which besides (7.86) also follows

$$s(t; a, b) = \frac{1}{2}\big(\Sigma - t + 4m\nu(t; a, b)\big) \, , \qquad \nu(t; a, b) = \frac{1}{4m}\sqrt{(t - \Sigma + 2a)^2 - 4b} \, ,$$

$$u(t; a, b) = \frac{1}{2}\big(\Sigma - t - 4m\nu(t; a, b)\big) \, , \qquad t_{(\pm)}(\nu; a, b) = \Sigma - 2a \pm 2\sqrt{(2m\nu)^2 + b} \, , \tag{7.88}$$

defining two hyperbola branches in the real (s, u) Mandelstam plane.[#21]

Under the assumption that no subtractions are necessary (cf. Chap. 11), one may thus straightforwardly write down generic HDRs for ν-even invariant amplitudes as functions of $(t; a, b)$ (cf. (7.24), hence no kinematical square root cuts are introduced by $\nu(t; a, b)$) according to

$$
\mathcal{A}_{\mathrm{ev}}(t; a, b) = \mathcal{A}_{\mathrm{ev}}^B(t; a, b) + \frac{1}{\pi} \int\limits_{-\infty}^{\tilde{t}_{\mathrm{th}}} \mathrm{d}t' \, \frac{\operatorname{Im} \mathcal{A}_{\mathrm{ev}}(t'; a, b)}{t' - t} + \frac{1}{\pi} \int\limits_{t_{\mathrm{th}}}^{\infty} \mathrm{d}t' \, \frac{\operatorname{Im} \mathcal{A}_{\mathrm{ev}}(t'; a, b)}{t' - t} \, ,
$$

$$
\frac{\mathcal{A}_{\mathrm{od}}}{\nu}(t; a, b) = \frac{\mathcal{A}_{\mathrm{od}}^B}{\nu}(t; a, b) + \frac{1}{\pi} \int\limits_{-\infty}^{\tilde{t}_{\mathrm{th}}} \mathrm{d}t' \, \frac{\operatorname{Im} \frac{\mathcal{A}_{\mathrm{od}}}{\nu}(t'; a, b)}{t' - t} + \frac{1}{\pi} \int\limits_{t_{\mathrm{th}}}^{\infty} \mathrm{d}t' \, \frac{\operatorname{Im} \frac{\mathcal{A}_{\mathrm{od}}}{\nu}(t'; a, b)}{t' - t} \, , \tag{7.89}
$$

where $\mathcal{A}^B$ denotes possible Born term contributions and the dispersive integrals represent the crossed-channel (now: s-/u-channel) and direct-channel (now: t-channel) contributions, respectively. Accordingly, the RHC starts at the physical threshold t_{th}, while the finite branch point of the LHC $\tilde{t}_{\mathrm{th}}$ is a function of the corresponding crossed-channel threshold s_{th}. Moreover, the physical t-channel limit is defined in the complex-t plane as approaching the RHC from above (i.e. replacing $t \to t + i\epsilon$ and taking the limit $\epsilon \to 0$) while due to $s \propto -t$ the LHC needs to be approached from below. Applying Cauchy's theorem as usual in the derivation of dispersion relations — i.e. integrating over a full circle with radius r in the complex-t plane circumventing both cuts by $\pm\epsilon_c$ and taking the limits $\epsilon_c \to 0$ (hermitian analyticity relating the discontinuities along the cuts with the pertinent imaginary parts, cf. (7.62)) as well as $r \to \infty$ (assuming the contributions of the arcs to vanish due to the asymptotic behavior of the amplitude) — then leads to the HDRs as given above.[#22]

It turns out advantageous, however, to replace the dependence on b by dependences on a and the Mandelstam variables. To this end, one rewrites b as a function of s and t for a given value of a,

$$
b(s, t; a) = (s - a)(\Sigma - s - t - a) \, , \tag{7.90}
$$

and hence for given s and a one considers a family of hyperbolae wherein all members are uniquely defined by t. Effectively, this replacement amounts to introducing the variables s and s' outside and inside the integrals, respectively. Due to the hyperbolic parameterization both the unprimed *external kinematics* (s, t, u) and the primed *internal kinematics* (s', t', u') are related by

$$
(s - a)(u - a) = b = (s' - a)(u' - a) \, , \qquad s + t + u = \Sigma = s' + t' + u' \, , \tag{7.91}
$$

where $u(s, t)$ and $u'(s', t')$ are only used for convenience and symmetry reasons. Repeatedly using the linearity of t in b (cf. (7.87), in analogy for the primed Mandelstam variables) yields

$$
\frac{\mathrm{d}t'}{\mathrm{d}s'} = \frac{\mathrm{d}}{\mathrm{d}s'} \left[g(s'; a)b + h(s'; a) \right] \quad \Rightarrow \quad \frac{\mathrm{d}t'}{t' - t} = \frac{\mathrm{d}s'}{s' - a} \frac{b - (s' - a)^2}{-b + (s' - a)(\Sigma - s' - a - t)}
$$

$$
= \mathrm{d}s' \left[\frac{1}{s' - s} + \frac{1}{s' - u} - \frac{1}{s' - a} \right] \, , \tag{7.92}
$$

[#21]Note that an equilateral hyperbolic parameterization is ideally suited to fulfill the first of the above requirements also in view of the hyperbolic boundaries of the physical regions, cf. (7.20) and Fig. 7.1 for the specific case of πN scattering.

[#22]Note that the order of limits is important in the derivation of dispersion relations: the physical limit $\epsilon \to 0$ is well-defined only *after* the contour limit $\epsilon_c \to 0$.

so that by taking care of the sign conventions for the physical limits one can recast the first HDR of (7.89) in the explicitly $s \leftrightarrow u$ crossing symmetric form

$$
\mathcal{A}_{\mathrm{ev}}(s,t;a) = \mathcal{A}_{\mathrm{ev}}^{B}(s,t;a) + \frac{1}{\pi} \int\limits_{s_{\mathrm{th}}}^{\infty} \mathrm{d}s' \left[\frac{1}{s'-s} + \frac{1}{s'-u} - \frac{1}{s'-a} \right] \mathrm{Im}\, \mathcal{A}_{\mathrm{ev}}(s',t';a)
$$

$$
+ \frac{1}{\pi} \int\limits_{t_{\mathrm{th}}}^{\infty} \mathrm{d}t' \, \frac{\mathrm{Im}\, \mathcal{A}_{\mathrm{ev}}(s',t';a)}{t'-t} \, , \tag{7.93}
$$

where under the integrals one has to use

$$
t'(s',s,t;a) = g(s';a)b(s,t;a) + h(s';a) \, ,
$$

$$
s'(t',s,t;a) = \frac{1}{2} \left[\Sigma - t' + \sqrt{(t'-\Sigma+2a)^2 - 4b(s,t;a)} \right] \, , \tag{7.94}
$$

respectively. By eliminating b one in particular simply recovers $\nu(s,t) = (s-u)/(4m)$ and in analogy $\nu(s',t') = (s'-u')/(4m)$, which both are obviously real and thus can be factorized out of the pertinent imaginary parts in (7.89). Thereby, defining the convenient abbreviation

$$
\nu'(s',t') = \nu(s',t') = \frac{2s' + t' - \Sigma}{4m} \, , \tag{7.95}
$$

and noting that

$$
\frac{\nu}{\nu'} \left[\frac{1}{s'-s} + \frac{1}{s'-u} - \frac{1}{s'-a} \right] = \frac{1}{s'-s} - \frac{1}{s'-u} \, , \tag{7.96}
$$

the second HDR of (7.89) eventually can be rewritten in analogy as

$$
\mathcal{A}_{\mathrm{od}}(s,t;a) = \mathcal{A}_{\mathrm{od}}^{B}(s,t;a) + \frac{1}{\pi} \int\limits_{s_{\mathrm{th}}}^{\infty} \mathrm{d}s' \left[\frac{1}{s'-s} - \frac{1}{s'-u} \right] \mathrm{Im}\, \mathcal{A}_{\mathrm{od}}(s',t';a) + \frac{1}{\pi} \int\limits_{t_{\mathrm{th}}}^{\infty} \mathrm{d}t' \, \frac{\mathrm{Im}\, \mathcal{A}_{\mathrm{od}}(s',t';a)}{t'-t} \, . \tag{7.97}
$$

For πN scattering, the corresponding HDRs for the Lorentz-invariant amplitudes thus read [161]

$$
A^{+}(s,t;a) = \frac{1}{\pi} \int\limits_{s_{+}}^{\infty} \mathrm{d}s' \left[\frac{1}{s'-s} + \frac{1}{s'-u} - \frac{1}{s'-a} \right] \mathrm{Im}\, A^{+}(s',t') + \frac{1}{\pi} \int\limits_{t_{\pi}}^{\infty} \mathrm{d}t' \, \frac{\mathrm{Im}\, A^{+}(s',t')}{t'-t} \, ,
$$

$$
A^{-}(s,t;a) = \frac{1}{\pi} \int\limits_{s_{+}}^{\infty} \mathrm{d}s' \left[\frac{1}{s'-s} - \frac{1}{s'-u} \right] \mathrm{Im}\, A^{-}(s',t') + \frac{1}{\pi} \int\limits_{t_{\pi}}^{\infty} \mathrm{d}t' \, \frac{\nu}{\nu'} \frac{\mathrm{Im}\, A^{-}(s',t')}{t'-t} \, ,
$$

$$
B^{+}(s,t;a) = N^{+}(s,t) + \frac{1}{\pi} \int\limits_{s_{+}}^{\infty} \mathrm{d}s' \left[\frac{1}{s'-s} - \frac{1}{s'-u} \right] \mathrm{Im}\, B^{+}(s',t') + \frac{1}{\pi} \int\limits_{t_{\pi}}^{\infty} \mathrm{d}t' \, \frac{\nu}{\nu'} \frac{\mathrm{Im}\, B^{+}(s',t')}{t'-t} \, ,
$$

$$
B^{-}(s,t;a) = N^{-}(s,t;a) + \frac{1}{\pi} \int\limits_{s_{+}}^{\infty} \mathrm{d}s' \left[\frac{1}{s'-s} + \frac{1}{s'-u} - \frac{1}{s'-a} \right] \mathrm{Im}\, B^{-}(s',t') + \frac{1}{\pi} \int\limits_{t_{\pi}}^{\infty} \mathrm{d}t' \, \frac{\mathrm{Im}\, B^{-}(s',t')}{t'-t} \, . \tag{7.98}
$$

Here, only the amplitudes $B^{\pm}$ contain Born term contributions $N^{\pm}$ due to the nucleon poles given by (cf. [171] for $\bar{N}^{\pm}$, i.e. the Born contributions without the term depending on a)[#23]

$$N^+(s,t) = \bar{N}^+(s,t) \ , \qquad \bar{N}^+(s,t) = g^2 \left[\frac{1}{m^2-s} - \frac{1}{m^2-u} \right] = \frac{g^2}{m} \frac{\nu}{\nu_B^2 - \nu^2} \ ,$$

$$N^-(s,t;a) = \bar{N}^-(s,t) - \frac{g^2}{m^2-a} \ , \qquad \bar{N}^-(s,t) = g^2 \left[\frac{1}{m^2-s} + \frac{1}{m^2-u} \right] = \frac{g^2}{m} \frac{\nu_B}{\nu_B^2 - \nu^2} \ ,$$
$$(7.99)$$

where the usual pseudoscalar πN coupling constant g and thereby the pseudovector πN coupling constant f are given by[#24]

$$\frac{g^2}{4\pi} = \frac{4m^2 f^2}{M_\pi^2} \approx 13.7 \ . \tag{7.100}$$

In order to express the integrands in terms of the corresponding CMS scattering angles according to

$$X(s',z_s') = X(s',t') \Big|_{t'=t'(s',z_s')} \ , \qquad X(t',z_t') = X(s',t') \Big|_{s'=s'(t',z_t')} \ , \qquad X \in \left\{ A^{\pm}, B^{\pm} \right\} \ , \tag{7.101}$$

we define

$$z_s'(s',t') = z_s(s',t') = 1 + \frac{t'}{2q'^2} \ , \qquad q'(s') = q(s') \ , \tag{7.102}$$

$$z_t'(s',t') = z_t(s',t') = \frac{m\nu'}{p_t' q_t'} \ , \qquad p_t'(t') = p_t(t') = ip_-'(t') \ , \qquad q_t'(t') = q_t(t') = iq_-'(t') \ ,$$

which leads to the relations

$$t'(s',z_s') = -2q'^2(1-z_s') \ , \qquad z_s'(s',s,t;a) = 1 - \frac{1}{2q'^2} \left[s' - \Sigma + a + \frac{b(s,t;a)}{s'-a} \right] \ ,$$

$$s'(t',z_t') = \frac{1}{2}(\Sigma - t' + 4p_t' q_t' z_t') \ , \qquad z_t'(t',s,t;a) = \frac{1}{4p_t' q_t'} \sqrt{(t' - \Sigma + 2a)^2 - 4b(s,t;a)} \ .$$
$$(7.103)$$

Note that b is linearly related to z_s' for the s-channel, but only to $z_t'^2$ for the t-channel, which will have important consequences in Chap. 10, where it will be shown that the HDRs (7.98) incorporate contributions from the direct channel as well as from the crossed channels, but not from double spectral regions, provided the parameters are chosen appropriately. Furthermore, starting from the defined ν-parity (7.26) of the amplitudes $A^{\pm}$ and $B^{\pm}$ due to crossing

---

[#23]The form of these nucleon pole terms easily follows from Cauchy's theorem via algebraic manipulations along the same lines as discussed for the integral contributions.

[#24]Note that [171] quotes a value of 14.28 based on [202]. For more information on conventions as well as the historical evolution of the value see [144, 145, 203, 204].

symmetry together with (7.99) as special case for $s' = m^2$ of the relations

$$\frac{1}{s'-s} + \frac{1}{s'-u} = \frac{2s'-(s+u)}{(s'-s)(s'-u)} = \frac{2(s'-m^2)+4m\nu_B}{(s'-m^2)\{(s'-m^2)+4m\nu_B\}+4m^2(\nu_B^2-\nu^2)}$$

$$= 4\frac{2s'-\Sigma+t}{(2s'-\Sigma+t)^2-(4m\nu)^2} = \frac{2(s'-s_0)+t}{(s'-s_0+\frac{t}{2})^2-4p_t^2q_t^2z_t^2} \ ,$$

$$\frac{1}{s'-s} - \frac{1}{s'-u} = \frac{s-u}{(s'-s)(s'-u)} = \frac{4m\nu}{(s'-m^2)\{(s'-m^2)+4m\nu_B\}+4m^2(\nu_B^2-\nu^2)}$$

$$= 4\frac{4m\nu}{(2s'-\Sigma+t)^2-(4m\nu)^2} = \frac{4p_tq_tz_t}{(s'-s_0+\frac{t}{2})^2-4p_t^2q_t^2z_t^2} \ , \tag{7.104}$$

one can easily check also for the dispersive integral representations in (7.98) that A^+ and B^- are indeed functions of ν^2, while A^- and B^+ are completely proportional to ν

$$\frac{A^-(s,t;a)}{4m\nu} = \frac{1}{\pi}\int\limits_{s_+}^\infty ds'\,\frac{\operatorname{Im}A^-(s',z_s')}{(s'-s)(s'-u)} + \frac{1}{\pi}\int\limits_{t_\pi}^\infty dt'\,\frac{\operatorname{Im}A^-(t',z_t')}{4p_t'q_t'z_t'(t'-t)} \ ,$$

$$\frac{B^+(s,t;a)}{4m\nu} = \frac{g^2}{(m^2-s)(m^2-u)} + \frac{1}{\pi}\int\limits_{s_+}^\infty ds'\,\frac{\operatorname{Im}B^+(s',z_s')}{(s'-s)(s'-u)} + \frac{1}{\pi}\int\limits_{t_\pi}^\infty dt'\,\frac{\operatorname{Im}B^+(t',z_t')}{4p_t'q_t'z_t'(t'-t)} \ , \tag{7.105}$$

which will be used in Chap. 13. Note that since $4p_t'q_t'z_t' = 4m\nu' = s' - u' = 2(s' - s_0) - 2q'^2(1 - z_s')$ is always real, one may rewrite the HDRs (7.105) in terms of reduced amplitudes $A^-(s',t')/\nu' = \frac{A^-}{\nu'}(\nu'^2,t')$ and $B^+(s',t')/\nu' = \frac{B^+}{\nu'}(\nu'^2,t')$ that are even in ν' according to

$$\frac{A^-}{\nu}(\nu^2,t;a) = \frac{2}{\pi}\int\limits_{s_+}^\infty ds'\,\frac{(s'-s_0+\frac{t'}{2})\operatorname{Im}\big[\frac{A^-}{\nu'}(\nu'^2,t')\big]}{(s'-s_0+\frac{t}{2})^2-4m^2\nu^2} + \frac{1}{\pi}\int\limits_{t_\pi}^\infty dt'\,\frac{\operatorname{Im}\big[\frac{A^-}{\nu'}(\nu'^2,t')\big]}{t'-t} \ ,$$

$$\frac{B^+}{\nu}(\nu^2,t;a) = \frac{g^2}{m}\frac{1}{\nu_B^2-\nu^2} + \frac{2}{\pi}\int\limits_{s_+}^\infty ds'\,\frac{(s'-s_0+\frac{t'}{2})\operatorname{Im}\big[\frac{B^+}{\nu'}(\nu'^2,t')\big]}{(s'-s_0+\frac{t}{2})^2-4m^2\nu^2} + \frac{1}{\pi}\int\limits_{t_\pi}^\infty dt'\,\frac{\operatorname{Im}\big[\frac{B^+}{\nu'}(\nu'^2,t')\big]}{t'-t} \ , \tag{7.106}$$

yielding, however, more involved angular kernels for the s-channel integrals.[#25]

In contrast, for usual fixed-t dispersion relations external and internal kinematics are related by

$$t = t' \ , \qquad s + t + u = \Sigma = s' + t' + u' \ . \tag{7.107}$$

It is remarkable that the HDRs have the simple form of (7.98) and (7.99), which by neglecting the terms depending on a (or equivalently for $|a| \to \infty$) reduce to the usual fixed-t dispersion relations [205] (cf. [171] for the standard notation), provided, however, that the t-channel integrals are discarded. Moreover, the hyperbolae then reduce to fixed-t lines, and thus we will refer to the limit $|a| \to \infty$ as "fixed-t limit" in the following.[#26]

[#25] While for the t-channel integrals the kernels simplify and reduce to Cauchy-type kernels like for A^+ and B^-, for the s-channel integrals the expansion into partial waves is complicated by the fact that ν' mixes the powers of z_s'.

[#26] As explained in Sect. 10.2, only the limit $a \to -\infty$ is compatible with range-of-convergence considerations.

Chapter 8

Partial-wave projection for the s-channel amplitudes

In this chapter, for the sake of completeness and convenience, we will collect some results of [161] and references therein [206–208] for the PWDRs for the s-channel partial waves derived from the HDRs (7.98), that we will need in the following as part of the full Roy–Steiner system.[#1]

The s-channel partial-wave amplitudes are conventionally denoted by $f_{l\pm}^I(W)$ with isospin (i.e. crossing) index $I \in \{+, -\}$ and total angular momentum $j = l\pm 1/2 = l\pm \geq 1/2$, whereby the orbital angular momentum can take the values $l \geq 0$ for $j = l+$ and $l \geq 1$ for $j = l-$. They obey the MacDowell symmetry relation [209] in the complex W-plane

$$f_{l+}^I(W) = -f_{(l+1)-}^I(-W) \qquad \forall\, l \geq 0 \,, \tag{8.1}$$

due to which only half of the W-plane is actually needed (corresponding to the full $s = (\pm W)^2$-plane), or which can be used the other way round to derive the partial waves with $j = l-$ from the ones with $j = l+$ via $W \to -W$

$$f_{l-}^I(W) = -f_{(l-1)+}^I(-W) \qquad \forall\, l \geq 1 \,. \tag{8.2}$$

As will be shown in the following, expanding the absorptive parts into s-channel and t-channel partial-wave amplitudes, respectively, and projecting onto the s-channel partial waves yields the result

$$
\begin{aligned}
f_{l+}^I(W) &= N_{l+}^I(W) \\
&+ \frac{1}{\pi} \int\limits_{W_+}^{\infty} dW' \sum_{l'=0}^{\infty} \left\{ K_{ll'}^I(W, W') \operatorname{Im} f_{l'+}^I(W') + K_{ll'}^I(W, -W') \operatorname{Im} f_{(l'+1)-}^I(W') \right\} \\
&+ \frac{1}{\pi} \int\limits_{t_\pi}^{\infty} dt' \sum_J \left\{ G_{lJ}(W, t') \operatorname{Im} f_+^J(t') + H_{lJ}(W, t') \operatorname{Im} f_-^J(t') \right\} \\
&= -f_{(l+1)-}^I(-W) \qquad \forall\, l \geq 0 \,. \tag{8.3}
\end{aligned}
$$

[#1]Correcting several typographical errors, adjusting the conventions, and partially extending the presentation in [161, 206–208] at the same time.

Here, $N_{l\pm}^I(W)$ represent the contributions due to the nucleon pole terms in the amplitudes $B^\pm$ as given in (7.98). Each s-channel partial wave $f_{l\pm}^I(W)$ is coupled to the absorptive parts of all other s-channel partial waves via the kernels $K_{ll'}^I(W, W')$, which contain the usual Cauchy kernel responsible for the physical cut and an analytically known remainder (denoted by dots below) containing only left-hand cut contributions

$$K_{ll'}^I(W, W') = \frac{\delta_{ll'}}{W' - W} + \dots \qquad \forall\, l, l' \geq 0 \, , \tag{8.4}$$

as well as to the absorptive parts of the t-channel partial waves $f_\pm^J(t)$ via the kernels $G_{lJ}(W, t')$ and $H_{lJ}(W, t')$, where the lower index $\pm$ denotes parallel(+) or antiparallel($-$) antinucleon–nucleon helicity and the total (t-channel) angular momentum J can take the values $J \geq 0$ or $J \geq 1$, respectively. Due to Bose statistics (i.e. crossing symmetry), the summations over J in (8.3) run over even/odd values of J for the crossing even/odd partial waves (upper index $I = +/-$), respectively, as explained in Sect. 7.2. Hence, the useful definitions

$$\epsilon^I = \begin{cases} \epsilon^+ = +1 \, , \\ \epsilon^- = -1 \, , \end{cases} \quad \tilde{\epsilon}_\pm = \frac{1 \pm \epsilon^I}{2} \, , \quad \tilde{\epsilon}_+ = \begin{cases} 1 \, , \\ 0 \, , \end{cases} \quad \tilde{\epsilon}_- = \begin{cases} 0 \, , \\ 1 \, , \end{cases} \quad \text{for} \begin{cases} I = + \text{ or } J \text{ even} \, , \\ I = - \text{ or } J \text{ odd} \, , \end{cases} \tag{8.5}$$

can be identified in this case with

$$\epsilon^I \doteq (-1)^J \, , \qquad \tilde{\epsilon}_\pm \doteq \frac{1 \pm (-1)^J}{2} \, . \tag{8.6}$$

In the following, the different contributions to (8.3) will be discussed in detail along the lines of [161].

8.1 Nucleon exchange

Using a shorthand notation for the z_s-projections of the invariant amplitudes

$$X_l^I(s) = \int_{-1}^1 dz_s \, P_l(z_s) X^I(s, t) \Big|_{t=t(s,z_s)=-2q^2(1-z_s)} \qquad \text{for } X \in \{A, B\} \, , \tag{8.7}$$

the well-known s-channel partial-wave projection formula, which is the source of the MacDowell symmetry relation (8.1), reads [210]

$$\begin{aligned} f_{l\pm}^I(W) &= \frac{1}{16\pi W} \Big\{ (E + m)\big[A_l^I(s) + (W - m)B_l^I(s)\big] \\ &\qquad + (E - m)\big[-A_{l\pm1}^I(s) + (W + m)B_{l\pm1}^I(s)\big] \Big\} \\ &= \frac{1}{16\pi W} \Big\{ (E(W) + m)\big[A_l^I(s) + (W - m)B_l^I(s)\big] \Big\} \\ &\qquad - \frac{1}{16\pi(-W)} \Big\{ (E(-W) + m)\big[A_{l\pm1}^I(s) + (-W - m)B_{l\pm1}^I(s)\big] \Big\} \, . \end{aligned} \tag{8.8}$$

Projecting the HDR Born terms $N^I(s,t)$ of (7.99) onto s-channel partial waves leads to accordingly symmetric nucleon pole contributions

$$N_{l+}^I(W) = \frac{g^2}{16\pi W}\left\{(E+m)(W-m)\left[\epsilon^I\frac{Q_l(y)}{q^2} + 2\delta_{l0}\left(\frac{1}{m^2-s} - \frac{\tilde{\epsilon}_-}{m^2-a}\right)\right]\right.$$
$$\left. + (E-m)(W+m)\left[\epsilon^I\frac{Q_{l+1}(y)}{q^2}\right]\right\}$$
$$= -N_{(l+1)-}^I(-W) \qquad \forall\, l \geq 0\,, \tag{8.9}$$

which by defining the abbreviation[#2]

$$\bar{N}_{l\pm}^I(W) = \frac{g^2}{16\pi W}\left\{(E+m)(W-m)\left[\epsilon^I\frac{Q_l(y)}{q^2} + \frac{2\delta_{l0}}{m^2-s}\right]\right.$$
$$\left. + (E-m)(W+m)\left[\epsilon^I\frac{Q_{l\pm1}(y)}{q^2} + \frac{2\delta_{l\pm1,0}}{m^2-s}\right]\right\} \tag{8.10}$$

for later convenience can also be written in the form

$$N_{l+}^+(W) = \bar{N}_{l+}^+, \qquad N_{l+}^-(W) = \bar{N}_{l+}^- - \frac{g^2}{4\pi}\frac{(E+m)(W-m)}{2W}\frac{\delta_{l0}}{m^2-a} \qquad \forall\, l \geq 0\,,$$
$$N_{l-}^+(W) = \bar{N}_{l-}^+, \qquad N_{l-}^-(W) = \bar{N}_{l-}^- - \frac{g^2}{4\pi}\frac{(E-m)(W+m)}{2W}\frac{\delta_{l1}}{m^2-a} \qquad \forall\, l \geq 1\,, \tag{8.11}$$

and where we have defined ($x_s(s,s')$ will be introduced in (8.31))

$$y(s) = 1 - \frac{s+m^2-\Sigma}{2q^2} = z_s(s,t(s,u=m^2)) = x_s(s,s'=m^2)\,, \tag{8.12}$$

and $Q_l(z)$ denote the Legendre functions of the second kind.

The $Q_l(z)$ obey a recursion relation similar to the one for the usual Legendre polynomials $P_l(z)$ (for $l \geq 0$)

$$(l+1)P_{l+1}(z) + lP_{l-1}(z) = (2l+1)zP_l(z)\,,$$
$$(l+1)Q_{l+1}(z) + lQ_{l-1}(z) = (2l+1)zQ_l(z) - \delta_{l0}\,, \tag{8.13}$$

which, together with $Q_l = P_l = 0$ for $l < 0$, leads in particular to (cf. (8.66) for the general formula)

$$Q_1(z) = P_1(z)Q_0(z) - 1\,, \qquad Q_2(z) = P_2(z)Q_0(z) - \frac{3}{2}z\,, \qquad Q_3(z) = P_3(z)Q_0(z) - \frac{5z^2}{2} + \frac{2}{3}\,. \tag{8.14}$$

From the Neumann integral representation for general complex argument z (cf. [211])

$$Q_l(z) = \frac{1}{2}\int_{-1}^{1}dx\,\frac{P_l(x)}{z-x} = (-1)^{l+1}Q_l(-z)\,, \tag{8.15}$$

[#2]Of course, also this form of the nucleon pole terms obeys the MacDowell symmetry relation (8.1), since the term proportional to $\delta_{l+1,0}$ or δ_{l0} vanishes for $\bar{N}_{l\pm}^I$ as a consequence of l starting at 0 or 1, respectively.

which leads to a cut along the real axis for $-1 \leq x \leq 1$, the boundary values on the upper and lower rim of the cut (i.e. for $z = y \pm i\epsilon$ with real y and $|y| \leq 1$) can be obtained by use of the symbolic principal value formula

$$\frac{1}{x - (y \pm i\epsilon)} = \mathcal{P}_x \frac{1}{x - y} \pm i\pi\delta(x - y) \, , \tag{8.16}$$

where $\mathcal{P}_x$ denotes the principal value integral over x. Thus one obtains for general real argument y

$$Q_l(y \pm i\epsilon) = Q_l^{\mathcal{P}}(y) \mp i\frac{\pi}{2} P_l(y) \, \theta(1 - y^2) \, , \tag{8.17}$$

and particularly for the lowest function

$$Q_0(y \pm i\epsilon) = \frac{1}{2} \int\limits_{-1}^{1} \frac{\mathrm{d}x}{y - x \pm i\epsilon} = \frac{1}{2} \log\left|\frac{1 + y}{1 - y}\right| \mp i\frac{\pi}{2} \, \theta(1 - y^2) \, . \tag{8.18}$$

From the form of $Q_0^{\mathcal{P}}(y)$ for real y

$$Q_0^{\mathcal{P}}(y) = \frac{1}{2} \log\left|\frac{1 + y}{1 - y}\right| = \begin{cases} \frac{1}{2} \log \frac{1+y}{1-y} = \mathrm{Artanh}\, y & \text{for } |y| < 1 \, , \\ \frac{1}{2} \log \frac{y+1}{y-1} = \mathrm{Arcoth}\, y & \text{for } |y| > 1 \, , \end{cases} \tag{8.19}$$

we can perform the analytic continuation for purely imaginary argument $z = iy$ with e.g. $y > 1$

$$Q_0(iy) = \frac{1}{2} \log \frac{iy + 1}{iy - 1} = \frac{1}{2} \log \frac{1 + iy}{1 - iy} - i\frac{\pi}{2} = i\left(\arctan y - \frac{\pi}{2}\right) = -Q_0(-iy) \, , \tag{8.20}$$

by choosing the cut of $\log z$ as usual along $-\infty \leq z \leq 0$ and taking the main branches for the phase $\arg z \in (-\pi, \pi]$ as well as for $\arctan y \in (-\pi/2, \pi/2]$. Thereby one can infer that $Q_l(iy)$ is imaginary/real for l even/odd, respectively. For general complex argument z with non-vanishing real part we may thus write

$$Q_0(z) = \frac{1}{2} \log \frac{1 + z}{1 - z} - i\frac{\pi}{2}\{\theta(\mathrm{Im}\, z) - \theta(-\mathrm{Im}\, z)\} \, , \qquad \log \frac{1 + z}{1 - z} = \log\left|\frac{1 + z}{1 - z}\right| + i \arg \frac{1 + z}{1 - z} \, . \tag{8.21}$$

Functions with $l \geq 1$ may then be obtained via either the recursion relation (8.13) or the reduction formula (8.66).

8.2   *s*- and *u*-channel exchange

By introducing a convenient matrix notation via

$$\mathbf{A}^I = \begin{pmatrix} A^I \\ B^I \end{pmatrix}, \qquad \mathbf{f}_l^I = \begin{pmatrix} f_{l+}^I \\ f_{(l+1)-}^I \end{pmatrix}, \tag{8.22}$$

the crossing properties of the even and odd invariant amplitude combinations (7.26) read

$$\mathbf{A}^I(\nu, t) = \epsilon^I \boldsymbol{\sigma}_3 \, \mathbf{A}^I(-\nu, t) \, , \qquad \boldsymbol{\sigma}_3 = \begin{pmatrix} 1 & 0 \\ 0 & -1 \end{pmatrix} . \tag{8.23}$$

While the *s*-channel partial-wave projection (8.8) can be rewritten as

$$\mathbf{f}_l^I(W) = \int\limits_{-1}^{1} dz_s \, \mathbf{R}^l(W, z_s) \mathbf{A}^I(s, t) \Big|_{t=t(s,z_s)} \, , \qquad (8.24)$$

where the projection kernel matrix is given by

$$\mathbf{R}^l(W, z_s) = \begin{pmatrix} R_{l,l+1}^1 & R_{l,l+1}^2 \\ R_{l+1,l}^1 & R_{l+1,l}^2 \end{pmatrix} \, , \qquad (8.25)$$

$$R_{kn}^1(W, z_s) = \frac{1}{16\pi W} \Big\{ (E+m) P_k(z_s) - (E-m) P_n(z_s) \Big\} = -R_{nk}^1(-W, z_s) \, ,$$

$$R_{kn}^2(W, z_s) = \frac{1}{16\pi W} \Big\{ (E+m)(W-m) P_k(z_s) + (E-m)(W+m) P_n(z_s) \Big\} = -R_{nk}^2(-W, z_s) ,$$

the *s*-channel partial-wave expansion, i.e. the inversion of (8.24), takes the form [205]

$$\mathbf{A}^I(s, t) \Big|_{t=t(s,z_s)} = \sum_{l=0}^{\infty} \mathbf{S}^l(W, z_s) \mathbf{f}_l^I(W) \, , \qquad (8.26)$$

with the expansion kernel matrix

$$\mathbf{S}^l(W, z_s) = \begin{pmatrix} S_{l+1,l}^1 & -S_{l,l+1}^1 \\ S_{l+1,l}^2 & -S_{l,l+1}^2 \end{pmatrix} \, ,$$

$$S_{kn}^1(W, z_s) = 4\pi \Big\{ \frac{W+m}{E+m} P_k'(z_s) + \frac{W-m}{E-m} P_n'(z_s) \Big\} = -S_{nk}^1(-W, z_s) \, ,$$

$$S_{kn}^2(W, z_s) = 4\pi \Big\{ \frac{1}{E+m} P_k'(z_s) - \frac{1}{E-m} P_n'(z_s) \Big\} = -S_{nk}^2(-W, z_s) \, . \qquad (8.27)$$

In accordance with the matrix form of the MacDowell symmetry relation (8.1)

$$\mathbf{f}_l^I(W) = -\boldsymbol{\sigma}_1 \mathbf{f}_l^I(-W) \, , \qquad \boldsymbol{\sigma}_1 = \begin{pmatrix} 0 & 1 \\ 1 & 0 \end{pmatrix} \, , \qquad (8.28)$$

these kernels obey the symmetry relations

$$\mathbf{R}^l(W, z_s) = -\boldsymbol{\sigma}_1 \mathbf{R}^l(-W, z_s) \, , \qquad \mathbf{S}^l(W, z_s) = -\mathbf{S}^l(-W, z_s) \boldsymbol{\sigma}_1 \, . \qquad (8.29)$$

With the definitions (7.102) the *s*- and *u*-channel terms of the HDRs (7.98) thus can be cast into the matrix form

$$\mathbf{A}^I(s, t) \Big|_{t=t(s,z_s)=-2q^2(1-z_s)}^{s+u} = \frac{1}{\pi} \int\limits_{s_+}^{\infty} ds' \, \mathbf{h}_s^I[s, s'; z_s] \, \text{Im} \, \mathbf{A}^I(s', t') \Big|_{t'=t'(s',z_s')=-2q'^2(1-z_s')} \, , \qquad (8.30)$$

where the HDR kernel matrix $\mathbf{h}_s^I$ is given by

$$\mathbf{h}_s^I(s, s'; z_s) = h_1 \boldsymbol{\sigma}_0 - \epsilon^I h_2 \boldsymbol{\sigma}_3 \, , \qquad \boldsymbol{\sigma}_0 = \mathbb{1}_2 = \begin{pmatrix} 1 & 0 \\ 0 & 1 \end{pmatrix} \, , \qquad x_s(s, s') = 1 - \frac{s + s' - \Sigma}{2q^2} \, ,$$

$$h_1(s, s') = \frac{1}{s' - s} - \frac{1}{2} \frac{1}{s' - a} \, , \qquad h_2(s, s'; z_s) = \frac{1}{2q^2} \frac{1}{x_s - z_s} + \frac{1}{2} \frac{1}{s' - a} \, , \qquad (8.31)$$

and $[s, s'; z_s]$ denotes that the whole integrand is to be understood as a function of these variables, which can be achieved by use of

$$z_s'(s, s'; z_s) = \alpha z_s + \beta, \qquad \alpha(s, s') = \frac{q^2}{q'^2} \frac{s - a}{s' - a}, \qquad \beta(s, s') = 1 - \alpha - \frac{s' - s}{s' - a} \frac{s + s' - \Sigma}{2q'^2}.$$
(8.32)

By expanding the absorptive part of the s- and u-channel HDR terms given in (8.30) into s-channel partial waves via (8.26) and projecting out s-channel partial waves again by means of (8.24), we arrive at the PWDRs

$$\mathbf{f}_l^I(W)\Big|^{s+u} = \frac{1}{\pi} \int\limits_{W_+}^{\infty} dW' \sum_{l'=0}^{\infty} \mathbf{K}^{ll', I}(W, W') \operatorname{Im} \mathbf{f}_{l'}^I(W'),$$
(8.33)

where the s- and u-channel kernel matrix is defined by

$$\mathbf{K}^{ll', I}(W, W') = 2W' \int\limits_{-1}^{1} dz_s \, \mathbf{R}^l(W, z_s) \mathbf{h}_s^I[W, W'; z_s] \mathbf{S}^{l'}(W', z_s').$$
(8.34)

Due to the symmetry relations

$$-\boldsymbol{\sigma}_1 \mathbf{K}^{ll', I}(-W, W') = \mathbf{K}^{ll', I}(W, W') = \mathbf{K}^{ll', I}(W, -W')\boldsymbol{\sigma}_1,$$
(8.35)

that follow from the relations (8.29), the s- and u-channel kernel matrix can be written with only one kernel function according to

$$\mathbf{K}^{ll', I}(W, W') = \begin{pmatrix} K_{ll'}^I(W, W') & K_{ll'}^I(W, -W') \\ -K_{ll'}^I(-W, W') & -K_{ll'}^I(-W, -W') \end{pmatrix},$$

$$K_{ll'}^I(W, W') = 2W' \int\limits_{-1}^{1} dz_s \left\{ \mathbf{R}^l(W, z_s) \mathbf{h}_s^I[W, W'; z_s] \mathbf{S}^{l'}(W', z_s') \right\}_{1,1},$$
(8.36)

where the subscript denotes the $1,1$-th element of the matrix in the curly brackets. The PWDRs (8.33) then take the form already stated in (8.3)

$$f_{l+}^I(W)\Big|^{s+u} = \frac{1}{\pi} \int\limits_{W_+}^{\infty} dW' \sum_{l'=0}^{\infty} \left\{ K_{ll'}^I(W, W') \operatorname{Im} f_{l'+}^I(W') + K_{ll'}^I(W, -W') \operatorname{Im} f_{(l'+1)-}^I(W') \right\}$$

$$= -f_{(l+1)-}^I(-W)\Big|^{s+u}.$$
(8.37)

Defining the structure

$$\varphi[a_{kn} | b(W, W')] = \frac{W'}{W} \Big\{ b(W, -W') a_{kn} + b(W, W') a_{k,n+1}$$

$$+ b(-W, -W') a_{k+1,n} + b(-W, W') a_{k+1,n+1} \Big\},$$
(8.38)

where $a_{kn}(s, s')$ is to be understood as a function invariant under sign changes in W and W', and introducing the kinematical abbreviations

$$\delta(W, W') = \frac{E + m}{E' + m}\left[W' + W\right] , \qquad E'(W') = E(W') ,$$

$$\varrho(W, W') = \frac{E + m}{E' + m}\left[W' - W + 2m\right] ,$$

$$\varkappa^I(W, W') = \frac{1}{2}\left[\delta(W, W') + \epsilon^I \varrho(W, W')\right] = \frac{E + m}{E' + m}\left[\tilde{\epsilon}_+(W' + m) + \tilde{\epsilon}_-(W - m)\right] , \quad (8.39)$$

as well as the angular kernels

$$U_{ll'}(s, s') = \frac{1}{2}\int\limits_{-1}^{1} \mathrm{d}z_s \; P_l(z_s)P'_{l'}(z'_s) , \qquad V_{ll'}(s, s') = \frac{1}{2}\int\limits_{-1}^{1} \mathrm{d}z_s \; \frac{P_l(z_s)P'_{l'}(z'_s)}{x_s - z_s} , \qquad (8.40)$$

the general s- and u-channel kernel function can be written as

$$\begin{aligned}
K_{ll'}^I(W, W') &= h_1\varphi\left[U_{ll'}\big|\delta(W, W')\right] - \frac{\epsilon^I}{2}\varphi\left[\frac{V_{ll'}}{q^2} + \frac{U_{ll'}}{s' - a}\bigg|\varrho(W, W')\right] \\
&= \frac{\varphi\left[U_{ll'}\big|\delta(W, W')\right]}{s' - s} - \epsilon^I\frac{\varphi\left[V_{ll'}\big|\varrho(W, W')\right]}{2q^2} - \frac{\varphi\left[U_{ll'}\big|\varkappa^I(W, W')\right]}{s' - a} . \qquad (8.41)
\end{aligned}$$

Since $\varphi[a_{kn}|b(W, W')]$ encodes the MacDowell symmetry (8.1) for both pairs (k, W) and (n, W'), we can decompose it in two ways

$$\begin{aligned}
\varphi\left[a_{kn}\big|b(W, W')\right] &= \varphi_1\left[a_{kn}\big|b(W, W')\right] - \varphi_1\left[a_{k+1,n}\big|b(-W, W')\right] , \\
&= \varphi_2\left[a_{kn}\big|b(W, W')\right] - \varphi_2\left[a_{k,n+1}\big|b(W, -W')\right] , \\
\varphi_1\left[a_{kn}\big|b(W, W')\right] &= \frac{W'}{W}\left\{b(W, -W')a_{kn} + b(W, W')a_{k,n+1}\right\} , \\
\varphi_2\left[a_{kn}\big|b(W, W')\right] &= \frac{W'}{W}\left\{b(W, -W')a_{kn} + b(-W, -W')a_{k+1,n}\right\} , \qquad (8.42)
\end{aligned}$$

and with the definitions

$$K_{ll'}^{I,i}(W, W') = \frac{\varphi_i\left[U_{ll'}\big|\delta(W, W')\right]}{s' - s} - \epsilon^I\frac{\varphi_i\left[V_{ll'}\big|\varrho(W, W')\right]}{2q^2} - \frac{\varphi_i\left[U_{ll'}\big|\varkappa^I(W, W')\right]}{s' - a} \qquad i \in \{1, 2\} , \qquad (8.43)$$

the kernels exhibit the following interrelations

$$K_{ll'}^I(W, W') = K_{ll'}^{I,1}(W, W') - K_{l+1,l'}^{I,1}(-W, W') = K_{ll'}^{I,2}(W, W') - K_{l,l'+1}^{I,2}(W, -W') , \quad (8.44)$$

that may be used to write down explicit expressions of the kernels in a compact form. However, for numerical evaluations a different prescription is preferable. The part of (8.41) that contains the s-channel cut can be decomposed according to

$$\begin{aligned}
\frac{\varphi\left[U_{ll'}\big|\delta(W, W')\right]}{s' - s} &= \frac{\gamma_{ll'}(W, W')}{W' - W} + \frac{1}{W' + W}\frac{W'}{W}\left\{\frac{E + m}{E' - m}U_{ll'} - \frac{E - m}{E' + m}U_{l+1,l'+1}\right\} , \\
\gamma_{ll'}(W, W') &= \frac{W'}{W}\left\{\frac{E + m}{E' + m}U_{l,l'+1} - \frac{E - m}{E' - m}U_{l+1,l'}\right\} . \qquad (8.45)
\end{aligned}$$

Using the identity

$$\int\limits_{-1}^{1} dz\, P'_{l'}(z)\big[P_{l\pm1}(z) - zP_l(z)\big] = \frac{2\delta_{ll'}}{2l+1}\left\{\begin{matrix} -l \\ l+1 \end{matrix}\right\} , \tag{8.46}$$

we can easily calculate its residue at the pole $W' = W$ (where $\alpha = 1$, $\beta = 0$, and thus $z'_s = z_s$)

$$\text{Res}\left[\frac{\gamma_{ll'}(W,W')}{W'-W}, W'=W\right] = \gamma_{ll'}(W,W) = U_{l,l'+1}(s,s) - U_{l+1,l'}(s,s) = \delta_{ll'} , \tag{8.47}$$

which together with the decompositions

$$U_{ll'}(W,W') = U_{ll'}(W,W) + (W'-W)\bar{U}_{ll'}(W,W') ,$$
$$\frac{W'}{W}\frac{E\pm m}{E'\pm m} = \frac{s'}{s}\frac{(W\pm W_+)(W\pm W_-)}{(W'\pm W_+)(W'\pm W_-)} = 1 + (W'-W)c_\pm ,$$
$$c_\pm(W,W') = \frac{(W'+W)\Sigma_- \pm 2mW'W}{2W'(E'\pm m)s} = \frac{(W'+W)W_+W_- \pm W'W(W_++W_-)}{(W'\pm W_+)(W'\pm W_-)s}$$
$$= -c_\mp(-W,-W') , \tag{8.48}$$

leads us to the alternative form of the kernels $K^I_{ll'}(W,W')$

$$K^I_{ll'}(W,W') = \frac{\delta_{ll'}}{W'-W} + \bar{K}^I_{ll'}(W,W') ,$$
$$\bar{K}^I_{ll'}(W,W') = \bar{U}_{l,l'+1}(W,W') - \bar{U}_{l+1,l'}(W,W') + c_+U_{l,l'+1} - c_-U_{l+1,l'}$$
$$+ \frac{1}{W'+W}\frac{W'}{W}\left\{\frac{E+m}{E'-m}U_{ll'} - \frac{E-m}{E'+m}U_{l+1,l'+1}\right\}$$
$$- \epsilon^I \frac{\varphi\big[V_{ll'}\big|\varrho(W,W')\big]}{2q^2} - \frac{\varphi\big[U_{ll'}\big|\varkappa^I(W,W')\big]}{s'-a} , \tag{8.49}$$

where the first term is the usual Cauchy kernel for the *s*-channel cut (contributing only for $l = l'$) and the kernels $\bar{K}^I_{ll'}(W,W')$ contain only the left-hand cut. In order to derive explicit expressions for the angular kernels $U_{ll'}(W = \sqrt{s}, W' = \sqrt{s'})$ from (8.40) and subsequently their regular parts $\bar{U}_{ll'}(W,W')$ from (8.48), we use the following expansion (cf. [211])

$$P_l(z_s) = \sum_{\lambda=0}^{l} a^l_\lambda x^\lambda , \qquad a^l_\lambda = \frac{(-1)^\lambda (l+\lambda)!}{(\lambda!)^2(l-\lambda)!} , \qquad x = \frac{1-z_s}{2} , \tag{8.50}$$

and hence

$$P'_{l'}(z'_s) = -\frac{1}{2}\sum_{\lambda'=0}^{l'-1}(\lambda'+1)a^{l'}_{\lambda'+1}x'^{\lambda'} , \qquad x' = \frac{1-z'_s}{2} = \omega + \alpha x ,$$
$$\omega(s,s') = \frac{1-(\alpha+\beta)}{2} = \frac{s'-s}{s'-a}\frac{s'+s-\Sigma}{4q'^2} , \tag{8.51}$$

together with the binomial theorem and the Saalschütz identity (cf. [211])

$$\sum_{\lambda=0}^{l}\frac{a^l_\lambda}{\mu+\lambda+1} = (-1)^l\frac{(\mu!)^2}{(\mu-l)!(\mu+l+1)!} \qquad (\mu \geq l) , \tag{8.52}$$

to arrive at the general expression for the angular kernel $U_{ll'}$

$$U_{ll'}(s, s') = \frac{(-1)^{l+1}}{2} \sum_{\lambda'=l}^{l'-1} (\lambda' + 1) a_{\lambda'+1}^{l'} \sum_{\mu=l}^{\lambda'} \binom{\lambda'}{\mu} \frac{(\mu!)^2}{(\mu - l)!(\mu + l + 1)!} \omega^{\lambda'-\mu} \alpha^\mu .$$ (8.53)

These kernels show the following asymptotic behavior

$$U_{ll'} \sim q^{2l} \quad \text{for} \quad q \to 0 , \qquad U_{ll'} \sim q'^{-2l'+2} \quad \text{for} \quad q' \to 0 , \qquad U_{ll'} \sim q'^{-4l} \quad \text{for} \quad q' \to \infty ,$$ (8.54)

and, in particular, the lowest kernels are given by (note that $U_{l0} = 0$ and $U_{l1} = \delta_{l0}$)

$$U_{ll'} = 0 \quad \text{for} \quad l' \le l , \qquad U_{l,l+1} = \alpha^l , \qquad U_{l,l+2} = (2l + 3)\beta\alpha^l ,$$

$$U_{l,l+3} = \frac{\alpha^l}{2}\left\{ (2l + 5)\left[\alpha^2 + (2l + 3)\beta^2\right] - (2l + 3) \right\} .$$ (8.55)

From (8.53) and (8.40) we can easily deduce for $W' = W$

$$U_{ll'}(W, W) = \sum_{\lambda'=l}^{l'-1} u_{ll'}^{\lambda'} = \begin{cases} 0 & \text{for } l' \le l \text{ or } l' - l \text{ even} , \\ 1 & \text{for } l' - l \text{ odd} , \end{cases}$$

$$u_{ll'}^{\lambda'} = \frac{(-1)^{l+\lambda'}(l' + \lambda' + 1)!}{2(\lambda' + 1)(l' - \lambda' - 1)!(\lambda' - l)!(l + \lambda' + 1)!} ,$$ (8.56)

which again yields $U_{l,l'+1}(W, W) - U_{l+1,l'}(W, W) = \delta_{ll'}$. By defining

$$\frac{q^2}{q'^2} = 1 + (W' - W)d_1 , \qquad d_1(W, W') = \frac{W' + W}{4q'^2}\left[\frac{\Sigma_-^2}{ss'} - 1\right] ,$$

$$\frac{s - a}{s' - a} = 1 + (W' - W)d_2 , \qquad d_2(W, W') = -\frac{W' + W}{s' - a} ,$$ (8.57)

we can rewrite the powers of α according to (note that $b_0 = 0$)

$$\alpha^\mu = 1 + (W' - W)b_\mu ,$$

$$b_\mu(W, W') = \sum_{k=0}^{\mu-1} \binom{\mu}{k+1} (W' - W)^k \left\{ d_1^{k+1} \left(\frac{s - a}{s' - a}\right)^\mu + d_2^{k+1} \right\}$$

$$= \frac{W' + W}{s' - a} \sum_{k=0}^{\mu-1} \binom{\mu}{k+1} \left(\frac{s' - s}{s' - a}\right)^k$$

$$\times \left\{ \left(\frac{s - a}{4q'^2}\left[\frac{\Sigma_-^2}{ss'} - 1\right]\right)^{k+1} \left(\frac{s - a}{s' - a}\right)^{\mu-(k+1)} + (-1)^{k+1} \right\} ,$$ (8.58)

which together with the definitions

$$\omega = (W' - W)\bar{\omega} , \qquad \bar{\omega}(W, W') = \frac{W' + W}{s' - a}\frac{s + s' - \Sigma}{4q'^2} ,$$

$$\tilde{U}_{ll'}(W, W') = \frac{(-1)^{l+1}}{2} \sum_{\lambda'=l}^{l'-1} (\lambda' + 1) a_{\lambda'+1}^{l'} \sum_{\mu=l}^{\lambda'-1} \binom{\lambda'}{\mu} \frac{(\mu!)^2}{(\mu - l)!(\mu + l + 1)!} \omega^{\lambda'-1-\mu} \alpha^\mu ,$$ (8.59)

allows us to give the explicit form of the "regular part" $\bar{U}_{ll'}$ of the angular kernel $U_{ll'}$ as

$$\bar{U}_{ll'}(W, W') = \sum_{\lambda'=l}^{l'-1} u_{ll'}^{\lambda'} b_{\lambda'} + \bar{\omega} \tilde{U}_{ll'} \,, \tag{8.60}$$

from which we can easily obtain the lowest $\bar{U}_{ll'}$ (note that $\bar{U}_{l0} = 0 = \bar{U}_{l1}$)

$$\bar{U}_{ll'} = 0 \quad \text{for} \quad l' \leq l \,, \qquad \bar{U}_{l,l+1} = b_l \,, \qquad \bar{U}_{l,l+2} = -(2l+3)\Big\{ b_{l+1} - b_l + 2\bar{\omega}\alpha^l \Big\} \,,$$

$$\bar{U}_{l,l+3} = (2l+5)(2l+3)\left\{ (l+2)\left[\frac{b_{l+2}}{2l+3} + \frac{b_l}{2l+5} \right] - b_{l+1} - \bar{\omega}\alpha^l(1 - \alpha + \beta) \right\} \,. \tag{8.61}$$

The angular kernels $V_{ll'}$ can be expressed by the kernels $U_{ll'}$ as follows: from the integral representation of $U_{ll'}$ (8.40) we can deduce that

$$P_{l'}'(z_s') = \sum_{n=0}^{l'-1} (2n+1) U_{nl'} P_n(z_s) \,, \tag{8.62}$$

and inserting this into the integral representation of $V_{ll'}$ (8.40) yields

$$V_{ll'} = \sum_{n=0}^{l'-1} (2n+1) U_{nl'} \left\{ \frac{1}{2} \int_{-1}^{1} dz_s \, \frac{P_n(z_s) P_l(z_s)}{x_s - z_s} \right\} \,. \tag{8.63}$$

By using the identity

$$\frac{1}{2} \int_{-1}^{1} dx \, \frac{P_n(x) P_l(x)}{z - x} = P_n(z) Q_l(z) \qquad \text{for} \quad n \leq l \,, \tag{8.64}$$

we can write (note that the sum vanishes for $l' \leq l+1$)

$$V_{ll'} = Q_l(x_s) P_{l'}'(x_s') - \sum_{n=l+1}^{l'-1} (2n+1) U_{nl'} \Big\{ P_n(x_s) Q_l(x_s) - P_l(x_s) Q_n(x_s) \Big\} \,,$$

$$x_s'(s, s') = \alpha x_s + \beta = 1 - \frac{s' + s - \Sigma}{2q'^2} = x_s(s', s) \,, \tag{8.65}$$

and with the aid of $W_{l-1}(z)$, which is a polynomial of degree $l-1$ in z defined by (cf. [211])

$$Q_l(z) = Q_0(z) P_l(z) - W_{l-1}(z) \,, \qquad W_{-1} = 0 \,, \tag{8.66}$$

leading to the integral representation

$$W_{l-1}(z) = \frac{1}{2} \int_{-1}^{1} dx \, \frac{P_l(z) - P_l(x)}{z - x} \,, \tag{8.67}$$

the angular kernels $V_{ll'}$ take the general form

$$V_{ll'}(s, s') = Q_l(x_s) P_{l'}'(x_s') - \bar{V}_{ll'} \,,$$

$$\bar{V}_{ll'}(s, s') = \sum_{n=l+1}^{l'-1} (2n+1) U_{nl'} \Big\{ P_l(x_s) W_{n-1}(x_s) - P_n(x_s) W_{l-1}(x_s) \Big\} \,. \tag{8.68}$$

The $\bar{V}_{ll'}$ only contribute for $l' \geq l + 2$

$$\bar{V}_{ll'} = 0 \quad \text{for} \ \ l' \leq l + 1 \,, \tag{8.69}$$

and we can immediately read off

$$V_{l0} = 0 \,, \qquad V_{l1} = Q_l(x_s) \,, \qquad V_{0l'} = Q_0(x_s) P'_{l'}(x'_s) - \sum_{n=1}^{l'-1} (2n+1) U_{nl'} W_{n-1}(x_s) \,, \tag{8.70}$$

where the second equation can also be seen directly by comparing (8.40) with (8.15). Furthermore one easily obtains the asymptotic behavior

$$V_{ll'} \sim q^{2l+2} \quad \text{for} \ \ q \to 0 \,, \qquad V_{ll'} \sim q'^{-2l'+2} \quad \text{for} \ \ q' \to 0 \,, \qquad V_{ll'} \sim q'^{-2l-2} \quad \text{for} \ \ q' \to \infty \,. \tag{8.71}$$

From (8.67) or from Christoffel's formula for $l \geq 1$ (cf. [211])

$$W_{l-1}(z) = \sum_{\lambda=0}^{\left\lfloor \frac{l-1}{2} \right\rfloor} \frac{2(l-\lambda) - (2\lambda+1)}{(l-\lambda)(2\lambda+1)} P_{l-(2\lambda+1)}(z) \,, \qquad \left\lfloor \frac{l-1}{2} \right\rfloor = \begin{cases} \frac{l}{2} - 1 & \text{for } l \geq 2 \text{ even} \,, \\ \frac{l-1}{2} & \text{for } l \geq 1 \text{ odd} \,, \end{cases} \tag{8.72}$$

both yielding (also in agreement with (8.14) and (8.66)) besides $W_{-1} = 0$

$$W_0 = 1 \,, \qquad W_1(z) = \frac{3}{2} z \,, \qquad W_2(z) = \frac{5}{2} z^2 - \frac{2}{3} \,, \tag{8.73}$$

where it is useful to note that $W_l(z)$ like $P_l(z)$ contains only even/odd powers of z for l even/odd, respectively, we can immediately deduce the non-vanishing angular kernels $U_{ll'}$, $\bar{U}_{ll'}$, and $V_{ll'}$ for $l' \leq 3$

$$U_{l1} = \delta_{l0} \,, \qquad U_{l2} = \alpha \delta_{l1} + 3\beta \delta_{l0} \,, \qquad U_{l3} = \alpha^2 \delta_{l2} + 5\alpha\beta \delta_{l1} + \frac{1}{2} \big\{ 5[\alpha^2 + 3\beta^2] - 3 \big\} \delta_{l0} \,,$$
$$\bar{U}_{l2} = b_1 \delta_{l1} - 3 \big\{ b_1 + 2\bar{\omega} \big\} \delta_{l0} \,,$$
$$\bar{U}_{l3} = b_2 \delta_{l2} + 5 \big\{ b_1 - b_2 - 2\bar{\omega}\alpha \big\} \delta_{l1} - 5 \big\{ 3b_1 - 2b_2 + 3\bar{\omega}(1 - \alpha + \beta) \big\} \delta_{l0} \,,$$
$$V_{l1} = Q_l(x_s) \,, \qquad V_{l2} = 3x'_s Q_l(x_s) - 3\alpha \delta_{l0} \,,$$
$$V_{l3} = P'_3(x'_s) Q_l(x_s) - \frac{5}{2} \alpha^2 \delta_{l1} - \frac{15}{2} \alpha \big\{ \alpha x_s + 2\beta \big\} \delta_{l0} \,, \tag{8.74}$$

needed for the kernels $K^I_{ll'}(W, W')$ for all combinations ($l \geq 0, l' \leq 2$) according to (8.49)

$$K^I_{l0}(W, W') = \left\{ \frac{1}{W' - W} + c_+ - \frac{W'}{W} \frac{\varkappa^I(W, W')}{s' - a} \right\} \delta_{l0}$$
$$- \frac{\epsilon^I}{2q^2} \frac{W'}{W} \big\{ \varrho(W, W') Q_l(x_s) + \varrho(-W, W') Q_{l+1}(x_s) \big\} \,,$$
$$K^I_{l1}(W, W') = \left\{ \frac{1}{W' - W} + b_1 + \alpha c_+ \right\} \delta_{l1} + \left\{ \frac{1}{W' + W} \frac{W'}{W} \left(\frac{E + m}{E' - m} - \alpha \frac{E - m}{E' + m} \right) \right.$$
$$\left. - 3 \big[b_1 + 2\bar{\omega} - \beta c_+ \big] \right\} \delta_{l0} - \frac{\epsilon^I}{2q^2} \frac{W'}{W} \left\{ \big[3x'_s \varrho(W, W') + \varrho(W, -W') \big] Q_l(x_s) \right.$$
$$\left. + \big[3x'_s \varrho(-W, W') + \varrho(-W, -W') \big] Q_{l+1}(x_s) - 3\alpha \varrho(W, W') \delta_{l0} \right\}$$

$$- \frac{1}{s'-a} \frac{W'}{W} \left\{ \alpha \varkappa^I(W,W')\delta_{l1} \right.$$

$$\left. + \left[3\beta\varkappa^I(W,W') + \varkappa^I(W,-W') + \alpha\varkappa^I(-W,W')\right]\delta_{l0} \right\},$$

$$K_{l2}^I(W,W') = \left\{ \frac{1}{W'-W} + b_2 + \alpha^2 c_+ \right\}\delta_{l2} + \left\{ \frac{\alpha}{W'+W}\frac{W'}{W}\left(\frac{E+m}{E'-m} - \alpha\frac{E-m}{E'+m}\right) \right.$$

$$\left. + 5\left[b_1 - b_2 - \alpha(2\bar\omega - \beta c_+)\right]\right\}\delta_{l1} + \left\{ \frac{\beta}{W'+W}\frac{W'}{W}\left(3\frac{E+m}{E'-m} - 5\alpha\frac{E-m}{E'+m}\right) \right.$$

$$\left. - 2(8b_1 - 5b_2) - 15\bar\omega(1-\alpha+\beta) + \frac{1}{2}(5[\alpha^2 + 3\beta^2] - 3)c_+ - \alpha c_- \right\}\delta_{l0}$$

$$- \frac{\epsilon^I}{2q^2}\frac{W'}{W}\left\{ -\alpha\left[15\left\{\frac{\alpha}{2}x_s + \beta\right\}\varrho(W,W') + 3\varrho(W,-W') + \frac{5}{2}\alpha\varrho(-W,W')\right]\delta_{l0} \right.$$

$$- \frac{5}{2}\alpha^2\varrho(W,W')\delta_{l1} + \left[P_3'(x_s')\varrho(W,W') + 3x_s'\varrho(W,-W')\right]Q_l(x_s)$$

$$\left. + \left[P_3'(x_s')\varrho(-W,W') + 3x_s'\varrho(-W,-W')\right]Q_{l+1}(x_s) \right\}$$

$$- \frac{1}{s'-a}\frac{W'}{W}\left\{ \alpha^2\varkappa^I(W,W')\delta_{l2} \right.$$

$$+ \alpha\left[5\beta\varkappa^I(W,W') + \varkappa^I(W,-W') + \alpha\varkappa^I(-W,W')\right]\delta_{l1}$$

$$+ \left[\frac{1}{2}(5[\alpha^2 + 3\beta^2] - 3)\varkappa^I(W,W') + 3\beta\varkappa^I(W,-W')\right.$$

$$\left.\left. + 5\alpha\beta\varkappa^I(-W,W') + \alpha\varkappa^I(-W,-W')\right]\delta_{l0} \right\}. \tag{8.75}$$

From $K_{l0}^I(W,W')$ in the form according to (8.41)

$$K_{l0}^I(W,W') = \frac{1}{2W}\frac{W'}{E'+m}\left\{ (E+m)\left[(W+W')\frac{2\delta_{l0}}{s'-s} + \epsilon^I(W-W'-2m)\frac{Q_l(x_s)}{q^2}\right] \right.$$

$$+ \epsilon^I(E-m)(W+W'+2m)\frac{Q_{l+1}(x_s)}{q^2}$$

$$\left. - (E+m)\left[\tilde\epsilon_+(W'+m) + \tilde\epsilon_-(W-m)\right]\frac{2\delta_{l0}}{s'-a} \right\}, \tag{8.76}$$

we can deduce that the nucleon pole terms (8.9) are reproduced by

$$N_{l+}^I(W) = -f^2 K_{l0}^I(W, -W' = m) = -N_{(l+1)-}^I(-W) \qquad \forall\, l \geq 0. \tag{8.77}$$

The explicit formulae for the additional non-vanishing angular kernels $U_{ll'}$, $\bar U_{ll'}$, and $V_{ll'}$ for $(l \leq 2, 4 \leq l' \leq 6)$ needed for calculating the additional higher kernels $K_{ll'}^I$ for $(l \leq 1, 3 \leq l' \leq 5)$ via (8.49) are displayed in App. C.1. Furthermore, we give the asymptotic behavior of the general kernel function $K_{ll'}^I(W,W')$, which can be inferred from the asymptotic behavior of the angular kernels (8.54) and (8.71),

$$\begin{array}{llll}
\text{for } q \to 0 & K_{ll'}^I(W,W') \sim q^{2l}, & K_{ll'}^I(-W,W') \sim q^{2l+2}, \\[4pt]
\text{for } q' \to 0 & K_{ll'}^I(W,W') \sim q'^{-2l'}, & K_{ll'}^I(W,-W') \sim q'^{-2l'-2}, \\[4pt]
\text{for } q' \to \infty & K_{ll'}^I(W,W') \sim q'^{-2l-1}, & \tag{8.78}
\end{array}$$

in agreement with the MacDowell symmetry relation (8.1). Alternatively, for $q \to 0$ and $q' \to \infty$ one could also use the expansion

$$Q_l(x_s) = \left(\frac{-2q^2}{s + s' - \Sigma}\right)^{l+1} + \mathcal{O}\left(\left(\frac{-2q^2}{s + s' - \Sigma}\right)^{l+2}\right) \quad \text{for } \frac{1}{x_s - 1} = \frac{-2q^2}{s + s' - \Sigma} \to 0 \,, \quad (8.79)$$

which easily follows from the integral representation (8.15) together with the orthogonality of the $P_l(z)$, while $(x_s - 1)^{-1} \to -2q^2/(s - s_-) \neq 0$ for $q' \to 0$. Either this expansion with $y(s) = x_s(s, s' = m^2)$ or the relation (8.77) can then be used to derive the asymptotic behavior of the nucleon pole terms

$$N_{l+}^I(W) \sim N_{(l+1)-}^I(-W) \sim q^{2l} \quad \text{for } q \to 0 \,. \tag{8.80}$$

8.3 t-channel exchange

With definitions (7.102) and relations (7.103) the t-channel terms of the HDRs (7.98) can be written as

$$\mathbf{A}^I(s, t)\Big|_{t=t(s, z_s)}^t = \frac{1}{\pi} \int_{t_\pi}^{\infty} dt' \, \mathbf{h}_t^I[s, t'; z_s] \, \mathrm{Im}\, \mathbf{A}^I(s', t')\Big|_{s'=s'(t', z_t')} \,, \tag{8.81}$$

where the HDR kernel matrix $\mathbf{h}_t^I$ is given by

$$\mathbf{h}_t^I(s, t'; z_s) = \frac{1}{2q^2} \frac{1}{x_t - z_s} \begin{pmatrix} \lambda_1^I & 0 \\ 0 & \lambda_2^I \end{pmatrix}, \qquad x_t(s, t') = 1 + \frac{t'}{2q^2} = z_s(s, t') \,,$$

$$\lambda_n^I(s, t'; z_s) = \left(\frac{\nu}{\nu'}\right)^{\frac{1 + (-1)^n \epsilon^I}{2}} \qquad \text{(with } x^0 \equiv 1 \;\; \forall \, x) \,, \tag{8.82}$$

and the integrand is to be understood as a function of $[s, t'; z_s]$ by using

$$z_t'(s, t'; z_s) = \frac{m\nu'}{p_t' q_t'} = \sqrt{\gamma z_s + \delta} \,, \qquad \gamma(s, t') = \frac{q^2(s - a)}{2p_t'^2 q_t'^2} \,, \tag{8.83}$$

$$\delta(s, t') = \frac{(t' - \Sigma + 2a)^2 - 4(s - a)(2q^2 + \Sigma - s - a)}{16 p_t'^2 q_t'^2} \,.$$

The t-channel partial-wave expansions of the invariant amplitudes read [212]

$$A^I(s', t')\Big|_{s'=s'(t', z_t')} = -\frac{4\pi}{p_t'^2} \sum_J (2J + 1)(p_t' q_t')^J \left\{ P_J(z_t') f_+^J(t') - \frac{m}{\sqrt{J(J+1)}} z_t' P_J'(z_t') f_-^J(t') \right\} \,,$$

$$B^I(s', t')\Big|_{s'=s'(t', z_t')} = 4\pi \sum_J \frac{2J + 1}{\sqrt{J(J+1)}} (p_t' q_t')^{J-1} P_J'(z_t') f_-^J(t') \,, \tag{8.84}$$

where it is crucial that the sums only run over even J for $I = +$ and odd J for $I = -$ due to Bose symmetry. Taken literally, the form (8.84) of the partial-wave expansions is only valid for $t' \geq t_N$ since below the two-particle thresholds t_N and t_π the CMS momenta p_t' of the nucleons and q_t' of the pions become purely imaginary and one has to use p_-' and q_-' instead, respectively (cf. (7.17) and [171]). Particularly, in the unphysical range $t' \in [t_\pi, t_N)$ — that we are interested in as the low-energy part of the integration range $t' \in [t_\pi, \infty)$ — we have

$q'_t \in \mathbb{R}$ but $p'_t, z'_t \in i\mathbb{R}$. However, the squares p'^2_t and q'^2_t are always real (albeit not necessarily positive, cf. (7.18)) and since the combination $p'_t q'_t z'_t = m\nu' = m(2s' + t' - \Sigma)$ is always real as well, so is z'^2_t. Due to the fact that the Legendre polynomials and their derivatives have definite parity $P_J(-z) = (-1)^J P_J(z)$ and $P'_J(-z) = (-1)^{J-1} P'_J(z)$ (i.e. they contain solely even/odd powers for J even/odd (for P_J) or odd/even (for P'_J), respectively), a closer look at the expansions (8.84) shows that in all cases only powers of the real combinations $p'_t q'_t z'_t$ and additional factors of powers of the likewise real squares p'^2_t and q'^2_t appear. Therefore, we can symbolically use these formulae for all kinematical ranges and factor out powers of the real squared momenta whenever necessary in order to form explicitly real quantities. This is especially important in view of these expansions being applied to the imaginary parts of the invariant amplitudes, which themselves have to be real, of course. By introducing the t-channel partial-wave amplitudes into the matrix notation via[#3]

$$\mathbf{f}^J = \begin{pmatrix} f^J_+ \\ f^J_- \end{pmatrix}, \tag{8.85}$$

the expansions (8.84) can be rewritten as

$$\mathbf{A}^I(s', t')\Big|_{s'=s'(t', z'_t)} = \sum_J \mathbf{T}^J(t', z'_t) \mathbf{f}^J(t') , \tag{8.86}$$

where the expansion kernel matrix is given by

$$\mathbf{T}^J(t', z'_t) = \zeta_J \begin{pmatrix} u_J & v_J \\ 0 & w_J \end{pmatrix}, \qquad\qquad \zeta_J(t') = 4\pi(2J+1)(p'_t q'_t)^{J-1} ,$$

$$u_J(t', z'_t) = -\frac{q'_t}{p'_t} P_J(z'_t) , \qquad\qquad v_J(t', z'_t) = \frac{m}{\sqrt{J(J+1)}} \frac{q'_t}{p'_t} z'_t P'_J(z'_t) ,$$

$$w_J(t', z'_t) = \frac{1}{\sqrt{J(J+1)}} P'_J(z'_t) . \tag{8.87}$$

As the sum only runs over even J for $I = +$ and odd J for $I = -$ and thus the full information on the crossing properties is already contained in the index J, we can redefine

$$\lambda^I_n(s, t'; z_s) = \lambda^J_n(s, t'; z_s) = \left(\frac{\nu}{\nu'}\right)^{\frac{1+(-1)^{n+J}}{2}} \qquad \text{(with } x^0 \equiv 1 \ \forall \, x) , \tag{8.88}$$

and omit the index I in favor of J in the following. If we expand the imaginary part of the t-channel HDR terms in (8.81) into t-channel partial waves via (8.86) and project out s-channel partial waves again by use of (8.24), we can obtain the following PWDRs

$$\mathbf{f}^I_l(W)\Big|^t = \frac{1}{\pi} \int\limits_{t_\pi}^{\infty} \mathrm{d}t' \sum_J \mathbf{G}^{lJ}(W, t') \operatorname{Im} \mathbf{f}^J(t') , \tag{8.89}$$

where the t-channel kernel matrix is defined by

$$\mathbf{G}^{lJ}(W, t') = \int\limits_{-1}^{1} \mathrm{d}z_s \, \mathbf{R}^l(W, z_s) \mathbf{h}^I_t[s, t'; z_s] \mathbf{T}^J(t', z'_t) . \tag{8.90}$$

[#3]In order to accommodate the fact that there is no f^0_- to the matrix notation, we define $f^0_- \equiv 0$ and in the following all corresponding quantities (e.g. integral kernels) are also understood to vanish.

Due to the symmetry relation

$$\mathbf{G}^{lJ}(-W,t') = -\boldsymbol{\sigma}_1 \mathbf{G}^{lJ}(W,t') \,, \tag{8.91}$$

which follows from (8.29) and is in accordance with the MacDowell symmetry (8.28), the t-channel kernel matrix can be expressed by two kernel functions

$$\mathbf{G}^{lJ}(W,t') = \begin{pmatrix} G_{lJ}(W,t') & H_{lJ}(W,t') \\ -G_{lJ}(-W,t') & -H_{lJ}(-W,t') \end{pmatrix} \,, \tag{8.92}$$

where in accordance with $f_-^0 \equiv 0$ for the matrix notation we set $H_{l0} \equiv 0$, and the PW-DRs (8.89) take the form already given in (8.3)

$$f_{l+}^I(W)\Big|^t = \frac{1}{\pi} \int\limits_{t_\pi}^\infty \mathrm{d}t' \sum_J \Big\{ G_{lJ}(W,t') \,\mathrm{Im}\, f_+^J(t') + H_{lJ}(W,t') \,\mathrm{Im}\, f_-^J(t') \Big\}$$

$$= -f_{(l+1)-}^I(-W)\Big|^t \,. \tag{8.93}$$

With the definitions

$$\psi\big[a_{kn}\big|d(W)\big] = d(W)a_{kn} + d(-W)a_{k+1,n} \,, \qquad \eta_J(W,t') = \frac{2J+1}{4Wq^2}\frac{(p_t'q_t')^J}{p_t'^2} \,, \tag{8.94}$$

and by introducing the angular kernels

$$A_{lJ}(s,t') = \frac{1}{2} \int\limits_{-1}^1 \mathrm{d}z_s \,\lambda_1^J \frac{P_l(z_s)P_J(z_t')}{x_t - z_s} \,, \qquad B_{lJ}(s,t') = \frac{1}{2} \int\limits_{-1}^1 \mathrm{d}z_s \,\lambda_2^J \frac{P_l(z_s)P_J'(z_t')}{x_t - z_s} \,,$$

$$C_{lJ}(s,t') = \frac{1}{2} \int\limits_{-1}^1 \mathrm{d}z_s \,\lambda_1^J \frac{P_l(z_s)z_t'P_J'(z_t')}{x_t - z_s} = JA_{lJ} + B_{l,J-1} \,, \tag{8.95}$$

we can write the kernel functions as

$$G_{lJ}(W,t') = -\eta_J\psi\big[A_{lJ}\big|E+m\big] \qquad\qquad\qquad\qquad \forall\, J \ge 0 \,,$$

$$H_{lJ}(W,t') = \frac{\eta_J}{\sqrt{J(J+1)}}\left\{\frac{p_t'}{q_t'}\psi\big[B_{lJ}\big|(W-m)(E+m)\big] + m\psi\big[C_{lJ}\big|E+m\big]\right\} \quad \forall\, J \ge 1 \,. \tag{8.96}$$

If we use the decomposition

$$\frac{\nu}{\nu'}\frac{1}{x_t - z_s} = \frac{\mu_1}{z_t'} + \frac{\mu_2}{z_t'}\frac{1}{x_t - z_s} \,, \qquad \mu_1(s,t') = -\frac{q^2}{2p_t'q_t'} \,, \qquad \mu_2(s,t') = \frac{2s+t'-\Sigma}{4p_t'q_t'} \,, \tag{8.97}$$

we get for the angular kernels for even J

$$A_{lJ}(s,t') = \frac{1}{2} \int\limits_{-1}^1 \mathrm{d}z_s \,\frac{P_l(z_s)P_J(z_t')}{x_t - z_s} \,,$$

$$B_{lJ}(s,t') = \frac{\mu_1}{2} \int\limits_{-1}^1 \mathrm{d}z_s \,P_l(z_s)\frac{P_J'(z_t')}{z_t'} + \frac{\mu_2}{2} \int\limits_{-1}^1 \mathrm{d}z_s \,\frac{P_l(z_s)P_J'(z_t')/z_t'}{x_t - z_s} \,, \tag{8.98}$$

and for odd J

$$A_{lJ}(s,t') = \frac{\mu_1}{2} \int\limits_{-1}^{1} \mathrm{d}z_s \, P_l(z_s) \frac{P_J(z'_t)}{z'_t} + \frac{\mu_2}{2} \int\limits_{-1}^{1} \mathrm{d}z_s \, \frac{P_l(z_s) P_J(z'_t)/z'_t}{x_t - z_s} \ ,$$

$$B_{lJ}(s,t') = \frac{1}{2} \int\limits_{-1}^{1} \mathrm{d}z_s \, \frac{P_l(z_s) P'_J(z'_t)}{x_t - z_s} \ , \tag{8.99}$$

from which we can infer that only even powers of z'_t occur and hence a square-root dependence on z_s is avoided. We now can work out the kernel functions explicitly, here given for all combinations ($l \geq 0, J \leq 2$) (remember $H_{l0} \equiv 0$)

$$G_{l0}(W,t') = -\frac{1}{4W q^2 p'^2_t} \Big\{ (E+m) Q_l(x_t) - (E-m) Q_{l+1}(x_t) \Big\} \ ,$$

$$G_{l1}(W,t') = \frac{3}{4} \Big\{ (2s+t'-\Sigma) G_{l0}(W,t') + \frac{E+m}{2W p'^2_t} \delta_{l0} \Big\} \ ,$$

$$H_{l1}(W,t') = \frac{1}{\sqrt{2}} \Big\{ \frac{3}{4} Z_l(W,t') - m G_{l1}(W,t') \Big\} \ ,$$

$$G_{l2}(W,t') = \frac{5}{16} \Big\{ \Big[6s(s+t'-\Sigma) + (t'-\Sigma)^2 + 2\Sigma^2_- \Big] G_{l0}(W,t') + 3\frac{(E+m)(s-a)}{W p'^2_t} \delta_{l0} \Big\} \ ,$$

$$H_{l2}(W,t') = \frac{15}{16\sqrt{6}} \Big\{ (2s+t'-\Sigma) Z_l(W,t') - m \Big[4s(s+t'-\Sigma) + (t'-\Sigma)^2 \Big] G_{l0}(W,t')$$

$$- 2\frac{E+m}{W} \Big[\frac{m(s-a)}{p'^2_t} + W - m \Big] \delta_{l0} \Big\} \ , \tag{8.100}$$

where we have defined

$$Z_l(W,t') = \frac{1}{W q^2} \Big\{ (E+m)(W-m) Q_l(x_t) + (E-m)(W+m) Q_{l+1}(x_t) \Big\} \ . \tag{8.101}$$

From the expansion (cf. (8.79))

$$Q_l(x_t) = \left(\frac{2q^2}{t'} \right)^{l+1} + \mathcal{O}\left(\left(\frac{2q^2}{t'} \right)^{l+2} \right) \quad \text{for} \quad \frac{1}{x_t - 1} = \frac{2q^2}{t'} \to 0 \ , \tag{8.102}$$

we can finally deduce the asymptotic behavior of the non-vanishing general kernel functions (8.96)

$$\begin{aligned}
&\text{for} \ \ q \to 0 &&G_{lJ}(W,t') \sim H_{lJ}(W,t') \sim q^{2l} \ , &&G_{lJ}(-W,t') \sim H_{lJ}(-W,t') \sim q^{2l+2} \ , \\
&\text{for} \ \ q'_t \to 0 &&G_{lJ}(W,t') \sim H_{lJ}(W,t') \sim 1 \ , \\
&\text{for} \ \ p'_t \to 0 &&G_{lJ}(W,t') \sim H_{lJ}(W,t') \sim p'^{-2}_t \ , \\
&\text{for} \ \ t' \to \infty &&G_{lJ}(W,t') \sim H_{lJ}(W,t') \sim t'^{J-l-2} \ , \tag{8.103}
\end{aligned}$$

in accordance with the MacDowell symmetry relation (8.1).

Chapter 9

Partial-wave projection for the t-channel amplitudes

For a complete system of Roy–Steiner equations (cf. [52,158]) we will need the analog of (8.3) for the t-channel partial-wave amplitudes $f_\pm^J(t)$,

$$
f_+^J(t) = \tilde{N}_+^J(t) + \frac{1}{\pi} \int\limits_{W_+}^{\infty} dW' \sum_{l=0}^{\infty} \left\{ \tilde{G}_{Jl}(t, W') \operatorname{Im} f_{l+}^I(W') + \tilde{G}_{Jl}(t, -W') \operatorname{Im} f_{(l+1)-}^I(W') \right\}
$$

$$
+ \frac{1}{\pi} \int\limits_{t_\pi}^{\infty} dt' \sum_{J'} \left\{ \tilde{K}_{JJ'}^1(t, t') \operatorname{Im} f_+^{J'}(t') + \tilde{K}_{JJ'}^2(t, t') \operatorname{Im} f_-^{J'}(t') \right\} \qquad \forall\, J \ge 0\,,
$$

$$
f_-^J(t) = \tilde{N}_-^J(t) + \frac{1}{\pi} \int\limits_{W_+}^{\infty} dW' \sum_{l=0}^{\infty} \left\{ \tilde{H}_{Jl}(t, W') \operatorname{Im} f_{l+}^I(W') + \tilde{H}_{Jl}(t, -W') \operatorname{Im} f_{(l+1)-}^I(W') \right\}
$$

$$
+ \frac{1}{\pi} \int\limits_{t_\pi}^{\infty} dt' \sum_{J'} \tilde{K}_{JJ'}^3(t, t') \operatorname{Im} f_-^{J'}(t') \qquad \forall\, J \ge 1\,, \tag{9.1}
$$

where $I = +/-$ if J is even/odd and the sum over J' runs over even/odd values of J' if J is even/odd (cf. Sect. 7.2). As for the s-channel case, the kernels for the corresponding t-channel partial waves can be split into the self-coupling Cauchy kernel and well-defined remainders

$$
\tilde{K}_{JJ'}^1(t, t') = \frac{\delta_{JJ'}}{t' - t} + \dots \qquad \forall\, J, J' \ge 0\,, \qquad \tilde{K}_{JJ'}^3(t, t') = \frac{\delta_{JJ'}}{t' - t} + \dots \qquad \forall\, J, J' \ge 1\,, \tag{9.2}
$$

but, in contrast to the s-channel case, only higher t-channel partial waves can couple to lower ones, since $\tilde{K}_{JJ'}^{1,2,3}(t, t') = 0$ for all $J' < J$, which will be a key ingredient in reducing the t-channel part (9.1) of the RS system to a MO problem in Sect. 12.3. Note furthermore that the f_-^J receive no contributions from the f_+^J. By virtue of crossing symmetry it is possible to use only half the interval in the cosine of the t-channel CMS scattering angle since $s \leftrightarrow u$ corresponds to $\nu \leftrightarrow -\nu$ and hence to $z_t \leftrightarrow -z_t$. If we introduce a matrix notation and define the z_t-projections of the invariant amplitudes in analogy to the s-channel

$$
\mathbf{A}_J^I(t) = \begin{pmatrix} A_J^I(t) \\ B_J^I(t) \end{pmatrix} = \int\limits_{-1}^{1} dz_t\, P_J(z_t) \mathbf{A}^I(s, t) \Big|_{s = s(t, z_t)}\,, \tag{9.3}
$$

we can easily show by using the crossing properties (8.23) that

$$\mathbf{A}_J^I(t) = 2 \int_0^1 \mathrm{d}z_t \, P_J(z_t) \frac{1}{2} \Big\{ \mathbb{1} + (-1)^J \epsilon^I \boldsymbol{\sigma}_3 \Big\} \mathbf{A}^I(t, z_t) \,, \tag{9.4}$$

which leads to the following projections for even J (cf. [212])

$$A_J^- = B_J^+ = 0 \,, \qquad A_J^+(t) = 2 \int_0^1 \mathrm{d}z_t \, P_J(z_t) A^+(t, z_t) \,, \qquad B_J^-(t) = 2 \int_0^1 \mathrm{d}z_t \, P_J(z_t) B^-(t, z_t) \,, \tag{9.5}$$

and for odd J

$$A_J^+ = B_J^- = 0 \,, \qquad A_J^-(t) = 2 \int_0^1 \mathrm{d}z_t \, P_J(z_t) A^-(t, z_t) \,, \qquad B_J^+(t) = 2 \int_0^1 \mathrm{d}z_t \, P_J(z_t) B^+(t, z_t) \,, \tag{9.6}$$

where the integrands of the non-vanishing integrals are effectively functions of $z_t^2 \propto \nu^2$. Even though for πN scattering using only $0 \leq z_t \leq 1$ rather than $-1 \leq z_t \leq 1$ is not as powerful as for the fully $s \leftrightarrow t \leftrightarrow u$ crossing symmetric case of $\pi\pi$ scattering [52], it is important to note that from both possible ranges of z_t it follows that the argument z_t^2 of the integrands is evaluated in the range $0 \leq z_t^2 \leq 1$. Actually, we will never constrain the t-channel scattering angle z_t to be positive, which will be important in Chap. 10. In the following, the different contributions to (9.1) will be discussed.

9.1 Nucleon exchange

Due to (9.4) the t-channel partial-wave projection, i.e. the inversion of (8.84), can be written as (cf. [212])

$$f_+^J(t) = -\frac{1}{4\pi} \int_0^1 \mathrm{d}z_t \, P_J(z_t) \Big\{ \frac{p_t^2}{(p_t q_t)^J} A^I(s,t) \Big|_{s=s(t,z_t)} - \frac{m}{(p_t q_t)^{J-1}} z_t B^I(s,t) \Big|_{s=s(t,z_t)} \Big\} \quad \forall \, J \geq 0 \,,$$

$$f_-^J(t) = \frac{1}{4\pi} \frac{\sqrt{J(J+1)}}{2J+1} \frac{1}{(p_t q_t)^{J-1}} \int_0^1 \mathrm{d}z_t \Big[P_{J-1}(z_t) - P_{J+1}(z_t) \Big] B^I(s,t) \Big|_{s=s(t,z_t)} \quad \forall \, J \geq 1 \,, \tag{9.7}$$

where $I = +/-$ if J is even/odd, such that the integrands are always functions of the squared angle z_t^2, $f_-^0 \equiv 0$ can be used to render the lower formula valid for $J = 0$, and also these formulae are valid literally only for $t \geq t_N$ though we can use them symbolically for all kinematical cases, cf. the discussion following (8.84). In order to carry out these projection integrals we rewrite s and u as functions of t and z_t via

$$s(t, z_t) = \frac{1}{2}(\Sigma - t + 4p_t q_t z_t) \,, \qquad u(t, z_t) = \frac{1}{2}(\Sigma - t - 4p_t q_t z_t) \,, \tag{9.8}$$

which allows us to cast the nucleon pole terms of the HDRs (7.98) into the form

$$\left\{\frac{1}{m^2-s}\pm\frac{1}{m^2-u}-\frac{1\pm1}{2(m^2-a)}\right\}\bigg|_{[t;z_t]}=\frac{1}{2p_tq_t}\left\{\frac{1}{\tilde{y}-z_t}\mp\frac{1}{(-\tilde{y})-z_t}\right\}-\frac{1\pm1}{2(m^2-a)}\ ,\quad(9.9)$$

where the upper/lower sign corresponds to even/odd J (i.e. to $I=+/-)^{\#1}$ and we have defined in analogy to (8.12) ($\tilde{x}_t(t,s')$ will be defined in (9.22))

$$\tilde{y}(t)=\frac{t-2M_\pi^2}{4p_tq_t}=\frac{m\nu_B}{p_tq_t}=z_t(s=m^2,t)=\tilde{x}_t(t,s'=m^2)\ .\qquad(9.10)$$

By defining in analogy to the Legendre polynomials of the second kind

$$\tilde{Q}_l(z)=\frac{1}{2}\int_0^1\mathrm{d}x\,\frac{P_l(x)}{z-x}\ ,\qquad(9.11)$$

from which we can deduce (cf. (8.15))

$$\tilde{Q}_l(z)+(-1)^{l+1}\tilde{Q}_l(-z)=Q_l(z)\ ,\qquad(9.12)$$

and by noting that the orthonormality of the Legendre polynomials yields

$$\frac{1\pm1}{2}\int_0^1\mathrm{d}z\,P_J(z)P_{l=2m}(z)=\frac{\delta_{Jl}}{2l+1}=\frac{1\mp1}{2}\int_0^1\mathrm{d}z\,P_J(z)P_{l=2n+1}(z)\qquad\forall\,J,l(m,n\in\mathbb{N}_0)\ ,$$
$$(9.13)$$

the nucleon pole terms of the PWDRs (9.1) can be written as (in analogy to (8.9))

$$\tilde{N}_+^J(t)=\frac{g^2}{4\pi}m\left\{\frac{\tilde{y}Q_J(\tilde{y})}{(p_tq_t)^J}-\delta_{J0}-\frac{1}{3}\frac{\delta_{J1}}{m^2-a}\right\}\qquad\forall\,J\geq0\ ,$$

$$\tilde{N}_-^J(t)=\frac{g^2}{4\pi}\frac{\sqrt{J(J+1)}}{2J+1}\left\{\frac{Q_{J-1}(\tilde{y})-Q_{J+1}(\tilde{y})}{(p_tq_t)^J}-\frac{\delta_{J1}}{m^2-a}\right\}\qquad\forall\,J\geq1\ ,\qquad(9.14)$$

which for later convenience may be expressed as (in analogy to (8.10))

$$\tilde{N}_+^J(t)=\hat{N}_+^J(t)-\frac{g^2}{4\pi}\frac{m}{3}\frac{\delta_{J1}}{m^2-a}\ ,\quad\hat{N}_+^J(t)=\frac{g^2}{4\pi}m\left\{\frac{\tilde{y}Q_J(\tilde{y})}{(p_tq_t)^J}-\delta_{J0}\right\}\ ,\qquad\forall\,J\geq0\ ,$$

$$\tilde{N}_-^J(t)=\hat{N}_-^J(t)-\frac{g^2}{4\pi}\frac{\sqrt{2}}{3}\frac{\delta_{J1}}{m^2-a}\ ,\quad\hat{N}_-^J(t)=\frac{g^2}{4\pi}\frac{\sqrt{J(J+1)}}{2J+1}\frac{Q_{J-1}(\tilde{y})-Q_{J+1}(\tilde{y})}{(p_tq_t)^J}\ ,\quad\forall\,J\geq1\ ,$$
$$(9.15)$$

and where we set in agreement with $f_-^0\equiv0$ and the above formula $\tilde{N}_-^0=\hat{N}_-^0\equiv0$. Note that for $t\in(t_\pi,t_N)$ due to $p_t\in i\mathbb{R}$ also $\tilde{y}\in i\mathbb{R}$ and hence we need the analytic continuations of $Q_l(z)$ as discussed in Sect. 8.1. However, the pole term projections (9.14), (9.15) are real for all t above the logarithmic branch point singularity at $t_\pi-(M_\pi^2/m)^2\approx3.98M_\pi^2$ of the nucleon cut (which is the left-hand cut for $\tilde{y}(t)^2\leq1$ along the real axis due to the z_t-projection of the

---

$^{\#1}$Alternatively, one may use prefactors containing either $(-1)^J$ or ϵ^I and $\tilde{\epsilon}_\pm$ here and in the following for the distinction of the two cases, cf. (8.6).

nucleon pole terms), since $\tilde{y}/(p_t q_t)$ and the squares p_t^2 and $\tilde{y}^2$ are always real and thus we can rewrite the projections solely in terms of real quantities due to the defined parity (8.15) of the $Q_J(\tilde{y})$. Finally, we comment on the asymptotic behavior for $p_t q_t \to 0$, particularly including the vicinity of the aforementioned logarithmic singularity. The ostensible poles in (9.14) are canceled by the asymptotics of $Q_J(\tilde{y})$ for $\tilde{y} \to \infty$. In this limit, we may abort the series representation of $Q_l(z)$ valid for $|z| > 1$ (cf. [211])

$$
\begin{aligned}
Q_l(z) &= \sqrt{\pi} \frac{\Gamma(l+1)}{\Gamma\left(\frac{2l+3}{2}\right)} (2z)^{-(l+1)} F\left(\frac{l+1}{2}, \frac{l+2}{2}; \frac{2l+3}{2}; z^{-2}\right) \\
&= \frac{2^l (l!)^2}{(2l+1)!} z^{-(l+1)} \left\{ 1 + \frac{(l+1)(l+2)}{2(2l+3)} z^{-2} \left[1 + \frac{(l+3)(l+4)}{4(2l+5)} z^{-2} \left\{ 1 + \dots \right\} \right] \right\},
\end{aligned} \quad (9.16)
$$

which is based on the hypergeometric series $F(a, b; c; z)$ and where $\Gamma(z)$ denotes the usual gamma function, after the first term and obtain the leading contributions

$$
\tilde{N}_+^J(t) = \frac{g^2}{4\pi} \frac{J!}{(2J+1)!!} m \left\{ \left(\frac{4}{t - 2M_\pi^2}\right)^J - \delta_{J0} - \frac{\delta_{J1}}{m^2 - a} \right\} + \mathcal{O}(p_t^2 q_t^2) \quad \forall\, J \geq 0,
$$

$$
\tilde{N}_-^J(t) = \frac{g^2}{4\pi} \frac{J!}{(2J+1)!!} \sqrt{\frac{J+1}{J}} \left\{ \left(\frac{4}{t - 2M_\pi^2}\right)^J - \frac{\delta_{J1}}{m^2 - a} \right\} + \mathcal{O}(p_t^2 q_t^2) \quad \forall\, J \geq 1. \quad (9.17)
$$

In particular, it follows that the leading contribution to $\tilde{N}_+^0$ vanishes, so that $\tilde{N}_+^0$ even involves zeros for $p_t q_t \to 0$. However, higher orders need to be taken into account in the approximations (9.17) (which can easily be done in a recursive fashion as indicated in (9.16)) in order to obtain precise numerical results in particular for $q_t \to 0$, since the pole terms vary rapidly in the vicinity of t_π. Note that (9.14) and (9.17) reduce to the results given in [171] (cf. also [213] for (9.14)), if the terms containing the hyperbola parameter a (that only contribute for $J = 1$ anyway) are dropped.

9.2   *s*- and *u*-channel exchange

We may rewrite the *t*-channel partial-wave projection (9.7) in matrix form as

$$
\mathbf{f}^J(t) = \int_0^1 \mathrm{d}z_t\, \tilde{\mathbf{T}}^J(t, z_t) \mathbf{A}^I(s, t) \Big|_{s = s(t, z_t)}, \quad (9.18)
$$

where the projection kernel is given by

$$
\tilde{\mathbf{T}}^J(t, z_t) = \tilde{\zeta}_J \begin{pmatrix} \tilde{u}_J & \tilde{v}_J \\ 0 & \tilde{w}_J \end{pmatrix}, \qquad \tilde{\zeta}_J(t) = \frac{1}{4\pi (p_t q_t)^{J-1}},
$$

$$
\tilde{u}_J(t, z_t) = -\frac{p_t}{q_t} P_J(z_t), \qquad \tilde{v}_J(t, z_t) = m z_t P_J(z_t),
$$

$$
\tilde{w}_J(t, z_t) = \frac{\sqrt{J(J+1)}}{2J+1} \left[P_{J-1}(z_t) - P_{J+1}(z_t) \right]. \quad (9.19)
$$

For the following, we need the matrix form of both *s*- and *u*-channel HDR terms (7.98) according to

$$
\mathbf{A}^I(s, t)\Big|_{s = s(t, z_t)}^{s+u} = \frac{1}{\pi} \int_{s_+}^\infty \mathrm{d}s'\, \mathbf{h}_s^I[t, s'; z_t] \operatorname{Im} \mathbf{A}^I(s', t') \Big|_{t' = t'(s', z_s')}, \quad (9.20)
$$

where the kernel matrix $\mathbf{h}_s^I$ is given in (8.31) and $[t, s'; z_t]$ denotes that the whole integrand is to be understood as a function of these variables, which can be done by using (9.8) and thus

$$\left\{ h_1 \mp h_2 \right\}\Big|_{[t,s';z_t]} = \left\{ \frac{1}{s'-s} \pm \frac{1}{s'-u} - \frac{1\pm 1}{2(s'-a)} \right\}\Big|_{[t,s';z_t]}$$

$$= \frac{1}{2p_t q_t}\left\{ \frac{1}{\tilde{x}_t - z_t} \mp \frac{1}{(-\tilde{x}_t) - z_t} \right\} - \frac{1\pm 1}{2(s'-a)} \ , \tag{9.21}$$

where the upper/lower sign corresponds to even/odd J and we have defined in analogy to (8.31)

$$\tilde{x}_t(t, s') = \frac{t + 2s' - \Sigma}{4p_t q_t} = z_t(s', t) \ . \tag{9.22}$$

According to (8.83), the relation between z_s' and z_t in (9.20) is given by[#2]

$$z_s'(t, s'; z_t) = \frac{z_t^2 - \tilde{\delta}}{\tilde{\gamma}} \ , \qquad \tilde{\gamma}(t, s') = \frac{q'^2(s'-a)}{2p_t^2 q_t^2} = \gamma(s', t) \ , \tag{9.23}$$

$$\tilde{\delta}(t, s') = \frac{(t - \Sigma + 2a)^2 - 4(s'-a)(2q'^2 + \Sigma - s' - a)}{16 p_t^2 q_t^2} = \delta(s', t) \ .$$

Expanding the absorptive parts of (9.20) into s-channel partial waves via (8.26) and projecting onto t-channel partial waves using (9.18) leads us to the PWDRs for the t-channel partial waves

$$\mathbf{f}^J(t)\Big|^{s+u} = \frac{1}{\pi}\int\limits_{W_+}^{\infty} dW' \sum_{l=0}^{\infty} \tilde{\mathbf{G}}^{Jl}(t, W')\,\mathrm{Im}\,\mathbf{f}_l^I(W') \ , \tag{9.24}$$

with the kernel matrix

$$\tilde{\mathbf{G}}^{Jl}(t, W') = 2W'\int\limits_0^1 dz_t \ \tilde{\mathbf{T}}^J(t, z_t)\mathbf{h}_s^I[t, W'; z_s']\mathbf{S}^l(W', z_s') \ . \tag{9.25}$$

As a remnant of the MacDowell symmetry, (8.29) induces the symmetry property

$$\tilde{\mathbf{G}}^{Jl}(t, -W') = \tilde{\mathbf{G}}^{Jl}(t, W')\boldsymbol{\sigma}_1 \ , \tag{9.26}$$

such that the parameterization with two kernel functions

$$\tilde{\mathbf{G}}^{Jl}(t, W') = \begin{pmatrix} \tilde{G}_{Jl}(t, W') & \tilde{G}_{Jl}(t, -W') \\ \tilde{H}_{Jl}(t, W') & \tilde{H}_{Jl}(t, -W') \end{pmatrix} \tag{9.27}$$

is justified, where again according to $f_-^0 \equiv 0$ we set $\tilde{H}_{0l} \equiv 0$ for the matrix notation. This reproduces the s- and u-channel part of (9.1)

$$f_+^J(t)\Big|^{s+u} = \frac{1}{\pi}\int\limits_{W_+}^{\infty} dW' \sum_{l=0}^{\infty} \left\{ \tilde{G}_{Jl}(t, W')\,\mathrm{Im}\,f_{l+}^I(W') + \tilde{G}_{Jl}(t, -W')\,\mathrm{Im}\,f_{(l+1)-}^I(W') \right\} \quad \forall\, J \geq 0 \ ,$$

$$f_-^J(t)\Big|^{s+u} = \frac{1}{\pi}\int\limits_{W_+}^{\infty} dW' \sum_{l=0}^{\infty} \left\{ \tilde{H}_{Jl}(t, W')\,\mathrm{Im}\,f_{l+}^I(W') + \tilde{H}_{Jl}(t, -W')\,\mathrm{Im}\,f_{(l+1)-}^I(W') \right\} \quad \forall\, J \geq 1 \ .$$

$$\tag{9.28}$$

[#2]Note that $\tilde{\delta}(t, s')$ depends linearly on a (i.e. $\tilde{\delta} = \mathcal{O}(a)$), which will be important when considering $|a| \to \infty$.

If we introduce the abbreviations (cf. (8.94))

$$
\tilde{\psi}\big[a_{kn}\big|d(W')\big] = d(W')a_{k,n+1} + d(-W')a_{kn} , \qquad \tilde{\eta}_J(t,W') = \frac{2W'}{(p_t q_t)^{J-1}} , \tag{9.29}
$$

we find for the kernel functions (in agreement with $\tilde{H}_{0l} \equiv 0$)

$$
\tilde{G}_{Jl}(t,W') = \tilde{\eta}_J \left\{ -\frac{p_t}{q_t}\tilde{\psi}\left[\tilde{A}_{Jl}\middle|\frac{W'+m}{E'+m}\right] + m\tilde{\psi}\left[\tilde{B}_{Jl}\middle|\frac{1}{E'+m}\right] \right\} \qquad \forall\, J \geq 0 ,
$$

$$
\tilde{H}_{Jl}(t,W') = \tilde{\eta}_J \frac{\sqrt{J(J+1)}}{2J+1}\tilde{\psi}\left[\tilde{C}_{Jl}\middle|\frac{1}{E'+m}\right] \qquad \forall\, J \geq 1 , \tag{9.30}
$$

where the angular kernels are given by

$$
\tilde{A}_{Jl}(t,s') = \int_0^1 \mathrm{d}z_t\, P_J(z_t)\big\{h_1 \mp h_2\big\}P_l'(z_s')\Big|_{[t,s';z_t]} ,
$$

$$
\tilde{B}_{Jl}(t,s') = \int_0^1 \mathrm{d}z_t\, P_J(z_t)z_t\big\{h_1 \pm h_2\big\}P_l'(z_s')\Big|_{[t,s';z_t]} ,
$$

$$
\tilde{C}_{Jl}(t,s') = \int_0^1 \mathrm{d}z_t\, \big[P_{J-1}(z_t) - P_{J+1}(z_t)\big]\big\{h_1 \pm h_2\big\}P_l'(z_s')\Big|_{[t,s';z_t]} = \tilde{A}_{J-1,l} - \tilde{A}_{J+1,l} . \tag{9.31}
$$

Decomposing these angular kernels according to

$$
\tilde{A}_{Jl}(t,s') = \frac{1}{p_t q_t}P_l'(\tilde{z}_s)Q_J(\tilde{x}_t) - \bar{A}_{Jl}(t,s') , \qquad \tilde{B}_{Jl}(t,s') = \frac{1}{p_t q_t}P_l'(\tilde{z}_s)\tilde{x}_t Q_J(\tilde{x}_t) - \bar{B}_{Jl}(t,s') ,
$$

$$
\tilde{C}_{Jl}(t,s') = \frac{1}{p_t q_t}P_l'(\tilde{z}_s)\big[Q_{J-1}(\tilde{x}_t) - Q_{J+1}(\tilde{x}_t)\big] - \bar{C}_{Jl}(t,s') , \tag{9.32}
$$

with the real quantity

$$
\tilde{z}_s(t,s') = \frac{\tilde{x}_t^2 - \tilde{\delta}}{\tilde{\gamma}} = 1 + \frac{t}{2q'^2} = z_s(s',t) \tag{9.33}
$$

and polynomial parts defined by

$$
\bar{A}_{Jl}(t,s') = \frac{1}{2}\int_{-1}^1 \mathrm{d}z_t\, P_J(z_t)\left\{ \frac{1}{p_t q_t}\frac{P_l'(\tilde{z}_s) - P_l'(z_s')}{\tilde{x}_t - z_t} + \frac{1\pm 1}{2(s'-a)}P_l'(z_s') \right\} ,
$$

$$
\bar{B}_{Jl}(t,s') = \frac{1}{2}\int_{-1}^1 \mathrm{d}z_t\, P_J(z_t)\left\{ \frac{1}{p_t q_t}\frac{\tilde{x}_t P_l'(\tilde{z}_s) - z_t P_l'(z_s')}{\tilde{x}_t - z_t} + \frac{1\mp 1}{2(s'-a)}z_t P_l'(z_s') \right\} ,
$$

$$
\bar{C}_{Jl}(t,s') = \frac{1}{2}\int_{-1}^1 \mathrm{d}z_t\, \big[P_{J-1}(z_t) - P_{J+1}(z_t)\big]\left\{ \frac{1}{p_t q_t}\frac{P_l'(\tilde{z}_s) - P_l'(z_s')}{\tilde{x}_t - z_t} + \frac{1\mp 1}{2(s'-a)}P_l'(z_s') \right\}
$$

$$
= \bar{A}_{J-1,l} - \bar{A}_{J+1,l} , \tag{9.34}
$$

the kernels $\tilde{G}_{Jl}$ and $\tilde{H}_{Jl}$ may be written in a recursive fashion

$$\tilde{G}_{Jl}(t,W') = \bar{G}_{Jl}(t,W') - \bar{G}_{J,l-1}(t,-W') , \qquad \bar{G}_{J,-1} = 0 \qquad \forall\, J \geq 0 , \tag{9.35}$$

$$\tilde{H}_{Jl}(t,W') = \bar{H}_{Jl}(t,W') - \bar{H}_{J,l-1}(t,-W') , \qquad \bar{H}_{J,-1} = 0 \qquad \forall\, J \geq 1 ,$$

$$\bar{G}_{Jl}(t,W') = \frac{\tilde{\eta}_J}{E'+m}\left\{ \frac{P'_{l+1}(\tilde{z}_s)}{p_t q_t}\left[-\frac{p_t}{q_t}(W'+m) + m\tilde{x}_t \right] Q_J(\tilde{x}_t) \right.$$

$$\left. + \frac{p_t}{q_t}(W'+m)\bar{A}_{J,l+1} - m\bar{B}_{J,l+1} \right\}$$

$$= \frac{2W'}{E'+m}\left\{ P'_{l+1}(\tilde{z}_s)\left[m\frac{\tilde{x}_t}{p_t q_t} - \frac{W'+m}{q_t^2} \right]\frac{Q_J(\tilde{x}_t)}{(p_t q_t)^{J-1}} \right.$$

$$\left. + \frac{W'+m}{q_t^2}\frac{\bar{A}_{J,l+1}}{(p_t q_t)^{J-2}} - m\frac{\bar{B}_{J,l+1}}{(p_t q_t)^{J-1}} \right\} ,$$

$$\bar{H}_{Jl}(t,W') = \frac{\tilde{\eta}_J}{E'+m}\frac{\sqrt{J(J+1)}}{2J+1}\left\{ \frac{P'_{l+1}(\tilde{z}_s)}{p_t q_t}\left[Q_{J-1}(\tilde{x}_t) - Q_{J+1}(\tilde{x}_t) \right] - \bar{C}_{J,l+1} \right\}$$

$$= \frac{2W'}{E'+m}\frac{\sqrt{J(J+1)}}{2J+1}\left\{ P'_{l+1}(\tilde{z}_s)\frac{Q_{J-1}(\tilde{x}_t) - Q_{J+1}(\tilde{x}_t)}{(p_t q_t)^J} - \frac{\bar{A}_{J-1,l+1} - \bar{A}_{J+1,l+1}}{(p_t q_t)^{J-1}} \right\} ,$$

keeping $\bar{C}_{J,l}$ just for convenience. Note that since $\tilde{x}_t/(p_t q_t)$ and the squares p_t^2 and $\tilde{x}_t^2$ are always real, $\bar{A}_{Jl}$ is real/imaginary for J even/odd and the other way round for $\bar{B}_{Jl}$ and $\bar{C}_{Jl}$. Therefore, we can conclude that the functions $\bar{G}_{Jl}$, $\bar{H}_{Jl}$ and hence the kernels $\tilde{G}_{Jl}$, $\tilde{H}_{Jl}$ are real for $t > t_\pi - (M_\pi^2/m)^2$, cf. the discussion following (9.15). The kernels for all combinations $(J \geq 0, l \leq 2)$ read explicitly

$$\tilde{G}_{J0}(t,W') = \frac{\tilde{\eta}_J}{E'+m}\left\{ \frac{1}{p_t q_t}\left(\left[-\frac{p_t}{q_t}(W'+m) + m\tilde{x}_t \right]Q_J(\tilde{x}_t) - m\delta_{J0} \right) \right.$$

$$\left. + \frac{p_t}{q_t}\frac{W'+m}{s'-a}\delta_{J0} - \frac{m}{3}\frac{\delta_{J1}}{s'-a} \right\} ,$$

$$\tilde{H}_{J0}(t,W') = \frac{\tilde{\eta}_J}{E'+m}\frac{\sqrt{J(J+1)}}{2J+1}\left\{ \frac{1}{p_t q_t}\left[Q_{J-1}(\tilde{x}_t) - Q_{J+1}(\tilde{x}_t) \right] - \frac{\delta_{J1}}{s'-a} \right\} ,$$

$$\tilde{G}_{J1}(t,W') = -\tilde{G}_{J0}(t,-W') + \frac{\tilde{\eta}_J}{E'+m}\left\{ \frac{3\tilde{z}_s}{p_t q_t}\left(\left[-\frac{p_t}{q_t}(W'+m) + m\tilde{x}_t \right]Q_J(\tilde{x}_t) - m\delta_{J0} \right) \right.$$

$$+ \frac{W'+m}{\tilde{\gamma}}\frac{p_t}{q_t}\left[\frac{1}{p_t q_t}\left\{ \delta_{J1} + 3\tilde{x}_t\delta_{J0} \right\} + \frac{1}{s'-a}\left\{ \frac{2}{5}\delta_{J2} + \left(1 - 3\tilde{\delta}\right)\delta_{J0} \right\} \right]$$

$$\left. - \frac{m}{\tilde{\gamma}}\left[\frac{1}{p_t q_t}\left\{ \frac{2}{5}\delta_{J2} + \tilde{x}_t\delta_{J1} + \delta_{J0} \right\} + \frac{1}{s'-a}\left\{ \frac{6}{35}\delta_{J3} + \left(\frac{3}{5} - \tilde{\delta}\right)\delta_{J1} \right\} \right] \right\}$$

$$= \bar{G}_{J1}(t,W') - \tilde{G}_{J0}(t,-W') ,$$

$$\tilde{H}_{J1}(t,W') = -\tilde{H}_{J0}(t,-W') + \frac{\tilde{\eta}_J}{E'+m}\frac{\sqrt{J(J+1)}}{2J+1}\left\{ \frac{3\tilde{z}_s}{p_t q_t}\left[Q_{J-1}(\tilde{x}_t) - Q_{J+1}(\tilde{x}_t) \right] \right.$$

$$\left. - \frac{1}{\tilde{\gamma}}\left[\frac{1}{p_t q_t}\left\{ \delta_{J2} + 3\tilde{x}_t\delta_{J1} \right\} + \frac{1}{s'-a}\left\{ \frac{2}{5}\delta_{J3} + 3\left(\frac{1}{5} - \tilde{\delta}\right)\delta_{J1} \right\} \right] \right\}$$

$$= \bar{H}_{J1}(t,W') - \tilde{H}_{J0}(t,-W') ,$$

$$
\begin{aligned}
\tilde{G}_{J2}(t, W') = {}& -\bar{G}_{J1}(t, -W') + \frac{\tilde{\eta}_J}{E' + m} \Bigg\{ \frac{P_3'(\tilde{z}_s)}{p_t q_t} \bigg(\Big[-\frac{p_t}{q_t}(W' + m) + m\tilde{x}_t \Big] Q_J(\tilde{x}_t) - m\delta_{J0} \bigg) \\
& + \frac{W' + m}{\tilde{\gamma}^2} \frac{p_t}{q_t} \bigg[\frac{1}{p_t q_t} \Big\{ \frac{3}{7}\delta_{J3} + \tilde{x}_t \delta_{J2} + \frac{5}{2}\Big(\frac{3}{5} + \tilde{x}_t^2 - 2\tilde{\delta}\Big)\delta_{J1} \\
& \qquad\qquad + \frac{15}{2}\tilde{x}_t\Big(\frac{1}{3} + \tilde{x}_t^2 - 2\tilde{\delta}\Big)\delta_{J0} \Big\} \\
& \qquad + \frac{1}{s' - a}\Big\{ \frac{4}{21}\delta_{J4} + 2\Big(\frac{3}{7} - \tilde{\delta}\Big)\delta_{J2} + \frac{15}{2}\Big(\frac{1 - \tilde{\gamma}^2}{5} - \frac{2}{3}\tilde{\delta} + \tilde{\delta}^2\Big)\delta_{J0} \Big\} \bigg] \\
& - \frac{m}{\tilde{\gamma}^2} \bigg[\frac{1}{p_t q_t}\Big\{ \frac{4}{21}\delta_{J4} + \frac{3}{7}\tilde{x}_t\delta_{J3} + \Big(\frac{6}{7} + \tilde{x}_t^2 - 2\tilde{\delta}\Big)\delta_{J2} \\
& \qquad\qquad + \frac{5}{2}\Big(\frac{3}{5} + \tilde{x}_t^2 - 2\tilde{\delta}\Big)\Big(\tilde{x}_t\delta_{J1} + \delta_{J0}\Big) \Big\} \\
& \qquad + \frac{1}{s' - a}\Big\{ \frac{20}{231}\delta_{J5} + \frac{3}{7}\Big(\frac{10}{9} - 2\tilde{\delta}\Big)\delta_{J3} + \frac{5}{2}\Big(\frac{3}{7} - \frac{6}{5}\tilde{\delta} + \tilde{\delta}^2 - \frac{\tilde{\gamma}^2}{5}\Big)\delta_{J1} \Big\} \bigg] \Bigg\} \\
= {}& \bar{G}_{J2}(t, W') - \bar{G}_{J1}(t, -W') \,, \\[6pt]
\tilde{H}_{J2}(t, W') = {}& -\bar{H}_{J1}(t, -W') + \frac{\tilde{\eta}_J}{E' + m} \frac{\sqrt{J(J+1)}}{2J + 1} \Bigg\{ \frac{P_3'(\tilde{z}_s)}{p_t q_t} \Big[Q_{J-1}(\tilde{x}_t) - Q_{J+1}(\tilde{x}_t) \Big] \\
& - \frac{1}{\tilde{\gamma}^2} \bigg[\frac{1}{p_t q_t}\Big\{ \frac{3}{7}\delta_{J4} + \tilde{x}_t\delta_{J3} + \frac{5}{2}\Big(\frac{3}{7} + \tilde{x}_t^2 - 2\tilde{\delta}\Big)\delta_{J2} + \frac{15}{2}\tilde{x}_t\Big(\frac{1}{5} + \tilde{x}_t^2 - 2\tilde{\delta}\Big)\delta_{J1} \Big\} \\
& \qquad + \frac{1}{s' - a}\Big\{ \frac{4}{21}\delta_{J5} + 2\Big(\frac{1}{3} - \tilde{\delta}\Big)\delta_{J3} + \frac{3}{2}\Big(\frac{3}{7} - 2\tilde{\delta} + 5\tilde{\delta}^2 - \tilde{\gamma}^2\Big)\delta_{J1} \Big\} \bigg] \Bigg\} \\
= {}& \bar{H}_{J2}(t, W') - \bar{H}_{J1}(t, -W') \,.
\end{aligned}
\tag{9.36}
$$

The explicit formulae for the polynomial parts $\bar{A}_{Jl}$, $\bar{B}_{Jl}$, and $\bar{C}_{J,l}$ for $(J \leq 2, l \leq 6)$ needed for calculating these kernels and furthermore the additional kernels $\tilde{G}_{Jl}$ and $\tilde{H}_{Jl}$ for $(J \leq 2, 3 \leq l \leq 5)$ via (9.35) are given in the App. C.2.[#3] As a check of our calculation we can reproduce the nucleon pole terms (9.14) by (cf. (8.77))

$$
\tilde{N}_+^J(t) = -f^2 \tilde{G}_{J0}(t, -W' = m) \quad \forall\, J \geq 0\,, \qquad \tilde{N}_-^J(t) = -f^2 \tilde{H}_{J0}(t, -W' = m) \quad \forall\, J \geq 1\,.
\tag{9.37}
$$

The asymptotic behavior of the general kernel functions (9.30) can be deduced to be

$$
\begin{aligned}
&\text{for } p_t q_t \to 0 \quad \tilde{G}_{Jl}(t, W') \sim \tilde{H}_{Jl}(t, W') \sim 1\,, \\
&\text{for } q' \to 0 \quad\;\; \tilde{G}_{Jl}(t, W') \sim \tilde{H}_{Jl}(t, W') \sim q'^{-2l}\,, \quad \tilde{G}_{Jl}(t, -W') \sim \tilde{H}_{Jl}(t, -W') \sim q'^{-2l-2}\,, \\
&\text{for } q' \to \infty \quad\;\; \tilde{G}_{Jl}(t, W') \sim \tilde{H}_{Jl}(t, W') \sim q'^{-2J}\,.
\end{aligned}
\tag{9.38}
$$

In particular, these kernels are finite for $p_t q_t \to 0$ and their precise form in this limit may be worked out in close analogy to the discussion of the pole terms in Sect. 9.1 based on (9.35). Note that both (9.37) and (9.38) obey the MacDowell symmetry relation (8.1), as they should.

[#3]Note that for $|a| \to \infty$, of all polynomial parts only the $\bar{B}_{0l}$ do not vanish completely and hence f_+^0 receives polynomial contributions from the kernels $\tilde{G}_{0l}$. These remaining contributions, however, are just those that cancel with the leading terms of the *S*-wave pole terms (9.14), cf. the discussion following (9.17) as well as the explicit kernels (9.36).

9.3   *t*-channel exchange

We need the *t*-channel HDR terms (8.81) in the form

$$\mathbf{A}^I(s,t)\Big|_{s=s(t,z_t)}^{t} = \frac{1}{\pi}\int\limits_{t_\pi}^{\infty} dt'\, \mathbf{h}_t^I[t,t';z_t]\, \mathrm{Im}\, \mathbf{A}^I(s',t')\Big|_{s'=s'(t',z_t')} \,, \tag{9.39}$$

where the kernel matrix $\mathbf{h}_t^I$ is given in (8.82) and the integrand can be written as a function of the variables $[t,t';z_t]$ by noting that

$$\frac{1}{2q^2}\frac{1}{x_t-z_s}\Big|_{[t,t';z_t]} = \frac{1}{t'-t} \,, \qquad \frac{\nu}{\nu'}\Big|_{[t,t';z_t]} = \frac{p_t q_t}{p_t' q_t'}\frac{z_t}{z_t'} \,, \tag{9.40}$$

and that z_t' and z_t are related by (cf. (8.32))

$$z_t'(t,t';z_t) = \sqrt{\tilde\alpha z_t^2 + \tilde\beta}\,, \qquad \tilde\alpha(t,t') = \frac{p_t^2 q_t^2}{p_t'^2 q_t'^2}\,, \qquad \tilde\beta(t,t') = \frac{t'-t}{16 p_t'^2 q_t'^2}(t+t'-2\Sigma+4a)\,. \tag{9.41}$$

Expanding the absorptive part of (9.39) into *t*-channel partial waves using (8.86) and projecting onto *t*-channel partial waves again via (9.18), we obtain the following PWDRs for the *t*-channel partial waves

$$\mathbf{f}^J(t)\Big|^{t} = \frac{1}{\pi}\int\limits_{t_\pi}^{\infty} dt' \sum_{J'} \tilde{\mathbf{K}}^{JJ'}(t,t')\, \mathrm{Im}\, \mathbf{f}^{J'}(t') \,, \tag{9.42}$$

where the summation runs over even/odd values of J' for even/odd values of J, accordingly, and the kernel matrix is defined by

$$\tilde{\mathbf{K}}^{JJ'}(t,t') = \int\limits_0^1 dz_t\, \tilde{\mathbf{T}}^J(t,z_t)\mathbf{h}_t^I[t,t';z_t]\mathbf{T}^{J'}(t',z_t')\,. \tag{9.43}$$

Calculating this kernel matrix shows that it can be written with three kernel functions as

$$\tilde{\mathbf{K}}^{JJ'}(t,t') = \begin{pmatrix} \tilde{K}_{JJ'}^1(t,t') & \tilde{K}_{JJ'}^2(t,t') \\ 0 & \tilde{K}_{JJ'}^3(t,t') \end{pmatrix} = \frac{\zeta_{JJ'}}{t'-t}\begin{pmatrix} u_{JJ'}(t,t') & v_{JJ'}(t,t') \\ 0 & w_{JJ'}(t,t') \end{pmatrix} \,,$$

$$\zeta_{JJ'}(t,t') = (2J'+1)\frac{(p_t' q_t')^{J'-1}}{(p_t q_t)^{J-1}} \,, \tag{9.44}$$

where we have defined different angular kernels for even J and J'

$$u_{JJ'} = \frac{p_t q_t'}{q_t p_t'}\int\limits_0^1 dz_t\, P_J(z_t)P_{J'}(z_t') \,,$$

$$v_{JJ'} = \frac{m}{\sqrt{J'(J'+1)}}\frac{p_t}{q_t p_t' q_t'}\int\limits_0^1 dz_t\, P_J(z_t)\Big\{q_t^2 z_t^2 - q_t'^2 z_t'^2\Big\}\frac{P_{J'}'(z_t')}{z_t'} \,,$$

$$w_{JJ'} = \frac{1}{2J+1}\sqrt{\frac{J(J+1)}{J'(J'+1)}}\frac{p_t q_t}{p_t' q_t'}\int\limits_0^1 dz_t\, \Big\{P_{J-1}(z_t) - P_{J+1}(z_t)\Big\}z_t\frac{P_{J'}'(z_t')}{z_t'} \,, \tag{9.45}$$

and for odd J and J'

$$u_{JJ'} = \frac{p_t^2}{p_t'^2} \int\limits_0^1 dz_t \, P_J(z_t) z_t \frac{P_{J'}(z_t')}{z_t'} \, ,$$

$$v_{JJ'} = \frac{m}{\sqrt{J'(J'+1)}} \left\{ 1 - \frac{p_t^2}{p_t'^2} \right\} \int\limits_0^1 dz_t \, P_J(z_t) z_t P_{J'}'(z_t') \, ,$$

$$w_{JJ'} = \frac{1}{2J+1} \sqrt{\frac{J(J+1)}{J'(J'+1)}} \int\limits_0^1 dz_t \, \left\{ P_{J-1}(z_t) - P_{J+1}(z_t) \right\} P_{J'}'(z_t') \, . \tag{9.46}$$

In this way, we recover the form of the *t*-channel part given in (9.1)

$$f_+^J(t) \Big|^t = \frac{1}{\pi} \int\limits_{t_\pi}^\infty dt' \sum_{J'} \left\{ \tilde{K}_{JJ'}^1(t,t') \operatorname{Im} f_+^{J'}(t') + \tilde{K}_{JJ'}^2(t,t') \operatorname{Im} f_-^{J'}(t') \right\} \qquad \forall \, J \geq 0 \, ,$$

$$f_-^J(t) \Big|^t = \frac{1}{\pi} \int\limits_{t_\pi}^\infty dt' \sum_{J'} \tilde{K}_{JJ'}^3(t,t') \operatorname{Im} f_-^{J'}(t') \qquad\qquad\qquad \forall \, J \geq 1 \, , \tag{9.47}$$

and according to $f_-^0 \equiv 0$ we set $\tilde{K}_{0J'}^3 \equiv 0 \equiv \tilde{K}_{J0}^2$.

From the projection integrals (9.45) and (9.46) together with the definitions (9.41) and

$$1 - \frac{p_t^2}{p_t'^2} = \frac{t'-t}{4p_t'^2} \, , \qquad q_t^2 z_t^2 - q_t'^2 z_t'^2 = \frac{t'-t}{4p_t'^2} \left\{ 4q_t^2 z_t^2 - \frac{1}{4}(t+t'-2\Sigma+4a) \right\} \, , \tag{9.48}$$

one can see that the off-diagonal term $v_{JJ'}$ is proportional to $t'-t$, as it should be. Note also that only even powers of z_t' and z_t occur in the projection integrals. Therefore the kernel functions $\tilde{K}_{JJ'}^1$, $\tilde{K}_{JJ'}^2$, and $\tilde{K}_{JJ'}^3$ are always real, since the prefactors contain only even powers of momenta. The integrals can be performed with the help of (cf. [211])

$$P_l(z) = \sum_{\lambda=0}^{\frac{l}{2}} a_{\lambda l}^{\mathrm{ev}} z^{2\lambda} \, , \qquad P_l(z) = \sum_{\lambda=0}^{\frac{l-1}{2}} a_{\lambda l}^{\mathrm{od}} z^{2\lambda+1} \, , \tag{9.49}$$

for even and odd values of l, respectively, where

$$a_{\lambda l}^{\mathrm{ev}} = \frac{(-1)^{\lambda+\frac{l}{2}}(2\lambda+l-1)!}{2^{l-1}\left(\frac{l}{2}-\lambda\right)!\left(\lambda+\frac{l}{2}-1\right)!(2\lambda)!} \, , \qquad a_{\lambda l}^{\mathrm{od}} = \frac{(-1)^{\lambda+\frac{l-1}{2}}(2\lambda+l)!}{2^{l-1}\left(\frac{l-1}{2}-\lambda\right)!\left(\lambda+\frac{l-1}{2}\right)!(2\lambda+1)!} \, , \tag{9.50}$$

which also follow from reordering the expansion

$$P_l(z) = \frac{1}{2^l} \sum_{\lambda=0}^{\lfloor \frac{l}{2} \rfloor} \frac{(-1)^\lambda (2l-2\lambda)!}{\lambda!(l-\lambda)!(l-2\lambda)!} z^{l-2\lambda} \, , \qquad \left\lfloor \frac{l}{2} \right\rfloor = \begin{cases} \frac{l}{2} & \text{for even } l \, , \\ \frac{l-1}{2} & \text{for odd } l \, . \end{cases} \tag{9.51}$$

In this way, the required non-vanishing integrals may be written for even J and J' as

$$\int_0^1 dz_t \, P_J(z_t) P_{J'}(z_t') = \sum_{\lambda'=\frac{J}{2}}^{\frac{J'}{2}} a_{\lambda'J'}^{\text{ev}} \sum_{\mu=\frac{J}{2}}^{\lambda'} \binom{\lambda'}{\mu} \tilde{\alpha}^\mu \tilde{\beta}^{\lambda'-\mu} \tilde{a}_{J\mu}^{\text{ev}} \, ,$$

$$\int_0^1 dz_t \, P_J(z_t) \Big\{ q_t^2 z_t^2 - q_t'^2 z_t'^2 \Big\} \frac{P_{J'}'(z_t')}{z_t'} = \sum_{\lambda'=\max\{\frac{J}{2},1\}}^{\frac{J'}{2}} 2\lambda' a_{\lambda'J'}^{\text{ev}}$$

$$\times \Bigg\{ q_t^2 \sum_{\mu=\max\{\frac{J}{2}-1,0\}}^{\lambda'-1} \binom{\lambda'-1}{\mu} \tilde{\alpha}^\mu \tilde{\beta}^{\lambda'-1-\mu} \tilde{a}_{J,\mu+1}^{\text{ev}} - q_t'^2 \sum_{\mu=\frac{J}{2}}^{\lambda'} \binom{\lambda'}{\mu} \tilde{\alpha}^\mu \tilde{\beta}^{\lambda'-\mu} \tilde{a}_{J\mu}^{\text{ev}} \Bigg\} \, ,$$

$$\int_0^1 dz_t \, \Big\{ P_{J-1}(z_t) - P_{J+1}(z_t) \Big\} z_t \frac{P_{J'}'(z_t')}{z_t'} = - \sum_{\lambda'=\frac{J}{2}+1}^{\frac{J'}{2}} 2\lambda' a_{\lambda'J'}^{\text{ev}} \sum_{\mu=\frac{J}{2}}^{\lambda'-1} \binom{\lambda'-1}{\mu} \tilde{\alpha}^\mu \tilde{\beta}^{\lambda'-1-\mu} \tilde{a}_{J+1,\mu+1}^{\text{od}}$$

$$+ \sum_{\lambda'=\max\{\frac{J}{2},1\}}^{\frac{J'}{2}} 2\lambda' a_{\lambda'J'}^{\text{ev}} \sum_{\mu=\max\{\frac{J}{2}-1,0\}}^{\lambda'-1} \binom{\lambda'-1}{\mu} \tilde{\alpha}^\mu \tilde{\beta}^{\lambda'-1-\mu} \tilde{a}_{J-1,\mu+1}^{\text{od}} \, , \qquad (9.52)$$

and for odd J and J' as

$$\int_0^1 dz_t \, P_J(z_t) z_t \frac{P_{J'}(z_t')}{z_t'} = \sum_{\lambda'=\frac{J-1}{2}}^{\frac{J'-1}{2}} a_{\lambda'J'}^{\text{od}} \sum_{\mu=\frac{J-1}{2}}^{\lambda'} \binom{\lambda'}{\mu} \tilde{\alpha}^\mu \tilde{\beta}^{\lambda'-\mu} \tilde{a}_{J,\mu+1}^{\text{od}} \, ,$$

$$\int_0^1 dz_t \, P_J(z_t) z_t P_{J'}'(z_t') = \sum_{\lambda'=\frac{J-1}{2}}^{\frac{J'-1}{2}} (2\lambda'+1) a_{\lambda'J'}^{\text{od}} \sum_{\mu=\frac{J-1}{2}}^{\lambda'} \binom{\lambda'}{\mu} \tilde{\alpha}^\mu \tilde{\beta}^{\lambda'-\mu} \tilde{a}_{J,\mu+1}^{\text{od}} \, ,$$

$$\int_0^1 dz_t \, \Big\{ P_{J-1}(z_t) - P_{J+1}(z_t) \Big\} P_{J'}'(z_t') = \sum_{\lambda'=\frac{J-1}{2}}^{\frac{J'-1}{2}} (2\lambda'+1) a_{\lambda'J'}^{\text{od}} \sum_{\mu=\frac{J-1}{2}}^{\lambda'} \binom{\lambda'}{\mu} \tilde{\alpha}^\mu \tilde{\beta}^{\lambda'-\mu} \tilde{a}_{J-1,\mu}^{\text{ev}}$$

$$- \sum_{\lambda'=\frac{J+1}{2}}^{\frac{J'-1}{2}} (2\lambda'+1) a_{\lambda'J'}^{\text{od}} \sum_{\mu=\frac{J+1}{2}}^{\lambda'} \binom{\lambda'}{\mu} \tilde{\alpha}^\mu \tilde{\beta}^{\lambda'-\mu} \tilde{a}_{J+1,\mu}^{\text{ev}} \, ,$$

$$(9.53)$$

with the definitions (for even and odd values of J, respectively)[#4]

$$\tilde{a}_{J\mu}^{\text{ev}} = \sum_{\lambda=0}^{\frac{J}{2}} \frac{a_{\lambda J}^{\text{ev}}}{2(\mu+\lambda)+1} = 2^J \frac{(\mu+\frac{J}{2})!(2\mu)!}{(\mu-\frac{J}{2})!(2\mu+J+1)!} = \frac{(2\mu)!}{(2\mu-J)!!(2\mu+1+J)!!} \qquad \left(\mu \geq \tfrac{J}{2}\right) ,$$

$$\tilde{a}_{J\mu}^{\text{od}} = \sum_{\lambda=0}^{\frac{J-1}{2}} \frac{a_{\lambda J}^{\text{od}}}{2(\mu+\lambda)+1} = 2^J \frac{(\mu+\frac{J-1}{2})!(2\mu-1)!}{(\mu-\frac{J+1}{2})!(2\mu+J)!} = \frac{(2\mu-1)!}{(2\mu-1-J)!!(2\mu+J)!!} \qquad \left(\mu \geq \tfrac{J-1}{2}\right) .$$

$$(9.54)$$

[#4] These identities are similar to the Saalschütz formula (8.52) employed in [206]. Note that $(-1)!! = 0!! = 1$.

We can conclude that the following kernels vanish (in addition to $\tilde{K}^3_{0J'} \equiv 0 \equiv \tilde{K}^2_{J0}$)

$$\mathbf{\tilde{K}}^{JJ'}(t,t') = 0 \quad \forall \, J' < J \, , \tag{9.55}$$

and by using the identities

$$(2J+1)a^{\text{ev}}_{\frac{J}{2},J}\tilde{a}^{\text{ev}}_{J,\frac{J}{2}} = 1 \, , \qquad\qquad J a^{\text{ev}}_{\frac{J}{2},J}\tilde{a}^{\text{od}}_{J-1,\frac{J}{2}} = 1 \qquad \text{for even } J \, ,$$

$$(2J+1)a^{\text{od}}_{\frac{J-1}{2},J}\tilde{a}^{\text{od}}_{J,\frac{J+1}{2}} = 1 \, , \qquad\qquad J a^{\text{od}}_{\frac{J-1}{2},J}\tilde{a}^{\text{ev}}_{J-1,\frac{J-1}{2}} = 1 \qquad \text{for odd } J \, , \tag{9.56}$$

it follows that the non-vanishing kernels for $J' = J$ take the form

$$\tilde{K}^1_{JJ}(t,t') = \frac{p_t^2}{p_t'^2}\frac{1}{t'-t} = \frac{1}{t'-t} - \frac{1}{t'-t_N} = \frac{t}{t'}\frac{1}{t'-t} - \frac{t_N}{t'}\frac{1}{t'-t_N} \qquad \forall \, J \geq 0 \, ,$$

$$\tilde{K}^2_{JJ}(t,t') = \sqrt{\frac{J}{J+1}}\frac{m}{4p_t'^2} = \sqrt{\frac{J}{J+1}}\frac{m}{t'-t_N} \qquad\qquad\qquad \forall \, J \geq 1 \, ,$$

$$\tilde{K}^3_{JJ}(t,t') = \frac{1}{t'-t} \qquad\qquad\qquad\qquad\qquad\qquad\qquad \forall \, J \geq 1 \, , \tag{9.57}$$

from which one can immediately read off the relation (valid for all J)

$$\tilde{K}^2_{JJ}(t,t') = m\sqrt{\frac{J}{J+1}}\left\{ \tilde{K}^3_{JJ}(t,t') - \tilde{K}^1_{JJ}(t,t') \right\} \, . \tag{9.58}$$

This together with

$$\tilde{K}^1_{02}(t,t') = \frac{5}{16}\frac{p_t^2}{p_t'^2}\left\{ t+t'-2\Sigma+6a \right\} \, , \qquad \tilde{K}^1_{13}(t,t') = \frac{7}{48}\frac{p_t^2}{p_t'^2}\left\{ t+t'-2\Sigma+10a \right\} \, ,$$

$$\tilde{K}^2_{02}(t,t') = \frac{5m}{16\sqrt{6}}\frac{p_t^2}{p_t'^2}\left\{ 4q_t^2 - 3(t+t'-2\Sigma+4a) \right\} \, ,$$

$$\tilde{K}^2_{13}(t,t') = \frac{7m}{64\sqrt{3}}\frac{1}{p_t'^2}\left\{ 8p_t^2 q_t^2 + (t'-t)(t+t'-2\Sigma+5a) \right\} \, ,$$

$$\tilde{K}^3_{13}(t,t') = \frac{7}{8\sqrt{6}}\left\{ t+t'-2\Sigma+5a \right\} \tag{9.59}$$

completes the calculation of the t-channel kernels with $(J \leq 3, J' \leq 3)$. Finally, from (9.52) and (9.53) we may infer the asymptotic behavior of the non-vanishing kernels

for $p_t \to 0$ $\quad \tilde{K}^1_{JJ'}(t,t') \sim p_t^2 \, , \qquad\qquad\qquad\qquad\quad \tilde{K}^2_{JJ'}(t,t') \sim \tilde{K}^3_{JJ'}(t,t') \sim 1 \, ,$

for $q_t \to 0$ $\quad \tilde{K}^1_{JJ'}(t,t') \sim \tilde{K}^2_{JJ'}(t,t') \sim \tilde{K}^3_{JJ'}(t,t') \sim 1 \, ,$

for $t \to \infty$ $\quad \tilde{K}^1_{JJ'}(t,t') \sim \tilde{K}^2_{JJ'}(t,t') \sim t^{J'-J} \, , \qquad\qquad\quad \tilde{K}^3_{JJ'}(t,t') \sim t^{J'-J-1} \, ,$

for $p'_t \to 0$ $\quad \tilde{K}^1_{JJ'}(t,t') \sim \tilde{K}^2_{JJ'}(t,t') \sim p_t'^{-2} \, , \qquad\qquad\quad \tilde{K}^3_{JJ'}(t,t') \sim 1 \, ,$

for $q'_t \to 0$ $\quad \tilde{K}^1_{JJ'}(t,t') \sim \tilde{K}^2_{JJ'}(t,t') \sim \tilde{K}^3_{JJ'}(t,t') \sim 1 \, ,$

for $t' \to \infty$ $\quad \tilde{K}^1_{JJ'}(t,t') \sim t'^{J'-J-2} \, , \qquad\qquad\qquad\qquad \tilde{K}^2_{JJ'}(t,t') \sim \tilde{K}^3_{JJ'}(t,t') \sim t'^{J'-J-1} \, .$

$$\tag{9.60}$$

Note that the self-coupling kernels $\tilde{K}^1_{JJ}$ and $\tilde{K}^3_{JJ}$ in (9.57) are independent of the value of J and that the kernel $\tilde{K}^2_{02}(t,t')$ exceptionally has better convergence properties

$$\tilde{K}^2_{02}(t,t') \sim p_t^2 \quad \text{for } p_t \to 0 \, , \qquad \tilde{K}^2_{02}(t,t') \sim 1 \quad \text{for } t' \to \infty \, . \tag{9.61}$$

Chapter 10

Ranges of convergence

There are three aspects of convergence in the Roy–Steiner PWHDR system constructed in Chaps. 8 and 9: first, the question of convergence of the integrals in the high-energy regime is linked to the number of necessary subtractions of the dispersion relations, which will be discussed in Chap. 13; for the rest of this chapter we may thus work as if no subtractions were necessary. Moreover, for the full system of RS equations to be valid, the convergence of both the pertinent partial-wave expansion of the (s- and t-channel) imaginary parts inside the integrals and the s- and t-channel partial-wave projection of the full HDR equations needs to be shown. Analyzing these two constraints (based on the Mandelstam representation of the invariant scattering amplitudes) will yield the ranges of convergence in s and t for (8.3) and (9.1), respectively, whereby the free hyperbola parameter a can actually be tuned in order to obtain the largest possible domain of validity. For the s-channel part (8.3) of the RS system the combined analysis of s- and t-channel constraints will lead to an optimal value of the hyperbola parameter a and a corresponding range of convergence in s of (cf. Sect. 10.3)

$$a = -23.19\, M_\pi^2 \quad \Rightarrow \quad s \in \left[s_+ = 59.64\, M_\pi^2, 97.30\, M_\pi^2\right]$$
$$\Leftrightarrow \quad W \in \left[W_+ = 1.08\, \text{GeV}, 1.38\, \text{GeV}\right], \tag{10.1}$$

while for the t-channel part (9.1) we will find (cf. Sect. 10.4)

$$a = -2.71\, M_\pi^2 \quad \Rightarrow \quad t \in \left[t_\pi = 4M_\pi^2, 205.45\, M_\pi^2\right]$$
$$\Leftrightarrow \quad \sqrt{t} \in \left[\sqrt{t_\pi} = 0.28\, \text{GeV}, 2.00\, \text{GeV}\right]. \tag{10.2}$$

Note that different choices of a for the s- and t-channel partial-wave projections are perfectly well justified, as we may start from different sets of HDRs, respectively. However, the choice of a is not only crucial for the ranges of convergence, but also influences the high-energy behavior of the imaginary parts as estimated by Regge asymptotics (cf. Chap. 11).

The reader not interested in the rather technical details of the derivation of the above results may skip this chapter without harm for the following discussion.[1]

---

[1] Note however that particularly in this case the devil is in the details: unfortunately, in the literature there are numerous errors floating around and especially the existing partial results for πN scattering are incomplete, not properly published and/or even totally inaccessible.
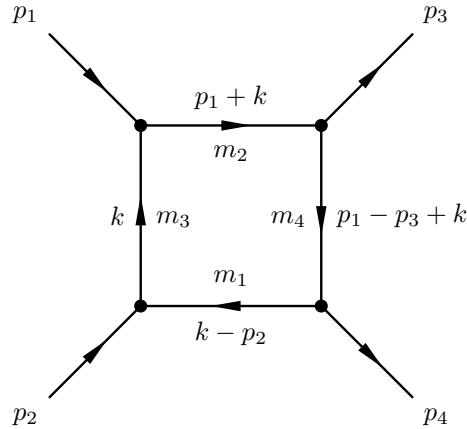
Figure 10.1: General box graph.

10.1   Boundaries of the double spectral regions

The following analysis is performed in the spirit of [158, 159, 171].[#2] The basic *assumption* is that the T-matrix element (and hence the invariant scattering amplitudes $\{A(s,t), B(s,t)\} \propto T(s,t)/(16\pi)$) fulfills Mandelstam analyticity [215], i.e. that it can be represented in terms of double spectral density functions ρ_{su}, ρ_{tu}, and ρ_{st} according to[#3]

$$T(s,t) = \frac{1}{\pi^2} \iint ds' du' \frac{\rho_{su}(s',u')}{(s'-s)(u'-u)} + \frac{1}{\pi^2} \iint dt' du' \frac{\rho_{tu}(t',u')}{(t'-t)(u'-u)}$$
$$+ \frac{1}{\pi^2} \iint ds' dt' \frac{\rho_{st}(s',t')}{(s'-s)(t'-t)} \,, \tag{10.3}$$

where the integration ranges are determined by the regions in the Mandelstam plane where the double spectral densities have support, which will be called double spectral regions in the following and whose boundaries will be the central objects of the following discussion. In order to study the consequences of unitarity in the 2-intermediate-particle approximation, we consider the general box graph displayed in Fig. 10.1 as a unitarity diagram, i.e. with on-shell intermediate particles. The discontinuities of the associated scalar box loop integral (in the non-cyclic conventions of [188] and with generic coupling g)

$$T_{\rm B}(s,t) = \frac{g^4}{i} \int \frac{d^4k}{(2\pi)^4} \frac{1}{\left((p_1+k)^2 - m_2^2\right)\left((p_1-p_3+k)^2 - m_4^2\right)\left((p_2-k)^2 - m_1^2\right)\left(k^2 - m_3^2\right)} \tag{10.4}$$

[#2]Note that the authors of [158] corrected their results for the boundaries of the double spectral regions in [214].

[#3]With respect to the discussion of the analyticity postulate of S-matrix theory in Sect. 7.4, this amounts to the additional assumption of analyticity also in the second (i.e. angular) Mandelstam variable; see e.g. [206] for the enlargement of the analyticity domain for πN scattering by assuming Mandelstam analyticity (compared to the analyticity domain axiomatically proven in [200]). Moreover, starting from dispersion relations along hyperbolas (in contrast to fixed-t lines) has proven successful in enlarging the domain of validity even further for Roy-type equations for $\pi\pi$ scattering, cf. [198, 216]. At any rate, Mandelstam analyticity can be justified in the framework of perturbation theory [215, 217, 218]. While for $\pi\pi$ scattering the validity of the Mandelstam representation can even be shown rigorously in a finite domain [219, 220], for πN scattering (involving unequal masses and spin) at least the uniqueness of amplitudes satisfying this representation is ensured by the MacDowell symmetry [221, 222].

can be calculated from the corresponding 2-particle form of the unitarity relation (7.61) (see e.g. [174, 175, 217]) or by using the Cutkosky cutting rules (as it was done already in the original work [187][#4]). The integral gives rise to the s-channel imaginary part (cf. (7.62))

$$\text{Im}_s\, T_{\text{B}}(s,t) = \frac{\text{Disc}_s\, T_{\text{B}}(s,t)}{2i} = \lim_{\epsilon \to 0} \frac{T_{\text{B}}(s+i\epsilon,t) - T_{\text{B}}(s-i\epsilon,t)}{2i}$$

$$= \frac{g^4}{16\pi} \frac{2s\sqrt{\lambda(s,m_1^2,m_2^2)}}{\sqrt{D}} \log \frac{ac - bd\cos\theta_s + \sqrt{D}}{ac - bd\cos\theta_s - \sqrt{D}}\, \theta\big(s - (m_1+m_2)^2\big)\,, \quad (10.5)$$

where (cf. (7.4) for the s-channel scattering angle)[#5]

$$D = (ac - bd\cos\theta_s)^2 - (a^2 - b^2)(c^2 - d^2)\,,$$
$$a = s^2 - s\big(p_1^2 + p_2^2 + m_1^2 + m_2^2 - 2m_3^2\big) - \big(m_1^2 - m_2^2\big)\big(p_1^2 - p_2^2\big)\,,$$
$$c = s^2 - s\big(p_3^2 + p_4^2 + m_1^2 + m_2^2 - 2m_4^2\big) - \big(m_1^2 - m_2^2\big)\big(p_3^2 - p_4^2\big)\,,$$
$$b = \sqrt{\lambda(s,m_1^2,m_2^2)}\sqrt{\lambda(s,p_1^2,p_2^2)}\,, \quad d = \sqrt{\lambda(s,m_1^2,m_2^2)}\sqrt{\lambda(s,p_3^2,p_4^2)}\,,$$
$$\cos\theta_s = \frac{s}{\sqrt{\lambda(s,p_1^2,p_2^2)}\sqrt{\lambda(s,p_3^2,p_4^2)}}\left\{ t - u + \frac{\big(p_1^2 - p_2^2\big)\big(p_3^2 - p_4^2\big)}{s} \right\}. \quad (10.6)$$

The corresponding double spectral density is then given by[#6]

$$\rho_{st}(s,t) = \frac{\text{Disc}_t\, \text{Disc}_s\, T_{\text{B}}(s,t)}{(2i)^2} = \lim_{\epsilon \to 0} \frac{\text{Im}_s\, T_{\text{B}}(s,t+i\epsilon) - \text{Im}_s\, T_{\text{B}}(s,t-i\epsilon)}{2i}$$

$$= \frac{g^4}{8} \frac{2s\sqrt{\lambda(s,m_1^2,m_2^2)}}{\sqrt{D}}\, \theta\big(s - (m_1+m_2)^2\big)\, \theta\big(t - (m_3+m_4)^2\big)\, \theta(D)\,, \quad (10.7)$$

such that $\theta(D)$ provides the non-trivial constraints on the support of $\rho_{st}(s,t)$ we were looking for. The boundaries (of the support) of the three double spectral densities of the full amplitude are determined by the corresponding lowest-lying intermediate states in the general box diagram and the explicit diagrams are depicted in Fig. 10.2 (remember that 3π states are forbidden by G-parity). The inelastic (referring to the intermediate state of the s-channel process) diagram (I) and the elastic diagram (II) yield the boundary of the support of ρ_{st}, from which due to $s \leftrightarrow u$ crossing symmetry directly follows the result for ρ_{ut}, while the "twisted" u-channel diagrams (III) and (IV) are relevant for calculating the boundary of the support of

---

[#4]As shown already in [223], the general result for the box graph in [187] lacks a factor of 2.

[#5]The kinematical abbreviations a and b defined here are not to be confused with the hyperbola parameters.

[#6]Note that both the result quoted in [188] and the original result for general masses of [217] for the imaginary part of the box integral (10.5) contain typographical errors. Remarkably, in both cases the same factor of $1/4$ is missing. For the resulting double spectral density (10.7) then [217] consequently lacks the factor of $1/4$, while [188] is now off by a factor of $1/2$. Our result, however, agrees with [160] and [174] (the latter unfortunately containing some typographical errors in the derivation). Noting in addition the missing factor of 2 in [187] as discussed in [223] (wherein also at least some of the errors in [217] are mentioned), we therefore fully agree with the authors of [199] (besides correcting the result for the corresponding unitarity integral of [215], they discuss similar errors in further references) in stating that (p. 152) *"there seem to be many possibilities of errors in this seemingly innocuous integral."* Interestingly, this statement is in line with a comment in [188] in the same context (p. 309): *"The analysis of complex singularities is indeed...complex!"*
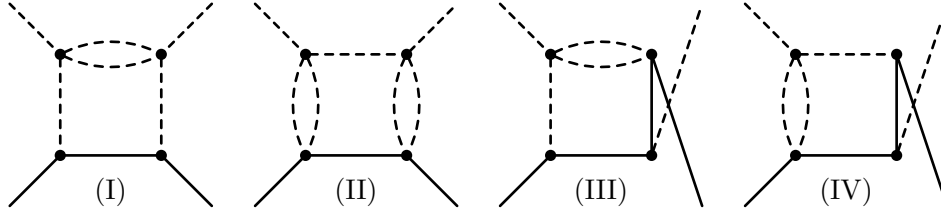
Figure 10.2: Box graphs constraining the boundaries of the double spectral regions. Solid lines denote nucleons and dashed lines denote pions. See main text for details.

ρ_{su}. Since for all four diagrams we have $d = b$ (the same external particles πN for in and out state being on-shell), we can write

$$D = 4b^2 \left\{ \frac{\cos\theta_s \mp 1}{2} \left[b^2 \frac{\cos\theta_s \pm 1}{2} - ca \right] + \left(\frac{c \mp a}{2} \right)^2 \right\} , \qquad (10.8)$$

with the upper signs being more convenient for (I,II) (where in addition $c = a$) and the lower signs being a good starting point for (III,IV), where it is important to note that the relations (10.6) (which are valid for the s-channel process only) need to be modified by $p_3 \leftrightarrow p_4$ and accordingly $t \leftrightarrow u$ (affecting only c and $\cos\theta_s$).[#7] This leads to (cf. the form of the double spectral density (10.7) with corresponding couplings)

$$\frac{D_{\mathrm{I,II}}(s,t)}{4s^2\lambda(s,m_1^2,m_2^2)} = t\, b_{\mathrm{I,II}}(s,t) , \qquad \frac{D_{\mathrm{III,IV}}(s,u)}{4s^2\lambda(s,m_1^2,m_2^2)} = b_{\mathrm{III,IV}}(s,u) , \qquad (10.9)$$

with boundary functions reading (cf. [171])

$$b_{\mathrm{I}}(s,t) = \left(t - 4M_\pi^2\right)\lambda\left(s, m^2, 4M_\pi^2\right) - 16M_\pi^4\left(s + 3\Sigma_-\right) ,$$
$$b_{\mathrm{II}}(s,t) = \left(t - 16M_\pi^2\right)\lambda\left(s, m^2, M_\pi^2\right) - 64M_\pi^4 s , \qquad (10.10)$$

for the boundary of ρ_{st} and thus $b_{\mathrm{I}}(u,t)$ and $b_{\mathrm{II}}(u,t)$ for the boundary of ρ_{ut}, as well as[#8]

$$b_{\mathrm{III}}(s,u) = \lambda\left(u, m^2, M_\pi^2\right)\lambda\left(s, m^2, 4M_\pi^2\right) - 16M_\pi^2\left[m^2 su - \Sigma_-^2\left(m^2 - t(s,u)\right)\right] ,$$
$$b_{\mathrm{IV}}(s,u) = \lambda\left(s, m^2, M_\pi^2\right)\lambda\left(u, m^2, 4M_\pi^2\right) - 16M_\pi^2\left[m^2 su - \Sigma_-^2\left(m^2 - t(s,u)\right)\right] , \qquad (10.11)$$

for the boundary of ρ_{su}, where we only need to consider $b_{\mathrm{III}}(s,u) = b_{\mathrm{IV}}(u,s)$ due to $s \leftrightarrow u$ symmetry. Due to $\theta(D)$, the whole support of all three double spectral densities is then given by the union of the regions allowed by the non-trivial constraints that the corresponding boundary functions be non-negative. Furthermore, trivial constraints arise from the lower kinematical bounds of the corresponding physical regions which are given by the asymptotes of the boundary functions in question, e.g. for the inelastic diagram (I) we find the asymptotes $s = (m + 2M_\pi)^2$ and $t = (2M_\pi)^2 = t_\pi$ and for the elastic diagram (II) we obtain $s = (m + M_\pi)^2 = s_+$ and $t = (4M_\pi)^2$.

[#7]Using the corresponding "untwisted" versions of diagrams (III,IV), this reduces to $t \leftrightarrow u$ in $\cos\theta_s$.

[#8]Note that the results for the πN double spectral region boundary functions b_{III} and b_{IV} given in the original work [218] are incomplete, while the formulae in e.g. [171, 212] are correct.

Therefore, by defining the following abbreviations for the solutions of the implicit equations

$$b_{\mathrm{I}}(s,t) \overset{!}{=} 0 \quad \Rightarrow \quad t = T_{\mathrm{I}}(s) \,, \qquad s = S_{\mathrm{I}}(t) \,,$$
$$b_{\mathrm{II}}(s,t) \overset{!}{=} 0 \quad \Rightarrow \quad t = T_{\mathrm{II}}(s) \,, \qquad s = S_{\mathrm{II}}(t) \,,$$
$$b_{\mathrm{III}}(s,u) \overset{!}{=} 0 \quad \Rightarrow \quad u = U_{\mathrm{III}}(s) \,, \qquad s = S_{\mathrm{III}}(u) \,, \tag{10.12}$$

the combined boundaries of the double spectral regions are given by

$$
\begin{aligned}
T_{st}(s) &= \min\{T_{\mathrm{I}}(s), T_{\mathrm{II}}(s)\} \,, & T_{ut}(u) &= T_{st}(u) \,, \\
S_{st}(t) &= \min\{S_{\mathrm{I}}(t), S_{\mathrm{II}}(t)\} \,, & U_{ut}(t) &= S_{st}(t) \,, \\
S_{su}(u) &= \min\{S_{\mathrm{III}}(s), U_{\mathrm{III}}(s)\} \,, & U_{su}(s) &= S_{su}(s) \,,
\end{aligned} \tag{10.13}
$$

where taking the minimum is to be understood as limited by the physical constraints for the corresponding reaction to actually happen. To be specific, the boundary of the support of e.g. ρ_{st} is described by

$$T_{st}(s) = \min\{T_{\mathrm{I}}(s), T_{\mathrm{II}}(s)\} = \begin{cases} T_{\mathrm{II}}(s) & \text{for } s_+ < s < (m + 2M_\pi)^2 \,, \\ \min\{T_{\mathrm{I}}(s), T_{\mathrm{II}}(s)\} & \text{for } (m + 2M_\pi)^2 < s \,, \end{cases} \tag{10.14}$$

with the functions

$$T_{\mathrm{I}}(s) = \frac{4M_\pi^2 \left(s - m^2 - 2M_\pi^2\right)^2}{\lambda\left(s, m^2, 4M_\pi^2\right)} > 4M_\pi^2 \qquad \forall \, s > (m + 2M_\pi)^2 \,,$$

$$T_{\mathrm{II}}(s) = \frac{16M_\pi^2 \left(s - \Sigma_-\right)^2}{\lambda\left(s, m^2, M_\pi^2\right)} > 16M_\pi^2 \qquad \forall \, s > s_+ \,, \tag{10.15}$$

again limited by the physical constraints, such that by definition $T_{st}(s) > t_\pi$ for $s > s_+$. Eventually, the boundaries of all three double spectral regions are shown in Fig. 10.3. The asymptotes of ρ_{st} are $s = s_+$ and $t = t_\pi$ and hence those of ρ_{ut} are $u = s_+$ and $t = t_\pi$, while the symmetric asymptotes of ρ_{su} are $s = s_+$ and $u = s_+$.

10.2 Lehmann ellipse constraints

The boundaries of the double spectral regions limit the range of validity of the hyperbolic dispersion relations in two ways:

1. The partial-wave expansions of the imaginary parts inside the HDR integrals (internal/primed kinematics) in the unphysical regions for both s- and t-channel partial waves converge only for CMS scattering angle cosines z' within the corresponding large Lehmann ellipses [188, 224]. These ellipses are the largest ellipses in the complex z'-plane centered at the origin with foci at $z' = \pm 1$ that do not reach into any double spectral region.

2. For a given value of the parameter a the hyperbolae $(s - a)(u - a) = b$ with asymptotes $s = a$ and $u = a$ must not enter any double spectral region for all values of the parameter b which are necessary for the partial-wave projections of the full HDR equations (external/unprimed kinematics) in given kinematical ranges. Trivial geometrical constraints on a arise already from the asymptotes of the double spectral regions.
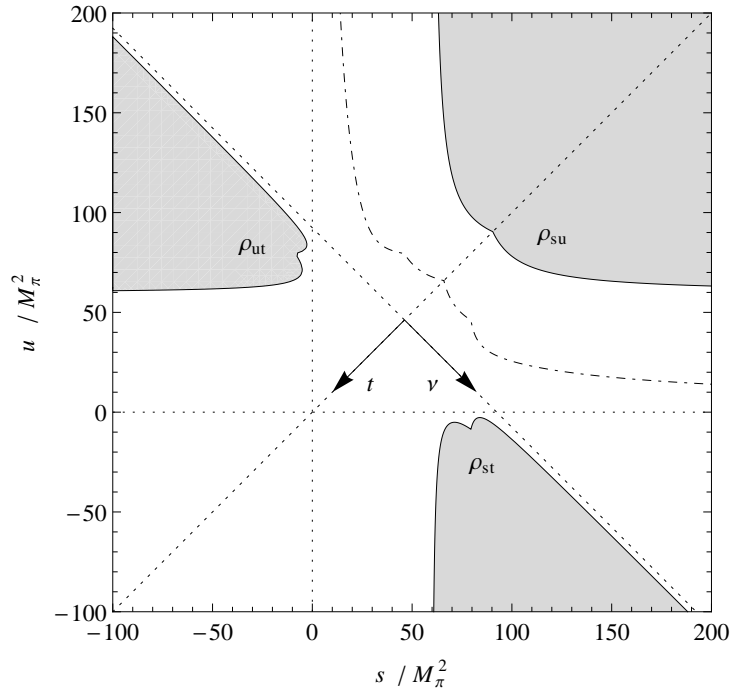
Figure 10.3: Double spectral regions for πN scattering (shaded) and boundaries of ρ_{st} and ρ_{ut} reflected in the corresponding scattering angle (dot-dashed).

In this section we will show how the (large) Lehmann ellipse constraint can be translated for a given a into a constraint on b each for both the expansions in s- and t-channel partial waves. For any allowed fixed a, the allowed values of b are those fulfilling both of the above requirements and the (limited) freedom in the choice of a in the construction of the HDRs can be used in order to optimize the convergence properties of the PWHDRs. In the two subsequent sections we will investigate numerically how these limits on b (for given a) yield the ranges of convergence of the full Roy–Steiner system via the restrictions that are necessary for both the projections onto s- and t-channel partial waves to converge.

For the partial-wave expansion of the s-channel contributions the Lehmann ellipse constraint states that the expansion converges for angles $z'_s(s', t') = 1 + 2s't'/\lambda_{s'}$ (cf. (7.102)) inside the ellipse

$$\frac{(\operatorname{Re} z'_s)^2}{A_s^2} + \frac{(\operatorname{Im} z'_s)^2}{B_s^2} = 1 \,, \qquad A_s^2 - B_s^2 = 1 \,, \tag{10.16}$$

with foci at $z'_s = \pm 1$ (corresponding to the physical constraint $-1 \leq z'_s \leq 1$), so that semimajor and semiminor axis A_s and B_s are related as given above. Since for given t' the angle z'_s is always real in the integration range $s' > s_+$, the maximal value of z'_s for given s' not entering the support of ρ_{st} follows from the corresponding maximally allowed value of t' (according to (10.14) for the internal (primed) variables) and thus reads

$$z_{s'}^{\max}(s') = 1 + \frac{2s'}{\lambda_{s'}} T_{st}(s') = A_s \qquad \forall \, s' > s_+ \,. \tag{10.17}$$

From the geometrical condition $-A_s \leq z'_s \leq A_s$ then follows

$$-z_{s'}^{\max} \leq z'_s \leq z_{s'}^{\max} \qquad \forall \, s' > s_+ \,, \tag{10.18}$$

and the lower bound due to this reflection in z'_s is actually stronger than the restrictions imposed by ρ_{su} as shown by the dot-dashed line in Fig. 10.3, where the z'_s-reflected boundary of the support of ρ_{st} for $\nu > 0$ is given by

$$u\Big(s, t\Big(s, -z_s\big(s, t = T_{st}(s)\big)\Big)\Big) = \frac{\Sigma_-^2}{s} + T_{st}(s) , \tag{10.19}$$

with the asymptote $u = t_\pi$ for $s \to \infty$ due to $T_{st}(s)$. Furthermore, due to $s \leftrightarrow u$ symmetry ρ_{ut} yields exactly the same constraints as ρ_{st} (including the z'_u-reflected boundary for $\nu < 0$) and hence we only need to consider the latter.[#9] The possible values of t' for given s' are then restricted by (cf. [171])

$$-\frac{\lambda_{s'}}{s'} - T_{st}(s') \leq t' \leq T_{st}(s') \qquad \forall\, s' > s_+ . \tag{10.20}$$

Via the linear relation (7.90) for the internal kinematics this range for t' can be translated into a range of allowed values of $b(s', t'; a)$ for given a according to (cf. (10.19))

$$b_s^-(s', a) \leq b \leq b_s^+(s', a) \qquad \forall\, s' > s_+ > a ,$$
$$b_s^-(s', a) = (s' - a)\big(\Sigma - s' - T_{st}(s') - a\big) ,$$
$$b_s^+(s', a) = (s' - a)\Big(\Sigma - s' + \frac{\lambda_{s'}}{s'} + T_{st}(s') - a\Big) = (s' - a)\bigg\{\frac{\Sigma_-^2}{s'} + T_{st}(s') - a\bigg\} , \tag{10.21}$$

where we have used that from the asymptotes $s = s_+$ and $u = s_+$ of the double spectral regions it is geometrically clear from Fig. 10.3 that the allowed values of the hyperbola's asymptotic parameter a are trivially limited to $a < s_+$ (independent of b) and hence here we have $s' > a$ for all $s' > s_+$. By invoking the asymptotes $s = t_\pi$ and $u = t_\pi$ of the z'-reflected boundaries of ρ_{st} and ρ_{ut} (cf. (10.19)) we can deduce that the allowed range of a is actually geometrically limited by $a < t_\pi$, which is the reason why the "fixed-t limit" $|a| \to \infty$ effectively reduces to $a \to -\infty$.[#10] Now, we may define the highest lower and the lowest upper bound

$$\tilde{b}_s^-(a) = \max_{s' > s_+} b_s^-(s', a) , \qquad \tilde{b}_s^+(a) = \min_{s' > s_+} b_s^+(s', a) , \tag{10.22}$$

as the maximum/minimum value of $b_s^{-/+}(s', a)$ within the integration range $s' > s_+$, which then finally determines the allowed values of b for given a by

$$\tilde{b}_s^-(a) \leq b \leq \tilde{b}_s^+(a) \qquad \forall\, s' > s_+ > a , \tag{10.23}$$

for the s-channel parts of the HDRs.

The Lehmann ellipse constraint for the partial-wave expansion of the t-channel contributions limits the convergence of the expansion to angles $z'_t(s', t') = m\nu'/(p'_t q'_t)$ (cf. (7.102)) inside an ellipse similar to (10.16) centered at the origin with foci at $z'_t = \pm 1$, i.e.

$$\frac{(\mathrm{Re}\, z'_t)^2}{A_t^2} + \frac{(\mathrm{Im}\, z'_t)^2}{B_t^2} = 1 , \qquad A_t^2 - B_t^2 = 1 . \tag{10.24}$$

[#9]Note that both the s- and u-channel physical regions fit well in between ρ_{st}, ρ_{ut}, and their reflected boundaries, cf. Fig. 7.1.

[#10]One can easily read off the range of convergence for fixed-t dispersion relations from Fig. 10.3 by considering lines of constant t, yielding $-25.81 M_\pi^2 \leq t \leq t_\pi$ in order not to enter the double spectral regions or the reflected boundaries.

The argument for the t-channel contributions is more intricate, since inside the integration range $t' > t_\pi$ the angle z'_t becomes purely imaginary for $t_\pi < t' < t_N$ and hence no relations similar to (10.18) are possible. However, as the relation between z'_t and b is non-linear anyway (cf. (7.103))

$$z'^2_t = \frac{(t' - \Sigma + 2a)^2 - 4b(s', t'; a)}{16p'^2_t q'^2_t} \, , \tag{10.25}$$

where all squares are real but not necessarily positive, we are interested in the resulting Lehmann ellipse constraint for z'^2_t. By squaring equation (10.24) for general complex z'_t we arrive at

$$\frac{\left(\text{Re}\,\{z'^2_t\} - \frac{1}{2}\right)^2}{\tilde{A}^2_t} + \frac{\left(\text{Im}\,\{z'^2_t\}\right)^2}{\tilde{B}^2_t} = 1 \, , \tag{10.26}$$

corresponding to an ellipse in the complex z'^2_t-plane shifted to the right by $(A^2_t - B^2_t)/2 = 1/2$. Hence, it is centered at $(1/2, 0)$ with the semimajor and semiminor axes given by

$$\tilde{A}_t = \frac{A^2_t + B^2_t}{2} = A^2_t - \frac{1}{2} \, , \qquad \tilde{B}_t = A_t B_t = A_t\sqrt{A^2_t - 1} \, , \tag{10.27}$$

such that the foci are at $1/2 \mp \sqrt{\tilde{A}^2_t - \tilde{B}^2_t} = 1/2 \mp 1/2$ (corresponding to the physical constraint $0 \le z'^2_t \le 1$). Since for $t' > t_\pi$ we have $z'^2_t = \text{Re}\,\{z'^2_t\}$, the geometrical condition $1/2 - \tilde{A}_t \le z'^2_t \le 1/2 + \tilde{A}_t$ leads to the analog of (10.18)

$$1 - A^2_t = -B^2_t \le z'^2_t \le A^2_t \, , \tag{10.28}$$

where it is important to note that on the right hand side the relation between z'_t and A_t is not fixed due to the squares, while the reflection bound on the left hand side again turns out to be more restrictive than the corresponding bound due to ρ_{su} and hence we only have to look at the boundaries of the support of ρ_{st} again. For the following it turns out to be advantageous to rewrite the boundary functions $b_{\text{I,II}}(s, t)$ of (10.10) in terms of (ν, t) since the quantity $\nu(z_t, t) = p_t q_t z_t / m$ is always real

$$b_{\text{I}}(\nu, t) = (t - 4M^2_\pi)\Big\{\frac{1}{4}(t - 4m\nu + 6M^2_\pi)^2 - 16m^2 M^2_\pi\Big\} + 8M^4_\pi\Big\{t - 4m\nu - \Sigma - 6\Sigma_-\Big\} \overset{!}{=} 0 \, ,$$

$$b_{\text{II}}(\nu, t) = (t - 16M^2_\pi)\Big\{\frac{1}{4}(t - 4m\nu)^2 - 4m^2 M^2_\pi\Big\} + 32M^4_\pi\Big\{t - 4m\nu - \Sigma\Big\} \overset{!}{=} 0 \, . \tag{10.29}$$

Solving these implicit quadratic equations for $\nu(t)$ yields the physical solutions (i.e. limited by the physical constraints and thus real, cf. [171])

$$\nu_{\text{I}}(t) = \frac{(t - 2M^2_\pi)(t + 4M^2_\pi) + 8M_\pi\sqrt{t}\sqrt{(t - 4M^2_\pi)m^2 + M^4_\pi}}{4m(t - 4M^2_\pi)} > 0 \qquad \forall\, t > 4M^2_\pi = t_\pi \, ,$$

$$\nu_{\text{II}}(t) = \frac{(t - 8M_\pi)^2 + 4M_\pi\sqrt{t}\sqrt{(t - 16M^2_\pi)m^2 + 16M^4_\pi}}{4m(t - 16M^2_\pi)} > 0 \qquad \forall\, t > 16M^2_\pi = 4t_\pi \, , \tag{10.30}$$

where each sign of the root is fixed by $z_t(\nu, t) = m\nu/(p_t q_t) \propto +\nu$ and therefore $z^{\text{max}}_t = +m\nu^{\text{max}}/(p_t q_t)$ in the physical t-channel region $t > 4m^2 = t_N$. Defining the (positive) combined upper bound on ν according to

$$N_{st}(t) = \min\{\nu_{\text{I}}(t), \nu_{\text{II}}(t)\} = \begin{cases} \nu_{\text{I}}(t) & \text{for } t_\pi < t < 4t_\pi \, , \\ \min\{\nu_{\text{I}}(t), \nu_{\text{II}}(t)\} & \text{for } 4t_\pi < t \, , \end{cases} \tag{10.31}$$

and resorting to the geometrical constraints of the original t-channel Lehmann ellipse (10.24) for z'_t, the maximally allowed value of the real angle $z'_t = \operatorname{Re} z'_t$ for given $t' > t_N$ not entering the support of ρ_{st} is given by

$$z^{\max}_{t'}(t') = \frac{m}{p'_t q'_t} N_{st}(t') = A_t \qquad \forall \, t' > t_N \,, \tag{10.32}$$

and thus (10.28) leads in this case to

$$1 - \frac{m^2}{p'^2_t q'^2_t} N_{st}(t')^2 \le z'^2_t \le \frac{m^2}{p'^2_t q'^2_t} N_{st}(t')^2 \qquad \forall \, t' > t_N \,. \tag{10.33}$$

In contrast, for $t_\pi < t' < t_N$ we have $p'_t = i p'_-$ with real p'_-. Accordingly, for the purely imaginary angle $z'_t = i \operatorname{Im} z'_t$ it follows from (10.24)

$$\left| \operatorname{Im} z'_t(t') \right| = \left| -\frac{m \nu'}{p'_- q'_t} \right| \le \frac{m}{p'_- q'_t} N_{st}(t') = B_t \quad \Rightarrow \quad B^2_t = -\frac{m^2}{p'^2_t q'^2_t} N_{st}(t')^2 \qquad \forall \, t_\pi < t' < t_N \,, \tag{10.34}$$

which plugged into (10.28) yields

$$\frac{m^2}{p'^2_t q'^2_t} N_{st}(t')^2 \le z'^2_t \le 1 - \frac{m^2}{p'^2_t q'^2_t} N_{st}(t')^2 \qquad \forall \, t_\pi < t' < t_N \,. \tag{10.35}$$

However, from both (10.33) with $p'^2_t > 0$ for all $t' > t_N$ and (10.35) with $p'^2_t < 0$ for all $t_\pi < t' < t_N$ we arrive at the same constraints on ν'^2 for given $t' > t_\pi$ (cf. [171])

$$\frac{p'^2_t q'^2_t}{m^2} - N_{st}(t')^2 \le \nu'^2 \le N_{st}(t')^2 \qquad \forall \, t' > t_\pi \,. \tag{10.36}$$

By virtue of the linear relation (cf. (7.88))

$$16 m^2 \nu'^2 = (t' - \Sigma + 2a)^2 - 4b \,, \tag{10.37}$$

this range for ν'^2 can then be translated into a range for $b(\nu'^2, t'; a)$ according to

$$b^-_t(t', a) \le b \le b^+_t(t', a) \qquad \forall \, t' > t_\pi > a \,, \tag{10.38}$$

$$b^-_t(t', a) = \frac{1}{4}(t' - \Sigma + 2a)^2 - 4 m^2 N_{st}(t')^2 \,,$$

$$b^+_t(t', a) = \frac{1}{4}(t' - \Sigma + 2a)^2 - 4 p'^2_t q'^2_t + 4 m^2 N_{st}(t')^2 = (t' - \Sigma)a + a^2 + \Sigma^2_- + 4 m^2 N_{st}(t')^2 \,,$$

where we have included the geometrical constraint on a as discussed below equation (10.21). Defining again the highest lower and the lowest upper bound

$$\tilde{b}^-_t(a) = \max_{t' > t_\pi} b^-_t(t', a) \,, \qquad \tilde{b}^+_t(a) = \min_{t' > t_\pi} b^+_t(t', a) \,, \tag{10.39}$$

as the maximum/minimum value of $b^{-/+}_t(s', a)$ within the integration range $t' > t_\pi$, we can finally give the range of allowed values of b for given a by

$$\tilde{b}^-_t(a) \le b \le \tilde{b}^+_t(a) \qquad \forall \, t' > t_\pi > a \,, \tag{10.40}$$

for the t-channel parts of the HDRs.

10.3 s-channel partial-wave projection

As mentioned before, it turns out that the constraints due to ρ_{ut} and ρ_{su} are equal to or weaker than the restrictions due to ρ_{st}. Therefore we only need to consider the corresponding constraints for the s-channel partial-wave projection of both the s-channel partial-wave-expanded and the t-channel partial-wave-expanded HDR parts. However, the strategy to find the optimal value of a and the corresponding range of convergence in s is the same in both cases: from the Lehmann ellipse constraint it follows that all allowed values of b must obey[#11]

$$\tilde{b}_{s,t}^-(a) \le b \le \tilde{b}_{s,t}^+(a) , \tag{10.41}$$

for all $s' > s_+$ and $t' > t_\pi$, i.e. within the corresponding integration ranges, respectively. The limits $-1 \le z_s \le 1$ of the scattering angle for the physical s-channel reaction (i.e. $s > s_+$) translates to

$$-4q^2 = -\frac{\lambda_s}{s} \le t \le 0 \qquad \forall\, s > s_+ , \tag{10.42}$$

and hence for given $a < s_+ < s$ the bounds on b due to the s-channel partial-wave projection are given by (cf. (10.21))

$$
\begin{aligned}
b_s^{\min}(s,a) &\le b \le b_s^{\max}(s,a) \qquad \forall\, s > s_+ > a , \\
b_s^{\min}(s,a) &= (s-a)(\Sigma - s - a) , \\
b_s^{\max}(s,a) &= (s-a)\Big(\Sigma - s + \frac{\lambda_s}{s} - a\Big) = (s-a)\Big\{\frac{\Sigma_-^2}{s} - a\Big\} .
\end{aligned}
\tag{10.43}
$$

The maximally allowed value of s for given a, $s_{s,t}^{\max}(a)$, is then the largest value of s such that for given a both $b_s^{\min}(s,a)$ and $b_s^{\max}(s,a)$ lie within the ranges $\big[\tilde{b}_{s,t}^-(a), \tilde{b}_{s,t}^+(a)\big]$, respectively. Equating the boundary values of b from both the s- and t-channel partial-wave expansions and the s-channel partial-wave projection yields

$$
\begin{aligned}
b_s^{\min}(s,a) &\overset{!}{=} \tilde{b}_{s,t}^-(a) &\Rightarrow& \quad s = s_{s,t}^-(a) , \\
b_s^{\max}(s,a) &\overset{!}{=} \tilde{b}_{s,t}^+(a) &\Rightarrow& \quad s = s_{s,t}^+(a) ,
\end{aligned}
\tag{10.44}
$$

where $s_{s,t}^-$ and $s_{s,t}^+$ denote the corresponding maximal solutions for given a, leads to two equations for the two wanted unknowns $\tilde{s}_{s,t}^{\max}$ and $\tilde{a}_{s,t}^s$ defined by

$$\tilde{s}_{s,t}^{\max} = \max_{a < s_+} s_{s,t}^{\max}(a) = s_{s,t}^{\max}(\tilde{a}_{s,t}^s) . \tag{10.45}$$

Explicitly, they follow from equating the maximal solutions

$$
\begin{aligned}
s_{s,t}^-(a) &\overset{!}{=} s_{s,t}^+(a) &\Rightarrow& \quad a = \tilde{a}_{s,t}^s , \quad s_{s,t}^-(\tilde{a}_{s,t}^s) = s_{s,t}^+(\tilde{a}_{s,t}^s) = \tilde{s}_{s,t}^{\max} , \\
s_{s,t}^\pm(a) &= \max\Big\{ s_{s,t}^{\pm(-)}(a), s_{s,t}^{\pm(+)}(a) \Big\} , \\
s_{s,t}^{-(\pm)}(a) &= \frac{\Sigma}{2} \pm \sqrt{\Big(\frac{\Sigma}{2} - a\Big)^2 - \tilde{b}_{s,t}^-(a)} , \\
s_{s,t}^{+(\pm)}(a) &= \frac{1}{2a}\Big\{ \big[a^2 + \Sigma_-^2 - \tilde{b}_{s,t}^+(a)\big] \pm \sqrt{\big[a^2 + \Sigma_-^2 - \tilde{b}_{s,t}^+(a)\big]^2 - 4a^2\Sigma_-^2} \Big\} ,
\end{aligned}
\tag{10.46}
$$

[#11]Note that the lower bounds coincide: $\tilde{b}_s^-(a) = \tilde{b}_t^-(a)$ for all $a < s_+$.
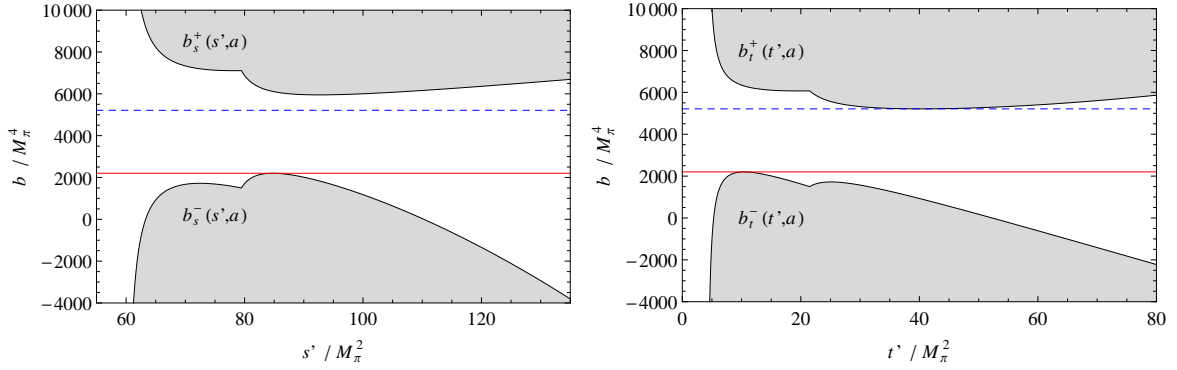
Figure 10.4: Allowed ranges of b for s-channel partial-wave projection with $a = \tilde{a}_t^s = -23.19\, M_\pi^2$ for s-channel (left) and t-channel (right) partial-wave expansion. Horizontal lines correspond to $\tilde{b}_t^-(a) = 2202\, M_\pi^4$ (solid) and $\tilde{b}_t^+(a) = 5212\, M_\pi^4$ (dashed).

where for $s > s_+ > \Sigma/2$ we have $s_{s,t}^- = s_{s,t}^{-(+)}$ and for in addition e.g. $a < 0$ we have $s_{s,t}^+ = s_{s,t}^{+(-)}$. The maximum value of the two other (i.e. minimal) solutions for $\tilde{a}_{s,t}$ then yields the highest lower bound on s and thus we can write

$$\tilde{s}_{s,t}^{\min} = \max\left\{s_+, s_{s,t}^{-(-)}(\tilde{a}_{s,t}^s), s_{s,t}^{+(+)}(\tilde{a}_{s,t}^s)\right\} \qquad \text{for } s > s_+ \text{ and } a < 0 \,. \tag{10.47}$$

For the s-channel parts, solving the equations numerically for all allowed $a < s_+$ leads to the following optimal value of a and corresponding range of convergence in $s > s_+ = 59.64\, M_\pi^2 = (1.08\,\text{GeV})^2$

$$\tilde{a}_s^s = -128.30\, M_\pi^2 \,, \quad s_+ < s < \tilde{s}_s^{\max} = 106.09\, M_\pi^2 \,, \quad \tilde{b}_s^-(\tilde{a}_s^s) = 26860\, M_\pi^4 \,, \quad \tilde{b}_s^+(\tilde{a}_s^s) = 34388\, M_\pi^4 \,, \tag{10.48}$$

in agreement with the unpublished App. E of [161].[#12]

For the t-channel parts, this procedure results in

$$\tilde{a}_t^s = -23.19\, M_\pi^2 \,, \quad s_+ < s < \tilde{s}_t^{\max} = 97.30\, M_\pi^2 \,, \quad \tilde{b}_t^-(\tilde{a}_t^s) = 2202\, M_\pi^4 \,, \quad \tilde{b}_t^+(\tilde{a}_t^s) = 5212\, M_\pi^4 \,. \tag{10.49}$$

In fact, it turns out that the s-channel constraints are weaker than the t-channel ones, which can also be deduced from Fig. 10.4, where the situation for $\tilde{a}_t^s = -23.19\, M_\pi^2$ is shown: for this a the range of b limited by $\tilde{b}_t^-(\tilde{a}_t^s)$ and $\tilde{b}_t^+(\tilde{a}_t^s)$ for the t-channel partial-wave expansion also lies within the allowed range of b for the s-channel partial-wave expansion and hence for the range of s given in (10.49) this range of b covers the interval $\left[b_s^{\min}(s, \tilde{a}_t^s), b_s^{\max}(s, \tilde{a}_t^s)\right]$ that is needed for the s-channel partial-wave projection. By construction, the resulting family of hyperbolae does cross neither any double spectral region nor their z'-reflected boundaries as depicted in Fig. 10.6(left), and thus (10.49) corresponding to $\tilde{W}^{\max} = \sqrt{\tilde{s}^{\max}} = \sqrt{97.30}\, M_\pi = 1.38\,\text{GeV}$ constitutes the result for the s-channel partial-wave projection, in agreement with [171].[#13]

[#12]App. E of [161] deals with finding the optimal values for the s-channel partial-wave projection of the s-channel partial-wave-expanded absorptive parts of the HDRs only and follows a similar scheme. The quoted results are $\tilde{s}_s^{\max} \gtrsim 105\, M_\pi^2$ for $\tilde{a}_s^s \approx -117\, M_\pi^2$.

[#13]As combined result for both s- and t-channel contributions, the numbers $\tilde{s}^{\max} = 97\, M_\pi^2$ for $\tilde{a}^s = -23\, M_\pi^2$

10.4   *t*-channel partial-wave projection

The relation between the range of b permitted by the Lehmann ellipse constraint (10.41) and the corresponding range of convergence in t for the projection of the HDR equations onto t-channel partial waves for given a is most easily established on the basis of the squared t-channel scattering angle z_t^2, which must cover the range

$$0 \leq z_t^2(t,a,b) = \frac{(t - \Sigma + 2a)^2 - 4b}{16 p_t^2 q_t^2} = \frac{(t - \Sigma + 2a)^2 - 4b}{(t - t_\pi)(t - t_N)} \leq 1 \;, \qquad (10.50)$$

for both the s-channel and t-channel partial-wave-expanded parts, since (as discussed after the t-channel partial-wave projection formulae (9.7)) the integrands are always functions of the real square z_t^2 even between the thresholds t_π and t_N and furthermore $0 \leq z_t^2 \leq 1$ is not only a necessary condition for $0 \leq z_t \leq 1$ but also equivalent to $-1 \leq z_t \leq 1$, which in turn is already sufficient to perform the partial-wave projections in our case (cf. the discussion in Chap. 9). Therefore, the range (10.50) of z_t^2 constitutes the necessary and sufficient condition not only for the physical region $t > t_N$ but for all kinematical regions. Obviously, for $t_\pi < t < t_N$ and given a, z_t^2 can only be non-negative for b non-negative and large enough. Translating (10.50) into ranges for b while taking care of the signs of p_t^2 and q_t^2 in the different kinematical regions yields (cf. (10.38))

$$b_t^{\min}(t,a) \leq b \leq b_t^{\max}(t,a) \qquad \forall\, t_\pi < t < t_N \;,$$

$$b_t^{\max}(t,a) \leq b \leq b_t^{\min}(t,a) \qquad \forall\, t > t_N \;(\text{or } t < t_\pi) \;,$$

$$b_t^{\min}(t,a) = \frac{1}{4}(t - \Sigma + 2a)^2 \geq 0 \;,$$

$$b_t^{\max}(t,a) = \frac{1}{4}(t - \Sigma + 2a)^2 - 4p_t^2 q_t^2 = (t - \Sigma)a + a^2 + \Sigma_-^2 \;, \qquad (10.51)$$

where the superscripts min/max refer to both the (at least partially) unphysical kinematical range $t > t_\pi$ needed in our Roy–Steiner system as well as the corresponding min/max values $0/1$ of z_t^2. Solving these equations for t yields (cf. $t_{(\pm)}(\nu = 0; a, b)$ of (7.88))

$$t_0^{(\pm)}(a, b_t^{\min}) = \Sigma - 2a \pm 2\sqrt{b_t^{\min}} \;, \qquad t_1(a, b_t^{\max}) = \Sigma - a + \frac{1}{a}\left[b_t^{\max} - \Sigma_-^2 \right] \;, \qquad (10.52)$$

and the range of convergence in t for given a is the kinematical range in which all values between $b_t^{\min}(t,a)$ and $b_t^{\max}(t,a)$ are covered by both intervals $[\tilde{b}_{s,t}^-(a), \tilde{b}_{s,t}^+(a)]$. Between the thresholds (i.e. for $t_\pi < t < t_N$) this amounts to the conditions $\tilde{b}_{s,t}^-(a) \leq b_t^{\min}(t,a)$ and $b_t^{\max}(t,a) \leq \tilde{b}_{s,t}^+(a)$, while below or above the thresholds (i.e. for $t < t_\pi$ or $t_N < t$) we have $\tilde{b}_{s,t}^-(a) \leq b_t^{\max}(t,a)$ and $b_t^{\min}(t,a) \leq \tilde{b}_{s,t}^+(a)$.[#14] Equivalently, we can demand that for given a the band $0 \leq z_t^2(t,a,b) \leq 1$ must be fully covered by the area between $z_t^2(t,a,\tilde{b}_{s,t}^-(a))$ and $z_t^2(t,a,\tilde{b}_{s,t}^+(a))$ in order to determine the range of validity in t. The situation that results from using the set (10.49) of optimal parameters for the s-channel partial-wave projection

---

are quoted in [171] without further explanation and giving only a vague reference for these numerical values, which is most probably meant to be [225]. However, roughly the same numbers are also given more recently in [165].

[#14]Accordingly, at the thresholds the respective min/max values are identical: $b_t^{\min}(t_\pi, a) = b_t^{\max}(t_\pi, a) = \left(a - \Sigma_-\right)^2 \geq 0$ and $b_t^{\min}(t_N, a) = b_t^{\max}(t_N, a) = \left(a + \Sigma_-\right)^2 \geq 0$.
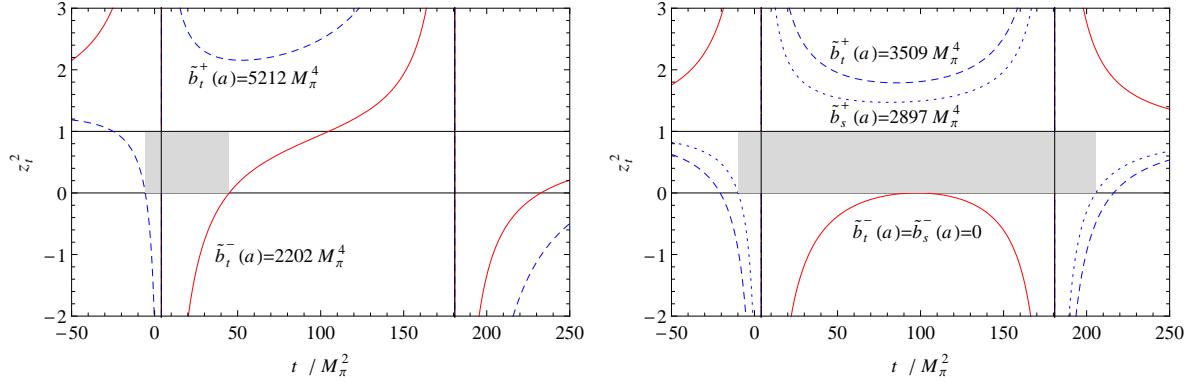
Figure 10.5: Ranges of convergence in t for t-channel partial-wave projection from full coverage (shaded area) of the physical band $0 \leq z_t^2 \leq 1$ for $a = \tilde{a}_t^s = -23.19\,M_\pi^2$ (left) and $a = \tilde{a}_{s,t}^t = -2.71\,M_\pi^2$ (right). Vertical lines indicate thresholds t_π and t_N.

derived in the previous section is shown in Fig. 10.5(left): the t-channel projection is then valid for $-5.63\,M_\pi^2 < t < 44.92\,M_\pi^2$ (denoted by the shaded area of coverage) and the reason for this rather low upper bound on t is that the curve for $\tilde{b}_t^- = 2202\,M_\pi^4$ changes sign between the thresholds and thus enters the critical band $0 \leq z_t^2 \leq 1$ which is hence no longer fully covered by the allowed area. Indeed, the range of convergence can be significantly improved if $z_t^2(t, a, \tilde{b}_{s,t}^-(a)) \leq 0$ (and of course also $z_t^2(t, a, \tilde{b}_{s,t}^+(a)) \geq 1$) for all t between the thresholds. From (10.50) it is clear that for $t \in (t_\pi, t_N)$ we have $z_t^2(t, a, b) \leq 0$ if and only if $b \leq (t - \Sigma + 2a)^2/4$, such that the curves for the lower limits $\tilde{b}_{s,t}^-(a)$ of b will be tangent to the zero axis provided that $\tilde{b}_{s,t}^-(a) = 0$. Solving this numerically yields

$$\tilde{b}_s^-(a) = \tilde{b}_t^-(a) \overset{!}{=} 0 \quad \Rightarrow \quad a = \tilde{a}_{s,t}^t = -2.71\,M_\pi^2\,, \tag{10.53}$$

which is unambiguous since it turns out that $\tilde{b}_{s,t}^-(a) > 0$ for $a < \tilde{a}_{s,t}^t$ as well as $\tilde{b}_{s,t}^-(a) < 0$ for $\tilde{a}_{s,t}^t < a < s_+$ (where we have used the numerical equality of the lower bounds for both s- and t-channel partial-wave expansion). Furthermore, the curves for $\tilde{b}_{s,t}^+(a)$ start to enter the critical band due to change of sign at t_N for $a > 2.58\,M_\pi^2$ and $a > 9.17\,M_\pi^2$, respectively (however, the geometrical constraint $a < t_\pi$ is partially tighter anyway). Thus $\tilde{a}_{s,t}^t$ is the smallest value of a such that the critical band is fully covered between the thresholds which is shown in Fig. 10.5(right). From this figure and equation (10.52) it is clear that in this case we can deduce the corresponding upper and lower bounds $t_{s,t}^{\min}(a)$ and $t_{s,t}^{\max}(a)$ on t by the intercepts $t_0^{(\pm)}(a, \tilde{b}_{s,t}^+(a))$ of $z_t^2(t, a, \tilde{b}_{s,t}^+(a))$ with the zero axis below and above the thresholds, respectively. Since moreover both $t_{s,t}^{\max}(a) = t_0^{(+)}(a, \tilde{b}_{s,t}^+(a))$ are strictly decreasing in the allowed ranges of a, the minimal allowed value $a = \tilde{a}_{s,t}^t$ is also the optimal one yielding $\tilde{t}_{s,t}^{\min} = t_0^{(-)}(\tilde{a}_{s,t}^t, \tilde{b}_{s,t}^+(\tilde{a}_{s,t}^t))$ and $\tilde{t}_{s,t}^{\max} = t_0^{(+)}(\tilde{a}_{s,t}^t, \tilde{b}_{s,t}^+(\tilde{a}_{s,t}^t))$. This procedure results in

$$\tilde{b}_s^+(\tilde{a}_{s,t}^t) = 2897\,M_\pi^4 \quad \Rightarrow \quad -9.84\,M_\pi^2 \leq t \leq 205.45\,M_\pi^2\,,$$
$$\tilde{b}_t^+(\tilde{a}_{s,t}^t) = 3509\,M_\pi^4 \quad \Rightarrow \quad -20.67\,M_\pi^2 \leq t \leq 216.28\,M_\pi^2\,, \tag{10.54}$$

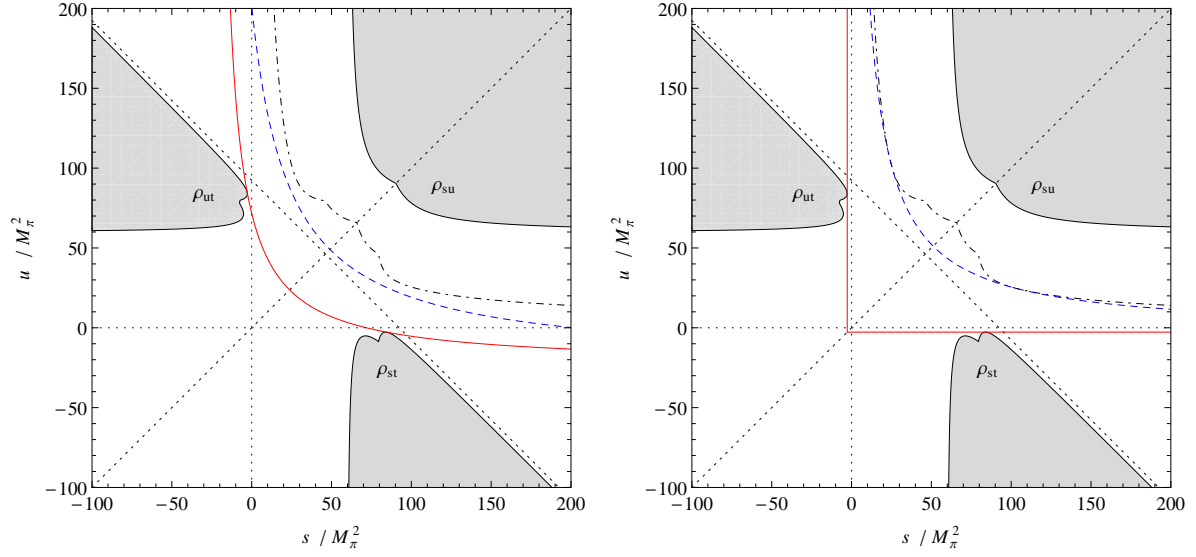where the s-channel Lehmann ellipse constraint proves slightly more restrictive.

Figure 10.6: Double spectral regions and limiting hyperbolae for s- and t-channel partial-wave projection. Left: for $a = \tilde{a}_t^s = -23.19\, M_\pi^2$ with $\tilde{b}_t^-(a) = 2202\, M_\pi^4$ (solid) and $\tilde{b}_t^+(a) = 5212\, M_\pi^4$ (dashed). Right: for $a = \tilde{a}_{s,t}^t = -2.71\, M_\pi^2$ with $\tilde{b}_{s,t}^-(a) = 0$ (solid) and $\tilde{b}_s^+(a) = 2897\, M_\pi^4$ (dashed).

Therefore the final result for the t-channel partial-wave projection reads

$$\tilde{a}_{s,t}^t = -2.71\, M_\pi^2 \, , \quad t_\pi < t < \tilde{t}_s^{\max} = 205.45\, M_\pi^2 \, , \quad \tilde{b}_{s,t}^-(\tilde{a}_{s,t}^t) = 0 \, , \quad \tilde{b}_s^+(\tilde{a}_{s,t}^t) = 2897\, M_\pi^4 \, , \tag{10.55}$$

which corresponds to $\sqrt{\tilde{t}^{\max}} = \sqrt{205.45}\, M_\pi = 2.00\,\mathrm{GeV}$. Again, ascertaining that the resulting family of hyperbolae does enter neither any double spectral region nor their z'-reflected boundaries, which is shown in Fig. 10.6(right), completes the derivation of the final result (10.55) for the t-channel partial-wave projection. Note that for each set of hyperbola parameters a and b only the "positive" branch of the hyperbola connecting the physical regions for the s- and u-channel (cf. Fig 7.1) is shown in Fig. 10.6; the corresponding "negative" branch yields the connection with the physical t-channel regions, however, not giving rise to any further constraints. It is interesting to note that the domain of validity in t is much bigger as the one in s, which is reflected by the possibility to use only the positive half $0 \leq z_t \leq 1$ of the range of the scattering angle due to Bose symmetry in the t-channel; in particular the range of convergence connects the physical regions for the s- and u-channel reactions, where $t \leq 0$, with the t-channel physical region $t \geq t_N$.

The complicated interplay between a, $\tilde{b}_{s,t}^\pm(a)$, and $z_t^2(t, a, b)$ in the different kinematical regions is the reason why it is not possible to treat the t-channel projection in analogy to the s-channel projection in the previous section: equating again the corresponding boundary values of b from both the s- and t-channel partial-wave expansions and the t-channel partial-wave projection and subsequently equating the corresponding maximal solutions in order to obtain $\tilde{t}_{s,t}^{\max}$ as the maximal upper limit on t for $t > t_N$ leads to entering or even crossing the critical band between the thresholds.

Chapter 11

Asymptotic regions and Regge theory

The asymptotic s- and t-channel contributions of the HDRs (7.98) to the invariant amplitudes are defined by splitting the corresponding integration ranges $s_+ \leq s' \leq \infty$ and $t_\pi \leq t' \leq \infty$ at some appropriate values $s_a = W_a^2$ and t_a, respectively, which yields the following asymptotic contributions

$$
A^+\big|_{\text{asym}}(s,t) = \frac{1}{\pi}\int\limits_{s_a}^{\infty} ds' \left[\frac{1}{s'-s} + \frac{1}{s'-u} - \frac{1}{s'-a}\right] \operatorname{Im} A^+(s',z_s') + \frac{1}{\pi}\int\limits_{t_a}^{\infty} dt' \frac{\operatorname{Im} A^+(t',z_t')}{t'-t} \ ,
$$

$$
A^-\big|_{\text{asym}}(s,t) = \frac{1}{\pi}\int\limits_{s_a}^{\infty} ds' \left[\frac{1}{s'-s} - \frac{1}{s'-u}\right] \operatorname{Im} A^-(s',z_s') + \frac{1}{\pi}\int\limits_{t_a}^{\infty} dt' \frac{s-u}{s'-u'} \frac{\operatorname{Im} A^-(t',z_t')}{t'-t} \ ,
$$

$$
B^+\big|_{\text{asym}}(s,t) = \frac{1}{\pi}\int\limits_{s_a}^{\infty} ds' \left[\frac{1}{s'-s} - \frac{1}{s'-u}\right] \operatorname{Im} B^+(s',z_s') + \frac{1}{\pi}\int\limits_{t_a}^{\infty} dt' \frac{s-u}{s'-u'} \frac{\operatorname{Im} B^+(t',z_t')}{t'-t} \ ,
$$

$$
B^-\big|_{\text{asym}}(s,t) = \frac{1}{\pi}\int\limits_{s_a}^{\infty} ds' \left[\frac{1}{s'-s} + \frac{1}{s'-u} - \frac{1}{s'-a}\right] \operatorname{Im} B^-(s',z_s') + \frac{1}{\pi}\int\limits_{t_a}^{\infty} dt' \frac{\operatorname{Im} B^-(t',z_t')}{t'-t} \ ,
$$

$$(11.1)$$

and the remaining non-asymptotic parts are given by the corresponding integrals over $s_+ \leq s' \leq s_a$ and $t_\pi \leq t' \leq t_a$, respectively, plus the nucleon pole terms $N^I(s,t)$ for the amplitudes $B^I(s,t)$. The internal (primed) kinematics are given by (cf. Sect. 7.4 and especially (7.88))

$$
s'(t';a,b) = \frac{1}{2}\left(\Sigma - t' + \sqrt{(t'-\Sigma+2a)^2 - 4b}\right) , \qquad t'(s';a,b) = -\frac{b}{s'-a} + \Sigma - s' - a \ ,
$$

$$
u'(t';a,b) = \frac{1}{2}\left(\Sigma - t' - \sqrt{(t'-\Sigma+2a)^2 - 4b}\right) ,
$$

$$(11.2)$$

where the parameter b is fixed by the external (unprimed) kinematics as

$$
(s-a)(\Sigma - s - t - a) = b = (s'-a)(u'-a) \ ,
$$

$$(11.3)$$

such that

$$
s'(u';a,b) = \frac{b}{u'-a} + a \ , \qquad u'(s';a,b) = \frac{b}{s'-a} + a \ .
$$

$$(11.4)$$

Thus (for given a and finite b), for the s-channel integrals we need the asymptotic behavior in the limit

$$s' \to \infty \quad \Rightarrow \quad t' \to -\infty \,, \quad u' \to a \,, \tag{11.5}$$

while in the t-channel integrals the asymptotic behavior is determined by

$$t' \to \infty \quad \Rightarrow \quad u' \to -\infty \,, \quad s' \to a \,. \tag{11.6}$$

From (11.1) the asymptotic parts of the s- and t-channel partial waves may then be deduced by the projection formulae (8.24) and (9.18) as

$$f_{l+}^I\big|_{\text{asym}}(W) = \int_{-1}^1 dz_s \left\{ R_{l,l+1}^1(W,z_s)\, A^I\big|_{\text{asym}}(W,z_s) + R_{l,l+1}^2(W,z_s)\, B^I\big|_{\text{asym}}(W,z_s) \right\} \,,$$

$$f_{(l+1)-}^I\big|_{\text{asym}}(W) = \int_{-1}^1 dz_s \left\{ R_{l+1,l}^1(W,z_s)\, A^I\big|_{\text{asym}}(W,z_s) + R_{l+1,l}^2(W,z_s)\, B^I\big|_{\text{asym}}(W,z_s) \right\} \,,$$

$$f_+^J\big|_{\text{asym}}(t) = \tilde{\zeta}_J(t) \int_0^1 dz_t \left\{ \tilde{u}_J(t,z_t)\, A^I\big|_{\text{asym}}(t,z_t) + \tilde{v}_J(t,z_t)\, B^I\big|_{\text{asym}}(t,z_t) \right\} \,,$$

$$f_-^J\big|_{\text{asym}}(t) = \tilde{\zeta}_J(t) \int_0^1 dz_t\, \tilde{w}_J(t,z_t)\, B^I\big|_{\text{asym}}(t,z_t) \,, \tag{11.7}$$

where for the t-channel partial waves we have again $I = +/-$ for even/odd J. Note that for these asymptotic contributions we do not expand the absorptive parts inside the integrals but take into account the high-energy behavior of the full invariant amplitudes as given by Regge theory [226]. Therefore, also for the driving terms (i.e. all contributions of the sums of the higher partial waves that are not treated dynamically, cf. [53, 158], as well as the asymptotic contributions of the lowest partial waves that are accounted for explicitly in solving the RS system) the integration ranges are limited by s_a and t_a in order to avoid double counting of the asymptotic regions. This procedure follows [53, 158], motivated by the observations that, first, for higher and higher energies one would be forced to explicitly use higher and higher partial waves as well in order to ensure the validity of the partial-wave expansion, and second, no available information in the asymptotic regime is lost without need. For the s-channel, in Sect. 15.2 we will explicitly demonstrate the matching of truncated sums of the lowest partial waves for $l \le 3$, $l \le 4$, and $l \le 5$ below W_a to the Regge model (cf. Sect. 11.1) above W_a.

In the following, for both channels the contributions from the asymptotic regions will be discussed in the framework of Regge theory; for a general introduction see e.g. [227].

11.1 s-channel asymptotics

First of all, contributions from t-channel Regge trajectories, i.e. the leading Pomeron ($I_t = 0$) trajectory $\alpha_P(t') \approx \alpha_P^{(0)} = 1$ (roughly independent of t' but with exponential residue function $\beta_P(t') = \sigma_P \exp\frac{b_P t'}{2}$, where σ_P represents the asymptotic total cross section value for $\pi\pi$ scattering and b_P is the width of the diffraction peak, cf. [53, 158]) as well as the ρ ($I_t = 1$)

and f ($I_t = 0$) trajectories $\alpha_\rho(t') = \alpha_\rho^{(0)} + \alpha_\rho^{(1)} t'$ (and $\alpha_f(t')$ in analogy) should be negligible, since due to (11.5) for $s' \to \infty$ they will behave as

$$\text{Im}\,\mathcal{A}(s', t') \sim \beta_P(t') s'^{\alpha_P(t')} \sim e^{\frac{b_P t'}{2}} s' \sim e^{-s'} s' \,,$$

$$\text{Im}\,\mathcal{A}(s', t') \sim \beta_\rho(t') s'^{\alpha_\rho(t')} \sim s'^{\alpha_\rho^{(0)} + t'\alpha_\rho^{(1)}} \sim s'^{-s'} \,, \tag{11.8}$$

leading to an exponential suppression.

Let us briefly review the *u*-channel exchange contributions to the *s*-channel reactions of backward πN scattering as discussed in [228]. The invariant amplitudes can be parameterized according to (cf. also [171])

$$A(s', u') = \sum_i \frac{\beta_i^A(u')\zeta_i(u')}{\Gamma\left(\alpha_i(u') - \frac{1}{2}\right)} \left(\frac{s'}{s_R}\right)^{\alpha_i(u') - \frac{1}{2}} , \qquad B(s', u') = \sum_i \frac{\beta_i^B(u')\zeta_i(u')}{\Gamma\left(\alpha_i(u') - \frac{1}{2}\right)} \left(\frac{s'}{s_R}\right)^{\alpha_i(u') - \frac{1}{2}} , \tag{11.9}$$

where both sums run over the four trajectories $i \in \{N_\alpha, N_\gamma, \Delta_\delta, \Delta_\beta\}$ and the Regge propagators $\zeta_i(u')$ are given by

$$\zeta_i(u') = \frac{1 + \mathcal{S}_i \exp\left(-i\pi\left[\alpha_i(u') - \frac{1}{2}\right]\right)}{\sin\left(\pi\left[\alpha_i(u') - \frac{1}{2}\right]\right)} \,. \tag{11.10}$$

Besides the scaling factor $s_R = 1\,\text{GeV}^2$, the following Regge residues $\beta_i^{A/B}(u')$ and Regge trajectories $\alpha_i(u')$ are employed

$$\beta_i^A(u') = a_i + b_i u' \,, \qquad \beta_i^B(u') = c_i + d_i u' \,, \qquad \alpha_i(u') = \alpha_i^{(0)} + \alpha' u' \,, \tag{11.11}$$

i.e. both the residues and the trajectories are linearly parameterized and for the latter an identical slope $\alpha_i^{(1)} = \alpha'$ is used for all i. The signature $\mathcal{S}_i = (-1)^{J_i - \frac{1}{2}}$ of the trajectory i is positive for N_α and Δ_β and negative for N_γ and Δ_δ. Since $\text{Im}\,\zeta_i(u') = -\mathcal{S}_i$, we may conclude that the imaginary parts of the invariant amplitudes in the *u*-channel isospin basis $I_u \in \{1/2 = N, 3/2 = \Delta\}$ can be written as

$$\text{Im}\,A^N(s', u') = \sum_{i \in \{N_\alpha, N_\gamma\}} \tilde{\beta}_i^A(u') \left(\frac{s'}{s_R}\right)^{\alpha_i(u') - \frac{1}{2}} ,$$

$$\text{Im}\,A^\Delta(s', u') = \sum_{i \in \{\Delta_\delta, \Delta_\beta\}} \tilde{\beta}_i^A(u') \left(\frac{s'}{s_R}\right)^{\alpha_i(u') - \frac{1}{2}} , \tag{11.12}$$

with the abbreviations

$$\tilde{\beta}_i^A(u') = -\frac{\mathcal{S}_i \beta_i^A(u')}{\Gamma\left(\alpha_i(u') - \frac{1}{2}\right)} \,, \tag{11.13}$$

and analogously for the B amplitudes. Using now the isospin crossing relations (7.41), we

	N_α	N_γ	Δ_δ	Δ_β
$a\,[\,\text{GeV}^{-1}]$	-60.68	47.22	-75.15	1419.99
$b\,[\,\text{GeV}^{-3}]$	326.52	-215.84	-138.75	3052.84
$c\,[\,\text{GeV}^{-2}]$	546.40	-101.11	64.16	-192.64
$d\,[\,\text{GeV}^{-4}]$	307.42	-128.04	86.77	-695.81
$\alpha^{(0)}$	-0.36	-0.62	0.03	-2.65
$\alpha'\,[\,\text{GeV}^{-2}]$			0.908	

Table 11.1: Regge model parameter values for backward πN scattering as given in [228].

finally obtain the absorptive parts

$$
\operatorname{Im} A^+(s', u'(s', t')) = +\frac{1}{3} \sum_{i \in \{N_\alpha, N_\gamma\}} \tilde{\beta}_i^A(u') \left(\frac{s'}{s_R}\right)^{\alpha_i(u')-\frac{1}{2}} + \frac{2}{3} \sum_{i \in \{\Delta_\delta, \Delta_\beta\}} \tilde{\beta}_i^A(u') \left(\frac{s'}{s_R}\right)^{\alpha_i(u')-\frac{1}{2}},
$$

$$
\operatorname{Im} A^-(s', u'(s', t')) = -\frac{1}{3} \sum_{i \in \{N_\alpha, N_\gamma\}} \tilde{\beta}_i^A(u') \left(\frac{s'}{s_R}\right)^{\alpha_i(u')-\frac{1}{2}} + \frac{1}{3} \sum_{i \in \{\Delta_\delta, \Delta_\beta\}} \tilde{\beta}_i^A(u') \left(\frac{s'}{s_R}\right)^{\alpha_i(u')-\frac{1}{2}},
$$

$$
\operatorname{Im} B^+(s', u'(s', t')) = +\frac{1}{3} \sum_{i \in \{N_\alpha, N_\gamma\}} \tilde{\beta}_i^B(u') \left(\frac{s'}{s_R}\right)^{\alpha_i(u')-\frac{1}{2}} + \frac{2}{3} \sum_{i \in \{\Delta_\delta, \Delta_\beta\}} \tilde{\beta}_i^B(u') \left(\frac{s'}{s_R}\right)^{\alpha_i(u')-\frac{1}{2}},
$$

$$
\operatorname{Im} B^-(s', u'(s', t')) = -\frac{1}{3} \sum_{i \in \{N_\alpha, N_\gamma\}} \tilde{\beta}_i^B(u') \left(\frac{s'}{s_R}\right)^{\alpha_i(u')-\frac{1}{2}} + \frac{1}{3} \sum_{i \in \{\Delta_\delta, \Delta_\beta\}} \tilde{\beta}_i^B(u') \left(\frac{s'}{s_R}\right)^{\alpha_i(u')-\frac{1}{2}},
$$

$$(11.14)$$

where the dependence on (s', t') can be translated into dependences on (s', z'_s) for the s-channel integrals and (t', z'_t) for the t-channel integrals via (7.103). For convenience we also give the numerical values of [228] for the 21 real parameters in Tab. 11.1.

As a byproduct, we can use these relations to infer the high-energy behavior of the HDR s-channel integrals: from the trajectory parameters given in Tab. 11.1 it follows that the high-energy tail of the integrals will be governed by the Δ_δ trajectory. Explicitly, for $u' \to a$ the integrands for A^+ and B^- will behave as

$$
s'^{-1} s'^{\alpha \Delta_\delta(a)-\frac{1}{2}} = s'^{\alpha' a - 1.47} = \begin{cases} s'^{-1.88} & \text{for } a = -23.19\,M_\pi^2\,, \\ s'^{-1.52} & \text{for } a = -2.71\,M_\pi^2\,, \end{cases} \tag{11.15}
$$

whereas the integrands for A^- and B^+ fall off faster by one power in s' (cf. (11.1) and (7.104)). We thus conclude that the s-channel part of the (unsubtracted) HDRs (7.98) converges in principle for $a < 26.57\,M_\pi^2$. Note that in order to investigate the behavior of these asymptotic contributions in the "fixed-t limit" $a \to -\infty$ (as discussed in Sect. 10.2) it is important to take the limits in the correct order, since $u' \to a$ only after $s' \to \infty$. Since $\alpha_i(u') - \frac{1}{2} < -1$ for sufficiently large and negative a, the s-channel Regge contributions vanish in the limit $s' \to \infty$ for such values of a. As will be shown in Sect. 15.3, these asymptotic contributions

are numerically small for the optimal value of a (and a reasonable choice of s_a) and thus they can be safely neglected for $a \to -\infty$, regardless of the pathological behavior of the Regge model due to the gamma function in this case.

11.2 *t*-channel asymptotics

Similarly to the previous section one could use Regge theory to describe the *t*-channel asymptotic region. However, the significance of these contributions in view of the corresponding low-energy region differs strongly from the *s*-channel: while contributing crucially to the dispersive integrals, the whole pseudophysical region $t_\pi \leq t \leq t_N$ cannot be constrained from experiment, but requires an analytic continuation. Within our system of Roy–Steiner equations this task naturally takes the form of a Muskhelishvili–Omnès problem, as will be explained in Chaps. 12 and 14. The solution of these equations becomes rather involved once other intermediate states than $\pi\pi$ are energetically allowed and start to produce significant inelastic effects, which happens roughly around $1\,\mathrm{GeV}$ (especially $\bar{K}K$ states above $\sqrt{t_K} = 0.99\,\mathrm{GeV}$ for e.g. $J = 0$, cf. Sect. 12.1). In view of the ensuing uncertainty of the *t*-channel partial waves even far below the $\bar{N}N$ threshold $\sqrt{t_N} = 1.88\,\mathrm{GeV}$, it is clear that the inclusion of physical phase-shift solutions above t_N — and even more so the modeling of the high-energy region — will be of little practical relevance (see also the discussion in Sect. 15.2.4). Moreover, in Chap. 13 we will derive a subtracted system of Roy–Steiner equations by introducing subtractions that are especially useful in order to suppress the dependence of our low-energy *t*-channel partial-wave solutions on input at higher energies, where these uncertainties become substantial. Finally , it will be shown explicitly in Sect. 15.3 that already the *s*-channel Regge contributions are numerically immaterial (in particular if subtractions are performed), which provides evidence that also the high-energy region in the *t*-channel can be safely ignored. Therefore, we will not consider the *t*-channel asymptotic region any further.

Chapter 12

Roy–Steiner system for πN scattering

In this chapter we first elaborate on the unitarity relations for the s- and especially the t-channel. Then, we collect the results for the partial wave hyperbolic dispersion relations of the previous Chaps. 8 and 9 in order to state the full Roy–Steiner system for πN scattering. Finally, we use the threshold behavior of the t-channel partial waves $f_\pm^J(t)$ in order to cast the t-channel part of the Roy–Steiner system in the form of a Muskhelishvili–Omnès problem.

12.1 Partial-wave unitarity relations

The reduced s-channel partial-wave amplitudes $f_{l\pm}^I(W)$ in the s-channel isospin basis $I_s \in \{1/2, 3/2\}$ are conventionally normalized according to (cf. (7.84) and e.g. [160, 171, 174])

$$f_{l\pm}^{I_s}(W) = \frac{1}{q} \frac{\left[S_{l\pm}^{I_s}(W)\right]_{\pi N \to \pi N} - 1}{2i} = \frac{1}{q} \frac{\eta_{l\pm}^{I_s}(W) e^{2i\delta_{l\pm}^{I_s}(W)} - 1}{2i} \overset{W < W_{\text{inel}}}{=} \frac{\sin\delta_{l\pm}^{I_s}(W)}{q} e^{i\delta_{l\pm}^{I_s}(W)} ,$$

$$(12.1)$$

where for the elastic form we have used the fact that the lowest inelastic intermediate state is $\pi\pi N$ and thus $\eta_{l\pm}^{I_s}(W) = 1$ below the inelastic threshold $W_{\text{inel}} = W_+ + M_\pi$. The s-channel partial wave unitarity relation corresponding to the normalization given above reads in its general form (i.e. including potential inelastic contributions to the imaginary parts, cf. (7.84)) as well as its elastic form (by considering πN intermediate states only, but including the possibility of charge exchange)

$$\text{Im} f_{l\pm}^{I_s}(W) = q\left|f_{l\pm}^{I_s}(W)\right|^2 \theta\left(W - W_+\right) + \frac{1 - \left(\eta_{l\pm}^{I_s}(W)\right)^2}{4q} \theta\left(W - W_{\text{inel}}\right)$$

$$\overset{W < W_{\text{inel}}}{=} q\left|f_{l\pm}^{I_s}(W)\right|^2 \theta\left(W - W_+\right) ,$$

$$(12.2)$$

leading to the branch cut for $W > W_+$.

For the (necessarily inelastic) t-channel partial wave unitarity relations one needs the dimensionless partial-wave amplitudes $t_J^{I_t}(t)$ of elastic $\pi\pi$ scattering. They are conventionally defined from the dimensionless isospin amplitudes of $\pi\pi \to \pi\pi$ via (given here as t-channel process in the isospin limit, i.e. with threshold energy $2M_\pi = \sqrt{t_\pi}$, t-channel isospin $I_t \in \{0, 1, 2\}$, total angular momentum $J = l$, and symmetry factors $\sqrt{S_f S_i} = 2$ for identical

pions, cf. (7.80) and [53, 160])

$$T^{I_t}(s,t) = 32\pi \sum_{J=0}^{\infty} (2J+1) t_J^{I_t}(t) P_J(\cos\theta^{\pi\pi}) , \qquad (12.3)$$

that are normalized according to

$$\frac{\mathrm{d}\sigma_{\pi\pi\to\pi\pi}^{I_t}}{\mathrm{d}\Omega} = \left| \frac{T^{I_t}(s,t)}{8\pi\sqrt{t}} \right|^2 . \qquad (12.4)$$

The corresponding elastic unitarity relation then takes the form (considering only $\pi\pi$ intermediate states, cf. (7.82))

$$\mathrm{Im}\, t_J^{I_t}(t) = \sigma_t^\pi \left| t_J^{I_t}(t) \right|^2 \theta\big(t - t_\pi\big) , \qquad \sigma_t^\pi = \frac{2q_t}{\sqrt{t}} = \sqrt{1 - \frac{t_\pi}{t}} , \qquad (12.5)$$

and hence the partial waves can be parameterized as

$$t_J^{I_t}(t) = \frac{1}{\sigma_t^\pi} \frac{\left[S_J^{I_t}(t) \right]_{\pi\pi\to\pi\pi} - 1}{2i} = \frac{1}{\sigma_t^\pi} \frac{\eta_J^{I_t}(t) e^{2i\delta_J^{I_t}(t)} - 1}{2i} \overset{\eta_J^{I_t}(t)=1}{=} \frac{\sin\delta_J^{I_t}(t)}{\sigma_t^\pi} e^{i\delta_J^{I_t}(t)} . \qquad (12.6)$$

The reduced t-channel πN partial-wave amplitudes $f_\pm^J(t)$ are related to πN helicity amplitudes $F_{\bar\lambda\lambda}(s,t)$ and dimensionless partial waves $F_\pm^J(t)$ via (cf. (7.78) and [171, 212])

$$F_{++}(s,t) = \quad F_{--}(s,t) = \frac{4\pi\sqrt{t}}{q_t} \sum_{J=0}^{\infty} (2J+1) F_+^J(t) P_J(\cos\theta_t) ,$$

$$F_{+-}(s,t) = -F_{-+}(s,t) = \frac{4\pi\sqrt{t}}{q_t} \sum_{J=1}^{\infty} \frac{2J+1}{\sqrt{J(J+1)}} F_-^J(t) \sin\theta_t P_J'(\cos\theta_t) ,$$

$$F_+^J(t) = \frac{q_t}{p_t} (p_t q_t)^J \frac{2}{\sqrt{t}} f_+^J(t) , \qquad F_-^J(t) = \frac{q_t}{p_t} (p_t q_t)^J f_-^J(t) , \qquad (12.7)$$

and they are normalized according to

$$\frac{\mathrm{d}\bar\sigma_{\pi\pi\to\bar N N}}{\mathrm{d}\Omega} = \frac{p_t}{q_t} \sum_{\bar\lambda,\lambda} \left| \frac{F_{\bar\lambda\lambda}(s,t)}{8\pi\sqrt{t}} \right|^2 = \frac{2p_t}{q_t} \left\{ \left| \frac{F_{++}(s,t)}{8\pi\sqrt{t}} \right|^2 + \left| \frac{F_{+-}(s,t)}{8\pi\sqrt{t}} \right|^2 \right\} = \frac{4p_t^2}{q_t^2} \frac{\mathrm{d}\bar\sigma_{\bar N N\to\pi\pi}}{\mathrm{d}\Omega} . \qquad (12.8)$$

The general formulae (12.7) and (12.8) are also valid for isospin even/odd parts $F_{\bar\lambda\lambda}^I(s,t)$ with crossing index $I = +/-$ and J even/odd, accordingly. Note that when referring to the t-channel isospin basis $I_t \in \{0,1\}$ like in the following, the isospin crossing coefficients c_J of (7.56) need to be included.

   In general, the t-channel partial waves may be parameterized as

$$f_\pm^J(t) = \left| f_\pm^J(t) \right| e^{i\varphi^J(t)} = \mathrm{Re}\, f_\pm^J(t) + i\,\mathrm{Im}\, f_\pm^J(t) . \qquad (12.9)$$

By considering now only $\pi\pi$ intermediate states in the region $t < (4M_\pi)^2$ (which is elastic w.r.t. $\pi\pi$ scattering but unphysical w.r.t. the πN t-channel) in the general unitarity relation (7.58) for $\bar N N \to \pi\pi$, the $f_\pm^J(t)$ can be shown to obey the "elastic" t-channel unitarity relation

$$\mathrm{Im}\, f_\pm^J(t) = \sigma_t^\pi \big(t_J^{I_t}(t) \big)^* f_\pm^J(t)\, \theta\big(t - t_\pi\big) \qquad \forall\, t \in [t_\pi, 16M_\pi^2) , \qquad (12.10)$$

where the coefficients c_J cancel and which leads to the branch cut for $t > t_\pi$. Since the imaginary part $\mathrm{Im}\, f_\pm^J(t)$ itself must be real, from (12.10) together with (12.6) and (12.9) one can immediately infer

$$f_\pm^J(t) = \left| f_\pm^J(t) \right| e^{i\delta_J^{I_t}(t)} \qquad \forall\, t \in [t_\pi, 16M_\pi^2)\,, \tag{12.11}$$

i.e. the phases of the t-channel partial waves $f_\pm^J(t)$ are given by the phases of the $\pi\pi$ partial waves $t_J^{I_t}(t)$ modulo π (by convention we choose the phases to coincide exactly), which is also known as Watson's final-state-interaction theorem [229].

Despite the fact that this theorem is valid rigorously only for a rather limited range in t, it is common practice to assume that further inelastic contributions due to 4π and other intermediate states can safely be ignored for $t \lesssim 40M_\pi^2 \approx 0.78\,\mathrm{GeV}^2$ in general (see e.g. [171] or [182]). However, as demonstrated in [230] in the context of the scalar pion form factor, for the S-wave this is certainly only true below the threshold $t_K = 4M_K^2 \approx 0.97\,\mathrm{GeV}^2$ for the production of $\bar{K}K$ intermediate states. While for the P-waves inelasticities effectively start to set in already around the $\pi\omega$ threshold at $0.85\,\mathrm{GeV}^2$, although nevertheless the $\pi\pi$ scattering P-wave inelasticity remains small at least for energies below $1\,\mathrm{GeV}$, for the D-waves we do not expect sizable deviations from elasticity in this energy range, since the $\pi\pi$ scattering D-wave is approximately elastic for even higher energies. Thus, for $t < t_K$ we will neglect everything except the 2π intermediate states in the following; especially Watson's theorem (12.11) is taken to be valid.

It is crucial to note that (12.10) is invariant under rescaling of $f_\pm^J(t)$ with real factors, whereas elastic unitarity relations as (12.2) (for $W < W_\mathrm{inel}$) and (12.5) are always nonlinear in the corresponding partial wave. Hence, fixing the normalization of all different partial waves that are needed in extended t-channel unitarity relations (i.e. allowing for additional intermediate states) in a consistent manner can only be done with resort to the corresponding elastic reactions, as we will now demonstrate for a system of coupled-channel equations with π, K and N degrees of freedom. Writing $T_{11} = T_{\pi\pi\to\pi\pi}$, $T_{12} = T_{\bar{K}K\to\pi\pi}$, $T_{13} = T_{\bar{N}N\to\pi\pi}$ etc. for the T-matrix elements and using the invariance of strong interactions under time reversal, the general unitarity relation reads in terms of matrix elements

$$S_{fj}^* S_{ji} = \delta_{fi}\,, \qquad S_{fi} = \delta_{fi} + iT_{fi} = \delta_{if} + iT_{if} = S_{if}\,. \tag{12.12}$$

In particular, one can read off the extended elastic unitarity relation for $\pi\pi \to \pi\pi$ and the extended unitarity relation for $\bar{N}N \to \pi\pi$ with $\pi\pi$, $\bar{K}K$, and $\bar{N}N$ intermediate states

$$\delta_{11} = 1 = |S_{11}|^2 + |S_{12}|^2 + |S_{13}|^2\,, \qquad \delta_{13} = 0 = S_{11}^* S_{13} + S_{12}^* S_{23} + S_{13}^* S_{33}\,, \tag{12.13}$$

and thus, by dropping the $\bar{N}N$ intermediate states in the second relation since we are finally interested in the extended t-channel unitarity relation of πN scattering in the region below the $\bar{N}N$ threshold, we get

$$2\,\mathrm{Im}\, T_{11} = |T_{11}|^2 + |T_{12}|^2 + |T_{13}|^2\,, \qquad 2\,\mathrm{Im}\, T_{13} = T_{11}^* T_{13} + T_{12}^* T_{23}\,. \tag{12.14}$$

Introducing now the reduced t-channel partial waves $g_J^{I_t}(t)$ of πK scattering (also given here as t-channel process with isospin $I_t = 0/1$ corresponding to $J = l$ even/odd due to Bose symmetry in $\pi\pi$, symmetry factors $\sqrt{S_f S_i} = \sqrt{2}$, and the partial waves being defined from

dimensionless isospin amplitudes, cf. (7.80) and [158])

$$G^{I_t}(s,t) = 16\pi\sqrt{2}\sum_{J=0}^{\infty}(2J+1)(k_t q_t)^J g_J^{I_t}(t) P_J(\cos\theta_t^{\pi K})\,, \qquad k_t = \sqrt{\frac{t}{4} - M_K^2} = \frac{\sqrt{t}}{2}\sigma_t^K\,,$$
(12.15)

the first relation of (12.14) may be decomposed in partial waves and performing the angular integrations of the phase space integrals (7.63) leads to[#1]

$$2\cdot 32\pi\,\mathrm{Im}\,t_J^{I_t}(t) = \frac{1}{2}\frac{1}{8\pi}\frac{2q_t}{\sqrt{t}}\left|32\pi\,t_J^{I_t}(t)\right|^2\theta\big(t-t_\pi\big) + \frac{1}{8\pi}\frac{2k_t}{\sqrt{t}}\left|16\pi\sqrt{2}\,(q_t k_t)^J g_J^{I_t}(t)\right|^2\theta\big(t-t_K\big)$$
$$+ \frac{2}{8\pi}\frac{2p_t}{\sqrt{t}}\frac{1}{c_J^2}\left\{\left|\frac{4\pi\sqrt{t}}{q_t}F_+^J(t)\right|^2 + \left|\frac{4\pi\sqrt{t}}{q_t}F_-^J(t)\right|^2\right\}\theta\big(t-t_N\big)\,, \qquad (12.16)$$

where the symmetry factor for the $\pi\pi$ intermediate state as well as all four different helicities of the $\bar{N}N$ states together with the isospin crossing coefficients c_J have been taken into account, such that the partial wave unitarity relation for $\pi\pi$ scattering (as t-channel process with $\pi\pi$, $\bar{K}K$ and $\bar{N}N$ intermediate states) takes the form

$$\mathrm{Im}\,t_J^{I_t}(t) = \sigma_t^\pi\left|t_J^{I_t}(t)\right|^2\theta\big(t-t_\pi\big) + (k_t q_t)^{2J}\sigma_t^K\left|g_J^{I_t}(t)\right|^2\theta\big(t-t_K\big)$$
$$+ \frac{t}{16q_t^2}\frac{\sigma_t^N}{c_J^2}\left\{\left|F_+^J(t)\right|^2 + \left|F_-^J(t)\right|^2\right\}\theta\big(t-t_N\big)\,. \qquad (12.17)$$

For $t < t_K$ (or if $I_t + J$ equals an odd number) this reproduces the elastic unitarity relation for $\pi\pi$ scattering (12.5), which corresponds to the relation (cf. (12.6))

$$\left[S_J^{I_t}(t)\right]_{\pi\pi\to\pi\pi} = 1 + i\frac{4q_t}{\sqrt{t}}t_J^{I_t}(t)\,\theta\big(t-t_\pi\big)\,. \qquad (12.18)$$

Comparing (12.17) with the elastic unitarity relation for the partial waves (cf. (12.13))

$$\left|\left[S_J^{I_t}(t)\right]_{\pi\pi\to\pi\pi}\right|^2 + \left|\left[S_J^{I_t}(t)\right]_{\pi\pi\to\bar{K}K}\right|^2 + 2\left\{\left|\left[S_+^J(t)\right]_{\pi\pi\to\bar{N}N}^{I_t}\right|^2 + \left|\left[S_-^J(t)\right]_{\pi\pi\to\bar{N}N}^{I_t}\right|^2\right\} = 1\,,$$
(12.19)

for the cases $t < t_N$ and $t \geq t_N$ successively, then allows to fix the normalizations of the partial wave S-matrix elements of the inelastic channels (both in the natural t-channel isospin basis $I_t \in \{0,1\}$) to[#2]

$$\left[S_J^{I_t}(t)\right]_{\pi\pi\to\bar{K}K} = i\frac{4(k_t q_t)^{J+\frac{1}{2}}}{\sqrt{t}}g_J^{I_t}(t)\,\theta\big(t-t_K\big)\,, \qquad \left[S_\pm^J(t)\right]_{\pi\pi\to\bar{N}N}^{I_t} = \frac{i}{c_J\sqrt{2}}\sqrt{\frac{p_t}{q_t}}F_\pm^J(t)\,\theta\big(t-t_N\big)\,.$$
(12.20)

[#1]Note that here S_{fi}, T_{fi} denote matrix elements and not the corresponding invariant amplitudes, cf. (7.59), such that the product of matrix elements is to be understood as an integration over the corresponding intermediate LIPS (respecting 4-momentum conservation and including potential symmetry factors) when rewriting these relations in terms of invariant amplitudes, cf. (7.61).

[#2]Note that our symmetric normalization of the helicity partial waves (7.78) together with (12.7) and (12.8) leads to an additional factor of $1/\sqrt{2}$ to $\left[S_\pm^J(t)\right]_{\pi\pi\to\bar{N}N}^{I_t}$ in comparison with [171] or [212], where one should read in addition $\left[S_\pm^J(t)\right]_{\pi\pi\to\bar{N}N} \equiv c_J\left[S_\pm^J(t)\right]_{\pi\pi\to\bar{N}N}^{I_t}$.

Inserting these S-matrix elements into (7.78) indeed reproduces the correctly normalized differential cross sections

$$\frac{\mathrm{d}\sigma^{I_t}_{\pi\pi\to\bar{K}K}}{\mathrm{d}\Omega} = \frac{k_t}{q_t}\left|\frac{G^{I_t}(s,t)}{8\pi\sqrt{t}}\right|^2 , \tag{12.21}$$

and (12.8), respectively. Furthermore, from the unitarity bound of the t-channel partial wave S matrix of πN scattering only (cf. (12.19)) together with its explicit form (12.20) and the relations (12.7) to the corresponding partial waves $f_\pm^J$ we can deduce that the partial waves fall off asymptotically at least as fast as (cf. [171])

$$f_+^J(t) \sim t^{-J+\frac{1}{2}} , \qquad f_-^J(t) \sim t^{-J} , \qquad \text{for } t\to\infty , \tag{12.22}$$

i.e. $f_\pm^J(t) \to 0$ for $t\to\infty$ by unitarity at least for all $J > 0$; this asymptotic vanishing is usually assumed to hold for the S-wave as well. By virtue of similar considerations, the normalization of the remaining partial waves in the second relation of (12.14) can be fixed. We can introduce the reduced t-channel partial waves $h_\pm^J(t)$ of KN scattering in analogy to the πN case via dimensionless helicity amplitudes (cf. (12.7) and [231, 232])

$$H_{++}(s,t) = \frac{4\pi\sqrt{t}}{k_t}\sum_{J=0}^{\infty}(2J+1)H_+^J(t)P_J(\cos\theta_t^{KN}) , \qquad\qquad H_+^J(t) = \frac{k_t}{p_t}(p_tk_t)^J\frac{2}{\sqrt{t}}h_+^J(t) ,$$

$$H_{+-}(s,t) = \frac{4\pi\sqrt{t}}{k_t}\sum_{J=1}^{\infty}\frac{2J+1}{\sqrt{J(J+1)}}H_-^J(t)\sin\theta_t^{KN}P_J'(\cos\theta_t^{KN}) , \quad H_-^J(t) = \frac{k_t}{p_t}(p_tk_t)^J h_-^J(t) , \tag{12.23}$$

where it is important to note that here in contrast to πN scattering also the combinations $I_t = 0$ with odd J and $I_t = 1$ with even J are allowed due to lack of Bose symmetry in $\bar{K}K$. In order not to bloat the notation we refrain from using an additional index for I_t and in the following e.g. $h_\pm^{J=\text{even/odd}}$ is always to be understood as $h_\pm^{(J=\text{even/odd},I_t=0/1)}$, respectively, and not $h_\pm^{(J=\text{odd/even},I_t=0/1)}$, since only the former can couple to the t-channel process $\pi\pi\to\bar{N}N$. The normalization is fixed by

$$\frac{\mathrm{d}\bar{\sigma}_{K\bar{K}\to\bar{N}N}}{\mathrm{d}\Omega} = \frac{p_t}{k_t}\sum_{\bar{\lambda},\lambda}\left|\frac{H_{\bar{\lambda}\lambda}(s,t)}{8\pi\sqrt{t}}\right|^2 = \frac{2p_t}{k_t}\left\{\left|\frac{H_{++}(s,t)}{8\pi\sqrt{t}}\right|^2 + \left|\frac{H_{+-}(s,t)}{8\pi\sqrt{t}}\right|^2\right\} = \frac{4p_t^2}{k_t^2}\frac{\mathrm{d}\bar{\sigma}_{\bar{N}N\to K\bar{K}}}{\mathrm{d}\Omega} , \tag{12.24}$$

so that the dimensionless partial-wave amplitudes $H_\pm^J(t)$ are related to the diagonal elements of the corresponding S-matrix according to

$$\left[S_\pm^J(t)\right]^{I_t}_{K\bar{K}\to\bar{N}N} = \frac{i}{c_J^{KN}}\sqrt{\frac{p_t}{k_t}}H_\pm^J(t)\,\theta(t-t_N) , \qquad c_J^{KN} = \frac{1}{2} \quad \forall\, J . \tag{12.25}$$

Simply plugging the partial wave matrix elements into the partial-wave projection of the second relation of (12.14) for either parallel or antiparallel antinucleon–nucleon helicities yields

$$\frac{2}{c_J}\sqrt{\frac{p_t}{2q_t}}\mathrm{Im}\,F_\pm^J(t) = \frac{4q_t}{\sqrt{t}}\left(t_J^{I_t}(t)\right)^*\frac{1}{c_J}\sqrt{\frac{p_t}{2q_t}}F_\pm^J(t)\,\theta(t-t_\pi)$$

$$+ \frac{4(k_tq_t)^{J+\frac{1}{2}}}{\sqrt{t}}\left(g_J^{I_t}(t)\right)^*2\sqrt{\frac{p_t}{k_t}}H_\pm^J(t)\,\theta(t-t_K) , \tag{12.26}$$

and hence the result for the extended t-channel unitarity relation for the t-channel partial waves $f^J_\pm(t)$, which extends (12.10) for $\bar{K}K$ intermediate states (but still neglecting heavier intermediate states), reads

$$\operatorname{Im} f^J_\pm(t) = \sigma^\pi_t \big(t^{I_t}_J(t)\big)^* f^J_\pm(t)\,\theta\big(t - t_\pi\big) + 2c_J\sqrt{2}\,k^{2J}_t \sigma^K_t \big(g^{I_t}_J(t)\big)^* h^J_\pm(t)\,\theta\big(t - t_K\big)\,. \tag{12.27}$$

Finally, we can use (12.19) to derive the inelasticities $\eta^{I_t}_J(t)$ of the $\pi\pi$ scattering amplitude that are consistent with (12.27). Below the $\bar{N}N$ threshold, inserting (12.6) and (12.20) into (12.19) leads to

$$\eta^{I_t}_J(t) = \sqrt{1 - 4\sigma^\pi_t \sigma^K_t (k_t q_t)^{2J}\big|g^{I_t}_J(t)\big|^2\,\theta\big(t - t_K\big)}\,. \tag{12.28}$$

12.2 Partial-wave hyperbolic dispersion relations

In order to use unitarity relations of the diagonal form (12.2) for the s-channel partial waves, we have to work in the s-channel isospin basis $I_s \in \{1/2, 3/2\}$ rather than in the isospin even/odd basis $I = +/-$ (as proposed in [160]), and therefore in analogy to (7.39) we define

$$\begin{pmatrix} X^{1/2} \\ X^{3/2} \end{pmatrix} = C_{s\nu} \begin{pmatrix} X^+ \\ X^- \end{pmatrix}\,, \qquad \begin{pmatrix} X^+ \\ X^- \end{pmatrix} = C_{\nu s} \begin{pmatrix} X^{1/2} \\ X^{3/2} \end{pmatrix}\,, \qquad \text{for } X \in \{f_{l\pm}, N_{l\pm}, K_{ll'}\}\,, \tag{12.29}$$

and the abbreviation

$$K^{1/2+3/2}_{ll'}(W, W') = K^{1/2}_{ll'}(W, W') + K^{3/2}_{ll'}(W, W') = 2K^+_{ll'}(W, W') + K^-_{ll'}(W, W')\,. \tag{12.30}$$

The full closed Roy–Steiner system of PWDRs for both s- and t-channel partial waves in the corresponding isospin bases $I_s \in \{1/2, 3/2\}$ and $I_t \in \{0, 1\}$ that follows from rewriting (8.3) and (9.1) reads (here, all sums run over both even and odd values and the formulae for the $f^I_{(l+1)-}$ are given explicitly for convenience)

$$
\begin{aligned}
f^{1/2}_{l+}(W) = {}& N^{1/2}_{l+}(W) \\
& + \frac{1}{\pi} \int_{W_+}^\infty \mathrm{d}W' \sum_{l'=0}^\infty \frac{1}{3}\Big\{ K^{1/2}_{ll'}(W, W')\operatorname{Im} f^{1/2}_{l'+}(W') + 2K^{3/2}_{ll'}(W, W')\operatorname{Im} f^{3/2}_{l'+}(W') \\
& \qquad + K^{1/2}_{ll'}(W, -W')\operatorname{Im} f^{1/2}_{(l'+1)-}(W') + 2K^{3/2}_{ll'}(W, -W')\operatorname{Im} f^{3/2}_{(l'+1)-}(W') \Big\} \\
& + \frac{1}{\pi} \int_{t_\pi}^\infty \mathrm{d}t' \sum_{J=0}^\infty \frac{\big(3 - (-1)^J\big)}{2}\Big\{ G_{lJ}(W, t')\operatorname{Im} f^J_+(t') + H_{lJ}(W, t')\operatorname{Im} f^J_-(t') \Big\}\,, \\
f^{3/2}_{l+}(W) = {}& N^{3/2}_{l+}(W) \\
& + \frac{1}{\pi} \int_{W_+}^\infty \mathrm{d}W' \sum_{l'=0}^\infty \frac{1}{3}\Big\{ K^{3/2}_{ll'}(W, W')\operatorname{Im} f^{1/2}_{l'+}(W') + K^{1/2+3/2}_{ll'}(W, W')\operatorname{Im} f^{3/2}_{l'+}(W') \\
& \qquad + K^{3/2}_{ll'}(W, -W')\operatorname{Im} f^{1/2}_{(l'+1)-}(W') + K^{1/2+3/2}_{ll'}(W, -W')\operatorname{Im} f^{3/2}_{(l'+1)-}(W') \Big\} \\
& + \frac{1}{\pi} \int_{t_\pi}^\infty \mathrm{d}t' \sum_{J=0}^\infty (-1)^J\Big\{ G_{lJ}(W, t')\operatorname{Im} f^J_+(t') + H_{lJ}(W, t')\operatorname{Im} f^J_-(t') \Big\}\,,
\end{aligned}
$$

$$f_{(l+1)-}^{1/2}(W) = N_{(l+1)-}^{1/2}(W)$$

$$- \frac{1}{\pi} \int\limits_{W_+}^{\infty} dW' \sum_{l'=0}^{\infty} \frac{1}{3} \Big\{ K_{ll'}^{1/2}(-W,W') \operatorname{Im} f_{l'+}^{1/2}(W') + 2K_{ll'}^{3/2}(-W,W') \operatorname{Im} f_{l'+}^{3/2}(W')$$

$$+ K_{ll'}^{1/2}(-W,-W') \operatorname{Im} f_{(l'+1)-}^{1/2}(W') + 2K_{ll'}^{3/2}(-W,-W') \operatorname{Im} f_{(l'+1)-}^{3/2}(W') \Big\}$$

$$- \frac{1}{\pi} \int\limits_{t_\pi}^{\infty} dt' \sum_{J=0}^{\infty} \frac{(3-(-1)^J)}{2} \Big\{ G_{lJ}(-W,t') \operatorname{Im} f_+^J(t') + H_{lJ}(-W,t') \operatorname{Im} f_-^J(t') \Big\},$$

$$f_{(l+1)-}^{3/2}(W) = N_{(l+1)-}^{3/2}(W)$$

$$- \frac{1}{\pi} \int\limits_{W_+}^{\infty} dW' \sum_{l'=0}^{\infty} \frac{1}{3} \Big\{ K_{ll'}^{3/2}(-W,W') \operatorname{Im} f_{l'+}^{1/2}(W') + K_{ll'}^{1/2+3/2}(-W,W') \operatorname{Im} f_{l'+}^{3/2}(W')$$

$$+ K_{ll'}^{3/2}(-W,-W') \operatorname{Im} f_{(l'+1)-}^{1/2}(W') + K_{ll'}^{1/2+3/2}(-W,-W') \operatorname{Im} f_{(l'+1)-}^{3/2}(W') \Big\}$$

$$- \frac{1}{\pi} \int\limits_{t_\pi}^{\infty} dt' \sum_{J=0}^{\infty} (-1)^J \Big\{ G_{lJ}(-W,t') \operatorname{Im} f_+^J(t') + H_{lJ}(-W,t') \operatorname{Im} f_-^J(t') \Big\}, \quad (12.31)$$

together with

$$f_+^J(t) = \tilde{N}_+^J(t) + \frac{1}{\pi} \int\limits_{W_+}^{\infty} dW' \sum_{l=0}^{\infty} \frac{1}{3} \Big\{ \tilde{G}_{Jl}(t,W') \Big[\operatorname{Im} f_{l+}^{1/2}(W') + \frac{1+3(-1)^J}{2} \operatorname{Im} f_{l+}^{3/2}(W') \Big]$$

$$+ \tilde{G}_{Jl}(t,-W') \Big[\operatorname{Im} f_{(l+1)-}^{1/2}(W') + \frac{1+3(-1)^J}{2} \operatorname{Im} f_{(l+1)-}^{3/2}(W') \Big] \Big\}$$

$$+ \frac{1}{\pi} \int\limits_{t_\pi}^{\infty} dt' \sum_{J'=J}^{\infty} \frac{1+(-1)^{J+J'}}{2} \Big\{ \tilde{K}_{JJ'}^1(t,t') \operatorname{Im} f_+^{J'}(t') + \tilde{K}_{JJ'}^2(t,t') \operatorname{Im} f_-^{J'}(t') \Big\} \quad \forall\, J \geq 0\,,$$

$$f_-^J(t) = \tilde{N}_-^J(t) + \frac{1}{\pi} \int\limits_{W_+}^{\infty} dW' \sum_{l=0}^{\infty} \frac{1}{3} \Big\{ \tilde{H}_{Jl}(t,W') \Big[\operatorname{Im} f_{l+}^{1/2}(W') + \frac{1+3(-1)^J}{2} \operatorname{Im} f_{l+}^{3/2}(W') \Big]$$

$$+ \tilde{H}_{Jl}(t,-W') \Big[\operatorname{Im} f_{(l+1)-}^{1/2}(W') + \frac{1+3(-1)^J}{2} \operatorname{Im} f_{(l+1)-}^{3/2}(W') \Big] \Big\}$$

$$+ \frac{1}{\pi} \int\limits_{t_\pi}^{\infty} dt' \sum_{J'=J}^{\infty} \frac{1+(-1)^{J+J'}}{2} \tilde{K}_{JJ'}^3(t,t') \operatorname{Im} f_-^{J'}(t') \quad \forall\, J \geq 1\,. \quad (12.32)$$

Note that in the above t-channel part (12.32) the sums over J' are limited to $J' \geq J$ due to (9.55). The preceding explicit equations illustrate the fact that (as already mentioned in Chap. 6) the unitarity-diagonal isospin states $I_s = 1/2$ and $I_s = 3/2$ are, however, coupled by the integral kernels. Conversely, working in the isospin even/odd basis $I = +/-$, the isospin states are mixed up by unitarity but not in the dispersion relations. Thus, the effective recoupling structure shown in Fig. 6.1 (center) arises independent of the chosen isospin basis.

12.3 The t-channel: from Roy–Steiner to Muskhelishvili–Omnès

12.3.1 Threshold behavior of the t-channel partial waves

The asymptotic behavior of $f_\pm^J(t)$ for $p_t \to 0$ and $q_t \to 0$ (which is equivalent to $t \to t_N = 4m^2$ and $t \to t_\pi = 4M_\pi^2$, respectively) can be derived directly from the partial-wave projection (9.7). Since $A^I(t, z_t)$ and $B^I(t, z_t)$ have definite symmetry properties under $s \leftrightarrow u$ and since $s - u = 4m\nu = 4p_t q_t z_t$, we can write down the expansions

$$A^I(t, z_t) = \sum_{J'} (p_t q_t)^{J'} P_{J'}(z_t) a_{J'}(t) \,, \qquad B^I(t, z_t) = \sum_{J'} (p_t q_t)^{J'} P_{J'}(z_t) b_{J'}(t) \,, \qquad (12.33)$$

where only even/odd values of J' contribute according to the symmetry properties of A^I and B^I (i.e. even J' for A^+, B^- and odd J' for A^-, B^+). Let us first consider the limit $p_t \to 0$, i.e. the behavior of $f_\pm^J(t)$ at the t-channel threshold t_N. As far as the leading asymptotic behavior is concerned, the functions $a_{J'}(t)$ and $b_{J'}(t)$ can be evaluated at $t = t_N$ and will thus be considered as constant coefficients in the following. Inserting these expansions into (9.7) (where J even/odd corresponds to $I = +/-$), we find for $J = 0$ that

$$f_+^0(t \to t_N) = \mathcal{O}(p_t^2) \qquad (12.34)$$

at the physical threshold, while for $J \geq 1$ we obtain

$$f_+^J(t \to t_N) = \frac{m b_{J-1}}{8\pi} \int_{-1}^{1} \mathrm{d}z_t P_J(z_t) z_t P_{J-1}(z_t) + \mathcal{O}(p_t^2) = \frac{m b_{J-1}}{8\pi} \frac{J}{2J+1} \frac{2}{2J-1} + \mathcal{O}(p_t^2) \,,$$

$$f_-^J(t \to t_N) = \frac{b_{J-1}}{8\pi} \frac{\sqrt{J(J+1)}}{2J+1} \int_{-1}^{1} \mathrm{d}z_t P_{J-1}(z_t) P_{J-1}(z_t) + \mathcal{O}(p_t^2)$$

$$= \frac{b_{J-1}}{8\pi} \frac{\sqrt{J(J+1)}}{2J+1} \frac{2}{2J-1} + \mathcal{O}(p_t^2) \,, \qquad (12.35)$$

such that

$$f_+^J(t \to t_N) = \mathcal{O}(1) \,, \qquad f_-^J(t \to t_N) = \mathcal{O}(1) \,, \qquad \forall\, J \geq 1 \,. \qquad (12.36)$$

However, the linear combination

$$\Gamma^J(t) = m \sqrt{\frac{J}{J+1}} f_-^J(t) - f_+^J(t) \qquad \forall\, J \geq 1 \,, \qquad (12.37)$$

which with $f_-^0 \equiv 0$ can also be generalized for the case $J = 0$ and which for $J = 1$ is closely related to the dispersive representation of the nucleon form factor, vanishes at threshold (cf. [171, 213, 233])

$$\Gamma^J(t \to t_N) = \mathcal{O}(p_t^2) \qquad \forall\, J \geq 1 \,. \qquad (12.38)$$

The same reasoning may be applied to the limit $q_t \to 0$ as well, but as A^I contributes at the same order as B^I in the expansion of $f_+^J(t)$, no relation between the threshold values of different amplitudes may be inferred for $q_t \to 0$:

$$f_+^J(t \to t_\pi) = \mathcal{O}(1) \qquad \forall\, J \geq 0 \,, \qquad f_-^J(t \to t_\pi) = \mathcal{O}(1) \qquad \forall\, J \geq 1 \,. \qquad (12.39)$$

In fact, the properties of $f_\pm^J(t)$ at the t-channel threshold are crucial to ensure convergence in the Roy–Steiner equations. From the partial-wave expansion (8.84) we can easily derive the leading contributions to the invariant amplitudes (given explicitly for $J \leq 2$)

$$\frac{A^+(\nu,t)}{4\pi} = -\frac{f_+^0(t)}{p_t^2} + \frac{15}{2}(m\nu)^2\frac{\Gamma^2(t)}{p_t^2} + \frac{5}{2}q_t^2 f_+^2(t) + \dots \,, \qquad \frac{B^+(\nu,t)}{4\pi} = \frac{15}{\sqrt{6}}m\nu f_-^2(t) + \dots \,,$$
$$\frac{A^-(\nu,t)}{4\pi} = 3m\nu\frac{\Gamma^1(t)}{p_t^2} + \dots \,, \qquad\qquad\qquad \frac{B^-(\nu,t)}{4\pi} = \frac{3}{\sqrt{2}}f_-^1(t) + \dots \,,$$

$$\tag{12.40}$$

demonstrating how the threshold behavior (12.34) and (12.38) ensures that the partial-wave expansion does not introduce spurious kinematical poles at $p_t \to 0$ into the expansion of the invariant amplitudes (as it must be) and thereby into the HDRs (7.98). To illustrate the consequences of this point, we briefly comment on the several places in our Roy–Steiner system (8.3) and (9.1) where the threshold behavior of $f_\pm^J(t)$ features:

1. Although $G_{lJ}(W,t')$ and $H_{lJ}(W,t')$ diverge as $p_t'^{-2}$ for $t' \to t_N$ according to (8.103), the relation

$$\text{Res}\left[H_{lJ}(W,t'), t' = t_N\right] = -m\sqrt{\frac{J}{J+1}}\,\text{Res}\left[G_{lJ}(W,t'), t' = t_N\right] \tag{12.41}$$

   together with (12.34) and (12.38) ensures that the corresponding integrals in (8.3) are well defined. We have checked that the explicit expressions in (8.100) fulfill this equation.

2. The $p_t'^{-2}$ divergence (9.60) of $\tilde{K}_{JJ'}^1(t,t')$ and $\tilde{K}_{JJ'}^2(t,t')$ for $t' \to t_N$ cancels in (9.1) provided that

$$\text{Res}\left[\tilde{K}_{JJ'}^2(t,t'), t' = t_N\right] = -m\sqrt{\frac{J'}{J'+1}}\,\text{Res}\left[\tilde{K}_{JJ'}^1(t,t'), t' = t_N\right]. \tag{12.42}$$

   This relation can easily be verified for the kernels given in (9.57) and (9.59), cf. (9.58).

3. Based on the asymptotic forms (9.17) of the pole-term projections $\tilde{N}_\pm^J(t)$, one may check their threshold behavior to be analogous to (12.34) and (12.38). Note that in this special case the relations hold for $q_t \to 0$ as well, since A^I does not contribute to the pole terms:

$$\tilde{N}_+^0(p_t q_t \to 0) = \mathcal{O}(p_t^2 q_t^2)\,,$$
$$m\sqrt{\frac{J}{J+1}}\tilde{N}_-^J(p_t q_t \to 0) - \tilde{N}_+^J(p_t q_t \to 0) = \mathcal{O}(p_t^2 q_t^2) \qquad \forall\, J \geq 1\,. \tag{12.43}$$

12.3.2   Muskhelishvili–Omnès problem for the *t*-channel partial waves

Using the properties of the kernel functions for t-channel exchange as given in Sect. 9.3 together with the threshold behavior of the partial waves as discussed in Sect. 12.3.1, we can rewrite the t-channel part (9.1) (i.e. working in the $I \in \{+, -\}$ s-channel isospin basis again for the

sake of brevity) of the (unsubtracted) Roy–Steiner system as

$$f_+^0(t) = \Delta_+^0(t) - \frac{1}{\pi} \int\limits_{t_\pi}^{\infty} dt' \frac{\operatorname{Im} f_+^0(t')}{t' - t_N} + \frac{1}{\pi} \int\limits_{t_\pi}^{\infty} dt' \frac{\operatorname{Im} f_+^0(t')}{t' - t} \,,$$

$$f_+^J(t) = \Delta_+^J(t) + \frac{1}{\pi} \int\limits_{t_\pi}^{\infty} dt' \frac{m\sqrt{\frac{J}{J+1}}\operatorname{Im} f_-^J(t') - \operatorname{Im} f_+^J(t')}{t' - t_N} + \frac{1}{\pi} \int\limits_{t_\pi}^{\infty} dt' \frac{\operatorname{Im} f_+^J(t')}{t' - t} \qquad \forall\, J \geq 1 \,,$$

$$f_-^J(t) = \Delta_-^J(t) + \frac{1}{\pi} \int\limits_{t_\pi}^{\infty} dt' \frac{\operatorname{Im} f_-^J(t')}{t' - t} \qquad \forall\, J \geq 1 \,, \tag{12.44}$$

where we have defined the abbreviations

$$\Delta_\pm^J(t) = \tilde{N}_\pm^J(t) + \bar{\Delta}_\pm^J(t) \,,$$

$$\bar{\Delta}_+^J(t) = \frac{1}{\pi} \int\limits_{W_+}^{\infty} dW' \sum_{l=0}^{\infty} \left\{ \tilde{G}_{Jl}(t, W') \operatorname{Im} f_{l+}^I(W') + \tilde{G}_{Jl}(t, -W') \operatorname{Im} f_{(l+1)-}^I(W') \right\}$$

$$+ \frac{1}{\pi} \int\limits_{t_\pi}^{\infty} dt' \sum_{J'=J+2}^{\infty} \frac{1 + (-1)^{J+J'}}{2} \left\{ \tilde{K}_{JJ'}^1(t, t') \operatorname{Im} f_+^{J'}(t') + \tilde{K}_{JJ'}^2(t, t') \operatorname{Im} f_-^{J'}(t') \right\} \qquad \forall\, J \geq 0 \,,$$

$$\bar{\Delta}_-^J(t) = \frac{1}{\pi} \int\limits_{W_+}^{\infty} dW' \sum_{l=0}^{\infty} \left\{ \tilde{H}_{Jl}(t, W') \operatorname{Im} f_{l+}^I(W') + \tilde{H}_{Jl}(t, -W') \operatorname{Im} f_{(l+1)-}^I(W') \right\}$$

$$+ \frac{1}{\pi} \int\limits_{t_\pi}^{\infty} dt' \sum_{J'=J+2}^{\infty} \frac{1 + (-1)^{J+J'}}{2} \tilde{K}_{JJ'}^3(t, t') \operatorname{Im} f_-^{J'}(t') \qquad \forall\, J \geq 1 \,, \tag{12.45}$$

for the inhomogeneities $\Delta_\pm^J(t)$, which besides the t-channel projections $\tilde{N}_\pm^J(t)$ of the nucleon pole terms contain the coupling to (in principle) all s-channel partial waves as well as to the higher t-channel partial waves. Note that $\Delta_\pm^J(t)$ only contains the left-hand cut and therefore it is real for all $t \geq t_\pi$. By virtue of (12.37) and the analogous definition

$$\Delta_\Gamma^J(t) = m\sqrt{\frac{J}{J+1}} \Delta_-^J(t) - \Delta_+^J(t) \,, \tag{12.46}$$

the equations (12.44) can be cast into the form of a Muskhelishvili–Omnès problem for $f_+^0(t)$, $f_-^J(t)$, and $\Gamma^J(t)$

$$f_+^0(t) = \Delta_+^0(t) + \frac{t - t_N}{\pi} \int\limits_{t_\pi}^{\infty} dt' \frac{\operatorname{Im} f_+^0(t')}{(t' - t_N)(t' - t)} \,,$$

$$\Gamma^J(t) = \Delta_\Gamma^J(t) + \frac{t - t_N}{\pi} \int\limits_{t_\pi}^{\infty} dt' \frac{\operatorname{Im} \Gamma^J(t')}{(t' - t_N)(t' - t)} \qquad \forall\, J \geq 1 \,,$$

$$f_-^J(t) = \Delta_-^J(t) + \frac{1}{\pi} \int\limits_{t_\pi}^{\infty} dt' \frac{\operatorname{Im} f_-^J(t')}{t' - t} \qquad \forall\, J \geq 1 \,, \tag{12.47}$$

where for $f_+^0(t)$ and $\Gamma^J(t)$ combining the integrals effectively yields one subtraction at the threshold t_N and the additional roots at $t' = t_N$ in the denominators get canceled by the threshold behavior of the numerators. The solution for $f_+^J(t)$ can then easily be recovered via (12.37).

How these equations (or their subtracted analogs derived in Sect. 13.6) can be used to determine $f_+^0(t)$, $f_\pm^1(t)$ and $f_\pm^2(t)$ with the help of Muskhelishvili–Omnès techniques will be described in the following (cf. Chaps. 13, 14, and 15). Note, however, that such an easy rewriting scheme is not possible for the *s*-channel part (8.3) of the Roy–Steiner PWHDRs, since in the corresponding *s*-channel integrals also $0 \leq l' \leq l$ contribute.

Chapter 13

Subtracted Roy–Steiner system for πN scattering

The Froissart–Martin bound [234–236] (see also [174]) limits the number of subtractions necessary for the convergence of the integrals in the high-energy regime to 2, since the total cross section does not increase faster than $\log^2 s$ for $s \to \infty$.[#1] The influence of the high-energy contributions to dispersion integrals may be reduced by means of suitable subtractions for the trade-off of introducing corresponding subtraction polynomials with subtraction constants that are a priori unknown. For the Muskhelishvili–Omnès integrals in (12.47) subtracting in t at subtraction points below t_π with the additional constraint $s = u$ in order to preserve crossing symmetry is favorable. A particularly useful choice is the subthreshold expansion, which amounts to subtracting in t at zero: first, it is very convenient for extrapolating to the Cheng–Dashen point in order to elaborate on the πN σ-term $\sigma_{\pi N}$ (cf. Sect. 7.1); second, subtracting at the subthreshold point facilitates matching to ChPT, which is expected to work best in the subthreshold region.[#2] To this end, we first briefly review the subthreshold expansion of the scattering amplitudes and then discuss its application in order to write down both the once- and twice-subtracted form of the hyperbolic dispersion relations (7.98).

13.1 Subthreshold expansion

The subthreshold expansion refers to the expansion of Born-subtracted amplitudes around the subthreshold point $(s = u = s_0, t = 0) = (\nu = 0, t = 0)$ (cf. Sect. 7.1), where the nucleon pole terms are subtracted since they are rapidly varying in this kinematical region. Subtracting the *pseudovector* Born terms (indicated by bars) yields

$$\bar{A}^+(s,t) = A^+(s,t) - \frac{g^2}{m} \,, \qquad \bar{B}^+(s,t) = B^+(s,t) - \bar{N}^+(s,t) \,,$$

$$\bar{A}^-(s,t) = A^-(s,t) \,, \qquad \bar{B}^-(s,t) = B^-(s,t) - \bar{N}^-(s,t) + \frac{g^2}{2m^2} \,, \qquad (13.1)$$

[#1]While the original Froissart bound assumes validity of the Mandelstam representation for the scattering amplitude, the result of Martin is based on somewhat less restrictive assumptions.

[#2]For the application of heavy-baryon ChPT to πN scattering in the subthreshold region see [237]. Conversely, analyticity and unitarity are used in [238] to stabilize the extrapolation of πN partial waves derived from ChPT amplitudes in the subthreshold region into the physical region, thus enabling the determination of the chiral parameters by matching to experimental information in terms of s-channel phase shifts.

while for the *pseudoscalar* Born-subtracted (indicated by tildes) amplitudes $\tilde{A}^{\pm}$ and $\tilde{B}^{\pm}$ the terms $-g^2/m$ and $+g^2/2m^2$ need to be dropped (cf. 7.99). Due to the crossing symmetry of the amplitudes (7.26) (similarly for HDRs (7.98), (7.105)) one can write the subthreshold expansion generically for crossing-even amplitudes as (cf. (7.105) as well as [171])

$$
X(\nu, t) = \sum_{m,n} x_{mn} (\nu^2)^m t^n , \quad X \in \left\{ \bar{A}^+, \tilde{A}^+, \frac{\bar{A}^-}{\nu}, \frac{\tilde{A}^-}{\nu}, \frac{\bar{B}^+}{\nu}, \frac{\tilde{B}^+}{\nu}, \bar{B}^-, \tilde{B}^-, \bar{D}^+, \tilde{D}^+, \frac{\bar{D}^-}{\nu}, \frac{\tilde{D}^-}{\nu} \right\} ,
$$
(13.2)

and thus explicitly for the pseudovector Born-subtracted amplitudes as

$$
\bar{A}^+(\nu, t) = \sum_{m,n=0}^{\infty} a_{mn}^+ \nu^{2m} t^n , \qquad\qquad \bar{B}^+(\nu, t) = \sum_{m,n=0}^{\infty} b_{mn}^+ \nu^{2m+1} t^n ,
$$

$$
\bar{A}^-(\nu, t) = \sum_{m,n=0}^{\infty} a_{mn}^- \nu^{2m+1} t^n , \qquad\qquad \bar{B}^-(\nu, t) = \sum_{m,n=0}^{\infty} b_{mn}^- \nu^{2m} t^n , \qquad (13.3)
$$

where the corresponding subthreshold parameters of the amplitudes $\bar{D}^{\pm} = \bar{A}^{\pm} + \nu \bar{B}^{\pm}$ are related by

$$
d_{mn}^+ = a_{mn}^+ + b_{m-1,n}^+ , \qquad d_{mn}^- = a_{mn}^- + b_{mn}^- .
$$
(13.4)

Note that due to $b_{-1,n}^+ = 0$ in particular

$$
d_{0n}^+ = a_{0n}^+ .
$$
(13.5)

From the expansions (cf. (7.104))

$$
\frac{1}{s'-s} - \frac{1}{s'-u} = \frac{4m\nu}{(s'-s_0)^2} + \mathcal{O}(\nu^3, \nu t) ,
$$

$$
\frac{1}{s'-s} + \frac{1}{s'-u} = \frac{2}{s'-s_0} - \frac{t}{(s'-s_0)^2} + \mathcal{O}(\nu^2, \nu^2 t, t^2) ,
$$
(13.6)

one then can read off the subthreshold expansions of the Born-unsubtracted amplitudes up to and including first order in ν and t[#3]

$$
A^+(\nu, t) = \frac{g^2}{m} + d_{00}^+ + d_{01}^+ t + \mathcal{O}(\nu^2, \nu^2 t, t^2) ,
$$

$$
A^-(\nu, t) = \nu a_{00}^- + \mathcal{O}(\nu^3, \nu t) , \qquad B^+(\nu, t) = g^2 \frac{4m\nu}{(m^2-s_0)^2} + \nu b_{00}^+ + \mathcal{O}(\nu^3, \nu t) ,
$$

$$
B^-(\nu, t) = g^2 \left[\frac{2}{m^2-s_0} - \frac{t}{(m^2-s_0)^2} \right] - \frac{g^2}{2m^2} + b_{00}^- + b_{01}^- t + \mathcal{O}(\nu^2, \nu^2 t, t^2) .
$$
(13.7)

13.2 Sum rules for the subthreshold parameters

In the following we will briefly explain how over-subtracting dispersion relations yields sum rules for the one-dimensional case (cf. for instance [174]) before deriving sum rules for the subthreshold parameters from the HDRs (7.98) at hand.

[#3]Note that for B^- the factor in square brackets is *not* proportional to ν_B.

Starting from a supposedly convergent dispersion relation (i.e. no subtractions necessary)

$$f(s) = \frac{1}{\pi} \int\limits_{s_1}^{s_2} \mathrm{d}s' \frac{\operatorname{Im} f(s')}{s' - s} \,, \tag{13.8}$$

we can utilize the general relation

$$\frac{1}{s' - s} = \sum_{i=0}^{n-1} \frac{(s - s_0)^i}{(s' - s_0)^{i+1}} + \frac{(s - s_0)^n}{(s' - s_0)^n} \frac{1}{s' - s} \qquad \forall \, n \geq 0 \,, \tag{13.9}$$

which directly follows from the formula for a partial sum of the geometric series, in order to derive the form of the n-times over-subtracted dispersion relation with identical fixed subtraction point s_0 for all subtractions[#4]

$$f(s) = \sum_{i=0}^{n-1} c_i (s - s_0)^i + \frac{(s - s_0)^n}{\pi} \int\limits_{s_1}^{s_2} \frac{\mathrm{d}s'}{(s' - s_0)^n} \frac{\operatorname{Im} f(s')}{s' - s} \,, \tag{13.10}$$

where the n subtraction constants, which are the coefficients c_i of the subtraction polynomial of order $n - 1$ in $(s - s_0)$, are given by

$$c_i = \frac{1}{\pi} \int\limits_{s_1}^{s_2} \mathrm{d}s' \frac{\operatorname{Im} f(s')}{(s' - s_0)^{i+1}} = \frac{1}{i!} \left[\left(\frac{\mathrm{d}}{\mathrm{d}s} \right)^i f(s) \right]_{s=s_0} \,. \tag{13.11}$$

The first equality for the c_i represents the convergent sum rules that the subtraction constants due to over-subtracting must obey, while the second equality, which can be inferred by differentiating both sides of the subtracted dispersion relation i times and evaluating at the subtraction point $s = s_0$ for all values of i, can be used to derive the explicit form of the sum rules. However, there are no sum rules for subtraction constants that are necessary for convergence reasons, which are thus a priori unknown.

Generalizing the above now to the two-dimensional case and noting that subtracting at the points $s_0 = \Sigma/2 < s_+$ and $t_0 = 0 < t_\pi$ corresponds to the subthreshold expansion around $(\nu = 0, t = 0)$ allows for the determination of sum rules for the subthreshold parameters. Matching the expansions (13.7) to the corresponding expansions of the HDRs (7.98) (or (7.105)) by equating the coefficients, where in addition to (13.6) we have

$$\frac{1}{t' - t} = \frac{1}{t'} \left\{ 1 + \frac{t}{t'} + \mathcal{O}(t^2) \right\} \,, \tag{13.12}$$

and it is crucial to keep track of all implicit dependences in the expansions, together with introducing the abbreviation

$$h_0(s') = \frac{2}{s' - s_0} - \frac{1}{s' - a} \,, \tag{13.13}$$

[#4]If the subtraction point is chosen away from the cut of $f(s)$ such that $\operatorname{Im} f(s_0) = 0$ (e.g. $s_0 < s_1$), the subtracted dispersion relation can also be written as unsubtracted dispersion relation for a subtracted function, i.e. $(f(s) - f(s_0))/(s - s_0)$ for $n = 1$.

then yields the following sum rules for the lowest subthreshold parameters

$$d_{00}^+ = -\frac{g^2}{m} + \frac{1}{\pi} \int\limits_{s_+}^{\infty} ds' \, h_0(s') \left[\text{Im}\, A^+(s', z_s')\right]_{(0,0)} + \frac{1}{\pi} \int\limits_{t_\pi}^{\infty} \frac{dt'}{t'} \left[\text{Im}\, A^+(t', z_t')\right]_{(0,0)} \,,$$

$$b_{00}^- = \frac{g^2}{2m^2} - \frac{g^2}{m^2 - a} + \frac{1}{\pi} \int\limits_{s_+}^{\infty} ds' \, h_0(s') \left[\text{Im}\, B^-(s', z_s')\right]_{(0,0)} + \frac{1}{\pi} \int\limits_{t_\pi}^{\infty} \frac{dt'}{t'} \left[\text{Im}\, B^-(t', z_t')\right]_{(0,0)} \,,$$

$$d_{01}^+ = \frac{1}{\pi} \int\limits_{s_+}^{\infty} ds' \left\{ h_0(s') \left[\partial_t \text{Im}\, A^+(s', z_s')\right]_{(0,0)} - \frac{\left[\text{Im}\, A^+(s', z_s')\right]_{(0,0)}}{(s' - s_0)^2} \right\}$$

$$+ \frac{1}{\pi} \int\limits_{t_\pi}^{\infty} \frac{dt'}{t'} \left\{ \left[\partial_t \text{Im}\, A^+(t', z_t')\right]_{(0,0)} + \frac{1}{t'} \left[\text{Im}\, A^+(t', z_t')\right]_{(0,0)} \right\} \,,$$

$$b_{01}^- = \frac{1}{\pi} \int\limits_{s_+}^{\infty} ds' \left\{ h_0(s') \left[\partial_t \text{Im}\, B^-(s', z_s')\right]_{(0,0)} - \frac{\left[\text{Im}\, B^-(s', z_s')\right]_{(0,0)}}{(s' - s_0)^2} \right\}$$

$$+ \frac{1}{\pi} \int\limits_{t_\pi}^{\infty} \frac{dt'}{t'} \left\{ \left[\partial_t \text{Im}\, B^-(t', z_t')\right]_{(0,0)} + \frac{1}{t'} \left[\text{Im}\, B^-(t', z_t')\right]_{(0,0)} \right\} \,,$$

$$\frac{a_{00}^-}{4m} = \frac{1}{\pi} \int\limits_{s_+}^{\infty} ds' \, \frac{\left[\text{Im}\, A^-(s', z_s')\right]_{(0,0)}}{(s' - s_0)^2} + \frac{1}{\pi} \int\limits_{t_\pi}^{\infty} \frac{dt'}{t'} \left[\frac{\text{Im}\, A^-(t', z_t')}{4p_t' q_t' z_t'}\right]_{(0,0)} \,,$$

$$\frac{b_{00}^+}{4m} = \frac{1}{\pi} \int\limits_{s_+}^{\infty} ds' \, \frac{\left[\text{Im}\, B^+(s', z_s')\right]_{(0,0)}}{(s' - s_0)^2} + \frac{1}{\pi} \int\limits_{t_\pi}^{\infty} \frac{dt'}{t'} \left[\frac{\text{Im}\, B^+(t', z_t')}{4p_t' q_t' z_t'}\right]_{(0,0)} \,. \tag{13.14}$$

The subscript $(0,0)$ indicates that z_s' and z_t' in the s- and t-channel integrals, respectively, are to be evaluated at $(\nu = 0,\, t = 0)$, which according to (7.103) and (7.90) amounts to using

$$\left[z_s'\right]_{(0,0)} = 1 - \frac{(s' - s_0)^2}{2q'^2(s' - a)} \,, \qquad\qquad \left[\partial_t z_s'\right]_{(0,0)} = \frac{s_0 - a}{2q'^2(s' - a)} \,,$$

$$\left[z_t'^2\right]_{(0,0)} = \frac{t'(t' - 4(s_0 - a))}{16 p_t'^2 q_t'^2} = 1 + \frac{t'4a - t_N t_\pi}{16 p_t'^2 q_t'^2} \,, \qquad \left[\partial_t z_t'^2\right]_{(0,0)} = \frac{s_0 - a}{4 p_t'^2 q_t'^2} \,, \tag{13.15}$$

where again we have used the fact that the t-channel integrands depend on the squared angle $z_t'^2$ only. Note that these sum rules as such are valid independent of the choice of a, but in practice one will incur an a-dependence once approximations are made (such as truncation of the partial-wave expansion, approximation of the high-energy region by Regge theory, etc.).

13.3   Subtracted hyperbolic dispersion relations

A single subtraction at $(\nu = 0, t = 0)$ only affects $A^+(\nu, t)$ and $B^-(\nu, t)$ since both $A^-(\nu, t)$ and $B^+(\nu, t)$ are proportional to ν. Based on the unsubtracted HDRs (7.98), the explicit

subthreshold expansions (13.7), and the corresponding sum rules (13.14), we obtain the once-subtracted HDRs

$$
A^+(s,t;a) = \frac{g^2}{m} + d_{00}^+ + \frac{1}{\pi} \int\limits_{t_\pi}^{\infty} dt' \left\{ \frac{\operatorname{Im} A^+(t', z_t')}{t' - t} - \frac{[\operatorname{Im} A^+(t', z_t')]_{(0,0)}}{t'} \right\} \tag{13.16}
$$

$$
+ \frac{1}{\pi} \int\limits_{s_+}^{\infty} ds' \left\{ \left[\frac{1}{s' - s} + \frac{1}{s' - u} - \frac{1}{s' - a} \right] \operatorname{Im} A^+(s', z_s') - h_0(s') \left[\operatorname{Im} A^+(s', z_s') \right]_{(0,0)} \right\},
$$

$$
B^-(s,t;a) = \bar{N}^-(s,t) - \frac{g^2}{2m^2} + b_{00}^- + \frac{1}{\pi} \int\limits_{t_\pi}^{\infty} dt' \left\{ \frac{\operatorname{Im} B^-(t', z_t')}{t' - t} - \frac{[\operatorname{Im} B^-(t', z_t')]_{(0,0)}}{t'} \right\}
$$

$$
+ \frac{1}{\pi} \int\limits_{s_+}^{\infty} ds' \left\{ \left[\frac{1}{s' - s} + \frac{1}{s' - u} - \frac{1}{s' - a} \right] \operatorname{Im} B^-(s', z_s') - h_0(s') \left[\operatorname{Im} B^-(s', z_s') \right]_{(0,0)} \right\},
$$

together with the unaltered equations (7.98) or (7.105) for A^- and B^+. Note that the dependence on a of the Born term contribution N^- is canceled by the sum rule (13.14) for b_{00}^-, which is why the subtraction constants are formally included in the subtracted nucleon pole terms in the following for convenience (i.e. preserving the generic form of the HDRs (7.98)).

Similarly, a second subtraction at $(\nu = 0, t = 0)$ yields the twice-subtracted HDRs

$$
A^+(s,t;a) = \frac{g^2}{m} + d_{00}^+ + d_{01}^+ t + \frac{1}{\pi} \int\limits_{t_\pi}^{\infty} dt' \left\{ \frac{\operatorname{Im} A^+(t', z_t')}{t' - t} \right.
$$

$$
\left. - \left(\frac{1}{t'} + \frac{t}{t'^2} \right) \left[\operatorname{Im} A^+(t', z_t') \right]_{(0,0)} - \frac{t}{t'} \left[\partial_t \operatorname{Im} A^+(t', z_t') \right]_{(0,0)} \right\}
$$

$$
+ \frac{1}{\pi} \int\limits_{s_+}^{\infty} ds' \left\{ \left[\frac{1}{s' - s} + \frac{1}{s' - u} - \frac{1}{s' - a} \right] \operatorname{Im} A^+(s', z_s') \right.
$$

$$
\left. - \left(h_0(s') - \frac{t}{(s' - s_0)^2} \right) \left[\operatorname{Im} A^+(s', z_s') \right]_{(0,0)} - h_0(s') \, t \left[\partial_t \operatorname{Im} A^+(s', z_s') \right]_{(0,0)} \right\},
$$

$$
B^-(s,t;a) = \bar{N}^-(s,t) - \frac{g^2}{2m^2} + b_{00}^- + b_{01}^- t + \frac{1}{\pi} \int\limits_{t_\pi}^{\infty} dt' \left\{ \frac{\operatorname{Im} B^-(t', z_t')}{t' - t} \right.
$$

$$
\left. - \left(\frac{1}{t'} + \frac{t}{t'^2} \right) \left[\operatorname{Im} B^-(t', z_t') \right]_{(0,0)} - \frac{t}{t'} \left[\partial_t \operatorname{Im} B^-(t', z_t') \right]_{(0,0)} \right\}
$$

$$
+ \frac{1}{\pi} \int\limits_{s_+}^{\infty} ds' \left\{ \left[\frac{1}{s' - s} + \frac{1}{s' - u} - \frac{1}{s' - a} \right] \operatorname{Im} B^-(s', z_s') \right.
$$

$$
\left. - \left(h_0(s') - \frac{t}{(s' - s_0)^2} \right) \left[\operatorname{Im} B^-(s', z_s') \right]_{(0,0)} - h_0(s') \, t \left[\partial_t \operatorname{Im} B^-(s', z_s') \right]_{(0,0)} \right\},
$$

$$A^-(s,t;a) = a_{00}^- \nu + \frac{\nu}{\pi} \int\limits_{t_\pi}^\infty dt' \left\{ \frac{\operatorname{Im} A^-(t',z_t')}{\nu'(t'-t)} - \frac{[\operatorname{Im} A^-(t',z_t')/\nu']_{(0,0)}}{t'} \right\}$$

$$+ \frac{1}{\pi} \int\limits_{s_+}^\infty ds' \left\{ \left[\frac{1}{s'-s} - \frac{1}{s'-u} \right] \operatorname{Im} A^-(s',z_s') - \frac{4m\nu \, [\operatorname{Im} A^-(s',z_s')]_{(0,0)}}{(s'-s_0)^2} \right\},$$

$$B^+(s,t;a) = \bar{N}^+(s,t) + b_{00}^+ \nu + \frac{\nu}{\pi} \int\limits_{t_\pi}^\infty dt' \left\{ \frac{\operatorname{Im} B^+(t',z_t')}{\nu'(t'-t)} - \frac{[\operatorname{Im} B^+(t',z_t')/\nu']_{(0,0)}}{t'} \right\}$$

$$+ \frac{1}{\pi} \int\limits_{s_+}^\infty ds' \left\{ \left[\frac{1}{s'-s} - \frac{1}{s'-u} \right] \operatorname{Im} B^+(s',z_s') - \frac{4m\nu \, [\operatorname{Im} B^+(s',z_s')]_{(0,0)}}{(s'-s_0)^2} \right\},$$

$$(13.17)$$

where A^- and B^+ can also be written as (cf. (7.105))

$$\frac{A^-(s,t;a)}{4m\nu} = \frac{a_{00}^-}{4m} + \frac{1}{\pi} \int\limits_{t_\pi}^\infty dt' \left\{ \frac{\operatorname{Im} A^-(t',z_t')}{4p_t'q_t'z_t'(t'-t)} - \frac{1}{t'} \left[\frac{\operatorname{Im} A^-(t',z_t')}{4p_t'q_t'z_t'} \right]_{(0,0)} \right\}$$

$$+ \frac{1}{\pi} \int\limits_{s_+}^\infty ds' \left\{ \frac{\operatorname{Im} A^-(s',z_s')}{(s'-s)(s'-u)} - \frac{[\operatorname{Im} A^-(s',z_s')]_{(0,0)}}{(s'-s_0)^2} \right\},$$

$$\frac{B^+(s,t;a)}{4m\nu} = \frac{g^2}{(m^2-s)(m^2-u)} + \frac{b_{00}^+}{4m} + \frac{1}{\pi} \int\limits_{t_\pi}^\infty dt' \left\{ \frac{\operatorname{Im} B^+(t',z_t')}{4p_t'q_t'z_t'(t'-t)} - \frac{1}{t'} \left[\frac{\operatorname{Im} B^+(t',z_t')}{4p_t'q_t'z_t'} \right]_{(0,0)} \right\}$$

$$+ \frac{1}{\pi} \int\limits_{s_+}^\infty ds' \left\{ \frac{\operatorname{Im} B^+(s',z_s')}{(s'-s)(s'-u)} - \frac{[\operatorname{Im} B^+(s',z_s')]_{(0,0)}}{(s'-s_0)^2} \right\}. \qquad (13.18)$$

These subtractions require modification of the nucleon pole term projections and the kernel functions for both the s- and t-channel contributions calculated in Chaps. 8 and 9 as well as the asymptotic contributions given in Chap. 11. The differences on the right hand side of the once-/twice-subtracted HDRs (13.16)/(13.17) (or (13.18)) compared to the unsubtracted HDRs (7.98) (or (7.105)) are the sources for corresponding additional contributions which will be derived in the subsequent sections. We will give the explicit formulae for both the once- and twice-subtracted case for convenience. Furthermore, some results will be given in the general n-times subtracted form, where $n \in \{0,1,2\}$ such that $n = 0$ denotes the unsubtracted case.[#5]

[#5]For the sake of simplicity, throughout this work we have chosen to count the number of subtractions according to the simultaneous expansion around s_0 and $t_0 = 0$, i.e. to expand in terms of Mandelstam variables directly. Alternatively, one may work with crossing-even amplitudes solely and expand around $\nu_0^2 = 0$ and t_0 simultaneously (note that $\nu^2 - \nu_0^2 \propto (\nu - \nu_0)$ and that both ν^2 and t are of $\mathcal{O}(\text{GeV}^2)$); the numbering of subtractions would then be in line with the indices of the subthreshold parameters (cf. (13.2); see, however, also the comment on (7.106)). Another possible counting (i.e. ordering) scheme derives from the observation that $A^\pm = \mathcal{O}(\text{GeV}^{-1})$ and $B^\pm = \mathcal{O}(\text{GeV}^{-2})$, which means that the $B^\pm$ amplitudes are relatively suppressed by one order in energy (and thus the reduced amplitude B^+/ν already by two orders): One may define the successive steps of the (subthreshold) expansion procedure via the (negative) orders of energy of the corresponding (subthreshold) expansion parameters in order to consistently account for the relative importance

13.4   Subtracted asymptotics

First, we show how to incorporate the effects due to the subtractions into the Regge prescription of the asymptotic parts (i.e. for $s' > s_a$ and $t' > t_a$, cf. (11.1)) of the corresponding subtracted HDRs (13.16) and (13.17). However, according to Sect. 11.2 all asymptotic t-channel contributions can be neglected.

For the high-energy tail $s' > s_a$ of the s-channel integrals, according to Sect. 11.1 the absorptive parts may generically be written as sums of Regge trajectory contributions

$$\operatorname{Im} X^{I_u}(s', u'(s', t')) = \sum_i \tilde{\beta}_i^X(u') \left(\frac{s'}{s_R}\right)^{\alpha_i(u')-\frac{1}{2}} \quad \text{for } X \in \{A, B\}\,, \tag{13.19}$$

with summands of the generic form (i.e. dropping the indices X and i for the time being)

$$\tilde{\beta}(u') = -\frac{\mathcal{S}\beta(u')}{\Gamma\left(\alpha(u') - \frac{1}{2}\right)}\,, \qquad \beta(u') = \beta^{(0)} + \beta^{(1)}u'\,, \qquad \alpha(u') = \alpha^{(0)} + \alpha'u'\,. \tag{13.20}$$

While the evaluation of the Regge contributions is straightforward in the un- and once-subtracted case, for two subtractions one furthermore needs the derivative

$$\left[\partial_t\left\{\tilde{\beta}(u')\left(\frac{s'}{s_R}\right)^{\alpha(u')-\frac{1}{2}}\right\}\right]_{(0,0)} = \left[\partial_t t'\right]_{(0,0)}\left[\frac{\mathcal{S}}{\Gamma\left(\alpha\left(u'(s',t')\right)-\frac{1}{2}\right)}\left(\frac{s'}{s_R}\right)^{\alpha\left(u'(s',t')\right)-\frac{1}{2}}\right]_{(0,0)}$$

$$\times \left[\beta^{(1)} + \alpha'\beta\left(u'(s',t')\right)\left\{\log\frac{s'}{s_R} - \Psi\left(\alpha\left(u'(s',t')\right)-\frac{1}{2}\right)\right\}\right]_{(0,0)}, \tag{13.21}$$

where $\Psi(z)$ denotes the digamma function, which is defined as the logarithmic derivative of the gamma function

$$\Psi(z) = \frac{\mathrm{d}}{\mathrm{d}z}\log\Gamma(z) = \frac{\Gamma'(z)}{\Gamma(z)}\,. \tag{13.22}$$

To this end, one may use $u'(s', t') = \Sigma - s' - t'$ and (cf. (13.15))

$$\left[t'\right]_{(0,0)} = -\frac{(s'-s_0)^2}{s'-a}\,, \qquad \left[\partial_t t'\right]_{(0,0)} = \frac{s_0 - a}{s'-a}\,. \tag{13.23}$$

After utilizing the crossing relations in order to rewrite the Regge contributions in the $I \in \{+, -\}$ isospin basis and expressing t' as well as the corresponding kernel functions in terms

---

of the successive terms in the subtraction polynomials on the full T-matrix element (which in turn is the fundamental quantity for the partial-wave expansion, cf. Sect. 7.3); in this scheme the "first subtraction" corresponds to expanding only A^+ up to $d_{00}^+ = \mathcal{O}(\mathrm{GeV}^{-1})$, the "second subtraction" at $\mathcal{O}(\mathrm{GeV}^{-2})$ comprises $a_{00}^- = d_{00}^- - b_{00}^-$ as well as b_{00}^-, and so forth. In contrast to the chosen counting scheme, besides $d_{01}^+ = \mathcal{O}(\mathrm{GeV}^{-3})$ this ordering would in particular suggest to account for $a_{10}^+ = d_{10}^+ - b_{00}^+ = \mathcal{O}(\mathrm{GeV}^{-3})$ instead of $b_{01}^- = d_{01}^- - a_{01}^- = \mathcal{O}(\mathrm{GeV}^{-4})$ at the next subtraction level (cf. (13.7) and Tab. 15.1). Note that this ordering automatically ensures the possibility to choose between working with $a_{mn}^\pm$ and $d_{mn}^\pm$ via (13.4), i.e. the expansion is independent of the decomposition of the T-matrix element into different sets of invariant amplitudes. Therefore, using both a_{10}^+ and b_{01}^- as well as in addition a_{01}^- (which is consistent with subtracting $A^\pm$ at least partially once more often than $B^\pm$, cf. also the discussion in [160]) would be the natural choice for extending the chosen subtraction scheme (allowing for d_{10}^+ and d_{01}^-), while furthermore accounting for $a_{10}^- = d_{10}^- - b_{10}^-$ and b_{10}^- would complete the $\mathcal{O}(\mathrm{GeV}^{-4})$.

of (s', z_s'), we can perform the partial-wave projections of the s-channel contributions onto both s- and t-channel partial waves according to (11.7), where again the implicit kinematical dependences have to be taken into account accordingly.

In the following we will demonstrate the projection onto the lowest t-channel partial waves with $J \leq 2$ explicitly. The n-times subtracted versions of (11.7) immediately lead to

$$f_+^0\big|_{\text{asym}}^{n\text{-sub}}(t) = \frac{1}{4\pi}\int_0^1 \mathrm{d}z_t\, p_t^2 \left\{ -A^+\big|_{\text{asym}}^{n\text{-sub}}(t, z_t) + 4mq_t^2 z_t^2 \frac{B^+\big|_{\text{asym}}^{n\text{-sub}}(t, z_t)}{4p_t q_t z_t} \right\},$$

$$f_+^1\big|_{\text{asym}}^{n\text{-sub}}(t) = \frac{1}{4\pi}\int_0^1 \mathrm{d}z_t\, z_t^2 \left\{ -4p_t^2 \frac{A^-\big|_{\text{asym}}^{n\text{-sub}}(t, z_t)}{4p_t q_t z_t} + m B^-\big|_{\text{asym}}^{n\text{-sub}}(t, z_t) \right\},$$

$$f_-^1\big|_{\text{asym}}^{n\text{-sub}}(t) = \frac{1}{4\pi}\int_0^1 \mathrm{d}z_t\, \frac{1 - z_t^2}{\sqrt{2}}\, B^-\big|_{\text{asym}}^{n\text{-sub}}(t, z_t),$$

$$f_+^2\big|_{\text{asym}}^{n\text{-sub}}(t) = \frac{1}{4\pi}\int_0^1 \mathrm{d}z_t\, \frac{3z_t^2 - 1}{2q_t^2} \left\{ -A^+\big|_{\text{asym}}^{n\text{-sub}}(t, z_t) + 4mq_t^2 z_t^2 \frac{B^+\big|_{\text{asym}}^{n\text{-sub}}(t, z_t)}{4p_t q_t z_t} \right\},$$

$$f_-^2\big|_{\text{asym}}^{n\text{-sub}}(t) = \frac{1}{4\pi}\int_0^1 \mathrm{d}z_t\, 2\sqrt{6}\, z_t^2(1 - z_t^2) \frac{B^+\big|_{\text{asym}}^{n\text{-sub}}(t, z_t)}{4p_t q_t z_t}, \tag{13.24}$$

again written in terms of quantities that are always real since $4p_t q_t z_t = 4m\nu$. Here, the asymptotic s-channel contributions to the invariant amplitudes for e.g. the twice-subtracted case read (i.e. as functions of (t, z_t), cf. (7.104) for the kernel functions and (9.23) for $z_s'(t, s'; z_t)$)

$$A^+\big|_{\text{s-asym}}^{2\text{-sub}}(t, z_t) = \frac{1}{\pi}\int_{s_a}^\infty \mathrm{d}s' \left\{ \left[\frac{2(s' - s_0) + t}{(s' - s_0 + \frac{t}{2})^2 - 4p_t^2 q_t^2 z_t^2} - \frac{1}{s' - a} \right] \operatorname{Im} A^+(s', z_s') \right.$$

$$- \left(h_0(s') - \frac{t}{(s' - s_0)^2} \right) \left[\operatorname{Im} A^+(s', z_s') \right]_{(0,0)}$$

$$\left. - h_0(s')\, t \left[\partial_t \operatorname{Im} A^+(s', z_s') \right]_{(0,0)} \right\},$$

$$\frac{A^-\big|_{\text{s-asym}}^{2\text{-sub}}(t, z_t)}{4p_t q_t z_t} = \frac{1}{\pi}\int_{s_a}^\infty \mathrm{d}s' \left\{ \frac{\operatorname{Im} A^-(s', z_s')}{(s' - s_0 + \frac{t}{2})^2 - 4p_t^2 q_t^2 z_t^2} - \frac{\left[\operatorname{Im} A^-(s', z_s') \right]_{(0,0)}}{(s' - s_0)^2} \right\}, \tag{13.25}$$

and analogously for $B^-(t, z_t)$ and $B^+(t, z_t)/(4p_t q_t z_t)$. For the evaluation of the imaginary parts in the integrands of (13.25) in the Regge model as discussed above, it is convenient to directly use

$$t'(s', t, z_t) = (s' - a) - 2(s' - s_0) - \frac{(a - s_0 + \frac{t}{2})^2 - 4p_t^2 q_t^2 z_t^2}{s' - a}. \tag{13.26}$$

Note that again only real squares of momenta and z_t occur and hence these formulae are valid in all kinematical regions. Furthermore, by rewriting the general t-channel partial-wave projections (9.7) for both even and odd J in terms of real quantities (i.e. ν-even amplitudes

and squares of momenta as well as squares of z_t) as above, the partial waves exhibit ostensible poles at t_π for all $J \geq 2$ and additionally at t_N for all $J \geq 3$, while from the discussion of their threshold behavior in Sect. 12.3.1 we know that these poles are immaterial. The reason for this behavior can be understood by first noting that for $p_t q_t \to 0$ the asymptotic (*s*-channel) contributions (13.25) no longer depend on z_t. The orthogonality of the Legendre polynomials $P_J(z_t)$ for even $J \geq 2$ and odd $J \geq 3$ then balances the poles and leads to the expected finite (but non-vanishing) values of the partial waves at both the pseudothreshold t_π and the threshold t_N (cf. the explicit case for $f_+^2(t)$ in (13.24)).

13.5 Subtracted kernels: *t*-channel partial-wave projection

Here, we give the modifications of the nucleon pole term projections and the kernel functions calculated in Chap. 9, that are required by the subtractions performed in Sect. 13.3. Note that the reduction from two subtractions to only one subtraction always entails omitting all terms proportional to δ_{J2} or the constants a_{00}^- and b_{00}^+ as well as terms whose t-dependence is trivially seen (e.g. higher subthreshold parameters).

To start with, the n-times subtracted nucleon pole term projections may be written as

$$\tilde{N}_\pm^J\big|^{n\text{-sub}}(t) = \hat{N}_\pm^J(t) + \Delta \hat{N}_\pm^J\big|^{n\text{-sub}}(t) \,,$$

$$\Delta \hat{N}_+^J\big|^{2\text{-sub}}(t) = -\frac{p_t^2}{4\pi}\left(\frac{g^2}{m} + d_{00}^+ + d_{01}^+ t - b_{00}^+ \frac{q_t^2}{3}\right)\delta_{J0}$$

$$+ \frac{m}{12\pi}\left(-\frac{g^2}{2m^2} + b_{00}^- + b_{01}^- t - a_{00}^- \frac{p_t^2}{m^2}\right)\delta_{J1} + \frac{b_{00}^+}{30\pi}\delta_{J2}$$

$$\xrightarrow{\text{1-sub}} -\frac{p_t^2}{4\pi}\left(\frac{g^2}{m} + d_{00}^+\right)\delta_{J0} + \frac{m}{12\pi}\left(-\frac{g^2}{2m^2} + b_{00}^-\right)\delta_{J1} \,,$$

$$\Delta \hat{N}_-^J\big|^{2\text{-sub}}(t) = \frac{\sqrt{2}}{12\pi}\left(-\frac{g^2}{2m^2} + b_{00}^- + b_{01}^- t\right)\delta_{J1} + \frac{b_{00}^+}{30\pi}\frac{\sqrt{6}}{2m}\delta_{J2}$$

$$\xrightarrow{\text{1-sub}} \frac{\sqrt{2}}{12\pi}\left(-\frac{g^2}{2m^2} + b_{00}^-\right)\delta_{J1} \,, \tag{13.27}$$

where for later convenience we have defined non-vanishing "corrections" also for the unsubtracted case (cf. (9.15))

$$\Delta \hat{N}_+^J\big|^{0\text{-sub}}(t) = -\frac{g^2}{4\pi}\frac{m}{3}\frac{\delta_{J1}}{m^2 - a} \,, \qquad \Delta \hat{N}_-^J\big|^{0\text{-sub}}(t) = -\frac{g^2}{4\pi}\frac{\sqrt{2}}{3}\frac{\delta_{J1}}{m^2 - a} \,, \tag{13.28}$$

which are constant and non-zero only for $J = 1$, in order to split off all terms that are either constant or contain subthreshold parameters. Note that for both one and two subtractions the full nucleon pole term projections fulfill the threshold relations (12.43) for $p_t \to 0$ but no longer for $q_t \to 0$. However, the subtraction-independent parts of the pole terms $\hat{N}_\pm^J$ still fulfill the relations (12.43) for $p_t q_t \to 0$.

The necessary update of the *s*-channel kernels $\tilde{G}_{Jl}$ and $\tilde{H}_{Jl}$ may be achieved by adding

$$\Delta \bar{A}_{Jl}\big|^{2\text{-sub}}(t, s') = \left\{\left(h_0(s') - \frac{t}{(s'-s_0)^2}\right)P_l'\left(\big[z_s'\big]_{(0,0)}\right) + h_0(s')\, t\, \big[\partial_t z_s'\big]_{(0,0)} P_l''\left(\big[z_s'\big]_{(0,0)}\right)\right\}$$

$$\times \delta_{J0} + \frac{4}{3}\frac{p_t q_t}{(s'-s_0)^2}P_l'\left(\big[z_s'\big]_{(0,0)}\right)\delta_{J1}$$

$$\xrightarrow{\text{1-sub}} h_0(s')P_l'\Big(\big[z_s'\big]_{(0,0)}\Big)\delta_{J0}\,,$$

$$\Delta\bar{B}_{Jl}\big|^{\text{2-sub}}(t,s') = \left\{\left(h_0(s') - \frac{t}{(s'-s_0)^2}\right)P_l'\Big(\big[z_s'\big]_{(0,0)}\Big) + h_0(s')\,t\,\big[\partial_t z_s'\big]_{(0,0)}P_l''\Big(\big[z_s'\big]_{(0,0)}\Big)\right\}$$

$$\times\frac{\delta_{J1}}{3} + \frac{4}{3}\frac{p_t q_t}{(s'-s_0)^2}P_l'\Big(\big[z_s'\big]_{(0,0)}\Big)\Big(\delta_{J0} + \frac{2}{5}\delta_{J2}\Big)$$

$$\xrightarrow{\text{1-sub}} h_0(s')P_l'\Big(\big[z_s'\big]_{(0,0)}\Big)\frac{\delta_{J1}}{3}\,,$$

$$\Delta\bar{C}_{Jl}\big|^{\text{2-sub}}(t,s') = \left\{\left(h_0(s') - \frac{t}{(s'-s_0)^2}\right)P_l'\Big(\big[z_s'\big]_{(0,0)}\Big) + h_0(s')\,t\,\big[\partial_t z_s'\big]_{(0,0)}P_l''\Big(\big[z_s'\big]_{(0,0)}\Big)\right\}$$

$$\times\delta_{J1} + \frac{4}{3}\frac{p_t q_t}{(s'-s_0)^2}P_l'\Big(\big[z_s'\big]_{(0,0)}\Big)\delta_{J2}$$

$$\xrightarrow{\text{1-sub}} h_0(s')P_l'\Big(\big[z_s'\big]_{(0,0)}\Big)\delta_{J1}\,, \tag{13.29}$$

respectively, to $\bar{A}_{Jl}$, $\bar{B}_{Jl}$, and $\bar{C}_{Jl}$ at the pertinent places in (9.35) leading to corresponding $\Delta\tilde{G}_{Jl}$ and $\Delta\tilde{H}_{Jl}$. Note that also in both the once- and twice-subtracted case $\Delta\bar{C}_{Jl} = \Delta\bar{A}_{J-1,l} - \Delta\bar{A}_{J+1,l}$ is still valid (for $J \geq 1$, here actually $\Delta\bar{C}_{Jl} = \Delta\bar{A}_{J-1,l}$).

The additional contributions to the t-channel kernels $\tilde{\mathbf{K}}^{JJ'}(t,t')$ for even J and J' read

$$\Delta\tilde{K}^1_{JJ'}\big|^{\text{2-sub}}(t,t') = -(2J'+1)(p_t'q_t')^{J'}\frac{p_t^2}{p_t'^2}\frac{1}{t'}\left\{\left(1+\frac{t}{t'}\right)\big[P_{J'}(z_t')\big]_{(0,0)} + t\big[\partial_t P_{J'}(z_t')\big]_{(0,0)}\right\}\delta_{J0}$$

$$\xrightarrow{\text{1-sub}} -(2J'+1)(p_t'q_t')^{J'}\frac{p_t^2}{p_t'^2}\frac{1}{t'}\big[P_{J'}(z_t')\big]_{(0,0)}\,\delta_{J0}\,,$$

$$\Delta\tilde{K}^2_{JJ'}\big|^{\text{2-sub}}(t,t') = \frac{2J'+1}{\sqrt{J'(J'+1)}}(p_t'q_t')^{J'}\frac{p_t^2}{p_t'^2}\frac{m}{t'}\left\{\left[\left(1+\frac{t}{t'}\right)\big[z_t'P_{J'}(z_t')\big]_{(0,0)}\right.\right.$$

$$\left.\left. + t\big[\partial_t(z_t'P_{J'}(z_t'))\big]_{(0,0)}\right]\delta_{J0} - \frac{1}{3}\frac{q_t^2}{q_t'^2}\left[\frac{P_{J'}'(z_t')}{z_t'}\right]_{(0,0)}\left(\delta_{J0} + \frac{2}{5}\frac{\delta_{J2}}{p_t^2 q_t^2}\right)\right\}$$

$$\xrightarrow{\text{1-sub}} \frac{2J'+1}{\sqrt{J'(J'+1)}}(p_t'q_t')^{J'}\frac{p_t^2}{p_t'^2}\frac{m}{t'}\big[z_t'P_{J'}(z_t')\big]_{(0,0)}\,\delta_{J0}\,,$$

$$\Delta\tilde{K}^3_{JJ'}\big|^{\text{2-sub}}(t,t') = -\frac{2J'+1}{\sqrt{J'(J'+1)}}(p_t'q_t')^{J'-2}\frac{\sqrt{6}}{15}\frac{1}{t'}\left[\frac{P_{J'}'(z_t')}{z_t'}\right]_{(0,0)}\delta_{J2}\xrightarrow{\text{1-sub}} 0\,, \tag{13.30}$$

while for odd J and J' one finds

$$\Delta\tilde{K}^1_{JJ'}\big|^{\text{2-sub}}(t,t') = -(2J'+1)(p_t'q_t')^{J'-1}\frac{p_t^2}{p_t'^2}\frac{1}{t'}\left[\frac{P_{J'}(z_t')}{z_t'}\right]_{(0,0)}\frac{\delta_{J1}}{3}\xrightarrow{\text{1-sub}} 0\,,$$

$$\Delta\tilde{K}^2_{JJ'}\big|^{\text{2-sub}}(t,t') = -\frac{2J'+1}{\sqrt{J'(J'+1)}}(p_t'q_t')^{J'-1}\frac{m}{t'}\left\{\left(1-\frac{p_t^2}{p_t'^2}+\frac{t}{t'}\right)\big[P_{J'}'(z_t')\big]_{(0,0)}\right.$$

$$\left. + t\big[\partial_t P_{J'}'(z_t')\big]_{(0,0)}\right\}\frac{\delta_{J1}}{3}$$

$$\xrightarrow{\text{1-sub}} -\frac{2J'+1}{\sqrt{J'(J'+1)}}(p_t'q_t')^{J'-1}\frac{m}{t'}\big[P_{J'}'(z_t')\big]_{(0,0)}\frac{\delta_{J1}}{3}\,,$$

$$\Delta\tilde{K}^3_{JJ'}\big|^{\text{2-sub}}(t,t') = -\frac{2J'+1}{\sqrt{J'(J'+1)}}(p_t'q_t')^{J'-1}\frac{\sqrt{2}}{t'}\left\{\left(1+\frac{t}{t'}\right)\big[P_{J'}'(z_t')\big]_{(0,0)}\right.$$

$$+ t \left[\partial_t P'_{J'}(z'_t)\right]_{(0,0)} \Big\} \frac{\delta_{J1}}{3}$$

$$\xrightarrow{\text{1-sub}} -\frac{2J'+1}{\sqrt{J'(J'+1)}}(p'_t q'_t)^{J'-1}\frac{\sqrt{2}}{t'}\left[P'_{J'}(z'_t)\right]_{(0,0)}\frac{\delta_{J1}}{3} \ . \tag{13.31}$$

Furthermore, $\mathbf{\Delta\tilde{K}}^{JJ'} = 0$ for $J > 2$ or $J' < J$, the latter being in agreement with (9.55). In all cases only even powers of z'_t and the primed momenta occur, so that the additional kernel terms are always real. Here, we refrain from explicitly expanding the Legendre polynomials using (9.49) as in Sect. 9.3, but only give one example to demonstrate this point (for even J'):

$$\left[\partial_t(z'_t P'_{J'}(z'_t))\right]_{(0,0)} = 2\left[\partial_t z'^2_t\right]_{(0,0)}\sum_{\lambda=1}^{\frac{J'}{2}} a^{\text{ev}}_{\lambda J'}\lambda^2\left[z'^2_t\right]_{(0,0)}^{\lambda-1} \ . \tag{13.32}$$

The general relation (cf. (9.58))

$$\frac{\Delta\tilde{K}^2_{JJ'}(t,t')}{m} = \sqrt{\frac{J}{J+1}}\Delta\tilde{K}^3_{JJ'}(t,t') - \sqrt{\frac{J'}{J'+1}}\Delta\tilde{K}^1_{JJ'}\Big|_{P'_{J'}(z'_t)\to\frac{z'_t}{J'}P'_{J'}(z'_t)}(t,t')$$

$$+ \frac{2(J+2)+1}{\sqrt{(J+2)((J+2)+1)}}p^2_t q^2_t \Delta\tilde{K}^3_{J+2,J'}(t,t') \ , \tag{13.33}$$

together with the explicit non-vanishing kernel contributions for $0 \le J' \le 3$ given by

$$\Delta\tilde{K}^1_{00}\big|^{\text{2-sub}}(t,t') = -\frac{p^2_t}{p'^2_t}\frac{1}{t'}\left(1+\frac{t}{t'}\right)\xrightarrow{\text{1-sub}}-\frac{p^2_t}{p'^2_t}\frac{1}{t'} \ , \qquad \Delta\tilde{K}^1_{11}\big|^{\text{2-sub}}(t,t') = -\frac{p^2_t}{p'^2_t}\frac{1}{t'} \ ,$$

$$\Delta\tilde{K}^1_{02}\big|^{\text{2-sub}}(t,t') = -\frac{15}{32}\frac{p^2_t}{p'^2_t}\left\{t+t'-4(s_0-a)-\left(1+\frac{t}{t'}\right)\frac{16p'^2_t q'^2_t}{3t'}\right\}$$

$$\xrightarrow{\text{1-sub}}-\frac{15}{32}\frac{p^2_t}{p'^2_t}\left\{t'-4(s_0-a)-\frac{16p'^2_t q'^2_t}{3t'}\right\} \ ,$$

$$\Delta\tilde{K}^1_{13}\big|^{\text{2-sub}}(t,t') = -\frac{35}{96}\frac{p^2_t}{p'^2_t}\left\{t'-4(s_0-a)-\frac{48p'^2_t q'^2_t}{5t'}\right\} \ ,$$

$$\Delta\tilde{K}^2_{11}\big|^{\text{2-sub}}(t,t') = -\frac{m}{\sqrt{2}}\frac{1}{t'}\left(1-\frac{p^2_t}{p'^2_t}+\frac{t}{t'}\right)\xrightarrow{\text{1-sub}}-\frac{m}{\sqrt{2}}\frac{1}{t'} \ , \qquad \Delta\tilde{K}^2_{22}\big|^{\text{2-sub}}(t,t') = -\frac{2m}{\sqrt{6}}\frac{1}{t'} \ ,$$

$$\Delta\tilde{K}^2_{02}\big|^{\text{2-sub}}(t,t') = \frac{15m}{16\sqrt{6}}\frac{p^2_t}{p'^2_t}\left\{t+t'-4(s_0-a)-q^2_t\frac{16p'^2_t}{3t'}\right\}\xrightarrow{\text{1-sub}}\frac{15m}{16\sqrt{6}}\frac{p^2_t}{p'^2_t}\left\{t'-4(s_0-a)\right\} \ ,$$

$$\Delta\tilde{K}^2_{13}\big|^{\text{2-sub}}(t,t') = -\frac{35m}{64\sqrt{3}}\left\{t+\left(1-\frac{p^2_t}{p'^2_t}\right)\left[t'-4(s_0-a)\right]-\left(1-\frac{p^2_t}{p'^2_t}+\frac{t}{t'}\right)\frac{16p'^2_t q'^2_t}{5t'}\right\}$$

$$\xrightarrow{\text{1-sub}}-\frac{35m}{64\sqrt{3}}\left\{t'-4(s_0-a)-\frac{16p'^2_t q'^2_t}{5t'}\right\} \ ,$$

$$\Delta\tilde{K}^3_{11}\big|^{\text{2-sub}}(t,t') = -\frac{1}{t'}\left(1+\frac{t}{t'}\right)\xrightarrow{\text{1-sub}}-\frac{1}{t'} \ , \qquad \Delta\tilde{K}^3_{22}\big|^{\text{2-sub}}(t,t') = -\frac{1}{t'} \ ,$$

$$\Delta\tilde{K}^3_{13}\big|^{\text{2-sub}}(t,t') = -\frac{35}{32\sqrt{6}}\left\{t+t'-4(s_0-a)-\left(1+\frac{t}{t'}\right)\frac{16p'^2_t q'^2_t}{5t'}\right\}$$

$$\xrightarrow{\text{1-sub}}-\frac{35}{32\sqrt{6}}\left\{t'-4(s_0-a)-\frac{16p'^2_t q'^2_t}{5t'}\right\} \ , \tag{13.34}$$

where we have also indicated the reductions for the case of one subtraction, ensures the threshold behavior (12.42) also for the additional terms. Further simplifications can be made by using

$$t + t' - 4(s_0 - a) = 4(p_t'^2 + q_t^2 + a) \qquad \text{or} \qquad \frac{16 p_t'^2 q_t'^2}{t'} = t' - 4s_0 + \frac{t_N t_\pi}{t'} , \qquad (13.35)$$

and for later convenience we also give the explicit complete forms of all those subtracted kernels with $0 \le J' \le 3$ that differ from their unsubtracted form (cf. (9.57) for $\tilde{\mathbf{K}}^{JJ}$):

$$\tilde{K}_{00}^1\big|^{\text{2-sub}}(t,t') = \frac{t^2}{t'^2}\tilde{K}_{JJ}^1(t,t') \overset{\text{1-sub}}{\longrightarrow} \frac{t}{t'}\tilde{K}_{JJ}^1(t,t') ,$$

$$\tilde{K}_{11}^1\big|^{\text{2-sub}}(t,t') = \frac{t}{t'}\tilde{K}_{JJ}^1(t,t') \overset{\text{1-sub}}{\longrightarrow} \tilde{K}_{JJ}^1(t,t') ,$$

$$\tilde{K}_{02}^1\big|^{\text{2-sub}}(t,t') = \frac{5}{8}\frac{p_t^2}{p_t'^2}\left\{\left(1+\frac{t}{t'}\right)\frac{t_N t_\pi}{4t'} - \frac{t}{t'}s_0\right\} = \frac{5}{32}\frac{p_t^2}{p_t'^2}\frac{1}{t'^2}\left\{(t'+t)t_N t_\pi - t't(t_N + t_\pi)\right\}$$

$$\overset{\text{1-sub}}{\longrightarrow} \frac{5}{16}\frac{p_t^2}{p_t'^2}\left\{t + \frac{t_N t_\pi}{2t'}\right\} ,$$

$$\tilde{K}_{13}^1\big|^{\text{2-sub}}(t,t') = \frac{7}{48}\frac{p_t^2}{p_t'^2}\left\{t + \frac{3t_N t_\pi}{2t'}\right\} \overset{\text{1-sub}}{\longrightarrow} \tilde{K}_{13}^1(t,t') ,$$

$$\tilde{K}_{11}^2\big|^{\text{2-sub}}(t,t') = \frac{tt_N}{t'^2}\tilde{K}_{11}^2(t,t') \overset{\text{1-sub}}{\longrightarrow} \frac{t_N}{t'}\tilde{K}_{11}^2(t,t') ,$$

$$\tilde{K}_{22}^2\big|^{\text{2-sub}}(t,t') = \frac{t_N}{t'}\tilde{K}_{22}^2(t,t') \overset{\text{1-sub}}{\longrightarrow} \tilde{K}_{22}^2(t,t') ,$$

$$\tilde{K}_{02}^2\big|^{\text{2-sub}}(t,t') = \frac{5m}{4\sqrt{6}}\frac{p_t^2 q_t^2}{p_t'^2}\frac{t_N}{t'} \overset{\text{1-sub}}{\longrightarrow} -\frac{5m}{8\sqrt{6}}\frac{p_t^2}{p_t'^2}\left\{t + \frac{t_\pi}{2}\right\} ,$$

$$\tilde{K}_{13}^2\big|^{\text{2-sub}}(t,t') = \frac{7m}{16\sqrt{3}}\left\{\frac{p_t^2}{p_t'^2}\left[2q_t^2 - t - \frac{t_N t_\pi}{4t'}\right] + \left[\left(1+\frac{t}{t'}\right)\frac{t_N t_\pi}{4t'} - \frac{t}{t'}s_0\right]\right\}$$

$$= \frac{7m}{16\sqrt{3}}\left\{-\frac{p_t^2}{p_t'^2}\left[\frac{t+t_\pi}{2} + \frac{t_N t_\pi}{4t'}\right] + \frac{1}{4t'^2}\left[(t'+t)t_N t_\pi - t't(t_N + t_\pi)\right]\right\}$$

$$\overset{\text{1-sub}}{\longrightarrow} \frac{7m}{16\sqrt{3}}\left\{\frac{p_t^2}{p_t'^2}\left[2q_t^2 - \left(t + t' - 4s_0 + 5a\right)\right] + \left[t + \frac{t_N t_\pi}{4t'}\right]\right\} ,$$

$$\tilde{K}_{11}^3\big|^{\text{2-sub}}(t,t') = \frac{t^2}{t'^2}\tilde{K}_{JJ}^3(t,t') \overset{\text{1-sub}}{\longrightarrow} \frac{t}{t'}\tilde{K}_{JJ}^3(t,t') ,$$

$$\tilde{K}_{22}^3\big|^{\text{2-sub}}(t,t') = \frac{t}{t'}\tilde{K}_{JJ}^3(t,t') \overset{\text{1-sub}}{\longrightarrow} \tilde{K}_{JJ}^3(t,t') ,$$

$$\tilde{K}_{13}^3\big|^{\text{2-sub}}(t,t') = \frac{7}{8\sqrt{6}}\left\{\left(1+\frac{t}{t'}\right)\frac{t_N t_\pi}{4t'} - \frac{t}{t'}s_0\right\} = \frac{7}{32\sqrt{6}}\frac{1}{t'^2}\left\{(t'+t)t_N t_\pi - t't(t_N + t_\pi)\right\}$$

$$\overset{\text{1-sub}}{\longrightarrow} \frac{7}{8\sqrt{6}}\left\{t + \frac{t_N t_\pi}{4t'}\right\} . \qquad (13.36)$$

still obeying the threshold-behavior relation (12.42). Note that at the level of two subtractions all these kernels are independent of a (which is, however, not true for only one subtraction and $J \ge 3$ or without subtracting), and that the exceptionally safe behavior of $\tilde{K}_{02}^2(t,t')$ at t_N (cf. (9.61)) is preserved irrespective of the number of subtractions:

$$\tilde{K}_{02}^2\big|^{n\text{-sub}}(t \to t_N, t') = \mathcal{O}(p_t^2) \qquad \forall\, n \ge 0 . \qquad (13.37)$$

13.6 Subtracted _t_-channel Muskhelishvili–Omnès problem

Now, using the subtracted kernels and pole terms as derived in the previous section leads to the subtracted analogs of the unsubtracted _t_-channel Muskhelishvili–Omnès problem (12.44), which we will state explicitly in the following for $J \leq 2$ (remember that the equations for $J \geq 3$ are unaltered for up to two subtractions). For one subtraction we can write

$$f_+^0(t) = \Delta_+^0\big|^{\text{1-sub}}(t) - \frac{t}{\pi}\int_{t_\pi}^{\infty} dt' \frac{\operatorname{Im} f_+^0(t')}{t'(t' - t_N)} + \frac{t}{\pi}\int_{t_\pi}^{\infty} dt' \frac{\operatorname{Im} f_+^0(t')}{t'(t' - t)} \ ,$$

$$f_+^1(t) = \Delta_+^1\big|^{\text{1-sub}}(t) + \frac{t_N}{\pi}\int_{t_\pi}^{\infty} dt' \frac{\frac{m}{\sqrt{2}}\operatorname{Im} f_-^1(t') - \operatorname{Im} f_+^1(t')}{t'(t' - t_N)} + \frac{t}{\pi}\int_{t_\pi}^{\infty} dt' \frac{\operatorname{Im} f_+^1(t')}{t'(t' - t)} \ ,$$

$$f_-^1(t) = \Delta_-^1\big|^{\text{1-sub}}(t) + \frac{t}{\pi}\int_{t_\pi}^{\infty} dt' \frac{\operatorname{Im} f_-^1(t')}{t'(t' - t)} \ ,$$

$$f_+^2(t) = \Delta_+^2\big|^{\text{1-sub}}(t) + \frac{1}{\pi}\int_{t_\pi}^{\infty} dt' \frac{m\sqrt{\frac{2}{3}}\operatorname{Im} f_-^2(t') - \operatorname{Im} f_+^2(t')}{t' - t_N} + \frac{1}{\pi}\int_{t_\pi}^{\infty} dt' \frac{\operatorname{Im} f_+^2(t')}{t' - t} \ ,$$

$$f_-^2(t) = \Delta_-^2\big|^{\text{1-sub}}(t) + \frac{1}{\pi}\int_{t_\pi}^{\infty} dt' \frac{\operatorname{Im} f_-^2(t')}{t' - t} \ , \tag{13.38}$$

while two subtractions yield

$$f_+^0(t) = \Delta_+^0\big|^{\text{2-sub}}(t) - \frac{t^2}{\pi}\int_{t_\pi}^{\infty} dt' \frac{\operatorname{Im} f_+^0(t')}{t'^2(t' - t_N)} + \frac{t^2}{\pi}\int_{t_\pi}^{\infty} dt' \frac{\operatorname{Im} f_+^0(t')}{t'^2(t' - t)} \ ,$$

$$f_+^1(t) = \Delta_+^1\big|^{\text{2-sub}}(t) + \frac{t_N t}{\pi}\int_{t_\pi}^{\infty} dt' \frac{\frac{m}{\sqrt{2}}\operatorname{Im} f_-^1(t') - \operatorname{Im} f_+^1(t')}{t'^2(t' - t_N)} + \frac{t^2}{\pi}\int_{t_\pi}^{\infty} dt' \frac{\operatorname{Im} f_+^1(t')}{t'^2(t' - t)} \ ,$$

$$f_-^1(t) = \Delta_-^1\big|^{\text{2-sub}}(t) + \frac{t^2}{\pi}\int_{t_\pi}^{\infty} dt' \frac{\operatorname{Im} f_-^1(t')}{t'^2(t' - t)} \ ,$$

$$f_+^2(t) = \Delta_+^2\big|^{\text{2-sub}}(t) + \frac{t_N}{\pi}\int_{t_\pi}^{\infty} dt' \frac{m\sqrt{\frac{2}{3}}\operatorname{Im} f_-^2(t') - \operatorname{Im} f_+^2(t')}{t'(t' - t_N)} + \frac{t}{\pi}\int_{t_\pi}^{\infty} dt' \frac{\operatorname{Im} f_+^2(t')}{t'(t' - t)} \ ,$$

$$f_-^2(t) = \Delta_-^2\big|^{\text{2-sub}}(t) + \frac{t}{\pi}\int_{t_\pi}^{\infty} dt' \frac{\operatorname{Im} f_-^2(t')}{t'(t' - t)} \ , \tag{13.39}$$

where it is important to note that _S_- and _D_-waves are coupled, as Δ_+^0 contains contributions from $J = 2$ according to (12.45). While the integrands containing the Cauchy kernel in (13.38) and (13.39) for $J = 0$ and $J = 1$ clearly show the corresponding number of subtractions at $t_0 = 0$, for $J = 2$ there is always one subtraction less or no subtraction at all. Note that the integrands containing linear combinations of the partial waves are proportional to

t_N/t' (if affected by the subtractions at all), which results in a suppressed internal high-energy dependence inside the integral due to division by t' without an increased external high-energy dependence due to multiplication with t_N rather than t as for a usual subtraction at zero.

The un- (12.44), once- (13.38) and twice-subtracted (13.39) equations are of the original form of the (subtracted) Muskhelishvili–Omnès problem with integrals of the absorptive parts times the Cauchy kernel, if the remaining t-independent integrals (which may, however, come with t-dependent prefactors) are absorbed into a redefinition of the inhomogeneities $\Delta_\pm^J(t)$ (cf. (14.1)). This problem is well defined due to the threshold behavior of the partial waves at $t = t_N$. However, the price for taking advantage of the convergence properties of the integrals this way is that reasonable approximations for the starting values for the partial waves are needed as input, since the solutions can only be found iteratively.

Therefore, we prefer to utilize the threshold behavior of the partial waves and use the linear combinations $\Gamma^J(t)$ in order to rewrite the equations in analogy to (12.47), i.e. to modify the original form of the (subtracted) Muskhelishvili–Omnès problem in a well-defined manner. The general n-times subtracted (with $n \in \{0, 1, 2\}$) versions of the Muskhelishvili–Omnès equations (12.47) for all J then read

$$
f_+^0(t) = \Delta_+^0 \big|^{n\text{-sub}}(t) + \frac{t^n(t - t_N)}{\pi} \int\limits_{t_\pi}^\infty dt' \frac{\mathrm{Im}\, f_+^0(t')}{t'^n(t' - t_N)(t' - t)} \,,
$$

$$
\Gamma^J(t) = \Delta_\Gamma^J \big|^{n\text{-sub}}(t) + \frac{t^{(n-J)\theta(n-J)}(t - t_N)}{\pi} \int\limits_{t_\pi}^\infty dt' \frac{\mathrm{Im}\, \Gamma^J(t')}{t'^{(n-J)\theta(n-J)}(t' - t_N)(t' - t)} \qquad \forall\, J \geq 1 \,,
$$

$$
f_-^J(t) = \Delta_-^J \big|^{n\text{-sub}}(t) + \frac{t^{(n-J+1)\theta(n-J)}}{\pi} \int\limits_{t_\pi}^\infty dt' \frac{\mathrm{Im}\, f_-^J(t')}{t'^{(n-J+1)\theta(n-J)}(t' - t)} \qquad \forall\, J \geq 1 \,, \qquad (13.40)
$$

where the Heaviside step function is to be understood in its right-continuous form, i.e. $\theta(0) = 1$. Again, the equations for $f_+^0(t)$ and $\Gamma^J(t)$ exhibit one additional subtraction at t_N, such that the combined number of subtractions for all $J \geq 0$ can be given as $(n - J + 1)\theta(n - J)$. For convenience, we also state the explicit formulae for $J \in \{1, 2\}$ for both one subtraction

$$
\Gamma^1(t) = \Delta_\Gamma^1 \big|^{1\text{-sub}}(t) + \frac{t - t_N}{\pi} \int\limits_{t_\pi}^\infty dt' \frac{\mathrm{Im}\, \Gamma^1(t')}{(t' - t_N)(t' - t)} \,,
$$

$$
f_-^1(t) = \Delta_-^1 \big|^{1\text{-sub}}(t) + \frac{t}{\pi} \int\limits_{t_\pi}^\infty dt' \frac{\mathrm{Im}\, f_-^1(t')}{t'(t' - t)} \,,
$$

$$
\Gamma^2(t) = \Delta_\Gamma^2 \big|^{1\text{-sub}}(t) + \frac{t - t_N}{\pi} \int\limits_{t_\pi}^\infty dt' \frac{\mathrm{Im}\, \Gamma^2(t')}{(t' - t_N)(t' - t)} \,,
$$

$$
f_-^2(t) = \Delta_-^2 \big|^{1\text{-sub}}(t) + \frac{1}{\pi} \int\limits_{t_\pi}^\infty dt' \frac{\mathrm{Im}\, f_-^2(t')}{t' - t} \,, \qquad (13.41)
$$

and two subtractions

$$\Gamma^1(t) = \Delta^1_\Gamma\big|^{\text{2-sub}}(t) + \frac{t(t - t_N)}{\pi} \int\limits_{t_\pi}^{\infty} dt' \frac{\operatorname{Im}\Gamma^1(t')}{t'(t' - t_N)(t' - t)} \ ,$$

$$f^1_-(t) = \Delta^1_-\big|^{\text{2-sub}}(t) + \frac{t^2}{\pi} \int\limits_{t_\pi}^{\infty} dt' \frac{\operatorname{Im} f^1_-(t')}{t'^2(t' - t)} \ ,$$

$$\Gamma^2(t) = \Delta^2_\Gamma\big|^{\text{2-sub}}(t) + \frac{t - t_N}{\pi} \int\limits_{t_\pi}^{\infty} dt' \frac{\operatorname{Im}\Gamma^2(t')}{(t' - t_N)(t' - t)} \ ,$$

$$f^2_-(t) = \Delta^2_-\big|^{\text{2-sub}}(t) + \frac{t}{\pi} \int\limits_{t_\pi}^{\infty} dt' \frac{\operatorname{Im} f^2_-(t')}{t'(t' - t)} \ , \tag{13.42}$$

as well as the terms in $\Delta^0_+(t)$ that couple the *D*- to the *S*-waves:

$$\Delta^0_+\big|^{\text{0-sub}}(t) = -\frac{5}{16}\frac{t - t_N}{\pi} \int\limits_{t_\pi}^{\infty} dt' \left\{ \left[t' + t - (t_N + t_\pi) + 6a \right] \frac{\operatorname{Im}\Gamma^2(t')}{t' - t_N} + \frac{m}{\sqrt{6}}\operatorname{Im} f^2_-(t') \right\} + \dots \ ,$$

$$\Delta^0_+\big|^{\text{1-sub}}(t) = -\frac{5}{16}\frac{t - t_N}{\pi} \int\limits_{t_\pi}^{\infty} \frac{dt'}{t'} \left\{ \left[t't + \frac{t_N t_\pi}{2} \right] \frac{\operatorname{Im}\Gamma^2(t')}{t' - t_N} + t_\pi \frac{m}{\sqrt{6}}\operatorname{Im} f^2_-(t') \right\} + \dots \ ,$$

$$\Delta^0_+\big|^{\text{2-sub}}(t) = -\frac{5}{16}\frac{t - t_N}{\pi} \int\limits_{t_\pi}^{\infty} \frac{dt'}{t'^2} \left\{ \frac{1}{2}\left[(t' + t)t_N t_\pi - t't(t_N + t_\pi) \right] \frac{\operatorname{Im}\Gamma^2(t')}{t' - t_N} + tt_\pi \frac{m}{\sqrt{6}}\operatorname{Im} f^2_-(t') \right\}$$
$$+ \dots \ , \tag{13.43}$$

which converge for $t' \to t_N$ due to the threshold behavior of Γ^2 and vanish for $t \to t_N$ due to the exceptional behavior of the (*n*-times subtracted) kernel $\tilde{K}^2_{02}$ (cf. (9.61) and (13.37)); the respective remainder denoted by dots above is then given by

$$\dots \doteq \tilde{N}^0_+\big|^{\text{n-sub}}(t) \tag{13.44}$$

$$+ \frac{1}{\pi} \int\limits_{W_+}^{\infty} dW' \sum_{l=0}^{\infty} \left\{ \tilde{G}_{0l}\big|^{\text{n-sub}}(t, W')\operatorname{Im} f^+_{l+}(W') + \tilde{G}_{0l}\big|^{\text{n-sub}}(t, -W')\operatorname{Im} f^+_{(l+1)-}(W') \right\}$$

$$+ \frac{1}{\pi} \int\limits_{t_\pi}^{\infty} dt' \sum_{J'=4}^{\infty} \frac{1 + (-1)^{J'}}{2} \left\{ \tilde{K}^1_{0J'}\big|^{\text{n-sub}}(t, t')\operatorname{Im} f^{J'}_+(t') + \tilde{K}^2_{0J'}\big|^{\text{n-sub}}(t, t')\operatorname{Im} f^{J'}_-(t') \right\} \ .$$

Note that this *D*- to *S*-wave coupling becomes independent of a by subtracting once or twice, while the corresponding *F*- to *P*-wave coupling also depends on a in the once-subtracted case (cf. (13.36)).

13.7 Subtracted kernels: *s*-channel partial-wave projection

Finally, we summarize the changes that are necessary if the subtracted versions of the hyperbolic dispersion relations are used for the *s*-channel projection as well.

The modified pole terms are given by

$$N_{l+}^I\big|^{\text{n-sub}}(W) = \bar{N}_{l+}^I(W) + \Delta\bar{N}_{l+}^I\big|^{\text{n-sub}}(W) = -N_{(l+1)-}^I\big|^{\text{n-sub}}(-W) \,,$$

$$\Delta\bar{N}_{l+}^+\big|^{\text{2-sub}}(W) = \frac{\delta_{l0}}{16\pi W}\left\{(E+m)\left[2\left(\frac{g^2}{m} + d_{00}^+ - 2q^2 d_{01}^+\right) + (W-m)(s-s_0-q^2)\frac{b_{00}^+}{m}\right]\right.$$

$$\left. - (E-m)\frac{q^2}{3}\left(4d_{01}^+ - (W+m)\frac{b_{00}^+}{m}\right)\right\}$$

$$+ \frac{\delta_{l1}}{16\pi W}(E+m)\frac{q^2}{3}\left(4d_{01}^+ + (W-m)\frac{b_{00}^+}{m}\right)$$

$$\xrightarrow{\text{1-sub}} \frac{\delta_{l0}}{8\pi W}(E+m)\left(\frac{g^2}{m} + d_{00}^+\right),$$

$$\Delta\bar{N}_{l+}^-\big|^{\text{2-sub}}(W) = \frac{\delta_{l0}}{16\pi W}\left\{(E+m)\left[(s-s_0-q^2)\frac{a_{00}^-}{m} + 2(W-m)\left(-\frac{g^2}{2m^2} + b_{00}^- - 2q^2 b_{01}^-\right)\right]\right.$$

$$\left. - (E-m)\frac{q^2}{3}\left(\frac{a_{00}^-}{m} - 4(W+m)b_{01}^-\right)\right\}$$

$$+ \frac{\delta_{l1}}{16\pi W}(E+m)\frac{q^2}{3}\left(\frac{a_{00}^-}{m} + 4(W-m)b_{01}^-\right)$$

$$\xrightarrow{\text{1-sub}} \frac{\delta_{l0}}{8\pi W}(E+m)(W-m)\left(-\frac{g^2}{2m^2} + b_{00}^-\right), \tag{13.45}$$

where in analogy to the t-channel projection we have defined unsubtracted "corrections" (cf. (8.11))

$$\Delta\bar{N}_{l+}^I\big|^{\text{0-sub}}(W) = -\tilde{\epsilon}_-\frac{g^2}{4\pi}\frac{(E+m)(W-m)}{2W}\frac{\delta_{l0}}{m^2-a} = -\Delta\bar{N}_{(l+1)-}^I\big|^{\text{0-sub}}(-W) \,. \tag{13.46}$$

The additional s-channel kernel contributions obeying the MacDowell symmetry (8.1) in both (W,l) and (W',l') can be written for all $(l \geq 0, l' \geq 0)$ in the symmetric form

$$\Delta K_{ll'}^I(W,W') = \widetilde{\Delta K}_{ll'}^I(W,W') - \widetilde{\Delta K}_{l,l'-1}^I(W,-W')$$

$$+ \widetilde{\Delta K}_{ll'}^I(W,W') - \widetilde{\Delta K}_{l,l'-1}^I(W,-W')$$

$$+ \frac{1}{3}\left\{\widetilde{\Delta K}_{ll'}^I(-W,W') - \widetilde{\Delta K}_{l,l'-1}^I(-W,-W')\right.$$

$$\left. - \widetilde{\Delta K}_{l-1,l'}^I(W,W') + \widetilde{\Delta K}_{l-1,l'-1}^I(W,-W')\right\},$$

$$\widetilde{\Delta K}_{ll'}^I\big|^{\text{2-sub}}(W,W') = -\frac{W'}{W}\left\{\varkappa^I(W,W')h_0(s') + \varkappa^{-I}(W,W')\frac{2(s-s_0)}{(s'-s_0)^2}\right\}P_{l'+1}'\left(\left[z_s'\right]_{(0,0)}\right)\delta_{l0}$$

$$= -\frac{W'}{W}\left\{\frac{\delta(W,W')(s'+s-2s_0) + \epsilon^I\rho(W,W')(s'-s)}{(s'-s_0)^2}\right.$$

$$\left. - \frac{\varkappa^I(W,W')}{s'-a}\right\}P_{l'+1}'\left(\left[z_s'\right]_{(0,0)}\right)\delta_{l0}$$

$$\xrightarrow{\text{1-sub}} -\frac{W'}{W}\varkappa^I(W,W')h_0(s')P_{l'+1}'\left(\left[z_s'\right]_{(0,0)}\right)\delta_{l0} \,,$$

$$\widetilde{\Delta K}_{ll'}^{I}\Big|^{\text{2-sub}}(W,W') = -\frac{W'}{W}2q^2\left\{\frac{\epsilon^I\rho(W,W')}{(s'-s_0)^2}P'_{l'+1}\Big(\left[z'_s\right]_{(0,0)}\Big)\right.$$

$$\left. - \varkappa^I(W,W')h_0(s')\left[\partial_t z'_s\right]_{(0,0)}P''_{l'+1}\Big(\left[z'_s\right]_{(0,0)}\Big)\right\}\delta_{l0} \xrightarrow{\text{1-sub}} 0\ , \quad (13.47)$$

where we have used that $\epsilon^{\pm I} = \pm\epsilon^I$. Note that for $l' = 0$ the term proportional to $(s'-a)^{-1}$ cancels against the corresponding term in $K_{l0}^I(W,W')$ of (8.75) like for the nucleon pole terms (cf. the relation (8.77)).

The additional contributions to G_{lJ} and H_{lJ} may be written as

$$\Delta G_{lJ}(W,t') = \widehat{\Delta G}_{lJ}(W,t') - \widehat{\Delta G}_{l+1,J}(-W,t') \qquad \forall\ (l \geq 0, J \geq 0)\ ,$$
$$\Delta H_{lJ}(W,t') = \widehat{\Delta H}_{lJ}(W,t') - \widehat{\Delta H}_{l+1,J}(-W,t') \qquad \forall\ (l \geq 0, J \geq 1)\ , \qquad (13.48)$$

where for even J

$$\widehat{\Delta G}_{lJ}\Big|^{\text{2-sub}}(W,t') = \frac{E+m}{2W}(2J+1)\frac{(p'_t q'_t)^J}{t'p'^2_t}\left\{\left[P_J(z'_t)\right]_{(0,0)}\delta_{l0}\right.$$

$$\left. - 2q^2\left(\frac{1}{t'}\left[P_J(z'_t)\right]_{(0,0)} + \left[\partial_t P_J(z'_t)\right]_{(0,0)}\right)\left(\delta_{l0} - \frac{\delta_{l1}}{3}\right)\right\}$$

$$\xrightarrow{\text{1-sub}} \frac{E+m}{2W}(2J+1)\frac{(p'_t q'_t)^J}{t'p'^2_t}\left[P_J(z'_t)\right]_{(0,0)}\delta_{l0}\ ,$$

$$\widehat{\Delta H}_{lJ}\Big|^{\text{2-sub}}(W,t') = -\frac{E+m}{2W}\frac{2J+1}{\sqrt{J(J+1)}}\frac{(p'_t q'_t)^J}{t'p'^2_t}\left\{\left(\frac{W-m}{2q'^2_t}(s-s_0)\left[\frac{P'_J(z'_t)}{z'_t}\right]_{(0,0)}\right.\right.$$

$$\left. + m\left[z'_t P'_J(z'_t)\right]_{(0,0)}\right)\delta_{l0} - 2q^2\left(\frac{W-m}{4q'^2_t}\left[\frac{P'_J(z'_t)}{z'_t}\right]_{(0,0)}\right.$$

$$\left.\left. + m\left[\frac{1}{t'}\left[z'_t P'_J(z'_t)\right]_{(0,0)} + \left[\partial_t(z'_t P'_J(z'_t))\right]_{(0,0)}\right]\right)\left(\delta_{l0} - \frac{\delta_{l1}}{3}\right)\right\}$$

$$\xrightarrow{\text{1-sub}} -\frac{E+m}{2W}\frac{2J+1}{\sqrt{J(J+1)}}\frac{(p'_t q'_t)^J}{t'p'^2_t}m\left[z'_t P'_J(z'_t)\right]_{(0,0)}\delta_{l0}\ , \qquad (13.49)$$

and for odd J

$$\widehat{\Delta G}_{lJ}\Big|^{\text{2-sub}}(W,t') = \frac{E+m}{2W}(2J+1)\frac{(p'_t q'_t)^{J-1}}{t'p'^2_t}\frac{1}{2}\left[\frac{P_J(z'_t)}{z'_t}\right]_{(0,0)}\left\{(s-s_0-q^2)\delta_{l0}+q^2\frac{\delta_{l1}}{3}\right\}\xrightarrow{\text{1-sub}}0,$$

$$\widehat{\Delta H}_{lJ}\Big|^{\text{2-sub}}(W,t') = -\frac{E+m}{2W}\frac{2J+1}{\sqrt{J(J+1)}}\frac{(p'_t q'_t)^{J-1}}{t'p'^2_t}\left\{\left(p'^2_t(W-m)+\frac{m}{2}(s-s_0)\right)\right.$$

$$\times\left[P'_J(z'_t)\right]_{(0,0)}\delta_{l0} - 2q^2\left(\frac{m}{4}\left[P'_J(z'_t)\right]_{(0,0)}\right.$$

$$\left.\left. + p'^2_t(W-m)\left[\frac{1}{t'}\left[P'_J(z'_t)\right]_{(0,0)} + \left[\partial_t P'_J(z'_t)\right]_{(0,0)}\right]\right)\left(\delta_{l0} - \frac{\delta_{l1}}{3}\right)\right\}$$

$$\xrightarrow{\text{1-sub}} -\frac{E+m}{2W}\frac{2J+1}{\sqrt{J(J+1)}}\frac{(p'_t q'_t)^{J-1}}{t'}(W-m)\left[P'_J(z'_t)\right]_{(0,0)}\delta_{l0}\ . \qquad (13.50)$$

Note that again only even powers of momenta and z'_t occur.

Chapter 14

Generalized Muskhelishvili–Omnès problem

In the following, we will assume to know the πN partial waves $f_\pm^J(t)$ above the matching point (i.e for $t \geq t_\mathrm{m}$) as well as the phases and inelasticity parameters of the $\pi\pi$ partial waves $t_J^{I_t}(t)$ for $4M_\pi^2 = t_\pi \leq t \leq t_\mathrm{m}$ and both the πK and KN partial waves $g_J^{I_t}(t)$ and $h_\pm^J(t)$, respectively, for $4M_K^2 = t_K \leq t \leq t_\mathrm{m}$. Note that the $h_\pm^J(t)$ are the most critical ones, as they are needed in the unphysical region requiring an analytic continuation.

Under these assumptions, we have to solve equations that are of the Muskhelishvili–Omnès type [166, 167]

$$f(t) = \Delta(t) + \frac{1}{\pi} \int\limits_{t_\pi}^{t_\mathrm{m}} \mathrm{d}t' \frac{T(t')^* f(t') + \sigma(t')}{t' - t} + \frac{1}{\pi} \int\limits_{t_\mathrm{m}}^{\infty} \mathrm{d}t' \frac{\mathrm{Im}\, f(t')}{t' - t} \tag{14.1}$$

for $f(t)$ in the range $t_\pi \leq t \leq t_\mathrm{m}$, where the physical values of the integrals are obtained in the limit $t \to t + i\epsilon$ and the discontinuity of $f(t)$ across the right hand cut is given by unitarity (cf. hermitian analyticity (7.62) and the extended t-channel unitarity relation (12.27))

$$\frac{\mathrm{Disc}\, f(t)}{2i} = \mathrm{Im}\, f(t) = T(t)^* f(t)\, \theta\big(t - t_\pi\big) + \sigma(t) \ . \tag{14.2}$$

Here, $\sigma(t) \propto \theta(t - t_\sigma)$ denotes all additional inelastic contributions due to additional intermediate channels that open at the corresponding threshold energies (like especially $\bar{K}K$ intermediate states for $t \geq t_K$ in (12.27)), the inhomogeneity $\Delta(t)$ contains potential left-hand cut contributions to $f(t)$ and is real for $t_\pi \leq t$, and the amplitude $T(t)$ is given by

$$T(t) = \frac{\eta(t)e^{2i\delta(t)} - 1}{2i} \ , \qquad 0 \leq \eta(t) \leq 1 \ , \qquad 1 - \eta(t) \propto \theta(t - t_\eta) \ . \tag{14.3}$$

For infinite matching point $t_\mathrm{m} = \infty$, the solution for the elastic case (i.e. $\eta(t) = 1$ and $\sigma(t) = 0$) can be found in the original work [167], while the impact of inelastic contributions is studied in [239, 240]. Conversely, finite-matching-point considerations for the elastic problem are given in [158, 241]. In the following, the generalized case with both inelasticities and a finite matching point will be considered.

14.1   Consistency condition

The consistency condition that the imaginary part Im $f(t)$ itself must be real involves some powerful constraints from equation (14.2). To see this, in addition to (14.3) we write

$$f(t) = |f(t)|e^{i\varphi(t)} , \qquad \sigma(t) = |\sigma(t)|e^{i\chi(t)} , \qquad |\sigma(t)| \propto \theta(t - t_\sigma) , \qquad (14.4)$$

which for $t \geq t_\pi$ (i.e. Im $f(t) \neq 0$ and thus $|f(t)| \neq 0$ and $\varphi(t) \neq 0$) together with the abbreviation $\tilde{\varphi}(t) = \varphi(t) - \delta(t)$ leads to the system of equations

$$\sin\varphi(t) = \frac{1+\eta(t)}{2}\sin\delta(t)\cos\tilde{\varphi}(t) + \frac{1-\eta(t)}{2}\cos\delta(t)\sin\tilde{\varphi}(t) + \frac{|\sigma(t)|}{|f(t)|}\cos\chi(t) ,$$

$$0 = \frac{1+\eta(t)}{2}\sin\delta(t)\sin\tilde{\varphi}(t) - \frac{1-\eta(t)}{2}\cos\delta(t)\cos\tilde{\varphi}(t) + \frac{|\sigma(t)|}{|f(t)|}\sin\chi(t) , \qquad (14.5)$$

and thereby to

$$\begin{pmatrix} \frac{1-\eta(t)}{2}\sin\delta(t) & \frac{1+\eta(t)}{2}\cos\delta(t) \\ \frac{1-\eta(t)}{2}\cos\delta(t) & -\frac{1+\eta(t)}{2}\sin\delta(t) \end{pmatrix} \begin{pmatrix} \cos\tilde{\varphi}(t) \\ \sin\tilde{\varphi}(t) \end{pmatrix} = \frac{|\sigma(t)|}{|f(t)|} \begin{pmatrix} \cos\chi(t) \\ \sin\chi(t) \end{pmatrix} . \qquad (14.6)$$

First, we prove the identity of the inelastic thresholds t_η and t_σ from (14.6), which of course is also necessary for or following from the consistency of the physical picture. For $t_\pi \leq t < t_\sigma$, the vanishing right-hand side (RHS) requires that the determinant of the coefficient matrix vanishes as well in order to ensure the existence of non-trivial solutions. In this way, we find

$$\frac{1 - \eta(t)^2}{4} = 0 , \qquad (14.7)$$

which can only be fulfilled for $\eta(t) = 1$ and hence we must demand $t_\eta \geq t_\sigma$. Conversely, for $t_\pi \leq t < t_\eta$ from $\eta(t) = 1$ follows

$$\frac{|\sigma(t)|}{|f(t)|}\frac{\cos\chi(t)}{\cos\delta(t)} = \sin\tilde{\varphi}(t) = -\frac{|\sigma(t)|}{|f(t)|}\frac{\sin\chi(t)}{\sin\delta(t)} , \qquad (14.8)$$

which admits non-trivial solutions only for $\sin(\delta(t) + \chi(t)) = 0$. Excluding this fine-tuning between the phases of $T(t)$ and $\sigma(t)$, we conclude that $|\sigma(t)| = 0$ and hence $t_\sigma \geq t_\eta$. Together this proves that

$$|\sigma(t)| = 0 \iff \eta(t) = 1 , \quad \text{or} \quad t_\sigma = t_\eta . \qquad (14.9)$$

For $t_\pi \leq t < t_\sigma$, i.e. in the elastic region, (14.6) reduces to

$$\cos\delta(t)\sin\tilde{\varphi}(t) = 0 = \sin\delta(t)\sin\tilde{\varphi}(t) , \qquad (14.10)$$

and thus $\tilde{\varphi}(t) = \varphi(t) - \delta(t) = 0 \mod \pi$, which is just Watson's theorem (12.11) again. For $t \geq t_\sigma$, however, we can gain information by inverting (14.6) leading to

$$\cos\tilde{\varphi}(t) = \frac{2}{1-\eta(t)}\frac{|\sigma(t)|}{|f(t)|}\sin(\delta(t) + \chi(t)) , \qquad \sin\tilde{\varphi}(t) = \frac{2}{1+\eta(t)}\frac{|\sigma(t)|}{|f(t)|}\cos(\delta(t) + \chi(t)) ,$$

$$(14.11)$$

and thus (cf. e.g. [240])

$$\varphi(t) = \delta(t) + \arctan\left(\frac{1 - \eta(t)}{1 + \eta(t)} \cot(\delta(t) + \chi(t))\right) \mod \pi \, ,$$

$$|f(t)| = 2|\sigma(t)|\sqrt{\left(\frac{\sin(\delta(t) + \chi(t))}{1 - \eta(t)}\right)^2 + \left(\frac{\cos(\delta(t) + \chi(t))}{1 + \eta(t)}\right)^2} \, , \tag{14.12}$$

both invariant under $\delta(t) + \chi(t) \to \delta(t) + \chi(t) + n\pi$ with $n \in \mathbb{Z}_0$. In this way, both the phase $\varphi(t)$ (by additionally requiring smoothness) and the modulus $|f(t)|$ of the complex function $f(t)$ are in principle completely fixed by the inelasticities in the full unitarity relation (14.2) in the inelastic region $t \geq t_\sigma$, i.e. above the onset of the first inelastic channel. Since for $t_\pi \leq t < t_\sigma$ the phase is known due to Watson's theorem, in the elastic region we only need to solve the Muskhelishvili–Omnès problem (14.1) for the modulus $|f(t)|$.

14.2   Homogeneous problem

To begin with, we consider the homogeneous problem with finite matching point (i.e. without inhomogeneity $\Delta(t)$, also neglecting the inelastic contributions $\sigma(t)$) for a function $f_0(t)$ with $\text{Im}\, f_0(t) \propto \theta(t - t_\pi)\theta(t_\mathrm{m} - t)$ (though this problem for itself is unphysical as long as $t_\mathrm{m} < \infty$ and $\sigma(t)$ is neglected)

$$f_0(t) = \frac{1}{\pi} \int_{t_\pi}^{t_\mathrm{m}} \mathrm{d}t' \frac{T(t')^* f_0(t')}{t' - t} \, , \tag{14.13}$$

since any function $f(t)$ solving the general problem (14.1) will then generate further solutions by setting $f(t) \to f(t) + cf_0(t)$ with $c \in \mathbb{R}$. Writing $t_\pm = t \pm i\epsilon$ and taking the difference of (14.13) evaluated in both limits (i.e. calculating the discontinuity with the physical amplitude $f_0(t)$ being identified with $f_0(t_+)$), we have (though $\eta(t) = 1$ for $t < t_\sigma$, we keep the inelasticity function $\eta(t)$ in preparation for the general, inhomogeneous case in the following section)

$$\left\{ \begin{matrix} f_0(t_+)\eta(t)e^{-2i\delta(t)} - f_0(t_-) = 0 \\ f_0(t_+) - f_0(t_-) = 0 \end{matrix} \right\} \quad \text{for} \quad \left\{ \begin{matrix} t_\pi \leq t \leq t_\mathrm{m} \\ t > t_\mathrm{m} \end{matrix} \right\} \, , \tag{14.14}$$

which is solved introducing the Omnès function $\Omega(t)$ defined by

$$\left\{ \begin{matrix} \Omega(t_+)e^{-2i\delta(t)} - \Omega(t_-) = 0 \\ \Omega(t_+) - \Omega(t_-) = 0 \end{matrix} \right\} \quad \text{for} \quad \left\{ \begin{matrix} t_\pi \leq t \leq t_\mathrm{m} \\ t > t_\mathrm{m} \end{matrix} \right\} \, , \tag{14.15}$$

such that we can write

$$\Omega(t) = \exp\left\{ \frac{1}{\pi} \int_{t_\pi}^{t_\mathrm{m}} \mathrm{d}t' \frac{\delta(t')}{t' - t} \right\} = |\Omega(t)| \exp\left\{ i\delta(t)\theta(t - t_\pi)\theta(t_\mathrm{m} - t) \right\} \, ,$$

$$|\Omega(t)| = \exp\left\{ \frac{1}{\pi} \fint_{t_\pi}^{t_\mathrm{m}} \mathrm{d}t' \frac{\delta(t')}{t' - t} \right\} = |\bar{\Omega}(t)|\, |t_\mathrm{m} - t|^{x(t)} \, , \qquad x(t) = \frac{\delta(t)}{\pi} \, ,$$

$$|\bar{\Omega}(t)| = |t - t_\pi|^{-x(t)} \exp\left\{ \frac{1}{\pi} \fint_{t_\pi}^{t_\mathrm{m}} \mathrm{d}t' \frac{\delta(t') - \delta(t)}{t' - t} \right\} \, , \tag{14.16}$$

where we have analytically separated the endpoint singularities of the principal value integral such that the remaining finite integral can be evaluated without any problems. The decomposition

$$f_0(t) = \Omega(t)\Sigma_0(t) \tag{14.17}$$

then leads to

$$\left\{ \begin{matrix} \Sigma_0(t_+)\eta(t) - \Sigma_0(t_-) = 0 \\ \Sigma_0(t_+) - \Sigma_0(t_-) = 0 \end{matrix} \right\} \quad \text{for} \quad \left\{ \begin{matrix} t_\pi \leq t \leq t_\mathrm{m} \\ t > t_\mathrm{m} \end{matrix} \right\} . \tag{14.18}$$

The first equation may be rewritten as

$$\frac{1 + \eta(t)}{2}\big(\Sigma_0(t_+) - \Sigma_0(t_-)\big) - \frac{1 - \eta(t)}{2}\big(\Sigma_0(t_+) + \Sigma_0(t_-)\big) = 0 , \tag{14.19}$$

where we can identify

$$\Sigma_0(t_+) - \Sigma_0(t_-) = 2i\,\mathrm{Im}\,\Sigma_0(t) , \qquad \Sigma_0(t_+) + \Sigma_0(t_-) = 2\mathrm{Re}\,\Sigma_0(t) , \tag{14.20}$$

since both $f_0(t)$ and $\Omega(t)$ are hermitian analytic functions and pass this property on to $\Sigma_0(t)$. As a consequence of this "reality condition" [239], both parts of (14.19) have to vanish separately, such that

$$\Sigma_0(t_+) - \Sigma_0(t_-) = 0 \qquad \forall\, t \geq t_\pi , \tag{14.21}$$

i.e. $\Sigma_0(t)$ has no right-hand cut, which of course was already clear from (14.18) for $\eta(t) = 1$. By assuming the reasonable asymptotic behavior $f_0(t) \to 0$ for $t \to \infty$ (cf. (12.22)), which yields $\Sigma_0(t) \to 0$ due to $\Omega(t) \to 1$ for a finite matching point, and by excluding essential singularities, the only analytic structures of $\Sigma_0(t)$ allowed by $f_0(t)$ and $\Omega(t)$ are poles at $t = t_\pi$ and $t = t_\mathrm{m}$. At these endpoints, according to (14.16) and due to $\delta(t_\pi) = 0$ the Omnès function behaves as (cf. [214])

$$\Omega(t) \sim |t - t_\pi|^{-x(t_\pi)} \sim 1 \quad \text{for } t \to t_\pi , \qquad \Omega(t) \sim |t_\mathrm{m} - t|^{x(t_\mathrm{m})} \quad \text{for } t \to t_\mathrm{m} . \tag{14.22}$$

In this way, the regularity of $f_0(t)$ excludes poles at $t = t_\pi$ and restricts the order of the poles at $t = t_\mathrm{m}$ to

$$n = \left\lfloor \frac{\delta(t_\mathrm{m})}{\pi} \right\rfloor \in \mathbb{N}_0 . \tag{14.23}$$

For later use we also define

$$n(t) = \lfloor x(t) \rfloor , \qquad \tilde{x}(t) = x(t) - n(t) \in (0, 1) , \qquad x = x(t_\mathrm{m}) , \qquad \tilde{x} = \tilde{x}(t_\mathrm{m}) , \tag{14.24}$$

i.e. suppression of the argument t denotes evaluation at the matching point t_m. Eventually, we find (for $t < t_\sigma$)

$$\Sigma_0(t) = \frac{\mathcal{P}_{n-1}(t)}{(t_\mathrm{m} - t)^n} , \tag{14.25}$$

where $\mathcal{P}_{n-1}(t)$ is an arbitrary real polynomial of degree $n-1$ that introduces n free parameters to the Omnès problem. For $n = 0$ the homogeneous solution vanishes according to $\mathcal{P}_{-1}(t) = 0$ and no free parameter enters the problem.

14.3 Inhomogeneous problem

The calculation for the general case goes along the same lines. Starting with

$$F(t) = f(t) - \Delta(t) = \frac{1}{\pi} \int_{t_\pi}^{t_m} dt' \frac{T(t')^* f(t') + \sigma(t')}{t' - t} + \frac{1}{\pi} \int_{t_m}^{\infty} dt' \frac{\operatorname{Im} f(t')}{t' - t} , \qquad (14.26)$$

we find that

$$\left\{ \begin{array}{r} F(t_+)\eta(t)e^{-2i\delta(t)} - F(t_-) = 2i\big(T(t)^*\Delta(t) + \sigma(t)\big) \\ F(t_+) - F(t_-) = 2i \operatorname{Im} f(t) \end{array} \right\} \quad \text{for} \quad \left\{ \begin{array}{c} t_\pi \le t \le t_m \\ t > t_m \end{array} \right\} , \qquad (14.27)$$

which via the analogous decomposition

$$F(t) = \Omega(t)\Sigma(t) \qquad (14.28)$$

corresponds to

$$\left\{ \begin{array}{r} \Sigma(t_+)\eta(t) - \Sigma(t_-) = \frac{2i}{|\Omega(t)|} e^{i\delta(t)}\big(T(t)^*\Delta(t) + \sigma(t)\big) \\ \Sigma(t_+) - \Sigma(t_-) = \frac{2i}{|\Omega(t)|} \operatorname{Im} f(t) \end{array} \right\} \quad \text{for} \quad \left\{ \begin{array}{c} t_\pi \le t \le t_m \\ t > t_m \end{array} \right\} . \qquad (14.29)$$

Rewriting the first equation as

$$\frac{1+\eta(t)}{2}\big(\Sigma(t_+) - \Sigma(t_-)\big) - \frac{1-\eta(t)}{2}\big(\Sigma(t_+) + \Sigma(t_-)\big) = \frac{2i}{|\Omega(t)|} e^{i\delta(t)}\big(T(t)^*\Delta(t) + \sigma(t)\big) \quad (14.30)$$

and inferring the hermitian analyticity of $\Sigma(t)$ in analogy to the homogeneous case, we can deduce from the reality condition that for $t_\pi \le t \le t_m$

$$2i \operatorname{Im} \Sigma(t) = \operatorname{Disc} \Sigma(t) = \Sigma(t_+) - \Sigma(t_-) = \frac{2}{1+\eta(t)} \frac{2i}{|\Omega(t)|} \operatorname{Re}\left\{ e^{i\delta(t)}\big(T(t)^*\Delta(t) + \sigma(t)\big) \right\} , \qquad (14.31)$$

and therefore together with (14.29) it follows

$$\Sigma(t) = \frac{1}{\pi} \int_{t_\pi}^{t_m} dt' \frac{\frac{2}{1+\eta(t')} \operatorname{Re}\left\{ e^{i\delta(t')}\big(T(t')^*\Delta(t') + \sigma(t')\big) \right\}}{|\Omega(t')|(t' - t)} + \frac{1}{\pi} \int_{t_m}^{\infty} dt' \frac{\operatorname{Im} f(t')}{|\Omega(t')|(t' - t)} . \qquad (14.32)$$

Using the identity (since $\Delta(t)$ is real for $t_\pi \le t$)

$$\operatorname{Re}\left\{ e^{i\delta(t)} T(t)^*\Delta(t) \right\} = \frac{1+\eta(t)}{2}\Delta(t)\sin\delta(t) , \qquad (14.33)$$

the general solution (i.e. including the homogeneous solution) for $t_\pi \le t \le t_m$ then reads

$$f(t) = \Delta(t) + \Omega(t)\left\{ \frac{\mathcal{P}_{n-1}(t)}{(t_m - t)^n} + \frac{1}{\pi} \int_{t_\pi}^{t_m} dt' \frac{\Delta(t')\sin\delta(t') + \frac{2}{1+\eta(t')} \operatorname{Re}\left\{\sigma(t')e^{i\delta(t')}\right\}}{|\Omega(t')|(t' - t)} \right.$$

$$\left. + \frac{1}{\pi} \int_{t_m}^{\infty} dt' \frac{\operatorname{Im} f(t')}{|\Omega(t')|(t' - t)} \right\} , \qquad (14.34)$$

which for $\sigma(t) \to 0$ reduces to the result quoted in [158,241] (up to the question of subtractions, cf. Sect. 14.4). The solution (14.34) may also be written in terms of a principal value integral for $t_\pi \leq t' \leq t_{\mathrm{m}}$ as

$$f(t) = \left[\Delta(t)\cos\delta(t) + \frac{2i}{1+\eta(t)}\mathrm{Re}\left\{\sigma(t)e^{i\delta(t)}\right\} + |\Omega(t)|\left\{ \frac{\mathcal{P}_{n-1}(t)}{(t_{\mathrm{m}}-t)^n} \right.\right. \tag{14.35}$$
$$\left.\left. + \frac{1}{\pi}\int\limits_{t_\pi}^{t_{\mathrm{m}}}\mathrm{d}t'\frac{\Delta(t')\sin\delta(t') + \frac{2}{1+\eta(t')}\mathrm{Re}\left\{\sigma(t')e^{i\delta(t')}\right\}}{|\Omega(t')|(t'-t)} + \frac{1}{\pi}\int\limits_{t_{\mathrm{m}}}^{\infty}\mathrm{d}t'\frac{\mathrm{Im}\, f(t')}{|\Omega(t')|(t'-t)} \right\}\right]e^{i\delta(t)} \,,$$

in accordance with [167] for $\sigma(t) \to 0$ and $t_{\mathrm{m}} \to \infty$. Based upon the parameterizations (14.4), we can finally decompose (14.35) into its real and imaginary part. For $t < t_\sigma$ (i.e. for t below the lowest inelastic threshold and hence $\sigma(t) = 0$) no imaginary part occurs in the prefactor and thus we can immediately read off both the phase $\varphi(t) = \delta(t)$ (in accordance with Watson's theorem (12.11)) and the modulus

$$|f(t)| = \Delta(t)\cos\delta(t) + |\Omega(t)|\left\{ \frac{\mathcal{P}_{n-1}(t)}{(t_{\mathrm{m}}-t)^n} + \frac{1}{\pi}\int\limits_{t_{\mathrm{m}}}^{\infty}\mathrm{d}t'\frac{\mathrm{Im}\, f(t')}{|\Omega(t')|(t'-t)} \right.$$
$$\left. + \frac{1}{\pi}\int\limits_{t_\pi}^{t_{\mathrm{m}}}\mathrm{d}t'\frac{\Delta(t')\sin\delta(t') + \frac{2|\sigma(t')|}{1+\eta(t')}\cos(\delta(t')+\chi(t'))}{|\Omega(t')|(t'-t)} \right\} \,. \tag{14.36}$$

For $t \geq t_\sigma$ (i.e. $\sigma(t) \neq 0$), the non-trivial imaginary part in the prefactor in (14.35) is non-zero; furthermore, the polynomial part due to the homogeneous solution vanishes. Decomposing (14.35) into real and imaginary parts again, inserting the resulting constraint into the equation for the generic real part of $f(t)$ and using the relations (14.11) for $\varphi(t) - \delta(t)$ reproduces the result (14.12) for $|f(t)|$. In this sense, (14.35) is consistent with (14.12) for $t \geq t_\sigma$. In particular, (14.35) carries no additional information that could help to pin down $|f(t)|$ independently of (14.12) above the inelastic threshold (i.e. for $t_\sigma \leq t \leq t_{\mathrm{m}}$).

14.4 Subtractions

Recalling (14.16) and (14.24), however, we note that for $x > 1$ the integrals of (14.36) in the present form do not converge. In order to ensure integrability for $t' \to t_{\mathrm{m}}$ suitable subtractions need to be performed. Let us begin with the case $1 < x < 2$, i.e. $n = 1$. The identity

$$\frac{1}{t'-t} = \frac{1}{t_{\mathrm{m}}-t}\left\{ 1 + \frac{t_{\mathrm{m}}-t'}{t'-t} \right\} = \frac{1}{t_{\mathrm{m}}-t}\left\{ \frac{t_{\mathrm{m}}}{t'} + \frac{t}{t'}\frac{t_{\mathrm{m}}-t'}{t'-t} \right\} \tag{14.37}$$

leads e.g. to

$$\int\limits_{t_{\mathrm{m}}}^{\infty}\mathrm{d}t'\frac{\mathrm{Im}\, f(t')}{|\Omega(t')|(t'-t)} = \frac{1}{t_{\mathrm{m}}-t}\left\{ t_{\mathrm{m}}\int\limits_{t_{\mathrm{m}}}^{\infty}\frac{\mathrm{d}t'}{t'}\frac{\mathrm{Im}\, f(t')}{|\Omega(t')|} + t\int\limits_{t_{\mathrm{m}}}^{\infty}\frac{\mathrm{d}t'}{t'}\frac{t_{\mathrm{m}}-t'}{|\Omega(t')|}\frac{\mathrm{Im}\, f(t')}{t'-t} \right\} \,, \tag{14.38}$$

where the second integral is now convergent. The first integral is still divergent, of course, but it does not depend on t any more and can thus be absorbed into a redefinition of the

(constant) polynomial $\mathcal{P}_0$ in (14.36) due to the common prefactor $(t_{\mathrm{m}} - t)^{-1}$. Note that by choosing the second identity of (14.37) rather than the first one we can additionally introduce a subtraction in the usual sense (i.e. in order to lessen the dependence of the integrals on the high-energy region), and that no more such additional subtractions are compatible with this redefinition procedure. For higher values of x this subtraction and redefinition prescription needs to be iterated, whereby all n parameters contained in the polynomial receive corresponding contributions. Applying this reasoning to both integrals of (14.36) for general x and using the highest number of subtractions allowed by the degree of the polynomial, the result for $t \leq t_\sigma \leq t_{\mathrm{m}}$ is given by[#1]

$$|f(t)| = \Delta(t)\cos\delta(t) + \frac{|\Omega(t)|}{(t_{\mathrm{m}} - t)^n} \Bigg\{ \mathcal{P}_{n-1}(t) + \frac{t^n}{\pi} \int\limits_{t_{\mathrm{m}}}^{\infty} \frac{\mathrm{d}t'}{t'^n} \frac{(t_{\mathrm{m}} - t')^n}{|\Omega(t')|} \frac{\operatorname{Im} f(t')}{t' - t}$$

$$+ \frac{t^n}{\pi} \int\limits_{t_\pi}^{t_{\mathrm{m}}} \frac{\mathrm{d}t'}{t'^n} \frac{(t_{\mathrm{m}} - t')^n}{|\Omega(t')|} \frac{\Delta(t')\sin\delta(t') + \frac{2|\sigma(t')|}{1+\eta(t')}\cos(\delta(t') + \chi(t'))}{t' - t} \Bigg\} . \tag{14.39}$$

In order to reduce the influence of the high-energy contributions on the Omnès integrals, subtractions may also be introduced already right from the beginning (14.1) by rewriting e.g.

$$\int\limits_{t_\pi}^{\infty} \mathrm{d}t' \frac{\operatorname{Im} f(t')}{t' - t} = \int\limits_{t_\pi}^{\infty} \mathrm{d}t' \frac{\operatorname{Im} f(t')}{t'} + t \int\limits_{t_\pi}^{\infty} \frac{\mathrm{d}t'}{t'} \frac{\operatorname{Im} f(t')}{t' - t} \tag{14.40}$$

and absorbing terms like the first one into a redefinition of $\Delta(t)$ at the cost of increasing the dependence of the solution of the Omnès problem on the starting value for $f(t)$ and thus potentially deteriorating its convergence properties when iterating the problem, cf. the discussion in Sect. 13.6. After l such subtractions, the analog of (14.39) becomes ($t \leq t_\sigma \leq t_{\mathrm{m}}$)

$$|f(t)| = \Delta(t)\cos\delta(t) + \frac{t^l |\Omega(t)|}{(t_{\mathrm{m}} - t)^n} \Bigg\{ \mathcal{P}_{n-1}(t) + \frac{t^n}{\pi} \int\limits_{t_{\mathrm{m}}}^{\infty} \frac{\mathrm{d}t'}{t'^{n+l}} \frac{(t_{\mathrm{m}} - t')^n}{|\Omega(t')|} \frac{\operatorname{Im} f(t')}{t' - t}$$

$$+ \frac{t^n}{\pi} \int\limits_{t_\pi}^{t_{\mathrm{m}}} \frac{\mathrm{d}t'}{t'^{n+l}} \frac{(t_{\mathrm{m}} - t')^n}{|\Omega(t')|} \frac{\Delta(t')\sin\delta(t') + \frac{2|\sigma(t')|}{1+\eta(t')}\cos(\delta(t') + \chi(t'))}{t' - t} \Bigg\}$$

$$= \Delta(t)\cos\delta(t) + t^l (t_{\mathrm{m}} - t)^{\tilde{x}(t)} |\bar{\Omega}(t)| \Bigg\{ \mathcal{P}_{n-1}(t) + \frac{(-t)^n}{\pi} \int\limits_{t_{\mathrm{m}}}^{\infty} \frac{\mathrm{d}t'}{t'^{n+l}} \frac{\operatorname{Im} f(t')}{(t' - t_{\mathrm{m}})^{\tilde{x}(t')} |\bar{\Omega}(t')| (t' - t)}$$

$$+ \frac{t^n}{\pi} \int\limits_{t_\pi}^{t_{\mathrm{m}}} \frac{\mathrm{d}t'}{t'^{n+l}} \frac{\Delta(t')\sin\delta(t') + \frac{2|\sigma(t')|}{1+\eta(t')}\cos(\delta(t') + \chi(t'))}{(t_{\mathrm{m}} - t')^{\tilde{x}(t')} |\bar{\Omega}(t')| (t' - t)} \Bigg\} . \tag{14.41}$$

This constitutes our final general result and e.g. for $l = 1$ and $n \in \{0, 1\}$ it reduces to the results quoted in [158] (for $\sigma(t) \to 0$, cf. (14.34)).

[#1]Of course, less subtractions can always be achieved by a suitable redefinition of the polynomial.

Note that for a finite matching point[#2] the use of subtracted Omnès functions involves no conceptual changes, since e.g. for one subtraction at zero the decomposition

$$\tilde{\Omega}(t) = \exp\left\{ \frac{t}{\pi} \int_{t_\pi}^{t_m} \frac{\mathrm{d}t'}{t'} \frac{\delta(t')}{t' - t} \right\} = \exp\left\{ -\frac{1}{\pi} \int_{t_\pi}^{t_m} \mathrm{d}t' \frac{\delta(t')}{t'} \right\} \Omega(t) \tag{14.42}$$

shows that the difference is just a multiplicative and t-independent constant that cancels in (14.41) between Omnès functions in the numerator and denominator (up to a redefinition of the polynomial). More generally, each l-times subtracted Omnès function

$$\Omega^{(l)}(t) = \exp\left\{ \left[\prod_{i=1}^{l}(t - t_i) \right] \frac{1}{\pi} \int_{t_\pi}^{t_m} \mathrm{d}t' \left[\prod_{i=1}^{l}(t' - t_i) \right]^{-1} \frac{\delta(t')}{t' - t} \right\} \tag{14.43}$$

with subtraction points $t_i < t_\pi$ also fulfills the defining property (14.15) of the general Omnès function and obeys the same behavior at the endpoints of integration for $t \to t_\pi$ and $t \to t_m$. However, the asymptotic behavior for $t \to \infty$ is given by $\Omega^{(0)}(t) = \Omega(t) \to 1$, $\Omega^{(1)}(t) \to \text{const}$ and $\Omega^{(l \geq 2)}(t) \to 0$, which is most easily seen for identical subtraction points $t_i = t_0$ for all i using (13.9).

14.5 Numerical treatment

The asymptotic behavior of the Omnès function $|\Omega(t)|$ for $t \to t_m$ requires some care in the numerical evaluation of the integrals in (14.41). Since by construction $\tilde{x} < 1$, the corresponding singularities for $t' \to t_m$ are integrable. However, this cusp generates large contributions to the integral and a fully numerical treatment would require a very careful distribution of mesh points in order to catch the effect. In the following, we will demonstrate how these endpoint singularities can be separated analytically (cf. the appendix of [158]). For the sake of simplicity, we discuss here only the case of $n = l = 0$ and vanishing inelasticities, which already displays all relevant features; the generalization is then straightforward. To this end, we split the integrals close to the matching point t_m and approximate $|\Omega(t)|$ by its asymptotic form in the proximity of t_m

$$|\Omega(t \approx t_m)| \approx |\bar{\Omega}(t_m)| \, |t_m - t|^x \, . \tag{14.44}$$

For $\tau \to 0^+$, we may thus rewrite the integrals above the matching point as

$$\int_{t_m}^{\infty} \mathrm{d}t' \frac{\mathrm{Im}\, f(t')}{|\Omega(t')|(t' - t)} = \int_{t_m+\tau}^{\infty} \mathrm{d}t' \frac{\mathrm{Im}\, f(t')}{|\Omega(t')|(t' - t)} + \frac{\mathrm{Im}\, f(t_m)}{|\bar{\Omega}(t_m)|} \int_{t_m}^{t_m+\tau} \frac{\mathrm{d}t'}{|t_m - t'|^x(t' - t)}$$

$$= \int_{t_m+\tau}^{\infty} \mathrm{d}t' \frac{\mathrm{Im}\, f(t')}{|\Omega(t')|(t' - t)} + \frac{\mathrm{Im}\, f(t_m)}{|\bar{\Omega}(t_m)|(t_m - t)^x} I_+(t) \, , \tag{14.45}$$

[#2]For $t_m \to \infty$ the subtraction is of course needed to ensure the convergence of the integral (for the usual assumptions on the behavior of the phase, e.g. $\lim_{t\to\infty} \delta(t) = \pi$). Furthermore, one subtraction at zero normalizes the Omnès function to unity: $\tilde{\Omega}(0) = 1$.

and similarly below the matching point either for $t_\pi \leq t < t_{\mathrm{m}} - \tau$ (whence $0 < \tilde{\tau}(t) < 1$) as

$$\int\limits_{t_\pi}^{t_{\mathrm{m}}} \mathrm{d}t' \frac{\Delta(t')\sin\delta(t')}{|\Omega(t')|(t'-t)} = \int\limits_{t_\pi}^{t_{\mathrm{m}}-\tau} \frac{\mathrm{d}t'}{t'-t}\left(\frac{\Delta(t')\sin\delta(t')}{|\Omega(t')|} - \frac{\Delta(t)\sin\delta(t)}{|\Omega(t)|}\right)$$
$$+ \frac{\Delta(t)\sin\delta(t)}{|\Omega(t)|}\log\frac{t_{\mathrm{m}}-\tau-t}{t-t_\pi} + \frac{\Delta(t_{\mathrm{m}})\sin\delta(t_{\mathrm{m}})}{|\bar{\Omega}(t_{\mathrm{m}})|(t_{\mathrm{m}}-t)^x}I_-(t)\,, \qquad (14.46)$$

where it is important to note that the log-term equals zero for $t = t_\pi$ since the phase vanishes at the $\pi\pi$ threshold, or for $t_{\mathrm{m}} - \tau \leq t \leq t_{\mathrm{m}}$ (whence $\tilde{\tau}(t) \geq 1$) as

$$\int\limits_{t_\pi}^{t_{\mathrm{m}}} \mathrm{d}t' \frac{\Delta(t')\sin\delta(t')}{|\Omega(t')|(t'-t)} = \int\limits_{t_\pi}^{t_{\mathrm{m}}-\tau} \frac{\mathrm{d}t'}{t'-t}\frac{\Delta(t')\sin\delta(t')}{|\Omega(t')|} + \frac{\Delta(t_{\mathrm{m}})\sin\delta(t_{\mathrm{m}})}{|\bar{\Omega}(t_{\mathrm{m}})|(t_{\mathrm{m}}-t)^x}\tilde{I}_-(t)\,, \qquad (14.47)$$

where the substitution $v(t') = (t'-t_{\mathrm{m}})/(t_{\mathrm{m}}-t)$ leads to the integrals (with $x \in (0,1)$)

$$I_\pm(t) = \int\limits_0^{\tilde{\tau}(t)} \frac{\mathrm{d}v}{v^x(1\pm v)} = \frac{\tilde{\tau}(t)^{1-x}}{1-x} \mp \int\limits_0^{\tilde{\tau}(t)} \mathrm{d}v\frac{v^{1-x}}{1\pm v}\,, \qquad \tilde{\tau}(t) = \frac{\tau}{t_{\mathrm{m}}-t}\,,$$

$$\tilde{I}_-(t) = \int\limits_0^{\tilde{\tau}(t)} \frac{\mathrm{d}v}{v^x(1-v)} = -\log|\tilde{\tau}(t)-1| + \frac{\tilde{\tau}(t)^{1-x}}{1-x} + \int\limits_0^{\tilde{\tau}(t)} \mathrm{d}v\frac{v^{1-x}-1}{1-v}\,. \qquad (14.48)$$

Separating the singularities as shown above, the remaining integrals can be solved by using standard integration routines. For sufficiently small τ (i.e. if τ is of the same order of magnitude as the discretization error of the integration routine), the above approximations are well justified and this procedure allows for a stable numerical evaluation of the Omnès integrals.

14.6 Continuity at the matching point

The continuity of the Omnès solution $f(t)$ at the matching point t_{m} (i.e. $t \to t_{\mathrm{m}}$ from below for fixed small but non-zero τ) is analytically ensured by the asymptotic forms of the corresponding integrals of (14.48) (with $0 < x < 1$, cf. the appendix of [158])

$$I_+(t_{\mathrm{m}}) = \int\limits_0^\infty \frac{\mathrm{d}v}{v^x(1+v)} = \frac{\pi}{\sin\pi x} = \pi\operatorname{cosec}\pi x\,,$$

$$\tilde{I}_-(t_{\mathrm{m}}) = \int\limits_0^\infty \frac{\mathrm{d}v}{v^x(1-v)} = -\pi\frac{\cos\pi x}{\sin\pi x} = -\pi\cot\pi x\,, \qquad (14.49)$$

that can be proven by relying on Cauchy's theorem and taking appropriate combinations of different paths in the complex plane.[#3] Taking equation (14.36) in the limit $t \to t_{\mathrm{m}}$ from

---

[#3]These results agree with those quoted in [158]. Though not essential here, it is interesting to note that both $\pi\operatorname{cosec}\pi x$ and $\pi\cot\pi x$ are meromorphic in the entire complex x-plane with single poles at all integers $n \in \mathbb{Z}_0$ with residues $(-1)^n$ and 1, respectively. Furthermore, we can identify $\pi\operatorname{cosec}\pi x = \Gamma(1-x)\Gamma(x)$ due to Euler's reflection formula for the usual gamma function, while the reflection formula for the digamma function $\Psi(x)$ defined in (13.22) reads $\pi\cot\pi x = \Psi(1-x) - \Psi(x)$. Due to their nice properties these functions are often used in the Sommerfeld–Watson transform in order to rewrite the sum of an infinite sequence as a contour integral, e.g. in the derivation of Regge theory (see for instance [174]).

below, plugging in these asymptotic forms of the integrals and using $x = \delta(t_\mathrm{m})/\pi$ indeed reduces the RHS to $|f(t_\mathrm{m})|$. This analytical equality may also be used as a check of the numerical evaluation.

However, the continuity of the first and higher derivatives is not ensured in a similar manner. Since the solution must not depend on the value of the matching point, an unphysical cusp or non-smooth behavior of the modulus of the solution at the matching point only indicates that the input in terms of the absorptive part is not precise enough or even physically inconsistent (so-called "non-analytic input", cf. [168,169]); moreover, the physical condition of a smooth behavior at the matching point ensures the uniqueness of the solution [168].[#4] Physically consistent input given, this smoothness constraint may be used in order to tune/estimate/fit the subtraction constants (i.e. subthreshold parameters, cf. e.g. [158]).

[#4]Furthermore, in [169] it is shown that also a matching point in the inelastic region admits a unique non-cusp solution provided that the inelasticity parameter η is known and sufficiently smooth.

Chapter 15

Solving the t-channel Muskhelishvili–Omnès problem

In this chapter the solution of the Muskhelishvili–Omnès problem for the lowest t-channel partial waves $f_\pm^J(t)$ with $J \in \{0,1,2\}$ will be discussed. First, the explicit analytical solutions will be stated. Then, the numerical input needed will be collected. Finally, the numerical results will be discussed.

15.1 Explicit analytical solutions

Here, we will give the explicit solutions for the n-times subtracted t-channel Muskhelishvili–Omnès problem (13.40) using the general results of Chap. 14. The crucial ingredient for the following discussion is Watson's theorem (12.11), which states that below the onset of inelasticities the phases $\varphi_\pm^J(t) = \delta_J(t)$ of the t-channel partial waves $f_\pm^J(t)$ are given by the corresponding $\pi\pi$ scattering phases $\delta_J^{I_t}(t)$ with $I_t \in \{0,1\}$, i.e. explicitly for $J \in \{0,1,2\}$[1]

$$\varphi_+^0(t) = \delta_0^0(t) = \delta_0(t)\,, \quad \varphi_\pm^1(t) = \delta_1^1(t) = \delta_1(t)\,, \quad \varphi_\pm^2(t) = \delta_2^0(t) = \delta_2(t)\,, \qquad \forall\, t \in [t_\pi, t_\sigma)\,. \tag{15.1}$$

These identities enter the solutions at two places: first, in this kinematical region we can use the same Omnès function Ω_J for both $f_\pm^J$ and thus also for the linear combination Γ^J. Second, in this range of t the linear relation (12.37) is also valid for the moduli such that after solving for $\left|\Gamma^J\right|$ we can recover

$$\left|f_+^J(t)\right| = m\sqrt{\frac{J}{J+1}}\left|f_-^J(t)\right| - \left|\Gamma^J(t)\right| \qquad \forall\, t \in [t_\pi, t_\sigma)\,. \tag{15.2}$$

Using once-subtracted (at $t_0 = 0$) Omnès functions in the finite matching point prescription, i.e. the integrals converge also in the limit $t_{\rm m} \to \infty$ for phases constant or smoothly approaching π above $t_{\rm m}$ and the Omnès functions themselves are normalized to unity at $t = 0$ (cf. (14.16) and (14.42)),

$$\Omega_J(t) = \exp\left\{\frac{t}{\pi}\int_{t_\pi}^{t_{\rm m}} \frac{{\rm d}t'}{t'}\frac{\delta_J(t')}{t'-t}\right\} = \left|\Omega_J(t)\right|\exp\left\{i\delta_J(t)\theta(t-t_\pi)\theta(t_{\rm m}-t)\right\}\,, \qquad \Omega_J(0) = 1\,,$$

---

[1]Though possible in principle, for the sake of simplicity we refrain from introducing J-dependent inelastic thresholds t_σ^J here (cf. the discussion in Sect. 12.1) as well as J-dependent matching points $t_{\rm m}^J$ (cf. Sect. 15.3.3).

$$\left|\Omega_J(t)\right| = \left|1 - \frac{t}{t_{\mathrm{m}}}\right|^{x_J(t)} \left|\frac{t}{t_\pi} - 1\right|^{-x_J(t)} \exp\left\{\frac{t}{\pi} \int\limits_{t_\pi}^{t_{\mathrm{m}}} \mathrm{d}t' \frac{\delta_J(t') - \delta_J(t)}{t'} \frac{1}{t' - t}\right\}, \qquad x_J(t) = \frac{\delta_J(t)}{\pi},$$

$$(15.3)$$

the general n-times subtracted (with $n \in \{0, 1, 2\}$) solutions of (13.40) for $t \in [t_\pi, t_{\mathrm{m}}]$ and for $t_{\mathrm{m}} < t_\sigma$ and $\lfloor \delta_J(t_{\mathrm{m}})/\pi \rfloor = 0$ (i.e. neglecting inelasticities and no occurrence of polynomial terms) read

$$f_+^0(t) = \Delta_+^0\big|^{n\text{-sub}}(t) + \Omega_0(t)\frac{t^n(t - t_N)}{\pi}\left\{\int\limits_{t_\pi}^{t_{\mathrm{m}}} \mathrm{d}t' \frac{\Delta_+^0\big|^{n\text{-sub}}(t')\sin\delta_0(t')}{t'^n(t' - t_N)|\Omega_0(t')|(t' - t)}\right.$$

$$\left. + \int\limits_{t_{\mathrm{m}}}^{\infty} \mathrm{d}t' \frac{\mathrm{Im}\, f_+^0(t')}{t'^n(t' - t_N)|\Omega_0(t')|(t' - t)}\right\},$$

$$\Gamma^J(t) = \Delta_\Gamma^J\big|^{n\text{-sub}}(t) + \Omega_J(t)\frac{t^{(n-J)\theta(n-J)}(t - t_N)}{\pi}\left\{\int\limits_{t_\pi}^{t_{\mathrm{m}}} \mathrm{d}t' \frac{\Delta_\Gamma^J\big|^{n\text{-sub}}(t')\sin\delta_J(t')}{t'^{(n-J)\theta(n-J)}(t' - t_N)|\Omega_J(t')|(t' - t)}\right.$$

$$\left. + \int\limits_{t_{\mathrm{m}}}^{\infty} \mathrm{d}t' \frac{\mathrm{Im}\, \Gamma^J(t')}{t'^{(n-J)\theta(n-J)}(t' - t_N)|\Omega_J(t')|(t' - t)}\right\} \qquad \forall\, J \geq 1,$$

$$f_-^J(t) = \Delta_-^J\big|^{n\text{-sub}}(t) + \Omega_J(t)\frac{t^{(n-J+1)\theta(n-J)}}{\pi}\left\{\int\limits_{t_\pi}^{t_{\mathrm{m}}} \mathrm{d}t' \frac{\Delta_-^J\big|^{n\text{-sub}}(t')\sin\delta_J(t')}{t'^{(n-J+1)\theta(n-J)}|\Omega_J(t')|(t' - t)}\right.$$

$$\left. + \int\limits_{t_{\mathrm{m}}}^{\infty} \mathrm{d}t' \frac{\mathrm{Im}\, f_-^J(t')}{t'^{(n-J+1)\theta(n-J)}|\Omega_J(t')|(t' - t)}\right\} \qquad \forall\, J \geq 1. \qquad (15.4)$$

Expanding these solutions about $t = 0$ and matching them to the original problem (13.40), as well as enforcing the correct threshold behavior for $p_t \to 0$, shows that the solutions indeed take the form of (15.4), i.e. no additional terms proportional to the corresponding lowest powers of t are generated by expanding (15.4), e.g. for $f_+^0(t) - \Delta_+^0\big|^{2\text{-sub}}(t)$ we have

$$\frac{t^2(t - t_N)}{t' - t} = \Omega_0(t)\frac{t^2(t - t_N)}{t' - t} + \mathcal{O}(t^3). \qquad (15.5)$$

Now, we can use the spectral representations of the inverse of the Omnès functions in the un-, once- and twice-subtracted form

$$\Omega_J^{-1}(t) = \frac{1}{\Omega_J(t)} = \frac{1}{\pi}\int\limits_{t_\pi}^{t_{\mathrm{m}}} \mathrm{d}t' \frac{\mathrm{Im}\, \Omega_J^{-1}(t')}{t' - t} = -\frac{1}{\pi}\int\limits_{t_\pi}^{t_{\mathrm{m}}} \mathrm{d}t' \frac{\sin\delta_J(t')}{|\Omega_J(t')|(t' - t)}$$

$$= 1 - \frac{t}{\pi}\int\limits_{t_\pi}^{t_{\mathrm{m}}} \mathrm{d}t' \frac{\sin\delta_J(t')}{t'|\Omega_J(t')|(t' - t)} = 1 - t\,\dot\Omega_J(0) - \frac{t^2}{\pi}\int\limits_{t_\pi}^{t_{\mathrm{m}}} \mathrm{d}t' \frac{\sin\delta_J(t')}{t'^2|\Omega_J(t')|(t' - t)}, \qquad (15.6)$$

using the derivative of the Omnès function[#2]

$$\dot{\Omega}_J(0) = \frac{\mathrm{d}}{\mathrm{d}t}\Omega_J(t)\Big|_{t=0} = \frac{1}{\pi}\int\limits_{t_\pi}^{t_\mathrm{m}}\mathrm{d}t'\frac{\delta_J(t')}{t'^2}\ , \tag{15.7}$$

in order to explicitly perform the integrals over terms that are either constant or come with appropriate factors of t' or $p_t'^2$, i.e. all terms involving the subthreshold parameters as well as the term proportional to $\delta_{J1}/(m^2 - a)$ for the unsubtracted case. For this purpose we define $\tilde{\Delta}_\pm^J(t)$ via removing all constant or subthreshold-parameter contributions from the inhomogeneities $\Delta_\pm^J(t)$ (cf. (12.45) and (13.27))

$$\tilde{\Delta}_\pm^J\big|^{n\text{-sub}}(t) = \Delta_\pm^J\big|^{n\text{-sub}}(t) - \Delta\hat{N}_\pm^J\big|^{n\text{-sub}}(t) = \hat{N}_\pm^J(t) + \bar{\Delta}_\pm^J\big|^{n\text{-sub}}(t)\ , \tag{15.8}$$

and thereby we obtain

$$f_+^0(t) = \tilde{\Delta}_+^0\big|^{n\text{-sub}}(t) + \Omega_0(t)\frac{t - t_N}{\pi}\bigg\{\chi_+^0\big|^{n\text{-sub}}(t)$$

$$+ t^n\bigg[\int\limits_{t_\pi}^{t_\mathrm{m}}\mathrm{d}t'\frac{\tilde{\Delta}_+^0\big|^{n\text{-sub}}(t')\sin\delta_0(t')}{t'^n(t' - t_N)|\Omega_0(t')|(t' - t)} + \int\limits_{t_\mathrm{m}}^\infty\mathrm{d}t'\frac{\mathrm{Im}\,f_+^0(t')}{t'^n(t' - t_N)|\Omega_0(t')|(t' - t)}\bigg]\bigg\}\ ,$$

$$\Gamma^J(t) = \tilde{\Delta}_\Gamma^J\big|^{n\text{-sub}}(t) + \Omega_J(t)\frac{t - t_N}{\pi}\bigg\{\chi_\Gamma^J\big|^{n\text{-sub}}(t)$$

$$+ t^{(n-J)\theta(n-J)}\bigg[\int\limits_{t_\pi}^{t_\mathrm{m}}\mathrm{d}t'\frac{\tilde{\Delta}_\Gamma^J\big|^{n\text{-sub}}(t')\sin\delta_J(t')}{t'^{(n-J)\theta(n-J)}(t' - t_N)|\Omega_J(t')|(t' - t)}$$

$$+ \int\limits_{t_\mathrm{m}}^\infty\mathrm{d}t'\frac{\mathrm{Im}\,\Gamma^J(t')}{t'^{(n-J)\theta(n-J)}(t' - t_N)|\Omega_J(t')|(t' - t)}\bigg]\bigg\}\quad \forall\,J \geq 1\ ,$$

$$f_-^J(t) = \tilde{\Delta}_-^J\big|^{n\text{-sub}}(t) + \Omega_J(t)\frac{1}{\pi}\bigg\{\chi_-^J\big|^{n\text{-sub}}(t)$$

$$+ t^{(n-J+1)\theta(n-J)}\bigg[\int\limits_{t_\pi}^{t_\mathrm{m}}\mathrm{d}t'\frac{\tilde{\Delta}_-^J\big|^{n\text{-sub}}(t')\sin\delta_J(t')}{t'^{(n-J+1)\theta(n-J)}|\Omega_J(t')|(t' - t)}$$

$$+ \int\limits_{t_\mathrm{m}}^\infty\mathrm{d}t'\frac{\mathrm{Im}\,f_-^J(t')}{t'^{(n-J+1)\theta(n-J)}|\Omega_J(t')|(t' - t)}\bigg]\bigg\}\quad \forall\,J \geq 1\ , \tag{15.9}$$

with

$$\chi_+^0\big|^{2\text{-sub}}(t) = -\frac{1}{16}\bigg\{\bigg[\frac{g^2}{m} + d_{00}^+ + t_\pi\frac{b_{00}^+}{12}\bigg]\big(1 - t\,\dot{\Omega}_0(0)\big) + \bigg[d_{01}^+ - \frac{b_{00}^+}{12}\bigg]t\bigg\}\ ,$$

$$\xrightarrow{1\text{-sub}} -\frac{1}{16}\bigg[\frac{g^2}{m} + d_{00}^+\bigg] \xrightarrow{0\text{-sub}} 0\ ,$$

[#2]Note that for $t_\mathrm{m} \to \infty$ (and neglecting inelasticities in the single-channel approximation) this quantity is closely related to the pion vector (charge) radius for $J = 1$: $\lim_{t_\mathrm{m}\to\infty}\dot{\Omega}_1 = \frac{1}{6}\langle r^2\rangle_\pi^V$.

$$\chi_\Gamma^J\big|^{\text{2-sub}}(t) = \frac{1}{12}\frac{a_{00}^-}{4m}\delta_{J1} \xrightarrow{\text{1-sub}} 0 \xrightarrow{\text{0-sub}} 0\,,$$

$$\chi_-^J\big|^{\text{2-sub}}(t) = \frac{\sqrt{2}}{12}\left\{\left[-\frac{g^2}{2m^2}+b_{00}^-\right](1-t\,\dot\Omega_1(0))+b_{01}^- t\right\}\delta_{J1} + \frac{\sqrt{6}}{15}\frac{b_{00}^+}{4m}\delta_{J2}$$

$$\xrightarrow{\text{1-sub}} \frac{\sqrt{2}}{12}\left[-\frac{g^2}{2m^2}+b_{00}^-\right]\delta_{J1} \xrightarrow{\text{0-sub}} 0\,. \tag{15.10}$$

Note that also in the unsubtracted case the explicit dependence on a cancels.[#3]

Finally, due to Watson's theorem (12.11) we can separate the unknown moduli from the known $\pi\pi$ phases for $t < t_\sigma$ and solve the MO problem for the moduli directly

$$\big|f_+^0(t)\big| = \tilde\Delta_+^0\big|^{n\text{-sub}}(t)\cos\delta_0(t) + (t-t_N)\frac{|\Omega_0(t)|}{\pi}\left\{\chi_0^J\big|^{n\text{-sub}}(t)\right.$$

$$\left. + t^n\left[\int_{t_\pi}^{t_{\rm m}}\mathrm{d}t'\,\frac{\tilde\Delta_+^0\big|^{n\text{-sub}}(t')\sin\delta_0(t')}{t'^n(t'-t_N)|\Omega_0(t')|(t'-t)} + \int_{t_{\rm m}}^{\infty}\mathrm{d}t'\,\frac{\operatorname{Im}f_+^0(t')}{t'^n(t'-t_N)|\Omega_0(t')|(t'-t)}\right]\right\},$$

$$\big|\Gamma^J(t)\big| = \tilde\Delta_\Gamma^J\big|^{n\text{-sub}}(t)\cos\delta_J(t) + (t-t_N)\frac{|\Omega_J(t)|}{\pi}\left\{\chi_\Gamma^J\big|^{n\text{-sub}}(t)\right.$$

$$ + t^{(n-J)\theta(n-J)}\left[\int_{t_\pi}^{t_{\rm m}}\mathrm{d}t'\,\frac{\tilde\Delta_\Gamma^J\big|^{n\text{-sub}}(t')\sin\delta_J(t')}{t'^{(n-J)\theta(n-J)}(t'-t_N)|\Omega_J(t')|(t'-t)}\right.$$

$$\left.\left. + \int_{t_{\rm m}}^{\infty}\mathrm{d}t'\,\frac{\operatorname{Im}\Gamma^J(t')}{t'^{(n-J)\theta(n-J)}(t'-t_N)|\Omega_J(t')|(t'-t)}\right]\right\} \qquad \forall\,J\geq 1\,,$$

$$\big|f_-^J(t)\big| = \tilde\Delta_-^J\big|^{n\text{-sub}}(t)\cos\delta_J(t) + \frac{|\Omega_J(t)|}{\pi}\left\{\chi_-^J\big|^{n\text{-sub}}(t)\right.$$

$$ + t^{(n-J+1)\theta(n-J)}\left[\int_{t_\pi}^{t_{\rm m}}\mathrm{d}t'\,\frac{\tilde\Delta_-^J\big|^{n\text{-sub}}(t')\sin\delta_J(t')}{t'^{(n-J+1)\theta(n-J)}|\Omega_J(t')|(t'-t)}\right.$$

$$\left.\left. + \int_{t_{\rm m}}^{\infty}\mathrm{d}t'\,\frac{\operatorname{Im}f_-^J(t')}{t'^{(n-J+1)\theta(n-J)}|\Omega_J(t')|(t'-t)}\right]\right\} \qquad \forall\,J\geq 1\,. \tag{15.11}$$

On the one hand, the subtraction-independent pole terms $\hat N_\pm^J$ are real for $t\geq t_\pi-(M_\pi^2/m)^2$ and grow rapidly with J for t in the vicinity of t_π, as discussed in Sect. 9.1. On the other

---

[#3]Actually, this has to be the case: e.g. the constant term proportional to $(m^2-a)^{-1}$ in the nucleon pole terms (7.99), which was introduced to the dispersion relations via the hyperbolic kinematical relations and which can be thought of as a contribution of the contour integral from the circle with infinite radius (i.e. for $|t|\to\infty$), leads to constant pole-term contributions to the partial waves (cf. (9.15) and (13.28)). These (unphysical) contributions do not vanish asymptotically, generate an unphysical behavior on a, and thus they must cancel in any (physical) solution. Hence, the dispersion integrals for the unsubtracted case both for the Omnès solution and the spectral representation of the Omnès function are strictly speaking not correct: there should be contributions from the contour at infinity. However, this problem can be solved most easily by removing all "dangerous" parts of the inhomogeneities via (15.6), which ensures that all these potential contributions from the contour at infinity cancel.

hand, in the elastic region the phases δ_J are given by the corresponding $\pi\pi$ scattering phases such that $\delta_J(t_\pi) = 0$ and thus $\mathrm{Im}\, f_\pm^J(t_\pi) = 0$. Since furthermore phenomenologically the $\pi\pi$ phases grow slower for higher J, we expect the partial waves $f_\pm^J$ (and thereby also their moduli $|f_\pm^J|$) to be increasingly dominated by the pole terms for increasing J and $t \to t_\pi$. However, we do not solve for f_+^J directly but for the linear combinations Γ^J, for which in turn the pole-term contributions $\hat{N}_\pm^J$ cancel at t_π, cf. Sect. 13.5. The pole-term domination of $|f_+^J|$ enters when calculating these parallel helicity moduli from the solutions for the $|\Gamma^J|$ and the (pole-term dominated) antiparallel helicity moduli $|f_-^J|$ via (15.2), where in addition the relative importance of the latter increases with J due to the factor $\sqrt{J/(J+1)}$. For $|f_+^J|$ both the pole-term domination and the dependence on $|f_-^J|$ will be explicitly demonstrated in Sect. 15.3.

15.2 Numerical input

In this section we will discuss all numerical input that is needed to solve the t-channel Muskhelishvili–Omnès problem (15.11) as given in Sect. 15.1.

15.2.1 $\pi\pi$ phases and Omnès functions

We use the (preliminary) $\pi\pi$ scattering phase shifts $\delta_J^{I_t}(t)$ of [154,155] for $J \in \{0, 1, 2\}$ with $I_t \in \{0, 1\}$ (and I_t even/odd for J even/odd) which are constructed for $\sqrt{t} \in [2M_\pi, 1.15\,\mathrm{GeV}]$.[#4] We reconstruct the phase shifts from the real and imaginary parts of the corresponding $\pi\pi$ scattering partial waves according to (cf. (12.6))

$$\delta_J^{I_t}(t) = \frac{1}{2}\left\{ \arctan \frac{2\sigma_t^\pi \,\mathrm{Re}\, t_J^{I_t}(t)}{1 - 2\sigma_t^\pi \,\mathrm{Im}\, t_J^{I_t}(t)} \mod \pi \right\} \overset{\eta_J^{I_t}(t)=1}{=} \arcsin \sqrt{\sigma_t^\pi \,\mathrm{Im}\, t_J^{I_t}(t)} \mod \pi \,,$$

(15.12)

using the fact that the inelasticity is proportional to the real part of the partial wave. Furthermore, we ensure both the vanishing at threshold $\delta_J^{I_t}(t_\pi) = 0$ as well as the correct square-root-power behavior above threshold by matching the phase shifts at and above t_π to Schenk-like parameterizations [53, 243]

$$\tan \delta_J^{I_t}(t) = \sigma_t^\pi q_t^{2J}\left\{ A_J^{I_t} + B_J^{I_t} q_t^2 + C_J^{I_t} q_t^4 + D_J^{I_t} q_t^6 \right\} \frac{t_\pi - r_J^{I_t}}{t - r_J^{I_t}} \,,$$

(15.13)

where the parameters $r_J^{I_t}$ denotes the point where the corresponding phase shift passes through $\pi/2$ (i.e. the squared mass of the first resonance). Therefore, δ_0^0 is linear, δ_1^1 cubic, and δ_2^0 quintic in σ_t^π.[#5] Furthermore, the Schenk parameters may be related to the coefficients of the threshold expansion

$$\mathrm{Re}\, t_J^{I_t}(t) = q_t^{2J}\left\{ a_J^{I_t} + b_J^{I_t} q_t^2 + c_J^{I_t} q_t^4 + d_J^{I_t} q_t^6 + \mathcal{O}(q_t^8) \right\} \,,$$

(15.14)

[#4]For $\pi\pi$ scattering the validity of the Roy equations can be shown rigorously for $t_\pi \leq t \leq 60M_\pi^2$ based on axiomatic field theory [52]. Assuming Mandelstam analyticity, this range can be extended to $t_\pi \leq t \leq 68M_\pi^2$ [242], which corresponds to $2M_\pi \leq \sqrt{t} \leq 1.15\,\mathrm{GeV}$ by reasoning along the lines of Chap. 10.

[#5]Here, we restrict ourselves to matching up to and including cubic powers of σ_t^π. While without this matching particularly the S-wave Omnès function Ω_0 exhibits an unphysical and sizable dint upwards just above t_π, matching up to and including also the fifth power of σ_t^π (as leading contribution for the D-waves) does not lead to significant changes.
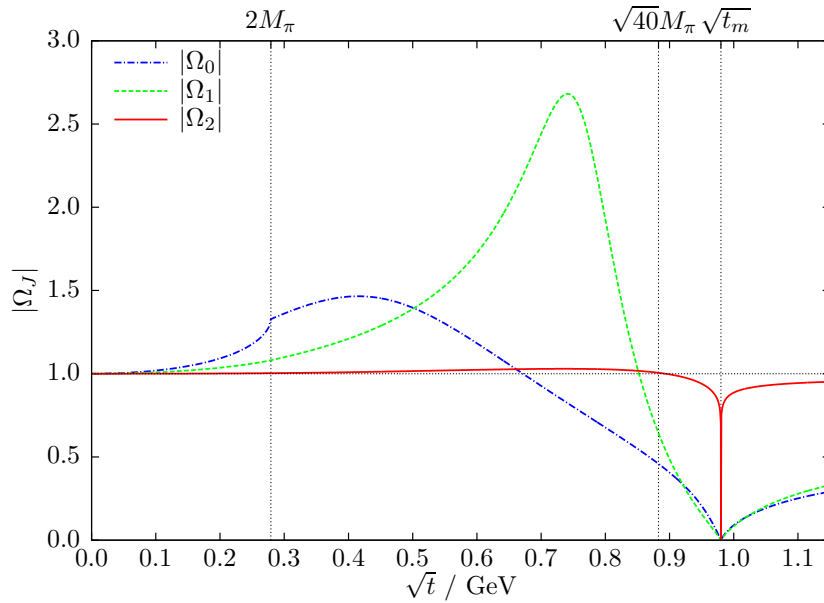
Figure 15.1: Moduli $|\Omega_J|$ of the lowest once-subtracted finite-matching-point Omnès functions for $\sqrt{t_{\mathrm{m}}} = 0.98\,\mathrm{GeV}$.

since in the elastic region (cf. (12.6))

$$\operatorname{Re} t_J^{I_t}(t) = \cot \delta_J^{I_t}(t) \operatorname{Im} t_J^{I_t}(t) = \frac{1}{\sigma_t^{\pi}} \frac{\tan \delta_J^{I_t}(t)}{1 + \tan^2 \delta_J^{I_t}(t)} \;, \tag{15.15}$$

such that e.g. for the scattering lengths $a_J^{I_t}$ and the effective ranges/volumes/etc. $b_J^{I_t}$ we get

$$a_J^{I_t} = A_J^{I_t} \;, \qquad b_J^{I_t} = B_J^{I_t} + \frac{4}{r_J^{I_t} - t_{\pi}} A_J^{I_t} + \delta_{J0} \frac{4}{t_{\pi}} \big(A_J^{I_t}\big)^3 \;. \tag{15.16}$$

In Fig. 15.1 we show the moduli $|\Omega_J|$ of the resulting once-subtracted finite-matching-point Omnès functions according to (15.3) for $J \in \{0, 1, 2\}$, where the choice $\sqrt{t_{\mathrm{m}}} = 0.98\,\mathrm{GeV}$ ensures that $x_J(t) \in (0,1)$ and hence $n_J = \lfloor x_J(t_{\mathrm{m}}) \rfloor = 0$ for $t \in [t_\pi, t_{\mathrm{m}}]$. Therefore all functions are normalized to unity at $t = 0$, finite for all t, and vanish at $t = t_{\mathrm{m}}$ due to the finite-matching-point prefactor $|t_{\mathrm{m}} - t|^{x_J(t)}$. Furthermore, for $J = 0$ the Omnès function exhibits a cusp (i.e. a discontinuity of the derivative) at the physical $\pi\pi$ threshold t_π and decreases approximately linearly over a wide range in t, for $J = 1$ it is fully dominated by the $\rho(770)$ peak, and for $J = 2$ it is almost flat (equaling 1 again roughly at the end of the KH80 energy range at $0.88\,\mathrm{GeV}$ and dropping rapidly above).[#6]

Using instead the parameterization of the $\pi\pi$ phases as given in [153] for the numerical evaluations in Sect. 15.3 leads to deviations in these Omnès functions and thereby the solutions of the Muskhelishvili–Omnès problem (15.11) which are much smaller, however, than the effects of the alterations described there.[#7]

[#6]Note that by construction these Omnès functions describe the contributions of the so-called two-pion continuum to the _t_-channel partial waves (assuming elastic $\pi\pi$ scattering). In fact, the importance of the two-pion continuum for the nucleon structure (i.e. the nucleon form factors, cf. Sect. 15.3.4) especially for the _P_-wave has lead to the _prediction_ of the ρ-resonance [244].

[#7]As stated in [171], the Karlsruhe–Helsinki dispersive partial-wave analyses KH78 and KH80 (see Sect. 15.2.2

15.2.2 Remarks on existing πN partial-wave analyses

Before summarizing the input from πN partial-wave analyses that will be used in the following, some general remarks are in order: first of all, we will use the time-honored Karlsruhe-Helsinki dispersive partial-wave analysis KH80 [170, 171] both as input for s-channel partial waves as well as subthreshold parameters and as reference for our MO t-channel partial-wave solutions, since KH80 is still the only consistent analysis for all the partial waves and parameters entailed in our Roy–Steiner framework. KH80 is based on $\pi N \to \pi N$ data only (besides isospin invariance) and uses Pietarinen's expansion method [246] in combination with conformal mapping techniques, aided in particular by fixed-t analyticity.[#8] Its solutions for both channels are given as tables in [171], wherein (p. 10) also an iteration uncertainty of about $3\,\%$ is stated for the given results of the iterative KH80 procedure.[#9] Since the KH80 partial-wave solutions exhibit sizable fluctuations, many efforts have been undertaken to improve the KH80 analysis. In [248], for instance, two different approaches to remove these fluctuations are advertised: on the one hand the subsequent Karlsruhe analysis KA84 [250] and on the other hand the πN s-channel PWHDRs proposed by [161] (mentioning work in progress, which is most probably contained in [225]). While KA84 indeed improves on KH80 especially for higher partial waves by using a modified PWDR framework and thereby smoothing KH80, unfortunately no consistent subthreshold parameters are derived in this framework.[#10] Moreover, according to [162, 165, 172] the KH80 analysis seems to suffer from internal inconsistencies (as well as KA84), hinting at possible issues with its analytic properties in the low-energy regime.[#11]Concerning HDRs on the other hand, in particular the pivotal role of the t-channel input for the reliability of the s-channel solutions of the PWHDRs of [161] is emphasized in [165]. Also for the continuously updated VPI/GWU(SAID) s-channel analyses, see e.g. [204, 252–254], at most the πN coupling constant and small subsets of the necessary subthreshold parameters are determined. For the t-channel partial waves in the unphysical region $t \in [t_\pi, t_N]$, there also exists an unpublished solution [213] extending the KH80 energy range $\sqrt{t} \in [2M_\pi, \sqrt{40}M_\pi = 0.88\,\text{GeV}]$ to roughly $1\,\text{GeV}$. While this solution is compatible with KH80 within the aforementioned range, it seems to suffer from internal inconsistencies for higher energies.[#12] For the t-channel partial waves in the physical region $t \geq t_N$, however, there exists a partial-wave analysis [255], which at least in principle could be used as

---

for more details) use as input the $\pi\pi$ phase shifts of [245], which are based on Roy-equation fits. In principle, the differences between these phase shifts and the recent results [153–155] are sources of discrepancies between the KH80 results and the solutions of the MO problem. However, this point is of minor importance for the results discussed in Sect. 15.3.

[#8]In general, analyticity constraints are necessary to get rid of ambiguities in πN partial-wave analyses, cf. [247]. Interestingly, the importance of a new and complete partial-wave analysis of πN scattering with hyperbolic analyticity constraints (in order to account for the t-channel properly) especially for determining $\sigma_{\pi N}$ was already pointed out a long time ago [162].

[#9]In [171], the results for the t-channel partial waves are quoted as KH78 solution, but according to [163] these tables are actually calculated from the KH80 s-channel solutions. Thus we will speak of the t-channel partial waves in [171] as KH80 solution as well. In general, KH80 is an update of KH78 including more recent data and particularly improved fixed-t analyticity constraints. Note, however, that according to [248] in particular the KH80 t-channel P-wave solutions as given in [249] are slightly wrong (there, notably, the t-channel partial wave solutions are given up to $\sqrt{t} \leq \sqrt{60}M_\pi = 1.08\,\text{GeV}$), whereas the results in [171] (given for $\sqrt{t} \leq \sqrt{40}M_\pi = 0.88\,\text{GeV}$) are correct.

[#10]For a comparison of KH80 with KA84 (and for an improvement of the formalism outlined in [206]), see [251].

[#11]For instance, *"indications for some fairly large systematic errors of unknown origin"* in both KH80 and KA84 are found in [172] (p. 178) when inspecting the πN S-wave scattering lengths.

[#12]There are e.g. rather obvious outliers (corresponding to unphysical jumps) in the phases.
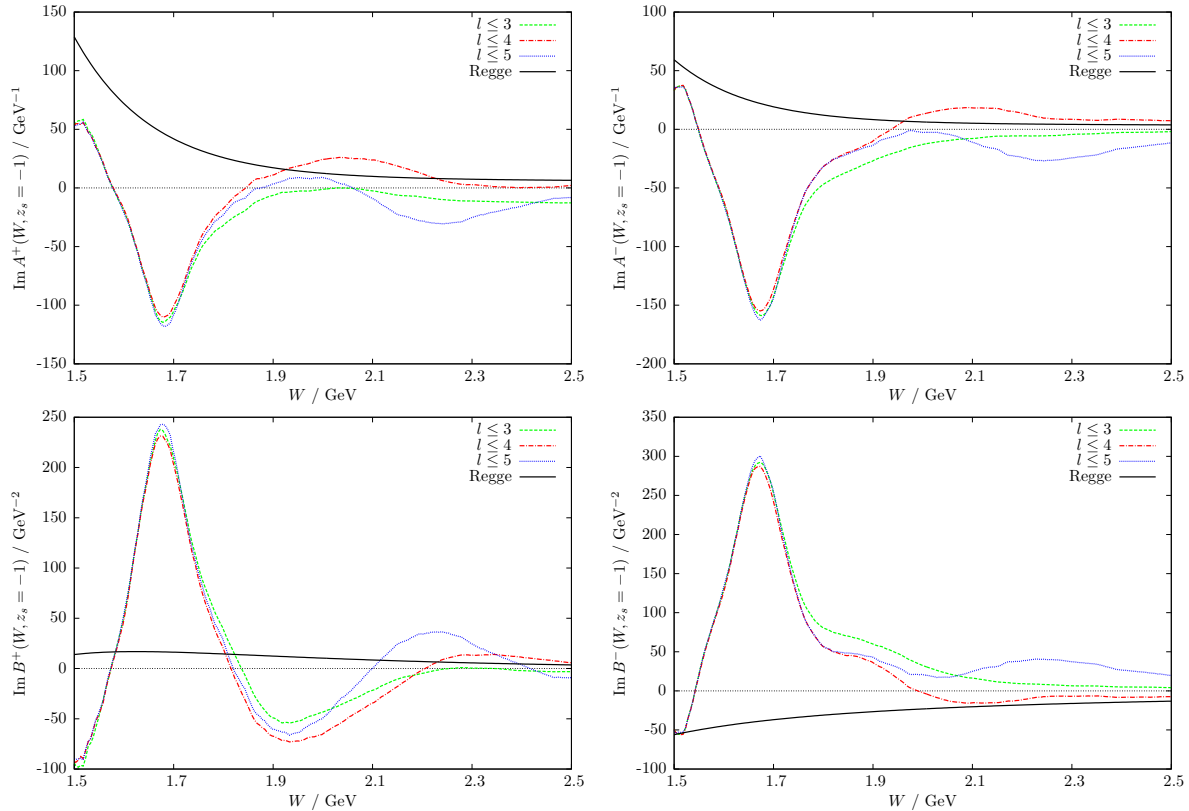
Figure 15.2: Matching of the *s*-channel absorptive parts between KH80 partial-wave contributions for $l \leq 3$, $l \leq 4$, and $l \leq 5$ and the πN backward scattering Regge model [228].

input.[#13] Finally, a partial update of the KH80 analysis including new data and using more computational power was reported in [259], but so far only results for forward πN scattering have been published [260].

15.2.3　*s*-channel partial waves

We use the KH80 solution for the *s*-channel partial waves from [254] for $W_+ \leq W \leq W_a = 2.5\,\text{GeV}$.[#14] On the one hand, this is roughly the same energy range as for the GWU "current solution" [254],[#15] so that we are able to compare between KH80 and GWU solutions as input. However, the effect of taking the current GWU solution instead as input for the *t*-channel Omnès problem (i.e. on the corresponding inhomogeneities $\tilde{\Delta}_{\pm}^{J}$) turns out to be much

---

[#13]Note also previous work on $\bar{N}N \to \pi\pi$: in particular, in [256] the πN invariant amplitudes are determined in the *t*-channel physical region by using (parametric) HDRs in order to be able to incorporate empirical information on the *s*-channel reaction. These results are then used as constraints in an analysis of the *t*-channel partial waves of πN scattering in [257] (for an energy-dependent update of this analysis see [258]).

[#14]Note that this corresponds to a slightly "smoothed" version of the original KH80 solution. We have checked, however, that both the effect of this smoothing of KH80 as well as the deviations induced by reading in the data for either KH80 or GWU solution from [254] in different energy steps (e.g. 2 MeV instead of 5 MeV, yielding effects especially close to threshold, but with smaller steps leading to an even more noisy behavior of the partial waves and thus the invariant amplitudes) are at least as small as the difference between KH80 and GWU solutions themselves.

[#15]While $W \leq 2.458\,\text{GeV}$ is stated for the solution SP06 [204], e.g. the update [253] already gives $W \leq 2.6\,\text{GeV}$.

smaller than the effects discussed in Sect. 15.3 and is hence neglected in the following. On the other hand, at $W_{\mathrm{a}} = 2.5\,\mathrm{GeV}$ a reasonable transition from the truncated sum of partial waves below W_{a} to the Regge model for the full invariant amplitudes above W_{a} can be achieved as we will demonstrate now (cf. Chap. 11). Summing up all partial waves with $l \leq 5$ would entail all 4-star resonances of [176], but of both 4-star resonances with $l = 5$, $N(2220)$ as $H_{1,9}$ and $\Delta(2420)$ as $H_{3,11}$ (spectroscopic notation: $l_{2I_s,2j}$), especially the latter one is mostly out of this energy range due to its broad width of roughly $700\,\mathrm{MeV}$. Hence we expect the best agreement with the Regge model [228], which is based on differential cross section and polarization data for πN backward scattering with $W \geq 3\,\mathrm{GeV}$ as discussed in Sect. 11.1, for $l \leq 4$ and a scattering angle of $z_s = -1$ corresponding to backward scattering. Since deviations between summing up contributions for $l \leq 3$, $l \leq 4$ and $l \leq 5$ start to show up around $1.5\,\mathrm{GeV}$ and we are interested in the matching to the Regge model at the end of the GWU range of validity around $2.5\,\mathrm{GeV}$, only this region is shown in Fig. 15.2 (in the spirit of [158]).[#16] Note that only $l \leq 4$ yields the correct sign compared to the Regge contribution in all four cases. Moreover, it turns out that for $l \leq 5$ the agreement is even worse than for $l \leq 3$. Hence, in the following all higher partial waves with $l \geq 5$ will be neglected below W_{a}. The higher kernel functions that are needed to account for these higher s-channel partial waves in both the s- and t-channel driving terms are collected in Apps. C.1 and C.2, respectively.

15.2.4 t-channel partial waves

Although it is tempting to employ direct experimental information in terms of the existing t-channel partial-wave analysis [255] as input above the physical threshold t_N, one would first need to fully account for the pseudophysical range $t_\pi \leq t \leq t_N$. However, as already mentioned before (cf. Sects. 11.2 and 12.1), there are significant inelastic contributions to the lowest partial waves already far below t_N (starting roughly around $\sqrt{t_N}/2$). In principle, there are several ways how inelasticities may be accommodated in a single-channel description of the t-channel MO problem. Since the general situation is similar for all of the lowest partial waves, in the following we will exemplarily discuss the S-wave f_+^0 (being the most important and also the most "problematic" partial wave at the same time), for which the assumption of elastic unitarity breaks down as soon as the $\bar{K}K$ channel opens, manifesting itself in the appearance of the $f_0(980)$ resonance.

First, inelastic contributions could be included directly in the solution of the MO equations using the formalism developed in Chap. 14, provided, however, that the inelasticities are sufficiently well known. The importance of this precondition becomes particularly obvious in view of the fact that above the onset of inelasticities the solutions are (in principle) fully determined by the (complete) inelasticities as discussed in Sects. 14.1 and 14.3. However, in the case of f_+^0 this method would in particular require knowledge of the $\bar{K}K \to \bar{N}N$ S-wave, but it is unclear how reliable input for this partial wave can be obtained independently from the present approach.

Second, one could retain a rather low matching point t_{m}, but try to model the energy region above t_{m} by means of a resonance description in order to establish a more meaningful matching condition. This strategy proved quite successful in $\gamma\gamma \to \pi\pi$ [159], where the input above the matching point is dominated by the $f_2(1270)$. However, in the case of the $f_0(980)$ this strategy is subject to several difficulties: its pole position is very close to the

---

[#16]Note that the absorptive parts $\mathrm{Im}\,A^\pm$ exhibit pronounced peaks at $W_+ + M_\pi$ (cf. Sect. 10.1). Of course, all imaginary parts are zero at the threshold W_+.

two-kaon threshold, such that the subtle interplay between the $\pi\pi$ and $\bar{K}K$ channels can certainly not be approximated by a simple Breit–Wigner (BW) description. To circumvent this problem, one would be compelled to further decrease the matching point and include the $f_0(980)$ dynamics by hand using a Flatté-like parameterization [261] (see also e.g. [262]), which is a modified relativistic version of the BW differential mass distribution. However, while the $f_0\pi\pi$ coupling constant has been thoroughly investigated [263] based on the recent dispersive analysis [153] (which yields phases that are basically consistent with the phases of [154, 155]), the f_0NN coupling constant is only very poorly known, with different meson-exchange models disagreeing significantly on the strength of the coupling and the continuation to the physical pole [264–267].

We conclude that including the $f_0(980)$ in our approach reliably as well as extending the energy range of our representation for f_+^0 beyond the two-kaon threshold will require a full solution of the underlying two-channel Omnès problem [173], whereas in this work we will content ourselves with the single-channel approximation.

Within the single-channel formalism, we thus can solve the MO problem for the lowest t-channel partial waves consistently in the elastic region only.[#17] Since furthermore iteration with the s-channel RS solutions (for which in turn accurate MO solutions are needed as input) as well as a consistent determination of the πN coupling and the subthreshold parameters is necessary to finally arrive at precise quantitative results for the partial waves of both channels, here we will only give qualitative results for the t-channel partial waves by comparing with KH80. Hence, in the following all t-channel absorptive parts above t_m are neglected (i.e. set to zero) and consequently also all t-channel Regge contributions are omitted (since $t_\mathrm{m} < t_\mathrm{a}$; cf. the discussion of the t-channel asymptotics in Sect. 11.2).[#18] Finally, also all higher partial waves with $J \geq 3$ are neglected.

15.2.5   Subthreshold parameters

To precisely determine the subthreshold parameters is not an easy task, since there simply is no experimental data available to analyze the t-dependence of the amplitudes close to $t = 0$ and thus means of analytic continuation or extrapolation are needed. Accordingly, in the literature there are only a few determinations of all parameters that enter the subtracted Roy–Steiner system. The KH80 results (cf. [171], wherein the error estimates are quoted to be *"based on deviations from the internal consistency"* and the total uncertainty to be *"somewhat larger"* (p. 275)) and all more recent dispersion theoretical analyses that we are aware of are collected in Tab. 15.1 (cf. [160]). Note that there are several determinations of only some of these parameters, which are therefore not listed in Tab. 15.1.[#19]

In [164] the subthreshold parameters are determined by means of interior dispersion relations together with fixed-t dispersion relations and by using as input the s-channel partial waves of both KA84 [250] and VPI/SP98 [252] (see also [272]) as well as the t-channel partial

---

[#17]Basically, the reconstruction of the partial waves above the matching point up to t_N via either inelasticities or resonance models fails to yield meaningful results in view of the deficient present knowledge of both the corresponding inelasticities and the couplings of $\pi\pi$ and $\bar{N}N$ to the pertinent resonances. Loosely speaking, the physical region turns out to be too far away from the onset of inelasticities in order to sufficiently constrain and thereby aid the reconstruction of the input absorptive parts in the range $t \in [t_\mathrm{m}, t_N]$.

[#18]Note that otherwise one would have to avoid double counting of the asymptotic regions of the t-channel partial waves in the MO problem.

[#19]E.g. $d_{00}^+ = -1.30/M_\pi$ and $d_{01}^+ = 1.27/M_\pi^3$ [252] as well as the same d_{00}^+ but $d_{01}^+ = 1.19/M_\pi^3$ [268] based on the VPI/SP98 solution [252], or $d_{00}^+ = (-1.20 \pm 0.03)/M_\pi$ and $d_{00}^- = a_{00}^- + b_{00}^- = (1.41 \pm 0.05)/M_\pi^2$ in [260].

	KH80	St(KA84)	St(SP98)	Oa(KH80)	Oa(SP98)	Fe
d_{00}^+ $[M_\pi^{-1}]$	-1.46 ± 0.10	-1.39 ± 0.02	-1.32 ± 0.02	-1.46 ± 0.04	-1.29 ± 0.02	-1.58
d_{01}^+ $[M_\pi^{-3}]$	1.14 ± 0.02	1.14 ± 0.01	1.15 ± 0.02	1.15 ± 0.11	1.23 ± 0.04	1.36
a_{00}^- $[M_\pi^{-2}]$	-8.83 ± 0.10	-8.82 ± 0.04	-8.97 ± 0.01	-9.26 ± 0.17	-8.92 ± 0.07	-8.47
b_{00}^+ $[M_\pi^{-3}]$	-3.54 ± 0.06	-3.49 ± 0.03	-3.48 ± 0.02	-3.56 ± 0.10	-3.42 ± 0.04	-7.90
b_{00}^- $[M_\pi^{-2}]$	10.36 ± 0.10	10.35 ± 0.02	10.45 ± 0.01	10.84 ± 0.18	10.37 ± 0.08	10.34
b_{01}^- $[M_\pi^{-4}]$	0.24 ± 0.01	0.22 ± 0.01	0.24 ± 0.01	0.26 ± 0.22	0.26 ± 0.10	0.14

Table 15.1: Subthreshold parameter values as given by KH80/Höhler [171], Stahov [164], Oades [269, 270], and Fettes (heavy-baryon ChPT, KA84) [271]. See main text for details.

waves of KH80 (and those of [213] in the consistent energy range).[20] In contrast, finite-contour dispersion relations are used in [269] to derive subthreshold parameter values — again for both KH80 and VPI/SP98 input (amongst others).[21] The subthreshold parameters are the standard expansion parameters for the Lorentz-invariant amplitudes, but neither these amplitudes nor the kinematical variables ν and t are "natural" for heavy-baryon ChPT and hence these values are not very satisfactory, cf. [270]. However, for comparison we also state the corresponding values for a third-order calculation [271, 273] as given in [271] (Fit 1 therein corresponding to KA84); note that according to [271, 274] some of the parameter values even deteriorate when calculated up to fourth order.

As can be seen already from the deviations between the different determinations of sub-threshold parameters in Tab. 15.1, the errors on the central values are in general unrealistically small (i.e. only statistical "fit errors" for specific input in a given framework, thus neglecting systematic errors). Hence we can conclude that there is no precise and consistent determination of the subthreshold parameters including realistic errors.

Since we want to compare our MO results with the KH80 solutions, for consistency we use the KH80 subthreshold parameters as given in Tab. 15.1 as well as the outdated KH80 πN pseudoscalar coupling value of 14.28 instead of the new value of 13.7 as given in (7.100).[22]

15.3 Numerical results

The numerical results that will be presented in this section are to be understood as a qualitative "KH80 consistency check" in order to show that the t-channel RS-MO machinery works, and as a first step towards a numerical analysis of the full Roy–Steiner system. In particular, by variation of either the coupling or the subthreshold parameters we can alter the results

---

[20]These are most probably the "new" subthreshold parameters mentioned in [247], where no explicit reference is given unfortunately.

[21]Note that some of the results of [269] are corrected in [270], where also a modified version of the finite-contour dispersion relations together with conformal mapping techniques is applied (it is mentioned therein that the subthreshold parameters do not change substantially). Since the applied fitting procedure does not respect the exact analytic equality of the parameters d_{0n}^+ and a_{0n}^+ (cf. (13.5)), however, the (corrected) values agree only within the given errors, but not exactly.

[22]Note that the πN coupling and the subthreshold parameters are related, as the difference $d_{00}^- - g^2/(2m)$ is given by an integral over a total cross section, cf. [160].
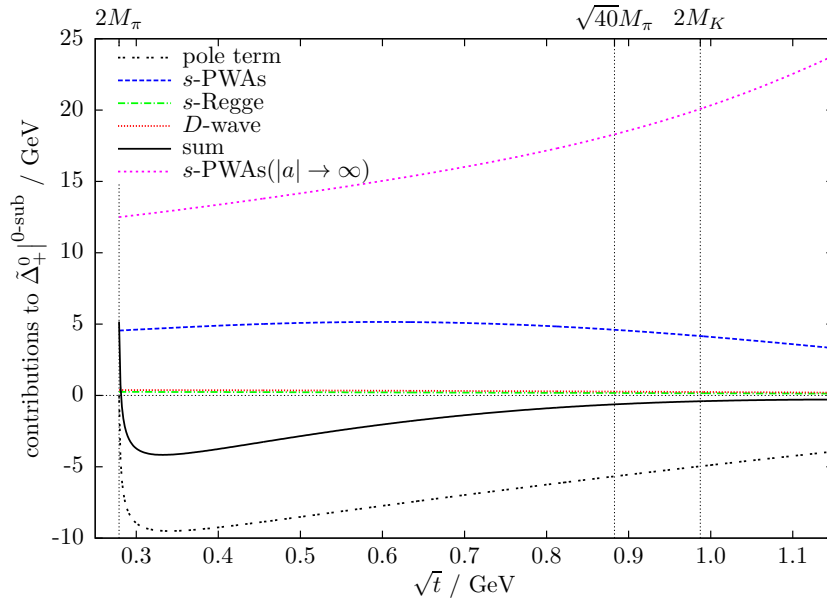
Figure 15.3: Contributions to the unsubtracted S-wave MO inhomogeneity $\tilde{\Delta}^0_+\big|^{\text{0-sub}}$. See main text for details.

significantly, since these variations produce the most sizable effects on the MO solutions compared to the other variations that will be discussed in the following. However, it is by no means clear a priori what the parameter values or their errors are, and only a self-consistent determination of all parameters and partial waves in a second step will allow for reliable quantitative results. Therefore, the necessary first task in this program is to check our method and the internal consistency of the KH80 results by using KH80 input as described in Sect. 15.2 and comparing our t-channel MO results with those of KH80. Moreover, we will investigate different systematic effects on the (subtracted) MO solutions $|f^J_\pm|$, which should prove valuable for the solution of the full system: after discussing exemplarily the importance of the different contributions to the MO inhomogeneities $\tilde{\Delta}^J_\pm(t)$, we will also discuss both the connection to the "fixed-t limit"[#23] and the effect of changing the matching point t_{m}. Except for the $a \to -\infty$ results, we will always use the optimal hyperbola parameter value of $a = -2.71\, M^2_\pi$ as obtained in Sect. 10.4.

15.3.1   Contributions to the inhomogeneities

In Figs. 15.3, 15.4, and 15.5 we show the different contributions to the MO inhomogeneities $\tilde{\Delta}^J_\pm(t)$ exemplarily for $\tilde{\Delta}^0_+$ for the un-, once-, and twice-subtracted case, respectively, from the $\pi\pi$ threshold t_π up to $1.15\,\text{GeV}$, also showing the upper limit of the KH80 solution as well as the $\bar{K}K$ threshold t_K as the uppermost limit of approximate elasticity for $J = 0$. We choose the S-wave for the following reasons: for $J = 0$ the nucleon pole term is zero at t_π and does not dominate all other contributions like it does for the higher partial waves; additionally, for the S-wave we can also show the coupling of the D-wave as leading contribution for the

---

[#23]Accordingly, the s-channel integral of the HDRs reduces to the fixed-t result, cf. Sect. 7.4 $a \to -\infty$. However, even in this limit the HDRs contain additional information as compared to fixed-t dispersion relations, since those do not provide equations for the t-channel partial waves in the first place.
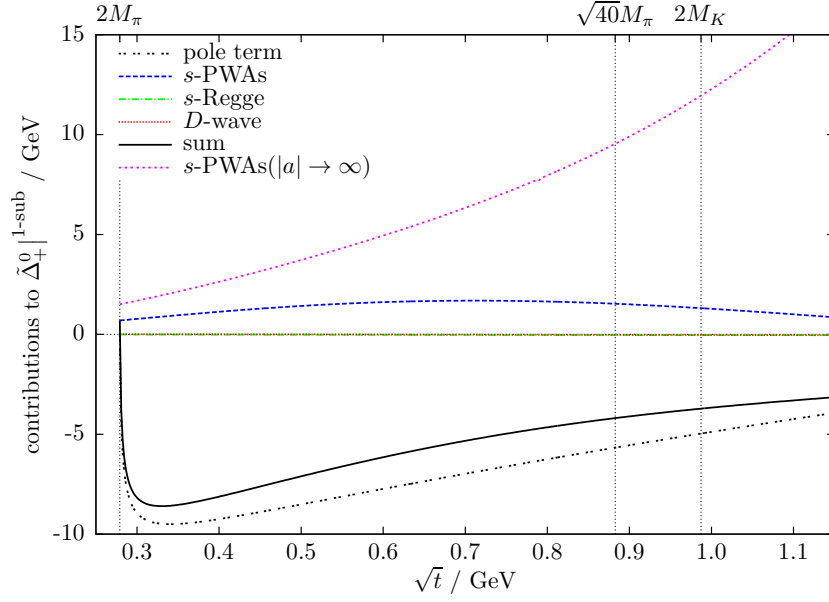
Figure 15.4: Contributions to the once-subtracted S-wave MO inhomogeneity $\tilde{\Delta}_+^0\big|^{\text{1-sub}}$.
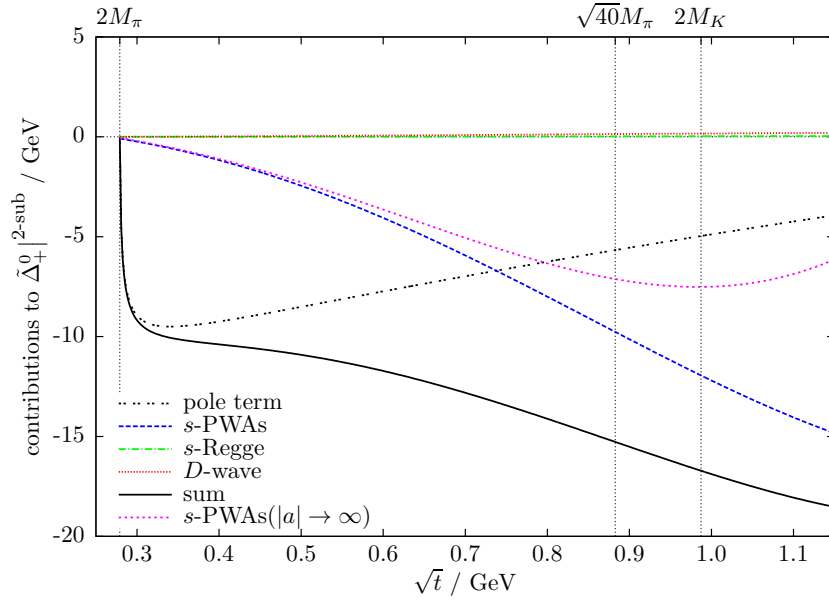
Figure 15.5: Contributions to the twice-subtracted S-wave MO inhomogeneity $\tilde{\Delta}_+^0\big|^{\text{2-sub}}$.

coupling of higher partial waves. The pole term $\hat{N}_+^0$ is independent of both the number of subtractions and a and thus serves as reference in all three plots (double-dashed). The s-channel contributions are shown separately for the sum of all partial waves with $l \leq 4$ in the range $W \in [W_+, W_a]$ (dashed) and the Regge contributions of the full invariant amplitudes for $W > W_a$ (dot-dashed). Even in the unsubtracted case both the s-channel Regge as well as the t-channel D-wave contributions (dotted) are very small and almost negligible in comparison to the other parts. From this it is also clear that the coupling of higher t-channel partial waves

(e.g. F-wave contributions to P-waves) can be completely omitted. The solid line denotes the sum of all these contributions and we have checked for $J \in \{0, 1, 2\}$ and $n \in \{0, 1, 2\}$ that the expected threshold behavior according to (12.34) and (12.38) (as for the corresponding partial waves) is indeed fulfilled. While all results are given for the optimal value of a unless stated otherwise, for comparison we also show the non-Regge s-channel contributions in the "fixed-t limit" $a \to -\infty$. Since this is a very drastic alteration (the Roy–Steiner system is not strictly valid in this case as will be explained below), the difference of this contributions for the two a values gives a very ample bound on the dependence on a. While the Regge contributions vanish for $a \to -\infty$ as discussed in Sect. 11.1, the D-wave coupling is not even well defined for $a \to -\infty$ in this framework as can be seen from the explicit a-dependence in the unsubtracted case leading to an infinite contribution, cf. (13.43). By comparing the three plots it is clearly seen that in the once-subtracted case all contributions except the pole term are suppressed, while in the twice-subtracted case an additional t-dependence is introduced such that they are strongly suppressed at t_π but at least the s-channel partial-wave contributions are comparable to the pole term around $0.75\,\mathrm{GeV}$. For small t, the differences between the two a values are also suppressed by each subtraction as expected.

15.3.2   Comparison with KH80

We will compare our un-, once-, and twice-subtracted MO solutions for $|f_\pm^J(t)|$ with $J \in \{0, 1, 2\}$ for $t \in [t_\pi, t_\mathrm{m}]$ with the KH80 results given as tables in [171]. Note that for $J \geq 2$ the un- and once-subtracted solutions coincide. The a-dependence (which is fully contained in $\tilde{\Delta}_\pm^J$) can be used as a crude measure for the systematic uncertainties due to neglecting t-channel input above t_m (i.e. "non-analytic" input), since the physical result must be independent of a.[#24] Thus, for the five lowest t-channel partial waves we show our "KH80 consistency MO solution" for the un-, once-, and twice-subtracted case, each for both the optimal value of a and $a \to -\infty$ in Figs. 15.6, 15.7 and 15.8. Here, we have chosen to use the same value of $\sqrt{t_\mathrm{m}} = 0.98\,\mathrm{GeV}$ for all considered partial waves, which in principle is not necessary; the effect of varying t_m will be explicitly investigated in Sect. 15.3.3. As discussed in Sects. 15.2.1 and 15.2.4, this choice is mainly motivated by the S-wave, since its phase is just below π at this energy (reaching π around the $\bar{K}K$ threshold $\sqrt{t_K} = 2M_K = 0.987\,\mathrm{GeV}$), so that no additional subtractions are necessary in the MO scheme, and furthermore at least for this partial wave the approximation of elasticity is severely broken for energies slightly above this matching point. In general, neglecting any t-channel input above the matching point as argued in Sect. 15.2.4 forces the MO solutions to go to zero at the matching point, i.e. $|f_\pm^J(t_\mathrm{m})| = 0$, according to the matching condition discussed in Sect. 14.6. Nevertheless, even for the S-wave we expect reasonable agreement with KH80 for this choice of t_m, since both KH80 and [213] suggest that the modulus $|f_+^0|$ has a minimum or even an approximate zero between $0.9\,\mathrm{GeV}$ and $\sqrt{t_K}$.[#25]

[#24]Numerically, we have checked that the limit $a \to -\infty$ can be safely approximated by $a = -10^6$ [GeV].

[#25]Note that despite neglecting (almost) all input absorptive parts above t_m, $|f(t_\mathrm{m})|$ may be fixed by hand to any (positive) finite value by using the second term on the RHS of (14.45) (containing the integral $I_+(t)$ for $t_\mathrm{m} \leq t < t_\mathrm{m} + \tau$, i.e. the asymptotic input contribution for $t \to t_\mathrm{m}$ from above) and tuning $\mathrm{Im}\, f(t_\mathrm{m})$ appropriately (given the phase $\delta(t_\mathrm{m})$), e.g. in order to estimate the numerical importance of input above t_m for the MO solutions. Unfortunately, this kind of input is obviously quite "non-analytic" for sizable non-zero $|f(t_\mathrm{m})|$ and hence produces a strong cusp at t_m (cf. Sect 14.6) thereby deteriorating the solutions already far below t_m. For this reason, the agreement between KH80 and the MO solutions becomes even worse in general when using a lower value $\sqrt{t_\mathrm{m}} = \sqrt{40}M_\pi = 0.88\,\mathrm{GeV}$ and taking the last data points of the corresponding KH80 partial-wave results in order to fix $|f_\pm^J(40M_\pi^2)|$. Ironically, a "smooth" matching to neglecting any input
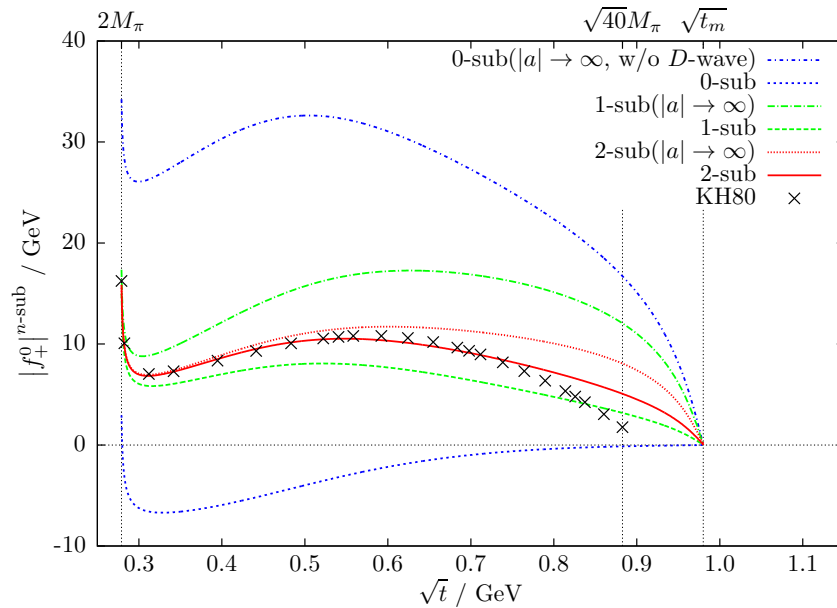
Figure 15.6: MO solutions for the S-wave. See main text for details.

In general, the solutions are fixed on both ends of the solution interval $[t_\pi, t_\mathrm{m}]$: on the right due to the input above t_m as discussed before and on the left due to the pole term, which becomes larger and thus more dominating with increasing J. Therefore the differences between the n-subtracted solutions and also the different a values decrease close to t_π. As they furthermore agree very well with the KH80 solution in the respective pole-term-dominated regions, we only show the remaining regions. Since the D-wave coupling for the unsubtracted case depends on a, this contribution is omitted for the $a \to -\infty$ limit (thus the solutions for the two a values do not coincide at t_π). Obviously, a negative modulus (i.e. the unsubtracted $|f_+^0|$ for optimal a and the once-subtracted $|f_+^1|$ for $a \to -\infty$) only indicates that too much input information is missing in this particular case in order to yield a reasonable solution — a problem that can be cured by subtractions. The general pattern is as expected: the effect of varying a is suppressed by both the subtraction procedure and higher J. Furthermore, the agreement with the KH80 solution is strongly aided by subtracting. This is clear since each subtraction power on the one hand suppresses the lacking input above t_m and on the other hand introduces additional consistent information via the subthreshold parameters as subtraction constants. Hence, the twice-subtracted solution for optimal a is our central "consistency result". The S-wave shows a nice convergence behavior in n, but around $0.8\,\mathrm{GeV}$ it starts to deviate from KH80, which is not surprising as the $f_0(980)$ is expected to have an important impact (cf. Sect. 15.2.4).[#26] As far as the P-waves are concerned, the numerical results confirm the analytic expectation that $|f_+^1|$ is much less well determined or constrained than $|f_-^1|$: basically, the MO equations for $|f_+^1|$ effectively contain one low-energy subtraction

---

above t_m could be achieved especially for the S-wave (and also for the linear combinations Γ^J, but not for f_-^J) for the unfeasible high value $t_\mathrm{m} = t_N$ at the physical threshold (due to the threshold behavior explained in Sect. 12.3.1) — just from where on input information is actually available.

[#26]Interestingly, we can find reasonable agreement with the unpublished (and partially inconsistent) result of [213] also for energies above the KH80 range by introducing the $f_0(980)$ resonance even via a (too) simple BW ansatz and adjusting by hand the f_0NN coupling constant accordingly. Small changes in this basically unknown coupling, however, lead to huge effects on the MO solution.
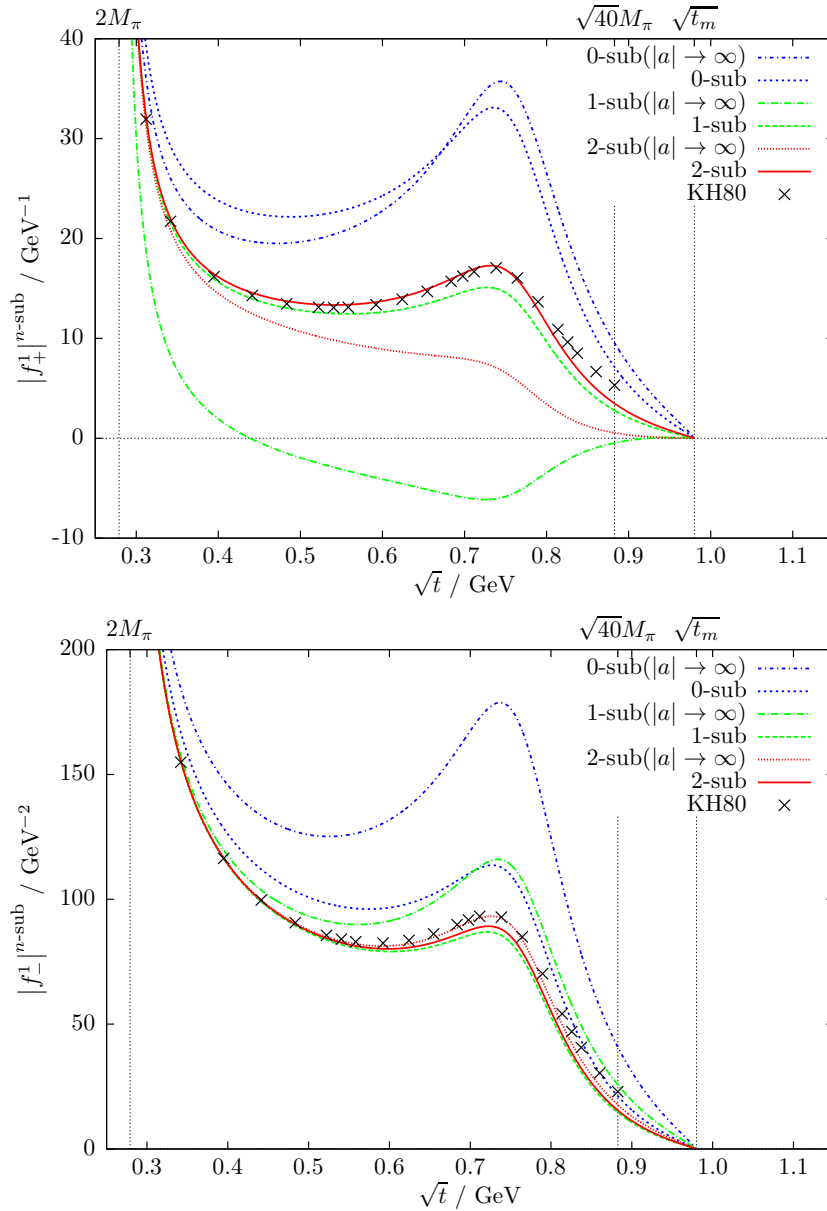
Figure 15.7: MO solutions for the *P*-waves.

less. Moreover, in the necessary intermediate step of solving the MO problem for $|\Gamma^1|$ the pole-term contributions $\hat{N}^J_\pm$ cancel at t_π (as discussed in Sect. 13.5) as for the *S*-wave and thus the solution for $|f^1_+|$ is less pole-term dominated and hence more sensitive to the values of the subthreshold parameters. Furthermore, the uncertainties of $|f^1_-|$ propagate into $|f^1_+|$ when calculating the latter from $|\Gamma^1|$ via (15.2). All this then leads to a rather slow convergence behavior in n for fixed a as well as the loss of the expected convergence pattern in n of the differences between the two a values (note especially the crossing of the unsubtracted solutions for different a values and the negative once-subtracted modulus). However, our central twice-subtracted result for $|f^1_+|$ agrees rather well with KH80 especially in the $\rho(770)$ peak, even though our result for $|f^1_-|$ (which enters $|f^1_+|$) seems to be systematically smaller than KH80.
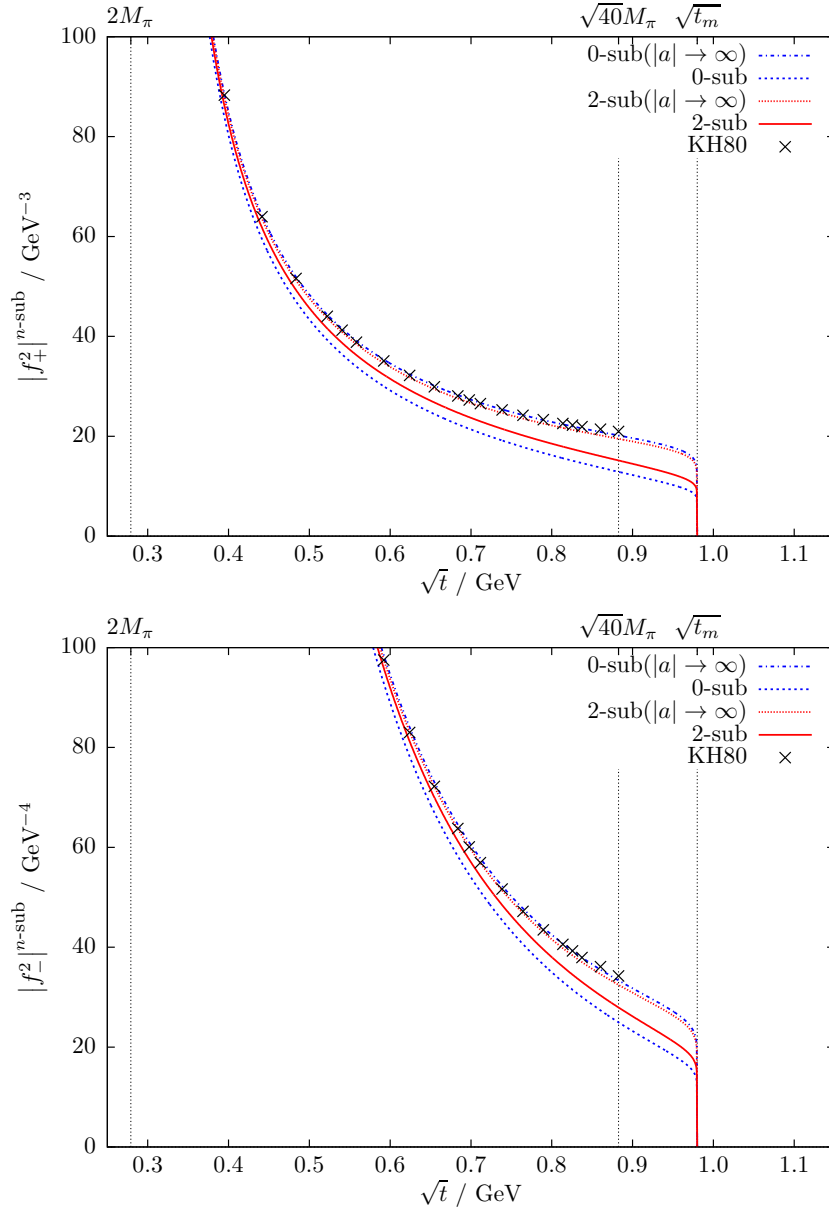
Figure 15.8: MO solutions for the D-waves. For $J \geq 2$ one subtraction has no effect.

Since this underestimation might be due to forcing the solution to go to zero at t_{m}, we will investigate the effect of using a higher value for t_{m} below. Nevertheless, the $a \to -\infty$ variant of the twice-subtracted solution for $|f_-^1|$ agrees well with KH80 in the ρ peak (though the agreement with KH80 becomes worse for $|f_-^1|$ in this limit). The D-wave results are systematically smaller than KH80 and the change from one (or equivalently zero) to two subtractions towards KH80 is roughly one third of this discrepancy and furthermore approximately of the same absolute size for both partial waves, which is probably due to calculating $|f_+^2|$ by using the result for $|f_-^2|$ together with the fact that $\chi_\Gamma^J = 0$ for all $J \neq 1$. For both $|f_+^2|$ and $|f_-^2|$ the accordance with KH80 (which is based on fixed-t dispersion relations) in the "fixed-t limit" $a \to -\infty$ is striking, the effect of varying a being much larger than the effect of subtractions.
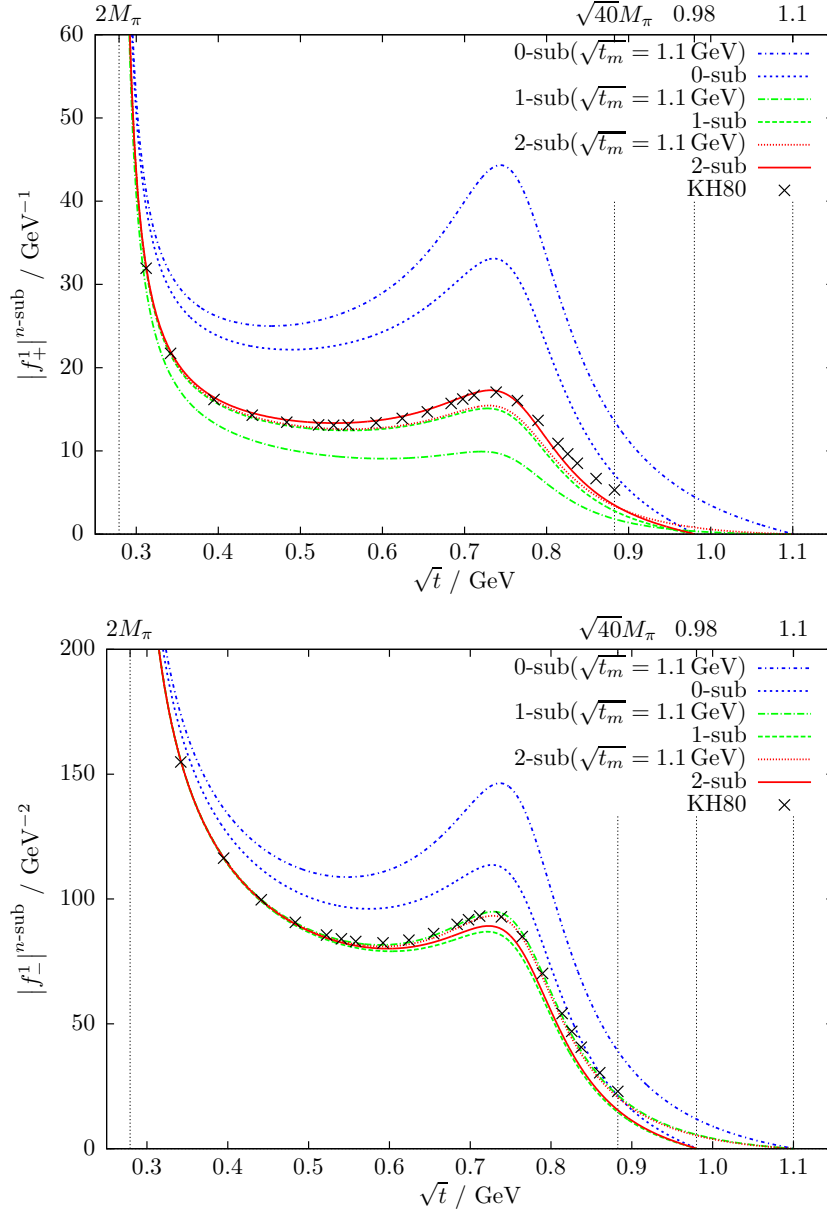
Figure 15.9: MO solutions for the P-waves with $\sqrt{t_{\mathrm{m}}} = 1.1\,\mathrm{GeV}$. See main text for details.

15.3.3 Variation of the matching point

Up to now we have used the S-wave-motivated value $\sqrt{t_{\mathrm{m}}} = 0.98\,\mathrm{GeV}$ for all considered partial waves. The effect of changing $\sqrt{t_{\mathrm{m}}}$ to $1.1\,\mathrm{GeV}$ is shown in Figs. 15.9 and 15.10 for the un-, once-, and twice-subtracted solutions for $J \in \{1, 2\}$. Again, for $J \geq 2$ the un- and once-subtracted solution coincide. For $J = 1$ it is generally assumed that 4π contributions can safely be neglected up to the $\pi\omega$ threshold around $0.92\,\mathrm{GeV}$; however, the $\pi\pi$ scattering P-wave inelasticity is small even above that energy and hence the impact of neglecting it (for both values of t_{m}) should be smaller than the effect of changing t_{m}. For $J = 2$ no substantial deviations from elasticity are expected, since the $\pi\pi$ scattering D-wave is essentially elastic
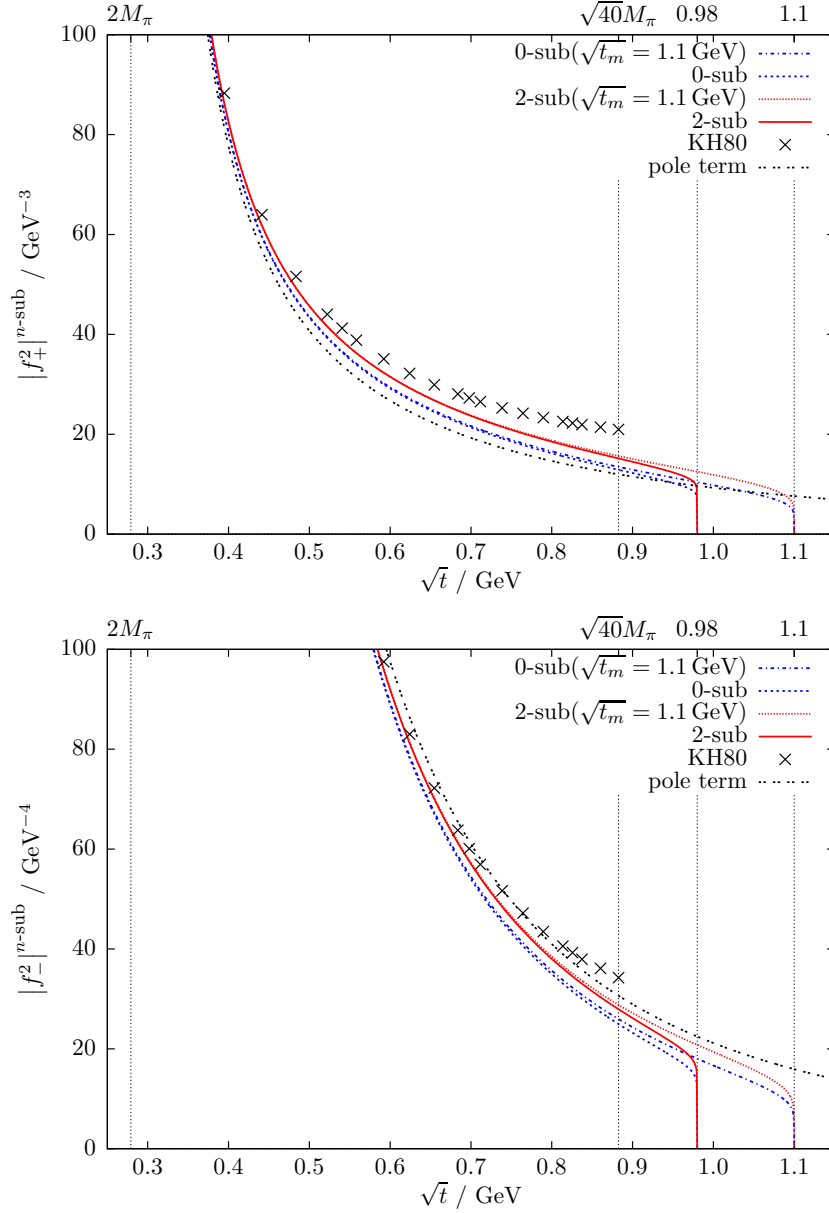
Figure 15.10: MO solutions for the D-waves with $\sqrt{t_{\mathrm{m}}} = 1.1\,\mathrm{GeV}$. For $J \geq 2$ one subtraction has no effect.

in this energy range. The P-wave solutions exhibit the expected behavior: the differences between the two matching point values become smaller with each subtraction, but the convergence behavior in n is again less good for $|f_+^1|$, where a higher value of t_{m} does not lead to a better agreement with KH80, while for $|f_-^1|$ already one subtraction in combination with the higher matching point yields description of the KH80 solution, which is even better than the twice-subtracted version for $a \to -\infty$ discussed before. Therefore we conclude that on the one hand the KH80 solution for $|f_-^1|$ can be reproduced well with a higher matching point already in the once-subtracted case, but on the other hand the KH80 solution for $|f_+^1|$ calls for a second subtraction and is hard to be accommodated in our MO scheme for energies above

roughly $0.8\,\text{GeV}$. The D-wave solutions, however, are hardly affected at all in the KH80 energy range by changing t_m. As discussed in Sect. 15.1, they are expected to be dominated by the pole terms $\hat{N}^2_\pm$, which for comparison are also shown in Fig. 15.10. While for $|f^2_-|$ the KH80 solution indeed agrees rather well with the pole term itself throughout the whole KH80 energy range, for $|f^2_+|$ there are "sizable" (w.r.t. the scale) deviations between KH80 and the pole term in this region, which again fits the picture that the partial wave with parallel helicity is both analytically and numerically less well constrained. Together with Fig. 15.8 we can conclude that in the limit $a \to -\infty$ for $|f^2_-|$ the net effect of adding the dispersive integrals to the pole term is very small, while for $|f^2_+|$ the corresponding dispersive contributions (which thus are not mainly induced by $|f^2_-|$ in this limit) are crucial for the agreement with KH80. For optimal a (and independent from the choice of t_m), though, these contributions deteriorate the agreement with KH80 (with respect to the pole term) for $|f^2_-|$, whereas improving the agreement for $|f^2_+|$; in this case the corrections to $|f^2_+|$ are effectively due to $|f^2_-|$.

15.3.4   Application to nucleon form factors

The t-channel partial waves considered in the previous sections are not only an integral part of any closed system of dispersion relations for πN scattering fully consistent with crossing symmetry, but also an essential ingredient to dispersive analyses of nucleon form factors. The contributions to the isovector spectral functions by two-pion intermediate states[27] in the case of the dimensionless electromagnetic Sachs form factors read [233] (cf. [275] as well as [171] for precise definitions and [276, 277] for recent applications)

$$\text{Im}\, G^v_E(t) = \frac{q^3_t}{m\sqrt{t}}\big(F^V_\pi(t)\big)^* f^1_+(t)\,\theta\big(t - t_\pi\big)\,, \qquad \text{Im}\, G^v_M(t) = \frac{q^3_t}{\sqrt{2t}}\big(F^V_\pi(t)\big)^* f^1_-(t)\,\theta\big(t - t_\pi\big)\,, \tag{15.17}$$

which due to the threshold behavior (12.38) of the t-channel partial waves obey

$$\text{Im}\, G^v_E(t \to t_N) - \text{Im}\, G^v_M(t \to t_N) = \mathcal{O}(p^2_t)\,, \tag{15.18}$$

while the imaginary part of the scalar form factor is determined by [278]

$$\text{Im}\,\sigma(t) = -\frac{3q_t}{4p^2_t\sqrt{t}}\big(F^S_\pi(t)\big)^* f^0_+(t)\,\theta\big(t - t_\pi\big) = \frac{\sigma^\pi_t}{2}\frac{3}{t_N - t}\big(F^S_\pi(t)\big)^* f^0_+(t)\,\theta\big(t - t_\pi\big)\,, \tag{15.19}$$

with the scalar and vector pion form factor $F^S_\pi(t)$ and $F^V_\pi(t)$, respectively.[28] In the case of the scalar form factors the approximation by $\pi\pi$ intermediate states breaks down as soon as the two-kaon threshold opens, and effects from $\bar{K}K$ intermediate states are known to be important for a dispersive description of $F^S_\pi(t)$ [230, 279]. In contrast, the two-pion contribution dominates in the vector channel, where inelasticities set in more smoothly. It is thus instructive to investigate the impact of our results for $|f^1_\pm(t)|$ on the spectral functions of the Sachs

---

[27]G-parity dictates that intermediate states of an even (odd) number of pions only contribute to the isovector (isoscalar) spectral functions; cf. Sect. 7.2.

[28]The relations (15.17) and (15.19) can be derived by explicitly calculating the corresponding pion loop integrals in terms of the πN T-matrix elements (7.22) in the t-channel CMS (i.e. effectively considering T^- for the vector form factors and T^+ for the scalar one); imposing current conservation as usual, the tensor decompositions of the resulting integrals over invariant amplitudes $A^\pm$ and $B^\pm$ (which are either even or odd in z_t) then automatically lead to explicit t-channel partial-wave projections according to (9.7) for P- and S-waves, respectively.

form factors. To illustrate the corresponding effects we approximate the vector pion form factor by a simple twice-subtracted Omnès representation (cf. [280] and references therein as well as (15.3))

$$F_\pi^V(t) = \exp\left\{\frac{\langle r^2\rangle_\pi^V}{6}t + \frac{t^2}{\pi}\int\limits_{t_\pi}^\infty \frac{\mathrm{d}t'}{t'^2}\frac{\delta_1(t')}{t'-t}\right\} = \left|F_\pi^V(t)\right|\exp\left\{i\delta_1(t)\theta\big(t-t_\pi\big)\right\}, \qquad F_\pi^V(0) = 1,$$

$$\left|F_\pi^V(t)\right| = \left|\frac{t}{t_\pi}-1\right|^{-x_1(t)}\exp\left\{t\left[\frac{\langle r^2\rangle_\pi^V}{6}-\frac{x_1(t)}{t_\pi}\right] + t^2\int\limits_{t_\pi}^\infty\frac{\mathrm{d}t'}{t'^2}\frac{x_1(t')-x_1(t)}{t'-t}\right\}, \qquad (15.20)$$

where the normalization ensures charge conservation (i.e. the constant part of the subtraction polynomial is fixed to zero) and Watson's theorem is fulfilled by construction, so that the phases in (15.17) cancel in the approximation of elasticity[#29]

$$\mathrm{Im}\,G_E^v(t) = \frac{\sigma_t^\pi}{8}\frac{t-t_\pi}{m}\left|F_\pi^V(t)\right|\left|f_+^1(t)\right|\theta\big(t-t_\pi\big),$$

$$\mathrm{Im}\,G_M^v(t) = \frac{\sigma_t^\pi}{8}\frac{t-t_\pi}{\sqrt{2}}\left|F_\pi^V(t)\right|\left|f_-^1(t)\right|\theta\big(t-t_\pi\big). \qquad (15.21)$$

For the mean square pion vector (or charge) radius we use $\langle r^2\rangle_\pi^V = 0.435\,\mathrm{fm}^2$ in accordance with [281] in order to ensure a decent description of form-factor data. However, the precise value of $\langle r^2\rangle_\pi^V$ is immaterial in the present context, since we merely wish to convey how the uncertainties in $|f_\pm^1|$ propagate into the spectral functions. Moreover, for the infinite-matching-point Omnès representation (15.20) in principle we need the phase δ_1 also in the high-energy regime. Since the numerical impact of the explicit assumption for the asymptotic behavior of the phase is suppressed by two subtractions, for our purpose of illustration we choose to simply keep the phase constant above $1.15\,\mathrm{GeV}$.[#30] The results for the once- and twice-subtracted versions of $|f_\pm^1|$ (the latter also for the "fixed-t limit" and a higher matching point value) together with the comparison to KH80 are depicted in Fig. 15.11.

As expected from the discussion in Sects. 15.3.2 and 15.3.3, the relative uncertainty in $\mathrm{Im}\,G_E^v$ is much larger than in $\mathrm{Im}\,G_M^v$, which is a result of the effectively lower number of subtractions in the calculation of $|f_+^1|$ and its enhanced subthreshold-parameter dependence. However, since $\mathrm{Im}\,G_M^v$ is much larger than $\mathrm{Im}\,G_E^v$, the absolute deviations between the individual curves are actually of comparable size in both cases. We conclude that a new determination of the subthreshold parameters from a full solution of our Roy–Steiner system should lead to improved central values and associated uncertainties for the two-pion contribution to the spectral functions of both form factors.

[#29]Strictly speaking, using any representation that goes beyond the two-pion approximation would be inconsistent unless the corresponding inelasticities are accounted for in the determination of $f_\pm^1$ and the unitarity relation (15.17) as well, as exemplified by the breakdown of Watson's theorem and the spectral functions becoming complex.

[#30]For instance, smoothly leading δ_1 to π at $t = \infty$ using e.g. $\delta_1(t) = \pi - \frac{c}{t-d}$ (with c and d adjusted for a smooth matching at $1.15\,\mathrm{GeV}$) instead does not lead to notable effects.
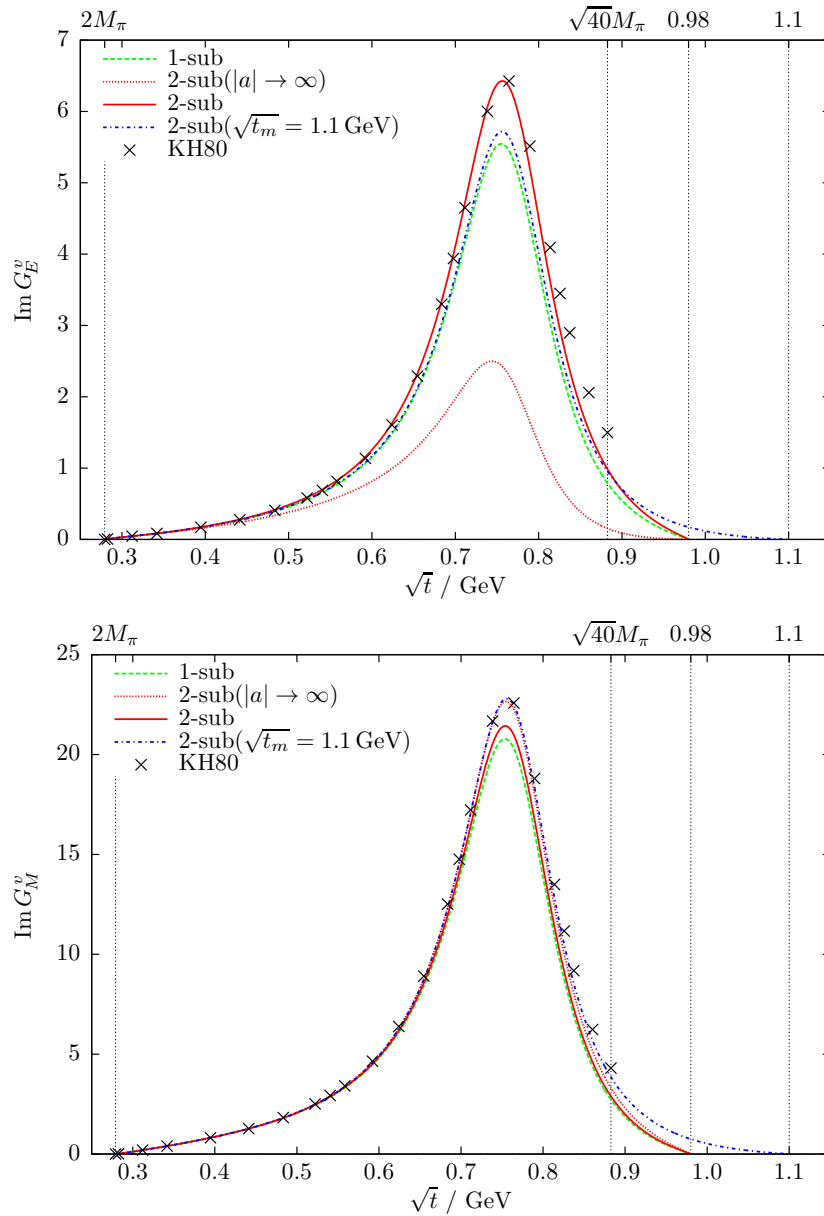
Figure 15.11: Two-pion-continuum contribution to $\operatorname{Im} G_E^v(t)$ and $\operatorname{Im} G_M^v(t)$.

Chapter 16

Conclusion

In this work we have derived a closed system of Roy–Steiner equations (i.e. partial-wave hyperbolic dispersion relations respecting analyticity, unitarity, and crossing symmetry) for πN scattering and analytically calculated all kernel functions for the lowest s- and especially the t-channel partial waves. Furthermore, we have constructed the corresponding unitarity relations in detail — including in particular inelastic contributions from $\bar{K}K$ intermediate states in the t-channel reaction — and thereby completed the Roy–Steiner system for πN scattering. To pin down the optimal value of the free hyperbola parameter a, assuming Mandelstam analyticity we have analyzed the domain of validity of the full system and determined a for both the s- and t-channel equations such that the corresponding range of convergence is maximized. We have accounted for the asymptotic contributions explicitly (in the s-channel) by means of a Regge model and found them to be numerically small. Subsequently, we have used the threshold behavior of the t-channel partial waves in order to cast the t-channel part of the Roy–Steiner system into the form of a Muskhelishvili–Omnès problem with a finite matching point. Furthermore, we have introduced subtractions at the subthreshold point in order to suppress the dependence on the high-energy region and derived the corresponding once- and twice-subtracted versions of our Roy–Steiner system and thereby the accordingly subtracted Muskhelishvili–Omnès equations. For this purpose, starting from the hyperbolic dispersion relations for πN scattering we have derived sum rules for the pertinent subtraction constants (i.e. subthreshold parameters) and calculated all necessary corrections to the kernel functions for both channels as well as the subtracted asymptotic contributions (which by subtracting, of course, get numerically immaterial). Moreover, we have developed a general (single-channel) Muskhelishvili–Omnès formalism that combines both the concepts of a finite matching point and the inclusion of inelasticities. However, the present knowledge of the pertinent couplings and partial waves is not sufficient to account for inelastic effects (particularly $\bar{K}K$ intermediate states) in this framework especially for the t-channel S-wave, while for the P- and higher partial waves already the elastic approximation yields reasonable results.

As a first step in solving the full Roy–Steiner system, we have then numerically solved the un-, once, and twice-subtracted Muskhelishvili–Omnès equations for the t-channel partial waves in the single-channel approximation (i.e. neglecting inelasticities). We have assessed the numerical importance of different input contributions for the Muskhelishvili–Omnès problem (in particular via the Muskhelishvili–Omnès inhomogeneities) by examining the behavior of the Muskhelishvili–Omnès solutions for the lowest t-channel partial waves ($J \in \{0, 1, 2\}$) with respect to varying both the input and/or the framework in many ways, including their

sensitivity to the $\pi\pi$ phase shifts, the number of subtractions ($n \in \{0, 1, 2\}$), variation of the finite matching point t_m, and taking the hyperbola parameter a to $-\infty$ (to some extent emulating fixed-t dispersion relations). In general, we have found consistency with the KH80 solutions and thereby confirmed the (approximate) self-consistency of the KH80 results for the s- and t-channel partial waves, the subthreshold parameters, and the (outdated) πN coupling constant — although there is clearly room for improvement on the KH80 analysis, especially regarding the analysis of the theoretical uncertainties. However, our analysis has shown that the structure of the equations renders the t-channel partial waves f_+^J systematically less well determined than their counterparts f_-^J both due to an enhanced sensitivity to the subtraction constants and an effectively lower number of subtractions. Finally, we have briefly discussed some consequences for nucleon form factors, in particular our analysis gives a first indication where the largest uncertainties in the spectral functions are to be expected.

The next step in the solution of our system of Roy–Steiner equations is the incorporation of $\bar{K}K$ intermediate states in a full two-channel Muskhelishvili–Omnès treatment of the t-channel S-wave, which has immediate consequences for the scalar form factor of the nucleon (and thereby also for the extraction of the πN σ-term) as discussed separately in [173] (which is not a part of this work). Having then thoroughly solved the t-channel part of the Roy–Steiner system also for the S-wave, the s-channel equations are solvable with techniques similar to those employed in the context of $\pi\pi$ Roy equations, and finally the iteration of the full system should determine the lowest partial waves as well as the subtraction parameters (as discussed in Chap. 6, cf. Fig. 6.2). We are confident that the framework proposed in this work eventually will allow for a reliable extrapolation to the Cheng–Dashen point and thus for an accurate determination of the πN σ-term.

Appendix C

Higher kernels for the *s*-channel driving terms

According to the general solution strategy for the full Roy–Steiner system as outlined in Chap. 6, only the lowest partial waves of both channels are solved for, namely those with $l \leq l_{\mathrm{d}}$ and $J \leq J_{\mathrm{d}}$, while the contributions of higher partial waves (i.e. the corresponding higher resonances) are collected as input in the respective driving terms. In the following, the higher kernel functions that are needed to incorporate higher *s*-channel partial waves as discussed in Sect. 15.2.3 are given.

C.1 *s*-channel partial-wave projection

Here, we display the explicit form of the additional angular kernels $U_{ll'}$, $\bar{U}_{ll'}$, and $V_{ll'}$ for $(l \leq 2, 4 \leq l' \leq 6)$ that are required for calculating the additional higher kernels $K_{ll'}^I$ for $(l \leq 1, 3 \leq l' \leq 5)$ via (8.49). From (8.53) we obtain

$$U_{04} = \frac{5}{2}\beta\Big\{7\alpha^2 + 7\beta^2 - 3\Big\}\,, \qquad U_{14} = \frac{1}{2}\alpha\Big\{7\alpha^2 + 35\beta^2 - 5\Big\}\,, \qquad U_{24} = 7\alpha^2\beta\,, \qquad \text{(C.1)}$$

$$U_{05} = \frac{1}{8}\Big\{15 - 70\big(\alpha^2 + 3\beta^2\big) + 63\big(\alpha^4 + 5\beta^4 + 10\alpha^2\beta^2\big)\Big\}\,,$$

$$U_{15} = \frac{7}{2}\alpha\beta\Big\{9\alpha^2 + 15\beta^2 - 5\Big\}\,, \qquad U_{25} = \frac{1}{2}\alpha^2\Big\{9\alpha^2 + 63\beta^2 - 7\Big\}\,,$$

$$U_{06} = \frac{21}{8}\beta\Big\{5 - 30\big(\alpha^2 + \beta^2\big) + 11\big(3\alpha^4 + 3\beta^4 + 10\alpha^2\beta^2\big)\Big\}\,,$$

$$U_{16} = \frac{1}{8}\alpha\Big\{35 - 126\big(\alpha^2 + 5\beta^2\big) + 33\big(3\alpha^4 + 35\beta^4 + 42\alpha^2\beta^2\big)\Big\}\,,$$

$$U_{26} = \frac{3}{2}\alpha^2\beta\Big\{33\alpha^2 + 77\beta^2 - 21\Big\}\,,$$

and (8.60) yields

$$\bar{U}_{04} = -5\Big\{7b_3 - 14b_2 + 9b_1 + \bar{\omega}\big[4 - 14\alpha(1-\alpha) + 7\beta(1-\alpha+\beta)\big]\Big\}\,, \qquad \text{(C.2)}$$

$$\bar{U}_{14} = 21b_3 - 35b_2 + 15b_1 - 35\bar{\omega}\alpha(1-\alpha+\beta)\,, \qquad \bar{U}_{24} = -7\Big\{b_3 - b_2 + 2\bar{\omega}\alpha^2\Big\}\,,$$

$$\bar{U}_{05} = 7\Big\{18b_4 - 5(9b_3 - 8b_2 + 3b_1) - \frac{15}{4}\bar{\omega}(1-\alpha+\beta)\big[(1-3\alpha)^2 + 3\beta^2\big]\Big\}\,,$$

$$\bar{U}_{15} = -7\Big\{12b_4 - 27b_3 + 20b_2 - 5b_1 + \bar{\omega}\alpha\big[2(5 - 15\alpha + 12\alpha^2) + 15\beta(1 - \alpha + \beta)\big]\Big\} \,,$$

$$\bar{U}_{25} = 36b_4 - 63b_3 + 28b_2 - 63\bar{\omega}\alpha^2(1 - \alpha + \beta) \,,$$

$$\bar{U}_{06} = -21\Big\{22(b_5 - 3b_4) + 5(15b_3 - 8b_2 + 2b_1) + \bar{\omega}\big[2(1 - 9\alpha + 31\alpha^2 - 22\alpha^3(2 - \alpha))$$
$$+ \frac{\beta}{4}(1 - \alpha + \beta)(3 - 11\alpha(6 - 13\alpha) + 33\beta^2)\big]\Big\} \,,$$

$$\bar{U}_{16} = 66(5b_5 - 14b_4) + 35(27b_3 - 12b_2 + 2b_1) - \frac{21}{4}\bar{\omega}\alpha(1 - \alpha + \beta)\big[(5 - 11\alpha)^2 + 55\beta^2\big] \,,$$

$$\bar{U}_{26} = -3\Big\{11(5b_5 - 12b_4) + 7(15b_3 - 4b_2) + \bar{\omega}\alpha^2\big[56 - 22\alpha(7 - 5\alpha) + 77\beta(1 - \alpha + \beta)\big]\Big\} \,,$$

where we refrain from spelling out explicitly the form of $b_\mu(W, W')$ for higher values of μ, as these functions follow directly from their definition (8.58). From (8.68) follows

$$\bar{V}_{04} = \frac{5}{6}\alpha\Big\{21(\alpha x_s)^2 + 63\beta(\alpha x_s) + 7\alpha^2 + 63\beta^2 - 9\Big\} \,, \tag{C.3}$$

$$\bar{V}_{14} = \frac{35}{6}\alpha^2\Big\{(\alpha x_s) + 3\beta\Big\} \,, \qquad \bar{V}_{24} = \frac{7}{3}\alpha^3 \,,$$

$$\bar{V}_{05} = \frac{105}{8}\alpha\Big\{3(\alpha x_s)^3 + 12\beta(\alpha x_s)^2 + \big(\alpha^2 + 18\beta^2 - 2\big)(\alpha x_s) + 4\beta\big(\alpha^2 + 3\beta^2 - 1\big)\Big\} \,,$$

$$\bar{V}_{15} = \frac{7}{8}\alpha^2\Big\{15(\alpha x_s)^2 + 60\beta(\alpha x_s) + 9\alpha^2 + 90\beta^2 - 10\Big\} \,, \qquad \bar{V}_{25} = \frac{21}{4}\alpha^3\Big\{(\alpha x_s) + 4\beta\Big\} \,,$$

$$\bar{V}_{06} = \frac{21}{40}\alpha\Big\{165(\alpha x_s)^4 + 825\beta(\alpha x_s)^3 + 5\big(11\alpha^2 + 330\beta^2 - 30\big)(\alpha x_s)^2$$
$$+ 25\beta\big(11\alpha^2 + 66\beta^2 - 18\big)(\alpha x_s) + 25 - 50\alpha^2 + 33\alpha^4 + 50\big(11\alpha^2 - 9\big)\beta^2 + 825\beta^4\Big\} \,,$$

$$\bar{V}_{16} = \frac{21}{40}\alpha^2\Big\{55(\alpha x_s)^3 + 275\beta(\alpha x_s)^2 + \big(33\alpha^2 + 550\beta^2 - 50\big)(\alpha x_s) + 5\beta\big(33\alpha^2 + 110\beta^2 - 30\big)\Big\} \,,$$

$$\bar{V}_{26} = \frac{3}{20}\alpha^3\Big\{77(\alpha x_s)^2 + 385\beta(\alpha x_s) + 2\big(33\alpha^2 + 385\beta^2 - 35\big)\Big\} \,.$$

C.2   *t*-channel partial-wave projection

The explicit forms of the polynomial parts $\bar{A}_{Jl}$, $\bar{B}_{Jl}$ and $\bar{C}_{J,l}$ from (9.34) for $(J \le 2, l \le 6)$ that are needed in order to calculate the kernels $\tilde{G}_{Jl}$ and $\tilde{H}_{Jl}$ for $(J \le 2, l \le 5)$ via (9.35) read

$$\bar{A}_{01} = \frac{1}{s' - a} \,, \qquad \bar{A}_{02} = \frac{3}{\tilde{\gamma}}\Big[\frac{\tilde{x}_t}{p_t q_t} + \frac{1}{s' - a}\Big\{\frac{1}{3} - \tilde{\delta}\Big\}\Big] \,, \tag{C.4}$$

$$\bar{A}_{03} = \frac{15}{2\tilde{\gamma}^2}\Big[\frac{\tilde{x}_t}{p_t q_t}\Big\{\tilde{x}_t^2 + \frac{1}{3} - 2\tilde{\delta}\Big\} + \frac{1}{s' - a}\Big\{\frac{1 - \tilde{\gamma}^2}{5} - \frac{2}{3}\tilde{\delta} + \tilde{\delta}^2\Big\}\Big] \,,$$

$$\bar{A}_{04} = \frac{35}{2\tilde{\gamma}^3}\Big[\frac{\tilde{x}_t}{p_t q_t}\Big\{\tilde{x}_t^4 + \tilde{x}_t^2\Big(\frac{1}{3} - 3\tilde{\delta}\Big) + \frac{1}{5} - \frac{3}{7}\tilde{\gamma}^2 - \tilde{\delta} + 3\tilde{\delta}^2\Big\}$$
$$+ \frac{1}{s' - a}\Big\{\frac{1}{7} - \frac{\tilde{\gamma}^2}{7}\Big(1 - 3\tilde{\delta}\Big) - \frac{3}{5}\tilde{\delta} + \tilde{\delta}^2 - \tilde{\delta}^3\Big\}\Big]$$

$$\bar{A}_{05} = \frac{315}{2\tilde{\gamma}^4}\Big[\frac{\tilde{x}_t}{p_t q_t}\Big\{\frac{\tilde{x}_t^6}{4} + \tilde{x}_t^4\Big(\frac{1}{12} - \tilde{\delta}\Big) + \tilde{x}_t^2\Big(\frac{1}{20} - \frac{\tilde{\gamma}^2}{6} - \frac{\tilde{\delta}}{3} + \frac{3}{2}\tilde{\delta}^2\Big)$$
$$+ \frac{1}{28} - \frac{\tilde{\gamma}^2}{3}\Big(\frac{1}{6} - \tilde{\delta}\Big) - \frac{\tilde{\delta}}{5} + \frac{\tilde{\delta}^2}{2} - \tilde{\delta}^3\Big\}$$

$$+ \frac{1}{s'-a}\left\{\frac{1}{36} - \frac{\tilde{\gamma}^2}{6}\left(\frac{1}{5} - \frac{\tilde{\gamma}^2}{14} - \frac{2}{3}\tilde{\delta} + \tilde{\delta}^2\right) - \frac{\tilde{\delta}}{7} + \frac{3}{10}\tilde{\delta}^2 - \frac{\tilde{\delta}^3}{3} + \frac{\tilde{\delta}^4}{4}\right\}\Bigg] \,,$$

$$\bar{A}_{06} = \frac{3465}{4\tilde{\gamma}^5}\Bigg[\frac{\tilde{x}_t}{p_t q_t}\left\{\frac{\tilde{x}_t^8}{10} + \tilde{x}_t^4\left(\frac{1}{50} - \frac{\tilde{\gamma}^2}{11} - \frac{\tilde{\delta}}{6} + \tilde{\delta}^2\right) + \tilde{x}_t^2\left(\frac{1}{70} - \frac{\tilde{\gamma}^2}{11}\left(\frac{1}{3} - 3\tilde{\delta}\right) - \frac{\tilde{\delta}}{10} + \frac{\tilde{\delta}^2}{3} - \tilde{\delta}^3\right)\right.$$

$$\left. + \frac{\tilde{x}_t^6}{2}\left(\frac{1}{15} - \tilde{\delta}\right) + \frac{1}{90} - \frac{\tilde{\gamma}^2}{11}\left(\frac{1}{5} - \frac{\tilde{\gamma}^2}{6} - \tilde{\delta} + 3\tilde{\delta}^2\right) - \frac{\tilde{\delta}}{14} + \frac{\tilde{\delta}^2}{5} - \frac{\tilde{\delta}^3}{3} + \frac{\tilde{\delta}^4}{2}\right\}$$

$$+ \frac{1}{s'-a}\left\{\frac{1}{110} - \frac{\tilde{\gamma}^2}{11}\left(\frac{1}{7} - \frac{\tilde{\gamma}^2}{6}\left(\frac{1}{3} - \tilde{\delta}\right) - \frac{3}{5}\tilde{\delta} + \tilde{\delta}^2 - \tilde{\delta}^3\right) - \frac{\tilde{\delta}}{18} + \frac{\tilde{\delta}^2}{7} - \frac{\tilde{\delta}^3}{5} + \frac{\tilde{\delta}^4}{6} - \frac{\tilde{\delta}^5}{10}\right\}\Bigg] \,,$$

$$\bar{A}_{11} = 0 \,, \qquad \bar{A}_{12} = \frac{1}{p_t q_t}\frac{1}{\tilde{\gamma}} \,, \qquad \bar{A}_{13} = \frac{1}{p_t q_t}\frac{5}{2\tilde{\gamma}^2}\left\{\tilde{x}_t^2 + \frac{3}{5} - 2\tilde{\delta}\right\} \,, \tag{C.5}$$

$$\bar{A}_{14} = \frac{1}{p_t q_t}\frac{35}{2\tilde{\gamma}^3}\left\{\frac{\tilde{x}_t^4}{3} + \tilde{x}_t^2\left(\frac{1}{5} - \tilde{\delta}\right) + \frac{1 - \tilde{\gamma}^2}{7} - \frac{3}{5}\tilde{\delta} + \tilde{\delta}^2\right\} \,,$$

$$\bar{A}_{15} = \frac{1}{p_t q_t}\frac{315}{2\tilde{\gamma}^4}\left\{\frac{\tilde{x}_t^6}{12} + \tilde{x}_t^4\left(\frac{1}{20} - \frac{\tilde{\delta}}{3}\right) + \tilde{x}_t^2\left(\frac{1}{28} - \frac{\tilde{\gamma}^2}{18} - \frac{\tilde{\delta}}{5} + \frac{\tilde{\delta}^2}{2}\right)\right.$$

$$\left. + \frac{1}{36} - \frac{\tilde{\gamma}^2}{3}\left(\frac{1}{10} - \frac{\tilde{\delta}}{3}\right) - \frac{\tilde{\delta}}{7} + \frac{3}{10}\tilde{\delta}^2 - \frac{\tilde{\delta}^3}{3}\right\} \,,$$

$$\bar{A}_{16} = \frac{1}{p_t q_t}\frac{3465}{4\tilde{\gamma}^5}\left\{\frac{\tilde{x}_t^8}{30} + \tilde{x}_t^4\left(\frac{1}{70} - \frac{\tilde{\gamma}^2}{33} - \frac{\tilde{\delta}}{10} + \frac{\tilde{\delta}^2}{3}\right) + \tilde{x}_t^2\left(\frac{1}{90} - \frac{\tilde{\gamma}^2}{11}\left(\frac{1}{5} - \tilde{\delta}\right) - \frac{\tilde{\delta}}{14} + \frac{\tilde{\delta}^2}{5} - \frac{\tilde{\delta}^3}{3}\right)\right.$$

$$\left. + \frac{\tilde{x}_t^6}{2}\left(\frac{1}{25} - \frac{\tilde{\delta}}{3}\right) + \frac{1}{110} - \frac{\tilde{\gamma}^2}{11}\left(\frac{1}{7} - \frac{\tilde{\gamma}^2}{18} - \frac{3}{5}\tilde{\delta} + \tilde{\delta}^2\right) - \frac{\tilde{\delta}}{18} + \frac{\tilde{\delta}^2}{7} - \frac{\tilde{\delta}^3}{5} + \frac{\tilde{\delta}^4}{6}\right\} \,,$$

$$\bar{A}_{21} = 0 \,, \qquad \bar{A}_{22} = \frac{2}{5\tilde{\gamma}}\frac{1}{s'-a} \,, \qquad \bar{A}_{23} = \frac{1}{\tilde{\gamma}^2}\left[\frac{\tilde{x}_t}{p_t q_t} + \frac{1}{s'-a}\left\{\frac{6}{7} - 2\tilde{\delta}\right\}\right] \,, \tag{C.6}$$

$$\bar{A}_{24} = \frac{7}{\tilde{\gamma}^3}\left[\frac{\tilde{x}_t}{p_t q_t}\left\{\frac{\tilde{x}_t^2}{3} + \frac{2}{7} - \tilde{\delta}\right\} + \frac{1}{s'-a}\left\{\frac{5}{21} - \frac{\tilde{\gamma}^2}{7} - \frac{6}{7}\tilde{\delta} + \tilde{\delta}^2\right\}\right] \,,$$

$$\bar{A}_{25} = \frac{21}{\tilde{\gamma}^4}\left[\frac{\tilde{x}_t}{p_t q_t}\left\{\frac{\tilde{x}_t^4}{4} + \tilde{x}_t^2\left(\frac{3}{14} - \tilde{\delta}\right) + \frac{5}{28} - \frac{\tilde{\gamma}^2}{6} - \frac{6}{7}\tilde{\delta} + \frac{3}{2}\tilde{\delta}^2\right\}\right.$$

$$\left. + \frac{1}{s'-a}\left\{\frac{5}{33} - \tilde{\gamma}^2\left(\frac{1}{7} - \frac{\tilde{\delta}}{3}\right) - \frac{5}{7}\tilde{\delta} + \frac{9}{7}\tilde{\delta}^2 - \tilde{\delta}^3\right\}\right] \,,$$

$$\bar{A}_{26} = \frac{231}{2\tilde{\gamma}^5}\left[\frac{\tilde{x}_t}{p_t q_t}\left\{\frac{\tilde{x}_t^6}{10} + \tilde{x}_t^4\left(\frac{3}{35} - \frac{\tilde{\delta}}{2}\right) + \tilde{x}_t^2\left(\frac{1}{14} - \frac{\tilde{\gamma}^2}{11} - \frac{3}{7}\tilde{\delta} + \tilde{\delta}^2\right)\right.\right.$$

$$\left. + \frac{2}{33} - \frac{\tilde{\gamma}^2}{11}\left(\frac{6}{7} - 3\tilde{\delta}\right) - \frac{5}{14}\tilde{\delta} + \frac{6}{7}\tilde{\delta}^2 - \tilde{\delta}^3\right\}$$

$$\left. + \frac{1}{s'-a}\left\{\frac{15}{286} - \frac{\tilde{\gamma}^2}{11}\left(\frac{5}{7} - \frac{\tilde{\gamma}^2}{6} - \frac{18}{7}\tilde{\delta} + 3\tilde{\delta}^2\right) - \frac{10}{33}\tilde{\delta} + \frac{5}{7}\tilde{\delta}^2 - \frac{6}{7}\tilde{\delta}^3 + \frac{\tilde{\delta}^4}{2}\right\}\right] \,,$$

$$\bar{B}_{01} = \frac{1}{p_t q_t} \,, \qquad \bar{B}_{02} = \frac{1}{p_t q_t}\frac{3}{\tilde{\gamma}}\left\{\tilde{x}_t^2 + \frac{1}{3} - \tilde{\delta}\right\} \,, \tag{C.7}$$

$$\bar{B}_{03} = \frac{1}{p_t q_t}\frac{15}{2\tilde{\gamma}^2}\left\{\tilde{x}_t^4 + \tilde{x}_t^2\left(\frac{1}{3} - 2\tilde{\delta}\right) + \frac{1 - \tilde{\gamma}^2}{5} - \frac{2}{3}\tilde{\delta} + \tilde{\delta}^2\right\} \,,$$

$$\bar{B}_{04} = \frac{1}{p_t q_t} \frac{35}{2\tilde{\gamma}^3} \left\{ \tilde{x}_t^6 + \tilde{x}_t^4 \left(\frac{1}{3} - 3\tilde{\delta} \right) + \tilde{x}_t^2 \left(\frac{1}{5} - \frac{3}{7}\tilde{\gamma}^2 - \tilde{\delta} + 3\tilde{\delta}^2 \right) \right.$$

$$\left. + \frac{1}{7} - \frac{\tilde{\gamma}^2}{7} \left(1 - 3\tilde{\delta} \right) - \frac{3}{5}\tilde{\delta} + \tilde{\delta}^2 - \tilde{\delta}^3 \right\} ,$$

$$\bar{B}_{05} = \frac{1}{p_t q_t} \frac{315}{2\tilde{\gamma}^4} \left\{ \frac{\tilde{x}_t^8}{4} + \tilde{x}_t^4 \left(\frac{1}{20} - \frac{\tilde{\gamma}^2}{6} - \frac{\tilde{\delta}}{3} + \frac{3}{2}\tilde{\delta}^2 \right) + \tilde{x}_t^2 \left(\frac{1}{28} - \frac{\tilde{\gamma}^2}{3} \left(\frac{1}{6} - \tilde{\delta} \right) - \frac{\tilde{\delta}}{5} + \frac{\tilde{\delta}^2}{2} - \tilde{\delta}^3 \right) \right.$$

$$\left. + \tilde{x}_t^6 \left(\frac{1}{12} - \tilde{\delta} \right) + \frac{1}{36} - \frac{\tilde{\gamma}^2}{6} \left(\frac{1}{5} - \frac{\tilde{\gamma}^2}{14} - \frac{2}{3}\tilde{\delta} + \tilde{\delta}^2 \right) - \frac{\tilde{\delta}}{7} + \frac{3}{10}\tilde{\delta}^2 - \frac{\tilde{\delta}^3}{3} + \frac{\tilde{\delta}^4}{4} \right\} ,$$

$$\bar{B}_{06} = \frac{1}{p_t q_t} \frac{3465}{4\tilde{\gamma}^5} \left\{ \frac{\tilde{x}_t^{10}}{10} + \tilde{x}_t^6 \left(\frac{1}{50} - \frac{\tilde{\gamma}^2}{11} - \frac{\tilde{\delta}}{6} + \tilde{\delta}^2 \right) + \tilde{x}_t^4 \left(\frac{1}{70} - \frac{\tilde{\gamma}^2}{11} \left(\frac{1}{3} - 3\tilde{\delta} \right) - \frac{\tilde{\delta}}{10} + \frac{\tilde{\delta}^2}{3} - \tilde{\delta}^3 \right) \right.$$

$$+ \frac{\tilde{x}_t^8}{2} \left(\frac{1}{15} - \tilde{\delta} \right) + \tilde{x}_t^2 \left(\frac{1}{90} - \frac{\tilde{\gamma}^2}{11} \left(\frac{1}{5} - \frac{\tilde{\gamma}^2}{6} - \tilde{\delta} + 3\tilde{\delta}^2 \right) - \frac{\tilde{\delta}}{14} + \frac{\tilde{\delta}^2}{5} - \frac{\tilde{\delta}^3}{3} + \frac{\tilde{\delta}^4}{2} \right)$$

$$\left. + \frac{1}{110} - \frac{\tilde{\gamma}^2}{11} \left(\frac{1}{7} - \frac{\tilde{\gamma}^2}{6} \left(\frac{1}{3} - \tilde{\delta} \right) - \frac{3}{5}\tilde{\delta} + \tilde{\delta}^2 - \tilde{\delta}^3 \right) - \frac{\tilde{\delta}}{18} + \frac{\tilde{\delta}^2}{7} - \frac{\tilde{\delta}^3}{5} + \frac{\tilde{\delta}^4}{6} - \frac{\tilde{\delta}^5}{10} \right\} ,$$

$$\bar{B}_{11} = \frac{1}{s'-a} \frac{1}{3} , \qquad \bar{B}_{12} = \frac{1}{\tilde{\gamma}} \left[\frac{\tilde{x}_t}{p_t q_t} + \frac{1}{s'-a} \left\{ \frac{3}{5} - \tilde{\delta} \right\} \right] , \tag{C.8}$$

$$\bar{B}_{13} = \frac{5}{2\tilde{\gamma}^2} \left[\frac{\tilde{x}_t}{p_t q_t} \left\{ \tilde{x}_t^2 + \frac{3}{5} - 2\tilde{\delta} \right\} + \frac{1}{s'-a} \left\{ \frac{3}{7} - \frac{\tilde{\gamma}^2}{5} - \frac{6}{5}\tilde{\delta} + \tilde{\delta}^2 \right\} \right] ,$$

$$\bar{B}_{14} = \frac{35}{2\tilde{\gamma}^3} \left[\frac{\tilde{x}_t}{p_t q_t} \left\{ \frac{\tilde{x}_t^4}{3} + \tilde{x}_t^2 \left(\frac{1}{5} - \tilde{\delta} \right) + \frac{1-\tilde{\gamma}^2}{7} - \frac{3}{5}\tilde{\delta} + \tilde{\delta}^2 \right\} \right.$$

$$\left. + \frac{1}{s'-a} \left\{ \frac{1}{9} - \frac{\tilde{\gamma}^2}{7} \left(\frac{3}{5} - \tilde{\delta} \right) - \frac{3}{7}\tilde{\delta} + \frac{3}{5}\tilde{\delta}^2 - \frac{\tilde{\delta}^3}{3} \right\} \right] ,$$

$$\bar{B}_{15} = \frac{105}{2\tilde{\gamma}^4} \left[\frac{\tilde{x}_t}{p_t q_t} \left\{ \frac{\tilde{x}_t^6}{4} + \tilde{x}_t^4 \left(\frac{3}{20} - \tilde{\delta} \right) + \tilde{x}_t^2 \left(\frac{3}{28} - \frac{\tilde{\gamma}^2}{6} - \frac{3}{5}\tilde{\delta} + \frac{3}{2}\tilde{\delta}^2 \right) \right. \right.$$

$$\left. + \frac{1}{12} - \tilde{\gamma}^2 \left(\frac{1}{10} - \frac{\tilde{\delta}}{3} \right) - \frac{3}{7}\tilde{\delta} + \frac{9}{10}\tilde{\delta}^2 - \tilde{\delta}^3 \right\}$$

$$\left. + \frac{1}{s'-a} \left\{ \frac{3}{44} - \tilde{\gamma}^2 \left(\frac{1}{14} - \frac{\tilde{\gamma}^2}{84} - \frac{\tilde{\delta}}{5} + \frac{\tilde{\delta}^2}{6} \right) - \frac{\tilde{\delta}}{3} + \frac{9}{14}\tilde{\delta}^2 - \frac{3}{5}\tilde{\delta}^3 + \frac{\tilde{\delta}^4}{4} \right\} \right] ,$$

$$\bar{B}_{16} = \frac{3465}{4\tilde{\gamma}^5} \left[\frac{\tilde{x}_t}{p_t q_t} \left\{ \frac{\tilde{x}_t^8}{30} + \tilde{x}_t^4 \left(\frac{1}{70} - \frac{\tilde{\gamma}^2}{33} - \frac{\tilde{\delta}}{10} + \frac{\tilde{\delta}^2}{3} \right) + \tilde{x}_t^2 \left(\frac{1}{90} - \frac{\tilde{\gamma}^2}{11} \left(\frac{1}{5} - \tilde{\delta} \right) - \frac{\tilde{\delta}}{14} + \frac{\tilde{\delta}^2}{5} - \frac{\tilde{\delta}^3}{3} \right) \right. \right.$$

$$\left. + \frac{\tilde{x}_t^6}{2} \left(\frac{1}{25} - \frac{\tilde{\delta}}{3} \right) + \frac{1}{110} - \frac{\tilde{\gamma}^2}{11} \left(\frac{1}{7} - \frac{\tilde{\gamma}^2}{18} - \frac{3}{5}\tilde{\delta} + \tilde{\delta}^2 \right) - \frac{\tilde{\delta}}{18} + \frac{\tilde{\delta}^2}{7} - \frac{\tilde{\delta}^3}{5} + \frac{\tilde{\delta}^4}{6} \right\}$$

$$+ \frac{1}{s'-a} \left\{ \frac{1}{130} - \frac{\tilde{\gamma}^2}{11} \left(\frac{1}{9} - \frac{\tilde{\gamma}^2}{6} \left(\frac{1}{5} - \frac{\tilde{\delta}}{3} \right) - \frac{3}{7}\tilde{\delta} + \frac{3}{5}\tilde{\delta}^2 - \frac{\tilde{\delta}^3}{3} \right) \right.$$

$$\left. \left. - \frac{\tilde{\delta}}{22} + \frac{\tilde{\delta}^2}{9} - \frac{\tilde{\delta}^3}{7} + \frac{\tilde{\delta}^4}{10} - \frac{\tilde{\delta}^5}{30} \right\} \right] ,$$

$$\bar{B}_{21} = 0 , \qquad \bar{B}_{22} = \frac{1}{p_t q_t} \frac{2}{5\tilde{\gamma}} , \qquad \bar{B}_{23} = \frac{1}{p_t q_t} \frac{1}{\tilde{\gamma}^2} \left\{ \tilde{x}_t^2 + \frac{6}{7} - 2\tilde{\delta} \right\} , \tag{C.9}$$

$$\bar{B}_{24} = \frac{1}{p_t q_t} \frac{7}{\tilde{\gamma}^3} \left\{ \frac{\tilde{x}_t^4}{3} + \tilde{x}_t^2 \left(\frac{2}{7} - \tilde{\delta} \right) + \frac{5}{21} - \frac{\tilde{\gamma}^2}{7} - \frac{6}{7} \tilde{\delta} + \tilde{\delta}^2 \right\} ,$$

$$\bar{B}_{25} = \frac{1}{p_t q_t} \frac{21}{\tilde{\gamma}^4} \left\{ \frac{\tilde{x}_t^6}{4} + \tilde{x}_t^4 \left(\frac{3}{14} - \tilde{\delta} \right) + \tilde{x}_t^2 \left(\frac{5}{28} - \frac{\tilde{\gamma}^2}{6} - \frac{6}{7} \tilde{\delta} + \frac{3}{2} \tilde{\delta}^2 \right) \right.$$
$$\left. + \frac{5}{33} - \tilde{\gamma}^2 \left(\frac{1}{7} - \frac{\tilde{\delta}}{3} \right) - \frac{5}{7} \tilde{\delta} + \frac{9}{7} \tilde{\delta}^2 - \tilde{\delta}^3 \right\} ,$$

$$\bar{B}_{26} = \frac{1}{p_t q_t} \frac{231}{2\tilde{\gamma}^5} \left\{ \frac{\tilde{x}_t^8}{10} + \tilde{x}_t^4 \left(\frac{1}{14} - \frac{\tilde{\gamma}^2}{11} - \frac{3}{7} \tilde{\delta} + \tilde{\delta}^2 \right) + \tilde{x}_t^2 \left(\frac{2}{33} - \frac{\tilde{\gamma}^2}{11} \left(\frac{6}{7} - 3\tilde{\delta} \right) - \frac{5}{14} \tilde{\delta} + \frac{6}{7} \tilde{\delta}^2 - \tilde{\delta}^3 \right) \right.$$
$$\left. + \tilde{x}_t^6 \left(\frac{3}{35} - \frac{\tilde{\delta}}{2} \right) + \frac{15}{286} - \frac{\tilde{\gamma}^2}{11} \left(\frac{5}{7} - \frac{\tilde{\gamma}^2}{6} - \frac{18}{7} \tilde{\delta} + 3\tilde{\delta}^2 \right) - \frac{10}{33} \tilde{\delta} + \frac{5}{7} \tilde{\delta}^2 - \frac{6}{7} \tilde{\delta}^3 + \frac{\tilde{\delta}^4}{2} \right\} ,$$

$$\bar{C}_{11} = \frac{1}{s' - a} , \qquad \bar{C}_{12} = \frac{3}{\tilde{\gamma}} \left[\frac{\tilde{x}_t}{p_t q_t} + \frac{1}{s' - a} \left\{ \frac{1}{5} - \tilde{\delta} \right\} \right] , \tag{C.10}$$

$$\bar{C}_{13} = \frac{15}{2\tilde{\gamma}^2} \left[\frac{\tilde{x}_t}{p_t q_t} \left\{ \tilde{x}_t^2 + \frac{1}{5} - 2\tilde{\delta} \right\} + \frac{1}{s' - a} \left\{ \frac{3}{35} - \frac{\tilde{\gamma}^2}{5} - \frac{2}{5} \tilde{\delta} + \tilde{\delta}^2 \right\} \right] ,$$

$$\bar{C}_{14} = \frac{105}{2\tilde{\gamma}^3} \left[\frac{\tilde{x}_t}{p_t q_t} \left\{ \frac{\tilde{x}_t^4}{3} + \tilde{x}_t^2 \left(\frac{1}{15} - \tilde{\delta} \right) + \frac{1}{35} - \frac{\tilde{\gamma}^2}{7} - \frac{\tilde{\delta}}{5} + \tilde{\delta}^2 \right\} \right.$$
$$\left. + \frac{1}{s' - a} \left\{ \frac{1}{63} - \frac{\tilde{\gamma}^2}{7} \left(\frac{1}{5} - \tilde{\delta} \right) - \frac{3}{35} \tilde{\delta} + \frac{\tilde{\delta}^2}{5} - \frac{\tilde{\delta}^3}{3} \right\} \right] ,$$

$$\bar{C}_{15} = \frac{315}{2\tilde{\gamma}^4} \left[\frac{\tilde{x}_t}{p_t q_t} \left\{ \frac{\tilde{x}_t^6}{4} + \tilde{x}_t^4 \left(\frac{1}{20} - \tilde{\delta} \right) + \tilde{x}_t^2 \left(\frac{3}{140} - \frac{\tilde{\gamma}^2}{6} - \frac{\tilde{\delta}}{5} + \frac{3}{2} \tilde{\delta}^2 \right) \right. \right.$$
$$\left. + \frac{1}{84} - \frac{\tilde{\gamma}^2}{3} \left(\frac{1}{10} - \tilde{\delta} \right) - \frac{3}{35} \tilde{\delta} + \frac{3}{10} \tilde{\delta}^2 - \tilde{\delta}^3 \right\}$$
$$\left. + \frac{1}{s' - a} \left\{ \frac{1}{132} - \tilde{\gamma}^2 \left(\frac{1}{70} - \frac{\tilde{\gamma}^2}{84} - \frac{\tilde{\delta}}{15} + \frac{\tilde{\delta}^2}{6} \right) - \frac{\tilde{\delta}}{21} + \frac{9}{70} \tilde{\delta}^2 - \frac{\tilde{\delta}^3}{5} + \frac{\tilde{\delta}^4}{4} \right\} \right] ,$$

$$\bar{C}_{16} = \frac{3465}{4\tilde{\gamma}^5} \left[\frac{\tilde{x}_t}{p_t q_t} \left\{ \tilde{x}_t^4 \left(\frac{3}{350} - \frac{\tilde{\gamma}^2}{11} - \frac{\tilde{\delta}}{10} + \tilde{\delta}^2 \right) + \tilde{x}_t^2 \left(\frac{1}{210} - \frac{\tilde{\gamma}^2}{11} \left(\frac{1}{5} - 3\tilde{\delta} \right) - \frac{3}{70} \tilde{\delta} + \frac{\tilde{\delta}^2}{5} - \tilde{\delta}^3 \right) \right. \right.$$
$$\left. + \frac{\tilde{x}_t^8}{10} + \frac{\tilde{x}_t^6}{2} \left(\frac{1}{25} - \tilde{\delta} \right) + \frac{1}{330} - \frac{\tilde{\gamma}^2}{11} \left(\frac{3}{35} - \frac{\tilde{\gamma}^2}{6} - \frac{3}{5} \tilde{\delta} + 3\tilde{\delta}^2 \right) - \frac{\tilde{\delta}}{42} + \frac{3}{35} \tilde{\delta}^2 - \frac{\tilde{\delta}^3}{5} + \frac{\tilde{\delta}^4}{2} \right\}$$
$$+ \frac{1}{s' - a} \left\{ \frac{3}{1430} - \frac{\tilde{\gamma}^2}{11} \left(\frac{1}{21} - \frac{\tilde{\gamma}^2}{6} \left(\frac{1}{5} - \tilde{\delta} \right) - \frac{9}{35} \tilde{\delta} + \frac{3}{5} \tilde{\delta}^2 - \tilde{\delta}^3 \right) \right.$$
$$\left. \left. - \frac{\tilde{\delta}}{66} + \frac{\tilde{\delta}^2}{21} - \frac{3}{35} \tilde{\delta}^3 + \frac{\tilde{\delta}^4}{10} - \frac{\tilde{\delta}^5}{10} \right\} \right] ,$$

$$\bar{C}_{21} = 0 , \qquad \bar{C}_{22} = \frac{1}{p_t q_t} \frac{1}{\tilde{\gamma}} , \qquad \bar{C}_{23} = \frac{1}{p_t q_t} \frac{5}{2\tilde{\gamma}^2} \left\{ \tilde{x}_t^2 + \frac{3}{7} - 2\tilde{\delta} \right\} , \tag{C.11}$$

$$\bar{C}_{24} = \frac{1}{p_t q_t} \frac{35}{2\tilde{\gamma}^3} \left\{ \frac{\tilde{x}_t^4}{3} + \tilde{x}_t^2 \left(\frac{1}{7} - \tilde{\delta} \right) + \frac{5}{63} - \frac{\tilde{\gamma}^2}{7} - \frac{3}{7} \tilde{\delta} + \tilde{\delta}^2 \right\} ,$$

$$\bar{C}_{25} = \frac{1}{p_t q_t} \frac{105}{2\tilde{\gamma}^4} \left\{ \frac{\tilde{x}_t^6}{4} + \tilde{x}_t^4 \left(\frac{3}{28} - \tilde{\delta} \right) + \tilde{x}_t^2 \left(\frac{5}{84} - \frac{\tilde{\gamma}^2}{6} - \frac{3}{7} \tilde{\delta} + \frac{3}{2} \tilde{\delta}^2 \right) \right.$$
$$\left. + \frac{5}{132} - \tilde{\gamma}^2 \left(\frac{1}{14} - \frac{\tilde{\delta}}{3} \right) - \frac{5}{21} \tilde{\delta} + \frac{9}{14} \tilde{\delta}^2 - \tilde{\delta}^3 \right\} ,$$

$$\bar{C}_{26} = \frac{1}{p_t q_t} \frac{1155}{4\tilde{\gamma}^5} \left\{ \frac{\tilde{x}_t^8}{10} + \tilde{x}_t^4 \left(\frac{1}{42} - \frac{\tilde{\gamma}^2}{11} - \frac{3}{14}\tilde{\delta} + \tilde{\delta}^2 \right) + \tilde{x}_t^2 \left(\frac{1}{66} - \frac{\tilde{\gamma}^2}{11}\left(\frac{3}{7} - 3\tilde{\delta} \right) - \frac{5}{42}\tilde{\delta} + \frac{3}{7}\tilde{\delta}^2 - \tilde{\delta}^3 \right) \right.$$

$$\left. + \frac{\tilde{x}_t^6}{2} \left(\frac{3}{35} - \tilde{\delta} \right) + \frac{3}{286} - \frac{\tilde{\gamma}^2}{11} \left(\frac{5}{21} - \frac{\tilde{\gamma}^2}{6} - \frac{9}{7}\tilde{\delta} + 3\tilde{\delta}^2 \right) - \frac{5}{66}\tilde{\delta} + \frac{5}{21}\tilde{\delta}^2 - \frac{3}{7}\tilde{\delta}^3 + \frac{\tilde{\delta}^4}{2} \right\} .$$

Bibliography

[1] C. Ditsche, B. Kubis, and U.-G. Meißner, "Electromagnetic corrections in $\eta \to 3\pi$ decays," *Eur. Phys. J.* **C 60** (2009) 83–105, `arXiv:0812.0344 [hep-ph]`.

[2] C. Ditsche, B. Kubis, and U.-G. Meißner, "Electromagnetic effects in $\eta \to 3\pi$," *PoS* **CD09** (2009) 043, `arXiv:0910.0210 [hep-ph]`. `http://pos.sissa.it/archive/conferences/086/043/CD09_043.pdf`.

[3] S. P. Schneider, B. Kubis, and C. Ditsche, "Rescattering effects in $\eta \to 3\pi$ decays," *JHEP* **1102** (2011) 028, `arXiv:1010.3946 [hep-ph]`.

[4] D. G. Sutherland, "Current algebra and the decay $\eta \to 3\pi$," *Phys. Lett.* **23** (1966) 384–385.

[5] J. S. Bell and D. G. Sutherland, "Current algebra and $\eta \to 3\pi$," *Nucl. Phys.* **B 4** (1968) 315–325.

[6] J. A. Cronin, "Phenomenological model of strong and weak interactions in chiral $U(3) \times U(3)$," *Phys. Rev.* **161** (1967) 1483–1494.

[7] H. Osborn and D. J. Wallace, "η–η' mixing, $\eta \to 3\pi$ and chiral Lagrangians," *Nucl. Phys.* **B 20** (1970) 23–44.

[8] A. Neveu and J. Scherk, "Final-state interaction and current algebra in $K \to 3\pi$ and $\eta \to 3\pi$ decays," *Annals Phys.* **57** (1970) 39–64.

[9] C. Roiesnel and T. N. Truong, "Resolution of the $\eta \to 3\pi$ problem," *Nucl. Phys.* **B 187** (1981) 293–300.

[10] S. Weinberg, "Phenomenological Lagrangians," *Physica* **A 96** (1979) 327–340.

[11] J. Gasser and H. Leutwyler, "Chiral perturbation theory to one loop," *Annals Phys.* **158** (1984) 142–210.

[12] J. Gasser and H. Leutwyler, "Chiral perturbation theory: Expansions in the mass of the strange quark," *Nucl. Phys.* **B 250** (1985) 465–516.

[13] J. Gasser and H. Leutwyler, "$\eta \to 3\pi$ to one loop," *Nucl. Phys.* **B 250** (1985) 539–560.

[14] R. Urech, "Virtual photons in chiral perturbation theory," *Nucl. Phys.* **B 433** (1995) 234–254, `arXiv:hep-ph/9405341`.

[15] R. Baur, J. Kambor, and D. Wyler, "Electromagnetic corrections to the decays $\eta \to 3\pi$," *Nucl. Phys.* **B 460** (1996) 127–142, `arXiv:hep-ph/9510396`.

[16] J. Bijnens and J. Gasser, "Eta decays at and beyond p^4 in chiral perturbation theory," *Phys. Scripta* **T 99** (2002) 34–44, `arXiv:hep-ph/0202242`.

[17] J. Kambor, C. Wiesendanger, and D. Wyler, "Final-state interactions and Khuri–Treiman equations in $\eta \to 3\pi$ decays," *Nucl. Phys.* **B 465** (1996) 215–266, `arXiv:hep-ph/9509374`.

[18] A. V. Anisovich and H. Leutwyler, "Dispersive analysis of the decay $\eta \to 3\pi$," *Phys. Lett.* **B 375** (1996) 335–342, `arXiv:hep-ph/9601237`.

[19] N. Beisert and B. Borasoy, "Hadronic decays of η and η' with coupled channels," *Nucl. Phys.* **A 716** (2003) 186–208, `arXiv:hep-ph/0301058`.

[20] B. Borasoy and R. Nißler, "Hadronic η and η' decays," *Eur. Phys. J.* **A 26** (2005) 383–398, `arXiv:hep-ph/0510384`.

[21] J. Bijnens and K. Ghorbani, "$\eta \to 3\pi$ at two loops in chiral perturbation theory," *JHEP* **0711** (2007) 030, `arXiv:0709.0230 [hep-ph]`.

[22] M. Gormley, E. Hyman, W. Lee, T. Nash, J. Peoples, *et al.*, "Experimental determination of the Dalitz-plot distribution of the decays $\eta \to \pi^+\pi^-\pi^0$ and $\eta \to \pi^+\pi^-\gamma$, and the branching ratio $\eta \to \pi^+\pi^-\gamma/\eta \to \pi^+\pi^-\gamma$," *Phys. Rev.* **D2** (1970) 501–505.

[23] J. G. Layter, J. A. Appel, A. Kotlewski, W. Lee, S. Stein, *et al.*, "Study of Dalitz-plot distributions of the decays $\eta \to \pi^+\pi^-\pi^0$ and $\eta \to \pi^+\pi^-\gamma$," *Phys. Rev.* **D7** (1973) 2565–2568.

[24] Crystal Barrel Collaboration, A. Abele *et al.*, "Momentum dependence of the decay $\eta \to \pi^+\pi^-\pi^0$," *Phys. Lett.* **B 417** (1998) 197–201.

[25] KLOE Collaboration, F. Ambrosino *et al.*, "Determination of $\eta \to \pi^+\pi^-\pi^0$ Dalitz plot slopes and asymmetries with the KLOE detector," *JHEP* **0805** (2008) 006, `arXiv:0801.2642 [hep-ex]`. `[arXiv:0707.2355 [hep-ex]]`.

[26] Serpukhov-Brussels-Annecy (Soviet-CERN) Collaboration, D. Alde *et al.*, "Neutral decays of the η meson," *Z. Phys.* **C 25** (1984) 225–229. [Yad. Fiz. **40** (1984) 1447].

[27] Crystal Barrel Collaboration, A. Abele *et al.*, "Decay dynamics of the process $\eta \to 3\pi^0$," *Phys. Lett.* **B 417** (1998) 193–196.

[28] Crystal Ball Collaboration, W. B. Tippens *et al.*, "Determination of the quadratic slope parameter in $\eta \to 3\pi^0$ decay," *Phys. Rev. Lett.* **87** (2001) 192001.

[29] M. N. Achasov, K. I. Beloborodov, A. V. Berdyugin, A. G. Bogdanchikov, A. V. Bozhenok, *et al.*, "Dynamics of $\eta \to 3\pi^0$ decay," *JETP Lett.* **73** (2001) 451–452. [Pisma Zh. Eksp. Teor. Fiz. **73** (2001) 511–512].

[30] KLOE Collaboration, F. Ambrosino *et al.*, "Measurement of the $\eta \to 3\pi^0$ slope parameter α with the KLOE detector," *Phys. Lett.* **B 694** (2010) 16–21, `arXiv:1004.1319 [hep-ex]`. [`arXiv:0707.4137 [hep-ex]`].

[31] CELSIUS-WASA Collaboration, M. Bashkanov *et al.*, "Measurement of the slope parameter for the $\eta \to 3\pi^0$ decay in the $pp \to pp\eta$ reaction," *Phys. Rev.* **C 76** (2007) 048201, `arXiv:0708.2014 [nucl-ex]`.

[32] C. Baglin, A. Bezaguet, B. Degrange, P. Musset, H. Bingham, *et al.*, "Heavy liquid chamber analysis of $\eta \to 3\pi$ and $\eta \to \gamma\gamma$ decay-modes," *Phys. Lett.* **B 29** (1969) 445–447.

[33] C. Baglin, A. Bezaguet, B. Degrange, P. Musset, A. Ferrando, *et al.*, "Heavy liquid bubble chamber analysis of η neutral decay modes: $\eta \to 3\pi^0$ and $\eta \to \gamma\gamma$," *Nucl. Phys.* **B 22** (1970) 66–84.

[34] Particle Data Group, J. Beringer *et al.*, "Review of particle physics," *Phys. Rev.* **D 86** (2012) 010001. [`http://pdg.lbl.gov`].

[35] F. W. Bullock, M. J. Esten, E. Fleming-Tompa, M. Govan, C. Henderson, *et al.*, "A determination of the branching ratio $(\eta \to 3\pi^0)/(\eta \to \pi^+\pi^-\pi^0)$," *Phys. Lett.* **B 27** (1968) 402–404.

[36] Crystal Barrel Collaboration, C. Amsler *et al.*, "η decays into three pions," *Phys. Lett.* **B 346** (1995) 203–207.

[37] CMD-2 Collaboration, R. R. Akhmetshin *et al.*, "Study of the process $e^+e^- \to \eta\gamma$ in c.m. energy range 600–1380 MeV at CMD-2," *Phys. Lett.* **B 509** (2001) 217–226, `arXiv:hep-ex/0103043`.

[38] M. N. Achasov, V. M. Aulchenko, K. I. Beloborodov, A. V. Berdyugin, A. G. Bogdanchikov, *et al.*, "Study of the $e^+e^- \to \eta\gamma$ process with Spherical Neutral Detector detector at the VEPP-2M e^+e^- collider," *Phys. Rev.* **D 74** (2006) 014016, `arXiv:hep-ex/0605109`.

[39] C. Ditsche, "Electromagnetic corrections in $\eta \to 3\pi$ decays," Master's thesis, University of Bonn, 2007.

[40] E. P. Wigner, "On the behavior of cross sections near thresholds," *Phys. Rev.* **73** (1948) 1002–1009.

[41] U.-G. Meißner, G. Müller, and S. Steininger, "Virtual photons in $SU(2)$ chiral perturbation theory and electromagnetic corrections to $\pi\pi$ scattering," *Phys. Lett.* **B 406** (1997) 154–160, `arXiv:hep-ph/9704377`. Erratum-ibid. **B 407** (1997) 454.

[42] U.-G. Meißner, "Hadron structure in the nonperturbative regime of QCD: Isospin symmetry and its violation," *Nucl. Phys.* **A 629** (1998) 72c–81c, `arXiv:hep-ph/9706367`.

[43] J. L. Rosner, "Effects of S-wave thresholds," *Phys. Rev.* **D 74** (2006) 076006, `arXiv:hep-ph/0608102`.

[44] B. Kubis, "Cusp effects in meson decays," *EPJ Web Conf.* **3** (2010) 01008, `arXiv:0912.3440 [hep-ph]`.

[45] P. Budini and L. Fonda, "Pion–pion interaction from threshold anomalies in k^+ decay," *Phys. Rev. Lett.* **6** (1961) 419–421.

[46] N. Cabibbo, "Determination of the $a_0 - a_2$ pion scattering length from $K^+ \to \pi^+\pi^0\pi^0$ decay," *Phys. Rev. Lett.* **93** (2004) 121801, `arXiv:hep-ph/0405001`.

[47] N. Cabibbo and G. Isidori, "Pion–pion scattering and the $K \to 3\pi$ decay amplitudes," *JHEP* **0503** (2005) 021, `arXiv:hep-ph/0502130`.

[48] NA48/2 Collaboration, J. R. Batley *et al.*, "Observation of a cusp-like structure in the $\pi^0\pi^0$ invariant mass distribution from $K^\pm \to \pi^\pm\pi^0\pi^0$ decay and determination of the $\pi\pi$ scattering lengths," *Phys. Lett.* **B 633** (2006) 173–182, `arXiv:hep-ex/0511056`.

[49] E. Gámiz, J. Prades, and I. Scimemi, "$K \to 3\pi$ final-state interactions at NLO in ChPT and Cabibbo's proposal to measure $a_0 - a_2$," *Eur. Phys. J.* **C 50** (2007) 405–422, `arXiv:hep-ph/0602023`.

[50] J. R. Batley, A. J. Culling, G. Kalmus, C. Lazzeroni, D. J. Munday, *et al.*, "Determination of the S-wave $\pi\pi$ scattering lengths from a study of $K^\pm \to \pi^\pm\pi^0\pi^0$ decays," *Eur. Phys. J.* **C 64** (2009) 589–608, `arXiv:0912.2165 [hep-ex]`.

[51] G. Colangelo, J. Gasser, and H. Leutwyler, "$\pi\pi$ scattering," *Nucl. Phys.* **B 603** (2001) 125–179, `arXiv:hep-ph/0103088`.

[52] S. M. Roy, "Exact integral equation for pion–pion scattering involving only physical region partial waves," *Phys. Lett.* **B 36** (1971) 353–356.

[53] B. Ananthanarayan, G. Colangelo, J. Gasser, and H. Leutwyler, "Roy equation analysis of $\pi\pi$ scattering," *Phys. Rept.* **353** (2001) 207–279, `arXiv:hep-ph/0005297`.

[54] G. Colangelo, J. Gasser, and H. Leutwyler, "The $\pi\pi$ S-wave scattering lengths," *Phys. Lett.* **B 488** (2000) 261–268, `arXiv:hep-ph/0007112`.

[55] KTeV Collaboration, E. Abouzaid *et al.*, "Detailed study of the $K_L \to \pi^0\pi^0\pi^0$ Dalitz plot," *Phys. Rev.* **D 78** (2008) 032009, `arXiv:0806.3535 [hep-ex]`.

[56] WASA-at-COSY Collaboration, C. Adolph *et al.*, "Measurement of the $\eta \to 3\pi^0$ Dalitz plot distribution with the WASA detector at COSY," *Phys. Lett.* **B 677** (2009) 24–29, `arXiv:0811.2763 [nucl-ex]`.

[57] Crystal Ball at MAMI (TAPS & A2) Collaboration, M. Unverzagt *et al.*, "Determination of the Dalitz plot parameter α for the decay $\eta \to 3\pi^0$ with the Crystal Ball at MAMI-B," *Eur. Phys. J.* **A 39** (2009) 169–177, `arXiv:0812.3324 [hep-ex]`.

[58] Crystal Ball at MAMI (A2) Collaboration, S. Prakhov *et al.*, "Measurement of the slope parameter α for the $\eta \to 3\pi^0$ decay with the Crystal Ball detector at the Mainz Microtron (MAMI-C)," *Phys. Rev.* **C 79** (2009) 035204, `arXiv:0812.1999 [hep-ex]`.

[59] G. Colangelo, J. Gasser, B. Kubis, and A. Rusetsky, "Cusps in $K \to 3\pi$ decays," *Phys. Lett.* **B 638** (2006) 187–194, `arXiv:hep-ph/0604084`.

[60] M. Bissegger, A. Fuhrer, J. Gasser, B. Kubis, and A. Rusetsky, "Cusps in $K_L \to 3\pi$ decays," *Phys. Lett.* **B 659** (2008) 576–584, `arXiv:0710.4456 [hep-ph]`.

[61] M. Bissegger, A. Fuhrer, J. Gasser, B. Kubis, and A. Rusetsky, "Radiative corrections in $K \to 3\pi$ decays," *Nucl. Phys.* **B 806** (2009) 178–223, `arXiv:0807.0515 [hep-ph]`.

[62] J. Gasser, B. Kubis, and A. Rusetsky, "Cusps in $K \to 3\pi$ decays: A theoretical framework," *Nucl. Phys.* **B 850** (2011) 96–147, `arXiv:1103.4273 [hep-ph]`.

[63] S. Lanz, "Berne–Lund–Valencia dispersive treatment of $\eta \to 3\pi$," in *Proceedings of the second International PrimeNet Workshop*. 2012. `arXiv:1204.5509 [nucl-ex]`.

[64] G. Colangelo, S. Lanz, H. Leutwyler, and E. Passemar, "Determination of the light quark masses from $\eta \to 3\pi$," *PoS* **EPS-HEP2011** (2011) 304. `http://pos.sissa. it//archive/conferences/134/304/EPS-HEP2011_304.pdf`.

[65] S. Lanz, "$\eta \to 3\pi$ and quark masses." To appear in the Proceedings of the seventh International Workshop on Chiral Dynamics, 2012. `http://wwwold.jlab.org/ conferences/CD12/tuesday/Lanz.pdf`.

[66] K. Kampf, M. Knecht, J. Novotný, and M. Zdráhal, "Analytical dispersive construction of $\eta \to 3\pi$ amplitude: First order in isospin breaking," *Phys. Rev.* **D 84** (2011) 114015, `arXiv:1103.0982 [hep-ph]`.

[67] M. Zdrahal, "Prague–Lund–Marseille (analytical) dispersive approach to $\eta \to 3\pi$," in *Proceedings of the second International PrimeNet Workshop*. 2012. `arXiv:1204.5509 [nucl-ex]`.

[68] A. Deandrea, A. Nehme, and P. Talavera, "Determination of light quark masses from $\eta \to 3\pi^0$," *Phys. Rev.* **D 78** (2008) 034032, `arXiv:0803.2956 [hep-ph]`.

[69] A. Nehme and S. Zein, "Electromagnetic corrections to the $\eta \to 3\pi$ neutral decay," `arXiv:1106.0915 [hep-ph]`.

[70] A. Nehme, "The eta decay into three neutral pions is mainly electromagnetic," `arXiv:1106.3491 [hep-ph]`.

[71] C.-O. Gullström, A. Kupść, and A. Rusetsky, "Predictions for the cusp in $\eta \to 3\pi^0$ decay," *Phys. Rev.* **C 79** (2009) 028201, `arXiv:0812.2371 [hep-ph]`.

[72] A. Kupść, A. Rusetsky, and C.-O. Gullström, "A step towards systematic studies of the cusp in $\eta \to 3\pi^0$ decay," *Acta Phys. Polon. Supp.* **2** (2009) 169–176. `http://www. actaphys.uj.edu.pl/sup2/abs/s2p0169.htm`.

[73] B. Kubis and S. P. Schneider, "The cusp effect in $\eta' \to \eta\pi\pi$ decays," *Eur. Phys. J.* **C 62** (2009) 511–523, `arXiv:0904.1320 [hep-ph]`.

[74] A. Starostin, "η and η' physics at MAMI," *Eur. Phys. J. ST* **198** (2011) 117–131.

[75] M. Unverzagt, "Light meson physics with Crystal Ball/MAMI and at BES-III," *J. Phys. Conf. Ser.* **349** (2012) 012015.

[76] CBELSA/TAPS Collaboration, M. Lang, "Upgrade for the CBELSA/TAPS experiment at ELSA for η and η' decays," *Int. J. Mod. Phys.* **E 19** (2010) 938–945.

[77] H.-B. Li, "η and η' physics at BES-III," *J. Phys.* **G 36** (2009) 085009, `arXiv:0902.3032 [hep-ex]`.

[78] G. Amelino-Camelia, F. Archilli, D. Babusci, D. Badoni, G. Bencivenni, *et al.*, "Physics with the KLOE-2 experiment at the upgraded DAΦNE," *Eur. Phys. J.* **C 68** (2010) 619–681, `arXiv:1003.3868 [hep-ex]`.

[79] L. C. Balkeståhl, "Dalitz plot analysis for $\eta \to \pi^+\pi^-\pi^0$ at KLOE," in *Proceedings of the second International PrimeNet Workshop*. 2012. `arXiv:1204.5509 [nucl-ex]`.

[80] WASA-at-COSY Collaboration, P. Adlarson and M. Zieliński, "Measurement of the $\eta \to \pi^+\pi^-\pi^0$ decay with WASA-at-COSY detector," *Int. J. Mod. Phys.* **A 26** (2011) 622–624, `arXiv:1009.5508 [hep-ex]`.

[81] P. Adlarson, "The $\eta \to \pi^+\pi^-\pi^0$ decay with WASA-at-COSY," in *Proceedings of the second International PrimeNet Workshop*. 2012. `arXiv:1204.5509 [nucl-ex]`.

[82] H. Leutwyler, "On the foundations of chiral perturbation theory," *Annals Phys.* **235** (1994) 165–203, `arXiv:hep-ph/9311274`.

[83] H. Neufeld and H. Rupertsberger, "The electromagnetic interaction in chiral perturbation theory," *Z. Phys.* **C 71** (1996) 131–138, `arXiv:hep-ph/9506448`.

[84] J. Gasser, A. Rusetsky, and I. Scimemi, "Electromagnetic corrections in hadronic processes," *Eur. Phys. J.* **C 32** (2003) 97–114, `arXiv:hep-ph/0305260`.

[85] G. Colangelo and G. Isidori, "An introduction to ChPT," `arXiv:hep-ph/0101264`.

[86] S. Scherer, "Introduction to chiral perturbation theory," *Adv. Nucl. Phys.* **27** (2003) 277, `arXiv:hep-ph/0210398`.

[87] V. Bernard and U.-G. Meißner, "Chiral perturbation theory," *Ann. Rev. Nucl. Part. Sci.* **57** (2007) 33–60, `arXiv:hep-ph/0611231`.

[88] B. Kubis, "An introduction to chiral perturbation theory," `arXiv:hep-ph/0703274`.

[89] B. Borasoy, "Introduction to chiral perturbation theory," `arXiv:hep-ph/0703297`.

[90] S. Scherer and M. R. Schindler, "A primer for chiral perturbation theory," *Lect. Notes Phys.* **830** (2012) 1–249.

[91] J. Gasser and H. Leutwyler, "Quark masses," *Phys. Rept.* **87** (1982) 77–169.

[92] G. Ecker, G. Müller, H. Neufeld, and A. Pich, "π^0–η mixing and CP violation," *Phys. Lett.* **B 477** (2000) 88–92, `arXiv:hep-ph/9912264`.

[93] G. Amoros, J. Bijnens, and P. Talavera, "QCD isospin breaking in meson masses, decay constants and quark mass ratios," *Nucl. Phys.* **B 602** (2001) 87–108, `arXiv:hep-ph/0101127`.

[94] H. Leutwyler, "Implications of $\eta\eta'$ mixing for the decay $\eta \to 3\pi$,"
Phys. Lett. **B 374** (1996) 181–185, `arXiv:hep-ph/9601236`.

[95] M. Gell-Mann, R. J. Oakes, and B. Renner, "Behavior of current divergences under
$SU(3) \times SU(3)$," *Phys. Rev.* **175** (1968) 2195–2199.

[96] R. F. Dashen, "Chiral $SU(3) \times SU(3)$ as a symmetry of the strong interactions,"
Phys. Rev. **183** (1969) 1245–1260.

[97] M. Gell-Mann, "The eightfold way: a theory of strong interaction symmetry."
California Institute of Technology, Synchrotron Laboratory Report No. CTSL-20
(1961), unpublished.

[98] S. Okubo, "Note on unitary symmetry in strong interactions,"
Prog. Theor. Phys. **27** (1962) 949–966.

[99] S. Weinberg, "The problem of mass," *Trans. New York Acad. Sci.* **38** (1977) 185–201.

[100] G. Colangelo, S. Dürr, A. Jüttner, L. Lellouch, H. Leutwyler, *et al.*, "Review of lattice
results concerning low-energy particle physics," *Eur. Phys. J.* **C 71** (2011) 1695,
`arXiv:1011.4408 [hep-lat]`.

[101] J. Laiho, E. Lunghi, and R. S. Van de Water, "Lattice QCD inputs to the CKM
unitarity triangle analysis," *Phys. Rev.* **D 81** (2010) 034503,
`arXiv:0910.2928 [hep-ph]`.

[102] J. Laiho, "Light quark physics from lattice QCD," *PoS* **Lattice 2010** (2010) 320,
`arXiv:1106.0457 [hep-lat]`. `http://pos.sissa.it/archive/conferences/105/`
`013/Lattice2010_013.pdf`. [updates at `http://www.latticeaverages.org`].

[103] A. Kastner and H. Neufeld, "The $K_{\ell3}$ scalar form factors in the standard model,"
Eur. Phys. J. **C 57** (2008) 541–556, `arXiv:0805.2222 [hep-ph]`.

[104] D. B. Kaplan and A. V. Manohar, "Current mass ratios of the light quarks,"
Phys. Rev. Lett. **56** (1986) 2004–2007.

[105] H. Leutwyler, "The ratios of the light quark masses,"
Phys. Lett. **B 378** (1996) 313–318, `arXiv:hep-ph/9602366`.

[106] J. Bijnens, "Violations of Dashen's theorem," *Phys. Lett.* **B 306** (1993) 343–349,
`arXiv:hep-ph/9302217`.

[107] J. F. Donoghue, B. R. Holstein, and D. Wyler, "Electromagnetic self-energies of
pseudoscalar mesons and Dashen's theorem," *Phys. Rev.* **D 47** (1993) 2089–2097.

[108] R. Baur and R. Urech, "On the corrections to Dashen's theorem,"
Phys. Rev. **D 53** (1996) 6552–6557, `arXiv:hep-ph/9508393`.

[109] A. Duncan, E. Eichten, and H. Thacker, "Electromagnetic splittings and light quark
masses in lattice QCD," *Phys. Rev. Lett.* **76** (1996) 3894–3897,
`arXiv:hep-lat/9602005`.

[110] J. Bijnens and J. Prades, "Electromagnetic corrections for pions and kaons: Masses and polarizabilities," *Nucl. Phys.* **B 490** (1997) 239–271, `arXiv:hep-ph/9610360`.

[111] J. F. Donoghue and A. F. Perez, "The Electromagnetic mass differences of pions and kaons," *Phys. Rev.* **D 55** (1997) 7075–7092, `arXiv:hep-ph/9611331`.

[112] B. Moussallam, "A sum rule approach to the violation of Dashen's theorem," *Nucl. Phys.* **B 504** (1997) 381–414, `arXiv:hep-ph/9701400`.

[113] B. Ananthanarayan and B. Moussallam, "Four-point correlator constraints on electromagnetic chiral parameters and resonance effective Lagrangians," *JHEP* **0406** (2004) 047, `arXiv:hep-ph/0405206`.

[114] B. V. Martemyanov and V. S. Sopov, "Light quark mass ratio from Dalitz plot of $\eta \to \pi^+\pi^-\pi^0$ decay," *Phys. Rev.* **D 71** (2005) 017501, `arXiv:hep-ph/0502023`.

[115] S. L. Adler, "Consistency conditions on the strong interactions implied by a partially conserved axial-vector current," *Phys. Rev.* **137** (1965) B 1022–1033. Erratum-ibid. **139** (1965) AB 2.

[116] S. L. Adler, "Consistency conditions on the strong interactions implied by a partially conserved axial-vector current. II," *Phys. Rev.* **139** (1965) B 1638–1643.

[117] J. J. Sakurai, *Modern Quantum Mechanics.* Addison-Wesley Publishing, 1995. [Prentice Hall Publications, 2007].

[118] M. Knecht and R. Urech, "Virtual photons in low-energy $\pi\pi$ scattering," *Nucl. Phys.* **B 519** (1998) 329–360, `arXiv:hep-ph/9709348`.

[119] M. Kolesár, "Analysis of discrepancies in Dalitz plot parameters in $\eta \to 3\pi$ decay," *Nucl. Phys. Proc. Suppl.* **219–220** (2011) 292–295, `arXiv:1109.0851 [hep-ph]`.

[120] R. Dalitz, "On the analysis of τ-meson data and the nature of the τ-meson," *Phil.Mag.* **44** (1953) 1068–1080. `http://www.tandfonline.com/doi/abs/10.1080/14786441008520365`.

[121] E. Fabri, "A study of τ-meson decay," *Nuovo Cim.* **11** (1954) 479–491.

[122] R. Nißler, *Topics in three flavor chiral dynamics.* Thesis, University of Bonn, 2007. `http://hss.ulb.uni-bonn.de/2008/1316/1316.htm`.

[123] A. Kupść, "Decays of η and η' mesons: An introduction," *Int. J. Mod. Phys.* **E 18** (2009) 1255–1270.

[124] G. Isidori, "Soft-photon corrections in multi-body meson decays," *Eur. Phys. J.* **C 53** (2008) 567–571, `arXiv:0709.2439 [hep-ph]`.

[125] J. Bijnens and F. Borg, "Isospin breaking in $K \to 3\pi$ decays. II. Radiative corrections," *Eur. Phys. J.* **C 39** (2005) 347–357, `arXiv:hep-ph/0410333`.

[126] D. R. Yennie, S. C. Frautschi, and H. Suura, "The infrared divergence phenomena and high-energy processes," *Annals Phys.* **13** (1961) 379–452.

[127] S. Weinberg, "Infrared photons and gravitons," *Phys. Rev.* **140** (1965) B516–B524.

[128] S. Weinberg, "Pion scattering lengths," *Phys. Rev. Lett.* **17** (1966) 616–621.

[129] M. Knecht and A. Nehme, "Electromagnetic corrections to charged pion scattering at low energies," *Phys. Lett.* **B 532** (2002) 55–62, `arXiv:hep-ph/0201033`.

[130] M. Abramowitz and I. A. Stegun, *Handbook of mathematical functions*. Dover Publications, 1965. [U.S. Government Printing Office, 1972].

[131] Particle Data Group, C. Amsler *et al.*, "Review of particle physics," *Phys. Lett.* **B 667** (2008) 1–1340.

[132] B. R. Holstein, "How large is F_π?," *Phys. Lett.* **B 244** (1990) 83–87.

[133] V. Bernard and E. Passemar, "Matching chiral perturbation theory and the dispersive representation of the scalar $K\pi$ form-factor," *Phys. Lett.* **B 661** (2008) 95–102, `arXiv:0711.3450 [hep-ph]`.

[134] J. Bijnens, G. Ecker, and J. Gasser, "Chiral perturbation theory," `arXiv:hep-ph/9411232 [hep-ph]`.

[135] J. Bijnens and I. Jemos, "A new global fit of the L_i^r at next-to-next-to-leading order in Chiral Perturbation Theory," *Nucl. Phys.* **B 854** (2012) 631–665, `arXiv:1103.5945 [hep-ph]`.

[136] C. Haefeli, M. A. Ivanov, and M. Schmid, "Electromagnetic low-energy constants in ChPT," *Eur. Phys. J.* **C 53** (2008) 549–557, `arXiv:0710.5432 [hep-ph]`.

[137] R. Baur and R. Urech, "Resonance contributions to the electromagnetic low-energy constants of chiral perturbation theory," *Nucl. Phys.* **B 499** (1997) 319–348, `arXiv:hep-ph/9612328`.

[138] A. Pinzke, "Estimating the electromagnetic chiral Lagrangian coefficients," `arXiv:hep-ph/0406107`.

[139] M. Walker, "$\eta \to 3\pi$," Master's thesis, University of Bern, 1998.

[140] S. Lanz, *Determination of the quark mass ratio Q from $\eta \to 3\pi$*. Thesis, University of Bern, 2011.

[141] C. Ditsche, M. Hoferichter, B. Kubis, and U.-G. Meißner, "Roy–steiner equations for pion–nucleon scattering," *JHEP* **1206** (2012) 043, `arXiv:1203.4758 [hep-ph]`.

[142] D. Gotta *et al.*, "Pionic hydrogen," *Lect. Notes Phys.* **745** (2008) 165–185.

[143] T. Strauch *et al.*, "Pionic deuterium," *Eur. Phys. J.* **A 47** (2011) 88, `arXiv:1011.2415 [nucl-ex]`.

[144] V. Baru, C. Hanhart, M. Hoferichter, B. Kubis, A. Nogga, and D. R. Phillips, "Precision calculation of the π^- deuteron scattering length and its impact on threshold πN scattering," *Phys. Lett.* **B 694** (2011) 473–477, `arXiv:1003.4444 [nucl-th]`.

[145] V. Baru, C. Hanhart, M. Hoferichter, B. Kubis, A. Nogga, and D. R. Phillips, "Precision calculation of threshold $\pi^- d$ scattering, πN scattering lengths, and the GMO sum rule," *Nucl. Phys.* **A 872** (2011) 69–116, `arXiv:1107.5509 [nucl-th]`.

[146] J. Gasser, "Hadron masses and sigma commutator in the light of chiral perturbation theory," *Annals Phys.* **136** (1981) 62–112.

[147] A. Bottino, F. Donato, N. Fornengo, and S. Scopel, "Size of the neutralino–nucleon cross-section in the light of a new determination of the pion–nucleon sigma term," *Astropart. Phys.* **18** (2002) 205–211, `arXiv:hep-ph/0111229`.

[148] J. R. Ellis, K. A. Olive, and C. Savage, "Hadronic uncertainties in the elastic scattering of supersymmetric dark matter," *Phys. Rev.* **D 77** (2008) 065026, `arXiv:0801.3656 [hep-ph]`.

[149] K. A. Olive, "The impact of XENON100 and the LHC on supersymmetric dark matter," `arXiv:1202.2324 [hep-ph]`.

[150] A. Walker-Loud, "Evidence for non-analytic light quark mass dependence in the baryon spectrum," `arXiv:1112.2658 [hep-lat]`.

[151] T. P. Cheng and R. F. Dashen, "Is $SU(2) \otimes SU(2)$ a better symmetry than $SU(3)$?," *Phys. Rev. Lett.* **26** (1971) 594–597.

[152] S. Descotes, N. H. Fuchs, L. Girlanda, and J. Stern, "Analysis and interpretation of new low-energy $\pi\pi$ scattering data," *Eur. Phys. J.* **C 24** (2002) 469–483, `arXiv:hep-ph/0112088`.

[153] R. García-Martín, R. Kamiński, J. R. Peláez, J. Ruiz de Elvira, and F. J. Ynduráin, "Pion–pion scattering amplitude. IV. Improved analysis with once subtracted Roy-like equations up to 1100 MeV," *Phys. Rev.* **D 83** (2011) 074004, `arXiv:1102.2183 [hep-ph]`.

[154] I. Caprini, G. Colangelo, and H. Leutwyler, "Regge analysis of the $\pi\pi$ scattering amplitude," *Eur. Phys. J.* **C 72** (2012) 1860, `arXiv:1111.7160 [hep-ph]`.

[155] I. Caprini, G. Colangelo, and H. Leutwyler. In preparation.

[156] B. Moussallam, "Couplings of light $I = 0$ scalar mesons to simple operators in the complex plane," *Eur. Phys. J.* **C 71** (2011) 1814, `arXiv:1110.6074 [hep-ph]`.

[157] B. Ananthanarayan and P. Büttiker, "Comparison of πK scattering in $SU(3)$ chiral perturbation theory and dispersion relations," *Eur. Phys. J.* **C 19** (2001) 517–528, `arXiv:hep-ph/0012023`.

[158] P. Büttiker, S. Descotes-Genon, and B. Moussallam, "A new analysis of πK scattering from Roy and Steiner type equations," *Eur. Phys. J.* **C 33** (2004) 409–432, `arXiv:hep-ph/0310283`.

[159] M. Hoferichter, D. R. Phillips, and C. Schat, "Roy–Steiner equations for $\gamma\gamma \to \pi\pi$," *Eur. Phys. J.* **C 71** (2011) 1743, `arXiv:1106.4147 [hep-ph]`.

[160] T. Becher and H. Leutwyler, "Low energy analysis of $\pi N \to \pi N$,"
JHEP **0106** (2001) 017, `arXiv:hep-ph/0103263`.

[161] G. E. Hite and F. Steiner, "New dispersion relations and their application to
partial-wave amplitudes," *Nuovo Cim.* **A 18** (1973) 237–270.

[162] R. Koch, "A new determination of the πN sigma term using hyperbolic dispersion
relations in the (ν^2, t) plane," *Z. Phys.* **C 15** (1982) 161–168.

[163] G. Höhler, "Determinations of the πN sigma term," *PiN Newslett.* **15** (1999) 123–126.

[164] J. Stahov, "The subthreshold expansion of the πN invariant amplitudes in dispersion
theory," *PiN Newslett.* **15** (1999) 13–18.

[165] J. Stahov, "Calculation of πN partial waves from hyperbolic dispersion relations," *PiN
Newslett.* **16** (2002) 116–120.

[166] N. I. Muskhelishvili, *Singular Integral Equations.* Wolters-Noordhoff Publishing, 1953.
[Dover Publications, 2008].

[167] R. Omnès, "On the solution of certain singular integral equations of quantum field
theory," *Nuovo Cim.* **8** (1958) 316–326.

[168] J. Gasser and G. Wanders, "One channel Roy equations revisited,"
Eur. Phys. J. **C 10** (1999) 159–173, `arXiv:hep-ph/9903443`.

[169] G. Wanders, "The role of the input in Roy's equations for $\pi\pi$ scattering,"
Eur. Phys. J. **C 17** (2000) 323–336, `arXiv:hep-ph/0005042`.

[170] R. Koch and E. Pietarinen, "Low-energy πN partial wave analysis,"
Nucl. Phys. **A 336** (1980) 331–346.

[171] G. Höhler, *Pion-Nukleon-Streuung: Methoden und Ergebnisse*, vol. **9b2** of
Landolt-Börnstein. Springer Verlag, 1983.

[172] J. Stahov, "Determination of πN low-energy parameters from forward dispersion
relations," *PiN Newslett.* **13** (1997) 174–180.

[173] M. Hoferichter, C. Ditsche, B. Kubis, and U.-G. Meißner, "Dispersive analysis of the
scalar form factor of the nucleon," *JHEP* **1206** (2012) 063,
`arXiv:1204.6251 [hep-ph]`.

[174] H. Burkhardt, *Dispersion Relation Dynamics.* North-Holland Publishing, 1969.

[175] T. W. B. Kibble, "Kinematics of general scattering processes and the Mandelstam
representation," *Phys. Rev.* **117** (1960) 1159–1162.

[176] Particle Data Group, K. Nakamura *et al.*, "Review of particle physics,"
J. Phys. **G 37** (2010) 075021.

[177] J. Hamilton and T. D. Spearman, "Low-energy pion scattering,"
Annals Phys. **12** (1961) 172–199.

[178] M. Döring, C. Hanhart, F. Huang, S. Krewald, and U.-G. Meißner, "Analytic properties of the scattering amplitude and resonances parameters in a meson exchange model," *Nucl. Phys.* **A 829** (2009) 170–209, `arXiv:0903.4337 [nucl-th]`.

[179] W. B. Kaufmann and G. E. Hite, "Tests of current algebra and partially conserved axial-vector current in the subthreshold region of the pion–nucleon system," *Phys. Rev.* **C 60** (1999) 055204.

[180] L. S. Brown, W. J. Pardee, and R. D. Peccei, "Adler-Weisberger theorem reexamined," *Phys. Rev.* **D 4** (1971) 2801–2810.

[181] V. Bernard, N. Kaiser, and U.-G. Meißner, "On the analysis of the pion–nucleon σ-term: The size of the remainder at the Cheng–Dashen point," *Phys. Lett.* **B 389** (1996) 144–148, `arXiv:hep-ph/9607245`.

[182] G. E. Hite, W. B. Kaufmann, and R. J. Jacob, "New evaluation of the πN sigma term," *Phys. Rev.* **C 71** (2005) 065201.

[183] S. L. Adler, "Sum rules for the axial-vector coupling-constant renormalization in β decay," *Phys. Rev.* **140** (1965) B 736–747. Erratum-ibid. **149** (1966) 1294, Erratum-ibid. **175** (1968) 2224.

[184] W. I. Weisberger, "Unsubtracted dispersion relations and the renormalization of the weak axial-vector coupling constants," *Phys. Rev.* **143** (1966) 1302–1309.

[185] G. E. Hite, R. J. Jacob, and M. D. Scadron, "Test of the partial conservation of axial-vector current limit in pion–nucleon scattering," *Phys. Rev.* **D 14** (1976) 1306–1310.

[186] J. R. Taylor, *Scattering Theory*. Wiley & Sons, 1972. [Dover Publications, 2006].

[187] R. E. Cutkosky, "Singularities and discontinuities of Feynman amplitudes," *J. Math. Phys.* **1** (1960) 429–433.

[188] C. Itzykson and J.-B. Zuber, *Quantum Field Theory*. McGraw-Hill, 1980. [Dover Publications, 2005].

[189] M. Jacob and G. C. Wick, "On the general theory of collisions for particles with spin," *Annals Phys.* **7** (1959) 404–428. [Annals Phys. **281** (2000) 774–799].

[190] D. A. Varshalovich, A. N. Moskalev, and V. K. Khersonskii, *Quantum Theory of Angular Momentum*. World-Scientific Publishing, 1988.

[191] J. T. Cushing, *Theory Construction and Selection in Modern Physics: The S Matrix*. Cambridge University Press, 1990.

[192] J. D. Bjorken and S. D. Drell, *Relativistic Quantum Fields*. McGraw-Hill, 1965. [Relativistische Quantenfeldtheorie, B.I. Wissenschaftsverlag, 1993].

[193] G. Barton, *Introduction to Dispersion Techniques in Field Theory*. W. A. Benjamin, 1965.

[194] R. J. Eden, P. V. Landshoff, D. I. Olive, and J. C. Polkinghorne, *The Analytic S-Matrix*. Cambridge University Press, 1966. [Cambridge University Press, 2002].

[195] G. F. Chew, *The Analytic S Matrix*. W. A. Benjamin, 1966.

[196] D. V. Shirkov, V. V. Serebryakov, and V. A. Meshcheryakov, *Dispersion Theories of Strong Interactions at Low Energy*. North-Holland Publishing, 1969.

[197] N. M. Queen and G. Violini, *Dispersion Theory in High-Energy Physics*. MacMillan Press, 1974.

[198] B. R. Martin, D. Morgan, and G. Shaw, *Pion–Pion Interactions in Particle Physics*. Academic Press, 1976.

[199] G. E. Brown and A. D. Jackson, *The Nucleon–Nucleon Interaction*. North-Holland Publishing, 1976.

[200] G. Sommer, "Extension of the axiomatic analyticity domain: Pion–nucleon scattering," *Nuovo Cim.* **A 52** (1967) 373–388.

[201] G. Sommer, "Present state of rigorous analytic properties of scattering amplitudes," *Fortsch. Phys.* **18** (1970) 577–688.

[202] D. V. Bugg, A. A. Carter, and J. R. Carter, "New values of pion–nucleon scattering lengths and f^2," *Phys. Lett.* **B 44** (1973) 278–280.

[203] J. J. de Swart, M. C. M. Rentmeester, and R. G. E. Timmermans, "The status of the pion–nucleon coupling constant," *PiN Newslett.* **13** (1997) 96–107, `arXiv:nucl-th/9802084`.

[204] R. A. Arndt, W. J. Briscoe, I. I. Strakovsky, and R. L. Workman, "Extended partial-wave analysis of πN scattering data," *Phys. Rev.* **C 74** (2006) 045205, `arXiv:nucl-th/0605082`.

[205] G. F. Chew, M. L. Goldberger, F. E. Low, and Y. Nambu, "Application of dispersion relations to low-energy meson–nucleon scattering," *Phys. Rev.* **106** (1957) 1337–1344.

[206] J. Baacke and F. Steiner, "πN partial wave relations from fixed-t dispersion relations," *Fortsch. Phys.* **18** (1970) 67–87.

[207] F. Steiner, "On the generalized πN potential. A new representation from fixed-t dispersion relations," *Fortsch. Phys.* **18** (1970) 43–65.

[208] F. Steiner, "Partial wave crossing relations for meson–baryon scattering," *Fortsch. Phys.* **19** (1971) 115–159.

[209] S. W. MacDowell, "Analytic properties of partial amplitudes in meson–nucleon scattering," *Phys. Rev.* **116** (1959) 774–778.

[210] W. R. Frazer and J. R. Fulco, "Partial-wave dispersion relations for pion–nucleon scattering," *Phys. Rev.* **119** (1960) 1420–1426.

[211] Bateman Manuscript Project Staff, *Higher Transcendental Functions*, vol. **1** of *Bateman Manuscript Project*. McGraw-Hill, 1953.

[212] W. R. Frazer and J. R. Fulco, "Partial-wave dispersion relations for the process $\pi + \pi \to N + \bar{N}$," *Phys. Rev.* **117** (1960) 1603–1609.

[213] E. Pietarinen, "A calculation of $\pi\pi \to N\bar{N}$ amplitudes in the pseudophysical region." University of Helsinki Preprint Series in Theoretical Physics HU-TFT-17-77, unpublished.

[214] S. Descotes-Genon and B. Moussallam, "The $K_0^*(800)$ scalar resonance from Roy–Steiner representations of πK scattering," *Eur. Phys. J.* **C 48** (2006) 553–560, arXiv:hep-ph/0607133.

[215] S. Mandelstam, "Determination of the pion–nucleon scattering amplitude from dispersion relations and unitarity. General theory," *Phys. Rev.* **112** (1958) 1344–1360.

[216] G. Auberson and L. Epele, "A tool for extending the analyticity domain of partial wave amplitudes and the validity of Roy-type equations," *Nuovo Cim.* **A 25** (1975) 453–466.

[217] S. Mandelstam, "Analytic properties of transition amplitudes in perturbation theory," *Phys. Rev.* **115** (1959) 1741–1751.

[218] S. Mandelstam, "Construction of the perturbation series for transition amplitudes from their analyticity and unitarity properties," *Phys. Rev.* **115** (1959) 1752–1762.

[219] A. Martin, "Extension of the axiomatic analyticity domain of scattering amplitudes by unitarity – I.," *Nuovo Cim.* **A 42** (1965) 930–953.

[220] A. Martin, "Extension of the axiomatic analyticity domain of scattering amplitudes by unitarity – II.," *Nuovo Cim.* **A 44** (1965) 1219–1244.

[221] S. W. MacDowell, "Analytic continuation of reduced pion-nucleon partial-wave amplitudes," *Phys. Rev.* **D 6** (1972) 3512–3515.

[222] F. F. K. Cheung and F. S. Chen-Cheung, "Uniqueness of amplitudes satisfying the Mandelstam representation," *Phys. Rev.* **D 5** (1972) 970–980.

[223] W. B. Rolnick, "Comment on the application of Cutkosky's rules," *Phys. Rev. Lett.* **16** (1966) 544–545.

[224] H. Lehmann, "Analytic properties of scattering amplitudes as functions of momentum transfer," *Nuovo Cim.* **10** (1958) 579–589.

[225] J. Stahov, *Dispersion relations on hyperbolas and higher pion–nucleon partial waves.* Thesis, University of Zagreb, 1983. [In Croatian].

[226] T. Regge, "Introduction to complex orbital momenta," *Nuovo Cim.* **14** (1959) 951–976.

[227] P. D. B. Collins, *An Introduction to Regge Theory and High Energy Physics.* Cambridge University Press, 1977.

[228] F. Huang, A. Sibirtsev, J. Haidenbauer, S. Krewald, and U.-G. Meißner, "Backward pion–nucleon scattering," *Eur. Phys. J.* **A 44** (2010) 81–92, `arXiv:0910.4275 [nucl-th]`.

[229] K. M. Watson, "Some general relations between the photoproduction and scattering of π mesons," *Phys. Rev.* **95** (1954) 228–236.

[230] B. Ananthanarayan, I. Caprini, G. Colangelo, J. Gasser, and H. Leutwyler, "Scalar form factors of light mesons," *Phys. Lett.* **B 602** (2004) 218–225, `arXiv:hep-ph/0409222`.

[231] H.-W. Hammer, *Vector neutral current form factors of the nucleon.* Thesis, University of Mainz, 1997.

[232] M. J. Musolf, H.-W. Hammer, and D. Drechsel, "Nucleon strangeness and unitarity," *Phys. Rev.* **D 55** (1997) 2741–2755, `arXiv:hep-ph/9610402`. Erratum-ibid. **D 62** (2000) 079901.

[233] W. R. Frazer and J. R. Fulco, "Effect of a pion–pion scattering resonance on nucleon structure. II," *Phys. Rev.* **117** (1960) 1609–1614.

[234] M. Froissart, "Asymptotic behavior and subtractions in the Mandelstam representation," *Phys. Rev.* **123** (1961) 1053–1057.

[235] M. Froissart, "Froissart bound," *Scholarpedia* **5** (2010) 10353.

[236] A. Martin, "Unitarity and high-energy behavior of scattering amplitudes," *Phys. Rev.* **129** (1963) 1432–1436.

[237] P. Büttiker and U.-G. Meißner, "Pion–nucleon scattering inside the Mandelstam triangle," *Nucl. Phys.* **A 668** (2000) 97–112, `arXiv:hep-ph/9908247`.

[238] A. Gasparyan and M. F. M. Lutz, "Photon– and pion–nucleon interactions in a unitary and causal effective field theory based on the chiral Lagrangian," *Nucl. Phys.* **A 848** (2010) 126–182, `arXiv:1003.3426 [hep-ph]`.

[239] T. N. Pham and T. N. Truong, "Muskhelishvili-Omnès integral equation with inelastic unitarity: Single- and coupled-channel equations," *Phys. Rev.* **D 16** (1977) 896–903.

[240] I. Caprini, "Omnès representations with inelastic effects for hadronic form factors," *Rom. J. Phys.* **50** (2005) 7–17. `http://www.nipne.ro/rjp/2005_50_1-2/0007_0018.pdf`.

[241] B. Ananthanarayan, P. Büttiker, and B. Moussallam, "πK sum rules and the $SU(3)$ chiral expansion," *Eur. Phys. J.* **C 22** (2001) 133–148, `arXiv:hep-ph/0106230`.

[242] J. L. Basdevant, J. C. Le Guillou, and H. Navelet, "Crossing and physical partial-wave amplitudes," *Nuovo Cim.* **A 7** (1972) 363–396.

[243] A. Schenk, "Absorption and dispersion of pions at finite temperature," *Nucl. Phys.* **B 363** (1991) 97–113.

[244] W. R. Frazer and J. R. Fulco, "Effect of a pion–pion scattering resonance on nucleon structure," *Phys.Rev.Lett.* **2** (1959) 365–368.

[245] C. D. Froggatt and J. L. Petersen, "Phase-shift analysis of $\pi^+\pi^-$ scattering between 1.0 GeV and 1.8 GeV based on fixed momentum transfer analyticity. II.," *Nucl. Phys.* **B 129** (1977) 89–110.

[246] E. Pietarinen, "Dispersion relations and experimental data," *Nuovo Cim.* **A 12** (1972) 522–531.

[247] G. Höhler, "Some results on πN phenomenology," *PiN Newslett.* **15** (1999) 7–12.

[248] R. Koch and M. Hutt, "A partial wave dispersion relation analysis of pion–nucleon scattering amplitudes," *Z. Phys.* **C 19** (1983) 119–128.

[249] G. Höhler, F. Kaiser, R. Koch, and E. Pietarinen, "Handbook of pion–nucleon scattering," *J. Phys. Data* **12-1** (1979) . [Published by Fachinformationszentrum Karlsruhe].

[250] R. Koch, "Improved πN partial waves, consistent with analyticity and unitarity," *Z. Phys.* **C 29** (1985) 597–609.

[251] R. Koch, "A calculation of low-energy πN partial waves based on fixed-t analyticity," *Nucl. Phys.* **A 448** (1986) 707–731.

[252] R. A. Arndt, R. L. Workman, I. I. Strakovsky, and M. M. Pavan, "πN elastic scattering analyses and dispersion relation constraints," `arXiv:nucl-th/9807087`.

[253] R. A. Arndt, W. J. Briscoe, I. I. Strakovsky, and R. L. Workman, "Partial-wave analysis and baryon spectroscopy," *Eur. Phys. J.* **A 35** (2008) 311–316.

[254] SAID Partial-Wave Analysis Facility. Data Analysis Center, Center for Nuclear Studies, George Washington University. `http://gwdac.phys.gwu.edu/`.

[255] A. V. Anisovich *et al.*, "Partial wave analysis of $\bar{p}p \to \pi^-\pi^+$, $\pi^0\pi^0$, $\eta\eta$ and $\eta\eta'$," *Nucl. Phys.* **A 662** (2000) 319–343, `arXiv:1109.1188 [hep-ex]`.

[256] B. R. Martin and G. C. Oades, "$\bar{N}N \to \pi\pi$ in the resonance region: (I) Invariant amplitudes," *Nucl. Phys.* **A 483** (1988) 669–685.

[257] B. R. Martin and G. C. Oades, "Partial-wave amplitudes and resonances in $\bar{p} + p \to \pi + \pi$," *Phys. Rev.* **C 56** (1997) 1114–1123, `arXiv:hep-ph/9703253`.

[258] B. R. Martin and G. C. Oades, "Amplitudes and resonances from an energy-dependent analysis of $\bar{p} + p \to \pi + \pi$," *Phys. Rev.* **C 57** (1998) 3492–3494, `arXiv:hep-ph/9802261`.

[259] M. E. Sainio, "Analyticity constrained pion–nucleon analysis," *PoS* **CD09** (2009) 013. `http://pos.sissa.it/archive/conferences/086/013/CD09_013.pdf`.

[260] P. Metsä, "Forward analysis of πN scattering with an expansion method," *Eur. Phys. J.* **A 33** (2007) 349–353, `arXiv:0705.4528 [hep-ph]`.

[261] S. M. Flatté, "Coupled-channel analysis of the $\pi\eta$ and $K\bar{K}$ systems near $K\bar{K}$ threshold," *Phys. Lett.* **B 63** (1976) 224–227.

[262] V. Baru, J. Haidenbauer, C. Hanhart, A. Kudryavtsev, and U.-G. Meißner, "Flatté-like distributions and the $a_0(980)$ / $f_0(980)$ mesons," *Eur. Phys. J.* **A 23** (2005) 523–533, `arXiv:nucl-th/0410099`.

[263] R. García-Martín, R. Kamiński, J. R. Peláez, and J. Ruiz de Elvira, "Precise determination of the $f_0(600)$ and $f_0(980)$ pole parameters from a dispersive data analysis," *Phys. Rev. Lett.* **107** (2011) 072001, `arXiv:1107.1635 [hep-ph]`.

[264] M. M. Nagels, T. A. Rijken, and J. J. de Swart, "Low-energy nucleon–nucleon potential from Regge-pole theory," *Phys. Rev.* **D 17** (1978) 768–776.

[265] P. M. M. Maessen, T. A. Rijken, and J. J. de Swart, "Soft-core baryon–baryon one-boson-exchange models. II. Hyperon–nucleon potential," *Phys. Rev.* **C 40** (1989) 2226–2245.

[266] V. G. J. Stoks, R. A. M. Klomp, C. P. F. Terheggen, and J. J. de Swart, "Construction of high-quality NN potential models," *Phys. Rev.* **C 49** (1994) 2950–2963, `arXiv:nucl-th/9406039`.

[267] T. A. Rijken, H. Polinder, and J. Nagata, "Extended-soft-core NN potentials in momentum space. II. Meson-pair exchange potentials," *Phys. Rev.* **C 66** (2002) 044009, `arXiv:nucl-th/0201020`.

[268] M. M. Pavan, I. I. Strakovsky, R. L. Workman, and R. A. Arndt, "The pion–nucleon sigma term is definitely large: Results from a GWU analysis of πN scattering data," *PiN Newslett.* **16** (2002) 110–115, `arXiv:hep-ph/0111066`.

[269] G. C. Oades, "Finite contour dispersion relations and the subthreshold expansion coefficients of the πN invariant amplitudes," *PiN Newslett.* **15** (1999) 307–310.

[270] B. R. Martin and G. C. Oades, "Threshold and subthreshold πN scattering amplitudes: Comparison with chiral perturbation theory predictions," *PiN Newslett.* **16** (2002) 133–137.

[271] N. Fettes, *Pion–nucleon physics in chiral perturbation theory*. Thesis, FZ Jülich / University of Bonn, 2000.

[272] M. M. Pavan, R. A. Arndt, I. I. Strakovsky, and R. L. Workman, "Determination of the πNN coupling constant in the VPI/GWU $\pi N \to \pi N$ partial-wave and dispersion relation analysis," *PiN Newslett.* **15** (1999) 171–175, `arXiv:nucl-th/9910040`. [Phys. Scripta **T87** (2000) 65–70].

[273] N. Fettes, U.-G. Meißner, and S. Steininger, "Pion–nucleon scattering in chiral perturbation theory. I. Isospin-symmetric case," *Nucl. Phys.* **A 640** (1998) 199–234, `arXiv:hep-ph/9803266`.

[274] N. Fettes and U.-G. Meißner, "Pion–nucleon scattering in chiral perturbation theory. II. Fourth order calculation," *Nucl. Phys.* **A 676** (2000) 311–338, `arXiv:hep-ph/0002162`.

[275] G. Höhler and E. Pietarinen, "Electromagnetic radii of nucleon and pion,"
Phys. Lett. **B 53** (1975) 471–475.

[276] M. A. Belushkin, H.-W. Hammer, and U.-G. Meißner, "Dispersion analysis of the
nucleon form factors including meson continua," *Phys. Rev.* **C 75** (2007) 035202,
`arXiv:hep-ph/0608337`.

[277] I. T. Lorenz, H.-W. Hammer, and U.-G. Meißner, "The size of the proton — closing in
on the radius puzzle," `arXiv:1205.6628 [hep-ph]`.

[278] J. Gasser, H. Leutwyler, and M. E. Sainio, "Form factor of the σ-term,"
Phys. Lett. **B 253** (1991) 260–264.

[279] J. F. Donoghue, J. Gasser, and H. Leutwyler, "The decay of a light Higgs boson,"
Nucl. Phys. **B 343** (1990) 341–368.

[280] F.-K. Guo, C. Hanhart, F. J. Llanes-Estrada, and U.-G. Meißner, "Quark mass
dependence of the pion vector form factor," *Phys. Lett.* **B 678** (2009) 90–96,
`arXiv:0812.3270 [hep-ph]`.

[281] G. Colangelo, "Hadronic contributions to a_μ below one GeV,"
Nucl. Phys. Proc. Suppl. **131** (2004) 185–191, `arXiv:hep-ph/0312017`.

Danksagung